LATE QUATERNARY VOLCANIC STRATIGRAPHY WITHIN A PORTION OF THE NORTHEASTERN TONGARIRO VOLCANIC CENTRE

A thesis presented as partial fulfilment of the requirements for the degree of

Doctor of Philosophy in Soil Science

By

Shane Jason Cronin

Massey University
Palmerston North
New Zealand

1996

Mount Ruapehu viewed from the east, July 1996.
Fresh tephra covers snow on the northern sector of the volcano.

ACKNOWLEDEGMENTS

I thank Vince Neall, Bob Stewart and Alan Palmer for all their help during the course of this study. The enthusiasm and passion they have for their science has taught me that geology is not just a job, nor a discipline, but a lifelong process of discovery.

In particular I thank Vince for "letting me loose" on this project, even if it seemed that I was heading in the wrong direction at times.

Cleland Wallace, John Kirkman, Brent Alloway and David Lowe have all provided valuable and highly appreciated input into various parts of this work, as have journal reviewers listed within the thesis.

I was the grateful benefactor of funding from the New Zealand Vice Chancellors Committee, the Helen E. Akers Scholarship fund (twice!), the Massey University Graduate Research Fund and the Tongariro Natural History Society.

Travel funding from the Royal Society of New Zealand (Young Scientists' Fund), Massey University Research Fund, and the New Zealand Vice Chancellors Committee (Claude McCarthy Fellowship) enabled me to attend two international conferences, which has greatly enhanced my Ph.D. experience.

I am grateful to Justlands, the Department of Conservation and the Rangipo Forest Trust for access into parts of the study area.

I thank all my contemporaries in the Department of Soil Science for making it such a relaxed and "down to earth" place to work, particularly John (pH) Morrell and Shivaraj (Bucket) Gurung.

Last but not least, I thank my family and Iris for their patient support during this work.

ABSTRACT

Investigation of the Late Quaternary volcanic stratigraphy within the andesitic Tongariro Volcanic Centre has elucidated the history of construction of the northeastern Ruapehu and eastern Tongariro ring plains and provided a lahar record for the Tongariro catchment. Volcaniclastic ring-plain sequences were correlated and dated using rhyolitic and andesitic marker tephras.

The identification of distal rhyolitic tephras in the area was improved by the application of discriminant function analysis (DFA) to their electron microprobe-determined glass chemistry. The Okaia, Omataroa and Hauparu Tephras and the Rotoehu Ash were identified for the first time in this area, providing a chronology for pre-22.6 ka ring-plain sequences not previously investigated.

DFA of ferromagnesian mineral chemistry proved useful for discrimination of andesitic tephras, with titanomagnetite being the most useful phase. Development of an andesitic tephrostratigraphy in pre-22.6 ka sequences was aided by clustering analysis and DFA. Seven andesitic marker tephras were identified using a range of parameters to supplement the rhyolitic tephrostratigraphy.

Using the tephrochronologic framework, 15 packages of lahar deposits were identified on the northeastern Ruapehu ring plain (from >64 to *c.* 5.2 ka) and six on the eastern Tongariro ring plain (from >22.6 to 11.9 ka). Lahar deposition on both ring plains was most voluminous and widespread during the last (Ohakean) and antepenultimate (Porewan) stadials of the last glacial (Otiran). Holocene lahars were restricted to a narrow sector of the northeastern Ruapehu ring plain. They appear to have been triggered mostly in response to large-scale tephra eruptions of Ruapehu and Tongariro, and mostly occurred along the path of the Mangatoetoenui Stream.

Lahar deposits and surfaces beside the Tongariro River were mapped in eight lahar hazard zones, with lahar recurrence intervals ranging from 1 in >15 000 years to 1 in 35 years. The largest number and volume of lahars in this catchment occurred in the period from 14.7 to 10 ka. The greatest population risk identified in the Tongariro catchment is part of Turangi, built within a 1 in 1000 year lahar-hazard zone. Other property and infrastructure at greater risk include the State Highway 1 bridge across the Mangatoetoenui Stream and the Rangipo Dam and Power Station, within a 1 in 35 year hazard zone.

The landscape of the northeastern Ruapehu and eastern Tongariro ring plains has developed in relation to late Quaternary climate changes in addition to volcanic activity. During the last and antepenultimate stadials of the last glacial, major ring-plain aggradation by lahars and streams occurred. This was probably in response to greater physical weathering and glacier action on the volcanic cones providing abundant sediment for lahars. During the warmer interstadials of the last glacial, soil development within andesitic ring plain material was greatest, particularly when the rate of soil accretion was low.

TABLE OF CONTENTS

PREFACE

CHAPTER ONE: INTRODUCTION, OBJECTIVES, OUTLINE OF STUDY AREA AND PREVIOUS WORK

CHAPTER 2: RHYOLITIC TEPHROCHRONOLOGY

CHAPTER 3: ANDESITIC TEPHROCHRONOLOGY

CHAPTER 4: PALEOSOL DEVELOPMENT AND PALEOCLIMATIC INVESTIGATIONS OF THE RING PLAIN SEQUENCE

CHAPTER 7: GEOLOGY AND LANDSCAPE DEVELOPMENT OF THE NORTHEASTERN TONGARIRO VOLCANIC CENTRE

CHAPTER 8: CONCLUSIONS

LIST OF TABLES

LIST OF PLATES

LIST OF FIGURES

CHAPTER 1: INTRODUCTION, OBJECTIVES, OUTLINE OF STUDY AREA AND PREVIOUS WORK

1.1 Introduction

Ruapehu and Tongariro are the two largest and youngest Quaternary volcanoes of the Tongariro Volcanic Centre in the central North Island of New Zealand. Both volcanoes are surrounded by ring plains composed dominantly of volcaniclastic deposits and lava flows. The ring plains are volumetrically as large or larger than the cone they surround. The ring plains provide arguably the best geologic record of the activity of the two volcanoes, because the cone itself is generally exposed to more severe physical weathering leading to greater erosion and loss of the stratigraphic record, and also older deposits tend to be buried by later erupted lavas. Of human importance, the geologic record contained within the ring plains provides information on the rates and magnitudes of tephra eruptives and lahars from the two volcanoes which are of the greatest threat to life and property.

1.2 Objectives of study

The manifold objectives of this study all branched from the main aim of establishing a stratigraphy for the northeastern Ruapehu and eastern Tongariro ring plains. Once this stratigraphy was developed, investigations were made into the chronology and rates of tephra eruptions, lahars, lava flows and also soil development and landscape stability. Prior to this study the last detailed work in this area of the ring plains was that of Topping (1973, and 1974). Topping's study was limited to the younger part of the stratigraphic record (<22.5 ka B.P.) and mostly to the Tongariro ring plain. The outcomes of this study were to be; (1) an improved assessment of the lahar hazards from Ruapehu volcano in conjunction with the previous studies of Purves (1990), Donoghue (1991) and Hodgson (1993) on other sectors of the volcano, (2) an assessment of the lahar hazards on the eastern Tongariro ring plain and the Tongariro River, (3) a better understanding of the eruptive history (particularly that of pre-22.5 ka tephra eruptives) from the two volcanoes, and (4) an overall synthesis of the landscape development of the NE Ruapehu and E Tongariro ring plains.

1.3 Methods

The initial part of the study was carried out in the field. The ring-plain areas were traversed and detailed section descriptions taken of all important exposures found. Effort was concentrated on the channels of rivers and streams which incise into the ring-plain deposits, affording the best exposure of the ring plain stratigraphy. Aerial photography was used where possible in conjunction with the field information to map deposits and/or surfaces using their coverbed stratigraphy. Previously dated tephra layers, both rhyolitic

and andesitic, were quickly found to be the most useful means of dating surfaces and deposits. Laboratory studies concentrated on the identification of these tephras and also on finding new marker tephra layers, particularly andesitic tephras.

Laboratory studies involved analysing the mineralogy of tephras as well as major element mineral and glass chemistry using the electron microprobe technique. Statistical methods were developed and used for both rhyolitic and andesitic tephra identification from the chemical analyses. Further laboratory studies were also conducted on buried soil materials to investigate former soil-forming, landscape and paleoclimatic conditions.

1.4 Geography of the study area

This study was confined to the NE Ruapehu and E Tongariro ring plains and is effectively the volcanic portion of the Tongariro River catchment (Fig. 1.1). The southern extent of the area lies along the watershed boundary between the Whangaehu River to the south and the Tongariro River to the north. Donoghue (1991) studied the Ruapehu ring plain in detail south of this boundary. The studied area encompasses the full eastern extent of the two ring plains which terminate against foothills of the Kaimanawa Mountains in the approximate position of the Tongariro River channel. The Round-the-Mountain Track on Ruapehu and a similar altitude (ca. 1300 m) on Tongariro marks the western boundary of study. North of State Highway 47A the study area narrowed to the general vicinity of the Tongariro River and its terraces.

The town of Turangi is the largest population centre within the area with a population of 4239 in 1991 (Department of Statistics, 1992). In addition, two smaller settlements, Rangipo and Tokaanu, and the Rangipo Prison lie within the study area. These settlements and other scattered dwellings are confined to the northern part of the area, while in the southern portion there are no permanent dwellings (Fig. 1.2).

The Turangi-Tokaanu area has been occupied by Maori of the Ngati Tuwharetoa tribe since the 16th century and European settlement began in the Tokaanu area as trout were released into the Tongariro River in the early 1900s (Clarke and Smith, 1986). Prior to 1964 less than 500 people lived in Turangi. The population swelled up to 7000 during the period of construction of the Tongariro Power Development from 1964 to 1983 (Mercer, 1973). Following completion of the Tongariro Power Development the population has dwindled and the town has become a service centre for a developing tourist industry. In addition, the town services extensive exotic forestry planting and the surrounding farming industry.

The southern part of the study area contains a large portion of the Tongariro National Park, while other parts of the area are Ngati Tuwharetoa tribal lands, Justice Department land and also Kaimanawa State Forest Park (Fig. 1.2).

A major arterial transport route, State Highway 1, runs through the centre of the area as well as three sets of high voltage electricity transmission lines. Parts of the major Tongariro power development are also contained within the area.

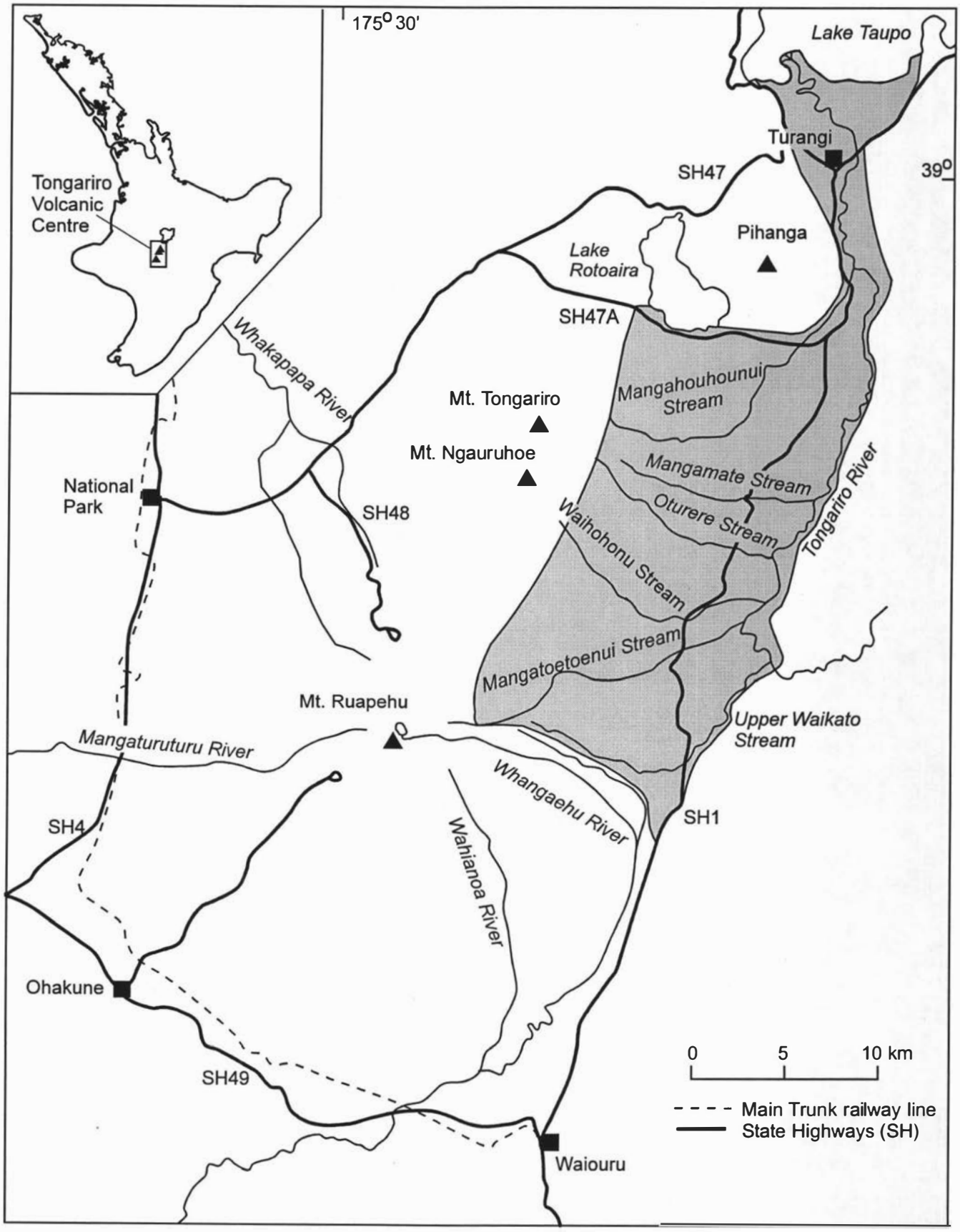

Figure 1.1. Location of the study area (shaded) within the Tongariro Volcanic Centre, central North Island, New Zealand

In this hydroelectric power scheme water is diverted from the southern tributaries of Ruapehu through an underground aqueduct into Lake Moawhango. Subsequently the water travels via a tunnel to the Rangipo Dam within the Tongariro River channel; water from the Wahianoa River is also diverted into the dam (Ministry of Works and Development, 1974). Water is then taken from the dam into the underground Rangipo Power station before being returned to the Tongariro River. A short distance downstream a variable proportion of the water is diverted through the Poutu Tunnel and Canal into Lake Rotoaira. A further tunnel is used to transfer water from Lake Rotoaira to the Tokaanu Power Station and eventually Lake Taupo via the Tokaanu Tailrace Canal (Fig. 1.2). This power development produces not only 1182 GWh of electricity from the two stations per annum, but adds extra water to Lake Taupo which in turn increases power generation at eight further hydroelectric power stations along the Waikato River. At the time of writing, the Rangipo Power Station is generating at only half of its capacity, because one of its two turbines needs to be replaced due to abrasion suffered from sediment in the water sourced from tephra and lahars from Ruapehu eruptions during September-November 1995.

1.5 Climate, soils and land use

The area studied ranges widely in physiography and altitude from the steep slopes of Ruapehu and Tongariro Volcanoes at ca. 1400 m to the flat surfaces of Turangi and surrounds at 360 m. There is a corresponding range in climatic conditions within this area. Turangi has a mean annual temperature of 12 °C with a relatively large range between the average daily maximum and minimum temperatures of 17-6.9 °C (Thompson, 1984). Away from the influence of the ocean, Turangi tends to have warm summer days and very cool winter evenings. The incidence of both ground and air frosts is high and the area is well sheltered from the prevailing westerly wind. Mean annual rainfall is in the order of 1600 mm (N.Z. Meteorological Service, 1980) with maximum falls in the late autumn and winter months and lower falls in the summer months. This produces a summer soil moisture deficit, while in winter runoff occurs (Thompson, 1984). In the higher altitude areas of Ruapehu and Tongariro rainfall is on average higher, up to 5000 mm, gale-force winds are common and temperatures are much lower. At 1500 m altitude the mean annual maximum to minimum temperature range is 9.4 to 2.3 °C. Heavy snow falls are common in the alpine areas and the winter snowline descends to the 1400-1500 m level.

Four main groups of soils occur within the study area (Fig. 1.3) all of which are azonal and intrazonal soils (Staff of Soil Bureau, 1968; Water and Soils Division, Ministry of Works and Development, 1979). In the areas close to the volcanoes the soils are typically recent soils developed from andesitic tephra erupted from Ruapehu and Tongariro volcanoes since the Taupo Tephra (1850 years B.P.; Froggatt and Lowe, 1990). These soils are known as the Ngauruhoe series and have limited production potential due to the harsh climatic conditions in which they occur.

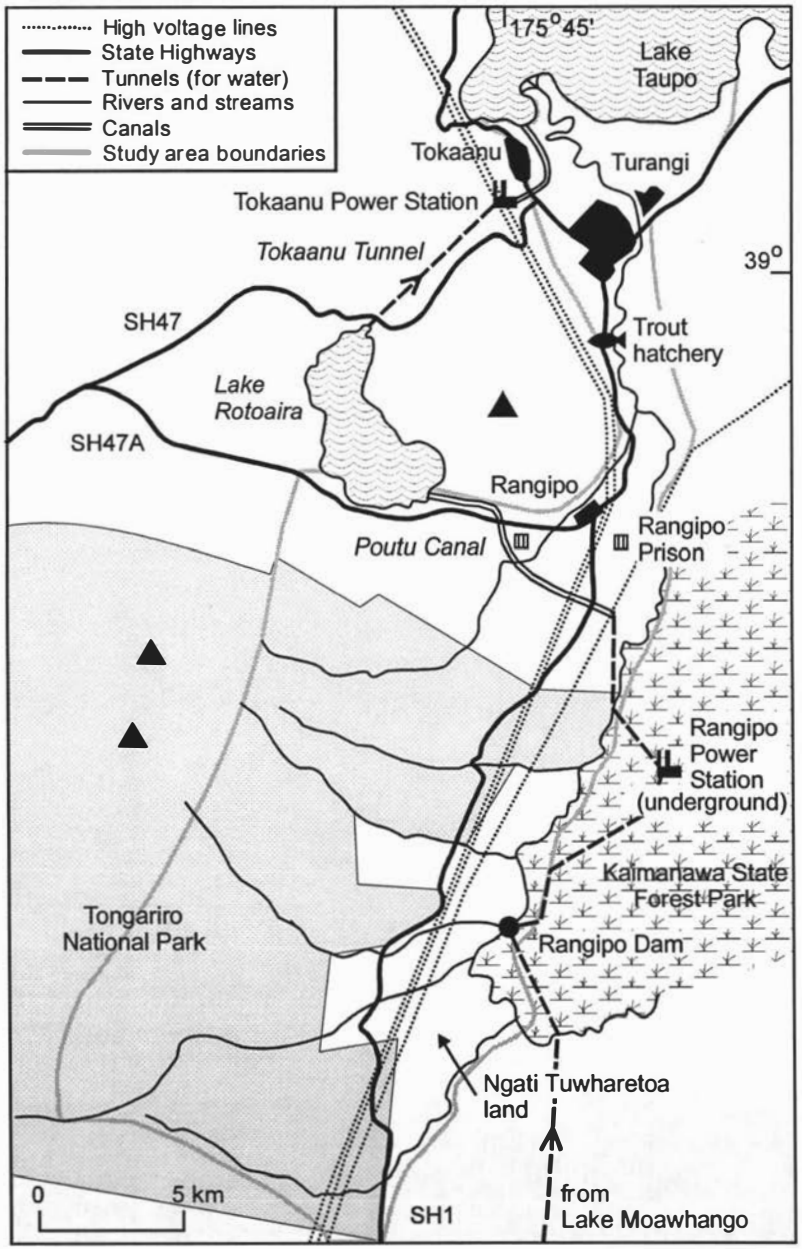

Figure 1.2. Infrastructure and land ownership within the studied area.

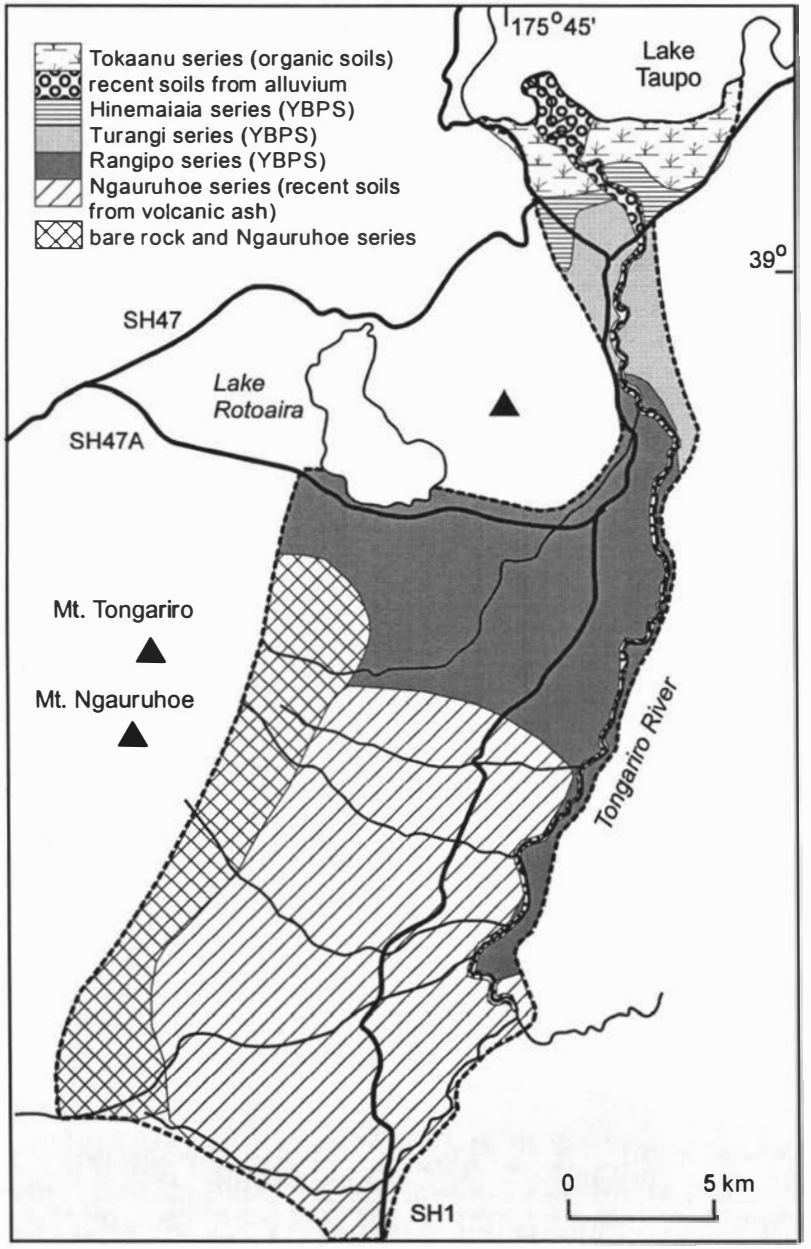

Figure 1.3. Soils of the study area. Data from; Staff of Soil Bureau (1968) and Water and Soils Division, M.W. and Development (1979).

Higher on the flanks of the volcanoes where the degree of erosion is higher areas of bare rock and scree occur.

Northeast of the two volcanoes the andesitic tephra covering on top of the Taupo Ignimbrite becomes thinner and the soils are yellow-brown pumice soils, developed directly into the Taupo Ignimbrite. Closer to the volcanoes the soils are Rangipo soils and further north and lower in altitude Turangi soils occur. Both of these soil series have potential for pastoral or exotic forestry use, while the Turangi series with more favourable climatic conditions can also be used for fodder cropping.

Within the low-lying area of the Tongariro River delta there is a mixture of recent soils from alluvium in areas near the present river course and organic soils in the swampy areas further away. The alluvium is composed in some cases of reworked Taupo Tephra and gives rise to another type of weakly developed yellow-brown pumice soil, the Hinemaiaia series. These soils are of low fertility and have few potential land uses, aside from low producing pastures. The whole area between Turangi and Lake Taupo is low lying and swampy and much of it is covered in peat in which is developed the Tokaanu series, an organic soil. This area has little potential agricultural use as there is difficulty in its drainage and very low gradient to the Lake, so it is best left as conservation reserve.

The actual land use in this area depends not only on the soils but also the land ownership or status. Much of the study area, particularly the southern part is undeveloped agriculturally (Fig. 1.4). Portions are within Tongariro National Park and Kaimanawa State Forest Park, and in addition parts of the Ngati Tuwharetoa land is undeveloped. In the northern part of the study area there are large areas of exotic forestry planting (Radiata Pine and Douglas Fir) on the NW slopes of Tongariro and also alongside the Tongariro River. Well developed pastoral lands are restricted to the Rangipo Prison farm and surrounds, and smaller areas near Turangi. Much of the swampy low-lying area between Lake Taupo and Turangi and Tokaanu is either poorly developed pasture or remains as undeveloped wetlands with a high conservation value.

1.6 Regional geologic setting

The current geological setting of New Zealand is dominated by the boundary between the Indo-Australian and Pacific plates which occurs through most of the length of the country (Fig. 1.5). The oblique angle of convergence of the two plates, the type of the crust along the boundary and the geometry of the plate boundary through New Zealand causes variations in the nature of the boundary (Cole and Lewis, 1981; Cole, 1986; Kamp, 1992). To the NE of New Zealand oceanic crust of the Pacific Plate is being subducted beneath the Australian Plate, forming the Tonga-Kermadec Island arc system which includes the Kermadec volcanoes. Farther south the angle of convergence between the two plates and subduction becomes more oblique through the central North Island of New Zealand.

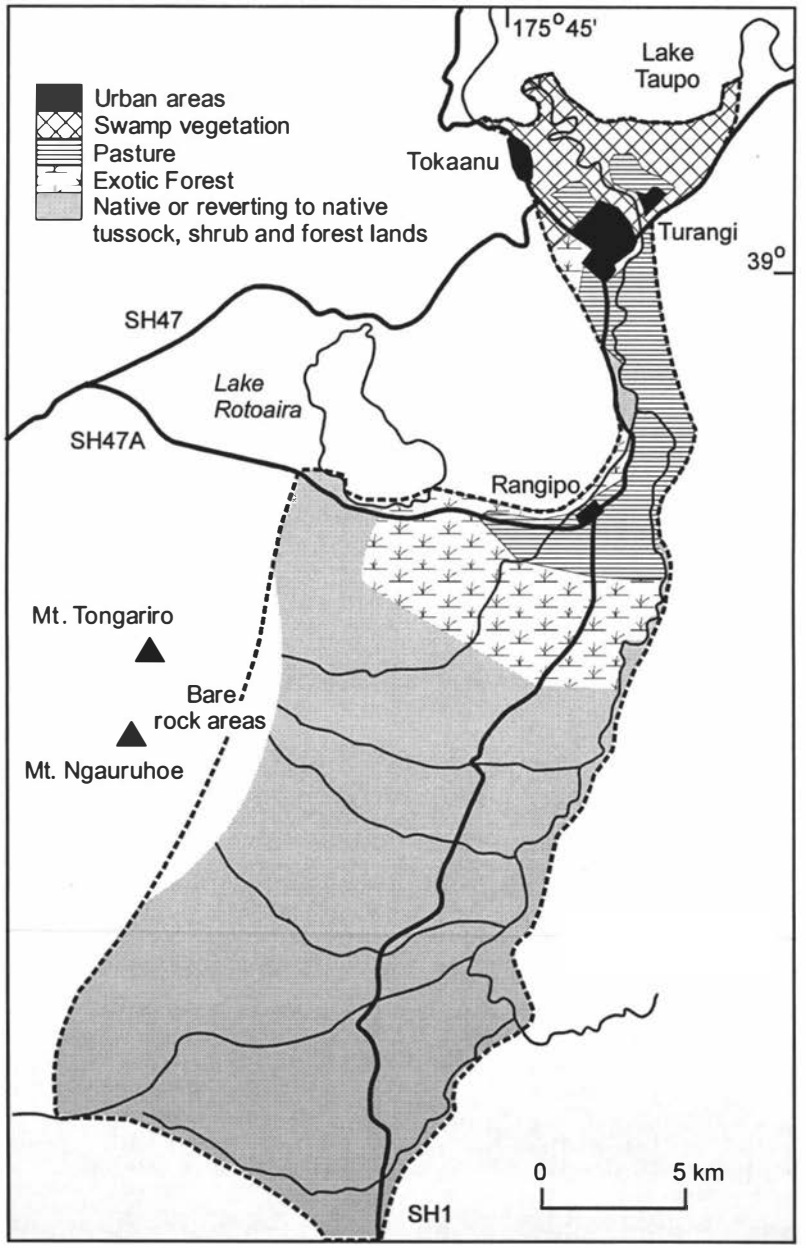

Figure 1.4. Vegatation/landuse within study area.

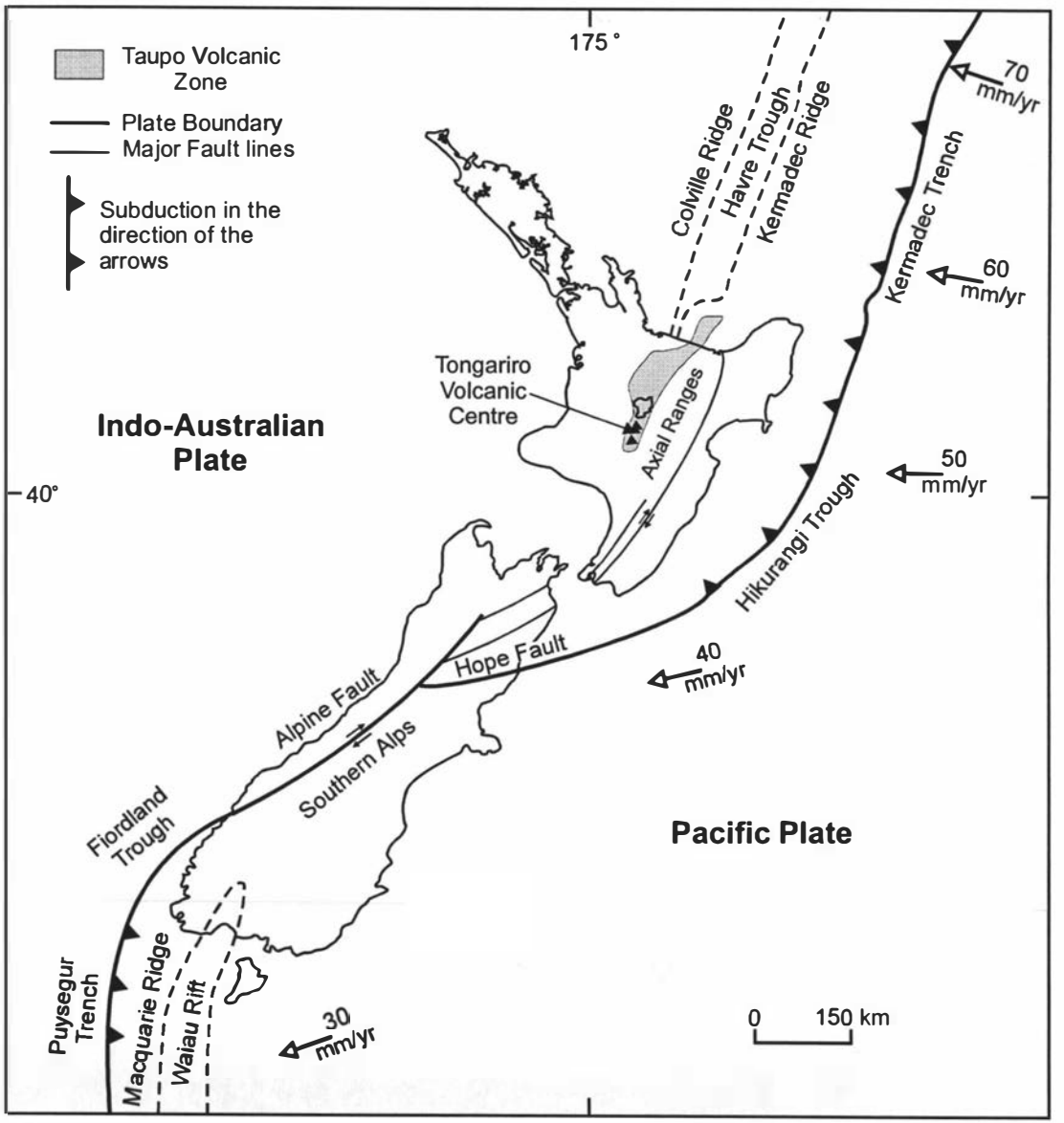

Figure 1.5. Major elements of the Pacific/Indo-Australian Plate boundary through New Zealand, and the positions of the Taupo Volcanic Zone and the Tongariro Volcanic Centre. Adapted from Cole and Lewis (1981).

Subduction is expressed in the central North Island by the development of a frontal ridge in E North Island; a volcanic front, including the andesitic and dacitic volcanoes of Ruapehu, Tongariro, Tauhara, Edgecumbe and White Island; and an ensialic marginal basin behind the volcanic front (Cole, 1990). Crustal spreading in the marginal basin has produced the voluminous Taupo Volcanic Zone (TVZ) rhyolitic volcanism in the Central North Island throughout the Quaternary (Wilson, *et al.*, 1984; Wilson *et al.*, 1986). TVZ volcanism appears to have begun at around 1.6 Ma (Pringle *et al.*, 1992; Soengkono *et al.*, 1992), reflecting the inception of the current orientation of the plate boundary.

The southern limit of subduction volcanism is marked approximately by Ruapehu volcano; from this latitude southward the decreasing angle of convergence of the two plates eventually gives rise to largely strike-slip motion between the two plates in the South Island (Fig. 1.5). Strike slip motion is taken up along a series of faults in Hawkes Bay and Wairarapa in the North Island and in the Hope Fault zone and Alpine Fault in the South Island. The component of convergence between the two plates in the South Island is represented by the uplift of the Southern Alps along the Alpine Fault Zone where there is continental-continental crust collision (Kamp *et al.*, 1989; Kamp and Tippett, 1993).

In the general vicinity of the study area there are three geologically distinct groups of rocks (Gregg, 1960). These are: (1) indurated Triassic-Jurassic greywacke/argillite rocks and their low grade (semi-schist) metamorphic equivalents; (2) weakly indurated Tertiary (Miocene-Pliocene) marine sediments; and (3) Quaternary volcanic rocks and deposits with associated volcaniclastic sediments.

The Triassic-Jurassic greywacke and argillite rocks make up the Kaimanawa Mountains in the eastern part of the area and are the basement of the volcanic terrain (Fig. 1.6). These rocks are equivalent to the Torlesse Terrane, an important and widely distributed basement terrane throughout New Zealand (Korsch and Wellman, 1988). These highly indurated and relatively unfossiliferous sedimentary rocks were originally deposited by turbidity currents in a deep ancestral basin and were sourced from a granitic continental mass. The sediments were then scraped from a subducting crustal slab to be accumulated as an accretionary wedge. Later deformation and metamorphism occurred in the late Mesozoic when the rocks were metamorphosed up to semi-schist grade in places. They have been uplifted to their present position over the last 2 million years during the Kaikoura Orogeny, relating to the propagation of the present boundary between the Pacific and Indo-Australian Plates through New Zealand.

Tertiary marine sediments within the area (Fig 1.6) were deposited on top of an eroded surface of the Mesozoic greywacke/argillite basement (Fleming, 1953; Gregg, 1960; Grindley, 1960; Williams, 1994). These sediments were deposited in the Miocene and Pliocene and include fossiliferous sandstone and siltstone with lenses of sub-bituminous coal, calcic sandstone and limestone units. They represent the encroachment and presence of a shallow sea over the region during Miocene and Pliocene times.

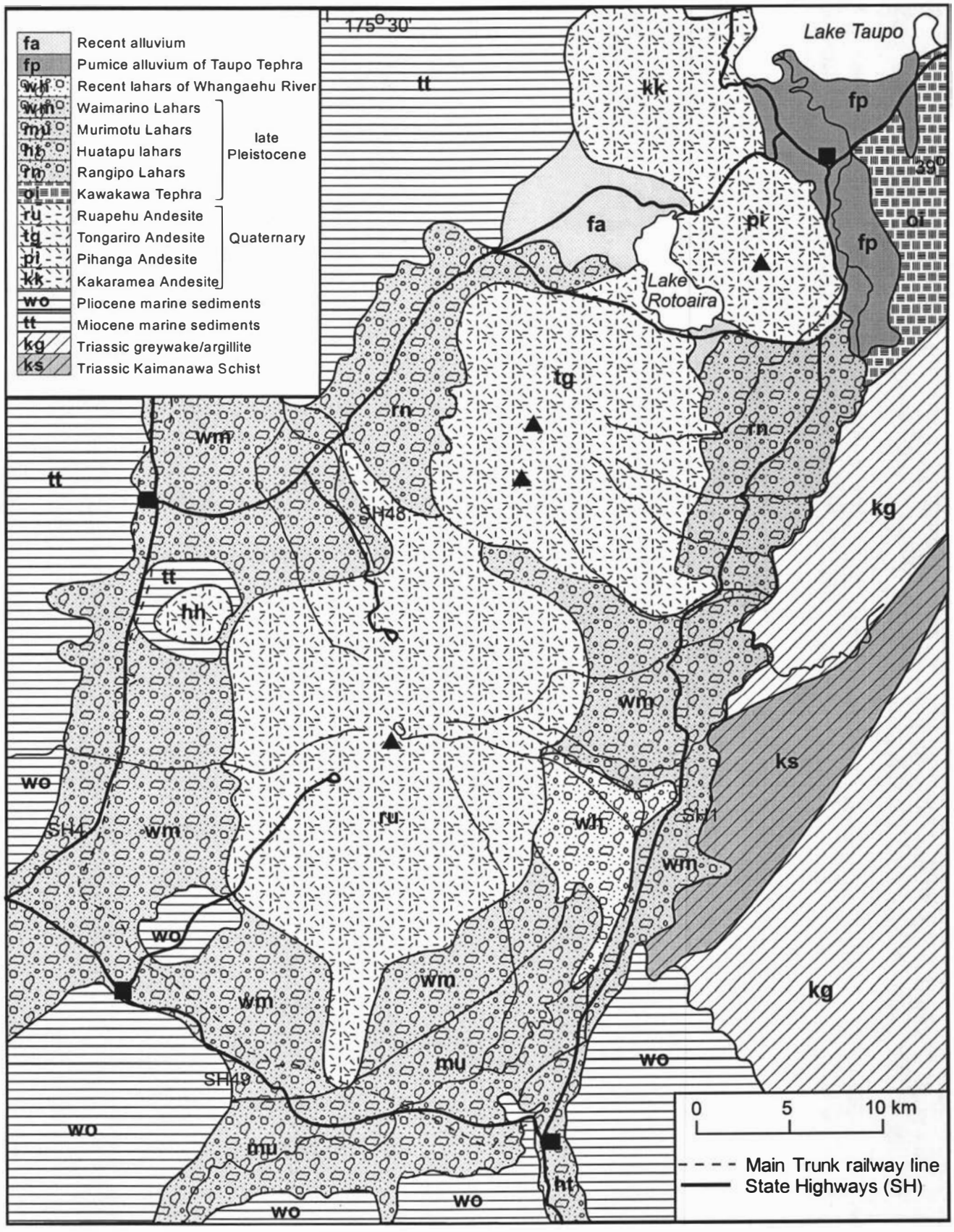

Figure 1.6. Sketch map of the geology of the region surrounding the study area (adapted from Grindley (1960) and Hay (1967).

Quaternary volcanic rocks cap the eroded remnants of these late Tertiary sediments (Fig. 1.6) and mostly consist of a series of andesitic stratovolcanoes of the Tongariro Volcanic Centre which are surrounded by aprons of volcaniclastic sediment and tephras. In addition, rhyolitic ignimbrites and reworked ignimbrite material from the Taupo volcano cover the northern part of the region (Fig. 1.6).

1.7 Tongariro Volcanic Centre

The Tongariro Volcanic Centre (TgVC) comprises four main volcanoes which lie at the southern terminus of the Taupo Volcanic Zone (Fig. 1.5 and 1.6; Plates 1 and 2). In addition to the four large andesitic volcanoes of Ruapehu, Tongariro, Kakaramea-Tihia and Pihanga (in order of descending size) there are several smaller outlying centres. The eruptives of TgVC are mostly calcalkaline medium-K basic and acid andesites with minor amounts of basalt and dacite (Cole *et al.*, 1986; Graham and Hackett, 1987). Within the porphyritic lavas the most common phenocrysts are plagioclase, hypersthene and augite, with minor amounts of hornblende and olivine. The TgVC eruptives are typical orogenic andesites consistent with the upper surface of the subducted Pacific Plate slab being 80 km below (Gamble *et al.*, 1990).

The oldest radiometrically dated lava from the TgVC is 0.27 ± 0.02 Ma (Hobden *et al.*, 1996); however, pebbles of TgVC lithology have been found in Lower Pleistocene conglomerates in the Wanganui region to the south (Fleming, 1953). Activity continues into the historic record for both Tongariro and Ruapehu volcanoes with the most recent eruptions being those of Ruapehu volcano in 1995-1996.

The pre-50 ka eruptive centres in the TgVC are aligned in a NW orientation, while the post-50 ka centres trend NNE, cross-cutting the old NW alignment (Hackett, 1985; Cole *et al.*, 1986). The eruptives from these two apparent sets of volcanism are petrologically distinct; the younger rocks are lower silica andesites than the older series and they contain more olivine-bearing lavas. The NNE trending vents are aligned with the young andesitic volcanoes of Mt. Edgecumbe, Whale Island and White Island and the orientation of the present subduction system, whereas the older NW trending system may represent an earlier orientation of subduction.

1.8 Previous work in and around the study area

The first mapping of the Tongariro region was carried out by Grange *et al.*, (1938). This reconnaissance mapping outlined the main components of the regional geology and the main volcanic features. Gregg (1960) described early geologic observations and records of the volcanic activity and provided a description of the volcanic and non-volcanic geology of the area including the Grange *et al.* (1938) maps. Later work by Grindley (1960) distinguished in greater detail several lava and lahar formations on and around Ruapehu. The Ruapehu ring plain was mapped as dominantly Waimarino Lahars (Fig. 1.6) determined to be of Last Glacial age.

Plate 1.1: View of the eastern flanks of Ruapehu volcano across its ring plain.

Plate 1.2 View of Tongariro volcano from the south-east. The large cone on the left is the most recently active vent, Ngauruhoe.

Two further lahar formations, the Hautapu, and Murimotu Lahars which form terraces in the Whangaehu valley were correlated to stadials of the Last Glacial and recent lahars were mapped in the Whangaehu Valley. Hay (1967) also mapped Murimotu Lahars on the NW flanks of Ruapehu. This deposit has been subsequently described as a 9.5 ka debris-avalanche deposit (Palmer and Neall, 1989). Mathews (1967) mapped and described the Tongariro massif as being a multiple volcano, made up of several small overlapping volcanic cones of varying age. Mathews also mapped paired Last Glacial moraines beside the Waihohonu Valley as well as in two valleys on the eastern flanks of the volcano.

The first detailed work on the stratigraphy of the Tongariro and Ruapehu ring plains was carried out by Topping (1974). Topping established a detailed chronology of late Pleistocene and Holocene distal rhyolitic tephras erupted from the TVZ calderas to the north which were interbedded within the andesitic ring plain sequence (Topping and Kohn, 1973). Using these tephra layers as time planes Topping developed a stratigraphy of andesitic tephras erupted from Tongariro and Ruapehu volcano from 13.8 ka B.P. to the present (Table 1.1) and mapped their distributions (Topping, 1973). The Tongariro Subgroup was defined to include all of these described tephra formations. Topping also noted the presence of Hinuera Formation gravels containing reworked Kawakawa Tephra and ranging in age from 22.59 ka B.P. to ca. 10 ka.

Hackett (1985) carried out a detailed study of Ruapehu and described four formations of lavas and associated volcaniclastic rocks which comprise the massif (Fig 1.7). Each of these formations represents a cone-building episode of Ruapehu. The Te Herenga Formation is the remnants of the oldest cone-building episode, the vents for which are thought to lie in the N-NW of Ruapehu (Hackett, 1985; Hackett and Houghton, 1989). The source vents for the next youngest, Wahianoa Formation are thought to lie in the SE of the present cone. Both the Te Herenga and Wahianoa Formations are of andesitic composition. The Mangawhero Formation occupies the present summit of Ruapehu and is of basaltic to dacitic composition. The lavas erupted in the post-glacial period belong to the Whakapapa Formation which includes eruptives from the present summit vents as well as several flank vents spread widely over the volcano.

The lavas of Ruapehu and the other volcanoes of the TgVC were further subdivided on the basis of petrology and geochemistry by Cole *et al.* (1986) and Graham and Hackett (1987). They defined six lava types on the volcano and its related vents characterised by their phenocryst species and geochemical similarities.

Prior to the present study the most recent work on the eastern ring plains was that of Donoghue (1991) who studied in detail the lahar and tephra stratigraphy of the Ruapehu ring plain to the south of the area investigated in this study. Purves (1990), in a landscape ecology study on the Rangipo Desert area of the SE Ruapehu ring plain also contributed to elucidating the lahar stratigraphy of the area. Donoghue (1991) and Purves (1990) significantly revised the lahar stratigraphy from the early mapping of Grindley (1960) and defined five new lahar formations dating from > 22.6 ka B.P to the present (Table 1.2).

Table 1.1. Stratigraphy of Tongariro Subgroup tephras and interbedded rhyolitic tephras described by Topping (1973, 1974) and Topping and Kohn (1973). Tephra ages are those currently accepted.

Formation*	Members	Source†	Age ka	Reference to age
Ngauruhoe Tephra		TgVC	ca. 1.8-0[1]	
Taupo Tephra (Unit Y)		Taupo	1.85[2]	Froggatt and Lowe (1990)
Mangatawai Tephra		Tongariro	2.5-1.85[2]	
unnamed andesitic ash		"		
Whakaipo Tephra		Taupo	2.7[2]	"
unnamed andesitic ash		TgVC		
Waimahia Tephra (Unit S)		Taupo	3.3[2]	"
Papakai Tephra		TgVC		
Hinemaiaia Tephra		Taupo	5.2-3.95[2]	Wilson (1993)
Papakai Tephra		TgVC		
Rotoma Ash		Oakataina	8.53[2]	Froggatt and Lowe (1990)
Papakai Tephra		TgVC		
Opepe Tephra (Unit E)		Taupo	9.05[2]	"
Papakai Tephra		TgVC		
Mangamate Tephra	Poutu Lapilli	Tongariro	ca. 9.7[1]	Topping (1973)
"	Wharepu Tephra	"	ca. 9.7[1]	"
Poronui Tephra (Unit C)		Taupo	9.81[2]	Froggatt and Lowe (1990)
Mangamate Tephra	Ohinepango Tephra	Tongariro	ca. 9.7[1]	Topping (1973)
"	Waihohonu Lapilli	"	ca. 9.7[1]	"
"	Oturere Lapilli	"	9.78[2]	"
Karapiti Tephra (Unit B)		Taupo	10.1[2]	Wilson (1993)
Okupata Tephra		Ruapehu	>9.79[2]	Topping (1973)
unnamed andesitic ash		TgVC		
?Rotorua Tephra		Okataina	13.08[2]	Froggatt and Lowe (1990)
unnamed andesitic ash		TgVC		
Puketarata Ash		Maroa	ca. 14[1]	"
unnamed andesitic ash		TgVC		
Rotoaira Tephra		Tongariro	13.8[2]	Topping (1973)
unnamed andesitic ash		TgVC		
Rerewhakaaitu Tephra		Okataina	14.7[2]	Froggatt and Lowe (1990)
unnamed andesitic ash		Tongariro		
Kawakawa Tephra	Oruanui Ignimbrite and Aokautere Ash	Taupo	22.59[2]	Wilson *et al.*, (1988)

* Taupo Volcanic Centre Unit nomenclature from Wilson (1993).

† TgVC = Tongariro and Ruapehu volcanoes, Tongariro includes the vent of Ngauruhoe.

[1] Estimated ages.

[2] Average or single ^{14}C ages on old (Libby) half life basis.

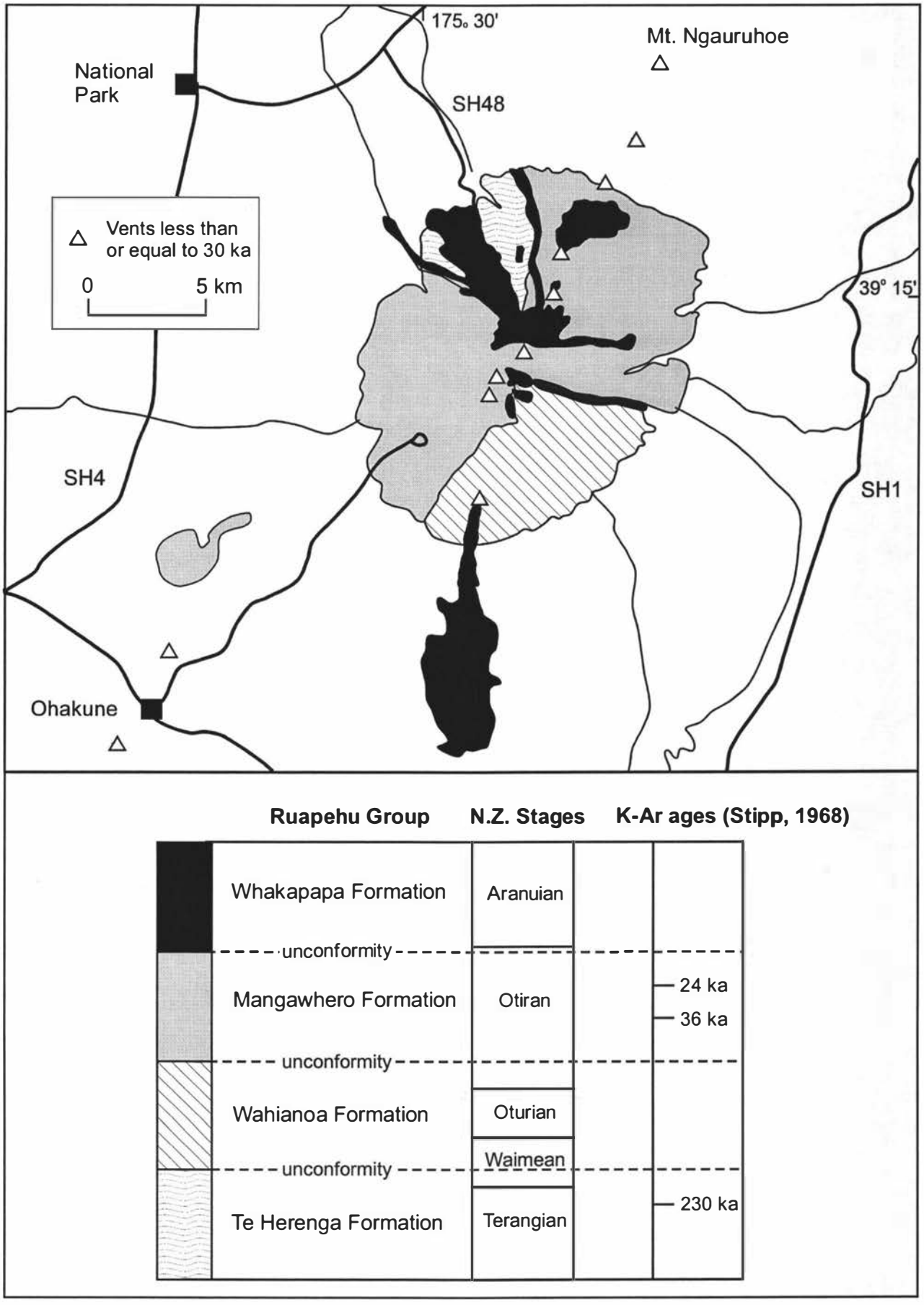

Figure 1.7. Generalised geologic map of Ruapehu volcano and related vents, adapted from Hackett (1985), with additions from Donoghue *et al* (1988) and Lecointre *et al* (1994).

Table 1.2. Stratigraphy of lahar formations on the SE Ruapehu ring plain, from Donoghue (1991) and Purves (1990).

Lahar formation	Age range (ka B.P.)	Tephra boundary marker beds
Onetapu Formation	1.85 - present	
		Taupo Tephra
		Waimahia Tephra
Manutahi Formation	3.28 - 4.60	
Mangaio Formation[1]	4.60	
Manutahi Formation	4.60 - 5.43	
		Motutere Tephra
Tangatu Formation	5.43 - 14.7	
		Rerewhakaaitu Tephra
Te Heuheu Formation	14.7 - > 22.6	
		no lower limit defined

[1] Mangaio Formation represents the deposits of a single event or a closely spaced series of events dated at 4.6 ka B.P. by Donoghue (1991). The other formations span the presented time ranges and include multiple events.

Based on the defined and mapped lahar formations Donoghue (1991) and Hodgson (1993) produced lahar hazard maps for the SE Ruapehu ring plain and the Whangaehu catchment.

Donoghue (1991) and Donoghue *et al.* (1995) also added to and revised the previously established rhyolitic and andesitic tephrostratigraphy developed by Topping (1973, 1974) and Topping and Kohn (1973) extending the stratigraphy to 22.6 ka B.P. Donoghue *et al.* (1995) revised the base of the Tongariro Subgroup from ca. 14 ka B.P. to ca. 10 ka B.P. and defined the Tukino Subgroup to include tephras aged between 10 and 22.6 ka B.P. They group all tephras erupted from the Tongariro Volcanic Centre since 22.6 ka B.P. into seven formations (Table 1.3). The major additions to the existing stratigraphy were the newly defined Tufa Trig and Bullot Formations. The Tufa Trig Formation with 18 members and the Bullot Formation with 23 lapilli members record the activity of Ruapehu volcano over the last 1.85 ka B.P. and the period 10 to 22.6 ka B.P. respectively. The definition of these two formations and mapping of the tephras within them contributed significantly to knowledge of the eruptive history of Ruapehu volcano.

1.9 Summary and conclusions from previous work

Geologic mapping of the study area and the surrounding region until the 1970's was concentrated on the volcanic cones with only reconnaissance work carried out on the ring plains. The ring plains of Ruapehu and Tongariro volcanoes were mapped as mostly Waimarino and Rangipo Lahars respectively. The Ruapehu ring plain also had smaller areas mapped in more detail. Topping (1973 and 1974) and Topping and Kohn (1974) constructed the first detailed late Pleistocene and Holocene andesitic and rhyolitic tephrostratigraphy of the area, defining the Tongariro Subgroup.

Table 1.3. Stratigraphy of andesitic and rhyolitic tephras on the SE Ruapehu ring plain, from Donoghue (1991) and Donoghue *et al*. (1995).

Subgroup	Formation	Members	Source	Age (ka)	Interbedded rhyolitic tephras
	Ngauruhoe Formation		Tongariro	ca. 1.85 - 0[1]	Kaharoa Tephra
	Tufa Trig Formation	Tf18 - Tf1	Ruapehu	ca. 1.85 - 0[1]	Kaharoa Tephra
				1.85[2]	Taupo Tephra
	Mangatawai Tephra		Tongariro	2.5 - 1.85[2]	Mapara Tephra
	Papakai Formation		TgVC	2.5 - 9.7[1]	Waimahia Tephra
					Hinemaiaia Tephra
					Whakatane Tephra
					Motutere Tephra
Tongariro Subgroup	Mangamate Formation	Poutu Lapilli	Tongariro	ca. 9.7[1]	
	"	Wharepu Tephra	"		
				9.81[2]	Poronui Tephra
	"	Ohinepango Tephra	"		
	"	Waihohonu Lapilli	"		
	"	Oturere Lapilli	"		
	"	Te Rato Lapilli	"	9.78[2]	
	unnamed tephra		TgVC		
				10.1[2]	Karapiti Tephra
	unnamed tephra		TgVC		
	Pahoka Tephra		Tongariro	ca. 10-9.8[1]	
	Bullot Formation (upper)		Ruapehu	ca. 10[1]	
	"	Ngamatea Lapilli-2	"		
	"	Ngamatea Lapilli-1	"		
	"	Pourahu Member	"		
	"	L18 - L17	"		
Tukino Subgroup	"	Shawcroft Lapilli	"		
	"	L16	"		
				11.85[2]	Waiohau Tephra
	"	L15 - L8	"		
				13.08[2]	? Rotorua Tephra
	"		"		
	Rotoaira Lapilli		Tongariro	13.8[2]	
	Bullot Formation (upper)	L15 - L8	Ruapehu		
				14.7[2]	Rerewhakaaitu Tephra
	Bullot Formation (middle)	L7b - L4	"		
				ca. 18.0[1]	Okareka Tephra[3]
	Bullot Formation (lower)	L3 - L1	"		
				22.6[2]	Kawakawa Tephra

[1] Estimated ages, references to ages the same as Table 1.1.
[2] Average or single ^{14}C ages on old (Libby) half life basis, references as for Table 1.1.
[3] Age from Nairn (1992).

Hackett (1985) described the stratigraphy of the Ruapehu cone and with Cole *et al.* (1986) and Graham and Hackett (1987) subdivided the lavas of TgVC on the basis of their mineralogy and geochemistry. Later work by Donoghue (1991) and Purves (1990) constructed a more detailed lahar stratigraphy of the SE Ruapehu ring plain with 5 lahar formations defined by dated tephra interbeds. Donoghue (1991) and Hodgson (1993) then were able to produce lahar hazard maps of the SE Ruapehu ring plain and Whangaehu River based on the lahar stratigraphy. Donoghue (1991) and Donoghue *et al.* (1995) revised and added to the existing tephrostratigraphy, adding the Tukino Subgroup to extend the stratigraphy to 22.6 ka B.P. Donoghue and co-workers also added a new stratigraphy of Ruapehu-sourced eruptives on the SE Ruapehu ring plain.

In conclusion, there are four areas in which geological investigations in the study area can add to that which has previously been carried out:

(1) The NE Ruapehu lahar and tephra stratigraphy up to 22.5 ka B.P. can be mapped using the framework established on the SE Ruapehu ring plain.

(2) The ring plain record older than 22.5 ka B.P. can be investigated to extend the existing lahar and tephra stratigraphy and the eruptive history of Ruapehu volcano. Both of these first two areas of investigation can contribute to a synthesis of the construction of the NE Ruapehu ring plain.

(3) The E Tongariro ring plain has not been investigated since the reconnaissance mapping of Grindley (1960) in which the entire area was mapped as the Rangipo Lahars. An investigation of the lahar and tephra stratigraphy in this area can potentially provide further information on the eruptive history of Tongariro volcano.

(4) By mapping the lahar stratigraphy on the NE Ruapehu and E Tongariro ring plains as well as along the Tongariro River a lahar hazard map for these areas can be constructed. In particular, knowledge of the lahar history of the Tongariro River, one of the most important drainage channels from TgVC is necessary because the town of Turangi (ca. 4200 population) is located on low surfaces beside the river. In addition the river is used for the Tongariro Power Development and all of its tributaries draining the volcanoes are crossed by the main transport arterial route of State Highway 1. The relevance of this issue is demonstrated by the generation of at least two lahars in the Mangatoetoenui Stream in 1995 which entered the Tongariro River. These lahars have seriously impacted on the Tongariro Power development by causing abrasion of turbines in the Rangipo Power Station necessitating the replacement of one of the two turbines, and also debris has accumulated behind the Rangipo Dam severely reducing its storage capacity. Serious effects on trout (a major tourist attraction and source of revenue for Turangi) also occurred and continue to occur at the time of writing due to much additional fine sediment remaining in the river system.

1.10 References

Clarke, C. and Smith, M., 1986. Turangi town centre, where to now? Taupo County Council Special Report, 15.

Cole, J.W., 1986. Distribution and tectonic setting of late Cenozoic volcanism in New Zealand. Royal Soc. of N.Z. Bull., 23: 7-20.

Cole, J.W., 1990. Structural control and origin of volcanism in the Taupo Volcanic Zone, New Zealand. Bull. Volcanol., 52: 445-492.

Cole, J.W. and Lewis, K.B., 1981. Evolution of the Taupo-Hikurangi subduction system. Tectonophysics, 72; 1-21.

Cole, J.W., Graham, I.J., Hackett, W.R., Houghton, B.F., 1986. Volcanology and petrology of the Quaternary composite volcanoes of Tongariro Volcanic Centre, Taupo Volcanic Zone. Royal Soc. of N.Z. Bull., 23: 224-250.

Department of Statistics, 1992. 1991 Census of Population and Dwellings, Waikato/Bay of Plenty Regional Report. Department of Statistics, Wellington, N.Z.

Donoghue, S.L., Neall, V.E., Palmer, A.S., 1988. Holocene geology of the upper Whangaehu River, Mt. Ruapehu. Geological Soc. of N.Z. Misc. Publ. 41a: 61.

Donoghue, S.L., 1991. Late Quaternary volcanic stratigraphy of the south-eastern sector of Mount Ruapehu ring plain, New Zealand. Unpub. PhD. thesis, Massey University, Palmerston North, N. Z.

Donoghue, S.L., Neall, V.E., Palmer, A.S., 1995. Stratigraphy and chronology of late Quaternary andesitic tephra deposits, Tongariro Volcanic Centre, New Zealand. J. Roy. Soc. of N.Z., 25: 115-206.

Fleming, C.A., 1953. The Geology of Wanganui Subdivision. N.Z. Geological Survey Bull., 52: 362 pp.

Froggatt, P.C. and Lowe, D. J., 1990. A review of late Quaternary silicic and some other tephra formations from New Zealand: their stratigraphy, nomenclature, distribution, volume and age. N.Z. J. Geol. and Geophys., 33: 89-109.

Gamble, J.A., Smith, I.E.M., Graham, I.J., Kokelaar, B.P., Cole, J.W., Houghton, B.F., Wilson, C.J.N., 1990. The petrology, phase relations and tectonic setting of basalts from the Taupo Volcanic Zone, New Zealand, and Kermadec Island Arc-Havre Trough, SW Pacific. J. Volcanol. and Geotherm. Res., 54: 265-290.

Graham, I.J., Hackett, W.R., 1987. Petrology of calc-alkaline lavas from Ruapehu volcano and related vents, Taupo Volcanic Zone, New Zealand. J. of Petrology, 28: 531-567.

Grange, L.I., Williamson, J.H., Hurst, J.A., 1938. Geological maps of Tongariro Subdivision, to accompany, N.Z. Geological Survey Bull, 40: 4 sheets.

Gregg, D.R., 1960. The geology of Tongariro Subdivision. N.Z. Geological Survey Bull., 40: 152pp.

Grindley, G.W., 1960. Geological map of New Zealand, 1st ed., 1: 250 000, Sheet 8, Taupo. D.S.I.R., Wellington.

Hackett, W.R., 1985. Geology and petrology of Ruapehu volcano and related vents. Unpub. thesis Victoria University of Wellington: 312 pp.

Hackett, W.R., Houghton, B.F., 1989. A facies model for a Quaternary andesitic composite volcano: Ruapehu, New Zealand. Bull. Volcanol., 51: 51-68.

Hay, R,F., 1967. Geological map of New Zealand, 1st ed., 1: 250 000, Sheet 7, Taranaki. D.S.I.R., Wellington.

Hobden, B.J., Houghton, B.F., Lanphere, M.A., Nairn, I.A., 1996. Growth of the Tongariro volcanic complex: new evidence from K-Ar age determinations. N.Z. J. Geol. and Geophys., 39: 151-154.

Hodgson, K.A., 1993. Late Quaternary lahars from Mount Ruapehu in the Whangaehu River valley. Unpub. PhD. thesis, Massey University, Palmerston North, N. Z.

Kamp, P.J.J., 1992. Tectonic architecture of New Zealand. In Soons, J.M. and Selby, M.J. (eds). Landforms of New Zealand, 2nd Edition, Longman Paul, Auckland: 1-30.

Kamp, P.J.J., Green. P.F., White, S.H., 1989. Fission track analysis reveals character of collisional tectonics in New Zealand. Tectonics, 8: 169-195.

Kamp, P.J.J, Tippett, J.M., 1993. Dynamics of Pacific Plate crust in the South Island (New Zealand) zone of oblique continent-continent convergence. J. Geophys. Res., 98(B9): 16 105-16 118.

Korsch, R.J., Wellman, H.W., 1988. The geological evolution of New Zealand and the New Zealand region. In Nairn, A.E.M., Stehli, F.G., Uyeda, S. (eds). The Ocean Basins and margins, Vol. 7B: 411-481. Plenium Publishing Corporation.

Lecointre, J.A., Neall, V.E., Palmer, A.S., 1994. A new lava field from the southwestern quadrant of the Ruapehu ring plain. Geological Soc. of N.Z. Misc. Publ. 80A: 111.

Mathews, W.H., 1967. A contribution to the geology of the Mount Tongariro massif, North Island, New Zealand. N.Z. J. Geol. and Geophys., 10: 1027-1038.

Mercer, E.V., (ed), 1973. Turangi "the town of the future". Papers from the Lions symposium 12-13 May 1973. Turangi Lions Club Inc., Turangi.

Ministry of Works and Development, 1974. New Zealand's latest power story, Tongariro Power Development. Ministry of Works and Development, Wellington, N.Z.

Nairn, I.A., 1992. The Te Rere and Okareka eruptive episodes - Okataina Volcanic Centre, Taupo Volcanic Zone, New Zealand. N.Z. J. Geol. and Geophys., 35: 93-108.

New Zealand Meteorological Service, 1980. Summary of climatological observations to 1980. New Zealand Meteorological Service Misc. Publ., 177.

Palmer, B.A., Neall, V.E., 1989. The Murimotu Formation - 9500 year old deposits of a debris avalanche and associated lahars, Mount Ruapehu, North Island, New Zealand. N.Z. J. Geol. and Geophys., 32: 477-486.

Pringle, M.S., McWilliams, M., Houghton, B.F., Lanphere, M.A., Wilson, C.J.N., 1992. $^{40}Ar/^{39}Ar$ dating of Quaternary feldspar: Examples from the Taupo Volcanic Zone, New Zealand. Geology, 20: 531-534.

Purves, A.M., 1990. Landscape ecology of the Rangipo Desert. Unpub. MSc. Thesis. Massey University, Palmerston North, N.Z.

Soengkono, S., Hochstein, M.P., Smith, I.E.M., Itaya, T., 1992. Geophysical evidence for widespread reversely magnetised pyroclastics in the western Taupo Volcanic Zone (New Zealand). N.Z. J. of Geol. and Geophys., 35: 47-55.

Staff of Soil Bureau, 1968. Soils of New Zealand, Part 1. N.Z. Soil Bureau Bull. 26 (1).

Stipp, J.J., 1968. The geochronology and petrogenesis of the Cenozoic volcanics of the North Island of New Zealand. Unpub. Ph.D. Thesis. Australian National University, Canberra.

Thompson, C.S., 1984. The weather and climate of the Tongariro Region. N. Z. Meteorological Service Misc. Publ., 115(14): 35pp.

Topping, W.W., 1973. Tephrostratigraphy and chronology of late Quaternary eruptives from the Tongariro Volcanic Centre, New Zealand. N. Z. J. Geol. and Geophys., 16: 397-423.

Topping, W.W., 1974. Some aspects of Quaternary history of Tongariro Volcanic Centre. Unpub. PhD. thesis, Victoria University of Wellington N. Z.

Topping, W.W., Kohn, B.P., 1973. Rhyolitic tephra marker beds in the Tongariro area, North Island, New Zealand. N.Z. J. Geol. and Geophys., 16: 375-395.

Water and Soils Division, Ministry of Works and Development, 1979. N. Z. Land Resource Inventory Worksheets, N102 Tokaanu and N112 Ngauruhoe and Bay of Plenty - Volcanic Region Landuse Capability Extended Legend (12pp). National Water and Soil Conservation Organisation, Ministry of Works and Development, Wellington, N.Z.

Williams, J.K., 1994. Some aspects of the Cenozoic geology of the Moawhango River region, in the army training area, Waiouru, North Island, New Zealand. Unpub. MSc. Thesis. Massey University, Palmerston North, N.Z.

Wilson, C.J.N., Rogan, A.M., Smith, I.E.M., Northey, D.J., Nairn, I.A., Houghton, B.F., 1984. Caldera volcanoes of the Taupo Volcanic Zone, New Zealand. J. Geophys. Res., 89(B10): 8463-8484.

Wilson, C.J.N, Houghton, B.F., Lloyd, E.F., 1986. Volcanic history and evolution of the Maroa-Taupo area, central North Island. Royal Soc. of N.Z. Bull., 23: 194-223.

Wilson, C.J.N., Switzur, R.V., Ward, A.P., 1988. A new ^{14}C age for the Oruanui (Wairakei) eruption, New Zealand. Geol. Mag., 125: 297-300.

Wilson, C.J.N., 1993. Stratigraphy, chronology, styles and dynamics of late Quaternary eruptions from Taupo Volcano, New Zealand. Phil. Trans. Roy. Soc. London A 343: 205-306.

CHAPTER 2: RHYOLITIC TEPHROCHRONOLOGY

2.1 Introduction

Rhyolitic tephra layers have played a key role in previous stratigraphic studies of the Tongariro and Ruapehu ring plains. In particular, Topping and Kohn (1973) and Donoghue *et al.* (1995) demonstrated the use of dated rhyolitic tephra layers to establish a stratigraphy of andesitic tephra layers and lahar deposits. In this study, one of the first approaches to establishing a stratigraphy on the NE Ruapehu and E Tongariro ring plains was to find and identify rhyolitic tephras in described sequences. In situations where the stratigraphy of a site was otherwise unclear, identification of a rhyolitic tephra layer within the sequence was an invaluable method of dating the sequence. In addition, in the older part of the ring plain sequences (> 40 ka B.P.), radiocarbon dating is impossible and identifying a rhyolitic tephra within a sequence became even more crucial.

The major problem encountered with using rhyolitic tephra layers was establishing their identity with confidence. Previous methods of rhyolitic tephra identification on the Tongariro and Ruapehu ring plains were based on stratigraphy, mineralogy and numerical comparisons of glass chemistry (Topping and Kohn, 1973; Donoghue, 1991). However, in many instances these methods were found to be insufficient to uniquely identify a particular tephra. Usually the existing methods could only narrow the field of possibilities, resulting in the necessity for a subjective decision of the tephras identity.

In this study, methods of improving the unique identification of rhyolitic tephras within the ring plain sequence were investigated. In particular the statistical analysis of major oxide glass chemistry was attempted. These studies form the paper below which is in press in the New Zealand Journal of Geology and Geophysics (Vol. 40 No. 2, 1997). The paper has multiple authors and the following lists each author's contribution to the work:

S. J. Cronin: Principal investigator

Carried out all: field description and sampling,
laboratory preparation of samples,
optical microscopy work,
electron microprobe analysis,
statistical programming and analysis,
manuscript preparation and writing

V.E. Neall, A.S. Palmer, R.B. Stewart: Advisers

Aided the study by: discussing results and methodology with SJC
editing and discussion of the manuscript

2.2 Additional methodology and notes

The problem of statistical closure discussed in the manuscript is due to the nature of compositional data; the component proportions (in this case, oxide weight proportions) must sum to unity (or close to unity) in compositional data. This is termed the constant sum constraint and causes a high degree of correlation or interdependence between the individual variables making up a composition (Aitchison, 1983 and 1986). However, discriminant function analysis (DFA) requires variables to be independent of one another. To remove the high correlation between the variables the log ratio transformation was developed by Aitchison (1983). The formula:

$$y_i = \log(x_i / x_d)$$

describes the transformation, where x_d is the score of the oxide chosen arbitrarily as the divisor, x_i some raw oxide score and y_i the transformed score (i can take values 1 to d-1). Not only does this procedure remove the statistical closure it reduces all of the composition variables to the same order of magnitude.

The SAS programs used for the DISCRIM, CANDISC and STEPDISC statistical analyses in the following study are presented in Appendix 1.

A listing of all electron microprobe analyses of rhyolitic tephra samples carried out in this study comprises Appendix 2.

2.3 METHODS OF IDENTIFYING LATE QUATERNARY RHYOLITIC TEPHRAS ON THE RING PLAINS OF RUAPEHU AND TONGARIRO VOLCANOES, NEW ZEALAND

Shane J. Cronin, V.E. Neall, A.S. Palmer and R.B. Stewart
Department of Soil Science, Massey University, Private Bag 11 222, Palmerston North, New Zealand.

New Zealand Journal of Geology and Geophysics 40, No. 2, in press.

Abstract On the ring plains of Ruapehu and Tongariro volcanoes, distal rhyolitic marker tephras provide a valuable stratigraphic framework. However, identification of many of these tephras has been imprecise. Here we provide a quantitative approach for identifying tephras within the ring-plain sequences. We extend from simple canonical discriminant function models of glass chemistry to show how these, in conjunction with other geological information, can be used in a practical field-based study. In two stratigraphically distinguishable groups (10-22 ka and 22-65 ka), we established discriminant models for possible tephra correlatives from standard glass analyses. Testing analyses from unknown tephras against the models classified 34 of the 41 samples with probabilities > 0.75 to tephras that were consistent with mineralogical and stratigraphic evidence. Unknowns with lower probabilities of classification had several possible correlatives. Some of these were improved when the tephras classified with > 0.75 probability, and which were consistent with stratigraphic and other evidence, were

added to the discriminant models. The improved classifications were due to an increased number of samples for each tephra and also because the added analyses were produced by the same EMP operator under the same instrument conditions. Classifications of other unknowns were improved by considering them as mixed tephras. In addition to more rigorously correlating several tephras previously identified in this area, four tephras have been identified in the area for the first time, the Okaia, Omataroa and Hauparu Tephras and the Rotoehu Ash. These occur as microscopic accumulations of rhyolitic glass shards within weathered andesitic tephra deposits.

2.4 Keywords

Ruapehu volcano, Tongariro volcano, ring plain, stratigraphy, rhyolitic tephra correlation, discriminant function analysis, Okaia Tephra, Omataroa Tephra, Hauparu Tephra, Rotoehu Ash.

2.5 Introduction

Tephra layers play an important part in stratigraphic studies throughout New Zealand and the surrounding sea floor. The most voluminous and best studied tephra layers are the rhyolitic eruptives from calderas of the Taupo Volcanic Zone in the central North Island of New Zealand. Over 30 dated, widespread, rhyolitic tephras have erupted over the last c. 65 ka and most have well-constrained radiocarbon ages (Vucetich and Pullar, 1969; 1973; Howorth, 1975; Vucetich and Howorth, 1976; Froggatt and Lowe, 1990). Primary tephra layers enable isochronous time horizons to be established in a wide range of depositional environments. In studies of the ring plains of andesitic volcanoes within the Tongariro Volcanic Centre, rhyolitic tephras enable relative ages to be assigned to andesitic tephras and lahar deposits in order to provide a basis for calculating eruption and volcanic hazard frequencies (Cronin *et al.*, 1996a; Cronin and Neall, in press). The tephras also are used for investigating the construction of the ring plains (Cronin *et al.*, 1996b) and for investigations of soil development on ring plain materials (Cronin *et al.*, 1996c).

Methods of rhyolitic tephra identification have become increasingly sophisticated over time as the need arose for identification of tephras in distal areas, where field criteria are less useful. Methods applied have involved mineralogical studies (e.g. Ewart, 1963; Randle *et al.*, 1971; Lowe, 1988) and chemical studies (e.g. Smith and Westgate, 1969; Kohn, 1970; Borchardt *et al.*, 1971; Froggatt, 1983; Stokes *et al.*, 1992). Chemical techniques have concentrated on glass and titanomagnetite, and in New Zealand, glass chemistry has assumed the greatest importance for chemical characterisation of tephras (e.g. Froggatt, 1983; Stokes *et al.*, 1992).

Stokes and Lowe (1988) introduced the use of canonical discriminant functions (DFA) with glass chemistry to New Zealand tephras and showed a theoretical discrimination of tephras from different volcanic sources. Stokes *et al.* (1992) went on to show a theoretical discrimination of several individual rhyolitic tephras from Okataina and

Taupo sources. Shane and Froggatt (1994) again demonstrated a theoretical discrimination of six rhyolitic tephras of widely varying ages from the Taupo Volcanic Zone. All of these studies have shown the potential of the DFA method to discriminate New Zealand rhyolitic tephras but did not go on to show these techniques used in a practical situation. The Shane and Froggatt (1994) study in particular, although providing a further demonstration of the statistical techniques, used tephras which ranged in age from 1.85 ka to 1.63 Ma that are unlikely to be confused stratigraphically.

Eighteen distal rhyolitic tephras have been identified on the ring plains of Tongariro and Ruapehu volcanoes ranging in age from ca. 0.8 to 22 ka. (Topping and Kohn, 1973; Donoghue *et al.*, 1995). In this study we focus on the time range between 10 and 65 ka and provide a practical demonstration of the use of discriminant function analysis (DFA) to identify the rhyolitic tephras present. We extend from the initial construction of DFA models by testing unknown tephras against the models and attempt different means of improving their classification performance.

2.6 Setting

Ruapehu volcano within the Tongariro Volcanic Centre, is a large, active, andesitic composite volcano, and forms the highest point in the North Island at 2797 m (Fig. 2.1). The current massif comprises a 110 km^3 cone with a volcaniclastic ring plain of similar volume surrounding it (Hackett and Houghton, 1989). Tongariro volcano is a slightly smaller andesitic massif made up of several coalescing volcanic cones (Mathews, 1967), the largest of which is the recently active cone of Ngauruhoe.

The ring plains of Ruapehu and Tongariro volcanoes are confined to the east by the Kaimanawa Mountains, and the Tongariro River is the approximate boundary of the eastern ring plains. The section localities where rhyolitic tephras were found in this study are shown in Fig. 2.1.

2.7 Methods

2.7.1 Sample Preparation and analysis

Rhyolitic tephra samples from macroscopic layers were cleaned in water using an ultrasonic probe; it was unnecessary to concentrate further glass. When tephra samples were scattered within fine andesitic ash or soil material they were cleaned in 0.2 M acid-oxalate reagent to disperse them and to remove short-range order and organic constituents (Blakemore *et al.*, 1987; Alloway *et al.*, 1992). Glass was then concentrated using a sodium polytungstate solution at a density of 2.45 Mg/m^3. Ferromagnesian minerals were concentrated from all samples using a Frantz Isodynamic Separator. Grain mounts of ferromagnesian minerals were prepared and assemblages described by point counting. Glass grains were mounted in epoxy resin plugs, which were ground to expose the grains and polished.

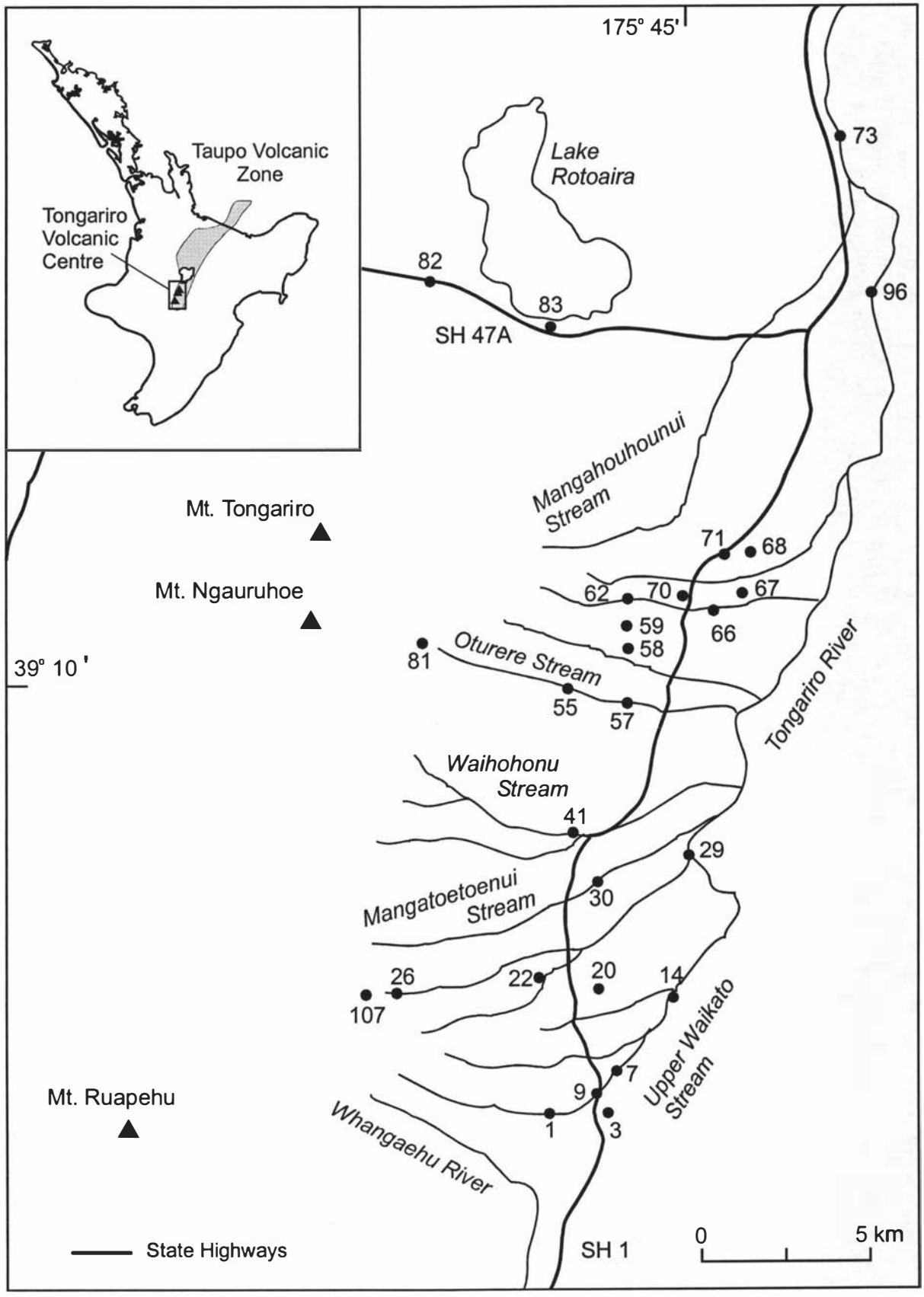

Figure 2.1. Location map of the eastern ring plains of Tongariro and Ruapehu volcanoes. Numbered dots indicate locations of sections where the rhyolitic tephras of this study were sampled; grid references are given in Table 2.2.

The major element chemistry was determined for polished individual grains on a JEOL-733 electron microprobe following the procedures and analytical conditions of Froggatt (1983). A 20 μm beam diameter was used when possible, otherwise a 10 μm beam was used with a beam current of 8 nA at an accelerating voltage of 15 kV. For each tephra sample at least 10 individual glass shards were analysed.

The glass chemistry was compared with published glass analyses carried out under the same analytical conditions and on the same instrument (Alloway, 1989; Donoghue, 1991; Froggatt, 1982; 1983; Froggatt and Solloway, 1986; Froggatt and Rogers, 1990; Lowe, 1988; Pillans and Wright, 1992; Stokes *et al.*, 1992; Pillans *et al.*, 1993; Shane and Froggatt, 1994; Carter *et al.*. 1995). Similarity coefficients, and coefficients of variation (Borchardt *et al.*, 1971), were calculated to compare the unknown samples with large volume tephra units in the same general time frame. However, these often provided two or three possible correlatives for a sample, even after their position in the stratigraphic column was considered, leaving the difficulty of choosing the most likely correlative. To improve on this correlation, canonical DFA was used.

2.7.2 Statistical Methods

Canonical DFA is a technique related to principal component analysis, which reduces the dimensionality of data such as compositional data which has a large number of independent variables. Canonical DFA produces a small number of linear combinations of the quantitative variables which best discriminate pre-defined groups of observations or analyses. This means that instead of working with ten oxide scores to discriminate groups of samples, one or two canonical variables contain the information. A reference set of analyses with pre-defined groupings must first be set up and canonical DFA is used to produce a discriminant model which can be used to classify unknown observations or analyses. The theory of DFA is outlined in many texts on multivariate analysis (e.g. Srivastava and Carter, 1983; Johnson and Wichern, 1992). The D^2 or Mahalanobis distance statistic is produced within the results of canonical DFA, and indicates the multivariate spacing between data groups in multi-dimensions (Srivastava and Carter, 1983). The D^2 statistic is therefore a useful measure of the separation of groups of samples (Stokes *et al.*, 1992) in place of the coefficients of variation and similarity coefficients first used with volcanic glass by Borchardt *et al.* (1971).

The studies of Beaudoin and King (1986) and Stokes and Lowe (1988), introduced the use of stepwise DFA methods which selected variables that had the greatest discriminating power. Stepwise DFA is further described by Srivastava and Carter (1983). In this study the SAS system programs DISCRIM, STEPDISC and CANDISC were used (SAS Institute Inc., 1989).

Prior to statistical analysis the data used in this study were transformed following the log-ratio procedure of Aitchison (1983, 1986) and Stokes and Lowe (1988) to avoid statistical closure, inherent in compositional data. We used MgO as the oxide divisor for this study, because of its moderate content and relatively low within, and between sample variance (Shane and Froggatt, 1994).

2.7.3 Tephra classification methodology

From the overall time interval of 10-65 ka, separate databases were established for two stratigraphically distinct groups of tephras (Table 2.1); those above and below the regional marker horizon of the Kawakawa Tephra (22.6 ka B.P., Wilson *et al.*, 1988). This enables two simpler discriminant models to be created rather than a single very complex model. All known tephras of significant volume within each time interval were included. Database 1 contained glass analyses of Karapiti, Waiohau, Rotorua, Rerewhakaaitu, Okareka and Te Rere Tephras. Database 2 contained analyses of Kawakawa, Okaia, Tihoi, Omataroa, Mangaone and Hauparu Tephras, and Rotoehu Ash. Analyses of Maketu Tephra were unavailable. The analyses were from published sources listed previously and unpublished data of SJC. Discriminant models were then created for each of these reference sets using the DISCRIM program.

Analyses of samples from the two stratigraphic intervals collected from the Ruapehu and Tongariro ring plains were tested against the discriminant functions calculated from the models. To improve any poor classifications resulting from this first model two further approaches were used. Firstly, unknown tephras that were correctly classified were added to the initial model to attempt to improve its performance in classifying the remaining unknowns. To satisfy the 'correctly classified' precondition, the overall probability of classification of a given sample with a particular tephra had to be high (>0.75), and this had to be consistent with all other evidence from stratigraphy, field observations and mineralogy. Secondly, in some cases where it appeared the sample was of a mixed origin, each component of the mixture was treated as a separate tephra for classification. Once again, any classifications made had to be consistent with other lines of evidence.

Table 2.1 Ages and sources of rhyolitic tephras within the two discriminant models used in this study.

Tephra name	Source*	Symbol	Age (Yrs B.P.)	Reference for age
Database 1, 10-22 ka tephras				
Karapiti Tephra	TVC	Kp	9820 ± 80†	Froggatt & Lowe (1990)
Waiohau Tephra	OVC	Wh	11850 ± 60†	"
Rotorua Tephra	OVC	Rr	13080 ± 50†	"
Rerewhakaaitu Tephra	OVC	Rk	14700 ±110†	"
Okareka Tephra	OVC	Ok	*c.* 18000‡	"
Te Rere Tephra	OVC	Te	21100 ± 320†	"
Database 2, 22.5-65 ka tephras				
Kawakawa Tephra	TVC	Kk	22590 ± 230†	Wilson *et al.* (1988)
Okaia Tephra	TVC	O	*c.* 23000‡	Froggatt & Lowe (1990)
Omataroa Tephra	OVC	Om	28220 ± 630†	"
Mangaone Tephra	OVC	Mn	27730 ± 350†	"
Hauparu Tephra	OVC	Hp	35870 ± 1270†	"
Tihoi Tephra	TVC	T	*c.* 46000‡	"
Rotoehu Ash	OVC	Re	64000 ± 4000§	Wilson *et al.* (1992)

* TVC = Taupo Volcanic Centre; OVC = Okataina Volcanic Centre.
† Denotes ^{14}C ages on old half life basis.
‡ Estimated stratigraphic age.
§ Whole rock K-Ar age.

2.8 Results

2.8.1 Ferromagnesian Assemblages

Table 2.2 Ferromagnesian mineral assemblages (modal %) and location of unknown tephra samples on the Ruapehu ring plain.

Sample number	Section number	Grid Ref. NZMS 260	Ferromagnesian mineralogy					
			opx	cpx	hb	bi	cu	tm
10-22 ka tephras								
93.5	20	T20/465127	52	41	5	-	tr	2
93.6	22	T20/453129	54	40	2	-	-	4
93.7	107	T20/430127	49	37	12	-	-	2
93.8	26	T20/435129	43	53	2	-	-	2
93.9	29	T20/498157	54	25	5	tr	tr	15
93.32	7	T20/469100	53	22	3	18	1	3
93.59	68	T19/505248	69	24	tr	-	-	7
94.7	20	T20/465127	48	16	15	-	-	21
94.9	30	T20/468162	50	30	1	-	-	19
94.21	55	T19/481211	58	40	tr	-	-	2
94.24	57	T19/486211	57	29	-	-	-	14
94.27	58	T19/485221	69	27	2	-	-	2
94.28	59	T19/495220	41	16	37	-	-	6
94.29	59	T19/495220	46	34	4	-	-	16
94.37	62	T19/485238	61	35	3	-	-	1
94.47	66	T19/496238	53	23	18	-	-	6
94.51	67	T19/504237	56	40	3	-	-	1
94.58	68	T19/505248	73	20	2	-	-	5
94.71	70	T19/488242	53	34	12	tr	-	1
94.74	71	T19/499247	68	26	2	-	-	4
94.79	73	T19/364544	67	15	6	-	-	2
95.2	81	T19/430238	61	37	1	-	-	1
95.3	81	T19/430238	53	35	8	tr	-	4
95.6	82	T19/423339	51	41	4	-	-	4
95.9	83	T19/448326	63	32	2	-	-	3
95.13	96	T19/549328	59	32	1	-	-	8
22.5-65 ka tephras								
93.1	1	T20/455088	30	44	18	-	-	8
93.3	3	T20/465095	53	37	2	-	-	8
93.17	41	T20/461170	35	18	33	-	-	14
93.33	7	T20/469100	32	15	37	-	-	16
7.37	7	"	58	39	-	-	-	3
7.36	7	"	66	28	-	-	-	6
9.37	9	T20/468102	63	27	6	-	-	4
9.36	9	"	66	23	4	-	-	7
9.35	9	"	68	20	10	-	-	2
9.33	9	"	59	35	3	-	-	3
9.25	9	"	79	19	2	-	-	tr
9.22	9	"	75	21	2	-	-	2
9.21	9	"	78	18	2	-	tr	2
14.23	14	T20/477112	77	19	1	-	-	3
14.22	14	"	79	19	1	-	tr	1

Abbreviations: opx = orthopyroxene, cpx = clinopyroxene, hb = hornblende, bi = biotite, cu = cummingtonite, tm = titanomagnetite; tr = trace quantities (< 1%).

The ferromagnesian assemblages for tephra samples studied are given in Table 2.2. These can be compared to the dominant mineral assemblages summarised by Froggatt

and Lowe (1990). The ferromagnesian assemblage is often useful to narrow down the possible correlatives of a tephra sample, but was rarely able to identify it uniquely. The assemblages are also found to be highly variable due to winnowing effects in distal localities and the common contamination of samples with andesitic tephra minerals. This contamination is evidenced by the presence of abundant clinopyroxene in many of the samples.

2.8.2 Glass chemistry and similarity coefficients

10-22 ka tephras

A correlation matrix with the similarity coefficients for the tephra samples from Ruapehu and Tongariro ring plain deposits in the 10-22 ka period with their potential correlatives is presented in Table 2.3. It has been reported that similarity coefficients for replicate analyses under the same microprobe operating conditions can deviate by around 10 % from the expected ideal value of 1.0 (Froggatt and Solloway, 1986; Stokes *et al.*, 1992). When different beam diameters are used, replicate analyses can have similarity coefficients as low as 0.88 (Pillans and Wright, 1992).

Table 2.3 Correlation matrix of similarity coefficients, comparing glass major oxide chemistry of rhyolitic tephras found in this study with published glass chemistry (Stokes *et al.*, 1992) from potential correlative tephras aged 10-22 ka. Tephra abbreviations from Table 2.1.

Sample	Kp	Wh	Rr	Rk	Ok	Te
93.5	0.76	0.85	0.81	0.81	0.78	0.80
93.6	0.84	0.91	0.91	0.85	0.82	0.93
93.7	0.78	0.87	0.86	0.82	0.80	0.86
93.8	0.77	0.81	0.82	0.78	0.75	0.82
93.9	0.78	0.92	0.83	0.88	0.87	0.86
93.32	0.80	0.93	0.88	0.88	0.79	0.69
93.59	0.80	0.92	0.88	0.88	0.85	0.88
94.7	0.85	0.94	0.90	0.87	0.84	0.94
94.9	0.94	0.81	0.92	0.75	0.72	0.88
94.21	0.86	0.91	0.93	0.85	0.82	0.94
94.24	0.91	0.77	0.88	0.72	0.70	0.84
94.27	0.80	0.94	0.84	0.94	0.91	0.88
94.28	0.79	0.92	0.84	0.94	0.92	0.86
94.29	0.82	0.90	0.84	0.92	0.91	0.86
94.37	0.86	0.93	0.90	0.87	0.84	0.95
94.47	0.74	0.84	0.77	0.85	0.84	0.81
94.51	0.84	0.94	0.90	0.87	0.84	0.93
94.58	0.81	0.90	0.86	0.87	0.86	0.89
94.71	0.79	0.95	0.84	0.93	0.90	0.87
94.74	0.84	0.93	0.90	0.86	0.83	0.92
94.79	0.85	0.70	0.80	0.67	0.65	0.77
95.2	0.84	0.93	091	0.87	0.84	0.93
95.3	0.79	0.93	0.84	0.93	0.91	0.88
95.6	0.88	0.91	0.93	0.85	0.82	0.96
95.9	0.84	0.90	0.93	0.85	0.81	0.93
95.13	0.86	0.93	0.91	0.87	0.83	0.94
Kp	-	0.81	0.89	0.76	0.75	0.91
Wh		-	0.86	0.92	0.89	0.89
Rr			-	0.80	0.78	0.93
Rk				-	0.97	0.84
Ok					-	0.81

Most of the tephra samples from this study in the 10-22 ka interval have similarity coefficients of ≥ 0.90 with published data for two or more of their possible correlatives. Similarity coefficients comparing published analyses of tephras in the 10-22 ka age range (Table 2.3) show a very high degree of correlation between almost all of the possible tephra combinations especially those from the same volcanic centre. The high degree of similarity between the glass chemistry of the tephras of this age range renders the similarity coefficient comparison technique ineffectual and a unique correlation can not be made for each unknown sample.

22-65 ka tephras

A correlation matrix of similarity coefficients for tephra samples from Ruapehu and Tongariro ring plain deposits in the 22-65 ka period with their potential correlatives is presented in Table 2.4. Again, most of the samples have more than one potential correlative with the similarity coefficient comparisons. In a comparison of published glass chemistry of the tephras in this time frame (Table 2.4), similarity coefficients indicate a high degree of correlation between all of these tephra combinations with the exception of Hauparu Tephra, which is distinctive. The high degree of similarity between most of the tephra units in this time frame render the similarity coefficient comparisons virtually unusable. This is particularly true for the study area, in which the stratigraphy beneath the Kawakawa tephra was completely unknown prior to this study.

Table 2.4 Correlation matrix of similarity coefficients, comparing glass major oxide chemistry of rhyolitic tephras found in this study with published glass chemistry from potential correlative tephras aged 22-65 ka. Tephra abbreviations from Table 2.1.

Sample	Kk*	O†	Om*	Mn*	Hp*	T†	Re*
95.1	0.82	0.83	0.82	0.79	0.76	0.78	0.78
93.3	0.90	0.90	0.92	0.89	0.72	0.83	0.85
93.17	0.88	0.88	0.93	0.89	0.73	0.81	0.82
93.33	0.86	0.87	0.88	0.87	0.74	0.82	0.82
7.37	0.85	0.85	0.83	0.82	0.72	0.80	0.81
7.36	0.92	0.90	0.89	0.81	0.70	0.69	0.87
9.37	0.83	0.85	0.83	0.81	0.72	0.78	0.82
9.36	0.92	0.92	0.90	0.81	0.68	0.76	0.87
9.35	0.87	0.87	0.87	0.84	0.75	0.85	0.83
9.33	0.90	0.90	0.89	0.86	0.70	0.87	0.87
9.25	0.73	0.73	0.73	0.74	0.86	0.67	0.69
9.22	0.73	0.75	0.80	0.80	0.85	0.68	0.68
9.21	0.95	0.95	0.93	0.88	0.68	0.87	0.91
14.23	0.77	0.79	0.82	0.83	0.85	0.71	0.72
14.22	0.91	0.93	0.90	0.85	0.68	0.87	0.90
Kk	-	0.97	0.89	0.85	0.68	0.90	0.90
O		-	0.91	0.87	0.69	0.87	0.88
Om			-	0.93	0.73	0.84	0.85
Mm				-	0.77	0.79	0.80
Hp					-	0.64	0.63
T						-	0.91

Source of analyses: * Pillans & Wright (1992); † Froggatt (1982).

2.8.3 Canonical discriminant function analyses of glass analyses

In both models the transformed oxide values of SiO_2, TiO_2, Al_2O_3, FeO, CaO, Na_2O and K_2O within the glasses were used.

10-22 ka tephras discrimination model

The initial discriminant model for the six 10-22 ka interval tephras comprises 185 glass analyses. This model can be represented as a plot of the first two (of five) canonical variates calculated from the log-transformed glass analyses (Fig. 2.2A). The mean compositions of each tephra group in the model are presented in Table 2.5. The D^2 statistics indicate good separation between each tephra group with values ranging between 8.9 and 102 (Table 2.6). The classification efficiencies (proportion of correctly identified glass shards based on reclassifying the original data with the calculated discriminant function) of this discriminant model are all high (Table 2.7); the lowest classification efficiency of 89 % is for the Rerewhakaaitu Tephra.

Stepwise DFA was attempted for the discriminant model to assess the oxides with the greatest discriminating power. All of the transformed oxides were highly discriminating, in the order of: K_2O, CaO, Na_2O, FeO, SiO_2, Al_2O_3 and TiO_2. The choice of K_2O, CaO and FeO near the top of the list of discriminating variables reflect their use by some workers in bivariate or trivariate plots to distinguish TVC and OVC sourced eruptives (e.g., Froggatt and Rogers, 1990; Pillans and Wright, 1992). However, five further oxides also provided discrimination according to STEPDISC, showing that much information is lost when only a subset of the available composition data is used; e.g. compare the plot of CaO vs. FeO for the analyses of the 10-22 ka tephras in Fig. 2.2B to the plot of the first two canonical variates in Fig. 2.2A.

Table 2.5 Mean electron microprobe glass compositions of tephras used in the initial 10-22 ka discriminant model.

	Karapiti	Waiohau	Rotorua	Rerewhakaaitu	Okareka	Te Rere
SiO_2	76.31 (1.08)	78.31 (0.70)	77.72 (0.40)	77.99 (0.33)	78.29 (0.27)	77.36 (0.26)
TiO_2	0.20 (0.06)	0.14 (0.05)	0.20 (0.04)	0.09 (0.03)	0.12 (0.03)	0.14 (0.04)
Al_2O_3	12.98 (0.38)	12.10 (0.27)	12.46 (0.16)	12.45 (0.24)	12.14 (0.13)	12.44 (0.14)
FeO	1.67 (0.24)	0.91 (0.13)	1.17 (0.15)	0.85 (0.11)	0.90 (0.10)	1.19 (0.11)
MgO	0.17 (0.03)	0.14 (0.03)	0.20 (0.03)	0.08 (0.02)	0.10 (0.03)	0.19 (0.02)
CaO	1.39 (0.14)	0.89 (0.12)	1.13 (0.14)	0.68 (0.11)	0.83 (0.08)	1.05 (0.11)
Na_2O	3.99 (0.33)	3.99 (0.43)	3.45 (0.26)	3.64 (0.15)	3.60 (0.17)	3.61 (0.13)
K_2O	3.06 (0.24)	3.38 (0.21)	3.50 (0.40)	4.12 (0.29)	3.89 (0.36)	3.85 (0.33)
n	45	52	13	27	33	15

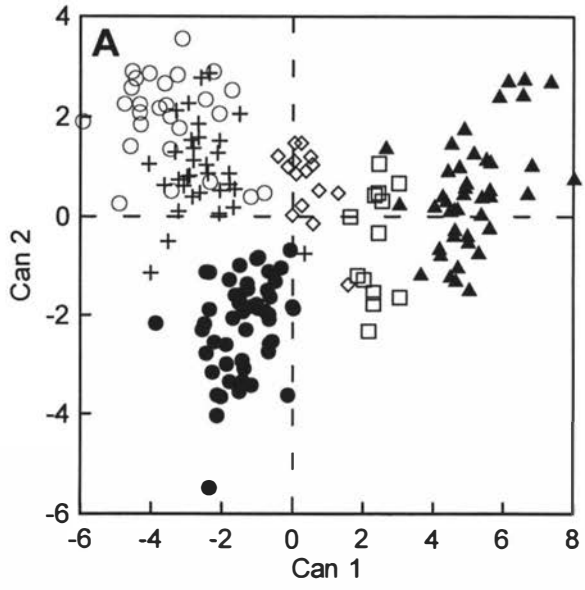

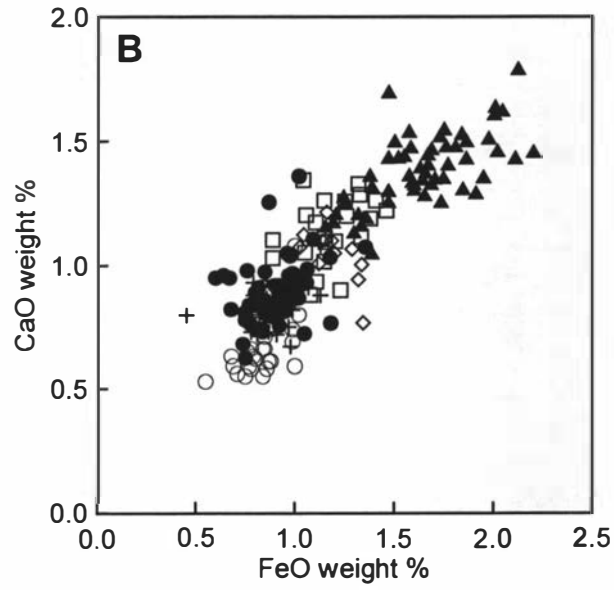

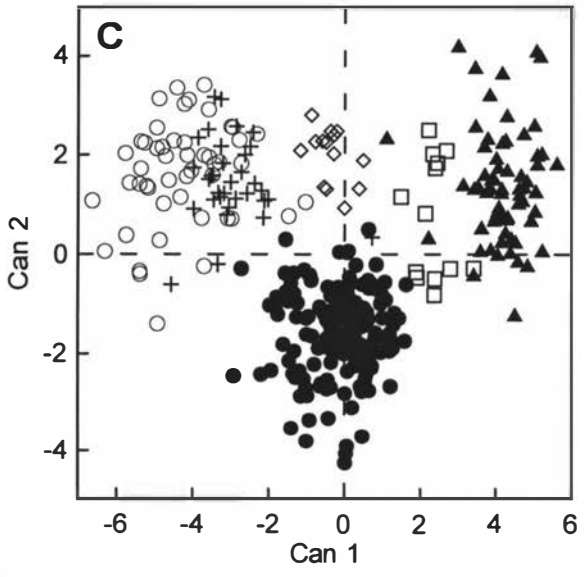

Symbol Key

▲= Kp ●= Wh □= Rr ○= Rk += Ok ◇= Te

Figure 2.2

A: Plot of the first two canonical variates (Can1 and Can 2) for tephras comprising the initial 10-22 ka rhyolitic glass discriminant model; D^2 values between groups are given in Table 2.6.

B: Plot of FeO vs, CaO weight % within the rhyolitic glass of the tephras comprising the the initial 10-22 ka discriminant model.

C: Plot of the first two canonical variates (Can 1 and Can 2) for tephras comprising the updated 10-22 ka rhyolitic glass discriminant model; D^2 values between tephra groups are given in Table 2.8.

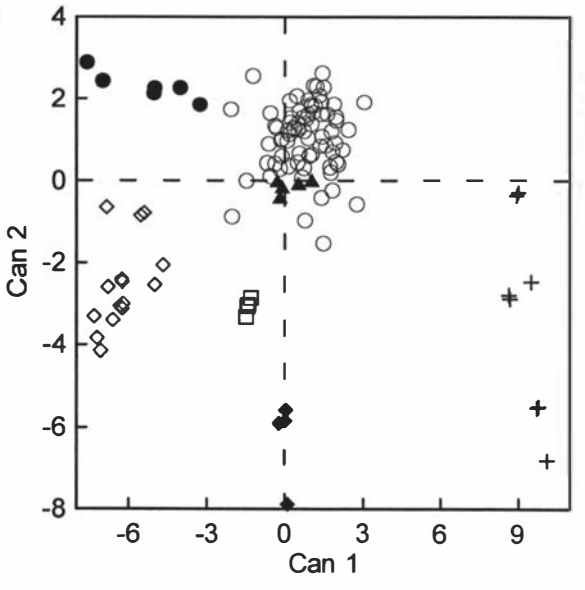

Symbol Key

○= Kk ▲= O □= Om += Hu ◆= Mg ●= T ◇= Re

Figure 2.3

Plot of the first two canonical variates (Can 1 and Can 2) for tephras comprising the 22-65 ka rhyolitic glass discriminant model; D^2 values between tephra groups are given in table 2.11.

Table 2.6 D^2 values and classification efficiencies of the initial discriminant model for the 10-22 ka tephras.

	Kp	Wh	Rr	Rk	Ok	Te
D^2 values between groups						
Kp	-	55	17	102	83	43
Wh		-	24	29	18	20
Rr			-	65	42	15
Rk				-	8.9	33
Ok					-	14
% correctly reclassified by model						
	98	100	100	89	97	93

Table 2.7 Probabilities of classification of unknown tephras in the 10-22 ka range with their potential correlatives, using the initial 10-22 ka tephra discriminant model.

Sample	*n*	Overall probability of classification					
		Kp	Wh	Rr	Rk	Ok	Te
Well classified samples							
93.5	8	-	0.79	0.04	-	-	0.17
93.6	11	-	0.98	0.01	-	-	0.01
93.7	9	-	0.83	0.10	-	-	0.07
93.32	9	-	-	-	0.88	0.12	-
94.7	9	-	0.78	0.09	-	-	0.13
94.9	10	0.87	-	0.13	-	-	-
94.21	9	-	0.79	0.03	0.08	0.05	0.05
94.24	10	1.00	-	-	-	-	-
94.37	10	-	0.85	0.14	-	-	0.01
94.47	11	-	-	-	0.93	0.07	-
94.51	9	-	0.94	0.05	-	-	0.01
94.58	8	-	0.91	-	-	0.09	-
94.74	10	-	0.99	0.01	-	-	-
94.79	6	1.00	-	-	-	-	-
95.2	9	-	0.98	0.02	-	-	-
95.3	9	-	-	0.14	0.82	0.04	-
95.6	10	-	0.89	0.09	-	-	0.02
95.9	10	-	0.95	0.04	-	-	0.01
95.13	9	-	0.81	0.19	-	-	-
Poorly classified samples							
93.8	14	0.07	0.35	0.26	0.09	-	0.23
93.9	11	-	0.61	-	0.37	0.01	0.01
93.59	10	0.10	0.27	0.09	0.44	0.06	0.04
94.27	9	-	0.64	0.02	0.23	0.10	0.01
94.28	10	0.01	0.18	0.15	0.30	0.31	0.05
94.29	8	-	0.01	0.09	0.30	0.29	0.31
94.71	10	-	0.38	-	0.11	0.33	0.18

n = number of analyses.

Classification of 10-22 ka unknown tephras

Twenty-six unknown tephra samples in this time range were tested against the initial discrimination model, 19 were classified with a particular tephra with overall (averaged over the number of analyses for each sample) probabilities exceeding 0.78 (Table 2.7). All of the 19 classifications were consistent with field, stratigraphic and mineralogical evidence. The remaining seven tephra samples had lower overall probabilities of classification to any one potential tephra correlative.

An updated discriminant model based on 351 analyses was constructed, with the addition of analyses from the 19 classified tephras to the initial model (Fig. 2.2C). The D^2 distances between tephra groups remained high, between 8.7 and 72 (Table 2.8), and so too did the classification efficiencies for each tephra. However, the improvement of this model over the initial one was with its classification of the remaining unknown tephras. This is because the updated model contained more analyses, and thus comprised better samples of the component tephra populations. Also the analyses added to form the updated model were carried out at the same time, by the same operator (SJC) as the remaining unknown samples awaiting classification. This was expected to reduce operator and instrument condition differences which may occur between the unknown analyses and those in the published literature or analysed at an earlier time. Small classification improvements were made with the seven formerly poorly classified tephra samples using the updated model (Table 2.9). Two tephras were well classified, while the remaining five were still poorly classified.

The next approach was to examine the possibility of mixed glass populations in the remaining unknown samples by classifying individual shards within each sample. It appears that each of the five poorly classified tephras contained two glass populations. One population was well classified whilst the other remained poorly classified (Table 2.9). The poorly classified population was later correlated with the Kawakawa Tephra using the 22-65 ka database. The presence of large volumes of Kawakawa Tephra and associated Hinuera Formation (Topping, 1974) in the study region provides a ready source of Kawakawa glass for admixing with these tephras.

Table 2.8 D^2 values and classification efficiencies of the updated discriminant model for the 10-22 ka tephras.

	Kp	Wh	Rr	Rk	Ok	Te
D^2 values between groups						
Kp	-	29	14	72	57	29
Wh		-	18	27	20	17
Rr			-	55	33	14
Rk				-	8.7	28
Ok					-	11
% correctly reclassified by model						
	96	97	100	84	97	93

22-65 ka tephras discriminant model

The initial discriminant model for seven of the largest volume tephras in this age range comprised 110 glass analyses (Fig. 2.3). The mean compositions of each tephra group in the model are presented in Table 2.10. The D^2 values between tephra groups range between 7.3 and 262 indicating good group separation (Table 2.11). The closest groups are the Kawakawa and the Okaia Tephras which were erupted from the same volcano within a short space of time (Froggatt and Lowe, 1990). The classification efficiencies of this discriminant model are high for all of the tephra groups; the lowest value of 93% is for the Kawakawa Tephra (Table 2.11).

Stepwise DFA of the analyses of this age group indicated that all of the transformed oxides were highly discriminating. The order in which the oxides were chosen was: K_2O, FeO, Al_2O_3, CaO, TiO_2, SiO_2 and Na_2O.

Table 2.9 Probabilities of classification of unknown tephras (that were poorly classified by the initial model) in the 10-22 ka range with their potential correlatives, using the updated 10-22 ka tephra discriminant model.

Sample	*n*	Overall probability of classification					
		Kp	Wh	Rr	Rk	Ok	Te
Samples with improved classifications							
93.9	11	-	0.95	-	0.05	-	-
94.27	9	-	0.98	0.01	0.01	-	-
*Mixed samples**							
93.8	14	0.07	0.35	0.26	0.09	-	0.23
93.8a	8	-	0.02	-	0.97	0.01	-
93.8b	6	0.10	0.15	0.28	0.13	-	0.34
93.59	10	0.13	0.29	0.04	0.47	0.04	0.03
93.59a	5	-	-	-	0.95	0.05	-
93.59b	5	0.33	0.47	0.11	-	-	0.09
94.28	10	0.01	0.18	0.15	0.30	0.31	0.05
94.28a	6	-	0.10	0.02	0.06	0.77	0.05
94.28b	4	0.10	0.44	0.05	0.35	0.01	0.05
94.29	8	-	0.01	0.09	0.30	0.29	0.31
94.29a	4	-	0.06	0.17	-	-	0.77
94.29b	4	-	0.03	0.28	0.36	0.32	0.01
94.71	10	-	0.38	-	0.11	0.33	0.18
94.71a	5	-	0.01	-	0.07	0.78	0.14
94.71b	5	-	0.46	0.12	0.23	0.10	0.09

n = number of analyses.
* For mixed samples, the first line is for all shards, (a) denotes the classified subset, and (b) the remaining unclassified subset.

Table 2.10 Mean electron microprobe compositions of tephras used in the 23-65 ka discriminant model.

	Kawakawa	Okaia	Omataroa	Mangaone	Hauparu	Tihoi	Rotoehu
SiO_2	78.36 (0.47)	78.48 (0.16)	78.17 (0.17)	78.36 (0.13)	76.05 (0.27)	78.47 (0.20)	78.87 (0.49)
TiO_2	0.14 (0.02)	0.11 (0.03)	0.15 (0.01)	0.17 (0.01)	0.33 (0.04)	0.09 (0.04)	0.13 (0.01)
Al_2O_3	12.24 (0.16)	12.55 (0.09)	12.30 (0.36)	12.76 (0.05)	13.09 (0.21)	12.53 (0.10)	12.08 (0.19)
FeO	1.19 (0.06)	1.15 (0.04)	1.14 (0.05)	1.12 (0.01)	1.75 (0.08)	1.01 (0.09)	0.92 (0.04)
MgO	0.13 (0.02)	0.15 (0.01)	0.15 (0.02)	0.19 (0.02)	0.35 (0.05)	0.10 (0.02)	0.12 (0.02)
CaO	1.07 (0.07)	1.08 (0.05)	1.07 (0.02)	1.14 (0.04)	1.73 (0.12)	0.79 (0.07)	0.77 (0.06)
Na_2O	3.50 (0.39)	3.45 (0.13)	3.84 (0.09)	3.80 (0.14)	4.09 (0.12)	3.34 (0.26)	3.46 (0.37)
K_2O	3.12 (0.17)	3.00 (0.20)	3.04 (0.21)	2.37 (0.20)	2.50 (0.33)	3.60 (0.13)	3.51 (0.29)
*n**	68	5	4	4	8	6	15

* each of the averaged analyses is itself a mean of usually 10 analyses.

Classification of the 22-65 ka unknown tephras

Fifteen unknown tephras were tested against the discriminant model as well as the sub-populations of the five mixed tephras mentioned previously from the 10-22 ka unknowns. All 15 of the unknown tephras were classified with probabilities of 0.7 or better (Table 2.12). All of the tephra samples older than the Kawakawa Tephra were microscopic glass accumulations within weathered andesitic tephras, thus little other corroborating evidence for these correlations was available. However, the correlations produced using the model were in the correct stratigraphic order considering the sampling positions.

Table 2.11 D^2 values and classification efficiencies of the discriminant model for the 22.5-65 ka tephras.

	Kk	O	Om	Mg	Hu	T	Re
D^2 values between groups							
Kk	-	7.3	25	77	98	45	64
O		-	18	59	106	40	61
Om			-	30	123	50	30
Mg				-	126	118	85
Hu					-	262	245
T						-	35
% correctly reclassified by model							
	93	100	100	100	100	100	100

Table 2.12 Probabilities of classification of unknown tephras in the 22.5-65 ka range with their potential correlatives, using the 22.5-65 ka tephra discriminant model.

Sample	*n*	Overall probability of classification						
		Kk	O	Om	Mg	Hu	T	Re
22.5-65 ka unknown tephra samples								
93.1	10	1.00	-	-	-	-	-	-
93.3	10	1.00	-	-	-	-	-	-
93.17	11	0.99	0.01	-	-	-	-	-
93.33	11	1.00	-	-	-	-	-	-
7.37	8	0.11	0.89	-	-	-	-	-
7.36	6	0.20	0.80	-	-	-	-	-
9.37	10	0.71	-	-	-	0.29	-	-
9.36	6	0.70	-	-	-	0.30	-	-
9.35	10	0.06	0.94	-	-	-	-	-
9.33	9	-	0.14	0.86	-	-	-	-
9.25	-	-	-	-	-	1.00	-	-
9.22	-	-	-	-	-	1.00	-	-
9.21	-	-	-	-	-	-	0.19	0.81
14.23	-	-	-	-	-	1.00	-	-
14.22	-	-	-	-	-	-	0.10	0.90
Unclassified subsets of mixed 10-22 ka group samples								
93.8b	6	1.00	-	-	-	-	-	-
93.59b	5	0.98	0.02	-	-	-	-	-
94.28b	4	0.73	-	-	-	-	0.27	-
94.29b	4	1.00	-	-	-	-	-	-
94.71b	5	0.70	0.30	-	-	-	-	-

n = number of analyses.

The unknown analyses not classified by the 10-22 ka model in the five mixed tephras were classified as Kawakawa Tephra with probabilities >0.7. This indicates that the five

mixed tephras were contaminated by reworked Kawakawa Tephra shortly after their deposition. The tephras were being deposited between 21.1 and 14.7 ka B.P., during a period when the climate was cool, dry and stormy (McGlone and Topping, 1983). Much erosion and deposition of ring plain deposits (including the Oruanui Ignimbrite member of the Kawakawa Tephra) by lahars and fluvial activity was occurring at this time on the ring plain (Cronin and Neall, in press). These conditions probably led to much Kawakawa Tephra glass being transported aerially and fluvially to contaminate the tephras and other ring plain deposits of this age.

2.9 Conclusions

In this study we have extended the scope of past DFA work and show a practical example of these statistical methods in action. From this work we have reached the following conclusions:

1) The creation of canonical discriminant models for potential tephra correlatives in two clearly defined stratigraphic intervals offers a considerable improvement on other methods for the identification of the tephras in this study.

2) Most unknown tephras in the two stratigraphic groups were classified using the initial discriminant models based on past analyses of the potential correlative tephras. However, small improvements in classification of unknown tephras were achieved by including correctly classified tephras into the model. This should only be done where all other corroborating evidence supports the statistical classification. The improvements were probably due to larger sample sizes in the updated model, and a reduction of differences in operators and instrument conditions between the unknown tephras being tested and the past analyses making up the initial model.

3) DFA enables the use of all of the glass analyses of a particular unknown tephra to be used to classify or identify it. We have shown this to be of great value for identifying mixed tephras in samples containing mixed glass populations. This approach will be especially practical when examining tephras which occur as microscopic concentrations in slowly accumulating sediments such as loess and aggrading soils. In these sediments there is a common mixing upwards of glass grains so that younger tephras need to be separated from a background of older shards into which they are mixed (Eden *et al.*, 1992).

4) In this study we have identified four previously undiscovered rhyolitic tephras in this area from glass concentrations within buried soil and andesitic ash. These are the Okaia, Omataroa and Hauparu Tephras and the Rotoehu Ash; they assist significantly in establishing a chronology for andesitic tephras and diamictons older than 22.6 ka B.P.

2.10 Acknowledgements

SJC gratefully acknowledges funding from the New Zealand Vice-Chancellor's Committee, Massey University Graduate Research Fund, the Helen E. Akers Scholarship

Fund, and the Department of Soil Science of Massey University. Ken Palmer (Victoria University of Wellington) is thanked for his introduction to the operation of the electron microprobe. Comments from two journal reviewers helped us to clarify our arguments, for which we are grateful.

2.11 References

Aitchison, J., 1983. Principal component analysis of compositional data. Biometrika 70: 57-65.

Aitchison, J., 1986. The statistical analysis of compositional data. Monographs on Statistics and Applied Probability. Chapman and Hall, London.

Alloway, B.V., 1989. Late Quaternary cover-bed stratigraphy and tephrochronology of north-eastern and central Taranaki, New Zealand. Unpublished Ph.D. thesis, Massey University, Palmerston North.

Alloway, B.V.; Neall, V.E.; Vucetich, C.G., 1992. Particle size analyses of Late Quaternary allophane-dominated andesitic deposits from New Zealand. Quat. Inter. 13/14: 167-174.

Beaudoin, A.B.; King, R.H., 1986. Using discriminant function analysis to identify Holocene tephras based on magnetite composition: a case study from the Sunwapta Pass area, Jasper National Park. Canadian J. of Earth Sci. 23: 804-812.

Blakemore, L.C.; Searle, P.L.; Daly, B.K., 1987. Methods for chemical analysis of soils. N. Z. Soil Bureau Scientific Rep. 80: 103pp.

Borchardt, G.A..; Harward, M.E.; Schmitt, R.A., 1971. Correlation of ash deposits by activation analysis of glass separates. Quat. Res. 1: 247-260.

Carter, L.; Nelson, C.S.; Neil, H.L.; Froggatt, P.C., 1995. Correlation, dispersal, and preservation of the Kawakawa Tephra and other late Quaternary tephra layers in the Southwest Pacific Ocean. N. Z. J. of Geol. and Geophys. 38: 29-46.

Cronin, S.J.; Neall, V.E., in press. A Late Quaternary stratigraphic framework for the northeastern Ruapehu and eastern Tongariro ring plains, New Zealand. N. Z. J. of Geol. and Geophys. 40.

Cronin, S.J.; Neall, V.E.: Palmer, A.S., 1996b. Geological history of the northeastern ring plain of Ruapehu volcano, New Zealand. Quat. Inter. 34-36: 21-28.

Cronin, S.J.; Neall, V.E., Palmer, A.S., 1996c. Investigation of an aggrading paleosol developed into andesitic ring-plain deposits, Ruapehu volcano, New Zealand. Geoderma 69: 119-135.

Cronin, S.J.; Neall, V.E.; Stewart, R.B.; Palmer, A.S., 1996a. A multiple-parameter approach to andesitic tephra correlation, Ruapehu volcano, New Zealand. J. Volcanol. and Geotherm. Res., 72: 199-215.

Donoghue, S.L., 1991. Late Quaternary volcanic stratigraphy of the southeastern sector of Mount Ruapehu ring plain, New Zealand. Unpub. Ph.D. thesis, Massey University, Palmerston North.

Donoghue, S.L.; Neall, V.E.; Palmer, A.S., 1995. Stratigraphy and chronology of late Quaternary andesitic tephra deposits, Tongariro Volcanic Centre, New Zealand. J. Roy. Soc. N. Z. 25: 115-206.

Eden, D.N.; Froggatt, P.C.; McIntosh, P.D., 1992. The distribution and composition of volcanic glass in late Quaternary loess deposits of southern South Island, New Zealand, and some possible correlations. N. Z. J. of Geol. and Geophys. 35: 69-79.

Ewart, A., 1963. Petrology and petrogenesis of the Quaternary pumice ash in the Taupo area, New Zealand. J. Petrology 4: 392-431.

Froggatt, P.C., 1982. A study of some aspects of the volcanic history of the Lake Taupo area, North Island, New Zealand. Unpub. Ph.D. thesis, Victoria University of Wellington, Wellington.

Froggatt, P.C., 1983. Towards a comprehensive Upper Quaternary tephra and ignimbrite stratigraphy in New Zealand using electron microprobe analysis of glass shards. Quat. Res. 19: 188-200.

Froggatt, P.C.; Solloway, G.J., 1986. Correlation of Papanetu Tephra to Karapiti Tephra, central North Island, New Zealand. N. Z. J. of Geol. and Geophys.29: 303-313.

Froggatt, P.C.; Lowe, D.J., 1990. A review of late Quaternary silicic and some other tephra formations from New Zealand: their stratigraphy, nomenclature, distribution, volume, and age. N. Z. J. of Geol. and Geophys. 33: 89-109.

Froggatt, P.C.; Rogers, G.M., 1990. Tephrostratigraphy of high altitude peat bogs along the axial ranges, North Island, New Zealand. N. Z. J. of Geol. and Geophys. 33: 111-124.

Hackett, W.R.; Houghton, B.F., 1989. A facies model for a Quaternary andesitic composite volcano: Ruapehu, New Zealand. Bull. Volcanol. 51: 51-68.

Howorth, R., 1975. New formations of Late Pleistocene tephras from Okataina Volcanic Centre, New Zealand. N. Z. J. of Geol. and Geophys. 18: 683-712.

Johnson, R.A.; Wichern, D.W., 1992. Applied multivariate statistical analysis (3rd Edition). Prentice-Hall Inc., New Jersey.

Kohn, B.P., 1970. Identification of New Zealand tephra layers by emission spectrographic analysis of their titanomagnetites. Lithos 3: 361-368.

Lowe, D.J., 1988. Stratigraphy, age, composition, and correlation of late Quaternary tephras interbedded with organic sediments in Waikato lakes, North Island, New Zealand. N. Z. J. of Geol. and Geophys. 31: 125-165.

Mathews, W.H., 1967. A contribution to the geology of the Mount Tongariro massif, North Island, New Zealand. N. Z. J. of Geol. and Geophys. 10: 1027-1038.

McGlone, M.S.; Topping, W.W., 1983. Late Quaternary vegetation, Tongariro region, central North Island, New Zealand. N. Z. J. of Botany 21: 53-76.

Pillans, B.J.; Wright, I., 1992. Late Quaternary tephrostratigraphy from the southern Havre Trough - Bay of Plenty, northeast New Zealand. N. Z. J. of Geol. and Geophys. 35: 129-143.

Pillans, B., McGlone, M., Palmer, A., Mildenhall, D., Alloway, B.; Berger, G., 1993. The Last Glacial Maximum in central and southern North Island: a paleoenvironmental reconstruction using the Kawakawa tephra formation as a chronostratigraphic marker. Palaeo., Palaeo., Palaeo. 101: 283-304.

Randle, K.; Gorton, G.G.; Kittleman, L.R., 1971. Geochemical and petrological characterisation of ash samples from Cascade Range volcanoes. Quat. Res. 1: 261-282.

SAS Institute Inc., 1989. SAS users guide: statistics. Version 6 Edition. Cary N.C., SAS Institute Inc., 1028 pp.

Shane, P.A.R., Froggatt, P.C., 1994. Discriminant function analysis of glass chemistry of New Zealand and North American tephra deposits. Quat. Res. 41: 70-81.

Smith, D. G. W.; Westgate, J.A., 1969. Electron probe technique for characterising pyroclastic deposits. Earth Planet. Sci. Lett. 5: 313-319.

Srivastiva, M.S.; Carter, E.M., 1983. An introduction to applied multivariate statistics. Elsevier Science Publishing Co. Inc., New York.

Stokes, S.: Lowe, D.J., 1988. Discriminant function analysis of late Quaternary tephras from five volcanoes in New Zealand using glass shard major element chemistry. Quat. Res. 30: 270-283.

Stokes, S.; Lowe, D.J.; Froggatt, P.C., 1992. Discriminant function analysis and correlation of Late Quaternary rhyolitic tephra deposits from Taupo and Okataina volcanoes, New Zealand, using glass shard major element composition. Quat. Inter. 13/14: 103-117.

Topping, W.W., 1974. Some aspects of the Quaternary history of the Tongariro Volcanic Centre, New Zealand. Unpub. Ph.D. thesis, Victoria University of Wellington, Wellington.

Topping, W.W.; Kohn, B.P., 1973. Rhyolitic tephra marker beds in the Tongariro area, North Island, New Zealand. N. Z. J. of Geol. and Geophys. 16: 375-395.

Vucetich, C.G.; Pullar, W.A., 1969. Stratigraphy and chronology of late Pleistocene volcanic ash beds in central North Island, New Zealand. N. Z. J. of Geol. and Geophys. 12: 784-837.

Vucetich, C.G.; Pullar, W.A., 1973. Holocene tephra formations erupted in the Taupo area and interbedded tephras from other volcanic sources. N. Z. J. of Geol. and Geophys. 16: 745-780.

Vucetich, C.G.; Howorth, R., 1976. Late Pleistocene tephrostratigraphy in the Taupo district, New Zealand. N. Z. J. of Geol. and Geophys. 19: 51-69.

Wilson, C.J.N.; Switzur, R.V.; Ward, A.P., 1988. A new ^{14}C age for the Oruanui (Wairakei) eruption, New Zealand. Geol. Mag. 125: 297-300.

Wilson, C.J.N.; Houghton, B.F.; Lanphere, M.A.; Weaver, S.D., 1992. A new radiometric age estimate for the Rotoehu Ash from Mayor Island volcano, New Zealand. N. Z. J. of Geol. and Geophys. 35: 371-374.

CHAPTER 3. ANDESTIC TEPHROCHRONOLOGY

3.1 Introduction

The work of Topping (1973, 1974) and Donoghue *et al.* (1995) has resulted in a well defined stratigraphy of Ruapehu- and Tongariro-sourced tephras since 22.6 ka B.P (Chapter 1: Table 1.3). The identification of these tephras in the ring plain area relies mostly on their physical appearance in conjunction with their stratigraphic position. In more distal areas the identification of TgVC-sourced tephras relies on other features such as characteristic mineralogy as well as chemistry of glass or phenocryst minerals (e.g. Lowe, 1988a; Donoghue *et al.*, 1991).

There were two ways in which this study was intended to add to previous andesitic tephrochronology work in the study area as well as to andesitic tephrochronolgy as a whole. The first contribution was to attempt additional methods of andesitic tephra identification such as the use of the major oxide chemistry of ferromagnesian phenocryst minerals within the tephras. To compare the chemical compositions of the tephras in this study, statistical methods similar to those used for the rhyolitic tephras in Chapter 2 were used. The second contribution of this study was to investigate the pre-22.6 ka B.P. andesitic tephrochronology of the NE Ruapehu and E Tongariro ring plains.

These two contributions have been written up as the following two papers. In the first study, the major oxide chemistry of hornblende and titanomagnetite phenocrysts of TgVC- and Egmont volcano (EV)-sourced tephras were used to test and develop the canonical discriminant function analysis (DFA) method. Once it was determined whether this method was able to distinguish between tephras from the two sources, discrimination between individual tephras from the same source was attempted. A well controlled sequence of EV-sourced tephras was chosen for this trial.

The second study involved combining many parameters to correlate the pre-22.6 ka B.P. sequence of andesitic tephras on the NE Ruapehu ring plain. Physical appearance, mineralogy and mineral chemistry were all used in combination to correlate this sequence. A statistical clustering method was used to establish tephra groupings which could then be discriminated using the DFA methods developed in the first study.

A listing of all electron microprobe analyses used in these studies comprises Appendix 3. The SAS programs used in the two studies are included in Appendix 1.

3.1.1 Photographs of the Upper Waikato Stream sequence

The following plates display part of the Upper Waikato Stream sequence and three of the marker units described on the basis of their appearance in Section 3.4. These plates were not included in either of the papers comprising this chapter.

Plate 3.1. Part of the Upper Waikato Stream sequence located at T20/468102 and represented in Figs. 3.6, 4.1 and 5.3. The exposure is ca. 30 m high.

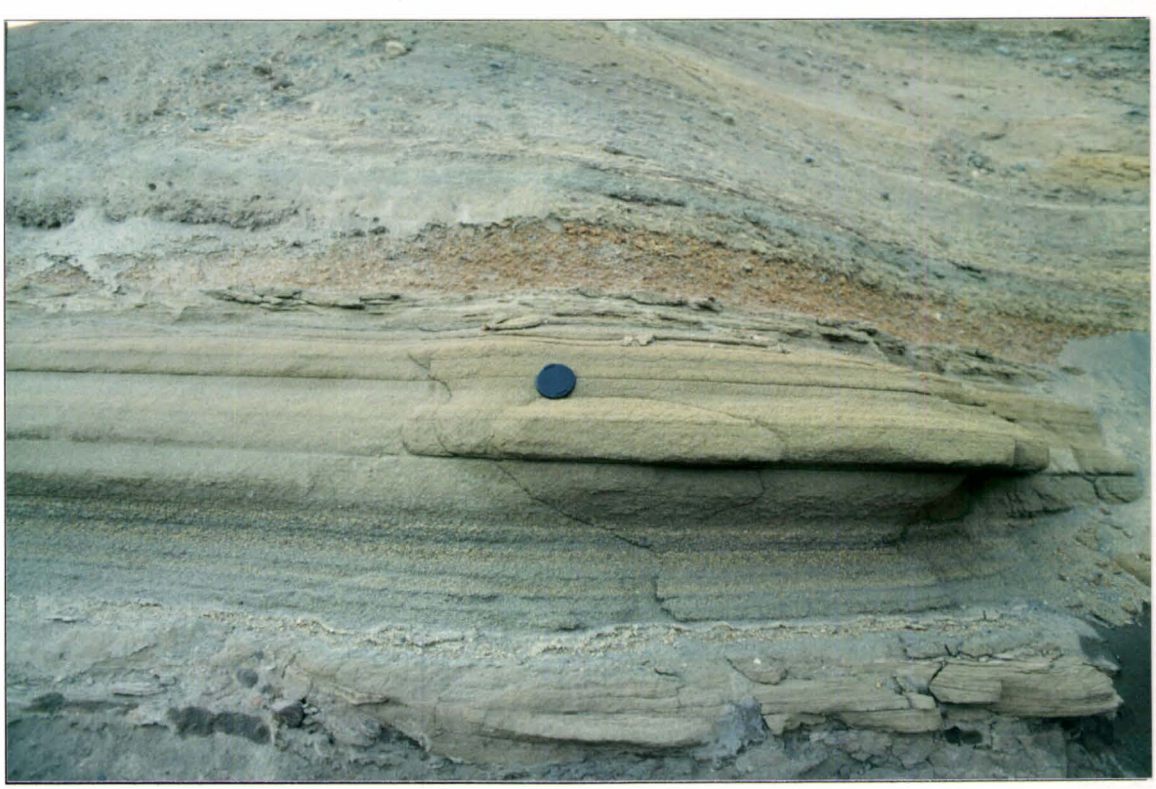

Plate 3.2. Marker Unit 1 tephra at T20/464098, see Fig. 3.6 for stratigraphic position and Section 3.4.6 for description. Lens cap is 50 mm in diameter.

Plate 3.3. Marker Unit 2 tephra at T20/469100; see Fig. 3.6 for stratigraphic position and Section 3.4.6 for description. Lens cap is 50 mm in diameter.

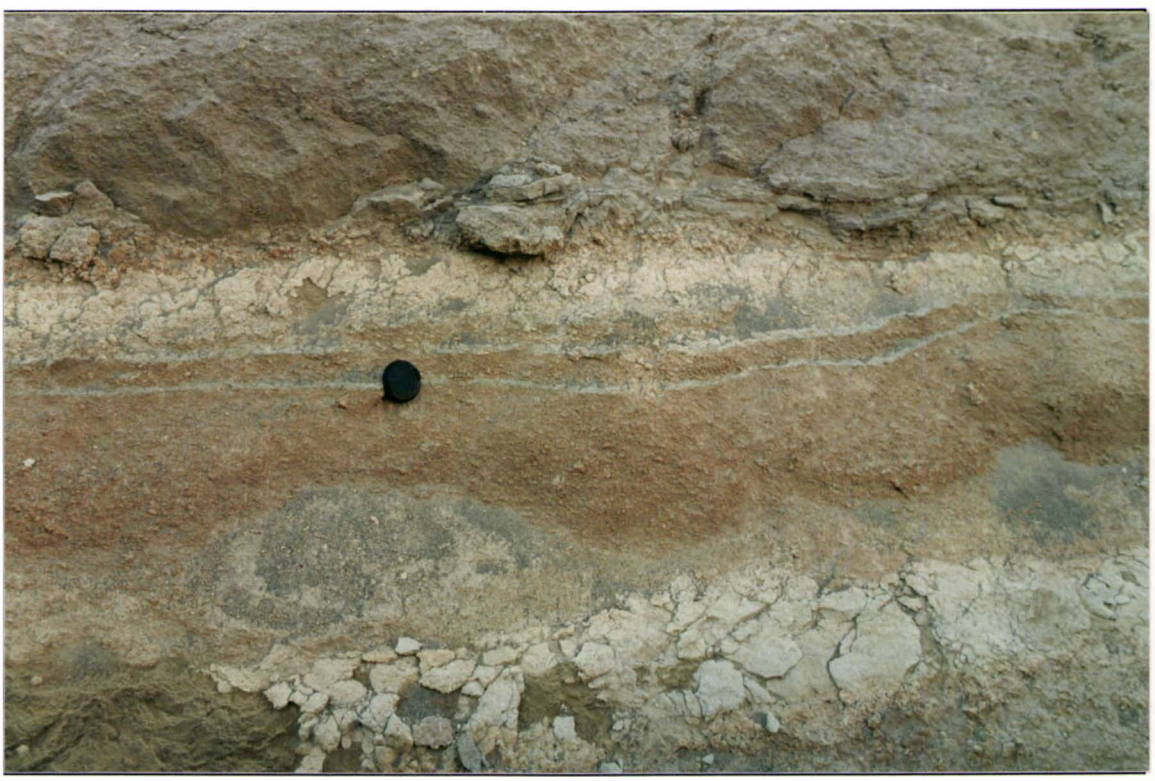

Plate 3.4. Marker Unit 3 tephra at T20/468102; see Fig. 3.6 for stratigraphic position and Section 3.4.6 for description. Lens cap is 50 mm in diameter.

3.2 Contributions of co-authors

Sourcing and identifying andesitic tephras using major oxide titanomagnetite and hornblende chemistry, Egmont volcano and Tongariro Volcanic Centre, New Zealand

Bulletin of Volcanology, 58: 33-40 (1996).

S.J. Cronin: Principal investigator
Carried out: sampling and laboratory preparation of TgVC tephras
electron microprobe analysis of TgVC tephras
all statistical programming and analysis
manuscript preparation and writing

R.C. Wallace: Co-investigator
Carried out: sampling and laboratory preparation of EV tephras
electron microprobe analysis of EV tephras
editing and discussion of the manuscript

V.E. Neall: Adviser: aided the study by discussing results and methodology as well as editing and discussion of the manuscript.

A multiple-parameter approach to andesitic tephra correlation, Ruapehu volcano, New Zealand

Journal of Volcanology and Geothermal Research, 72: 199-215 (1996).

S.J. Cronin: Principal investigator
Carried out: sampling and laboratory preparation of tephras
optical microscopy
electron microprobe analysis
statistical programming and analysis
manuscript preparation and writing

V.E. Neall, R.B. Stewart, A.S. Palmer: Advisers
aided the study by discussing results and methodology with SJC as well as editing and discussion of the manuscript.

3.3 SOURCING AND IDENTIFYING ANDESITIC TEPHRAS USING MAJOR OXIDE TITANOMAGNETITE AND HORNBLENDE CHEMISTRY, EGMONT VOLCANO AND TONGARIRO VOLCANIC CENTRE, NEW ZEALAND

S. J Cronin, R C. Wallace, and V. E Neall
Department of Soil Science, Massey University, Private Bag 11 222, Palmerston North, New Zealand

1996, Bulletin of Volcanology, 58: 33-40.

Abstract. Canonical discriminant function analysis was employed to discriminate between electron microprobe-determined titanomagnetite and hornblende analyses from Egmont volcano and Tongariro Volcanic Centre. Data sets of 436 titanomagnetite and 206 hornblende analyses from the two sources were used for the study. Titanomagnetite chemistry provided the best discrimination between these two sources with classification efficiencies of 99 % for sample averages and 95 % for individual analyses. The difference between sources for hornblende chemistry was less marked, but classification efficiencies of 100 % for sample averages and 87 % for individual analyses were achieved. Using the same methods, a preliminary discrimination of individual Egmont volcano-sourced tephras was attempted. Titanomagnetite chemistry enabled the discrimination of several individual tephras or at least pairs of tephra units, but hornblende chemistry provided little discrimination. This technique provides an improvement on previous methods for chemically distinguishing distal tephra from the two sources as well as potentially identifying individual tephras from a particular source. A major advantage over previous discrimination techniques is that individual analyses can be classified with a known probability of group membership (with groups such as volcano source or an individual tephra unit). Tephras in a depositional environment where mixing is common such as within soil, loess and marine sequences, can be sourced or identified more easily with classification of individual grains.

Key words: Tephrostratigraphy-Egmont volcano-Tongariro Volcanic Centre-discriminant function analysis-DFA.

3.3.1 Introduction

The stratigraphic importance of tephra layers is well recognised in Quaternary studies world-wide as well as in New Zealand (e.g. Thorarinsson, 1949; Pullar, 1967; Lowe, 1990). Tephrochronology studies in New Zealand have mostly concentrated on the many, widespread and voluminous rhyolitic tephras erupted from calderas within the Taupo Volcanic Zone (e.g. Vucetich and Pullar, 1969 and 1973; Froggatt, 1983; Froggatt and Lowe, 1990). Studies of andesitic tephrochronology have been fewer in New Zealand due to the more restricted distribution of andesitic tephras, the ease with which

they weather, apparent difficulties involved in their identification, and their perceived limited use in petrographic studies. Andesitic tephrochronology has however proved to be important in studies on and around the two major andesitic volcanic areas in the North Island (Fig. 3.1); Egmont volcano and Tongariro Volcanic Centre (e.g. Kohn and Neall, 1973; Topping, 1973; Donoghue *et al.*, 1995), as well as in distal regions (Lowe, 1988a; Wallace, 1987; Eden *et al.*, 1993). In these areas andesitic tephras have been used to either complement the rhyolitic tephra record or provide greater stratigraphic resolution.

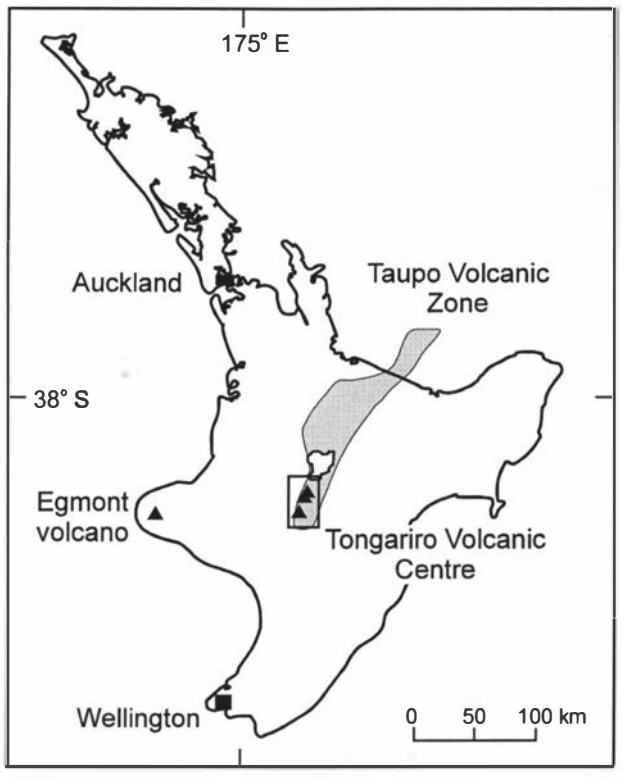

Fig 3.1. North Island of New Zealand with locations of Egmont volcano and Tongariro Volcanic Centre.

Methods of rhyolitic tephra identification have become increasingly sophisticated as the need arises for accurate and reliable identification of tephras in distal areas, where field criteria are sometimes ambiguous. Methods have involved mineralogical criteria, (e.g. Randle *et al.*, 1971; Lowe, 1988) as well as chemical criteria, (e.g. Smith and Westgate, 1969; Kohn, 1970; Borchardt *et al.*, 1971; Froggatt, 1983; Wallace, 1987; Stokes *et al.*, 1992). Chemical techniques have mostly involved glass and titanomagnetite, and in New Zealand glass chemistry has achieved the most widespread use for chemical characterisation of tephra (e.g. Froggatt, 1983; Stokes *et al.* 1992).

Andesitic tephra identification methods in New Zealand have followed those developed for rhyolitic tephras. However in distal areas of tephra accumulation it remains difficult to distinguish Tongariro Volcanic Centre- (TgVC) and Egmont volcano- (EV) sourced tephras because they have similar mineralogy, and mixing occurs. The greatest difficulty with the identification of andesitic tephras results from them being more easily

weathered in most depositional environments than rhyolitic tephras (Kirkman and McHardy, 1980; Lowe 1986). There are major differences in glass chemistry between the two centres, (Wallace *et al.*, 1986) but rapid weathering, renders andesitic glass unusable for tephra identification in most circumstances. Mineralogy is often but not always useful for distinguishing EV- and TgVC-sourced distal tephras. Lowe (1988a) distinguished EV tephras by a ferromagnesian assemblage of clinopyroxene + hornblende ± orthopyroxene, compared with orthopyroxene + clinopyroxene ± olivine ± hornblende for TgVC tephras. However, Wallace *et al.* (1986) concluded that olivine and orthopyroxene are more abundant in EV-sourced tephras than previously thought, and several TgVC-sourced tephra layers also lie outside of the general assemblage fields defined by Lowe (Donoghue *et al.*, 1991; Cronin *et al.*, 1996). Mineral assemblages may also be affected by winnowing (Juvigné and Shipley, 1983), weathering (Hodder *et al.*, 1991), and pedogenic mixing (Wallace, 1987).

Titanomagnetite trace element chemistry has been shown to be useful in distinguishing individual EV tephras, (Kohn and Neall, 1973; Wallace *et al.*, 1986) as well as distinguishing between EV- and TgVC-sourced tephras (Kohn and Neall, 1973; Lowe, 1988a). Kohn and Neall (1973) used emission spectrographic analyses on bulk samples of titanomagnetites, but this technique is unsuitable in any environment where there is potential mixing of tephra layers, such as in loess and soil. The elements which provided the greatest discrimination of sources were, chromium, vanadium, nickel, and manganese. Lowe (1988a) used a bivariate plot of Cr_2O_3 vs. MnO wt % to show a provisional difference between tephras from the two sources.

Hornblende chemistry has also been used to distinguish between EV- and TgVC-sourced tephras. Wallace (1987) used MgO, FeO and K_2O content of hornblende to distinguish between EV- and Taupo Volcanic Zone-sourced tephras and Eden *et al.* (1993), used calcium and silicon to discriminate between TgVC and EV hornblendes. These approaches may be useful but they do not use the full range of chemistry data available. Other mineral phases which have been used to discriminate individual tephras or provide limited discrimination between EV and TgVC sources are olivine, clinopyroxene, and plagioclase (Lowe, 1988a; Donoghue *et al.*, 1991).

Compared to bivariate plots, a more statistically powerful technique which uses the total chemistry of a sample in comparing and contrasting compositional data is canonical discriminant function analysis (DFA). DFA was introduced to tephra studies by Borchardt *et al.* (1971) using rhyolitic glass analyses, and has since been applied to titanomagnetite major element analyses to discriminate tephras in Canada (King *et al.*, 1982; Beaudion and King, 1986). In New Zealand, DFA using major oxide glass analyses has been used to discriminate volcanic source areas as well as some individual rhyolitic eruptives (Stokes and Lowe, 1988; Stokes *et al.*, 1992; Shane and Froggatt, 1994).

This study was firstly aimed at discriminating between TgVC- and EV-sourced andesitic tephras by using canonical DFA of all titanomagnetite and hornblende major oxides. The second step was to apply this methodology on the same data set in a preliminary investigation to discriminate individual tephra eruptives from one of the

sources. We also present here preliminary results from our investigation of EV-sourced tephras.

3.3.2 Methods

Tephra samples were taken from localities proximal to EV and TgVC. Phenocryst phases were extracted, mounted in epoxy resin, cut and polished.

Phenocrysts of titanomagnetite and hornblende were analysed in this study. Orthopyroxene, clinopyroxene and plagioclase were not used because they display strong oscillatory zoning in TgVC tephras and the chemical variation within a single grain was as great as the variation between samples. Olivine was also not targeted because it was not present in many of the tephras. The chemistry of the titanomagnetites and hornblendes varied less within each sample population and there was no observable oscillatory zoning. Further advantages of using titanomagnetite are that it is relatively stable during weathering (Ruxton, 1968) and is easy to separate from a sample.

The analyses were carried out with a JEOL JXA-733 electron microprobe using an accelerating voltage of 15 kV, a 12 nA beam current, and a 3 μm beam diameter. Mineral standards of the Victoria University of Wellington collection were analysed routinely to check for any machine drift. Between six and ten titanomagnetite and hornblende crystals were analysed where possible from each tephra sample.

3.3.3 Statistical Methods

Canonical discriminant function analyses (DFA) were used to discriminate between the Egmont and Tongariro mineral analyses. This is a technique related to principle component analysis that reduces the dimensionality of data, such as compositional analyses, which consist of a large number of variables. Canonical DFA enables the derivation of a small number of linear combinations of the quantitative variables which best discriminate pre-defined groups of observations or analyses. This means that instead of working with ten oxide scores to discriminate groups of samples, one or two canonical variables contain the information. Before identification of an unknown tephra can be undertaken, a reference set of data with known associations must be established. The canonical DFA from this known set is used to produce a discriminant model which then can be used to classify unknown data. The analyses obtained in this study from EV and TgVC enable the creation of a discriminant model. The theory of DFA has been outlined by many authors (e.g. Srivastava and Carter, 1983; Johnson and Wichern, 1992) but is not discussed further here. As part of canonical DFA the Mahalanobis distance statistic or D^2 value is often calculated. It indicates the multivariate spacing between data groups in multiple dimensions (Srivastava and Carter, 1983). The D^2 statistic is therefore a measure of the separation of groups of samples (Stokes *et al.*, 1992), in a similar manner to the coefficients of variation and similarity coefficients of Borchardt *et al.* (1971).

Beaudion and King (1986), and Stokes and Lowe (1988) used a technique which selected variables that had the greatest discriminating power. This subset of highly discriminating variables was shown to improve classification within groups and discrimination between groups. This method is known as stepwise DFA and is further described by Srivastava and Carter (1983), and Stokes and Lowe (1988).

In this study the SAS system programs STEPDISC and CANDISC were used (SAS Institute Inc., 1985). These programs perform stepwise DFA and canonical DFA respectively.

Prior to statistical analysis the data used in this study were transformed in the manner described by Aitchison (1983) and Stokes and Lowe (1988). This is necessary due to the statistical problem of closure in compositional data. The pre-treatment used is termed a log ratio transformation, whereby one oxide score is used to divide into all of the other scores and the logarithm (base 10) is taken of each of these ratios. Use of the logarithm constrains component scores to being greater than zero.

3.3.4 Discrimination between sources

Titanomagnetite

In this study 300 titanomagnetite phenocrysts were analysed from 70 individual TgVC-sourced tephra units, and 136 from 11 individual EV-sourced tephra units. The tephra units sampled range in age from ca. 3-35 ka. The mean titanomagnetite compositions for each centre are presented in Table 3.1. The analyses were normalised and then transformed with the log-ratio transformation using SiO_2 as the oxide divisor. The choice of oxide for the divisor was found to have no effect on the discriminating ability of the DFA (Stokes and Lowe, 1988).

Table 3.1. Titanomagnetite and hornblende average chemistry from the two tephra sources.

	Titanomagnetite		Hornblende	
Oxide wt%	Tongariro	Egmont	Tongariro	Egmont
SiO_2	0.18 (0.16)	0.18 (0.06)	43.13 (1.55)	42.62 (1.33)
TiO_2	10.66 (2.22)	9.09 (1.40)	2.22 (0.65)	3.35 (1.95)
Al_2O_3	4.00 (1.10)	3.91 (1.32)	12.46 (1.43)	11.99 (2.30)
FeO	80.81 (2.02)	82.65 (1.79)	12.77 (1.17)	11.99 (0.83)
MnO	0.42 (0.19)	0.68 (0.20)	0.33 (0.15)	0.25 (0.13)
MgO	3.13 (0.68)	3.35 (0.65)	14.51 (0.78)	14.27 (0.66)
CaO	nd	nd	11.58 (0.62)	12.06 (0.39)
Na_2O	nd	nd	2.34 (0.34)	2.50 (0.12)
K_2O	nd	nd	0.58 (0.27)	0.96 (0.09)
Cr_2O_3	0.42 (0.38)	0.07 (0.07)	nd	nd
n	300	136	117	89

n = number of analyses to calculate the mean, standard deviations in brackets.
nd = not determined

Two SAS data sets were created for DFA, one using the mean analyses for each tephra unit, and one using all of the individual analyses. Shane and Froggatt (1994) found that mean analyses produced better discrimination than individual glass shard analyses for New Zealand rhyolitic tephras. The total spread of the data is however better indicated by individual analyses.

The variables used in both databases were transformed TiO_2, Al_2O_3, FeO, MnO, MgO and Cr_2O_3. Canonical DFA of the means data set produced very good separation between the EV and TgVC sample groups. A plot of the first two canonical variates is used to illustrate the separation (Fig. 3.2A). The D^2 value of 18.1 between groups indicates a good separation of the two groups with very little overlap occurring. The efficiency of group classification is presented in Table 3.2. The stepwise procedure STEPDISC selected the most discriminating variables in order of Cr_2O_3, MnO, TiO_2, FeO and Al_2O_3. Using these variables it was possible to achieve a group separation almost as good as using all of the oxides. The Cr_2O_3 values in the EV-sourced tephras are very low, close to detection limits of the microprobe. Removing Cr_2O_3 from the DFA reduces the degree of separation of the two tephra groups to a D^2 value of 12.3 (Fig. 3.2B, Table 3.2). The most discriminating variables now become MnO, FeO, TiO_2, and MgO.

Canonical DFA using all of the data including Cr_2O_3 also produced very good group separation (Fig. 3.2C). There is very little overlap between the two groups and the D^2 value of 13.1 is still high indicating good separation (Table 3.2). The STEPDISC procedure selected the most discriminating variables in order of Cr_2O_3, MnO, TiO_2, MgO, and FeO. Removing Cr_2O_3 from the DFA reduced the D^2 value between the source groups to 7.2 but still enabled a good classification of the groups (Table 3.2). The most discriminating variables became MnO, FeO, TiO_2, and MgO.

Hornblende

117 hornblende analyses were obtained from 23 individual TgVC-sourced tephras, and 89 analyses from 11 individual EV-sourced tephras. A further 15 hornblende analyses from 5 EV-sourced tephras were also available (Lowe, 1987). The mean hornblende compositions for each centre are presented in Table 3.1. The analyses were normalised and transformed with the log-ratio transformation using Na_2O as the oxide divisor. As for titanomagnetite, two SAS data sets were created, one with the average analysis for each tephra, the other with all of the analyses. The same transformed oxides were used in both data sets: SiO_2, TiO_2, Al_2O_3, FeO, MnO, MgO, CaO, and K_2O.

Canonical DFA of the average data produced a good separation of the TgVC and EV tephras (Fig. 3.3A). The D^2 value of 9.9 is not as high as for the titanomagnetite averages separation, but still indicates the volcanic centre groups are well separated with no overlap (Table 3.2). The STEPDISC procedure selected the most discriminating variables in order of K_2O, MnO, SiO_2, CaO, and MgO.

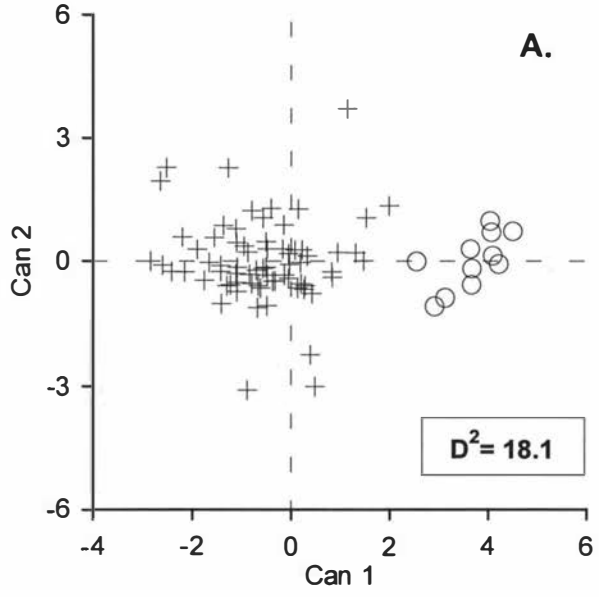

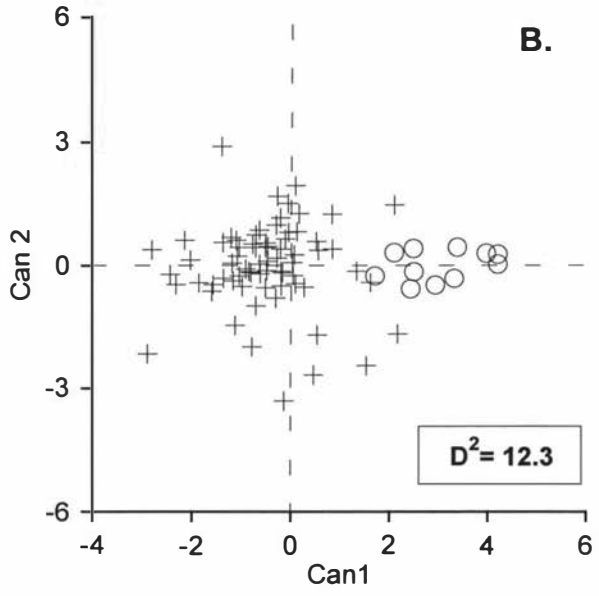

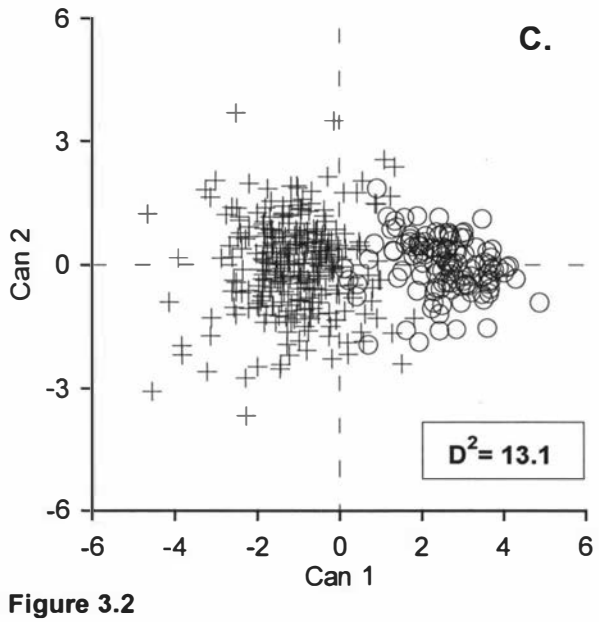

Figure 3.2

Plots of the first and second canonical variates (Can 1 and Can 2) for titanomagnetite data together with D^2 values between source groups. Circles represent EV data and Crosses TgVC data. (A) Sample mean data with all oxide variables, (B) sample mean data excluding Cr_2O_3, (C) all individual analyses using all oxides.

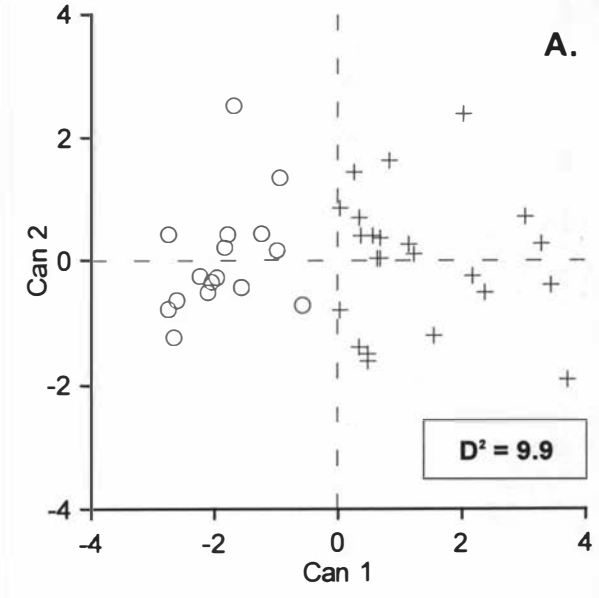

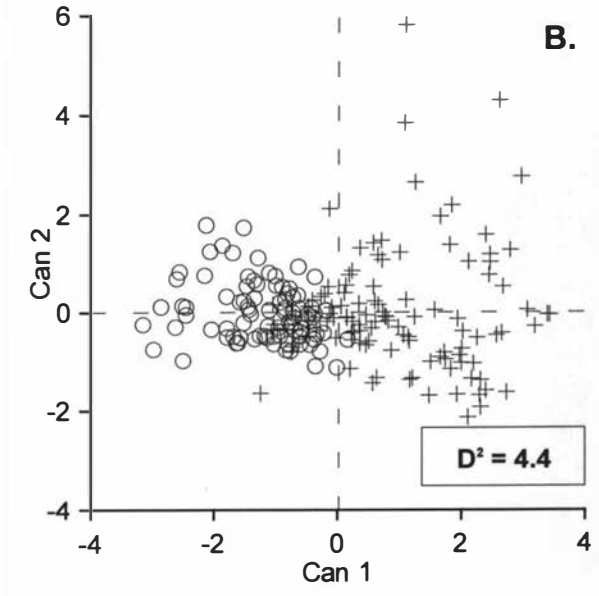

Figure 3.3

Plots of the first and second canonical variates (Can 1 and Can2) for hornblende data together with D^2 values between source groups. Circles represent EV and Crosses TgVC data. (A) Sample mean data, (B) all individual analyses.

Canonical DFA using all of the individual analyses produced a reasonable separation of samples from the two sources (Fig. 3.3B). There is a small degree of overlap between groups and the D^2 value is correspondingly lower at 4.4 (Table 3.2). The STEPDISC procedure selected all of the variables as being highly discriminating but in the order of K_2O, MnO, SiO_2, MgO, FeO, TiO_2, Al_2O_3, and CaO.

Table 3.2. Classification efficiency of the between-source discriminant functions.

Actual group	Number of observations	Classified group membership		Overall classification efficiency (%)
		TgVC	EV	
Titanomagnetite				
Mean data				
TgVC	70	69	1	
EV	11	-	11	98.8
Mean data excluding Cr_2O_3				
TgVC	70	65	5	
EV	11	-	11	93.8
Individual data				
TgVC	300	285	15	
EV	136	7	129	95.0
Individual data excluding Cr_2O_3				
TgVC	300	277	23	
EV	136	12	124	91.9
Hornblende				
Mean data				
TgVC	23	23	-	
EV	16	-	16	100.0
Individual data				
TgVC	117	93	24	
EV	89	2	87	87.4

3.3.5 Discrimination of individual Egmont volcano-sourced tephras

Titanomagnetite

An EV-source subset of the individual titanomagnetite analyses database described in the previous section was used to attempt discrimination of individual tephras. The analyses from each tephra unit in Table 3.3 were grouped separately except for samples Tariki a, Tariki b,c,d and, Tariki e, f which were combined as a single group representing Tariki tephra. The separation of these tephra units appeared very promising with the canonical DFA approach (Fig. 3.4A, Table 3.4). D^2 distances between many of the tephras were very high and their degree of classification was also good (Table 3.4). Four tephra units were not as well separated from all of the others; Konini Tephra and Kaponga Tephra analyses appear very closely related, also Mahoe Tephra and Poto Tephra (members f, g) were also very closely related. The most discriminating variables were chosen as MnO, MgO, FeO, TiO_2 and Al_2O_3.

Table 3.3. Egmont-sourced tephras used in the discrimination study.

Tephra unit (Alloway *et al.*, 1995)	Symbol	Estimated age (ca. ka B.P.)
Manganui Tephra	Mg	2.9 - 3.3
Inglewood Tephra	Il	3.6 - 3.7
Mangatoki Tephra	Mt	4.1 - 4.6
Tariki Tephra, e, f	Tr	4.6 -5.2
Tariki Tephra, d, c, b		
Tariki Tephra, a		
Waipuku Tephra	Wp	5.0 - 5.2
Kaponga Tephra	Kp	5.3 - 10.0
Konini Tephra	Kn	10.1 -10.4
Mahoe Tephra	Mh	10.4 - 12.0
Poto Tephra, f, g	Pt	22.5

Hornblende

An EV-source subset of the database of hornblende individual analyses was used for this discrimination. The analyses from each tephra unit in Table 3.3 were grouped in the same manner as for the titanomagnetite data. The DFA enabled very little discrimination of the individual tephra units (Fig 3.4B). The D^2 distances were very low between many of the tephra sample groups, and within many tephra groups there was a large spread of data. The classification efficiency was also very low with this data (Table 3.4). The only tephra unit which was effectively discriminated was the Manganui tephra.

Table 3.4. Classification efficiencies of the discriminant function analyses for the individual Egmont-sourced tephras.

Actual group*	Number of observations	Classified group membership									Overall classification efficiency (%)
		Mg	Il	Mt	Tr	Wp	Kp	Kn	Mh	Pt	
Titanomagnetite											
Mg	11	11									
Il	4		2	2							
Mt	10			10							
Tr	38			4	28	6					83.3
Wp	11				1	10					
Kp	6						6				
Kn	13						4	9			
Mh	12								11	1	
Pt	9								1	8	
Hornblende											
Mg	3	3									
Il	9		6	2	1						
Mt	7			2		3				1	
Tr	20	1	2	2	7	1	1	2		4	
Wp	8			1	1	6					55.9
Kp	4		1				3				
Kn	4				1			3			
Mh	5	1		1					3		
Pt	8			1	1			1		5	

* Tephra abbreviations from Table 3.3.

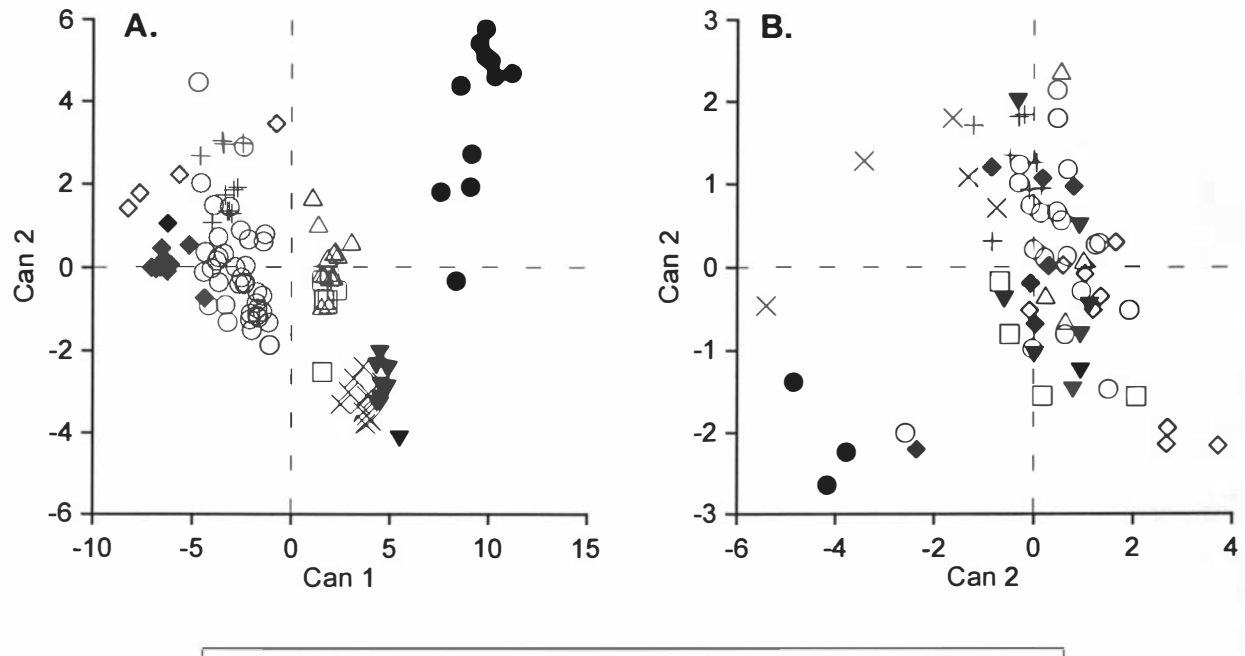

A: titanomagnetite

D^2	Il	Mt	Tr	Wp	Kp	Kn	Mh	Pt
Mg	237.1	256.5	162.7	166.7	79.4	72.3	82.0	68.1
Il	-	11.7	28.9	20.3	76.8	78.6	122.5	140.0
Mt		-	14.4	14.1	65.8	70.0	108.1	127.1
Tr			-	6.4	21.5	22.8	50.9	64.6
Wp				-	36.4	31.9	76.8	89.9
Kp					-	4.0	10.0	13.6
Kn						-	16.6	21.3
Mh							-	2.2

B: hornblende

D^2	Il	Mt	Tr	Wp	Kp	Kn	Mh	Pt
Mg	37.9	21.1	27.8	27.3	27.6	35.0	15.1	27.6
Il	-	5.6	4.0	9.5	8.0	9.8	21.6	4.4
Mt		-	1.4	1.9	4.7	5.8	8.2	3.1
Tr			-	3.0	5.9	4.8	10.7	2.2
Wp				-	9.9	8.3	7.8	5.7
Kp					-	6.6	16.0	6.2
Kn						-	15.5	5.7
Mh							-	12.9

Figure 3.4 Plots of the first and second canonical variates (Can1 and Can 2) for Egmont-sourced tephras together with D^2 values between tephra groups (tephra abbreviations from Table 3.3). (A) Using titanomagnetite data, (B) using hornblende data.

3.3.6 Summary and Conclusions

Both phenocryst phases examined in this study can be used with the Canonical DFA method to easily and accurately discriminate tephras from EV and TgVC. Titanomagnetite is preferable for this distinction because:
(1) there are greater differences in titanomagnetite chemistry between sources, (2) it occurs within nearly all samples, (3) it is relatively stable during weathering, (4) it is rapidly and easily separated from a bulk sample.

Canonical DFA of the mean tephra analyses for both of the mineral phases enabled better classification efficiencies of the two volcanic sources and correspondingly larger D^2 values, which is consistent with the findings of Shane and Froggatt (1994). To apply this technique to discriminating tephras in soil and loess we prefer however, to use a discrimination model based on all of the individual analyses. The analysis of each individual grain of an unknown sample can then be classified by the discriminant model and mixed tephra populations can easily be identified and accounted for.

Using this canonical DFA method the probability of any given sample belonging to either of the volcano source groups can be assessed. In situations where unknown samples are close to or within the region of overlap between source groups the probability of group membership is important and can be reported with any correlation made.

For the discrimination of individual analyses, titanomagnetite appears very promising. Using the limited database available we can show good discrimination of several individual tephra units, or at least pairs of the stratigraphically closest units, with mostly high D^2 values and classification efficiencies. Hornblende provided very little discrimination between tephra groups due to the large spread of data for each tephra as well as small differences in chemistry between tephra groups; only one tephra was clearly discriminated.

The most easily distinguished tephra unit, the Manganui tephra was erupted from the parasitic cone of Fanthams Peak on the side of Egmont volcano, whereas the others were probably erupted from the main vent region (Alloway *et al.*, 1995). This tephra unit is also easily discriminated by its characteristic field appearance and mineralogy.

The difference in discriminating abilities of titanomagnetite and hornblende may be related to the petrology of the Egmont volcano system. Stewart *et al.* (in press) describe titanomagnetite as an early crystallising and stable phase in EV magmas, while hornblende was formed when the melts reached the base of the crust, and on subsequent rising the hornblende was partially resorbed. Stewart *et al.* (in press) also suggest that these hornblende phenocrysts are largely xenocrysts entrained from lower crustal and upper mantle sources. This may explain the large spread in the hornblende data for each tephra unit as well as the difficulty in separating the individual tephras.

The results of this study demonstrate the potential of the methods described for future tephra discrimination studies of EV and TgVC units as well as providing a more rigorous method of discriminating tephras from the two sources in distal areas. As well as the advantages of DFA for tephra identification reported by others, (Stokes *et al.*,

1992; Shane and Froggatt, 1994) this method is ideal for tephra layers which may be mixed within soil, loess or marine sequences. Using individual grain analyses and their probabilities of group membership, mixed tephra populations can be easily discriminated.

3.3.7 Acknowledgements

We wish to thank David Lowe for the use of his hornblende analyses, and Ken Palmer (Victoria University of Wellington) for his introduction to the electron microprobe. Thanks are also extended to R.B. Stewart and A.S. Palmer for helpful criticism of an earlier version of this manuscript, as well as P. Froggatt and an anonymous reviewer for their useful comments.

3.4 A MULTIPLE-PARAMETER APPROACH TO ANDESITIC TEPHRA CORRELATION, RUAPEHU VOLCANO, NEW ZEALAND

S. J. Cronin, V. E. Neall, R. B. Stewart, A. S. Palmer
Department of Soil Science, Massey University, Private Bag 11 222, Palmerston North, New Zealand

1996, Journal of Volcanology and Geothermal Research, 72: 199-215.

Abstract

A multi-parameter approach was used to correlate andesitic tephras in a complex tephra sequence ranging in age from ca. 23 ka to ca. 75 ka on the eastern ring plain of Ruapehu volcano, North Island. Field properties, combined with ferromagnesian mineral assemblages and mineral compositions, were required to map and correlate this sequence. Three tephra units could be identified based on their unique physical appearance, but other tephras could not be correlated on this basis alone. Hornblende and olivine proved to be valuable marker minerals enabling further distinction of two of the marker units recognised by field properties, as well as defining two further marker tephras. Unweathered titanomagnetite crystals, present in all of the tephras, were subjected to major element analysis by electron microprobe. Canonical discriminant function analysis (DFA) of these analyses enabled the grouping and discrimination of tephra units, further aiding the identification of defined marker units, as well as defining new marker units. The titanomagnetite chemistry showed a strong relationship to the ferromagnesian mineralogy, showing that the ferromagnesian phenocrysts formed from the same melt or under the same melt conditions prior to eruption of each tephra. Canonical DFA was also applied to hornblende and olivine mineral analyses to identify further marker beds and to confirm identifications of previously defined units. This statistical analysis was found to be invaluable in reducing the large amount of

compositional data from this study into a useable form for andesitic tephra correlation and mapping.

3.4.1 Introduction

Andesitic tephrochronology plays an important role in the relative and numerical dating of sediments and geomorphic surfaces on the ring plains of composite volcanoes and surrounding areas. The techniques for andesitic tephra correlation in New Zealand are however less well developed than those for the rhyolitic tephra record of the central North Island. In previous studies of the ring plains of Ruapehu and Tongariro, tephrochronology has played an important role in assigning numerical and relative ages to ring plain surfaces and sediments (Topping, 1973; Topping and Kohn, 1973; Donoghue *et al.*, 1995). However studies have been restricted mostly to the younger parts of the ring plain record (< ca. 23 ka.) in which distal rhyolitic tephras present can be correlated to the well established record of the Taupo and Okataina volcanic centres (Froggatt and Lowe, 1990; Wilson, 1993).

In this study, ring plain deposits ranging from ca. 23 ka. up to 75 ka are investigated. Radiocarbon dating is less useful in this time frame and fewer rhyolitic tephras are present, with ages less well constrained than those of the post 23 ka record. This constraint places more emphasis on the role of andesitic tephras as local marker horizons for relative dating of surfaces and sediments. In this study we have used multiple criteria to correlate stratigraphic successions and surfaces in different parts of the ring plain. In particular to extend from physical tephra characteristics and mineralogy, canonical discriminant function analysis of titanomagnetite, olivine and hornblende phenocryst compositions were used to correlate andesitic tephras.

3.4.2 Setting

Ruapehu volcano within the Tongariro Volcanic Centre, is a large, active, andesitic stratovolcano, and the highest point in the North Island at 2797 m. Its latest eruption was in 1995. The current massif comprises a 110 km^3 cone surrounded by a volcaniclastic ring plain of similar volume (Hackett and Houghton, 1989). The adjacent Tongariro volcano is a slightly smaller andesitic massif made up of several coalescing volcanic cones (Mathews, 1967), the largest of which is the recently active cone of Ngauruhoe.

The ring plains of Ruapehu and Tongariro volcanoes are confined to the east by the Kaimanawa Mountains, with the boundary marked by the Tongariro River. The dominant wind direction is from the west, thus the andesitic tephras are generally thickest on the ring plain to the east of the volcanoes.

The principal reference sections used in this study are exposed along Upper Waikato Stream (Fig. 3.5), on the north-eastern Ruapehu ring plain.

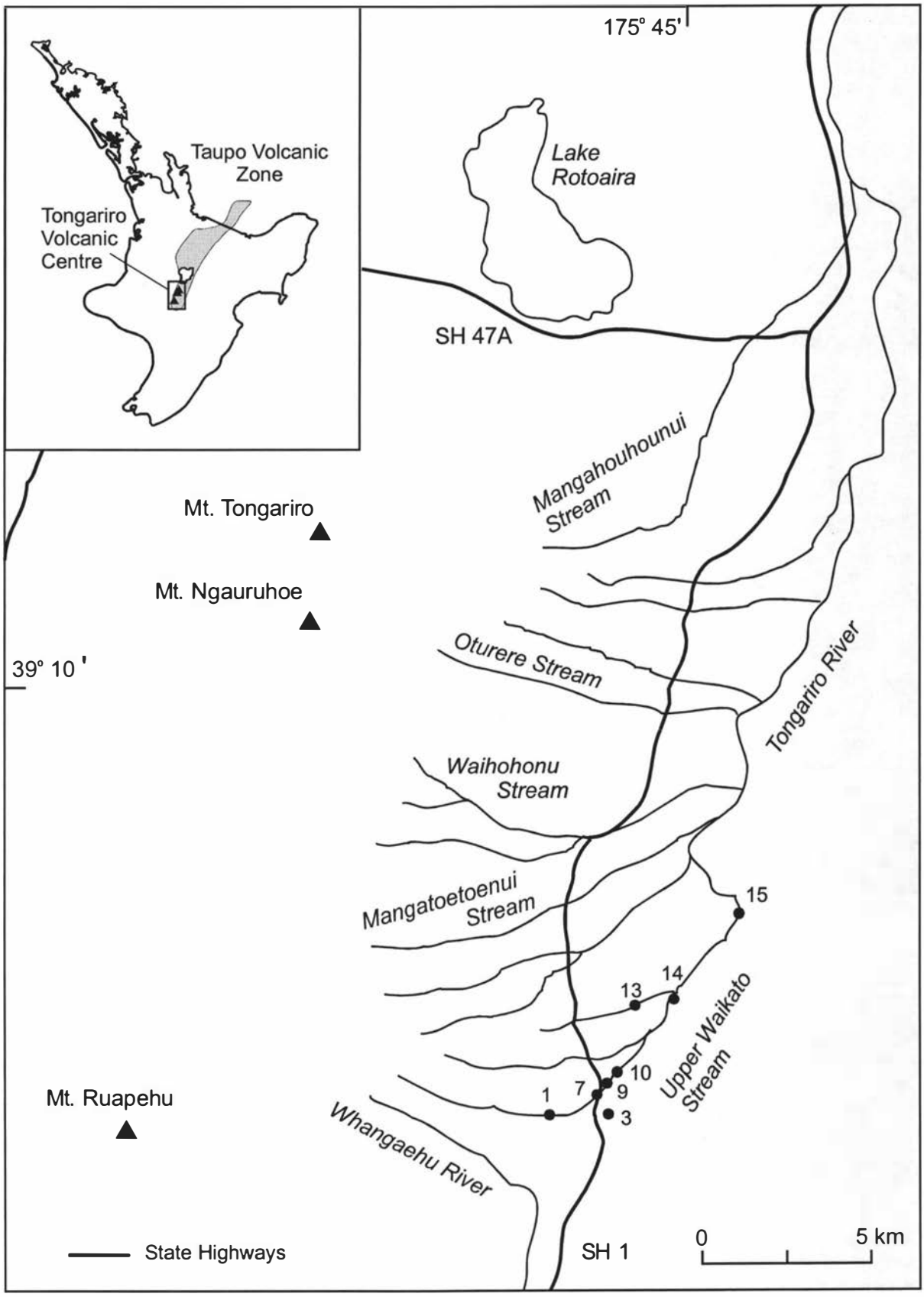

Figure 3.5. Location map of the eastern ring plains of Tongariro and Ruapehu volcanoes. Numbered dots indicate locations of principal reference sections, numbers correspond to section descriptions contained within Appendix 4.

This stream is immediately north of the catchment boundary where present drainage from the eastern flanks of Ruapehu is split between the Whangaehu River to the south and the Tongariro River system to the north.

3.4.3 Methods

A composite stratigraphy of the principal reference sections was first established, providing the longest and most complete record of deposition in the area. The andesitic tephras in this master section were then characterised according to their physical appearance and mineralogy. The simplest and most valuable stratigraphic markers were those which possessed a unique physical appearance enabling their recognition in other areas. The next most valuable markers were those that possessed a unique mineralogy enabling their discrimination from other tephras in the sequence. Those andesitic tephras that could be reliably identified in other sections based on these criteria were few and further fingerprinting was deemed necessary.

The major element composition of various mineral phases and andesitic glass were then determined using an electron microprobe for as many of the andesitic tephras as possible. The largest pumice clasts of each tephra sample were cleaned in water with an ultrasonic probe, crushed and their ferromagnesian minerals separated using a Frantz Isodynamic Separator. The mineral grains were then mounted in an epoxy resin plug which was cut and polished (Froggatt and Gosson, 1982).

The phases targeted for analysis were titanomagnetite, olivine and hornblende; some analyses were also obtained from andesitic glass, orthopyroxene and clinopyroxene. Orthopyroxene, clinopyroxene, and plagioclase were not used because these minerals all displayed strong oscillatory zoning and greater compositional variation than titanomagnetite, olivine and hornblende. Andesitic glass was poorly preserved in these samples, being present only in some of the younger tephras and in tephras preserved within lignite.

Analyses were carried out on a JEOL JXA-733 electron microprobe, employing an accelerating voltage of 15 kV and a 12 nA beam current. A beam diameter of 3 μm was used for the mineral phases and 10 μm with a 8 nA beam current for the andesitic glass (Froggatt, 1983). Mineral standards of the Victoria University of Wellington collection were analysed routinely to correct any machine drift. Between six and ten analyses of individual titanomagnetite crystals were obtained where possible from each tephra sample. Six to ten analyses of hornblende, olivine and andesitic glass were obtained from the samples containing these phases. The resulting data were then examined using traditional oxide plot techniques and statistical analysis.

3.4.4 Statistical methods

Canonical discriminant function analyses were used to establish groups of samples which could be used for correlation and stratigraphic purposes. Canonical discriminant function

analysis (DFA) is a technique related to principal component analysis, which reduces the dimensionality of data such as compositional data that has scores on a large number of independent variables. Canonical DFA enables the derivation of a small number of linear combinations of the quantitative variables which best discriminate pre-defined groups of observations or analyses. A reference set of observations or analyses with pre-defined groupings must first be set up and canonical DFA is used to produce a discriminant model which can be used to classify unknown observations or analyses. The theory of DFA is outlined in many texts on multivariate analysis such as Srivastava and Carter (1983) and Johnson and Wichern (1992). The D^2 or Mahalanobis distance statistic is produced within the results of canonical DFA, and indicates the multivariate spacing between data groups in multi-dimensions (Srivastava and Carter, 1983). The D^2 statistic is then a useful statistic measure of the separation of groups of samples (Stokes *et al.*, 1992), in a manner similar to the numerical coefficients of variation and similarity coefficients of Borchardt *et al.* (1971).

DFA was first used to discriminate tephras by Borchardt *et al.* (1971), based on instrumental neutron activation analysis of glasses. King *et al.*(1982) and Beaudoin and King (1986) used this type of DFA on titanomagnetite major element chemistry to identify Holocene-aged tephras in western Canada. In New Zealand, Stokes and Lowe (1988) and Stokes *et al.* (1992) demonstrated the use of canonical DFA to discriminate volcanic source areas and later some individual eruptive units, using major element glass analyses. A similar study but including trace and rare earth element analyses was reported by Shane and Froggatt (1994).

These DFA studies also introduced the use of methods which selected variables that had the greatest discriminating power. This method is known as stepwise DFA and is further described by Srivastava and Carter (1983), Stokes and Lowe (1988) and Stokes *et al.* (1992).

Cluster analysis, another form of multivariate analysis, involves the placement of observations into groups suggested by the data only, without any prior groups being established (Johnson and Wichern, 1992). A form of cluster analysis was used by King *et al.* (1982) and was shown to be ineffective in obtaining a clear, objective discrimination of groups. It was, however, useful as a preliminary technique to examine any major groupings in the data prior to the use of canonical DFA.

In this study the SAS system programs CLUSTER, STEPDISC and CANDISC were used (SAS Institute Inc., 1985). These programs perform cluster analysis, stepwise DFA and canonical DFA, respectively.

Prior to statistical analysis the compositional data used in this study was pre-treated to avoid statistical closure, in the manner described by Aitchison (1983, 1986) and Stokes and Lowe (1988). The pre-treatment used is termed a log ratio transformation, whereby one oxide score is used to divide into all of the other scores and the logarithm (base 10) is taken of each of these ratios. The oxide chosen as the divisor for all of the analyses in this study was MnO, for its moderate abundance and relatively low pooled and within sample variance (Stokes and Lowe, 1988; Shane and Froggatt, 1994).

3.4.5 Stratigraphy and distribution of 23-75 ka andesitic tephras

The age of the andesitic tephras in this study is constrained at the top by the Kawakawa Tephra, dated at 22 590 ± 230 years B.P. (Wilson *et al.*, 1988). The age of the base of the tephra sequence is less well defined and is marked by a large thickness of lahar and stream flow deposits correlated to marine $\delta^{18}O$ stage 4 (65-75 ka; Cronin *et al.*, 1996). Throughout the sequence, however, additional dated rhyolitic tephras occur which lend further time control. These rhyolitic tephras are found as glass shards and mineral grains scattered over several centimetres in a matrix of fine-grained andesitic ash. Their identification has been achieved using a combination of electron microprobe major element glass shard chemistry, ferromagnesian mineral assemblages and stratigraphic position (Cronin *et al.*, in press). The microscopic tephras are identified as the Taupo Volcanic Centre-sourced Okaia Tephra and the Okataina Volcanic Centre-sourced Omataroa Tephra, Hauparu Tephra and Rotoehu Ash. The ages of these units are given in Table 3.5, and their relative stratigraphic positions in Fig. 3.6.

Table 3.5 Rhyolitic tephras identified within the eastern ring plain sequence, Ruapehu.

Tephra name	Source[a]	Age (Yrs BP)	Reference for age
Kawakawa Tephra	TVC	22 590 ± 230[1]	Wilson et al. (1988)
Okaia Tephra	TVC	ca. 23 000[2]	Froggatt and Lowe (1990)
Omataroa Tephra	OVC	28 220 ± 630[1]	Froggatt and Lowe (1990)
Hauparu Tephra	OVC	35 870 ± 1270[1]	Froggatt and Lowe (1990)
Rotoehu Ash	OVC	64 000 ± 4000[3]	Wilson et al. (1992)

[a] TVC = Taupo Volcanic Centre; OVC = Okataina Volcanic Centre.
[1] Denotes ^{14}C ages on old half life basis.
[2] Estimated stratigraphic age.
[3] Whole rock K-Ar age of enclosing lavas.

Andesitic tephras occur throughout the entire sequence at Upper Waikato Stream (Fig. 3.6). The tephras occur as individual pumice lapilli units or as accumulations of fine ash representing the products of several eruptions over time. The lapilli and coarse ash units were used for correlation and fingerprinting studies. Over 60 individual andesitic lapilli units are interbedded within fine ash as well as fluvial and lahar deposits.

The distribution of these tephras is not well delimited because their exposure in other sectors of the ring plain is sporadic. They are generally distributed to the east of Ruapehu Volcano and thin rapidly away from their axes of dispersal. Distal equivalents of some of these andesitic lapilli units are mapped to the south in the Rangitikei River valley, lying stratigraphically above the Porewan loess as middle Tongariro Subgroup tephras (Leamy *et al.* 1973; Milne and Smalley, 1979). Andesitic ash on top of a Porewan loess correlative further to the east in Hawkes Bay is also commonly found (A.P. Hammond, *pers. comm.*, 1995). Partial isopachs of two of the marker horizons are shown in Fig. 3.7. The limited distribution information of these tephras would suggest a Ruapehu volcano source for most of the lapilli units rather than Tongariro volcano.

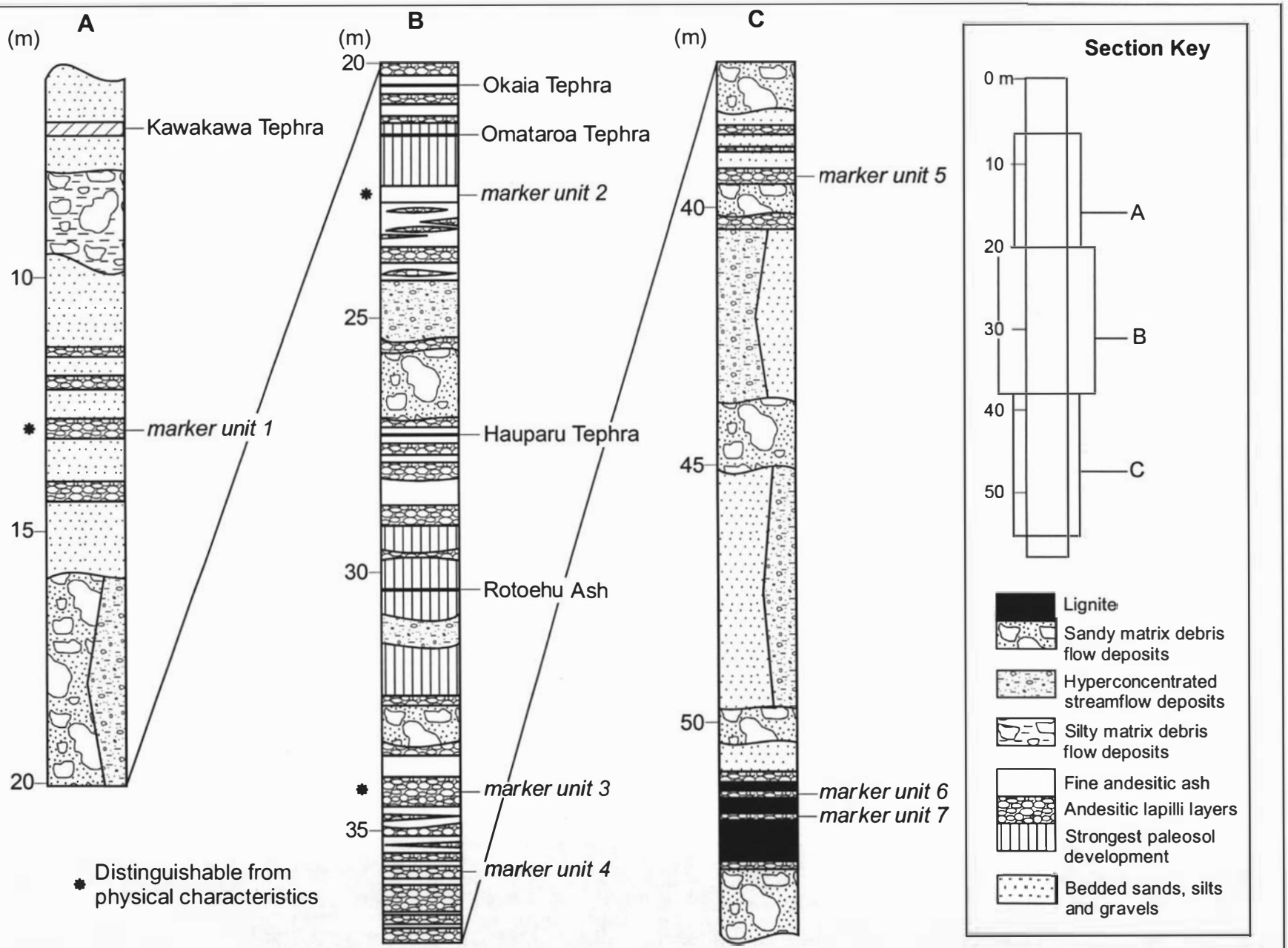

Figure 3.6 Composite stratigraphic sequence from principal reference sections observed in the Upper Waikato Stream area with positions of andesitic and rhyolitic marker tephras shown.

3.4.6 Physical properties and mineralogy of 23-75 ka andesitic tephras

The coarse-grained andesitic tephra are dominantly fine-medium pumice lapilli which are highly vesicular with very fine vesicles; the proportion of lithic components is usually <10 % by volume. The pumice is soft, highly weathered, and ranges from yellow to reddish brown. The degree of weathering, colour, and hardness of the pumice lapilli changes markedly from site to site, depending largely on individual site hydrology. In a single outcrop an individual tephra may range from a pale yellow soft pumiceous lapilli to a reddish brown very firm pumiceous lapilli unit. This makes these parameters virtually unusable for discriminating and correlating the tephra units from place to place even on a very large scale with sites as little as 100 m apart. Shower bedding and graded bedding are also relatively common features and so can only be used in combination with other means to correlate units.

Three units can be uniquely identified from the other tephras in the sequence by their physical properties alone (other marker units can additionally be identified using compositional and mineralogy data). The properties of the three units at the principal reference sections are given below, and their stratigraphic positions are shown in Fig. 3.6.

Unit 1 is an approximately 400-500 mm thick grey and olive brown lithic coarse ash mixed with yellow and yellow-brown coarse pumice ash. It is well shower-bedded with alternating 50 mm beds dominated either by grey lithic ash or yellow pumice ash giving a distinctive striped appearance. The basal 20 mm is composed of yellow fine pumice lapilli. The Kawakawa and Okaia Tephras overlie and underlie this unit, respectively, giving a stratigraphic age of ca. 23 ka. The only other tephras found in this area that have a similar appearance to this are members of the Mangamate Tephra described by Topping (1973). The Mangamate Tephra is easily distinguished by stratigraphic position, having been erupted ca.10 ka from Tongariro volcano.

Unit 2 is a grey, fine ash tuff, which is very hard and breaks up into blocks. It is showerbedded on a 10 mm scale from very fine to medium ash and contains abundant accretionary lapilli ranging in diameter from 1 to 5 mm within three ca. 40 mm layers. The unit totals ca. 200 mm in thickness. The Omataroa Tephra overlies this unit within a paleosol and the Hauparu Tephra underlies it, giving a stratigraphic age range of 28-36 ka. No other tephra found in the study area bears any resemblance to this unit.

Unit 3 is a reddish brown and strong brown fine pumice lapilli and coarse ash mixed with grey lithic coarse ash. Two distinctive 10 mm thick bands of grey lithic-dominated coarse ash 20 mm apart occur near the top of the unit. This unit is ca. 300 mm thick. The Rotoehu Ash occurs above the unit giving a minimum stratigraphic age of 64 ka.

Apart from these three units, there are no other tephra units which can be positively correlated based on their physical features alone. Marker Units 4 and 5 are discriminated on the basis of hornblende and olivine chemistry respectively, while Units 6 and 7 are discriminated using a combination of mineralogy and titanomagnetite chemistry.

3.4.7 Mineralogy

The andesitic tephras commonly contain phenocrysts of plagioclase, orthopyroxene, clinopyroxene and titanomagnetite. Some units also contain hornblende and olivine phenocrysts with rare illmenite and chrome spinel. The dominant ferromagnesian assemblage is:

1. orthopyroxene + clinopyroxene > titanomagnetite ± olivine ± hornblende.

This assemblage accounts for 90 % of the tephras in this sequence. Hornblende and olivine occur only in small quantities (<2% by volume) in most of the lapilli. Two other ferromagnesian mineral assemblages are also observed in the tephra sequence, and can be characterised as hornblende-dominant and olivine-dominant:

2. Olivine > orthopyroxene + clinopyroxene > titanomagnetite.
3. Hornblende > orthopyroxene + clinopyroxene > titanomagnetite.

These assemblages are restricted in their occurrence within the sequence and hence can be used to correlate individual units or small sequences of units to provide further marker beds for stratigraphic study.

The bulk of the tephras fit the "type 1" petrological classification of Ruapehu lavas (Cole *et al.*, 1986; Graham and Hackett, 1987), although much less hornblende occurs in the lavas. The olivine-dominant assemblages fit into the "type 5" lava classification. The lavas with "type 5" mineralogy are generally found in satellite vents rather than on the main Ruapehu cone from where the olivine-dominant tephra appears to have been erupted (Marker unit 1, Fig. 3.7A). No hornblende-dominant mineral assemblages are recognised in Ruapehu lavas but rare hornblende-bearing lavas are described from Tongariro volcano (Cole, 1978).

Only one tephra has a ferromagnesian mineral assemblage dominated by olivine, (55 % by volume) namely Unit 1 as described previously. This distinctive mineralogy adds to the versatility of this marker bed because it can be identified from its mineralogy in localities where its distinctive physical features may not be evident, e.g. in distal areas or off the dispersal axis. The tephra directly above Unit 1 also contains appreciable olivine (ca. 20% by volume), but all other tephras throughout the entire sequence contain mostly 0-2% by volume olivine. Abundant olivine has only been described previously in Tongariro volcano-sourced members of the Mangamate Tephra (Lowe, 1988a; Donoghue *et al.*, 1991).

Hornblende is another valuable marker mineral because it occurs in only 11 of the tephras in the sequence and mostly in very minor quantities (<1% by volume). It does, however, occur in greater quantities in two tephras at the very base of the sequence. In these tephras the hornblende content is >5% and in one is up to 30% by volume. The units do not have diagnostic physical features, but they can be used as marker horizons because of their distinctive hornblende rich-mineralogy. The stratigraphic positions of these two tephras (Units 6 and 7) are shown in Fig. 3.6. Both tephras are medium-coarse grade ash and are interbedded within the lignite near the base of the principal reference section.

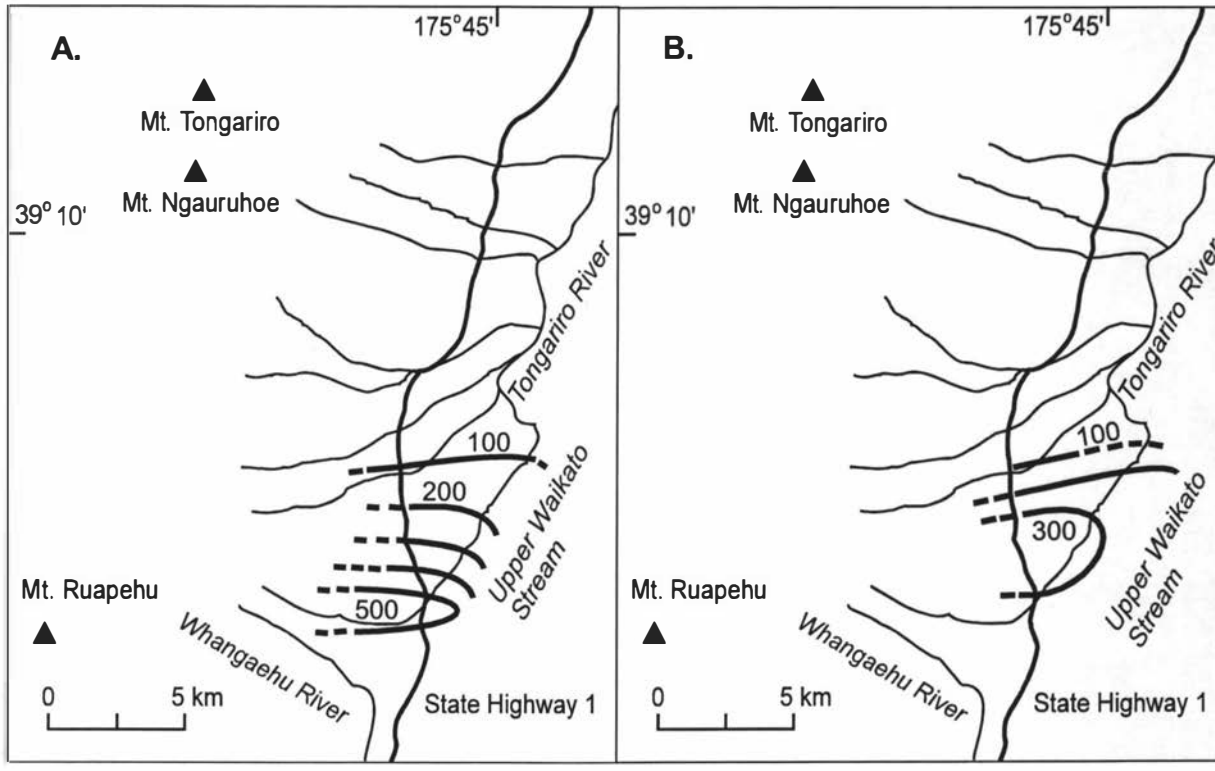

Figure 3.7. Partial andesitic tephra isopach maps, thickness given in millimetres. (A) Marker Unit 1, (B) Marker Unit 3.

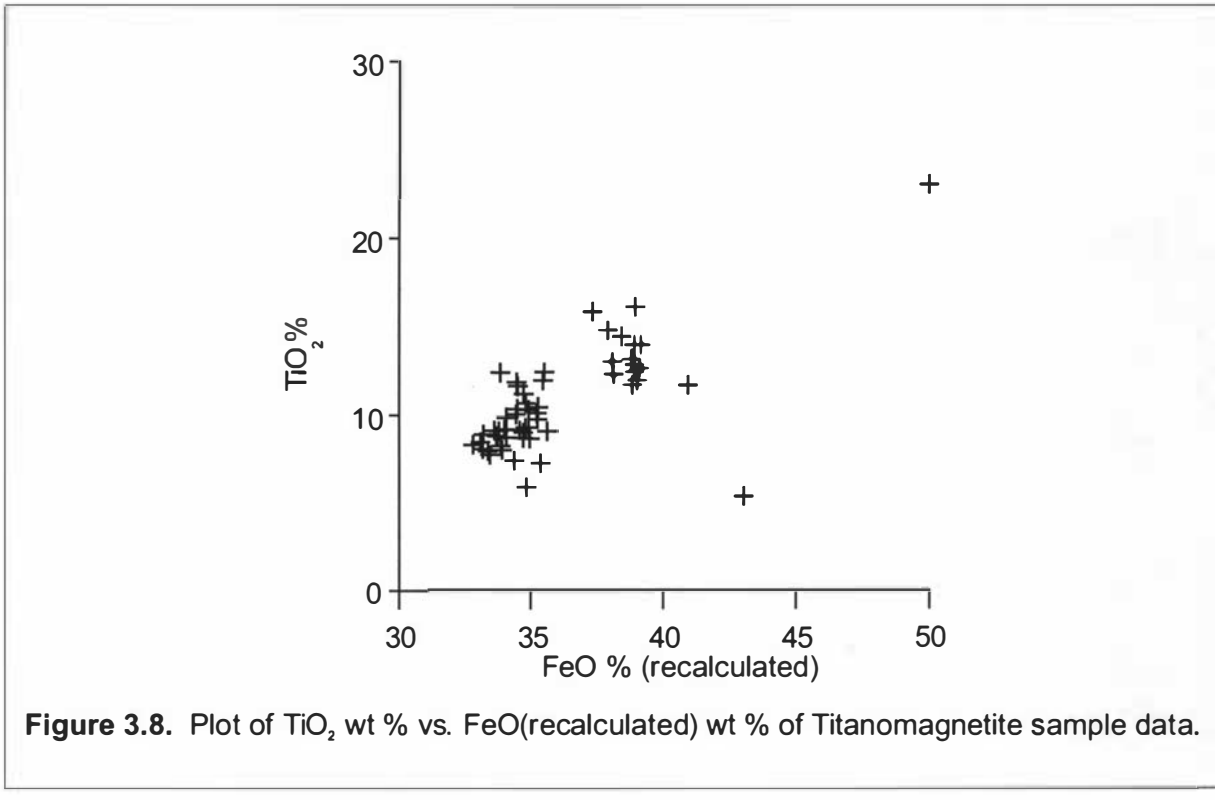

Figure 3.8. Plot of TiO_2 wt % vs. FeO(recalculated) wt % of Titanomagnetite sample data.

The Rotoehu Ash occurs stratigraphically higher in the sequence giving a minimum age of 64 ka for Units 6 and 7. Hornblende is also found in small quantities within the previously described marker Unit 3, further enabling its identification as a marker horizon. Hornblende has been previously described only in Tongariro-sourced members of the Mangamate Tephra (Donoghue *et al.*, 1991). Although units 4 and 5 intervene stratigraphically they are distinguished on the basis of their hornblende and olivine chemistry rather than mineralogy and are discussed later in the text.

3.4.8 Mineral chemistry of 23-75 ka andesitic tephras

Table 3.6 Mean electron microprobe analyses of final titanomagnetite, hornblende and olivine groupings.

Titanomagnetite	Group 1	Group 2	Group 3	Group 4
SiO_2	0.11 (0.08)	0.27 (0.10)	0.19 (0.10)	0.15 (0.05)
TiO_2	21.76 (3.95)	8.91 (2.32)	10.19 (2.28)	10.98 (2.21)
Al_2O_3	1.09 (0.27)	1.87 (0.32)	3.75 (0.80)	4.49 (1.01)
FeO	74.78 (5.04)	81.39 (2.27)	81.85 (2.22)	79.78 (2.25)
MnO	0.30 (0.07)	0.42 (0.01)	0.41 (0.08)	0.39 (0.08)
MgO	1.68 (0.37)	1.69 (0.66)	2.82 (0.65)	3.40 (0.64)
Cr_2O_3	0.07 (0.03)	0.20 (0.13)	0.42 (0.21)	0.46 (0.21)
n	12	12	48	234

Hornblende	Group hb1	Group hb2	Group hb3
SiO_2	41.92 (1.23)	42.20 (0.88)	43.81 (0.30)
TiO_2	2.46 (0.53)	2.57 (0.60)	1.25 (0.03)
Al_2O_3	12.93 (1.26)	13.20 (0.94)	12.58 (0.28)
FeO	12.64 (1.14)	12.31 (0.61)	14.55 (0.36)
MnO	0.30 (0.13)	0.32 (0.11)	0.35 (0.14)
MgO	13.94 (0.92)	14.63 (0.65)	14.05 (0.22)
CaO	12.32 (0.61)	11.60 (0.59)	11.05 (0.21)
Na_2O	2.53 (0.22)	2.49 (0.13)	2.03 (0.05)
K_2O	0.85 (0.15)	0.61 (0.27)	0.28 (0.06)
Cl	0.11 (0.11)	0.08 (0.08)	0.05 (0.01)
n	30	31	7

Olivine	Group ol1	Group ol2	Group ol3	Group ol4
SiO_2	38.87 (0.88)	36.91 (0.14)	38.51 (1.14)	36.12 (0.28)
TiO_2	0.04 (0.02)	0.12 (0.01)	0.04 (0.03)	0.02 (0.01)
Al_2O_3	0.03 (0.01)	0.35 (0.17)	0.06 (0.02)	0.07 (0.04)
FeO	14.39 (3.94)	31.45 (1.30)	18.11 (3.52)	24.44 (0.25)
MnO	0.24 (0.08)	0.49 (0.05)	0.34 (0.15)	0.44 (0.01)
MgO	46.20 (3.48)	30.13 (1.57)	42.64 (2.78)	38.65 (0.60)
CaO	0.14 (0.02)	0.34 (0.04)	0.14 (0.03)	0.08 (0.02)
Na_2O	0.03 (0.03)	0.13 (0.03)	0.05 (0.03)	0.10 (0.05)
K_2O	0.03 (0.02)	0.04 (0.01)	0.07 (0.07)	0.04 (0.01)
Cl	0.02 (0.01)	0.03 (0.01)	0.03 (0.02)	0.04 (0.02)
n	53	12	46	8

Analyses obtained using a 12 nA beam current at 15 kV, with a 3 μm beam.
Standard deviation in brackets.

All olivine phenocrysts analysed from tephras studied are forsteritic, ranging in composition from fo_{74} to fo_{87} (Table 3.6). The olivine phenocrysts are not zoned and do not display skeletal morphologies as described by Donoghue *et al*. (1991). Hornblende compositions range from edenite to pargasite (Table 3.6). Clinopyroxene compositions fall in the augite field and orthopyroxenes all lie within the enstatite field. Titanomagnetite occurs in a range of ulvöspinel compositions (Table 3.6). The mineral chemistry was used to identify any further marker horizons that could be used for stratigraphic study.

3.4.9 Titanomagnetite (discrimination of marker Units 1, 2 and 6)

Titanomagnetite chemistry has been used in several studies to correlate tephra marker beds. In New Zealand, Kohn (1970) demonstrated the use of titanomagnetite composition to distinguish rhyolitic tephras. Kohn and Neall (1973) were able to group andesitic Egmont volcano (EV) tephras into chemically distinct groups and correlate distal andesitic tephras. Distal Tongariro Volcanic Centre-(TgVC) and EV-sourced tephras can also be separated on the basis of their chemistry (Kohn and Neall, 1973; Lowe, 1988a). All of these methods relied on bivariate plots to display differences in selected elements and thus only a small subset of the available composition information is used. King *et al*. (1982) and Beaudoin and King (1986) used DFA on titanomagnetite compositions to separate individual distal tephra marker beds in Canada.

In this study 306 titanomagnetite analyses were made on 53 tephra samples. As a first approach for classification, a number of two oxide plots were examined. The only useful plot for grouping the analyses into coherent groups was the plot of TiO_2 vs. FeO (recalculated) (Fig. 3.8). FeO recalculation was from stoichiometry (Droop, 1987). This plot indicates a tightly clustered group of low TiO_2 and FeO (recalculated) content samples and a group with higher contents of both oxides; two samples are outliers from these groups. The two outlying samples are those from the marker units 1 and 6.

The titanomagnetite oxide analyses were averaged for each sample before being entered into a SAS datafile. The transformed oxides used in the following statistical analyses were SiO_2, TiO_2, Al_2O_3, FeO (total as determined by microprobe), MgO, and Cr_2O_3. The first approach was assess any 'natural' grouping in the data by using the SAS program CLUSTER (SAS Institute Inc., 1985). The cluster analysis resulted in the recognition of four groups. The Mahalanobis statistics (D^2) between the groups are large, with the closest groups having a D^2 value of 8 between them (Fig. 3.9, Table 3.7). The membership of these groups was examined and a relationship between the ferromagnesian mineral assemblage and the clusters was found. Cluster Group 1, contains only one sample, the hornblende-rich marker Unit 6. This unit is well separated from the others in the cluster analysis. Cluster Group 3 contains six samples, five of which are hornblende-bearing. Cluster Group 2 contains ten samples, eight of which contain olivine. Cluster Group 4 contains the bulk of the samples which have mineral assemblages mostly without appreciable olivine or hornblende. There is, however, mixing of samples which have mineral assemblages that do not conform to the group in which

the clustering process has placed them. Clustering techniques are usually only an exploratory technique to examine multivariate data (SAS Institute Inc., 1985). The grouping of the samples on the basis of their ferromagnesian mineral assemblage as suggested by the clustering was then tested further.

All of the samples were assigned a group according to their ferromagnesian mineral assemblage. These groups were tested using canonical DFA with all the log ratio-transformed oxide scores. The SAS program CANDISC was used (SAS Institute Inc.,1985). The groups were compiled as follows:

Group 1 hornblende-rich samples (>5%)
Group 2 olivine-rich samples (>10%)
Group 3 hornblende-bearing samples (>0.5%)
Group 4 all other samples.

All of these groups were well discriminated by canonical DFA with high D^2 values ranging from 158 to 10 between groups (Fig. 3.9B, Table 3.7). The marker units which are particularly well separated by this analysis are Unit 2 and Unit 6 (Group 1) and Unit 1 (Group 2). Samples of the hornblende bearing tephras in the sequence can also be distinguished from the rest, which may also help to narrow down tephra correlations. If an unknown sample is analysed, this statistical analysis should result in a more precise identification of its possible correlatives. The mean compositions of the titanomagnetites in these four groups are presented in Table 3.6.

Stepwise DFA was used to select a subset of variables which enabled the greatest separation between groups. The SAS program STEPDISC was used (SAS Institute Inc., 1985). The variables TiO_2, Cr_2O_3, MgO, FeO and Al_2O_3 were chosen in order as the most discriminating variables. Using these variables in the DFA produced a group separation almost identical to using all of the variables (Table 3.7). Cr_2O_3 was chosen as a highly discriminating variable in the analysis but the contents of this oxide is close to the microprobe detection limits in many of the tephras. With Cr_2O_3 removed from the analysis good group separation is still produced (Fig. 3.9C, Table 3.7). The order of the remaining variables discriminating power becomes, TiO_2, Al_2O_3, FeO, and MgO.

The well defined DFA groupings show that the differences in major element titanomagnetite composition correlates with differences in phenocryst assemblages of the tephras. Most notably, the hornblende bearing and olivine rich tephras have a different titanomagnetite composition to one another and to the rest of the tephras. Aside from the tephra correlation implications as previously mentioned, the statistical groupings therefore also provide petrological information. In these tephras it appears that the phenocryst phases are genetically related, if not crystallising from the same melt at least the same melt composition for each tephra. This relationship and the fact that all of the tephras examined have a single population of titanomagnetite compositions indicates little magma mixing occurring in this suite of tephras contrasting with a younger Ruapehu-sourced, silica-rich tephra described by Donoghue *et al.* (1995).

The groupings of titanomagnetite samples are not just simply related to the ferromagnesian mineralogy. Other factors appear to affect the group membership. The

TiO_2 vs. FeO(recalculated) plot described previously shows two main groupings of samples with two outlying samples. The groupings suggested by these two elements were tested using the CANDISC program:

Group H	High TiO_2 and FeO(recalculated) content
Group L	Low TiO_2 and FeO(recalculated) content
Group 1	as defined previously (Hornblende rich samples)
Group 2	as defined previously (Olivine rich samples).

This procedure clearly separated the groups defined on this basis (Fig. 3.9D, Table 3.7). These groupings, which are characterised by different relative contents of TiO_2 and FeO(recalculated), could be indicating different eruptive sources e.g. Tongariro vs. Ruapehu, or different batches of magma over time. There appears to be no clear division of Tongariro-sourced and Ruapehu-sourced tephras between Groups H and L. The major element titanomagnetite chemistry does not appear to differ consistently for the two volcanoes for this set of samples.

Investigating the order of eruption of the tephras indicates that the mixing of groups over time is not random. There are two instances in the tephra record where the titanomagnetites are dominantly of group H, otherwise they are group L. Group H samples, characterised by higher TiO_2 and FeO contents may indicate the introduction of a more basic melt at these times. This corresponds with greater quantities of olivine present within the group H tephras. In some cases the greater proportions of olivine are replaced by higher relative quantities of orthopyroxene, hornblende or titanomagnetite in the ferromagnesian mineral assemblage. The outlying groups are again the samples from the marker Unit 1 and Units 2 and 6 as described previously.

Table 3.7 D^2 values between titanomagnetite groupings.

Group Definition	D^2	Group 2	Group 3	Group 4
Cluster Grouping (Fig. 3.9A)	Group 1 (marker Unit 6)	177	104	118
	Group 2	-	32	11
	Group 3		-	8
Mineralogical Groupings (Fig. 3.9B)	Group 1 (Marker Units 2, 6)	158	46	50
	Group 2 (Marker Unit 1)	-	82	149
	Group 3		-	10
Mineralogical Groupings with STEPDISC variables	Group 1 (Marker Units 2, 6)	158	45	49
	Group 2 (Marker Unit 1)	-	82	148
	Group 3		-	10
Mineralogical Groupings with reduced variables (Fig. 3.9C)	Group 1 (Marker Units 2, 6)	72	26	41
	Group 2 (Marker Unit 1)	-	59	109
	Group 3		-	8
		Group L	Group 2	Group 1
Chemically defined Groupings (Fig. 3.9D)	Group H	9	119	95
	Group L	-	95	122
	Group 2		-	174

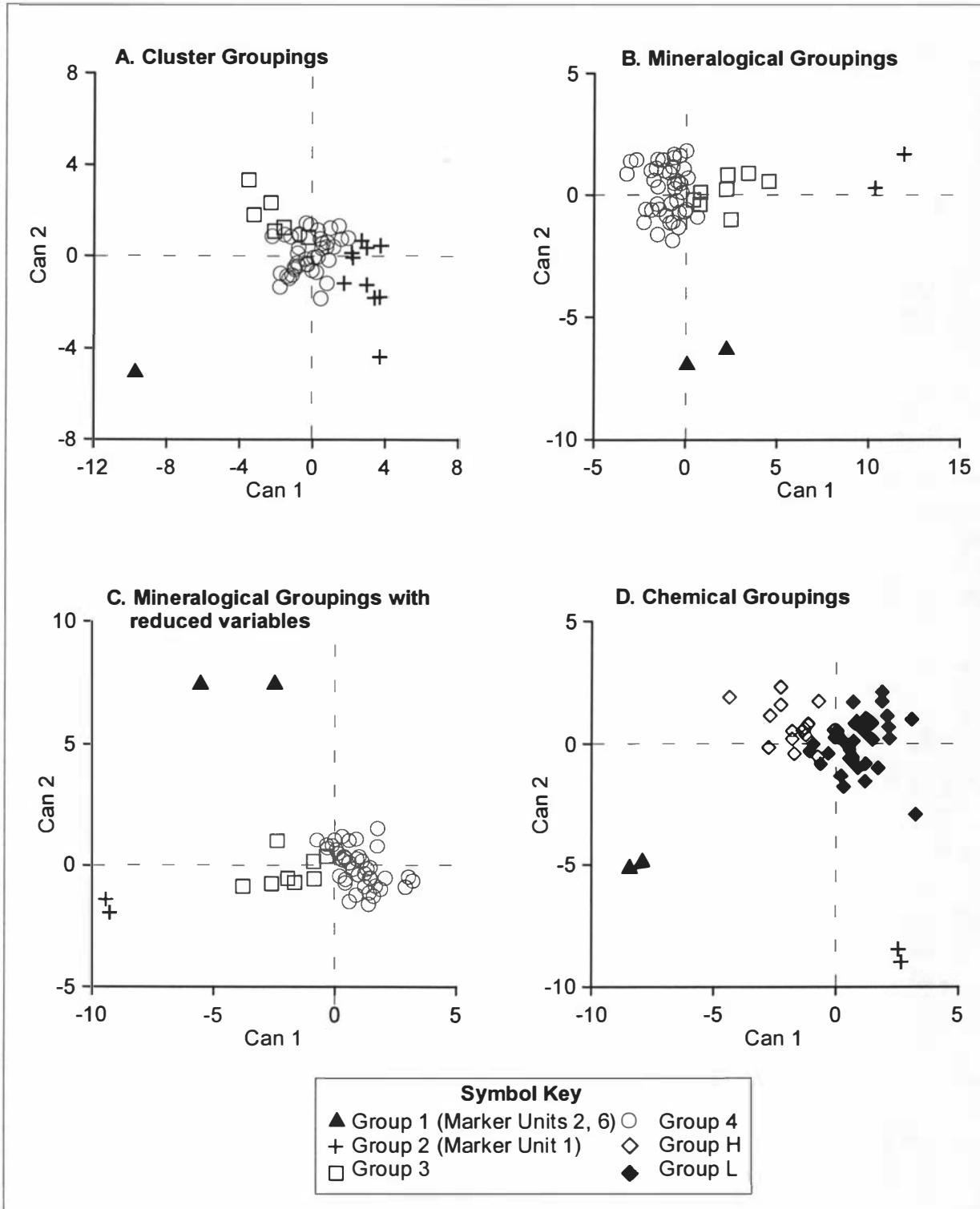

Figure 3.9. Plots of the first two canonical variables (Can 1 and Can2) for titanomagnetite data.
(A) Cluster defined groupings.
(B) Mineralogical groupings.
(C) Mineralogical groupings with reduced variables (Cr_2O_3 omitted).
(D) Chemically defined groupings (derived from the TiO_2 vs. FeO (recalculated) plot).

3.4.10 Hornblende (discrimination of marker Unit 4)

Hornblende chemistry has been used in New Zealand tephra studies as a tool to separate eruptives from EV, TgVC and Taupo Volcanic Zone (TVZ) rhyolitic centres (Lowe, 1988b; Froggatt and Rogers, 1990; Eden *et al.*, 1993). Eden *et al.* (1993) used a plot of the atomic proportions of Ca vs. Si to separate EV, TgVC, and TVZ-rhyolitic hornblendes. In this study the hornblende chemistry of individual eruptive units within the tephra sequence was examined to attempt to identify marker horizons in the same manner as for titanomagnetite. A plot of the atomic proportions of Ca and Si did not show any separation or grouping of samples, and no other two oxide plots proved to be useful in distinguishing any marker units.

Clustering analysis was applied to the transformed hornblende data in the same manner as for titanomagnetite. As there are only 11 hornblende-bearing tephras analysed in this sequence, the mean analyses of each sample cannot be used in the multivariate statistical procedures due to the lack of sufficient degrees of freedom. As a result, individual analyses were used in the following procedures rather than means. The clustering procedure produced three groups of samples with good separation, Groups hb1, hb2 and hb3 (Fig. 3.10A, Table 3.8). Several tephra samples had all of their analyses contained within a single group, but some of the samples had one or two of their analyses in another cluster grouping.

The hornblende cluster groups were then refined by keeping the analyses of each tephra sample within a single group (*i.e.* assuming a single population for each tephra sample). Canonical DFA of the refined hornblende groups produced better discrimination with higher D^2 values (Fig. 3.10B, Table 3.8), indicating that there are no mixed populations of hornblendes in these samples. The STEPDISC program chose, in order, K_2O, FeO, TiO_2, Al_2O_3, MgO, CaO, and SiO_2 as the most discriminating variables. Using this subset of variables the group separation was almost as good as using all of the variables (Table 3.8).

The hornblende groupings enable the discrimination of marker Unit 4 from the other hornblende bearing tephras. The refined Group hb3 is well separated from the other groups and consists of analyses of marker Unit 4 (Fig. 3.6). This unit had not been uniquely identified with any of the methods described previously. Group hb2 contains the analyses of several tephra samples but they all lie within the same part of the sequence, in the middle part of the record below the distinctive, previously described marker Unit 3 (Fig 3.6). Group hb1 contains the tephra samples which are at the very base of the sequence, including marker Unit 6. Group hb1 also contains the distinctive marker Unit 2, but this is able to be identified on the basis of its field appearance. The hornblende major element chemistry can be used to potentially place an unknown tephra sample in a specific part of the sequence, and in the case of one tephra (marker Unit 4) uniquely identify it.

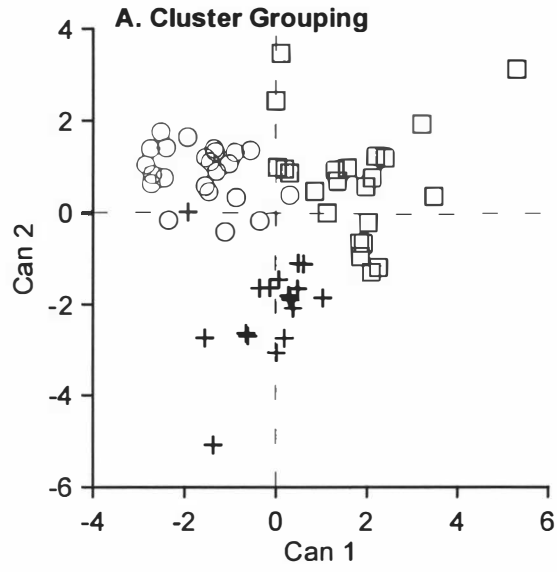

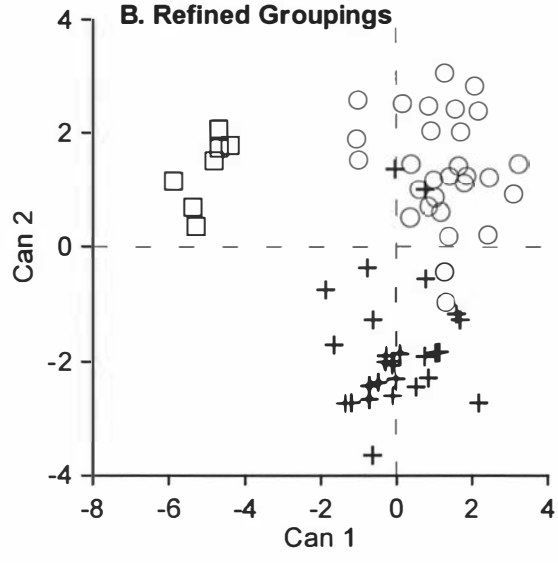

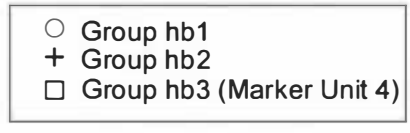

Figure 3.10. Plots of the first two canonical variables for hornblende data. (A) Cluster defined groupings. (B) Refined cluster-defined groups.

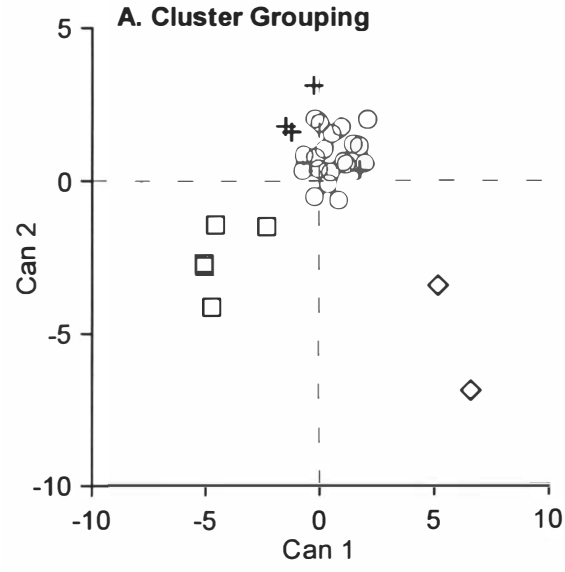

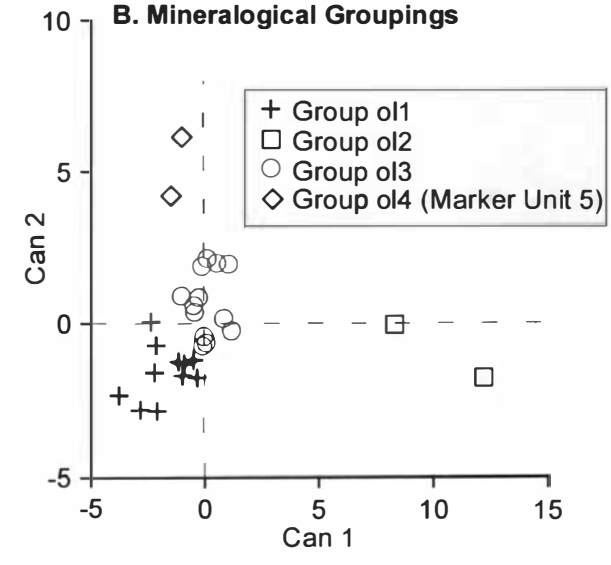

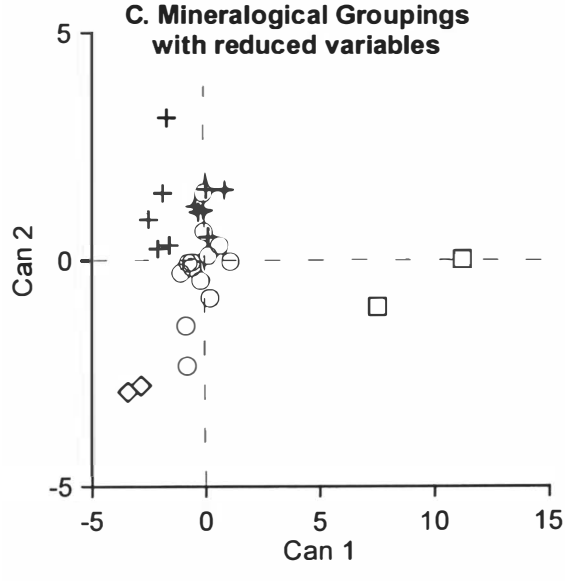

Figure 3.11. Plots of the first two canonical variables for olivine data. (A) Cluster defined groupings. (B) Mineralogical groupings. (C) Mineralogical groupings with reduced variables.

Table 3.8 D^2 values between hornblende groupings.

Group definition	D^2	Group hb2	Group hb3
Cluster Groupings	Group hb1	11	11
(Fig. 3.10A)	Group hb2	-	11
		Group hb2	Group hb3 (Marker Unit 4)
Refined Groupings	Group hb1	11	39
(Fig. 3.10B)	Group hb2	-	35
Refined Groupings with	Group hb1	9	37
STEPDISC variables	Group hb2	-	34

3.4.11 Olivine (discrimination of marker Unit 5)

Olivine has been used in New Zealand tephrochronology studies for distinguishing Egmont- and Tongariro-sourced tephras. Lowe (1988a) pointed out the presence of forsteritic olivine within TgVC-sourced tephras but very little olivine within EV-sourced tephras. Donoghue *et al.* (1991), used the morphology and chemistry of olivine phenocrysts to identify individual tephra members of the Tongariro volcano-sourced Mangamate Tephra Formation.

Almost half of the tephras within this sequence contain olivine and approximately half of the olivine-bearing tephras contain more than trace amounts (>0.5%) of olivine phenocrysts. No skeletal forms of olivine analogous to those described by Donoghue *et al.* (1991) in the Mangamate Tephra Formation were seen. In this study 119 grains of olivine were analysed from 16 tephras. Bivariate oxide plots showed no consistent groupings of samples that were easily discernible by eye because oxide values are very similar from one analysis to another.

Clustering analysis was applied to the transformed olivine data in the same manner as for titanomagnetite. The oxide variables used were SiO_2, Al_2O_3, FeO, MgO, CaO, and Na_2O, the other oxides reported in Table 3.6 were too low and close to microprobe detection limits. Four groupings resulted, which were separated by significant D^2 spacings (Fig. 3.11A, Table 3.9). The group membership of tephra units was found to be dominantly (but not exactly) the same as the previously defined titanomagnetite groupings. With this in mind, groups were defined on a similar basis to the titanomagnetite groups for canonical DFA:

Group ol1 Olivine rich samples (>5%)
Group ol2 Hornblende bearing samples
Group ol3 All other samples
Group ol4 Marker Unit 5

Group ol4 had to be defined to contain analyses of a tephra sample which did not fit into any of the other groups (marker Unit 5). These four groups were well separated using DFA (Fig. 3.11B; Table 3.9). The STEPDISC procedure chose, in order: MgO, SiO_2 Al_2O_3, CaO, and FeO as the most discriminating variables. Using this subset of variables,

group separation almost as good as using all of the variables was achieved (Table 3.9). The DFA was also tried without the STEPDISC chosen oxides Al_2O_3 and CaO which are of low content in these olivines. The resultant discrimination is still good for all groups but was reduced between groups ol1 and ol3 (Fig. 3.11C, Table 3.9).

Using these statistical techniques with olivine analyses from the tephra sequence the group separation defined by the titanomagnetite chemistry is able to be corroborated. Thus the olivine chemistry appears to be as sensitive to the ferromagnesian assemblage as the titanomagnetite chemistry. One further tephra unit can be uniquely identified in the sequence on the basis of its olivine chemistry. This is the unit represented by Group ol4, corresponding to marker Unit 5 (Fig. 3.6).

Table 3.9 D^2 values between olivine groupings.

Group definition	D^2	Group ol2	Group ol3	Group ol4 (Marker Unit 5)
Cluster Groupings (Fig. 3.11A)	Group ol1	40	11	89
	Group ol2	-	35	113
	Group ol3		-	66
Mineralogical Groupings (Fig. 3.11B)	Group ol1	145	9	46
	Group ol2	-	106	169
	Group ol3		-	22
Mineralogical Groupings with STEPDISC variables	Group ol1	142	7	34
	Group ol2	-	106	166
	Group ol3		-	18
Mineralogical Groupings with reduced variables (Fig. 3.11C)	Group ol1	107	1.8	19
	Group ol2	-	93	161
	Group ol3		-	15

3.4.12 Other phases

Lowe (1988a) found some provisional separation between EV and TgVC pyroxenes using analyses from the phenocryst cores. The pyroxene grains of the present sequence, however, were too strongly compositionally zoned to attempt chemical correlation and discrimination between individual eruptives.

Andesitic glass chemistry was shown to be effective in discriminating EV and TgVC tephras (Lowe, 1988a; Stokes and Lowe, 1988). The preservation of andesitic glass is, however, poor in most sedimentary environments, and very poor in the New Zealand soil environment (Neall, 1977; Kirkman and McHardy, 1980). Very few glass analyses could be obtained from the andesitic tephras in this sequence, and those that were obtained were considered unreliable due to the degree of weathering and hydration of the glass.

3.4.13 Conclusions

1) In this andesitic tephra sequence, ranging in age from ca. 23 ka to 75 ka, correlation of individual units over the eastern Ruapehu ring plain has been achieved through a variety of laboratory and field methods (Table 3.10). Seven units can be distinguished as marker beds over the eastern Ruapehu ring plain. This enables relative dating of ring plain deposits and surfaces, where other dating methods are less useful or more expensive.

Table 3.10 Summary of the criteria for identification of andesite marker tephras in this study.

Tephra marker	Unique field appearance	Characteristic mineralogy	Unique titanomagnetite chemistry	Unique hornblende chemistry	Unique olivine chemistry
Unit 1	✓	olivine rich	✓		
Unit 2	✓	hornblende rich	✓		
Unit 3	✓	hornblende bearing			✓
Unit 4		hornblende bearing		✓	
Unit 5		-			✓
Unit 6		hornblende rich	✓		
Unit 7		hornblende rich			

2) Three tephra units within this sequence are able to be identified over the eastern Ruapehu ring plain based on their unique field appearances; no other units can be uniquely identified on this basis. The field-based marker units are termed Units 1, 2, and 3.

3) The ferromagnesian mineral assemblage is another valuable identification criterion. The presence of >50 % modal olivine and > 5% modal hornblende are useful in further characterising Units 1 and 2, respectively. The presence of large quantities of hornblende (>5 to 30% by volume) enables the identification of two further tephra units near the base of the sequence, marker Units 6 and 7. Further identification of marker beds relies on electron microprobe analyses of phenocryst minerals.

4) The use of statistical clustering methods on electron microprobe-determined mineral compositions was found to have limited use in accurately grouping and discriminating mineral data, but was a valuable reconnaissance technique. Canonical DFA was used to distinguish groupings of sample data which were refined from clustering analysis by using other factors such as ferromagnesian mineral assemblage.

5) The grouping and discrimination of tephras using their titanomagnetite major element analyses reflected the tephra ferromagnesian mineral assemblage. Four distinct chemical groups were defined:

Group 1 hornblende-rich samples (>5%)
Group 2 olivine-rich samples (>10%)
Group 3 hornblende-bearing samples
Group 4 all other samples

This implies that all of the phenocrysts in these andesitic tephras were formed together in the same crystallising event or under the same magmatic conditions, and that these conditions are also reflected by the titanomagnetite chemistry. Titanomagnetite mineral chemistry was used to further discriminate marker Units 1, 2, and 6, as well as narrow down the identification of the other units. This is especially useful in situations such as distal areas where the ferromagnesian mineral assemblage is not well represented. The titanomagnetite chemistry also indicates episodes of changing melt composition during the eruptive history of Ruapehu volcano. Two episodes, thought to represent a more basic melt composition were seen.

6) Marker Units 2 and 6 are able to be further identified on the basis of hornblende composition and one other unit is able to be uniquely identified: marker Unit 4. The remaining hornblende bearing units are specifically grouped according to their stratigraphic position, enabling correlation to a general part of the sequence if not a specific tephra unit.

7) Olivine chemistry corroborates the groupings of tephra samples based on their titanomagnetite analyses, giving further means of identifying Unit 2 and the groups defined by the titanomagnetites. One other tephra unit can also be uniquely identified by its olivine chemistry: marker Unit 5.

8) In this study the usefulness of a multi-parameter approach and the statistical analysis of data for andesitic tephra correlation has been shown. In an andesitic ring plain environment very few tephra units can be discriminated by physical features alone as the physical appearances of small-medium volume andesitic tephra units change over very small distances. Detailed field mapping needs to be combined with increasingly diverse techniques to be able to correlate such tephras. The described statistical methods have proven useful in conjunction with more traditional methods currently used for andesitic tephra fingerprinting and correlation.

3.4.14 Acknowledgements

SJC gratefully acknowledges funding from the New Zealand Vice-Chancellor's Committee, Massey University Graduate Research Fund, and the Helen E. Akers Scholarship Fund. We thank K. Palmer for introduction to the use of the electron microprobe, and B. Roser and D. Lowe for their thoughtful reviews and comments.

3.5 Combined reference list

Aitchison, J., 1983. Principal component analysis of compositional data. Biometrika, 70: 57-65.

Aitchison, J., 1986. The Statistical Analysis of Compositional Data. Monographs on Statistics and Applied Probability. Chapman and Hall, London.

Alloway, B.V., Neall, V.E., Vucetich, C.G., 1995. Late Quaternary (post 28 000 year B.P.) tephrostratigraphy of northeast and central Taranaki, New Zealand. J. Roy. Soc. N.Z., 25: 385-458.

Beaudoin, A.B. and King, R.H., 1986. Using discriminant function analysis to identify Holocene tephras based on magnetite composition: a case study from the Sunwapta Pass area, Jasper National Park. Can. J. Earth Sci., 23: 804-812.

Borchardt, G.A.., Harward, M.E. and Schmitt, R.A., 1971. Correlation of ash deposits by activation analysis of glass separates. Quat. Res., 1: 247-260.

Cole, J.W., 1978. Andesites of the Tongariro Volcanic Centre, North Island, New Zealand. J. Volcanol. Geotherm. Res., 3: 121-153.

Cole, J.W., Graham, I.J., Hackett, W.R. and Houghton, B.F., 1986. Volcanology and petrology of the Quaternary composite volcanoes of Tongariro Volcanic Centre, Taupo Volcanic Zone. In: Smith, I.E.M. Late Cenozoic volcanism in New Zealand. Roy. Soc. N.Z. Bull., 23: 225-250.

Cronin, S.J., Neall, V.E. and Palmer, A.S., 1996. The geological history of the north-eastern ring plain of Ruapehu Volcano, New Zealand. Quat. Inter., 34-36: 21-28.

Donoghue, S.L., Neall, V.E. and Palmer A.S. 1995. Stratigraphy and chronology of late Quaternary andesitic tephra deposits, Tongariro Volcanic Centre, New Zealand. J. Roy. Soc. N.Z., 25: 115-206.

Donoghue, S.L., Stewart, R.B. and Palmer, A.S., 1991. Morphology and chemistry of olivine phenocrysts of Mangamate Tephra, Tongariro Volcanic Centre, New Zealand. J. Roy. Soc. N.Z., 21: 225-236.

Droop, G.T.R., 1987. A general equation for estimating Fe^{2+} concentrations in ferromagnesian silicates and oxides from microprobe analyses, using stoichiometric criteria. Min. Mag., 51: 431-435.

Eden, D. N., Froggatt, P.C., Trustrum, N.A. and Page, M.J., 1993. A multiple-source Holocene tephra sequence from Lake Tutira, Hawkes Bay, New Zealand. N.Z. J. Geol. Geophys., 36: 233-242.

Froggatt, P.C., 1983. Towards a comprehensive Upper Quaternary tephra and ignimbrite stratigraphy in New Zealand using electron microprobe analysis of glass shards. Quat. Res., 19: 188-200.

Froggatt, P.C. and Gosson, G.J., 1982. Techniques for the preparation of tephra samples for mineral or chemical analysis and radiometric dating. Geology Department, Victoria University of Wellington Publication 23 (12 pp.).

Froggatt, P.C. and Lowe, D.J., 1990. A review of late Quaternary silicic and some other tephra formations from New Zealand: their stratigraphy, nomenclature, distribution, volume, and age. N.Z. J. Geol. Geophys., 33: 89-109.

Froggatt, P.C. and Rogers G.M., 1990. Tephrostratigraphy of high-altitude peat bogs along the axial ranges, North Island, New Zealand. N.Z. J. Geol. Geophys., 33: 111-124.

Graham, I.J. and Hackett, W.R., 1987. Petrology of calc-alkaline lavas from Ruapehu volcano and related vents, Taupo Volcanic Zone, New Zealand. J. Petrol., 28: 531-567.

Hackett, W.R. and Houghton, B.F., 1989. A facies model for a Quaternary andesitic composite volcano: Ruapehu, New Zealand. Bull. Volcanol., 51: 51-68.

Hodder, A.P.W., de Lange, P.J., Lowe, D.J., 1991. Dissolution and depletion of ferromagnesian minerals from Holocene tephra layers in an acid bog, New Zealand, and its implications for tephra correlation. J. Quat. Sci., 6: 195- 208.

Johnson, R.A. and Wichern, D.W., 1992. Applied Multivariate Statistical Analysis (3rd Edition). Prentice-Hall Inc, New Jersey.

Juvigné, E., Shipley, S., 1983. Distribution of the heavy minerals in the downwind tephra lobe of the May 18, 1980 eruption of the Mount St. Helens (Washington, USA). Eiszeitalter U. Gegenwart 33: 1-7.

King, R.H., Kingston, M.S. and Barnett, R.L., 1982. A numerical approach to the classification of magnetites from tephra in southern Alberta. Can. J. Earth Sci., 19: 2012-2019.

Kirkman, J.H. and McHardy, W.J., 1980. A comparative study of the morphology, chemical composition and weathering rhyolite and andesite glass. Clay Minerals, 15: 165-173.

Kohn, B.P., 1970. Identification of New Zealand tephra layers by emission spectrographic analysis of their titanomagnetites. Lithos, 3: 361-368.

Kohn, B.P. and Neall, V.E., 1973. Identification of late Quaternary tephras for dating Taranaki lahar deposits. N.Z. J. Geol. Geophys., 16: 781-792.

Leamy, M.L., Milne, J.D.G., Pullar, W.A. and Bruce, J.G., 1973. Paleopedology and soil stratigraphy in the New Zealand Quaternary succession. N.Z. J. Geol. Geophys., 16: 723-744.

Lowe, D.J., 1986. Controls on the rates of weathering and clay mineral genesis in airfall tephras: a review and New Zealand case study. In: Colman, S.M., Dethier, D.P. (eds). Rates of chemical weathering of rocks and minerals. Academic Press, Orlando: 265-330.

Lowe, D.J., 1987. Studies on late Quaternary tephras in the Waikato and other regions in northern North Island, New Zealand, based on distal deposits in lake sediments and peats. Unpub. PhD thesis, University of Waikato, Hamilton, New Zealand.

Lowe, D.J., 1988a. Stratigraphy, age, composition, and correlation of late Quaternary tephras interbedded with organic sediments in Waikato lakes, North Island, New Zealand. N.Z. J. Geol. Geophys., 31: 125-165.

Lowe, D.J., 1988b. Late Quaternary volcanism in New Zealand: towards an integrated record using distal airfall tephras in lakes and bogs. J. Quat. Sci., 3: 111-120.

Lowe, D.J., 1990. Tephra studies in New Zealand: an historical review. J. Roy. Soc. N.Z.,20: 119-150.

Mathews, W.H., 1967. A contribution to the geology of the Mount Tongariro massif, North Island, New Zealand. N.Z. J. Geol. Geophys., 10: 1027-1038.

Milne, J.D.G. and Smalley, I.J., 1979. Loess deposits in the southern part of the North Island of New Zealand: an outline stratigraphy. Acta Geologica Academiae Scientarium Hungaricae, 22: 197-204.

Neall, V.E., 1977. Genesis and weathering of Andisols in Taranaki, New Zealand. Soil Sci., 123: 400-408.

Pullar, W.A., 1967. Uses of volcanic ash beds in geomorphology. Earth Sci. J., 1: 164-177.

Randle, K., Gorton, G.G., Kittleman, L.R., 1971. Geochemical and petrological characterisation of ash samples from Cascade Range volcanoes. Quat. Res., 1: 261-282

Ruxton, B.P., 1968. Rates of weathering of Quaternary volcanic ash in north-eastern Papua. 9th International Congress of Soil Science Transactions Vol. 4, Paper 38: 367-376

SAS Institute Inc., 1985. SAS Users guide: Statistics. Version 5 Edition, SAS Institute Inc., Cary N.C., 956 pp.

Shane, P.A.R. and Froggatt, P.C., 1994. Discriminant function analysis of glass chemistry of New Zealand and North American tephra deposits. Quat. Res., 41:70-81.

Smith, D.G.W., Westgate, J.A., 1969. Electron probe technique for characterising pyroclastic deposits. Earth Planet. Sci. Lett., 5: 313-319.

Srivastiva, M.S. and Carter, E.M., 1983. An Introduction to Applied Multivariate Statistics. Elsevier Science Publishing Co. Inc., New York.

Stewart, R.B., Price, R.C., Smith, I.E.M., (in press). Evolution of high-K arc magma, Egmont volcano, Taranaki, New Zealand: evidence from mineral chemistry. J. Volcanol. Geotherm. Res.

Stokes, S. and Lowe, D.J., 1988. Discriminant function analysis of late Quaternary tephras from five volcanoes in New Zealand using glass shard major element chemistry. Quat. Res., 30: 270-283.

Stokes, S., Lowe, D.J. and Froggatt, P.C., 1992. Discriminant function analysis and correlation of Late Quaternary rhyolitic tephra deposits from Taupo and Okataina volcanoes, New Zealand, using glass shard major element composition. Quat. Inter., 13/14: 103-117.

Thorarinsson, S., 1949. Some tephrochronological contributions to the volcanology and glaciology of Iceland. Geografiska Annaler, 31: 239-256.

Topping, W.W., 1973. Tephrostratigraphy and chronology of late Quaternary eruptives from the Tongariro Volcanic Centre, New Zealand. N.Z. J. Geol. Geophys., 16: 397-423.

Topping, W.W. and Kohn, B.P., 1973. Rhyolitic tephra marker beds in the Tongariro area, North Island, New Zealand. N.Z. J. Geol. Geophys., 16: 375-395.

Vucetich, C.G., Pullar, W.A., 1969. Stratigraphy and chronology of late Pleistocene volcanic ash beds in central North Island, New Zealand. N.Z. J. Geol. Geophys., 12: 784-837.

Vucetich, C.G., Pullar, W.A., 1973. Holocene tephra formations erupted in the Taupo area and interbedded tephras from other volcanic sources. N.Z. J. Geol. Geophys. 16: 745-780.

Wallace, R.C., Alloway, B.V., Stewart, R.B., Neall, V.E., 1986. Mineral chemistry as an indicator of petrogenisis at Egmont volcano. Abstracts of the International Volcanological Congress, 1986 New Zealand: 23.

Wallace, R.C., 1987. The mineralogy of the Tokomaru Silt Loam and the occurrence of cristobalite and tridymite in selected North Island soils. Unpub. Ph.D. thesis, Massey University, New Zealand.

Wilson, C.J.N., 1993. Stratigraphy, chronology, styles and dynamics of late Quaternary eruptions from Taupo volcano, New Zealand. Phil. Trans. Roy. Soc. London A, 343: 205-306.

Wilson, C.J.N., Houghton, B.F., Lanphere, M.A. and Weaver, S.D., 1992. A new radiometric age estimate for the Rotoehu Ash from Mayor Island volcano, New Zealand. N.Z. J. Geol. Geophys., 35: 371-374.

Wilson, C.J.N., Switzur, R.V. and Ward, A.P., 1988. A new ^{14}C age for the Oruanui(Wairakei) eruption, New Zealand. Geol. Mag., 125: 297-300.

CHAPTER 4: PALEOSOL DEVELOPMENT AND PALEOCLIMATIC INVESTIGATIONS OF THE RING PLAIN SEQUENCE

4.1 Introduction

In the previous two chapters a stratigraphic framework of rhyolitic and andesitic tephras has been established for the older ring-plain sequences found on the NE Ruapehu and E Tongariro ring plains. The first way in which the stratigraphic framework has been applied was the investigation through time of weathering and soil development within the ring plain sequence. In particular the stratigraphic framework allowed the sequence of weathering and soil development on the ring plains to be correlated to other investigations of the New Zealand late Quaternary paleoclimatic record.

In the following published study, parameters of weathering and soil development in the ring plain sequences, particularly the clay mineralogy, were investigated. In this way past climatic and soil development conditions on the ring plain areas were elucidated. The sequence of soil development was compared to other paleosol sequences in other areas of the North Island of New Zealand using the interbedded tephra layers as time planes.

The following paper has multiple authors and the contributions of each author to the work were:

S.J. Cronin: Principal investigator
Carried out all: field description and sampling
laboratory preparation of samples
optical microscopy work
chemical, XRD and DTA analyses
grainsize and soil-physical analyses
manuscript preparation and writing

V.E. Neall and A.S. Palmer: Advisers
Aided the study by: discussion of methodology and results
editing and discussion of the manuscript

4.2 INVESTIGATION OF AN AGGRADING PALEOSOL DEVELOPED INTO ANDESITIC RING-PLAIN DEPOSITS, RUAPEHU VOLCANO, NEW ZEALAND.

Shane J. Cronin, Vincent E. Neall, and Alan S. Palmer
Department of Soil Science, Massey University, Private Bag 11222, Palmerston North, New Zealand.

Geoderma, 69 (1996) 119-135.

Abstract Within a sequence of andesitic volcaniclastic deposits on the north-eastern ring plain of Ruapehu volcano is a ca.10 m-thick sequence of weathered andesitic tephras. Weathering and paleosol development is most evident in 3.6 m of fine ash in this sequence. The age of these tephras are constrained between ca. 23-70 ka by dated rhyolite tephras erupted from central North Island volcanoes. Mineralogy of the fine ash deposits reveals their origin, and the processes involved in their soil development. The fine ash deposits are almost totally locally derived either as primary volcanic ash or fines reworked from the ring plain itself by aeolian processes. Aerosolic quartz input associated with regional loess deposition during the cool climatic episodes of mid-$\delta^{18}O$ stage 3 and $\delta^{18}O$ stage 4 is very low, having been diluted by rapid accumulation of andesitic tephras in these episodes. The observed weathering features and secondary minerals within the ash sequence were derived from a complex combination of factors including climate change, accretion rate, and post-depositional modification. Relatively strong weathering development in two parts of the ash sequence is correlated with two widespread soil development episodes during the Last Glacial observed throughout the southern North Island. The accretion rate of the soil surface at these times also affected the expression of climate-related weathering. Formation of allophane (with an Al/Si ratio of 2:1) and ferrihydrite occurred near the soil surface as the ash was accreting. The amount of allophane and ferrihydrite through the sequence appears to be inversely related to the accretion rate of the soil surface. Upon burial of the ash materials by a thick (>20 m) sequence of lahar and tephra deposits, halloysite was later formed in the buried ash. The leaching of silica from the thick overburden of volcaniclastics into the ash material as well as perched water is thought to have decreased the Al/Si ratio in the soil solution and thus promoted the formation of halloysite from weathering andesitic glass.

4.3 Introduction

Preserved on the eastern ring plain of Ruapehu volcano is a >50 m thick sequence of volcaniclastic deposits which have accumulated over the last ca. 75 ka (Cronin, *et al.*, 1996). Within this sequence the contrasting morphologies of the deposits indicate the intensity of surficial weathering has varied over time. During the cold climatic episodes of marine $\delta^{18}O$ stages 2 and 4, near-continuous aggradation of diamictons occurred over the entire eastern Ruapehu ring plain (diamicton is a non genetic term for poorly sorted

sediments which contain a wide variety of particle sizes; Flint, 1960). The diamictons of this sequence generally contain pebble- to boulder-sized clasts which are supported by a sand-silt matrix. The aggradation of the diamictons is thought to be a reflection of unstable conditions on Ruapehu volcano, and the mechanism of deposition is thought to be dominantly by lahars (volcanic mud-flows). Within the periods of rapid aggradation on the ring plain there appears to have been little opportunity for the preservation of any air fall tephra or volcanic loess. The only tephras preserved in the diamicton sequences are the very large lapilli units and these have been reworked and eroded in many places. There is no soil development evident within the "packages" of diamictons.

During the mild climatic episodes of $\delta^{18}O$ Stage 3, deposition on the ring plain was dominated by tephra and volcanic loess accession. Soil development is evident throughout these deposits but is most strongly exhibited in the fine ash material. Diamictons still occur in the sequence but were separated by significant time intervals. The aim of this study was to characterise the origin of the fine ash deposits and to investigate the paleosol-forming environment throughout the sequence of tephra and volcanic loess deposits. This was achieved through field interpretation of the deposits coupled with mineralogical studies.

4.4 Setting

Ruapehu volcano within the Tongariro Volcanic Centre, is a large, active, andesitic, stratovolcano, and the highest point in the North Island at 2797 m. The current massif comprises a 110 km^3 cone with an apron of volcaniclastic deposits surrounding it of similar volume (Hackett and Houghton, 1989). The apron of volcaniclastic deposits is termed the ring plain. The area of this study is located along the Upper Waikato Stream of the north-eastern ring plain (Chapter 3: Fig. 3.5). Exposed in continuous stream bank exposures in this and adjacent streams are the deposits described in this paper. The altitude of the area ranges from 900 to 1100 m above sea level.

The Ruapehu region has a cool-temperate climate with numerous frosts and snow-falls, and a mean annual temperature of 10 °C at 600 m (McGlone and Topping, 1977). The orographic influence of Ruapehu volcano on the predominantly westerly airflow increases the rainfall on the higher slopes of the volcano compared to surrounding areas. The average annual rainfall varies from 1600 mm at 900 m to 2400 mm at 1100 m altitude on the eastern side of the volcano (N.Z. Meteorological Service, 1973).

4.5 Stratigraphy

The tephra dominant portion of this section of the ring plain sequence occurs between two "packages" of diamictons (Fig. 4.1). Time control is provided by the presence of five rhyolitic tephras erupted from central North Island volcanoes to the north (Table 4.1). The four oldest tephras occur as rhyolitic glass shards and minerals dispersed over several centimetres within a matrix of fine andesitic ash. The identification of these tephras was

made on the basis of characteristic mineralogy and electron-microprobe major element glass chemistry.

Table 4.1. Rhyolitic tephra identified within the north-eastern ring plain sequence.

Tephra Name	Source	Age	Reference for age
Kawakawa Tephra	TVC	22 590 ± 230[1]	Wilson et al., (1988)
Okaia Tephra	TVC	ca. 23 000	Froggatt and Lowe, (1990)
Omataroa Tephra	OVC	28 220 ± 630[1]	Froggatt and Lowe, (1990)
Hauparu Tephra	OVC	35 870 ± 1270[1]	Froggatt and Lowe, (1990)
Rotoehu Ash	OVC	64 000 ± 4000[2]	Wilson et al., (1992)

TVC = Taupo Volcanic Centre
OVC = Okataina Volcanic Centre
[1] Denotes ^{14}C ages based on old half life (years B.P.)
[2] Whole rock K-Ar age (years)

4.6 Physical description

The ash materials of this study are 20 to 30 m below the present soil surface. The diamictons interbedded with, and above and below the tephra and volcanic loess sequence have a sandy matrix supporting clasts of andesitic lava; the clasts can be over 1 m in diameter. All of the diamictons contain 5-10% by volume andesitic pumice lapilli but in an extreme case up to 60%. Two of the diamicton units in this sequence are firmly cemented, while the others are unconsolidated.

The andesitic tephra occur as individual pumice lapilli and coarse ash beds or as accumulations of fine ash representing the products of several eruptions over time. The coarser andesitic tephra are dominantly fine pumice lapilli which are highly and very finely vesicular; the proportion of lithic components is usually <10% by volume. The pumice is soft, highly weathered, and ranges from yellow to reddish-brown. The pumice lapilli occur interbedded with fine ash throughout the sequence. A high frequency of pumice lapilli units within fine ash is here considered to represent more rapid accumulation of the surface compared to slower accretion where pumice lapilli are fewer within the fine ash.

The finer grained andesite ash ranges in texture from fine sandy loam to loam. A few zones within the ash column contain the occasional pumice lapilli clasts while most of these deposits are uniformly fine grained <2 mm. The ash is dominantly yellow-brown and brown and some sites have lower chroma colours but little or no evidence of mottling. It is firm when moist and dries into very strong blocks. Very little soil structure is seen apart from coarse blockiness when the ash material is dry. Root rhizomorphs are abundant throughout all of the fine ash. Two zones of more strongly weathered ash with common to very common root rhizomorphs were noted (Fig. 4.1). The upper zone is dark brown, contains finely disseminated charcoal fragments, and has the greatest abundance of root rhizomorphs.

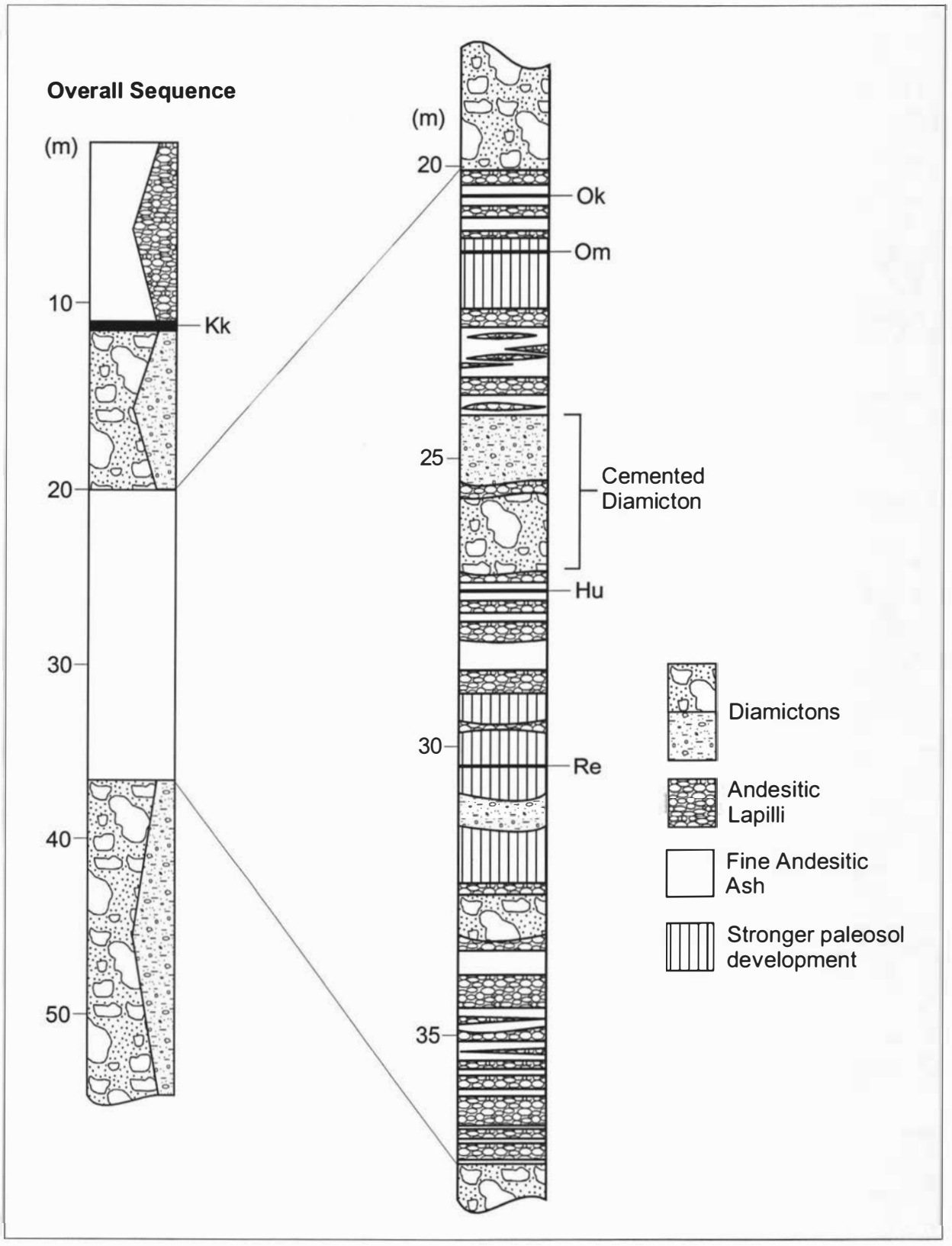

Figure 4.1. Stratigraphic column of part of the northeastern Ruapehu ring-plain sequence with paleosol development and its position within the overall ring plain sequence. Kk = Kawakawa Tephra, Ok = Okaia Tephra, Om = Omataroa Tephra, Hu = Hauparu Tephra, Re = Rotoehu Ash.

The lower zone is not as well expressed but contains a greater abundance of root rhizomorphs than the surrounding ash, as well as finely disseminated charcoal fragments.

The dry bulk density of the ash material ranges from 0.68 to 0.86 Mg m^{-3} (Table 4.2). The lowest bulk densities are in the upper part of the ash column within the upper zone of stronger weathering. The highest bulk densities are within the lower zone of stronger weathering.

Table 4.2. Soil physical properties of selected ash samples.

Sample depth (m)	Dry bulk density (Mg m^{-3})	Field-moist gravimetric water content at -1.5 MPa (%)	Air-Dry gravimetric water content at -1.5 MPa (%)	Gravimetric water content of air dry soil <2mm (%)
0.4-0.5	0.68	78	50	13
0.9-1.0	0.68	96	52	23
1.5-1.6	0.86	64	51	15
1.8-1.9	0.80	81	50	10
3.5-3.6	0.75	75	39	15

4.7 Mineralogy of ash grade material

Selected mineralogy of the ash grade material was investigated to identify the provenance of the material and to elucidate the soil forming processes occurring in the ash. The fine ash was channel sampled at 10 cm intervals through its 3.6 m thickness.

4.8 Methods

Quartz, cristobalite, and plant opal were concentrated from the whole soil (<2 mm) using the method of Henderson *et al.* (1972). Each soil sample was subjected to repeated dissolution in 6 *M* hydrochloric acid at 80 °C followed by 0.5 *M* sodium hydroxide at 100 °C. After this procedure the sample was dissolved in 30% hydroflurosilicic acid at 15-16 °C. Henderson *et al.* (1972), went on to further concentrate the silica minerals by heavy liquid separation but this step was not necessary here as sufficient quartz and cristobalite were present for identification using X-Ray Diffraction (XRD).

The quantities of quartz and cristobalite in the concentrated sample were estimated with XRD from the 33.4 nm and 40.6 nm reflections respectively. Standards were prepared for both cristobalite and quartz with a matrix of ash from the sampling site which had a negligible content of quartz or cristobalite. The results of the determinations calculated for the bulk soil (<2 mm) are shown in Fig. 4.3A and B. The reflection counts from the standard mixtures were reproducible within 10% or better, giving rise to precision of ± 10% in the sample determinations. The quantities of plant opal were not estimated but its presence was noted in all samples under a polarising microscope.

Halloysite was identified in the bulk soil (<2 mm) using the XRD methods described by Churchman *et al.* (1984). Initially a 101 nm reflection and occasionally a

poorly defined peak in the region of 74 nm were obtained for ground samples mixed into a slurry and dried on a ceramic tile. After spraying the sample with formamide the 101-102 nm peak sharpened and enlarged considerably and any reflection around 74 nm was reduced to background levels. This test indicates that the intermittent 74 nm reflection was not due to kaolinite but to a hydrated form of halloysite which upon addition of formamide expanded to give reflections around 102 nm. Following heating of the sample at 110 °C the 102 nm reflection disappeared, and a small peak at 74 nm was seen. The disappearance of the 102 nm peak indicated that mica minerals are not present.

To confirm the identification of halloysite the 1-2 μm fractions of selected ash samples were separated by settling after dispersion of the sample with 1:1 ammonium hydroxide. These samples were then examined under a transmission electron microscope, where the characteristic tubular and spherical morphologies of halloysite particles enabled their identification, after Kirkman (1981).

The quantity of halloysite was assessed throughout the ash sequence (Fig. 4.3C) using Differential Thermal Analysis (DTA) following the methods of Whitton and Churchman (1987). The depth of the dehydroxylation endotherm at around 540-550 °C was used to estimate the halloysite content. Standards were prepared using an andesite ash matrix with negligible halloysite content. Standard results were reproducible within 10%, giving rise to a precision of ± 10% in the sample estimates.

Amorphous constituents of the fine ash material were estimated using two methods. The first is an indirect method for estimating the short range order and organic constituents (SROCO) in a soil (Alloway *et al.*, 1992a). Air-dried soil (<2 mm) is shaken in the dark for 24 hours in 0.2 *M* acid-oxalate reagent (pH 3.0), at a ratio of 100 ml of reagent to 1g of soil. SROCO content is the weight of material dissolved from the soil. Air dry analysis does not however take into account the weight of water present within the structure of, or held tightly by the short range order minerals such as allophane. A moisture correction factor is then applied here to account for the water held by the air dry soil before and after extraction. The SROCO content of the ash materials (Fig. 4.3D) ranges from around 3-9 % of the oven dry bulk soil.

The other, more quantitative method used is that of Parfitt and Wilson (1985) using oxalate and pyrophosphate extractable chemistry. Bulk soil samples (<2 mm) were extracted with acid-oxalate and pyrophosphate reagents following the procedures of Blakemore *et al.* (1987). The Si, Al, and Fe content of the acid-oxalate extracts (Sio, Alo, and Feo), and the Al content of the pyrophosphate extract (Al*p*) were assessed using flame atomic absorption. The acid-oxalate dissolves the short-range order and organic constituents, while the Al*p* provides an estimate of the aluminium in Al-humus complexes. The established methodology is then to asses the Al/Si ratio for allophane from (Alo-Al*p*)/Sio multiplied by 28/27 to give the atomic ratio. The Sio content is then multiplied by a factor corresponding to the atomic ratio to give the percentage of allophane in the soil sample (Fig. 4.3E). Ferrihydrite content of the ash materials was estimated (Fig. 4.3F) by multiplying Feo by 1.7 after Childs (1985).

The grain size distribution through the fine ash material (Fig. 4.2) was estimated using the method of Alloway *et al*. (1992a). Short range order and organic constituents (SROCO) are extracted from a sample with 0.2 *M* acid-oxalate reagent, and crystalline clay, silt and sand fractions are then assessed using a combination of wet and dry sieving.

The water content at a matric potential of -1.5 MPa was determined gravimetrically after 24 hrs soaking and 7 days to equilibrate under the matric potential.

4.9 Results and discussion

The grain size is variable throughout the thickness of ash but shows no trends with depth, apart from the relative abundance of SROCO + crystalline clay near the top of the ash column (Fig. 4.2). The grain size variability reflects additions of air fall ash of varying grades which makes up the sequence. The field moist and air dry gravimetric water content measured at a matric potential of -1.5 MPa is high to very high for the ash (Table 4.2). The -1.5 MPa water content is highest where the clay + SROCO content is highest.

4.9.1 Primary ash mineralogy

All of the ash samples have been studied under a polarising microscope. Major phases present are plagioclase, orthopyroxene, and clinopyroxene, in order of abundance. The three major phases make up usually >90% by volume of the mineral phases observed. Hornblende and titanomagnetite occur in about half of the samples in quantities usually <5% by volume of the mineral component, but sometimes up to 10%. Highly vesicular and microlite-rich andesitic glass is seen within all samples and comprises over 50% of grains counted in most samples. The andesitic glass is always partially weathered and brown in colour, but not completely replaced by secondary minerals as observed by Kirkman and McHardy (1980) in andesitic glass of tephras from Egmont volcano in western North Island.

4.9.2 Siliceous phases

The quartz content of these ash units is very low throughout the entire range of samples (Fig. 4.3A). The peak of 0.5% quartz at the top of the sampling sequence is due to the presence of the quartz-bearing Okaia Tephra (sourced from Taupo Volcano). No quartz was found in andesitic lapilli units and the small amount of quartz within the ash deposits is here regarded to be a result of aerosolic addition.

A small increase in the quartz content occurs near the top of the sequence in a more strongly weathered zone below the Okaia Tephra, with fewer pumice lapilli interbeds present. This suggests a more slowly accumulating soil surface at this time, providing an opportunity for greater weathering and larger quantities of quartz to be deposited onto the soil surface.

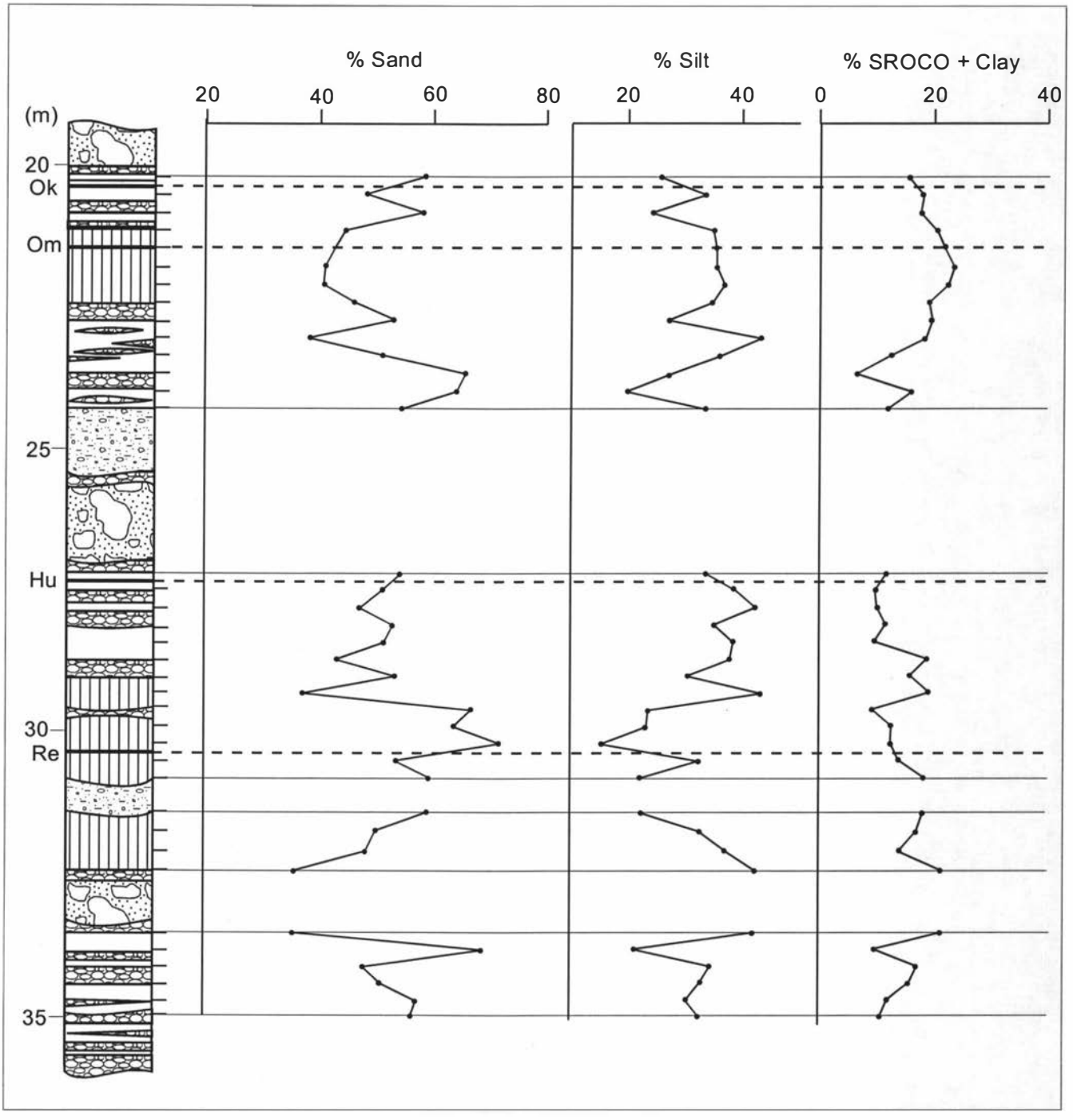

Figure 4.2. Grain size distribution within the fine ash materials assessed using the method of Alloway *et al.* (1992a). Coarse ash/lapilli beds and diamictons were not sampled. Ok = Okaia Tephra, Om = Omataroa Tephra, Hu = Hauparu Tephra and Re = Rotoehu Ash. Lithology symbols given in Fig 4.1.

A previous study of aerosolic quartz within andic materials in Taranaki (Alloway *et al.*, 1992b), showed two peaks of quartz accumulation corresponding with oxygen isotope stages 2 and 4, and very little quartz in deposits accumulating during $\delta^{18}O$ stage 3 (*c.* 25-60 ka B.P.). Quartz accumulation was correlated with episodes of regional loess deposition throughout the southern North Island in $\delta^{18}O$ stages 2, and 4. A loess deposition episode during $\delta^{18}O$ stage 3 did not correspond to a quartz peak in the sequence studied by Alloway *et al.* (1992b) in Taranaki.

The ash deposits studied here on the Ruapehu ring plain accumulated mostly during $\delta^{18}O$ stage 3 and part of $\delta^{18}O$ stage 4. Regional loess deposition occurred during both $\delta^{18}O$ stages 3 and 4, throughout the southern North Island (Milne and Smalley, 1979; Palmer, 1985; Alloway *et al.*, 1988; Pillans, 1994). Neither of these regional loess deposition episodes are indicated by a quartz peak in the Ruapehu ash sequence even though source areas in the Wanganui hill country to the south-west, or the Kaimanawa Mountains to the east potentially could have supplied quartz to the site. This indicates that the accumulation rate of the ash in this sequence was too high to preserve appreciable quartz and/or the climate was insufficiently severe to mobilise the quartz source.

The quartz content in the Ruapehu ring plain ash sequence appears to be a function of the accretion rate of the soil surface rather than of climate change and consequent loess deposition as indicated by the study of Alloway *et al.* (1992b).

The cristobalite content throughout the ash column (Fig. 4.3B) is highly variable from <0.5 to 4%. The origin of cristobalite in volcanic soils has been attributed to both pedogenesis (Lowe, 1986), and as a primary phase from the volcanic parent material (Mizota, *et al.*, 1987). The amount of cristobalite within selected andesite pumice lapilli layers interbedded in the sequence has been estimated using the same methods used for the ash samples. The content of cristobalite in the pumice lapilli was of a similar range to that in the ash material. The cristobalite in the ash material was also in a highly crystalline form as indicated by its sharp X-ray reflections and its presence was noted as microlites within weathered andesitic glass. The cristobalite content of the samples is thus most likely a reflection of the primary composition of the ash, and indicates that the cristobalite content of the erupted ash changed rapidly over time.

4.9.3 Secondary minerals

The secondary minerals which have been identified within the ash sequence are halloysite, allophane and ferrihydrite.

The halloysite content within the ash sequence ranges from 10 to 25 % of whole soil (<2 mm). The highest contents are found in the lower zone of strong weathering. Halloysite within the deposits occurs in two morphological forms, as hollow tubes and as spheres or ellipsoids. The spherical form is dominant. Kirkman (1981) proposed that the tubular particles formed from feldspar and the spheres from rhyolite glass. Due to the

virtual absence of rhyolite glass in this sequence it is considered that the spherical halloysite is here formed from andesitic glass.

The allophane content of the ash calculated using the method of Parfitt and Wilson (1985), is very low throughout the sequence (Fig. 4.3E), ranging from 1 to 4%. The trend of allophane content in the sequence is very similar to the SROCO trend, with higher values recorded near the top within the upper zone of strong weathering. The range of estimated ferrihydrite contents is from 0.3 to 1.6%, showing a similar trend to the allophane content (Fig. 4.3F).

The calculated allophane and ferrihydrite contents are lower than the SROCO contents of the ash material. Al*p* content within the ash sequence is barely detectable ranging from 0 to 0.02%, indicating that there is little organic material present which could be making up the rest of the SROCO estimate. This difference was also noted by Alloway *et al.* (1992b), although they did not take into account the water held by allophane, ferrihydrite and humus complexes in air dried samples. In air dried allophane-rich soils significant water is held within the particles and within the structure of SROCO constituents (Table 4.2). This water is measured as a weight difference in the SROCO estimation as the SROCO minerals have been dissolved, but is not seen in the Si and Al content of the extracted solution, leading to overestimation in the SROCO method compared to the Parfitt and Wilson (1985) method.

Even after a moisture correction factor is applied to the Ruapehu ash SROCO estimates, they are still higher than the calculated allophane + ferrihydrite. Either the Parfitt and Wilson (1985) empirical method underestimates the allophane within these samples or the acid-oxalate reagent is partially dissolving other phases, contributing to the SROCO estimate. The SROCO extractions were carried out in the dark and past studies have shown that under these conditions very little dissolution of crystalline minerals is expected (e.g. Fey and Le Roux, 1977; Wada, 1977; Parfitt and Childs, 1988). The differences between the two methods is probably due to a combination of, longer extraction times used in the SROCO method (2 successive 24 hour extractions compared to a single 2 or 4 hour extraction), inaccuracies in recovering and weighing the undissolved sample fraction in the SROCO method, and a possible lack of understanding of which phases are being attacked by the oxalate reagent in long extraction times in these tephric samples.

The formation of allophane and halloysite from volcanic ash in New Zealand conditions has been addressed in many studies (e.g. Parfitt *et al.*, 1983 and 1984; Lowe, 1986; Singleton *et al.*, 1989; Parfitt and Kimble, 1989). The overall conclusion from these studies is that volcanic glass can weather directly to either allophane or halloysite; which mineral is formed depends on the Al/Si ratio of the soil solution. When the Al/Si ratio is low in soil solution, halloysite is formed and when the ratio is high allophane is formed. This model does not require allophane to be formed as an intermediary which later transforms to halloysite, as in the model of Kirkman (1975).

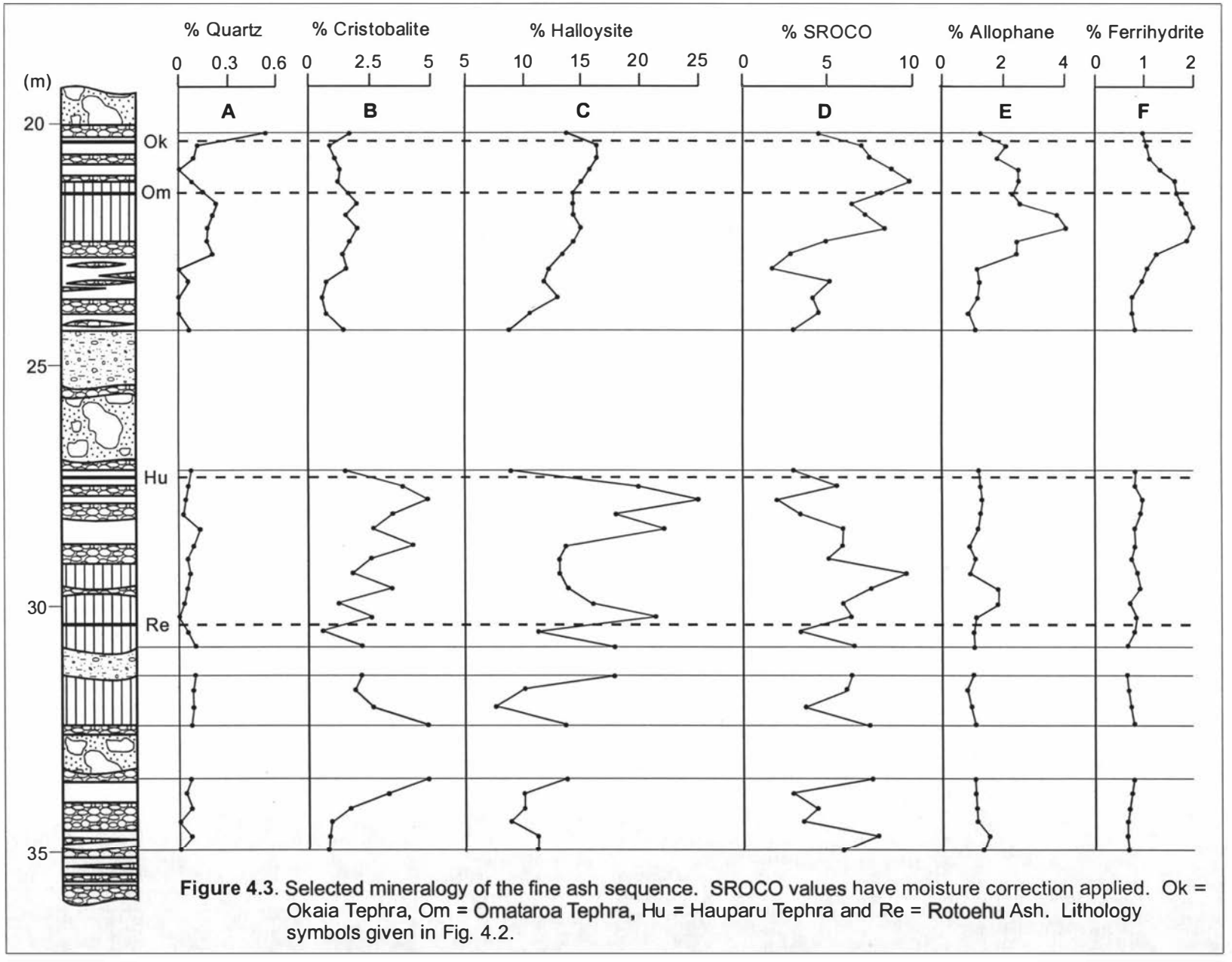

Figure 4.3. Selected mineralogy of the fine ash sequence. SROCO values have moisture correction applied. Ok = Okaia Tephra, Om = Omataroa Tephra, Hu = Hauparu Tephra and Re = Rotoehu Ash. Lithology symbols given in Fig. 4.2.

There are many factors which can decrease the Al/Si ratio in soil solution (Lowe, 1986) and thus promote the formation of halloysite from volcanic glass. These factors include low rainfall, poor or impeded drainage, and deep burial of ash deposits. Strong evidence for poor drainage is not seen in the form of common mottling and gleying features in the ash deposits but the dominant brown colouring of the ash deposits could mask all but very strong gleying processes. Some of the diamictons within the sequence have a sandy matrix and may not provide a large impediment to drainage, however others have a clay-rich matrix or are cemented and may impede drainage. The deposits are presently buried by at least 20 m of tephra and diamictons which is likely to have played an important role in their weathering. Dissolved silica has probably leached down into the sequence of ash deposits from the sediments and tephras above. This supply of silica would have promoted the formation of halloysite from the weathering andesitic glass by reducing the Al/Si ratio in soil solution, especially where drainage is impeded. In this sequence it is likely that the effects of both deep and rapid burial of the ash deposits, and poor drainage conditions created by water perching on or below interbedded diamictons have had the greatest effect on formation of secondary minerals.

The Al/Si atomic ratio of the allophane present in the ash sequence is 2:1 or greater throughout the entire sequence. The 2:1 allophane is coexisting in the ash with halloysite. This is at odds with the findings of Parfitt *et al.*, (1984) who found that when allophane and halloysite were coexisting in a rhyolitic ash bed in a moderate or low leaching environment (<200 mm of percolation/year), the allophane had an Al/Si ratio of close to 1:1. Allophane with an Al/Si ratio of 2:1 was formed under conditions of greater leaching (>250 mm a year), and no halloysite was formed under these conditions. The paleosol sequence is not near the current soil surface and modern plant roots do not affect it; thus the allophane is not considered to be modified by modern processes. The allophane may also have lost Si post-formation, thus increasing its Al/Si ratio, but past studies have shown that 2:1 allophane can persist in soils for hundreds of thousands of years in buried soil environments similar to the Ruapehu ring plain sequence (e.g. Kirkman, 1981; Stevens and Vucetich, 1985; Lowe, 1986; Lowe and Percival, 1993), so this affect is not thought to be dominant in the sequence.

The coexistence of allophane with a 2:1 Al/Si ratio and appreciable halloysite in the Upper Waikato Stream ash deposits may indicate that the two minerals were formed at different times in the weathering history of the ash materials due to a change in the weathering environment. If halloysite is forming from the weathering ash while tephra and ring-plain sediments are being deposited above, the 2:1 allophane may be remnant from weathering of the ash material when it was originally in an acid leaching environment, at or near the soil surface. If this is the case then the trends shown in the allophane content may indicate the length of time the soil surface was stable, or a record of the accumulation rate. Where the soil surface is stable for a longer time more allophane is formed. This agrees with field observation of stronger weathering features and a low frequency of pumice lapilli additions where there is greatest allophane content in the top of the ash sequence. This also correlates with the preferential concentration of quartz in

the sequence at this point, due to slower accumulation rates and more intensive weathering. The trend of ferrihydrite contents of the ash parallels that of allophane, and indicates that the ferrihydrite is likely to have been formed when the ash was at or near the soil surface at the same time as allophane.

The lower zone of observed relatively strong weathering within the fine ash does not show a peak in allophane or ferrihydrite content. This could be due to the soil surface accumulating too quickly to produce favourable conditions for the formation of allophane and ferrihydrite. Field observation at this point shows that there is a much greater frequency of pumice lapilli additions to the sequence at this time, indicating a relatively high rate of deposition.

In this sequence of andesitic tephra with very little rhyolitic glass present, the Al/Si ratio of the soil solution appears to be driving the formation of the secondary minerals as found by Singleton *et al.* (1989), rather than the Al/Si ratio of the parent glass as found by Kirkman and McHardy (1980). The parent glass composition obviously has an effect on the soil solution composition. As it weathers, andesite glass will release more Al into solution than rhyolite glass reflecting their initial Al content differences. The result of this is observed in soils from Taranaki which contain large quantities of allophane (Alloway *et al.*, 1992b). In the ash materials on the Ruapehu ring-plain sequence the effect of the weathering andesitic glass composition on the soil solution is considered to be overshadowed by the other environmental factors of rapid burial and impeded drainage. This is reflected by the dominance of halloysite as a weathering product and only a limited time for allophane formation when the ash material was at or near the surface.

4.10 Relationship of Ruapehu ring-plain sequence to climate record for southern North Island

The observed features of stronger weathering and more abundant root rhizomorphs within parts of the ash sequence could be indicating the climate was warmer during these periods of deposition than at other periods within the sequence. The effect of climate change during the period of deposition on these ash deposits would have been overprinted onto the effect of accumulation rate discussed previously.

The timing and nature of climate oscillations within southern North Island, New Zealand has been well documented (Palmer, 1985; Alloway *et al.*, 1992b and 1992c; Pillans, 1994), and landscape events can be shown to be related to the marine $\delta^{18}O$ record (Fig. 4.4). The presence of identified rhyolitic tephras provide time planes which enable correlation of features in the ash sequence to the established climate record of the southern North Island. The range in age of the deposits within this sequence is from *c.* 24 to 70 ka, mostly during $\delta^{18}O$ stage 3.

Within the upper zone of strong weathering, the presence of the Omataroa Tephra (ca. 28.2 ka; Table 4.1) correlates this weathering period with a widespread soil development episode in loess sequences of the southern North Island (Fig. 4.4; Milne and Smalley, 1979 ; Leamy *et al.*, 1973; Palmer, 1985; Alloway *et al.*, 1988; Pillans 1988).

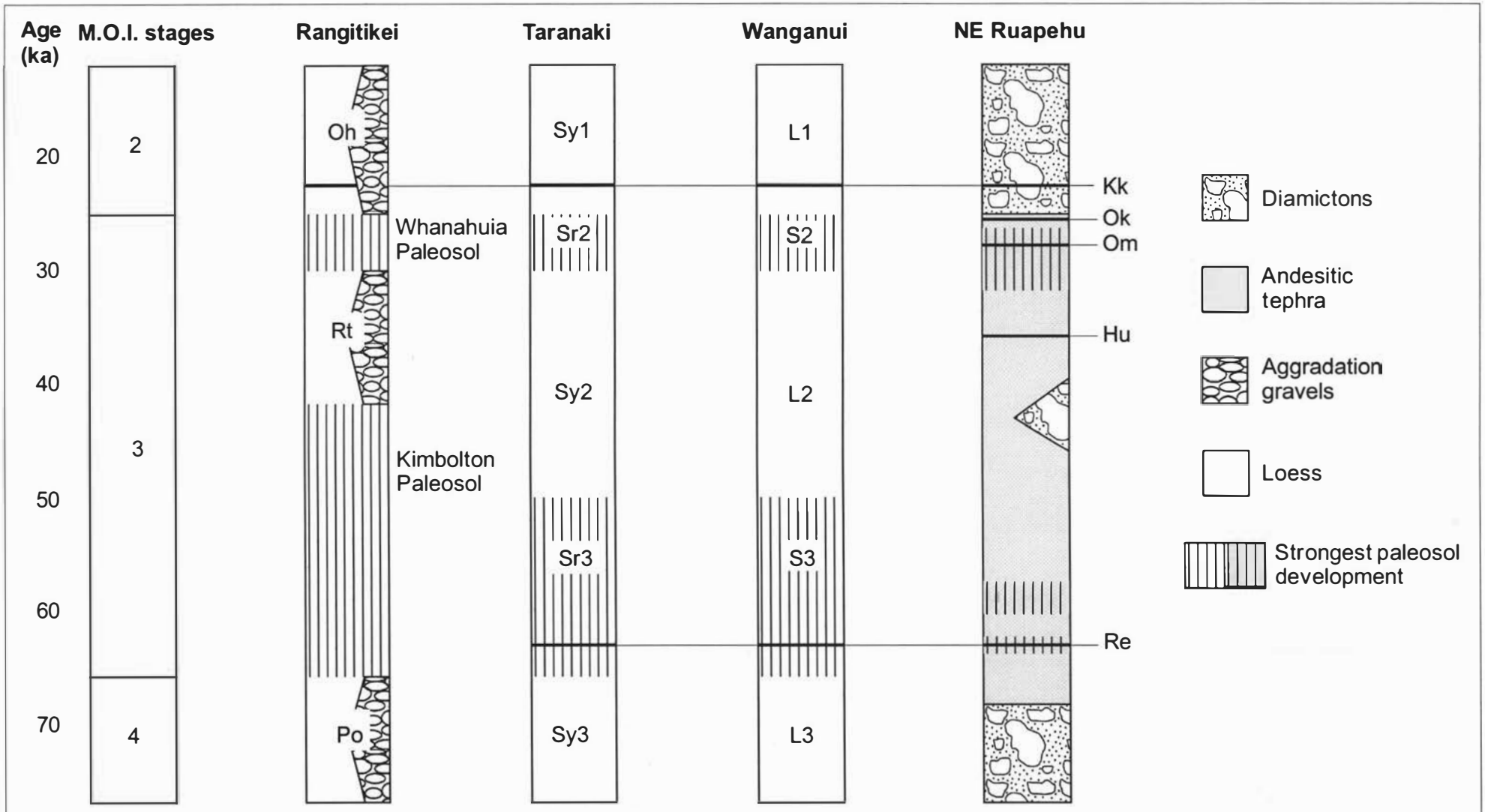

Figure 4.4. The relationship of the northeastern Ruapehu ring-plain sequence with deep sea ^{18}O isotope record (M.O.I. Stages; Shackleton *et al.*, 1990), and southern North Island loess stratigraphy from the Rangitikei valley (Leamy *et al.*, 1973; Milne and Smalley, 1979), Wanganui (Pillans, 1988; 1994), and Taranaki (Alloway *et al.*, 1988). Oh = Ohakea loess, Rt = Rata loess and Po = Porewa loess L1 = loess 1, S2 = buried soil 2 etc. Sy1 = loess 1 correlative, Sr2 = buried soil 2 correaltive etc. Kk = Kawakawa Tephra, Ok = Okaia Tephra, Om = Omataroa Tephra, Hu = Hauparu Tephra and Re = Rotoehu Ash.

This soil development is represented by one of the weakest of the Last Glacial paleosols. In the ash sequence from eastern Ruapehu the weathering of this paleosol is further enhanced by relatively slow accretion of the soil surface as discussed previously.

Within the lower zone of strong weathering, the presence of the Rotoehu Ash (ca. 64 ka; Table 4.1) indicates this weathering episode was contemporaneous with another period of widespread soil development on loess throughout the southern North Island (Fig. 4.4; Milne and Smalley, 1979; Leamy *et al.*, 1973; Palmer, 1985; Alloway *et al.*, 1988; Pillans, 1988). This soil development is represented by very strong paleosols throughout the southern North Island. In the eastern Ruapehu sequence the intensity of soil development was probably hindered by rapid accretion of tephra at the soil surface.

The cool climatic episode in late $\delta^{18}O$ stage 3, represented by loess deposition in the southern North Island (Fig. 4.4), is not evidenced in the Ruapehu sequence. Quartz input is swamped by a high accretion rate of andesite ash and lapilli. The only manifestations of a cool climate are less observable weathering features, less root rhizomorphs, and lower amounts of allophane and ferrihydrite in the ash deposited during this time. There were intervals of slow deposition within this time frame evidenced by low frequencies of pumice lapilli layers at various levels in the sequence. In these parts of the sequence the weathering development may have been slow under a cool and possibly dry climate.

4.11 Conclusions

The provenance of ash material within the sequence is almost entirely local, and represents continuous deposition of andesite ash and lapilli. If there is any redeposited material of ash grade within the sequence it is very locally derived volcanic loess blown from other parts of the ring plain. The input of material from outside of the local area such as regional loess deposition recorded in other parts of the southern North Island is very low. Although source areas proximal to the study area exist (< 10 km away), aerosolic quartz input into this sequence appears to have been diluted by an overwhelming component of rapidly accumulating locally derived ash and lapilli.

Weathering zones within the ash materials on the eastern Ruapehu ring plain are correlated to mild climate episodes during the Last Glacial, contemporaneous with periods of widespread soil development on loess throughout the southern North Island (Fig. 4.4; Leamy *et al*, 1973; Palmer, 1985; Alloway, *et al.*, 1988; Pillans, 1988). However, weathering features within the ash materials on the eastern Ruapehu ring plain are not only a function of the climate when the ash was accumulating, but are also strongly dependent on the accretion rate of the soil surface. Slow tephra accretion enhanced weathering features during the development of the soil on fine ash deposited during late $\delta^{18}O$ stage 3. Rapid tephra accretion during the development of the soil in fine ash deposited during early $\delta^{18}O$ stage 3 may have reduced the expression of weathering features and secondary minerals in the ash at this time.

The weathering minerals within this ash sequence appear to have been formed in two separate periods in the history of the ash sequence. This is deduced from the coexistence of halloysite in appreciable quantities (10-25% of bulk soil <2 mm) with allophane which has an Al/Si atomic ratio of >2:1. Allophane is present in small quantities according to estimates using the Parfitt and Wilson (1985) method. The sequence can be regarded as an aggrading sequence of Entisols and Andisols in which the rapid accretion of the soil surface is hindering further development of the soil. The allophane and ferrihydrite content of the ash material shows a distribution which has an inverse relationship with the accumulation rate indicated by quartz content, field observations of pumice lapilli frequency and weathering features. The allophane and ferrihydrite content is greatest where the accumulation rate of the ash appears lowest. This indicates that allophane and ferrihydrite in this sequence were formed from weathering andesitic glass when the ash material was at or near the surface. Subsequent, rapid burial of the ash and poor drainage conditions in the sequence probably hindered further formation of allophane as silica leached from the deposits above to decrease the Al/Si ratio in soil solution and thus prevent further allophane formation (Parfitt *et al.*, 1984; Singleton *et al.*, 1989).

Halloysite probably formed after the burial of the ash materials. As silica was leached down from tephra and diamictons above, the Al/Si ratio in the soil solution was decreased, and the formation of halloysite was promoted from weathering andesitic glass (Parfitt *et al.*, 1984; Singleton *et al.*, 1989). The peaks in concentration of halloysite within the ash profile may relate to where the drainage is impeded as water and silica move down the profile. The drainage impediment could be a textural change within the ash or a diamicton interbedded within the sequence. The highest contents of halloysite occur beneath a large cemented diamicton unit (Fig. 4.1), exemplifying this interpretation.

The now buried ash sequence represents a continuously accreting Entisol/Andisol. The weathering features and secondary minerals within the sequence are a function of a complex mix of accretion rate, late Quaternary climate change, and post-depositional weathering.

4.12 Acknowledgements

This work forms part of the Ph.D. research of Shane Cronin and we gratefully acknowledge funding from the New Zealand Vice Chancellors Committee, Massey University Graduate Research Fund, the Helen E. Akers Scholarship fund, and the Department of Soil Science of Massey University. J.S. Whitton is thanked for his help with mineral analyses, J.H. Kirkman and R.B. Stewart are thanked for their comments on an earlier version of the manuscript. We also wish to thank B.V. Alloway and R.L. Parfitt for their comprehensive reviews of the manuscript.

4.13 References

Alloway, B.V., Neall, V.E. and Vucetich, C.G., 1988. Localised loess deposits in north Taranaki, North Island, New Zealand. In: Loess - Its distribution geology and soils, Eden, D.N., and Furkert, R.J. (eds). A.A. Balkema Publishers, Rotterdam.

Alloway, B.V., Neall, V.E. and Vucetich, C.G., 1992a. Particle size analyses of Late Quaternary allophane-dominated andesitic deposits from New Zealand. Quat. Int., 13/14, 167-174.

Alloway, B.V., Stewart, R.B., Neall, V.E. and Vucetich, C.G., 1992b. Climate of the Last Glaciation in New Zealand, based on aerosolic quartz influx in an andesitic terrain. Quat. Res., 38, 170-179.

Alloway, B.V., McGlone, M.S., Neall, V.E. and Vucetich, C.G., 1992c. The role of Egmont-sourced tephra in evaluating the paleoclimatic correspondence between the bio- and soil-stratigraphic records of central Taranaki, New Zealand. Quat. Int., 13/14, 187-194.

Blakemore, L.C., Searle, P.L. and Daly, B.K., 1987. Methods for chemical analysis of soils. N. Z. Soil Bureau Scientific Rep., 80.

Childs, C.W., 1985. Towards understanding soil mineralogy. II Notes on ferrihydrite. N. Z. Soil Bureau Lab.Rep., CM7, DSIR, New Zealand.

Churchman, G.J., Whitton, J.S., Claridge, G.G.C. and Theng, B.K.G., 1984. Intercalation method using formamide for differentiating halloysite from kaolinite. Clays and Clay Min., 32, 241-248.

Cronin, S.J., Neall, V.E. and Palmer, A.S., 1996. The geological history of the north-eastern ring plain of Ruapehu Volcano, New Zealand. Quat. Int., 34-36: 21-28.

Fey, M, and Le Roux, J., 1977. Properties and quantitative estimation of poorly crystalline components in sesquoxidic soil clays. Clays and Clay Min., 25, 285-294.

Flint, R.V., 1960. Diamictite, a substitute term for symmictite. Geol. Soc. of America Bull., 71, 1809.

Froggatt, P.C. and Lowe, D.J., 1990. A review of late Quaternary silicic and some other tephra formations from New Zealand: their stratigraphy, nomenclature, distribution, volume, and age. N. Z. J. of Geol. and Geophys., 33, 89-109.

Hackett, W.R. and Houghton, B.F., 1989. A facies model for a Quaternary andesitic composite volcano: Ruapehu, New Zealand. Bull. Volcanol., 51, 51-68.

Henderson, J.H., Clayton, R.N., Jackson, M.L., Syers, J.K., Rex, R.W., Brown, J.L., and Sachs, I.B., 1972. Cristobalite and quartz isolation from soils and sediments by hydroflurosilicic acid treatment and heavy liquid separation. Soil Sci. Soc. America Proc., 36, No. 5, 830-835.

Kirkman, J.H., 1975. Clay mineralogy of some tephra beds of the Rotorua area, North Island, New Zealand. Clay Min., 10, 437-449.

Kirkman, J.H., 1981. Morphology and structure of halloysite in New Zealand tephras. Clays and Clay Min., 29, 1-9.

Kirkman, J.H., and McHardy, W.J., 1980. A comparative study of the morphology, chemical composition and weathering rhyolite and andesite glass. Clay Min., 15, 165-173.

Leamy, M.L., Milne, J.D.G., Pullar, W.A. and Bruce, J.G., 1973. Paleopedology and soil stratigraphy in the New Zealand Quaternary succession. N. Z. J. of Geol. and Geophys., 16, 723-744.

Lowe, D.J., 1986. Controls on the rates of weathering and clay mineral genesis in airfall tephras: a review and New Zealand case study. In: Colman, S.M., and Dethier, D.P. (eds) Rates of chemical weathering of rocks and minerals. Academic Press, Orlando, pp. 265-330.

Lowe, D.J. and Percival, H.J., 1993. Clay mineralogy of tephras and associated paleosols and soils, and hydrothermal deposits, North Island. Guide book for New Zealand pre-conference field trip F.1. 10th International Clay Conference, Adelaide, Australia.

McGlone, M.S. and Topping, W.W., 1977. Aranuian (post-glacial) pollen diagrams from the Tongariro region, New Zealand. N. Z. J. of Botany, 15, 749-760.

Milne, J.D.G. and Smalley, I.J., 1979. Loess deposits in the southern part of the North Island of New Zealand: an outline stratigraphy. Acta Geologica Academiae Scientarium Hungaricae, 22, 197-204.

Mizota, C., Toh, N. and Matsuhisa, Y., 1987. Origin of cristobalite in soils derived from volcanic ash in temperate and Tropical regions. Geoderma, 39, 323-330.

New Zealand Meteorological Service, 1973. Rainfall normals for New Zealand, 1941-1970. Misc. Publ., 145.

Palmer, A.S., 1985. The Last Interglacial record in Wairarapa Valley, New Zealand. In: Pillans, B.J. (ed). Proceedings of the second CLIMANZ conference 1985. Publication No.31 of Geology Department, Victoria University of Wellington, N.Z.

Parfitt, R.L. and Childs, C.W., 1988. Estimation of forms of Fe and Al: A review, and analysis of contrasting soils by dissolution and Moessbauer methods. Australian J. of Soil Res., 26, 121-144.

Parfitt, R.L. and Kimble, J.M., 1989. Conditions for formation of allophane in soils. Soil Sci. Soc. of America J., 53, 971-977.

Parfitt, R.L., Russell, M. and Orbell, G.E., 1983. Weathering sequence of soils from volcanic ash involving allophane and halloysite, New Zealand. Geoderma, 29, 41-57.

Parfitt, R.L., Saigusa, M. and Cowie, J.D., 1984. Allophane and halloysite formation in a volcanic ash bed under different moisture conditions. Soil Sci., 138, 360-364.

Parfitt, R.L., and Wilson, A.D., 1985. Estimation of allophane and halloysite in three sequences of volcanic soils, New Zealand. Catena Suppl. 7, 1-8.

Pillans, B.J., 1988. Loess chronology in Wanganui Basin, New Zealand. In: Loess - Its distribution geology and soils, Eden, D.N., and Furkert, R.J. (eds). A.A. Balkema Publishers, Rotterdam.

Pillans, B.J., 1994. Direct marine-terrestrial correlations, Wanganui Basin, New Zealand: the last 1 million years. Quat. Sci. Reviews, 13, 189-200.

Shackleton, N.J., Berger, A. and Peltier, W.R., 1990. An alternative astronomical calibration of the lower Pleistocene timescale based on ODP Site 677. Trans. Roy. Soc. of Edinburgh: Earth Sci., 81, 251-261.

Singleton, P.L., McLeod, M. and Percival, H.J., 1989. Allophane and halloysite content and soil solution silicon in soils from rhyolitic volcanic material, New Zealand. Australian J. of Soil Res., 27, 67-77.

Stevens, K.F., and Vucetich, G.C., 1985. Weathering of Upper Quaternary tephras in New Zealand. Part II Clay minerals. Chem. Geol., 53, 237-247.

Wada, K., 1977. Allophane and Imogolite. In: Minerals in Soil Environments, Dixon, J.B., and Weed, S.B. (eds), 603-638. Soil Sci. Soc. of America, Madison, Wisconsin.

Whitton, J.S. and Churchman, G.J., 1987. Standard methods for mineral analysis of soil survey samples for characterisation and classification in New Zealand Soil Bureau. N.Z. Soil Bureau Sci. Rep., 79.

Wilson, C.J.N., Switzur, R.V. and Ward, A.P., 1988. A new ^{14}C age for the Oruanui (Wairakei) eruption, New Zealand. Geol. Mag., 125, 297-300.

Wilson, C.J.N., Houghton, B.F., Lanphere, M.A. and Weaver, S.D., 1992. A new radiometric age estimate for the Rotoehu ash from Mayor Island volcano, New Zealand. N. Z. J. of Geol. and Geophys., 35, 371-374.

CHAPTER 5: THE LAHAR RECORD AND CONSTRUCTION OF THE NORTHEASTERN RUAPEHU AND EASTERN TONGARIRO RING PLAINS

5.1 Introduction

The NE Ruapehu and E Tongariro ring plains are composed of laharic, fluvial and glacial sediments as well as tephra and lava lithologies. However, the ring plains are volumetrically dominated by volcaniclastic diamictons deposited by lahars. Thus by dating and mapping these lahars, the timing and landform construction of much of the ring plain areas can be established. In addition, the timing of lahars can be used to assess the lahar hazard, which is contained in the following chapter.

The rhyolitic and andesitic tephra stratigraphy of Topping (1973), Donoghue *et al.*, (1995), and that established in Chapters 2 and 3 were used to date and map lahar deposits on the ring plain areas studied. Once the lahar deposits were dated and mapped, the distribution and timing of lahars in conjunction with information from the paleosol record developed in Chapter 4 was used to elucidate the construction of the ring plain areas studied. In this way a history of the timing of construction of various ring plain areas was established. In addition, the influence of climatic and volcanic events on the ring plain construction is explained.

This part of the study is in press within the New Zealand Journal of Geology and Geophysics, Vol. 40, No. 2 (1997). The contributions of the two authors to the study were as follows:

S.J. Cronin: Principal investigator
Carried out all: field descriptions and sampling
tephra and lahar correlation and mapping
preparation and writing of the manuscript

V.E. Neall: Adviser
Aided the study by: discussion of results and methodology
editing and discussion of the manuscript

5.2 A LATE QUATERNARY STRATIGRAPHIC FRAMEWORK FOR THE NORTHEASTERN RUAPEHU AND EASTERN TONGARIRO RING PLAINS, NEW ZEALAND

Shane J. Cronin and Vincent E. Neall
Department of Soil Science, Massey University, Private Bag 11 222, Palmerston North, New Zealand

New Zealand Journal of Geology and Geophysics 40, No. 2.

Abstract The northeastern Ruapehu and eastern Tongariro ring plains record a complex sequence of episodic lahar sedimentation. Using andesitic and rhyolitic tephrostratigraphy, fifteen lahar episodes are recognised in the northeastern Ruapehu ring-plain record ranging in age from >65 to 5 ka, and five in the Tongariro ring-plain record ranging in age from >23 to 14 ka. The most voluminous and widespread lahar deposition occurred during cool and stormy climatic periods equivalent in age to marine $\delta^{18}O$ stages 2 and 4. In these periods, accelerated physical weathering on the volcanoes supplied erosion debris, while large areas of snow and ice acted as sources of water to form lahars triggered by a variety of mechanisms. Lahar distribution after c. 22.5 ka was affected by two landform changes in the area at about this time. First, a large lava flow was emplaced along the boundary between Ruapehu and Tongariro ring plains shortly before 22.5 ka, effectively separating the two ring plains since. Second, Last Glacial moraines along the Whangaehu and Mangatoetoenui Rivers have blocked direct drainage from the Ruapehu summit region to a large sector of the northeastern ring plain, including the Upper Waikato Stream, formerly an important lahar path. These moraines have directed subsequent lahars (after c. 15 ka) along their current routes (active in 1995) in the Whangaehu and Mangatoetoenui catchments. Lahar deposition in the study area during this time is linked to large, explosive andesitic eruptions impacting on catchments where retreating glaciers provided water for lahar generation.

5.3 Keywords
Ruapehu volcano, ring plain, volcanic stratigraphy, lahars, Late Quaternary, paleoclimatic change.

5.4 Introduction

Ring-plain sediments of composite volcanoes provide a valuable record of past eruptive and sedimentary events that may not be preserved closer to source. The sedimentary record of the ring plain can often be dated precisely using interbedded tephras and radiometric techniques to provide a stratigraphic record of such events missing on the volcano. In the central North Island of New Zealand, coalescing ring plains of the eastern flanks of Tongariro and Ruapehu volcanoes are incised by numerous stream channels

that expose a detailed record of their ring-plain sediments and structure. A well-established rhyolitic tephra record from the North Island (Froggatt and Lowe, 1990) and the developing andesitic tephrochronology in the Tongariro Volcanic Centre (TgVC - Topping, 1973; Donoghue *et al.*, 1995; Cronin *et al.*, 1996(a)) provide a good chronological framework for the ring-plain deposits. The aim of this study was to elucidate the stratigraphy and construction of the northeastern Ruapehu and eastern Tongariro ring plains, based on detailed investigations of sections in streams draining the eastern flanks of the volcanoes.

5.5 Setting

Tongariro and Ruapehu are the two largest and most recently active volcanoes of TgVC (Gregg, 1960). Ruapehu is presently active. It is, the highest peak in the North Island at 2797 m, comprising a 110 km^3 composite cone with a ring plain of similar volume surrounding it (Hackett and Houghton, 1989). Tongariro volcano is a slightly smaller massif constructed from several coalescing volcanic cones, the largest of which is the recently active cone of Ngauruhoe (Mathews, 1967). Tongariro volcano is also surrounded by an extensive ring plain. The ring-plain deposits of these volcanoes are confined in the east by the Kaimanawa Mountains and extend down drainage channels to the north and south. Sections examined in this study are along streams indicated in Fig. 5.1.

5.6 Time control

Eighteen dated rhyolitic tephras erupted from Taupo Volcanic Zone calderas to the north are preserved within the TgVC ring-plain sediments (Topping and Kohn, 1973; Donoghue *et al.*, 1995; Cronin *et al.*, 1996(a)). The rhyolitic tephras are identified using combinations of their stratigraphic position, field appearance, mineralogy, and major element glass chemistry. In addition, dated andesitic tephras erupted from Tongariro and Ruapehu volcanoes provide valuable stratigraphic markers (Topping, 1973; Donoghue, *et al.*, 1995). They are identified using their characteristic field appearances, stratigraphic position and occasionally their mineralogy. The names and ages of marker tephras used in this study are listed in Table 5.1.

5.7 Terminology and identification of ring plain deposits

Ring-plain sediments range greatly in their nature and mode of deposition. At one end of the depositional series are well-bedded silts, sands, and gravels deposited by streamflow mechanisms. At the other end of the series are poorly sorted, matrix-supported units deposited by debris flow mechanisms. A whole range of deposits intermediate in character occur between these two extremes.

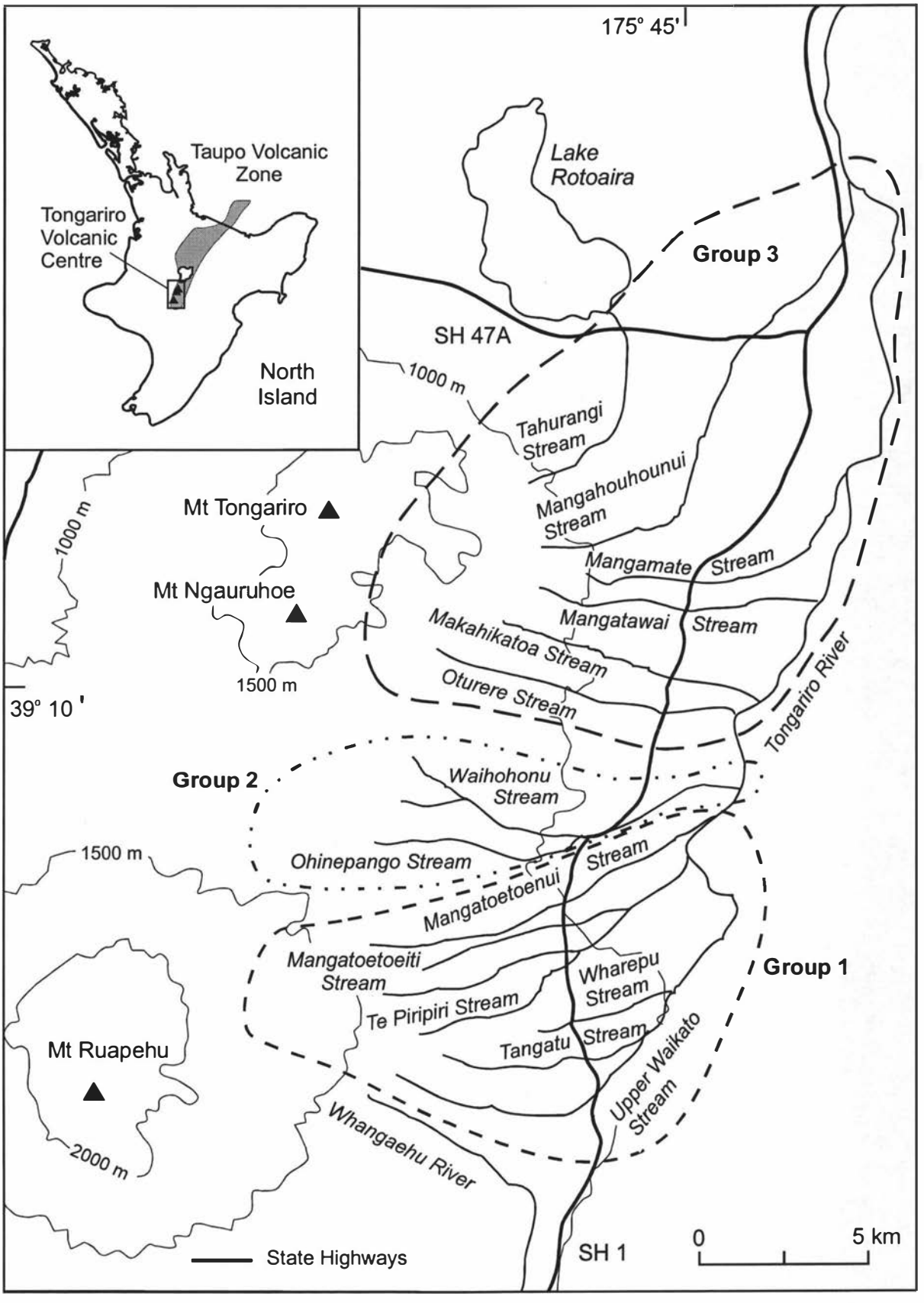

Figure 5.1 Location of Tongariro Volcanic Centre including Mts. Tongariro, Ngauruhoe and Ruapehu, and the streams dissecting the eastern Ruapehu and Tongariro ring plains. The streams are discussed in the text in three groups; labelled Groups 1, 2 and 3 on the map.

Table 5.1. Tephra coverbeds used in this study.

Tephra layers	Abbreviation	Source[a]	Age (ka)	Reference to age
Ngauruhoe Tephra	Ng	TgV	ca. 1.8-0[1]	Donoghue (1991)
Taupo Tephra (Unit Y)	Tp	TVC	1.85[2]	Froggatt and Lowe (1990)
Mangatawai Tephra	Mgt	TgV	2.5-1.85[2]	Donoghue (1991)
Waimahia Tephra (Unit S)	Wm	TVC	3.3[2]	Froggatt and Lowe (1990)
Hinemaiaia Tephra (Units I-R)	Hm	TVC	5.2-3.95[2]	Wilson (1993)
Motutere Tephra (Units G-H)	Mt	TVC	5.8-5.3[2]	"
Mangamate Tephra (Mm), Poutu Lapilli	Pt	TgV	ca. 9.7[1]	Topping (1973)
Mm, Wharepu Tephra	Wp	TgV	ca. 9.7[1]	"
Poronui Tephra (Unit C)	Po	TVC	9.81[2]	Froggatt and Lowe (1990)
Mm, Ohinepango Tephra	Oh	TgV	ca. 9.7[1]	Topping (1973)
Mm, Waihohonu Lapilli	Wa	TgV	ca. 9.7[1]	"
Mm, Oturere Lapilli	Ot	TgV	9.78[2]	"
Karapiti Tephra (Unit B)	Kp	TVC	10.1[2]	Wilson (1993)
Pahoka Tephra	Pk	TgV	ca. 10-9.8[1]	Topping (1973)
Bullot Formation (Bt), Pourahu Member	Ph	RV	ca. 10[1]	Donoghue (1991)
Waiohau Tephra	Wh	OVC	11.85[2]	Froggatt and Lowe (1990)
Rotorua Tephra	Rr	OVC	13.08[2]	"
Rotoaira Tephra	Ra	TgV	13.8[2]	Topping (1973)
Rerewhakaaitu Tephra	Rk	OVC	14.7[2]	Froggatt and Lowe (1990)
Kawakawa Tephra	Kk	TVC	22.59[2]	Wilson *et al.*, (1988)
Okaia Tephra	Ok	TVC	ca. 23[1]	Froggatt and Lowe (1990)
Omataroa Tephra	Om	OVC	28.22[2]	"
Hauparu Tephra	Hu	OVC	35.87[2]	"
Rotoehu Ash	Re	OVC	64[3]	Wilson *et al.*, (1992)

[a] TgV = Tongariro volcano, RV = Ruapehu volcano, TVC = Taupo Volcanic Centre, OVC = Okataina Volcanic Centre.
[1] Estimated ages.
[2] Average or single ^{14}C ages on old (Libby) half life basis.
[3] Whole rock K-Ar age.

We use the Smith and Fritz (1989) definition of the term "lahar" in this study as: "a rapidly flowing mixture of rock debris and water (other than normal streamflow) from a volcano". This definition encompasses volcano-derived hyperconcentrated streamflows and debris flows. The definition is restricted to the process and does not include the deposit. The use of the terms "debris flow" and "hyperconcentrated" streamflow follow that of Smith

(1986), Pierson and Costa (1987), and Scott (1988). Table 5.2 outlines the characteristic features of the sediments within the ring-plain sequence, and relates their observed lithologies and sedimentary features to their interpreted emplacement mechanisms.

Table 5.2. Sedimentary features of ring plain deposits and their inferred mode of deposition.

Sediment type	Observed features	Inferred mode of deposition (after Smith, 1986)
Bedded sands, silts and gravels	-Variable grainsize, silt, sand and gravels in layers and lenses -Individual layers and lenses well sorted -Strong development of dominantly wavy and cross bedding -Clast supported -Maximum clast diameter 0.2 m	Normal streamflow
Horizontally/planar bedded sands	-Grain size dominantly med-coarse sand, supporting common pebbles and rare cobbles -boulders -Poorly sorted -Clast supported -Horizontal bedding discontinuous but overall planar or horizontal fabric -Larger clasts often in pebble or cobble "strings" -Maximum clast diameter 1 m	Hyperconcentrated streamflow
Sandy-matrix massive diamictons	-Very poorly sorted -Matrix supported -Matrix dominantly med-coarse sand -unbedded, mostly ungraded and occasionally normally graded -Maximum clast diameter 1-3 m	Debris flow
Silty-matrix massive diamictons	-Features as above except matrix dominated by silt and clay -can contain hydrothermally altered pumice and lithic clasts -ungraded, and normally graded	Debris flow

5.8 Present channel geography

A large number of sections were examined in several streams. Measured sections at different locations along the length of each stream (e.g. Mangatoetoenui Stream Fig. 5.2) were compared and correlated to obtain a composite stratigraphic column for each stream (Fig. 5.3, 5.5 and 5.6). The streams can be split into three catchment groups. Group 1 comprises Upper Waikato, Tangatu, Wharepu, Te Piripiri, Mangatoetoeiti and Mangatoetoenui Streams (Fig. 5.1) which drain the northeastern flanks of Ruapehu volcano. Ohinepango and Waihohonu Streams form Group 2 which drain a sector of northeastern Ruapehu volcano as well as the southeastern sector of Tongariro volcano. Group 3 comprises Oturere, Makahikatoa, Mangatawai, Mangamate, Mangahouhounui,

and Tauhurangi Streams which drain the eastern and northeastern flanks of Tongariro volcano. The three stream catchment groups receive lahars from different source areas and potentially provide different sets of information about the sources, timing, and distribution of lahar events on the eastern flanks of the two volcanoes.

5.9 Group 1 - Northeastern Ruapehu streams (Fig. 5.3)

A clear boundary exists between drainage from the northeastern and southeastern flanks of Ruapehu. To the southeast a large active fan of Holocene laharic and stream sediments has been formed by the Whangaehu River (Palmer *et al.*, 1993). The fan sediments have been deposited by lahar events that are channelled down the upper part of Whangaehu River and avulse their courses on the relatively unconfined lower ring plain (Palmer *et al.*, 1993). This route has been the major path for Ruapehu lahars in historic times (e.g., 1953, 1969, and 1975; Gregg, 1960; Nairn *et al.*, 1979), including 1995.

All drainage channels north of the Whangaehu River drain northeast into the Tongariro River. There is no historical evidence of lahars overflowing northward from the Whangaehu fan into the Tongariro. However, restricted lahar deposits younger than c. 2 ka are present in the upper portions of the Upper Waikato Stream, and are thought to originate from the Whangaehu catchment (Donoghue, 1991). This suggests that some lahars may have overflowed into the Upper Waikato Stream in the recent geologic past.

Of the northeastern Ruapehu streams, the Mangatoetoenui is the only channel to have an historic record of lahars (Nairn *et al.*, 1979), including at least one lahar in the 1995 eruptive sequence.

A correlation diagram for the sequences in the six main drainage channels from northeastern Ruapehu is presented in Fig. 5.3. Fifteen episodes of lahar deposition are recognised and numbered consecutively R01-R15 from youngest to oldest. These episodes are recognised by debris flow and hyperconcentrated streamflow deposits, each episode containing a single lahar or series of lahars within a short time interval. The stratigraphic ages of the diamicton packages are determined from their tephra interbeds (Fig. 5.4).

Upper Waikato and Tangatu Streams contain the longest stratigraphic records, although Tangatu Stream sections show evidence of extensive coverbed stripping and erosional unconformities. The surfaces around Tangatu Stream do not appear to have stabilised until immediately before the eruption of the Hinemaiaia Tephra, c. 5 ka B.P.

In Upper Waikato Stream, the oldest and also the thickest diamicton sequence recorded is R15, which comprises the deposits of several lahars. Rotoehu Ash (c. 64 ka) occurs as glass shards scattered throughout fine andesitic ash overlying lahar deposits of episode R14, thus providing a minimum age for R14 and R15. R13 comprises the deposit of a single lahar whilst R12 contains deposits of two. Andesitic pumice lapilli are abundant within both R12 and R13 and as a pinching shower-bedded tephra between them. R11 consists of a complicated collection of deposits of numerous lahars.

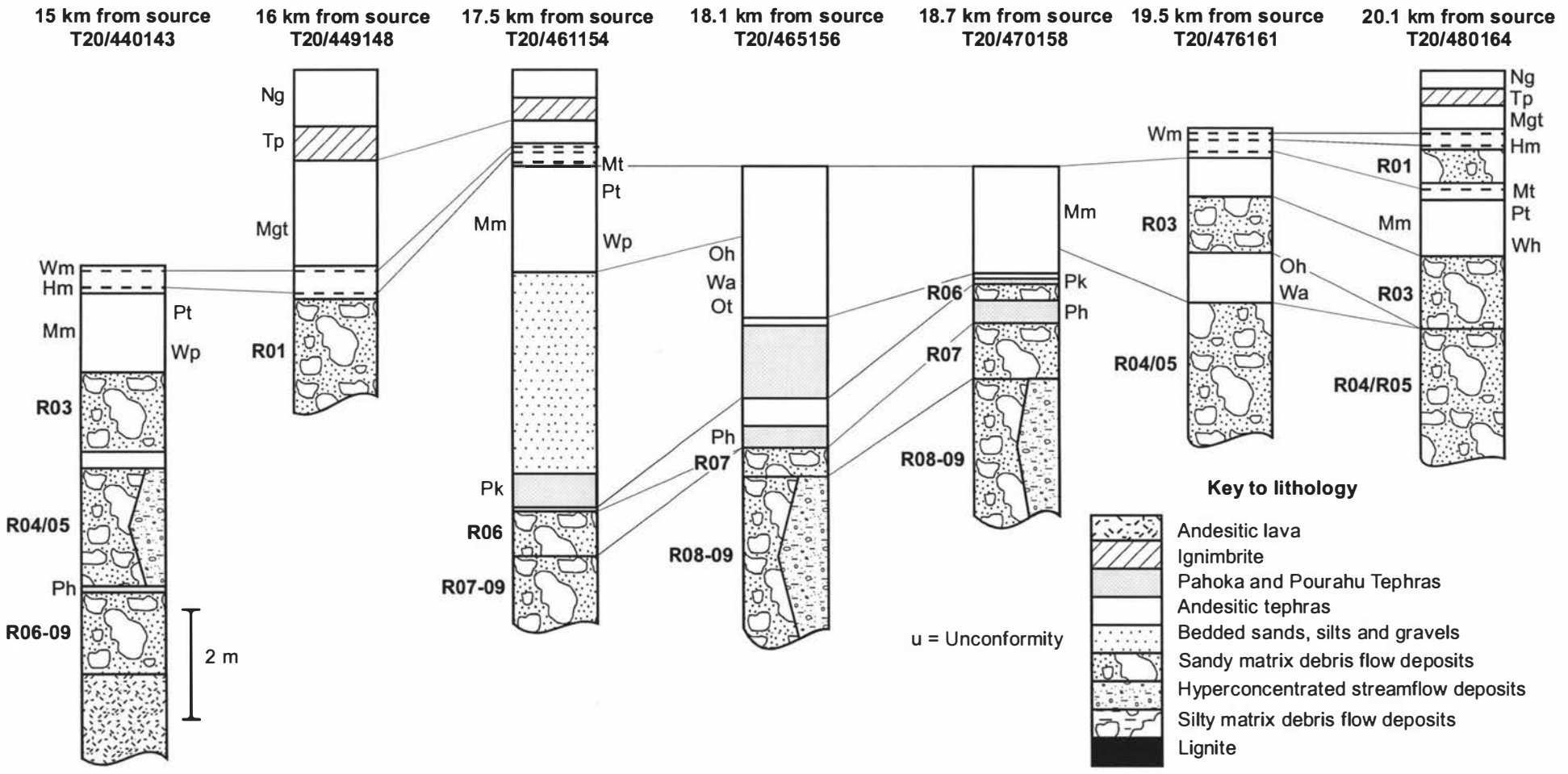

Figure 5.2 A Sequence of selected measured sections in the direction of stream flow in the Mangatoetoenui Stream. These sections and others were used to produce the composite section shown in Fig. 5.3.

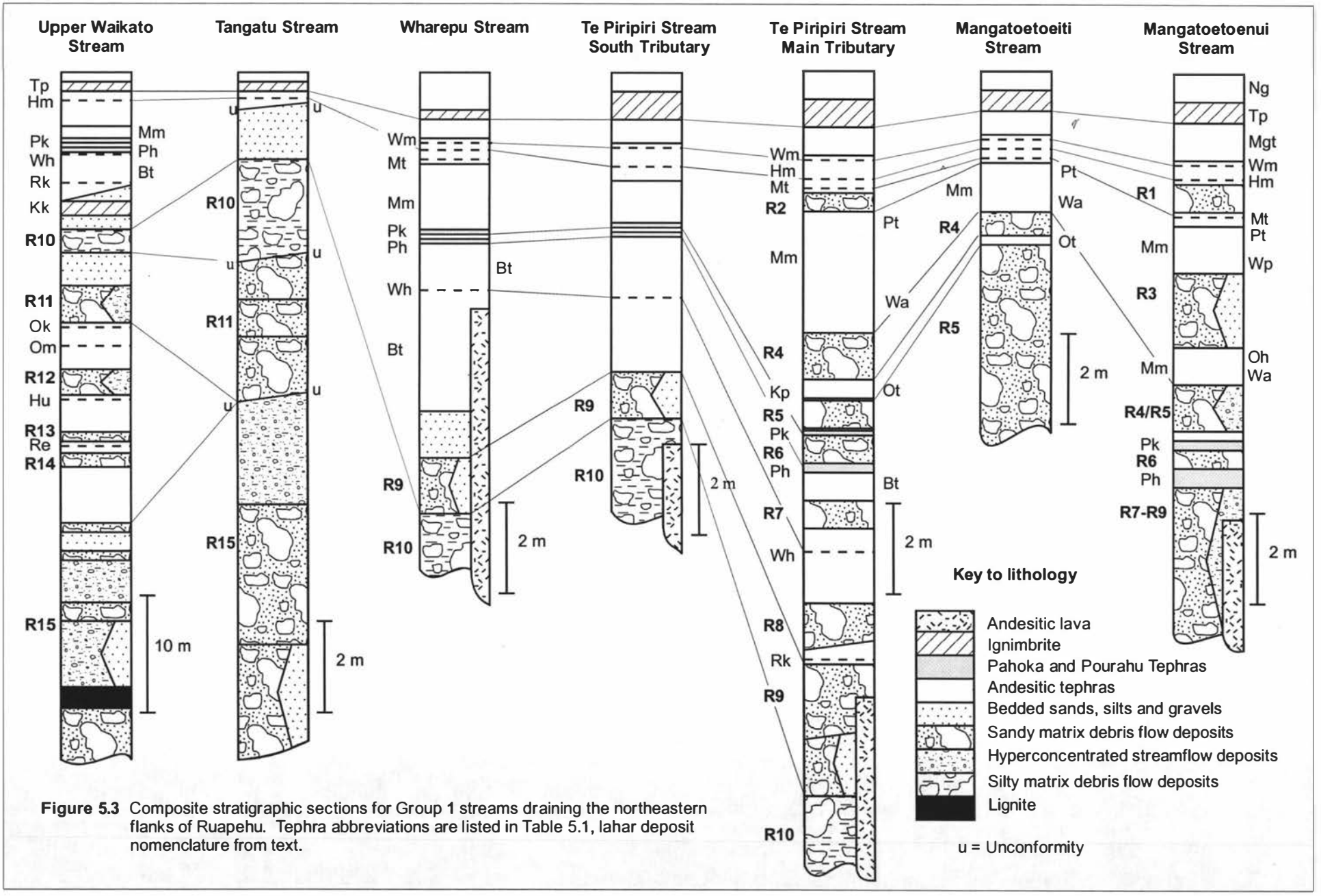

Figure 5.3 Composite stratigraphic sections for Group 1 streams draining the northeastern flanks of Ruapehu. Tephra abbreviations are listed in Table 5.1, lahar deposit nomenclature from text.

Other than in the Upper Waikato and Tangatu Streams, lahar deposits of episodes older than R10 are only well preserved along the Desert Road Fault scarp beside the Whangaehu River.

The youngest lahar deposit in the Upper Waikato Stream sequence is from the R10 episode. This is part of an overall aggradation package of sediments deposited during the Last Glacial Maximum. The R10 deposit is a lithologically distinctive unit. It has a yellowish brown to brown silt and clay-rich matrix which supports pebbles to large boulders. These clasts are subangular to angular, multi-coloured and multi-lithologic, including abundant, red, yellow and white, hydrothermally altered soft clasts. In many places this deposit comprises two or three flow units separated by thin (5 mm) clay laminae. The uppermost flow unit exhibits crude normal grading with large boulders concentrated at the base. The lower one or two flow units are finer grained and ungraded. Unit R10 is generally the lowest unit exposed in the streams north of Tangatu Stream.

The stream sections between Tangatu and Mangatoetoenui Streams collectively record nine episodes of lahar deposition younger than R10. Wharepu Stream and small surrounding streams, including the southern tributary of the Te Piripiri, all record essentially the same sequence, R10 and R09. The R09 sequence comprises the deposits of several lahars below the Rerewhakaaitu Tephra. The main Te Piripiri Stream channel records the southernmost occurrence of six lahar deposits younger than R09. These six units (R08, R07, R06, R05, R04 and R02) are all deposits of single lahars and are well constrained in age by enclosing tephra layers (Fig. 5.4). Units R04 and R05 are correlated to the fragmentary sequence within Managatoetoeiti Stream and R04-R09 can be traced into Mangatoetoenui Stream sections. In the latter sequence, two further lahar deposits are preserved; R03, together with the youngest recorded episode R01 (5.2-5.3 ka).

5.10 Group 2 - Streams draining both volcanoes (Fig. 5.5)

The Ohinepango and Waihohonu Streams drain the area between the Tongariro and Ruapehu massifs and have the potential to receive sediment from both volcanoes. The records in these streams are complicated by the presence of a large lava flow and its associated autobreccia deposits. The composite stream section for Ohinepango Stream (Fig. 5.5) shows a sequence of lahar deposits, which can be correlated to units in the neighbouring Mangatoetoenui Stream. Most notably, the distinctive R10 debris flow deposit is present below the Kawakawa Formation and the lava flow. Sections showing the stratigraphic relationships between the lava flow and Kawakawa Formation occur in the adjacent Waihohonu Stream. The age of the lava flow is well constrained between R10 (and the underlying Okaia Tephra) and the Kawakawa Formation, i.e. between c. 23 ka and 22.6 ka B.P. The Ohinepango Stream sections also record R11, R07, R06, and R04 lahar deposits (Fig. 5.4). The Waihohonu Stream has a much larger proportion of its headwaters on the slopes of Tongariro volcano. Here there are more fluvial deposits

throughout the sequence, as well as three lahar deposits which are equivalent in age to R09, R07 and R06 (Fig. 5.4).

Figure 5.4 Stratigraphy of lahar deposition episodes on the north-eastern Ruapehu and eastern Tongariro ring plains.

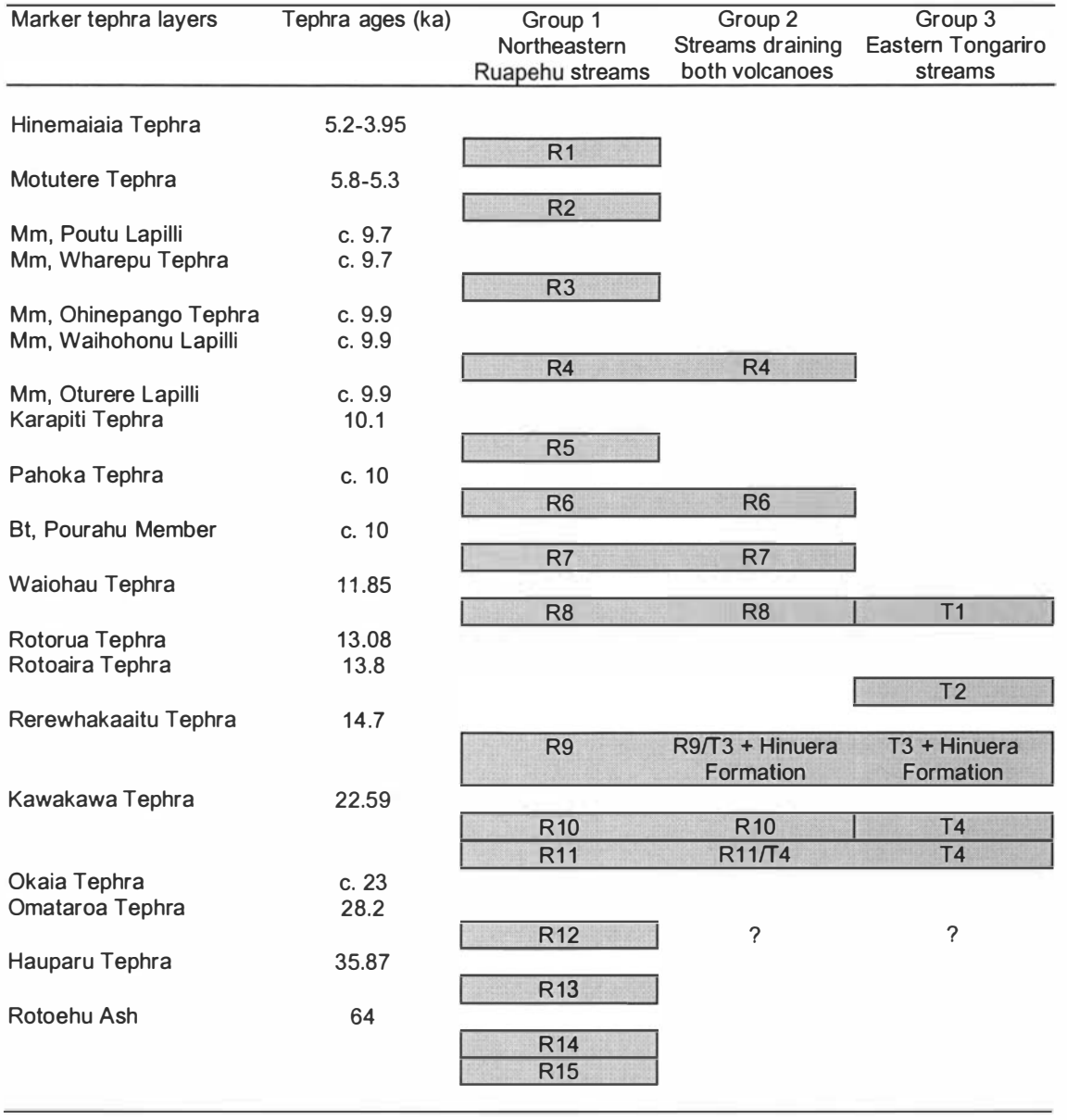

5.11 Group 3 - Eastern and northeastern Tongariro streams (Fig. 5.6)

Five lahar deposition episodes are recognised in the stream sequences from Oturere to Tahurangi Streams. These are mostly well constrained in age although more unconformities are present in the sequences (Fig. 5.4, 5.6). The oldest deposition episode (T5) consists of two lahar deposits interbedded with fluvial deposits.

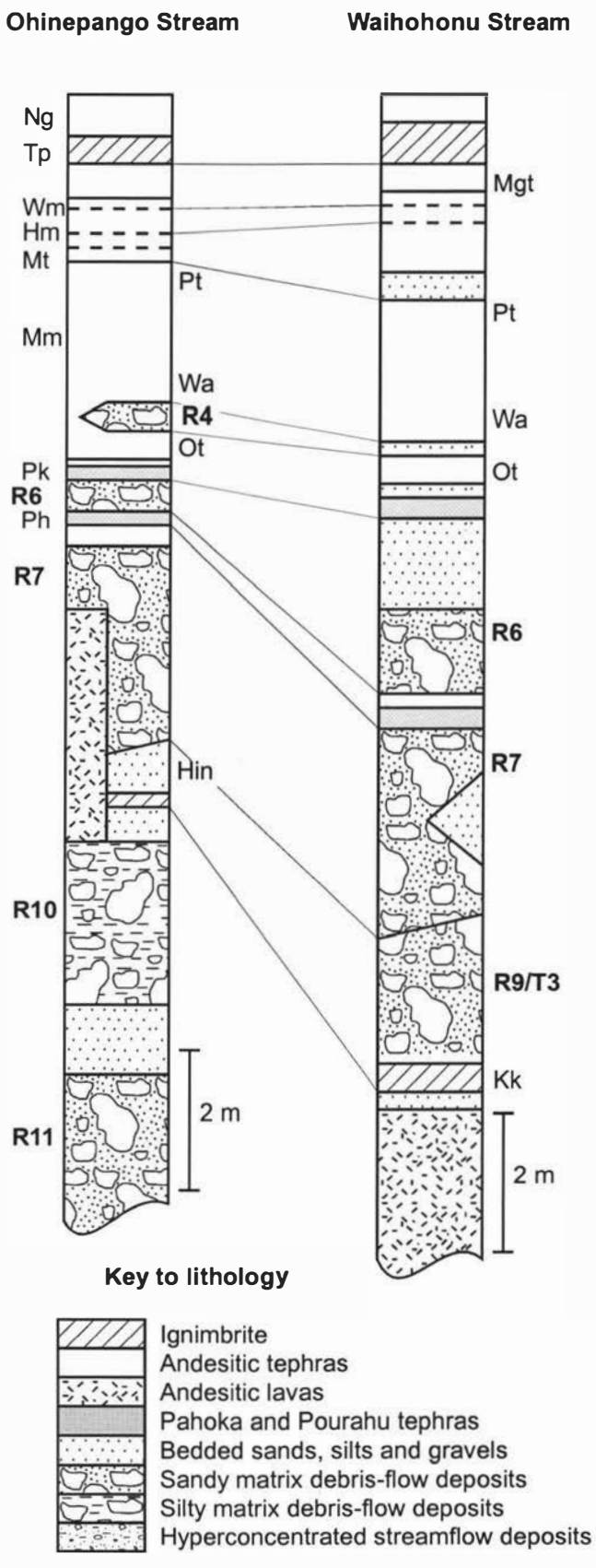

Figure 5.5 Composite stratigraphic sections for Group 2 streams draining the northeastern flanks of Ruapehu and southeastern flanks of Tongariro. Tephra abbreviations are listed in Table 5.1, lahar deposit nomenclature from text.

T5 is preserved beneath a presently unidentified rhyolitic tephra, which is also below an unconformity in the Mangatawai Stream sequence; hence the ages of the T5 units are not well constrained. T4, which commonly consists of several lahar deposits, occurs directly below the Kawakawa Formation, roughly equivalent in age to R10 and R11. Unit T3 comprises lahar deposits that are laterally equivalent to Hinuera Formation fluvial sediments, that are commonly found within the Tongariro streams and are equivalent in age to R09. T2 consists of a distinctive, bright yellow silty matrix debris flow deposit which contains dominantly pebble-sized pumice supported within the matrix and is only recognised in the Oturere, Makahikatoa and Mangatawai Streams. No evidence of lahars equivalent in age to the younger episodes in the Ruapehu streams is recognised in the Tongariro streams; the youngest deposit T1 is equivalent in age to R8 (11.85-13.08 ka B.P.).

5.12 Lahar distribution on the eastern ring-plain sectors from 23 ka to the present

The areal distribution of each episode of lahar deposition has been mapped from the stream sections and supplementary field data (Fig. 5.7-5.9). The distribution of the oldest units (R12-R15, and T5) cannot be mapped because only a few deep sections expose these units.

Lahar units of the two oldest mappable episodes have the largest distribution. R11 and T4 lahar deposits are found over the entire northeastern Ruapehu and eastern Tongariro ring plains (Fig. 5.7A). This indicates that active lahar sedimentation was occurring over the entire eastern ring plains before the eruption of the Kawakawa Formation during the early part of the Last Glacial Maximum. Streamflow deposition was also occurring over large areas of the ring plains during this time. R10 lahar deposits, however, were derived solely from the northeastern flanks of Ruapehu (Fig. 5.7B), and are lithologically distinct from the contemporaneous R11 and T4 lahars.

In the period following the Kawakawa eruption and before the Rerewhakaaitu eruption (i.e. the latter part of the Last Glacial Maximum) much of the area continued to be inundated by lahar and fluvial deposits. Contemporaneous lahar episodes occurred from northeastern Ruapehu sources (R09) and eastern Tongariro sources (T3), coupled with stream sedimentation and reworking of Kawakawa Formation to form Hinuera Formation deposits. In the same time interval, formation of two major landscape features had a major effect on subsequent lahar distribution. The first was a large lava flow which was emplaced between the present Waihohonu and Oturere Streams (Fig 5.7C) immediately before the eruption of the Kawakawa Tephra. This extensive lava flow served as a divide, effectively isolating lahars with a source in the northeastern Ruapehu and eastern Tongariro catchments. The second landscape feature was deposition of a series of glacial moraines along the Whangaehu and Mangatoetoenui Streams (Fig 5.7C). These moraines blocked the direct drainage from the eastern Ruapehu flanks to a sector of the northeastern Ruapehu ring plain between the present Upper Waikato Stream to the southern tributary of Te Piripiri Stream.

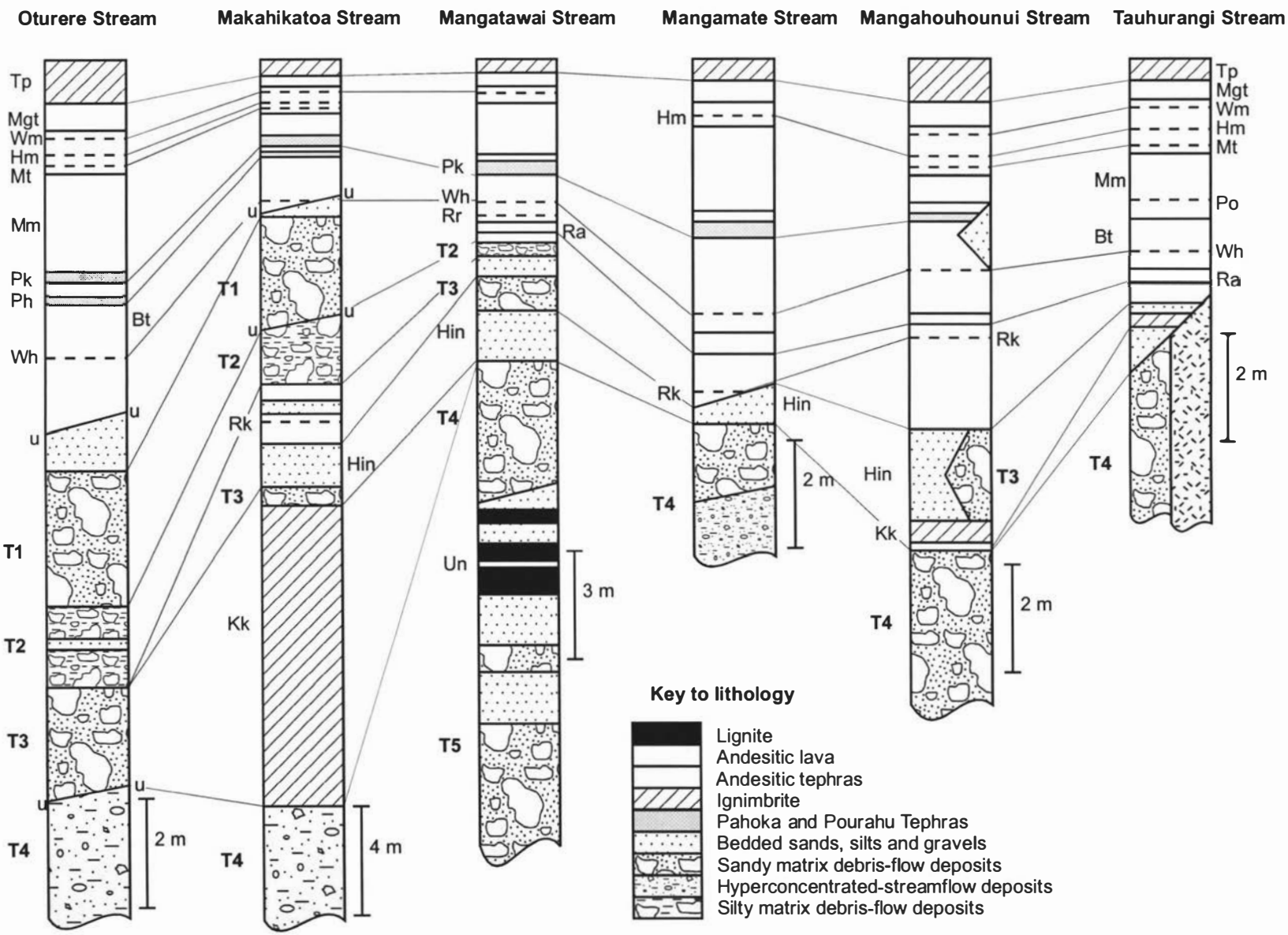

Figure 5.6 Composite stratigraphic sections for Group 3 streams draining the eastern flanks of Tongariro. Tephra abbreviations listed in Table 5.1, lahar deposit nomenclature from text.

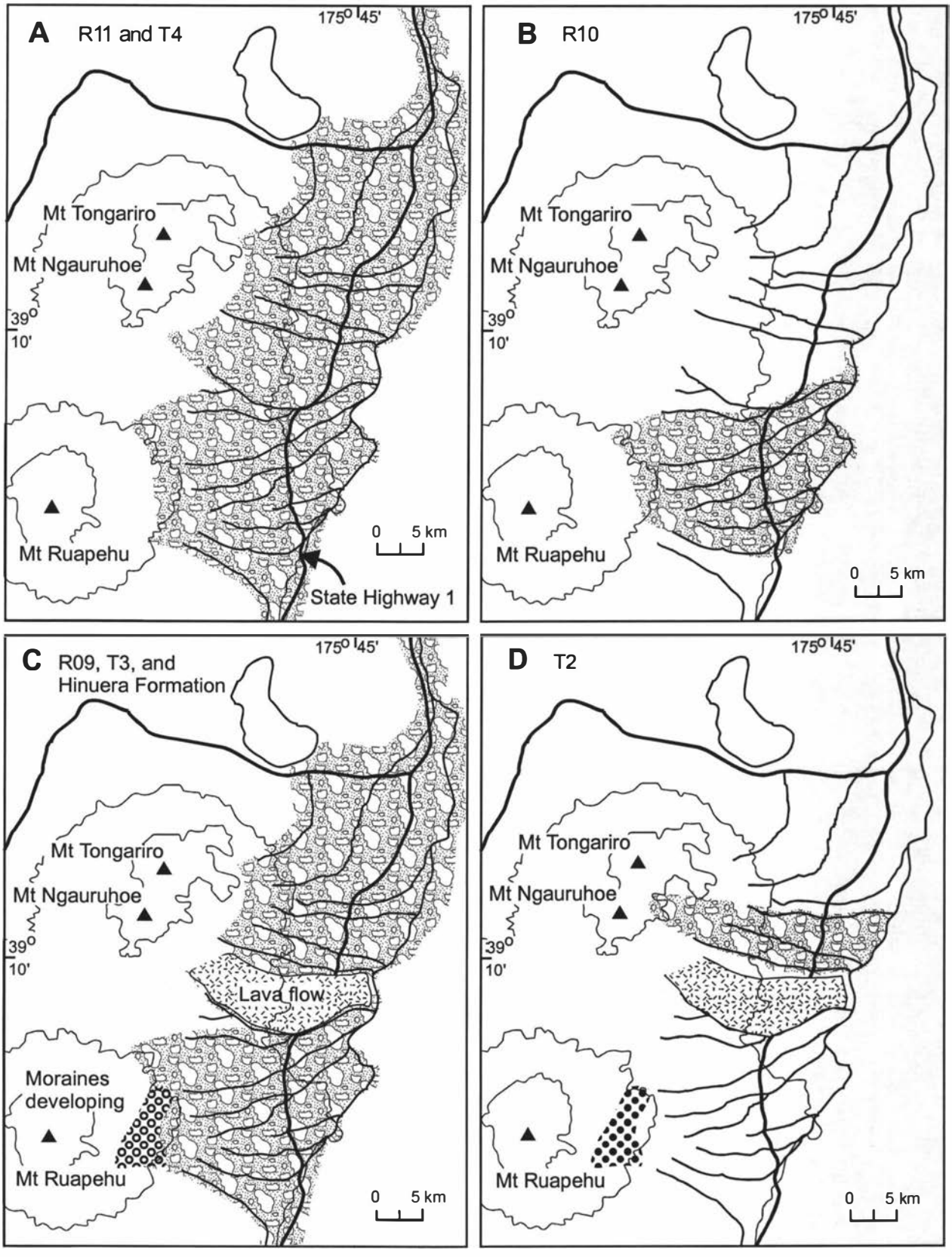

Figure 5.7 Distribution of deposits from lahar episodes: (A) R11/T4, (B) R10, (C) R09/T3 and the Hinuera Formation, (D) T2. Ages of the deposition episodes are given in Fig. 5.4.

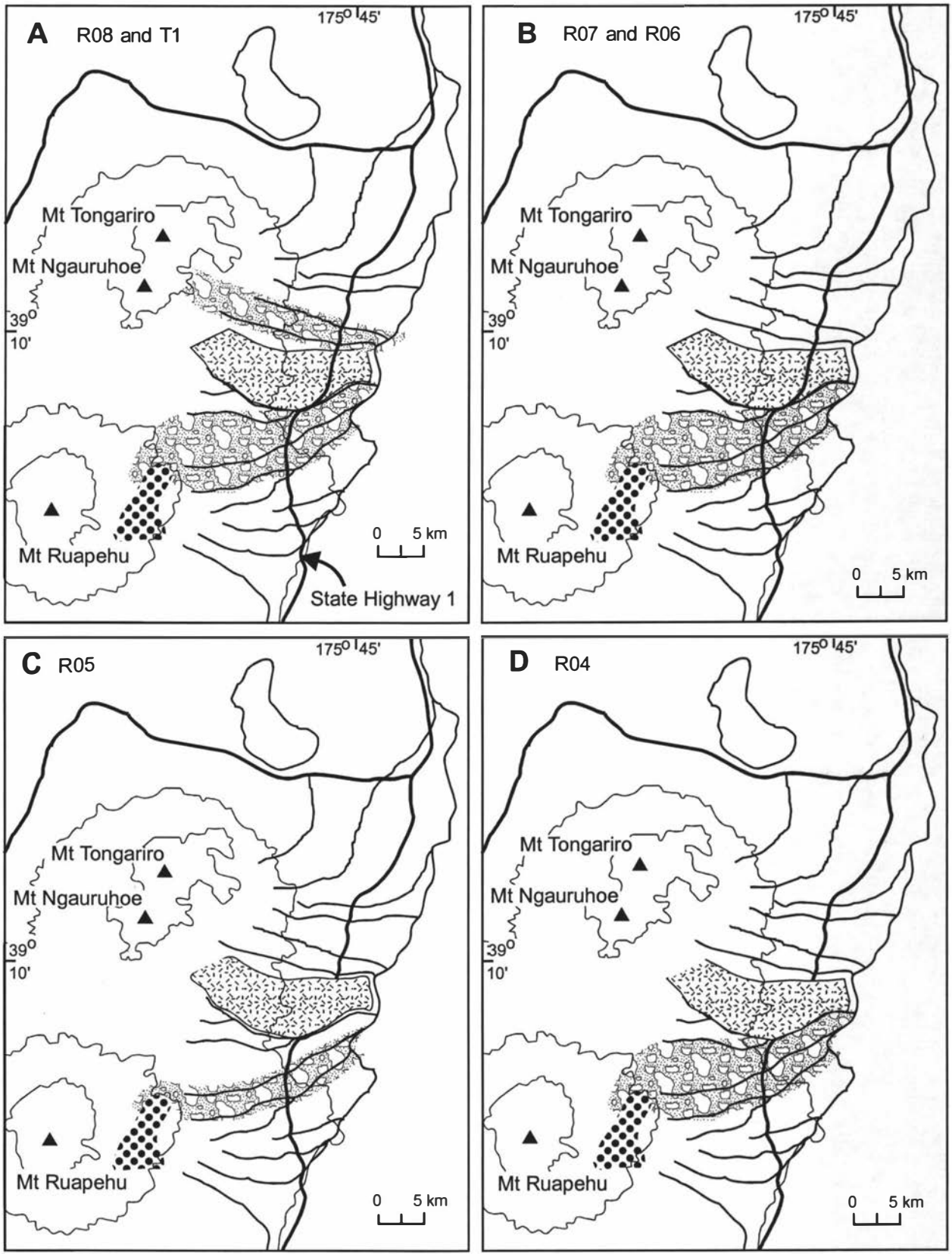

Figure 5.8 Distribution of deposits from lahar episodes: (A) R08/T1, (B) R07 and R06, (C) R05, (D) R04. Ages of deposition episodes given in Fig. 5.4.

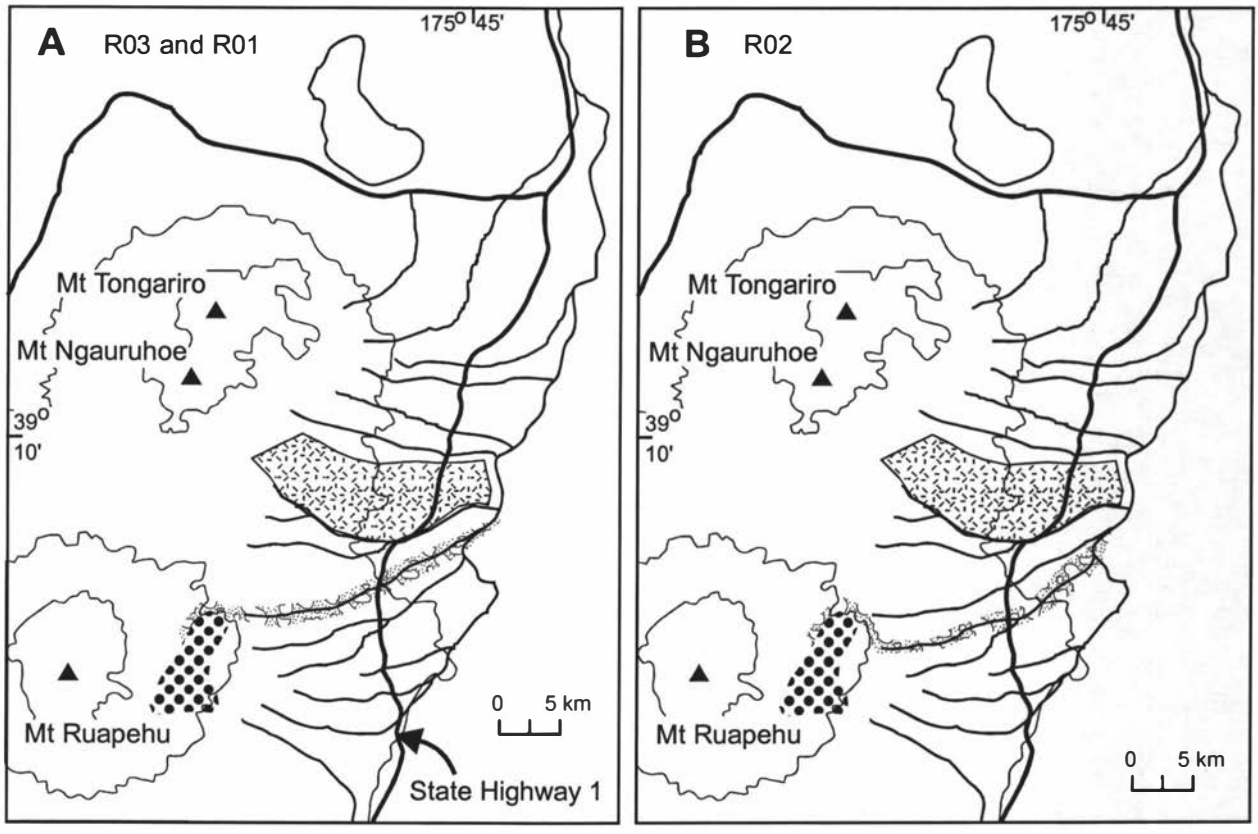

Figure 5.9 Distribution of deposits from lahar episodes; (A) R03 and R01 and (B) R02; ages of episodes are given in Fig. 5.4.

With the exception of small overflows from the Whangaehu catchment, there have been no lahars in this ring plain sector since. Lahars generated on the eastern Ruapehu flanks since the formation of the moraine ridges have been directed to the southeast into the Whangaehu (Donoghue 1991) or to the northeast, dominantly into the Mangatoetoenui catchment.

All of the lahars after the R09/T3 depositional episode were distributed over much narrower sectors of the ring plains. Their distribution was partially controlled by the lava flow and moraines as previously discussed, together with deepening of drainage channels following the Last Glacial Maximum. T2 episode lahars were distributed only within the Oturere-Mangatawai Stream sector of the Tongariro ring plain (Fig. 5.7D). The youngest lahar episode on the eastern Tongariro ring plain, T1, occurred within the same time range as R08 on the northeastern Ruapehu ring plain. The deposits of these two episodes are confined to areas on either side of the large lava flow between Waihohonu and Oturere Streams (Fig. 5.8A). The distribution of R08 lahars is typical of many of the subsequent deposition episodes on the northeastern Ruapehu ring plain. R07, R06 and R04 lahars all covered the same sector between Waihohonu Stream and the northern tributary of Te Piripiri Stream (Fig. 5.8B, 5.8D). R05 lahar deposits have a narrower distribution within this zone, between the northern tributary of Te Piripiri Stream and Mangatoetoenui Stream (Fig. 5.8C). The three youngest lahar events occurred within the same ring plain sector but were confined to single stream channels - R02 along the northern Te Piripiri Stream tributary, and R03 and R01 within Mangatoetoenui Stream (Fig. 5.9A, 5.9B). The youngest lahar to cross the northeastern Ruapehu ring plain was generated on 28 October 1995, and flowed down Mangatoetoenui Stream channel to the Tongariro River (i.e. similar to the path in Fig. 5.9A).

5.13 Source and generation of lahars

A framework for the eruptive activity of Tongariro and Ruapehu volcanoes in the period during which these lahars were generated is contained in Table 5.3. The oldest lahar deposition episode, R15, consists of a thick sequence of debris flow and hyperconcentrated streamflow deposits interbedded with gravelly fluvial sediments derived from Ruapehu volcano. A moderate frequency of large-scale eruptions during this time is reflected by a few layers of andesitic pumice lapilli preserved between the fluvial beds of the sequence. However, very little pumice is found within the lahar and fluvial sediments themselves. In addition, no paleosols are preserved and there is no evidence for major unconformities. These deposits thus appear to represent a period of intermittent volcanic activity with continuous syn- and post-eruptive aggradation on the eastern sector of the Ruapehu ring plain. A lignite deposit within these sediments (Fig. 5.3) contains a grassland and shrubland palynoflora (M.S. McGlone 1995, *pers. comm.*). Above these deposits is a paleosol with the Rotoehu Ash preserved near its base. This enables correlation of the R15 sequence to a widespread period of river aggradation and loess deposition in the lower North Island during the cool climate of marine δ^{18} O Stage **4**

(Milne and Smalley, 1979; Pillans, 1988; Cronin *et al.*, 1996(b)). During this period the climate in the region is interpreted from previous palynofloral studies (McGlone and Topping, 1983) as having been cool and stormy, with episodes of erosion and widespread cover-bed stripping. The harsher climate would have accelerated physical weathering processes on the volcanoes and thereby provided a ready source of loose sediment on the cone supplementing that produced by eruptions.

Table 5.3 Summary of the eruptive activity of Ruapehu and Tongariro volcanoes for the last 75 ka based on the ring plain tephra record (Topping, 1973; Donoghue *et al.*, 1995; Cronin *et al.*, 1996(a)).

Time period (ka B.P.)	Tongariro volcano	Ruapehu volcano	Mapping units
0 - 1.85	frequent, low volume and low magnitude eruptions	frequent (1 per 100 years), low volume and low magnitude eruptions	Tufa Trig and Ngauruhoe Formations
1.8 - 2.5	frequent, low volume and low magnitude eruptions	infrequent, low volume and low magnitude eruptions	Mangatawai Tephra
2.5 - 9.7	frequent, low volume and low magnitude eruptions	infrequent, low volume and low magnitude eruptions	Papakai Formation
9.7 - 10	very frequent (1 per < 50 years), large volume and large magnitude eruptions		Mangamate Tephra and Pahoka Tephra
c. 10		1 large volume and large magnitude eruption	Okupata Tephra
c. 10		1 large volume and large magnitude eruption including a pyroclastic flow	Pourahu Member of Bullot Formation
c. 10 - 22.5	1 large volume and large magnitude eruption	moderately frequent (1 per 500 years), large volume and large magnitude eruptions	Bullot Formation and Rotoaira Lapilli
22.5 - 35.8		moderate-low frequency (1 per 800 years), large volume and large magnitude eruptions.	Unnamed
35.8 - 64		very low frequency (1 per 7 ka), large volume and large magnitude eruptions and frequent low volume and low magnitude eruptions.	Unnamed
64 - c. 75		moderately frequent (1 per 600 years), large volume and large magnitude eruptions and frequent low volume and low magnitude eruptions.	Unnamed

Redeposition of this loose material then appears to have taken place by lahars or normal streamflow. These were probably triggered by a number of different mechanisms, such as storms, slope failures, avalanches, glacial collapse and eruptive events. A greater volume of ice and snow on the upper volcano during this cool period may have provided an additional water source for lahar formation. Scouring and melting of glacier ice and snow has been an important mechanism in the formation of lahars in many historical eruptions (Major and Newhall, 1989; Pierson *et al.*, 1990; Waitt *et al.*, 1994). In addition, at the beginning of the 1995 Ruapehu eruptive sequence, augmentation of lahar volumes by eroded snow from the summit glaciers was an important process (Cronin *et al.*, in press).

Deposits of the next three lahar episodes R14, R13 and R12 are interbedded within thick andesitic tephra deposits from infrequent but large-scale eruptions of

Ruapehu (Table 5.3), and also contain pumice lapilli within their matrices. R12 deposits in particular contain a 0.2 m-thick andesitic pumice lapilli layer interbedded between debris flow units. R13 and R14 comprise the deposits of single lahar events. All three episodes appear to have accompanied, and were probably caused by sub-plinian tephra eruptions at Ruapehu. The age of these deposits ranges from c. 65-35 ka, during a period of relatively mild and settled climate in the Tongariro region (McGlone and Topping, 1983).

R11 and its stratigraphic equivalent on the Tongariro ring plain, T4, were then deposited before the eruption of the Kawakawa Formation (before 22.6 ka B.P., Wilson *et al.*, 1988). These deposits are thick continuous sequences of debris flow, hyperconcentrated streamflow, and coarse fluvial deposits with occasional andesitic lapilli layers interbedded in the R11 deposits. They are widespread over all the examined sectors of both ring plains and indicate that abundant sediment was available on the volcanoes at this time for redeposition. The mechanisms of deposition of these units were likely to be the same as for the R15 lahar deposition episode. The frequency of large-scale eruptions in the interval when R11 and T4 were deposited was moderate-low (Table 5.3). However, this interval was the beginning of the greatest period of environmental destabilisation in the North Island of New Zealand (marine δ^{18} O stage 2, or the Last Glacial Maximum - 23-13 ka) over the last c. 120 ka (Pillans *et al.*, 1993).

R10 is the deposit of a single event or a closely spaced series of lahar pulses within the same time period as R11 and T4. However, this unit is lithologically distinct from them. It has a clay-rich silty matrix and hydrothermally altered clasts, indicating that it has been derived from a collapse of a hydrothermally altered section of the former Ruapehu cone.

The R09/T3 lahar deposition episode represents lahar aggradation during the Last Glacial Maximum (marine δ^{18}O stage 2) after the Kawakawa eruption. It is coeval with deposits of redeposited Kawakawa ignimbrite mixed with andesitic sand and gravels, which have been previously mapped as Hinuera Formation in the northern sector of Tongariro ring plain (Topping and Kohn, 1973). R09/T3 deposits are also widespread over much of the ring plain examined. They appear to have ceased accumulating immediately before the eruption of the Rerewhakaaitu Tephra. This is coincident with climatic conditions beginning to ameliorate in the Tongariro region (McGlone and Topping, 1977). The frequency of large scale eruptions during this period was moderate (Table 5.3), although this activity continued after widespread lahar deposition had ceased.

Deposits of the subsequent lahar episodes are distributed over much narrower sectors of the two ring plains. This is a result of both landform changes, as discussed previously, as well as seemingly reduced availability of loose sediment on the flanks of the two volcanoes with climatically induced landscape stability after the Last Glacial Maximum. Where lahars continued to be deposited they appear to have been more channellised than previously. This is probably due to incision of stream channels following the Last Glacial Maximum when more water and less sediment became available. On the eastern Tongariro ring plain, the Oturere-Mangatawai Stream sector

was the only area active following the Last Glacial Maximum where the deposits of two lahar episodes, T1 and T2, are preserved. T2 deposits are rich in andesitic pumice (up to 30 % by volume) and appear to be associated with the eruption of Rotoaira Tephra from Tongariro volcano at 13.8 ka (Topping, 1973). T1, the youngest lahar deposit on the Tongariro ring plain, is within the same time frame as the first of eight lahar episodes on the northeastern Ruapehu ring plain, restricted between the main tributary of the Te Piripiri and Waihohonu Streams.

During the time of the lahar deposition episodes R08/T1 to R02 (c. 13-9 ka) both volcanoes were erupting thick sub-plinian tephra layers with a high frequency, including the Mangamate and Pahoka Tephras from Tongariro (Topping, 1973) and the younger Bullot Formation tephras from Ruapehu (Donoghue *et al.*, 1995). Several of the lahar deposition episodes appear to be directly associated with these eruptives. The most notable are: R06 with the Pourahu Member of the Bullot Formation, R05 with Pahoka Tephra, R04 with Oturere Lapilli member of the Mangamate Tephra, R03 with Ohinepango/Waihohonu Tephra members of the Mangamate Tephra, and R02 with the Poutu Lapilli member of the Mangamate Tephra. The association with explosive volcanism provides a triggering mechanism and a large volume of source material for these lahar episodes but it does not completely explain their consistently restricted area of deposition.

The Waihohonu and Oturere Streams on the Tongariro ring plain and the Mangatoetoenui Stream on the Ruapehu ring plain all have evidence of glacial moraines in their headwaters (Mathews, 1967; Hackett, 1985; McArthur and Shephard, 1990). None of the other streams examined in this study do. The Waiohau Tephra (11.85 ka B.P.) occurs near the base of the coverbed sequence on the moraines beside Waihohonu Stream, the Rerewhakaaitu Tephra (14.7 ka B.P.) on the Oturere Stream moraines, and the Pourahu Tephra (c. 10 ka) on Mangatoetoenui Stream moraines. This suggests the glacier in the former Oturere valley retreated before the glaciers in the Waihohonu and Mangatoetoenui valleys. This retreat is also reflected by the cessation of frequent lahars in the Oturere Stream after T1 at c. 14 ka, in the upper Waihohonu Stream (upstream of the confluence with Ohinepango Stream) from c. 15 ka, and the Mangatoetoenui Stream (where a glacier still exists on the upper volcano slopes) at c. 9ka. The presence of three retreating glaciers at these times provides a potential source of snow and water for lahar formation when eruptive products landed on them. Also moraine deposits are a ready source of sediment. Thus, the lahar record suggests these catchments were predisposed to lahar formation compared to other catchments without glaciers. Furthermore, units such as the Pourahu Member of the Bullot Formation had an associated pyroclastic flow (Donoghue *et al.*, 1995), which could have melted a large amount of snow and ice to form the lahars of the R06 episode.

The youngest lahar deposition episode occurred between 5.3 and 5.2 ka B.P. in the Mangatoetoenui Stream when the climate was wetter and milder than the present (McGlone and Topping, 1977). The activity of the two andesite volcanoes had reduced in magnitude at this time, with fine ash of the Papakai Formation accumulating slowly on the

ring plain. This single lahar event could have had many triggering mechanisms, the most likely being an eruption which was not large enough to be represented individually in the tephra record.

The 1995 lahar in the Mangatoetoenui Stream was a dominantly monolithologic unit derived from the sudden rainfall-induced failure of large thicknesses of tephra (up to 80 cm thick) erupted onto the Mangatoetoenui Glacier.

5.14 Summary and Conclusions

Using the coverbed stratigraphy of rhyolitic and andesitic tephra, 15 lahar episodes are recognised in the northeastern Ruapehu ring-plain record, ranging in age from >65 to 5 ka. Five episodes are recognised on the eastern Tongariro ring plain ranging in age from >23 to 14 ka.

The two main periods of lahar and fluvial aggradation were from c. 75-65 ka and 23 to 14 ka, corresponding to the two coolest periods of the Last Glacial (marine $\delta^{18}O$ Stages 4 and 2). The cool and stormy climate of these times coupled with an expanded area of glaciers appeared to result in greater sediment supply for lahar formation. Greater volumes of snow and ice also increased the availability of water for lahar generation. The triggering mechanisms for these lahars could have been eruptive activity, storm events, slope failures, avalanches and glacier collapses.

Two events during the period c. 23-14.7 ka B.P. strongly influenced the distribution of subsequent lahars. Firstly, the eastern Tongariro and Ruapehu ring plains were separated by a large lava flow emplaced between the present Waihohonu and Oturere Streams immediately before 22.5 ka. Secondly, Last Glacial Maximum moraines along the upper Whangaehu and Mangatoetoenui valleys blocked lahars from the upper eastern flanks of Ruapehu to the ring-plain sector between the Upper Waikato and Te Piripiri Streams. Subsequent lahars generated on the eastern Ruapehu flanks have thus been channelled to the southeast down the Whangaehu catchment and northeast into mostly the Mangatoetoenui catchment.

Many of the late glacial and postglacial lahar episodes appear to be related to plinian and sub-plinian tephra eruptions of Tongariro and Ruapehu volcanoes. However, both tephra deposition and water supply were required to form lahars. It appears major lahars at this time were formed only where tephra fell onto catchments with valley glaciers.

The cessation of lahars on the eastern flanks of Tongariro before 11.6 ka B.P. coincided with vegetational stabilisation of the volcanic slopes and glacial moraines. On the northeastern Ruapehu ring plain, lahar deposition continued until 5.2 ka B.P., possibly because the glaciers were slower to retreat, particularly in the Mangatoetoenui catchment.

5.15 Acknowledgements

We gratefully acknowledge funding from the New Zealand Vice-Chancellor's Committee,

Massey University Graduate Research Fund, the Helen E. Akers Scholarship Fund, and the Department of Soil Science of Massey University. We also thank A.S. Palmer, R.B. Stewart and J.A. Lecointre for their useful reviews of an earlier version of the manuscript, and B.F. Houghton and A.W. Walton for their comprehensive and useful reviews.

5.16 References

Cronin, S.J., Neall, V.E. and Palmer, A.S., 1996(b). Investigation of an aggrading paleosol developed into andesitic ring plain deposits, Ruapehu volcano, New Zealand. Geoderma, 69: 119-135.

Cronin, S.J., Neall, V.E., Stewart, R.B. and Palmer, A.S., 1996(a). A multiple parameter approach to andesitic tephra correlation, Ruapehu volcano, New Zealand. J. Volcanol. and Geotherm. Res. 72, 199-215.

Cronin, S.J., Neall, V.E., Lecointre, J.A., Palmer, A.S., in press. Unusual "snow slurry" lahars from Ruapehu volcano, New Zealand, September 1995. Geology.

Donoghue, S.L., 1991. Late Quaternary volcanic stratigraphy of the south-eastern sector of Mount Ruapehu ring plain, New Zealand. Unpub. PhD thesis, Massey University, Palmerston North, New Zealand.

Donoghue, S.L., Neall, V.E. and Palmer, A.S., 1995. Stratigraphy and chronology of late Quaternary andesitic tephra deposits, Tongariro Volcanic Centre, New Zealand. J. Roy. Soc. N. Z., 25: 115-206.

Froggatt, P.C. and Lowe, D.J., 1990. A review of late Quaternary silicic and some other tephra formations from New Zealand: their stratigraphy, nomenclature, distribution, volume, and age. N. Z. J. Geol. and Geophys., 33: 89-109.

Gregg, D.R., 1960. The geology of Tongariro Subdivision. N. Z. Geol. Survey Bull., 40.

Hackett, W.R., 1985. The geology and petrology of Ruapehu volcano and related vents. Unpub. PhD Thesis, Victoria University of Wellington, New Zealand.

Hackett, W.R. and Houghton, B.F., 1989. A facies model for a Quaternary andesitic composite volcano: Ruapehu, New Zealand. Bull. Volcanol., 51: 51-68.

Major, J.J. and Newhall, C.G., 1989. Snow and ice perturbation during historical volcanic eruptions and the formation of lahars and floods; a global review. Bull. Volcanol., 52: 1-27.

Mathews, W.H., 1967. A contribution to the geology of the Mount Tongariro massif, North Island, New Zealand. N. Z. J. Geol. and Geophys., 10: 1027-1038.

McArthur, J.L. and Shepherd, M.J., 1990. Late Quaternary glaciation of Mt. Ruapehu, North Island, New Zealand. J. Roy. Soc. N. Z., 20: 287-296.

McGlone, M.S. and Topping, W.W., 1977. Aranuian (post-glacial) pollen diagrams from the Tongariro region, New Zealand. N. Z. J. of Botany, 15: 749-760.

McGlone, M.S. and Topping, W.W., 1983. Late Quaternary vegetation, Tongariro region, central North Island, New Zealand. N. Z. J.. Botany, 21: 53-76.

Milne, J.D.G. and Smalley I.J., 1979. Loess deposits in the southern part of the North Island of New Zealand: an outline stratigraphy. Acta Geologica Academiae

Scientarium Hungaricae, 22: 197-204.

Nairn, I.A., Wood, C.P and Hewson C.A.Y., 1979. Phreatic eruptions of Ruapehu: April 1975. N. Z. J. Geol. and Geophys., 22: 155-173.

Palmer, B.A., Purves, A.M. and Donoghue, S.L., 1993. Controls on the accumulation of a volcaniclastic fan, Ruapehu composite volcano, New Zealand. Bull. Volcanol., 55: 176-189.

Pierson, T.C. and Costa, J.E., 1987., A rheologic classification of subaerial sediment-water flows. G.S.A. Reviews in Engineering Geology, VII: 1-12.

Pierson, T.C., Janda, R.J., Thouret, J.-C. and Borrero, C.A., 1990. Perturbation and melting of snow and ice by the 13 November 1985 eruption of Nevado del Ruiz, Colombia, and consequent mobilisation, flow and deposition of lahars. J. Volcanol. and Geotherm. Res., 41: 17-66.

Pillans, B.J., 1988. Loess chronology in Wanganui Basin, New Zealand. In: Eden, D.N. and Furkert, R.J. (eds) Loess - Its Distribution Geology and Soils: 175-191. A.A. Balkema, Rotterdam.

Pillans, B., McGlone, M., Palmer, A., Mildenhall, D., Alloway, B., Berger, G., 1993. The Last Glacial Maximum in central and southern North Island: a paleoenvironmental reconstruction using the Kawakawa tephra formation as a chronostratigraphic marker. Pal., Pal., Pal., 101: 283-304.

Scott, K.M., 1988. Origins, behaviour, and sedimentology of lahars and lahar-runout flows in the Toutle-Cowlitz River system. U.S.G.S. Prof. Pap. 1447-A: 76pp.

Smith, G.A., 1986. Coarse-grained nonmarine volcaniclastic sediment: Terminology and deposition process. G.S.A. Bull., 97: 1-10.

Smith, G.A. Fritz, W.J., 1989. Volcanic influences on terrestrial sedimentation. Geology 17: 375-376.

Topping, W.W., 1973. Tephrostratigraphy and chronology of late Quaternary eruptives from the Tongariro Volcanic Centre, New Zealand. N. Z. J. Geol. and Geophys., 16: 397-423.

Topping, W.W. and Kohn B.P., 1973. Rhyolitic tephra marker beds in the Tongariro area, North Island, New Zealand. N. Z. J. Geol. and Geophys., 16: 375-395.

Waitt, R.B., Gardner, C.A., Pierson, T.C., Major, J.J., Neal, C.A., 1994. Unusual ice diamicts emplaced during the December 15, 1989 eruption of Redoubt Volcano, Alaska. J. of Volcanol. and Geotherm Res. 62: 409-428.

Wilson, C.J.N., Switzur, R.V. and Ward, A.P., 1988. A new ^{14}C age for the Oruanui (Wairakei) eruption, New Zealand. Geol. Mag.,125: 297-300.

Wilson, C.J.N., Houghton, B.F., Lanphere, M.A. and Weaver, S.D., 1992. A new radiometric age estimate for the Rotoehu Ash from Mayor Island volcano, New Zealand. N. Z. J. Geol. and Geophys., 35: 371-374.

Wilson, C.J.N., 1993. Stratigraphy, chronology, styles and dynamics of late Quaternary eruptions from Taupo Volcano, New Zealand. Phil. Trans. Roy. Soc. of London A, 343: 205-306.

CHAPTER 6: LAHAR HISTORY AND LAHAR HAZARD OF THE TONGARIRO RIVER

6.1 Introduction

The Tongariro River drains a large portion of the northeastern Tongariro Volcanic Centre and thus has the potential of being a conduit for devastating lahars as has happened in the geological past. Built beside the river, Turangi, a town of more than 4 000 people is potentially at risk from these lahars. The aim of this chapter is also one of the main objectives of the overall study outlined in Chapter 1 - to establish what is the hazard to Turangi and the surrounding area from lahars in the Tongariro River.

This part of the study relies on many of the developments made in previous chapters. Using the rhyolitic and andesitic tephrochronology established for the study area in Chapters 2 and 3, the lahar stratigraphy along the Tongariro River was investigated in the same manner as for Chapter 5. By combining the Tongariro River stratigraphy with that developed for the northeastern Ruapehu and eastern Tongariro ring plains (Chapter 5), the lahar hazards of the entire Tongariro River catchment have been assessed.

This part of the study has been written as a manuscript which has been submitted to the New Zealand Journal of Geology and Geophysics. The manuscript has multiple authors and the contributions of the authors were as follows:

S. J. Cronin: Principal investigator

Carried out all:	Field descriptions and sampling
	Tephra and lahar correlation and mapping
	Drawing and designation of zones on the hazard map
	Preparation and writing of the manuscript

V. E. Neall

A.S. Palmer: Advisers

Aided the study by:	Discussion of methodology and lahar hazard designation
	Editing and discussion of the manuscript and lahar hazard map

6.2 LAHAR HISTORY AND LAHAR HAZARD OF THE TONGARIRO RIVER, NORTHEASTERN TONGARIRO VOLCANIC CENTRE, NEW ZEALAND

Shane J. Cronin, V.E. Neall and A.S. Palmer
Department of Soil Science, Massey University, Private Bag 11 222, Palmerston North, New Zealand.

Submitted to: *New Zealand Journal of Geology and Geophysics*

Abstract Laharic surfaces beside the Tongariro River have been mapped and dated using andesitic and rhyolitic marker tephras. Coupling the stratigraphic record obtained with that of the Tongariro and Ruapehu ring plains, has enabled a history of lahars occurring in the Tongariro River to be compiled. This has formed the basis of a lahar hazard map for the entire catchment. Eight lahar hazard zones with assigned recurrence intervals ranging from 1 in 35 years to 1 in >15 000 years have been mapped. Lahar surfaces between the ages of 14.7 and 9.8 ka B.P. cover the greatest areas, while younger lahar surfaces are confined to lower and restricted surfaces closer to the present river channel. Holocene lahar deposits along the Tongariro River are not as well preserved as older units, probably because the Holocene lahars were confined to a more deeply incised channel where their deposits were more readily eroded following emplacement. All recorded lahars in the Tongariro catchment post-11.85 ka B.P. have been derived from Ruapehu volcano. The Mangatoetoenui Stream has been the conduit for the greatest number of Holocene lahars and for all of the historic ones. Most of Turangi is built on a surface which has not been inundated by a lahar since c. 10 ka B.P. However, the area identified where high risk affects the greatest population is part of Turangi, having been inundated by a lahar since 1850 years B.P. The infrastructure at greatest risk includes the State Highway 1 bridge across the Mangatoetoenui Stream and the Rangipo Dam and power station.

6.3 Keywords

Volcanic hazards, volcanic risk, lahar hazard map, lahars, Ruapehu volcano, Tongariro volcano, Tongariro River, Late Quaternary lahars, Holocene Lahars.

6.4 Introduction

The Tongariro catchment drains the northeastern portion of the Tongariro Volcanic Centre and includes the northeastern flanks of Ruapehu volcano and the eastern and northeastern flanks of Tongariro volcano. Lahars can enter the Tongariro River via a large number of tributary channels draining these two volcanoes. The most recent example was a small lahar from Ruapehu volcano in October 1995.

At risk from lahars along the Tongariro River is the town of Turangi with a population of 4239 in 1991 (Department of Statistics, 1992). Two smaller settlements, Rangipo and Tokaanu and the Rangipo Prison lie farther from the river, but are also located on laharic and fluvial surfaces. The Tongariro Power Development which utilises both the Tongariro river channel and water from its tributaries is also at risk from lahars. In 1995 laharic and fluvial sediment filled a large portion of the Rangipo dam, sited within the Tongariro River channel. This and additional sediment over the following few months led to excessive wear of turbine blades in the Rangipo Power Station. Also at risk from lahars along the Tongariro River is tourist revenue from trout fishing and other recreational activities.

To assess the lahar hazards within the Tongariro River and its surrounds we have mapped the laharic surfaces and sediments along the River and dated them using rhyolitic and andesitic cover- and interbeds. Combining this with a knowledge of the lahar stratigraphy on the northeastern Ruapehu and eastern Tongariro ring plains (Cronin and Neall, in press) we have produced an integrated lahar hazard map for the entire Tongariro catchment.

6.5 Setting

Tongariro and Ruapehu are the two largest and most recently active volcanoes of the Tongariro Volcanic Centre (Gregg, 1960). Ruapehu was last active in 1996. It is the highest peak in the North Island at 2797 m and consists of a 110 km^3 composite cone with a surrounding ring plain of similar volume, comprising mainly volcaniclastic deposits (Hackett and Houghton, 1989). Tongariro volcano is a slightly smaller massif made up of several coalescing volcanic cones, the largest of which is the recently active cone of Ngauruhoe (Mathews, 1967; Nairn and Self, 1978). Tongariro volcano is also surrounded by an extensive ring plain. The ring plain deposits of these two volcanoes are confined in the east by the Kaimanawa Mountains and extend down drainage channels to the north and south.

The Upper Waikato Stream is the southern boundary of the volcanic portion of the Tongariro catchment (Fig. 6.1). South of this boundary (a low divide on the Whangaehu fan), drainage from the flanks of Ruapehu flows southwards into the Whangaehu River. From its origins at the junction of the Waipakihi River and Upper Waikato Stream, the Tongariro River flows for 47 km before entering Lake Taupo. Its gradient ranges from 1 m drop in 43 m to 1 m in 225 m, before it becomes meandering within a delta formed into Lake Taupo. Along its path, 9 major and several other smaller streams rising from the flanks of the Ruapehu and Tongariro volcanoes join the River.

6.6 Terminology

The word lahar is here used to describe, "a rapidly flowing mixture of rock debris and water (other than normal streamflow) from a volcano" (Smith and Fritz, 1989).

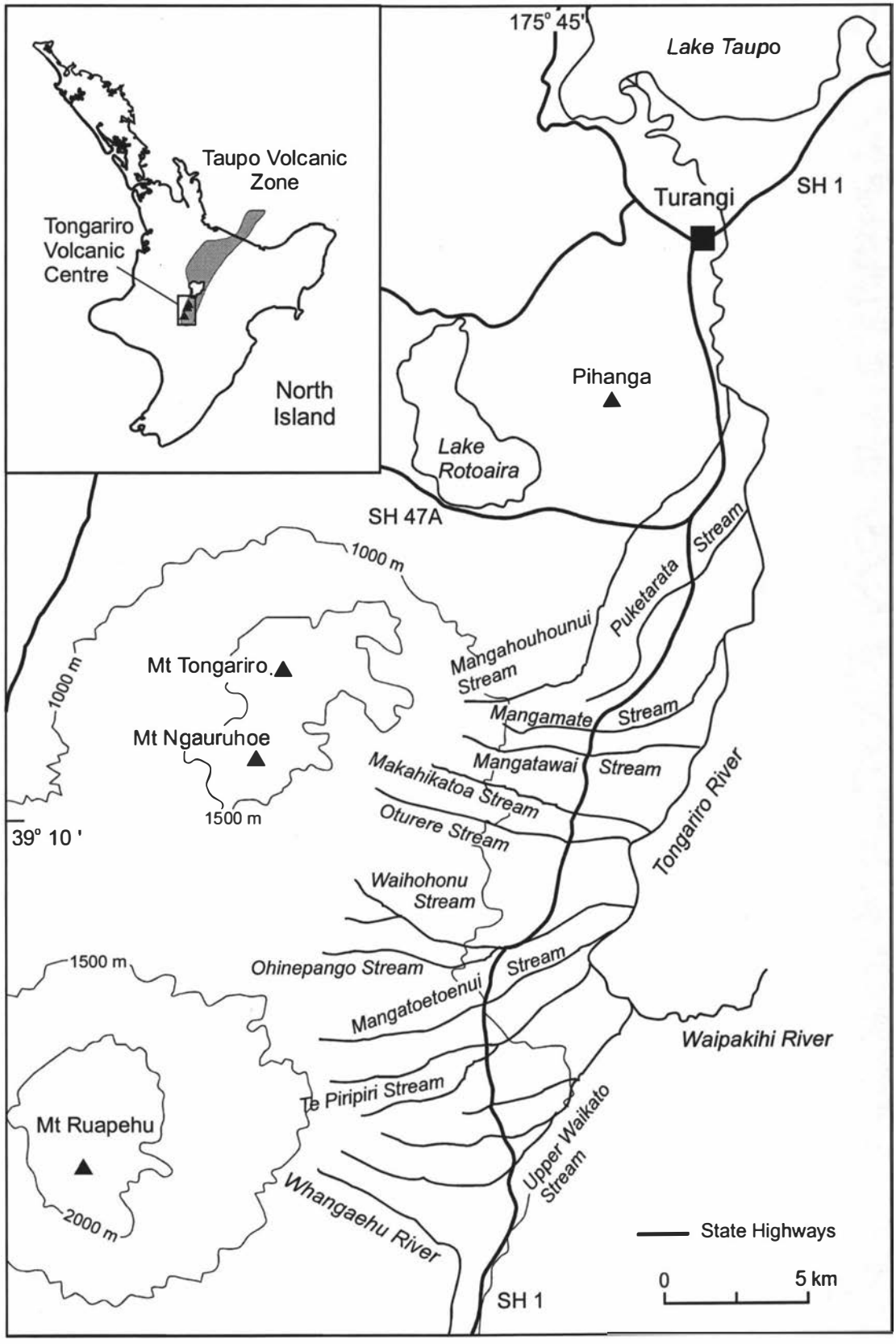

Figure 6.1 Location of the Tongariro catchment, draining the northeastern Tongariro Volcanic Centre in the central North Island of New Zealand. The nine major tributary streams which drain from Ruapehu and Tongariro volcanoes into the Tongariro River are labelled.

Lahars are generally subdivided on the basis of differing sediment concentrations and resulting differences in rheology. A continuum of flow behaviour and rheology occurs between normal Newtonian streamflow and plastic plug-flows (Pierson and Costa, 1987). Most lahars fall into two main rheologic categories which have been defined on the basis of field and laboratory experiment observations; debris flows and hyperconcentrated streamflows.

Hyperconcentrated streamflows are defined as containing 20-60% sediment by volume (Beverage and Culbertson, 1964). More importantly however, the onset of hyperconcentrated streamflow behaviour is when a sediment-water mixture begins to attain a measurable yield strength (i.e. it becomes a non-Newtonian fluid). Sediment is supported within these flows dominantly by clast-clast collisions/interactions and turbulence, and deposition is by a rapid grain by grain settling process at the base of the flow (Pierson and Scott, 1985; Smith, 1986). Deposits typical of hyperconcentrated flows are usually sand dominated, horizontally bedded, poorly sorted and clast supported.

When the sediment concentration in the flow approaches 60% (the actual content varies according to the particle-size distribution of the sediment), yield strengths of the flow increase markedly. At this stage the flow begins to behave like a laminar flowing, single-phase plug rather than sediment suspended in water (Pierson and Costa, 1987). Clast support in these flows is by matrix support and buoyancy, and deposition is *en masse*, the deposits representing a frozen state of the flow. Debris flow deposits are dominantly matrix supported, massive and very poorly sorted (Smith, 1986).

6.7 Hazards of Lahars

The hazards posed by lahars have been vividly portrayed by a number of disasters throughout the world in recent history. In 1953, in a local example, 151 people were killed when their train plunged into the Whangaehu River as a lahar undermined the rail bridge (Stillwell *et al.*, 1954). In 1985, the town of Armero in Colombia and 23 000 of its inhabitants were inundated by lahars from Nevado del Ruiz (Pierson *et al.*, 1990; Voight, 1990). In 1991 and following years, lahars in rivers radiating outward from Mt. Pinatubo in the Philippines caused at least 143 fatalities. They destroyed bridges and inundated towns, roads and huge areas of arable land, forcing the evacuation of more than 70 000 people (Philippine Institute of Volcanology and Seismology, 1992; Pierson *et al.*, 1992).

Hazard to life from lahars results from their high speeds and sediment concentrations. People and animals are swept away or entombed in sediment. Bridges and other man-made structures are also easily destroyed by large, highly competent flows. Lahars can also deposit sediment across large areas of productive land, not only destroying crops but potentially resulting in a permanent loss of production. Other hazards can result from the acidity, toxicity and heat of some types of lahars.

6.8 Methods

The surfaces and sediments in this study have been dated using andesitic and rhyolitic tephra cover- and interbeds. Lahar surfaces were mapped from field exposures and using aerial photographs. Eighteen dated rhyolitic tephras erupted from Taupo Volcanic Zone calderas are preserved within the Ruapehu and Tongariro ring plain and Tongariro River sequences (Topping and Kohn, 1973; Donoghue *et al.*, 1995; Cronin and Neall, in press). These tephras were identified by their stratigraphic positions, physical appearances, mineralogy and glass chemistry (Cronin *et al.* in press(a)). In addition, 11 dated andesitic tephras erupted from Tongariro and Ruapehu volcanoes occur within the sequences (Topping, 1973; Donoghue *et al.*, 1995). These and further andesitic marker tephras were identified by a similar range of methods as those used for the rhyolitic tephras (Cronin *et al.*, 1996). All the marker tephras discussed in this study are listed in Table 5.1 (Chapter 5).

Laharic deposits within the stratigraphic sequences were interbedded with fluvial sediments, tephras and lava flows. The laharic deposits were distinguished from fluvial sediments by their laterally continuous and characteristic sedimentology outlined previously.

In constructing the lahar hazard map, laharic surfaces of differing ages were delineated into zones and a lahar recurrence interval was assigned to each zone. For the three youngest zones this was a simple process of calculating the ratio of the number of lahars in a given time, e.g. within the historic record (100-150 years), or since the Taupo Tephra (1850 years B.P.; Froggatt and Lowe, 1990). For older lahar surfaces this approach yields results which are not considered valid, e.g. a surface mapped in this study has not been inundated by a lahar since c. 10 ka B.P. This surface comprises the deposits of several lahars, and using tephra interbeds various recurrence intervals can be calculated. Since 13.8 ka B.P. the recurrence interval is 1 in 2 800 years, and since 22.6 ka B.P. it is 1 in 3 200 years. These intervals are not representative of a surface which has not been crossed by a lahar in the last 10 ka, nor are they representative of the actual frequency of the lahar deposition (from 22.5 to 13.8 ka B.P.=1 in 4 400 years, and from 13.8 to 10 ka B.P.=1 in 800 years). In situations such as this, the approach in this study was to assign a recurrence interval based on the last time a given surface was inundated by a lahar.

6.9 Lahar history of the Tongariro River

6.9.1 Stratigraphic record within the tributary streams

The number and timing of lahars entering the Tongariro River may be obtained from the lahar record preserved within its volcanic sourced tributaries (Cronin and Neall, in press). This indicates that prior to the eruption of the Rerewhakaaitu Tephra (14.7 Ka B.P.), multiple lahars occurred within almost all of its major tributaries (Table 6.2). In contrast,

Holocene lahars are restricted to three streams on the northeastern Ruapehu ring plain. The Mangatoetoenui Stream has contributed the largest number of post-glacial lahars to the Tongariro River. During the 1995/96 eruption episode of Ruapehu volcano, the only lahars to enter the Tongariro River travelled down the Mangatoetoenui Stream.

6.9.2 Stratigraphic record within the Tongariro River valley

6.9.2A *Highest surface*

The oldest exposed sequences in the Tongariro River valley form the highest surface, which is commonly 15-30 m above the present river level. This surface is extensive throughout the catchment between Upper Waikato Stream and the town of Turangi. Sections through it are described in exposures at various locations along the Tongariro River (Fig. 6.2). Close to the Tongariro River the surface has been eroded and subsequently been infilled by the Taupo Ignimbrite. As a result of this infilling, lahar surfaces of differing ages have been buried to form a single younger surface. This complexity is exemplified by the difference in age of the lahars comprising the highest surface described at Site 1 with those at Sites 2 and 3 which have been overlain by 4 to 6 m of pumiceous ignimbrite to form a laterally continuous surface. At Sites 2 and 3 beneath the pumice veneer are formerly lower and younger laharic surfaces than at Site 1.

Sites 2 to 7 from 1.5 to 36 km down the river all have coverbed sequences of similar ages. At Site 2, the lahar deposits above an unconformity are younger than any recorded in the Upper Waikato Stream and are probably derived from the Te Piripiri catchment. Sites 2 to 5 all record the deposits of several lahars below either the Pourahu or the Pahoka Tephras (c. 9.8-10 ka B.P.). At Sites 6 and 7 the Pahoka and Pourahu tephras have thinned beyond recognition, but the lower members of Mangamate Tephra and the Poronui Tephra are present, providing a minimum age of c. 9.7-9.8 ka B.P. for the underlying lahar deposits. None of the many lahars younger than 10 ka B.P. that are recorded by deposits in the Te Piripiri,
Mangatoetoenui or Waihohonu Streams (Table 6.2) are represented in any of the sections described through this high surface.

The Rotoaira Tephra preserved at Site 6 provides a lower age limit for a package of several lahar deposits. This indicates that this lahar package was probably derived from the Te Piripiri, Mangatoetoenui, Waihohonu, Oturere, and Makahikatoa catchments. Lahar deposits preserved below the Kawakawa Tephra at Sites 6 and 7 could have been derived from lahars in any of the tributary streams (Table 6.2).

The post-Kawakawa lahars described in the Tongariro valley sequences cannot be individually correlated downstream on the basis of lithology or stratigraphy. However, consistent changes in the sedimentology of the overall package of post-22.6 ka B.P. lahar deposits are observed. In the upstream sites most of the deposits are: coarse grained - containing pebbles-large boulders, matrix-supported with a sandy or silty matrix, poorly sorted and massive.

Table 6.2 Number and timing of lahars in tributary catchments of the Tongariro River, based on the exposed stratigraphic record in each catchment (Cronin & Neall in press).

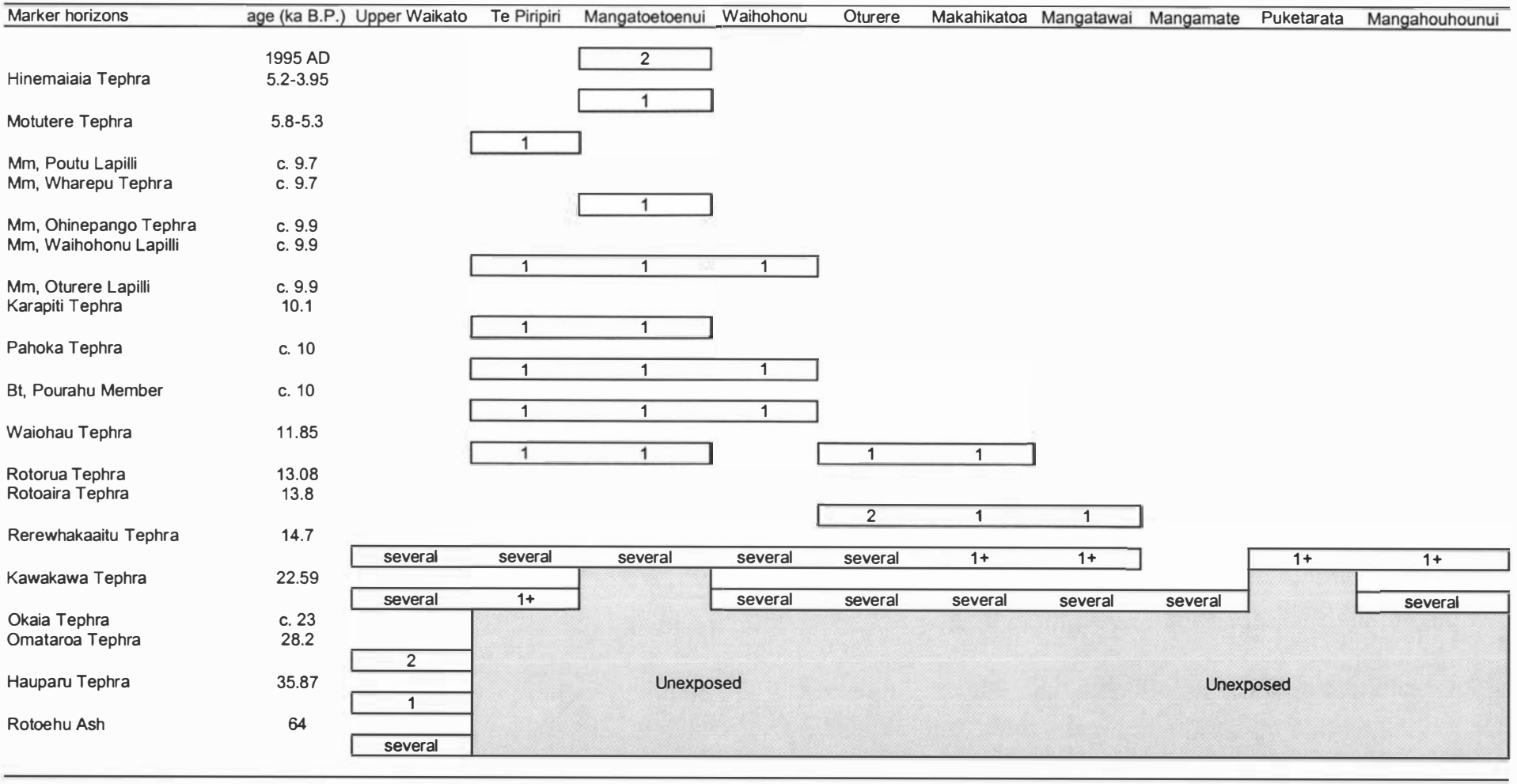

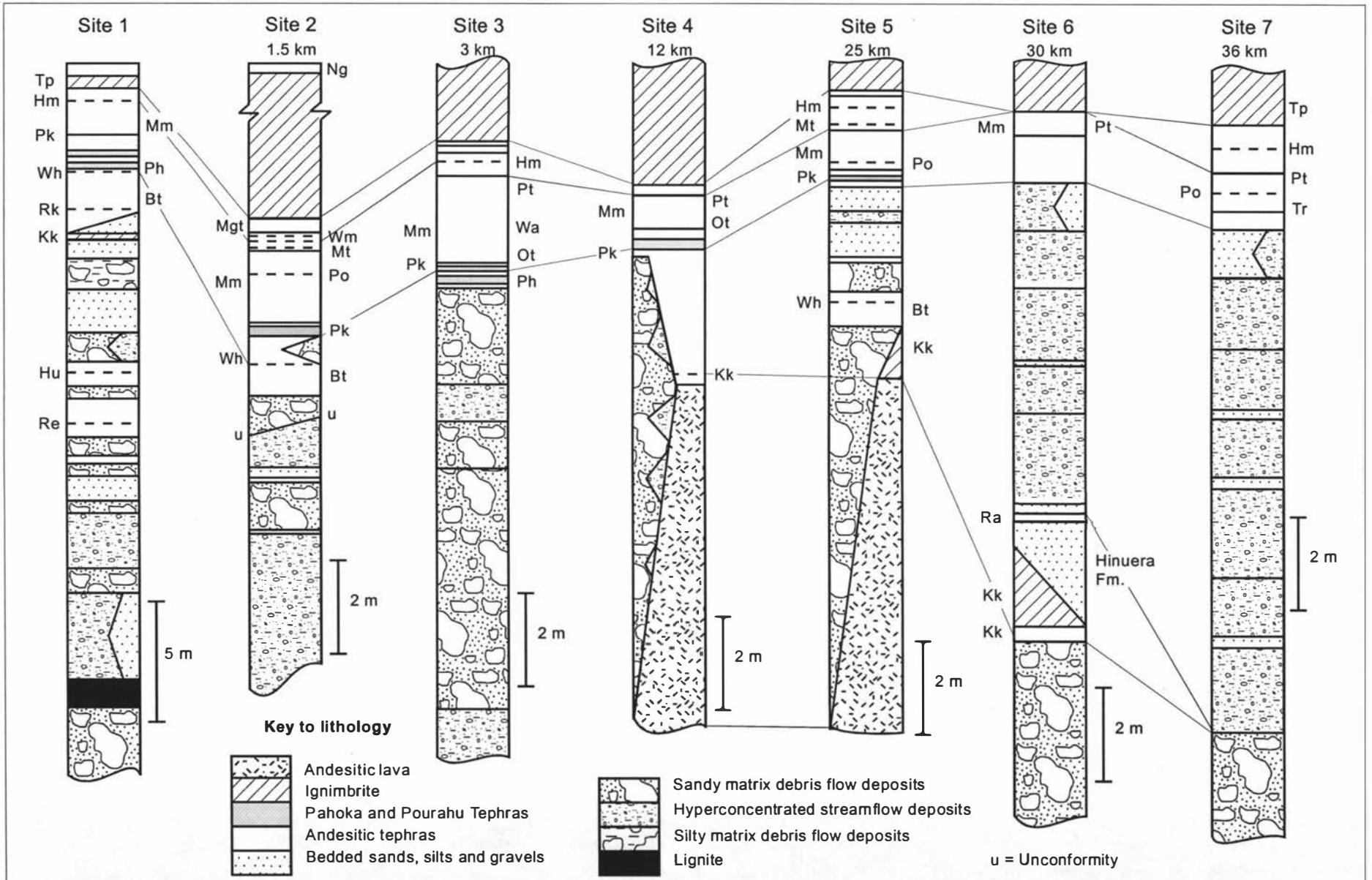

Figure 6.2 Stratigraphy of sections preserved through the highest laharic surface beside the Tongariro River. Sites 1-7 are labelled on Figs. 4 and 5. Sites 2-7 are located at the labelled distances downstream of the start of the Tongariro River (at the junction of the Waipakihi River and the Upper Waikato Stream).

In contrast in downstream sites the deposits are: dominated by sands and large clast poor; clast-supported; weakly planar or horizontally bedded with rare larger clasts in horizontal "strings".

These changes in sedimentology indicate changes in the rheology of many of the lahars as they travelled downstream. In upstream localities, the deposits indicate the lahars were likely to be debris flows, depositing sediment *en masse*. The downstream deposits imply finer-grained, more dilute hyperconcentrated streamflows, with incremental deposition of many thin layers to build up each deposit. These lahars appear to have transformed from debris flow to hyperconcentrated streamflow between c. 25 and 29 km along the Tongariro River. This was probably due to loss of sediment from the flows by deposition and their dilution by incorporating river water in their paths. Similar lahar transformations have been described by Pierson and Scott (1985) at Mt. St. Helens, and Cronin *et al.* (in press(b)) in 1995 lahars in the Whangaehu River.

6.9.2B *Lower surfaces*

Small areas of low surfaces are preserved close to the main channel in the upper reaches of the river. These are flood plains, composed of recent (post-1850 years B.P.), coarse (bouldery and cobbly) alluvial deposits, mostly with no stratigraphy exposed. In the lower reaches from the town of Turangi northwards, the lower surfaces are extensive. Where the surfaces are more extensive, only those preserving a stratigraphy were described. In all described exposures, lahar stratigraphy is very difficult to interpret because of extensive fluvial reworking of lahar deposits and poor preservation of tephra marker beds. However, a sequence of at least four lahar deposits is preserved in a small number of exposures (Fig. 6.3).

At Site A (Fig. 6.3) two pre-Taupo Tephra lahar deposits are preserved, with a variable thickness of fluvial sands between them. Deposit 2 is unconsolidated and finer-grained than the large boulder-bearing, and firmly compacted deposit 3. Site A has been inundated by the River since the deposition of Taupo Pumice, but this deposit is not laharic. At Site B a similar stratigraphy is preserved, and the sedimentologies of lahar deposits 2 and 3 are also similar to Site A. Lahar deposit 2 was probably emplaced soon before the Taupo Ignimbrite, because little or no reworking or soil development is evident at the top of the lahar deposit. Site B also preserves the deposit of at least one lahar beneath lahar deposit 3. Downstream, at Site C the lahar deposit preserved at the base of the sequence is correlated to deposit 3 from its grainsize characteristics, sedimentology and firmly compacted nature. The Hinemaiaia Tephra (Hm on Fig. 6.3) provides a minimum age for this lahar. Lahar deposit 2 is not preserved at this site.

At Sites D and E, which are on lower surfaces than the first three localities, the basal lahar deposits are correlated to lahar deposit 2, because of their unconsolidated nature and finer grainsize than deposit 3. Large parts of the upper portions of lahar deposit 2 at these sites and many others are reworked, the fine grained matrix having been elutriated leaving a cobbly-bouldery matrix-poor clast-supported deposit.

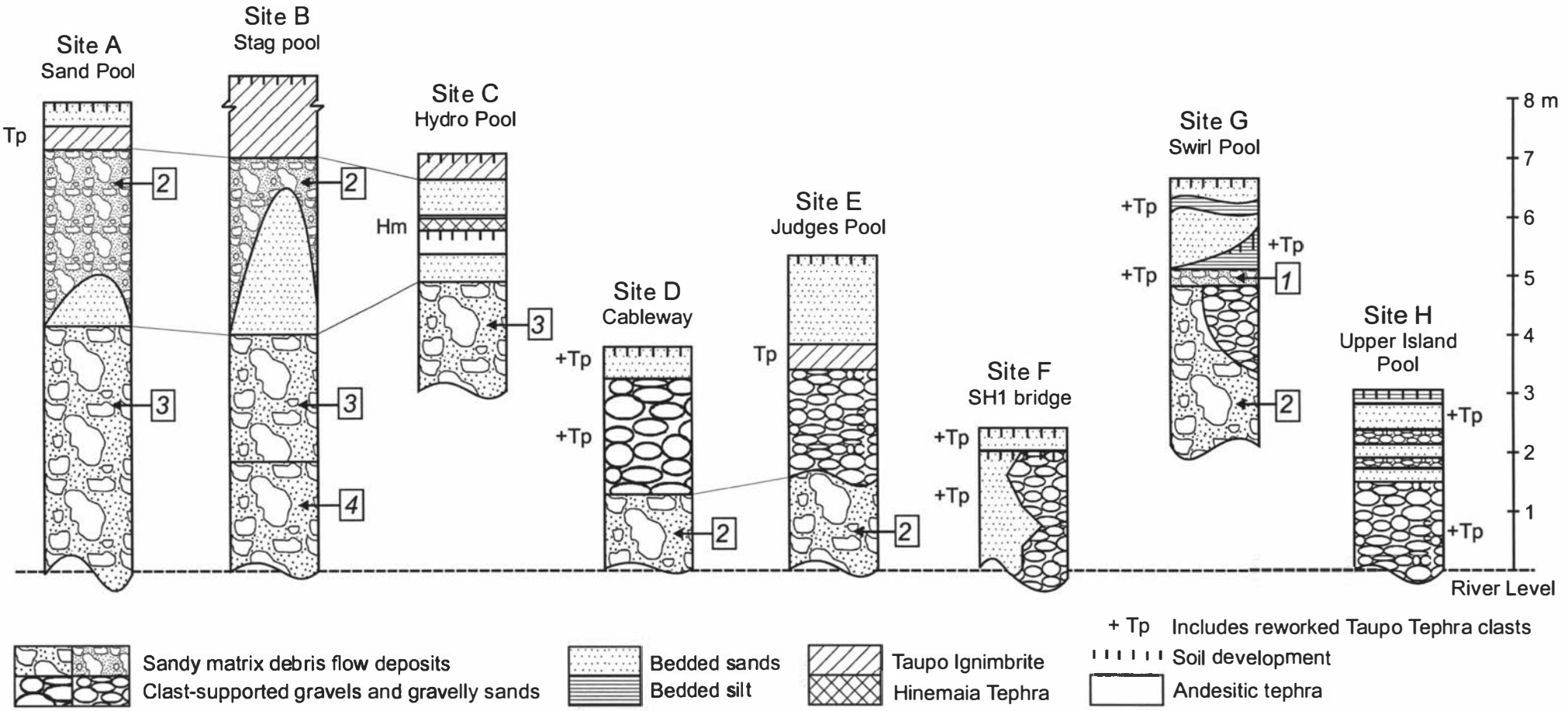

Figure 6.3 Stratigraphy of sections through the lower laharic surfaces alongside the Tongariro River. Sites A to G are located on Figs. **4** and **5.**

Sites F and H exemplify many of the lowest surface exposures where only bedded sands and clast-supported cobbles and boulders are preserved. In these sites the lahar deposits appear to have been completely eroded or reworked. At site G the youngest (pre-1995) lahar deposit in the Tongariro catchment is preserved (lahar deposit 1). This deposit contains reworked Taupo Tephra clasts, indicating a post-1850 year B.P. age. Alluvial sands and silts with two episodes of weak soil development occur above the lahar deposit providing no definite minimum age. Lahar deposit 2 is also preserved at Site G, and in many places its upper portion is reworked.

The deposit 4 lahar was probably derived from either Te Piripiri or Mangatoetoenui Streams, based on the presence of lahar deposits in a similar stratigraphic position (Table 6.2 and Cronin and Neall, in press). The lahar that emplaced deposit 3 was probably derived from the Mangatoetoenui Stream, where a lahar deposit in the same stratigraphic position has been described. Lahar deposits 2 and 1 are not preserved in upstream areas, thus it is difficult to assess from which catchments they were derived. However, in the late Holocene many lahars were derived from Ruapehu volcano in the Whangaehu catchment (the Onetapu Formation, Donoghue, 1991; Hodgson, 1993; Palmer *et al.*, 1993). So deposits 2 and 1 are likely to be from Ruapehu, and given the 1995 example, the Mangatoetoenui Stream was their probable conduit.

The fact that the youngest lahar deposits are not well preserved in the Tongariro catchment can be explained by comparison to the 1995 lahars in the Whangaehu catchment (Cronin *et al.*, in press(b)). Of 35 lahars recorded in the Whangaehu River from September to December 1995, one year later only a few localities preserve the deposits from only one of these - the largest. However, large amounts of reworked deposits occur. The reason for reworking of the 1995 lahar deposits is that they were mostly confined to the river channel, so streamflow remobilised them immediately following their deposition. The same circumstances probably applied to lahar deposits within the Tongariro River in the late Holocene when the channel was incised almost as deeply as at present. In contrast, during the late glacial and early post-glacial period, the Tongariro River was probably not confined to a deeply incised channel. This resulted in emplacement of lahar deposits across a broad area, now represented by the highest lahar surface preserved extensively throughout the catchment.

6.10 Lahar hazards in the Tongariro River

The lahar hazard map of the Tongariro catchment (Figs. 6.4 and 6.5) is based on the lahar stratigraphy and mapped extent of laharic surfaces in the catchment as described above. Each lahar hazard zone was derived from a mapped laharic surface of known or inferred age. Each assignment is based on the age of the youngest lahar to cross the surface.

6.10.1 *1 in >15 000 year zone*

This zone includes the most extensive surfaces in the Tongariro catchment. The laharic surfaces included within this zone comprise lahar deposits older than the Rerewhakaaitu Tephra (14.7 ka B.P.). Almost all of the eastern ring plain of Tongariro volcano and large parts of the northeastern Ruapehu ring plain comprise laharic surfaces of this age. In the southern part of the mapped area, near the Upper Waikato Stream, the zone includes lahar surfaces which are pre-Kawakawa Tephra age. A small patch of a pre-Kawakawa Tephra surface is also preserved immediately south of Turangi township (Fig. 6.5). On the Ruapehu ring plain the lahar deposits within this hazard zone belong to the Te Heuheu Formation (Donoghue, 1991). On Tongariro volcano these lahar deposits were previously mapped as the Rangipo Lahars (Grindley, 1960). This extensive zone and the large number of lahars that comprise these surfaces (Table 6.2 and Cronin and Neall, in press) indicate that lahars were a common occurrence across large areas of both ring plains during and following the Last Glacial Maximum.

At risk within this zone is the village of Rangipo and part of the Rangipo Prison, State Highway 1 and other secondary roads. In addition, high voltage transmission lines and the Poutu Canal cross this zone.

6.10.2 *1 in 12 000 year zone*

This zone covers small areas alongside the Oturere and Makahikatoa Streams on the Tongariro ring plain and lower slopes. It represents a lahar path following deposition of the Rotorua Tephra but prior to the eruption of Waiohau Tephra (11.85 ka B.P.). The zone is crossed by State Highway 1 and high voltage transmission lines, but mostly includes unpopulated land covered by native forest.

6.10.3 *1 in 10 000 year zone*

This zone represents a lahar surface recognised by its oldest marker coverbed being either the Pourahu, Pahoka, or Poronui Tephra, all of which are between the ages of 9.8-10 ka B.P. This surface covers a sector of the northeastern Ruapehu ring plain, and comprises deposits of several post-glacial lahars which flowed down the Te Piripiri, Mangatoetoenui, and Waihohonu Streams (Table 6.2). The surface pinches out in the central reaches of the Tongariro River where lahars of this age were probably confined to an incised channel. Immediately upstream of the Rangipo prison the lahar surface again spreads out to cover a large area between Rangipo and Turangi. Much of Turangi township is built on this surface as well as the Rangipo Prison and a few other outlying houses. Also at risk on the surface are numerous roads, telephone lines, high voltage transmission lines, as well as large areas of pastoral land and livestock.

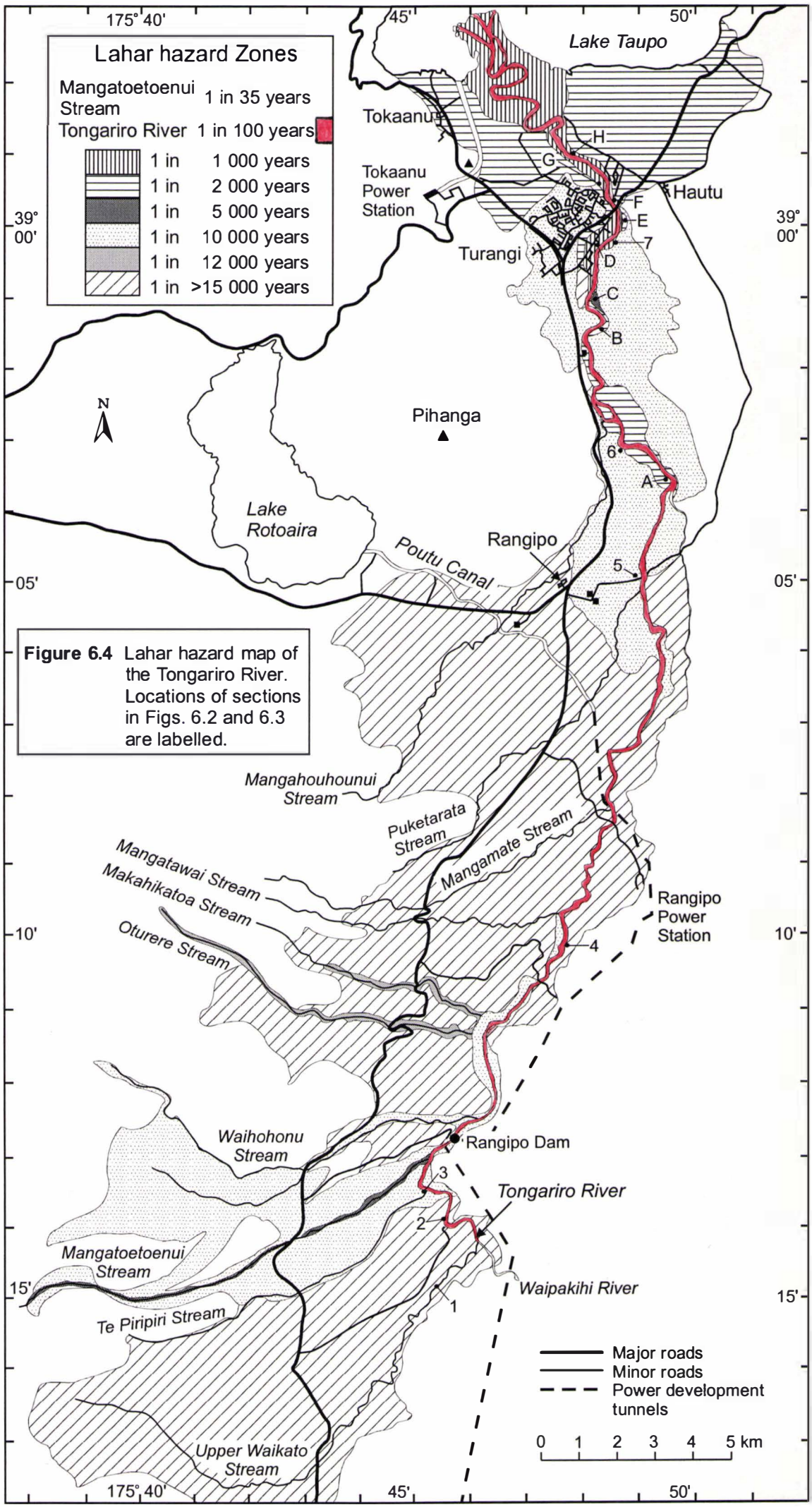

Figure 6.4 Lahar hazard map of the Tongariro River. Locations of sections in Figs. 6.2 and 6.3 are labelled.

6.10.4 *1 in 5 000 year zone*

Two small areas of this hazard zone are delineated, along Mangatoetoenui Stream (Fig. 6.4) and a small area south of Turangi township (Fig. 6.5). These surfaces were last inundated by a lahar between the time of the eruptions of the Hinemaiaia and Motutere Tephras (Table 6.2, c. 5.2-5.3 ka B.P.). Both of these areas are unpopulated and are not used for agricultural production.

6.10.5 *1 in 2 000 year zone*

Surfaces within this zone are extensive only in the lower reaches of the Tongariro River (Fig. 6.5). The last lahar to inundate this surface was immediately prior to the Taupo Tephra eruption. Upstream of Turangi these surfaces are confined close to the present river channel but fan outwards north of the town. Parts of Turangi, and Tokaanu and many outlying houses are built on this surface. An airstrip, the Turangi sewage treatment area, the Tongariro trout hatchery and many roads (including State Highway 1) are also within this zone. Large portions of the zone are also in pastoral production.

6.10.6 *1 in 1 000 year zone*

This zone includes areas which are interpreted to have been crossed by a lahar since the eruption of the Taupo Tephra (1.85 ka B.P.). Only a few localities within this zone preserve deposits of a post-Taupo Tephra lahar because many of the deposits have been reworked by subsequent fluvial action. The area covered by this zone extends from Turangi to the delta in Lake Taupo (Fig. 6.5). In the Tongariro delta region, where exposure is poor, the extent of the zone has been delimited by consideration of the soil map of this region (Water and Soils Division, Ministry of Works and Development, 1979). The mapped extent of the 1 in 1 000 year zone corresponds to "Recent soils from alluvium", whilst "Organic soils" beyond the limit of these lahars, occur in the surrounding swampy area. Parts of Turangi are included within the zone as well as a few outlying houses and the State Highway 1 Bridge across the river.

6.10.7 *1 in 100 year zone*

This zone comprises the channel of the Tongariro River into which at least one lahar flowed during the 1995 eruption sequence of Ruapehu (Cronin *et al.*, in press(b)). Europeans did not settle in the Turangi region until the early 1900's (Clarke and Smith, 1986), so that continuous records were not available until this time. Although the 1995 lahar did not pass beyond the Rangipo Dam in the Tongariro River, a 1 in 100 year hazard zone is still applied to the remainder of the river channel because this would probably be the case without human intervention.

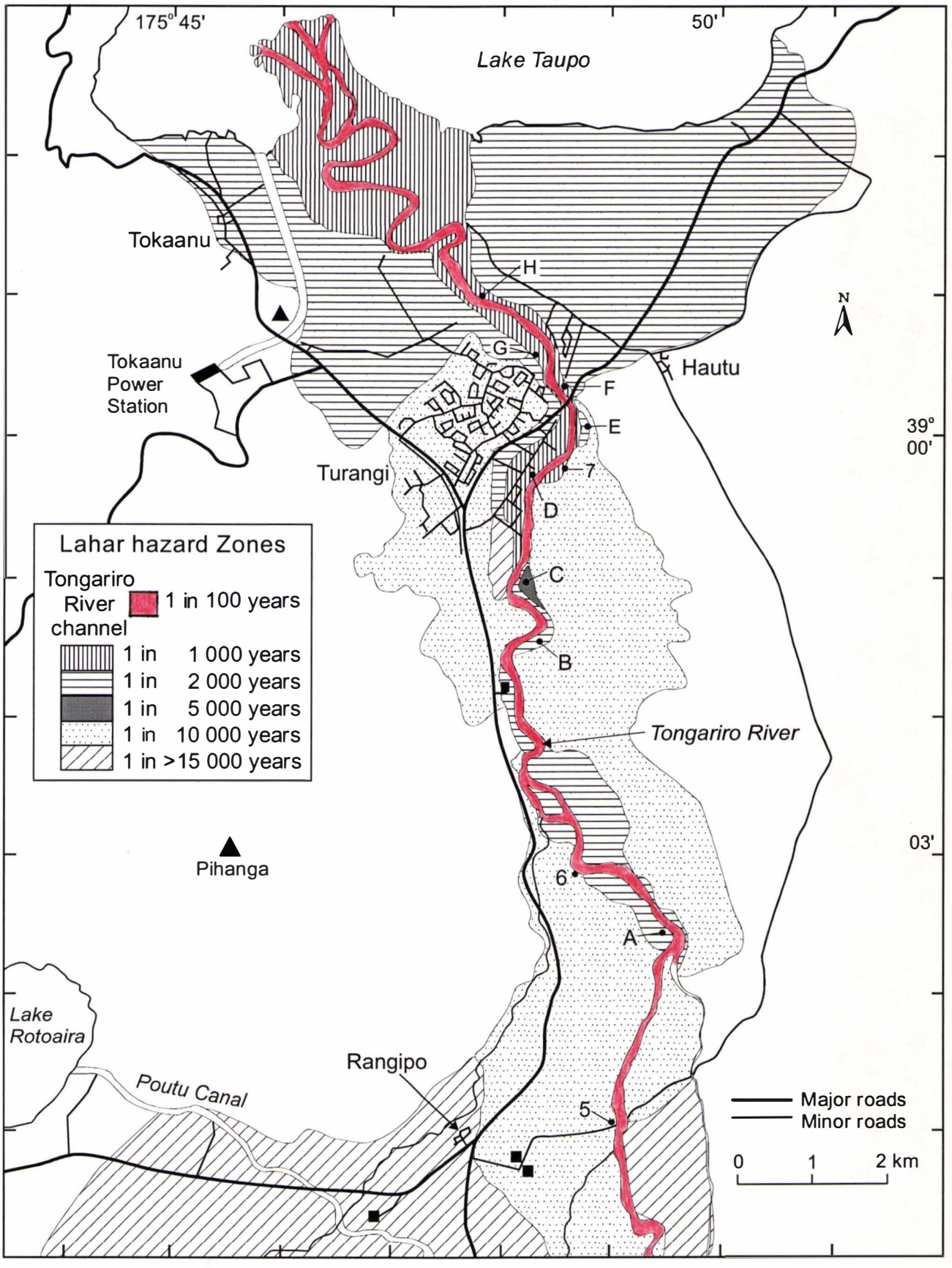

Figure 6.5 Enlargement of lahar hazard map for Turangi and its surrounds. This area contains the greatest population and most of the youngest laharic surfaces in the Tongariro catchment. Location of sections in Figs. 6.2 and 6.3 are labelled.

6.10.8 *1 in 35 year zone*

This zone includes the channel of the Mangatoetoenui Stream which was affected by at least two lahars in the 1995 eruption sequence of Ruapehu (Cronin *et al.*, in press(b)), and also by lahars in the 1895 and 1975 Ruapehu eruptions (Allen, 1902; Nairn *et al.*, 1979). Observations of Ruapehu volcano have been made for ca. 140 years (Gregg, 1960), and four lahars recorded during this time equates to a 1 in 35 year recurrence interval.

6.11 Discussion

The areas of greatest lahar hazard in the catchment are obviously the lowest lying areas closest to the Tongariro River and Mangatoetoenui Stream. The area of greatest risk in the catchment is where the highest lahar hazard and greatest vulnerability of people and property are combined. Although the entire town of Turangi is built on laharic surfaces, much of it is on a surface which has not been inundated by lahars since 10 ka B.P. However, parts of Turangi and many outlying houses are on surfaces which have been covered by much younger lahars. Thus, the area of greatest human risk in this catchment is where houses are built within the 1 in 1 000 year hazard zone in part of Turangi. One of the greatest property risks in the area has already been identified by lahar impacts during the 1995 Ruapehu eruption sequence. The Rangipo Dam became substantially infilled with sediment from lahars sourced within the Mangatoetoenui catchment. This dam retains water to be used for power generation in the underground Rangipo Power Station. Sandy and silty sediment within water piped to the power station led to severe wear of the turbine blades, necessitating replacement of one of them (ECNZ pers. comm., 1995). The State Highway 1 bridge crossing the Mangatoetoenui Stream on the Desert Road is probably the bridge at greatest risk from lahars in the Tongariro catchment.

The source of most lahars in the period 14.7-10 ka B.P. in the Tongariro catchment has been Ruapehu volcano, particularly via the Mangatoetoenui and Te Piripiri Streams. All Holocene lahars have also come from Ruapehu and most of these were sourced within Mangatoetoenui Stream.

Lahars in the Tongariro catchment have been attributed to a variety of generation mechanisms, including flank collapse, eruptions, glacier collapse and storms. The most readily identifiable are those related to tephra eruptions of either Tongariro or Ruapehu (Cronin and Neall, in press). Almost all of the Holocene lahars have been linked to large-scale tephra eruptions from either volcano. The 1995 lahars followed this pattern, but were of a smaller scale than most Holocene lahars.

Unlike the Whangaehu River, the Tongariro River tributaries do not directly drain Crater Lake, nor are they as close to the Lake as the Mangaturuturu, Whakapapaiti and Whakapapanui catchments. Thus, lahars generated by water expelled during small scale eruptions through the Lake have not occurred with the same frequency in the Tongariro

tributaries as they have in the other catchments. Two lahars derived from surges from Crater Lake were produced in the Mangatoetoenui Stream during eruptions in 1895 and 1975. In contrast, 19 lahars derived from Crater Lake are recorded in the Whangaehu Catchment prior to 1995 (Hodgson, 1993), and a further 26 occurred during the 1995 Ruapehu eruptive sequence (Cronin *et al.*, in press(b)).

During 1995, events in the Mangatoetoenui Stream indicate another mechanism for creating lahars that enter the Tongariro River during eruptions of Ruapehu. These lahars were caused when large amounts of tephra fell onto Mangatoetoenui Glacier, following several eruptions throughout September and early October 1995. The largest of these eruptions on October 11-12 contributed the greatest volume of tephra. Heavy rains in the following weeks caused collapse, rilling and remobilisation of saturated tephra to form lahars (Cronin *et al.*, in press(b)).

A further potential lahar generating mechanism in this catchment is the eruption of hot pyroclastic flows onto the Mangatoetoenui Glacier, which could rapidly entrain and melt snow and ice. Lahars caused by these mechanisms occurred on Nevado del Ruiz, where relatively small scale eruptions led to huge, devastating lahars (Pierson *et al.*, 1990). Evidence of only one pyroclastic flow has been recorded on Ruapehu at c. 10 ka B.P. (Donoghue et al., 1995) but most notably a lahar associated with this event is recorded in the Mangatoetoenui catchment (Cronin and Neall, in press).

Another possible way for lahars to enter the Tongariro River is via overflow of a large lahar from the Whangaehu River into Upper Waikato Stream. Deposits recording such an event have not been described in this study, but are described by Donoghue (1991). During the 1995 eruption sequence of Ruapehu this situation almost eventuated. Several lahars between September 18 and 25 gradually built up the base level of the Whangaehu channel on the upper ring plain by several metres until on September 25 the largest lahars flooded into small tributaries which flow northwards before rejoining the Whangaehu River farther downstream. These northeastward-flooding lahars travelled to within 300 m of tributaries of Upper Waikato Stream. If diversion of the main Whangaehu River channel into this route were to occur, lahars would probably overflow into Upper Waikato Stream. Incision of the Whangaehu River through the aggraded lahar deposits over the following few months has temporarily reduced this risk. If the northeastward flowing channels become further incised during heavy rainstorms, headward erosion could lead to capture of the main Whangaehu River channel. A northeastward course of the River would then lead to a new route within 300 m of Upper Waikato Stream. Hence the potential for riverbank erosion and overflow northwards could lead to future lahars being directed into the Tongariro River.

6.11.1 Mitigation of hazards

Three areas are identified where hazards of lahars in the Tongariro River can be mitigated.

1) Warning of lahars. Given adequate warning of a lahar, areas at risk can be evacuated and loss of life minimised. Currently there is no lahar warning device installed on the Tongariro River or any of its tributaries. Although monitoring of flow levels is carried out by ECNZ for managing the Tongariro Power Development, a purpose-built lahar warning gauge would provide the best and most timely warning.
2) Containment of small lahars. Lahars of a certain volume could be potentially retained behind the Rangipo Dam, particularly if the dam were emptied in preparation for such a lahar. The same strategy was advised and utilised in the Swift Reservoir to contain a lahar from Mt. St. Helens in 1980 (Crandell and Mullineaux, 1978; Schuster, 1981). Containment of a lahar in the Rangipo Dam would create problems for the power development but could potentially reduce downstream impacts. However, if the lahar were larger than the dam capacity, the facility could be destroyed in attempting to contain it.
3) Planning of future expansion of Turangi. Parts of Turangi have expanded onto surfaces within the 1 in 2000 and 1 in 1000 year lahar hazard zones across the River from the main area of town. In planning future housing expansion of the town, building within the 1 in 10 000 year zone should be encouraged over areas of greater hazard.

6.12 Conclusions

The greatest number and thickness of lahar deposits in the exposed record of the Tongariro catchment are from lahars occurring between 14.7 and 9.8 ka B.P. Consequently the preserved laharic surfaces of greatest area are also of this age. Deposits of Holocene lahars are confined to restricted surfaces, closer to the present river channel. These deposits are less well preserved than the older units because they were probably confined to a more deeply incised channel than during late glacial and early post-glacial times.

The town of Turangi and many outlying houses are built on surfaces that are laharic in origin. However, lahars have not inundated a large proportion of the town since c. 10 ka years B.P. Lower-lying parts of Turangi, closer to the Tongariro River and other outlying houses are built on surfaces which have been inundated by much younger lahars. The area identified with the greatest human risk are the lowest-lying parts of Turangi, which were last inundated by a lahar less than 1850 years B.P. Mitigation of this risk could be provided by a lahar warning system and careful planning of future urban development in Turangi.

The Mangatoetoenui Stream tributary is identified as the most important lahar conduit for the Tongariro catchment during the Holocene. It has also been the only lahar conduit in this catchment in historic times. Consequently, infrastructure at greatest risk of damage from lahars includes the State Highway 1 bridge crossing Mangatoetoenui Stream, the Rangipo Dam, the Rangipo Power Station that it supplies, and the Poutu Canal intake structure.

6.13 Acknowledgements

SJC gratefully acknowledges funding from the New Zealand Vice-Chancellor's Committee, Massey University Graduate Research Fund, the Helen E. Akers Scholarship Fund and the Tongariro Natural History Society. We thank J.A. Lecointre for his comments on an earlier version of the manuscript.

References

Allen, G.F., 1902. Supplementary edition of Willis' guide book of new routes for tourists. Willis, Wanganui: 240 pp.

Beverage, J.P., Culbertson, J.K., 1964. Hyperconcentrations of suspended sediment. J. Hydraul. Div., American Soc. of Civil Engineers, 90: 117-126.

Clarke, C., Smith, M., 1986. Turangi town centre, where to now? Taupo County Council Special Report, 15.

Crandell, D.R., Mullineaux, D.R., 1978. Potential hazards from future eruptions of Mount St. Helens volcano, Washington. U.S.G.S. Bull., 1383-C: 26 pp.

Cronin, S.J., Neall, V.E., in press. A late Quaternary stratigraphic framework for the northeastern Ruapehu and eastern Tongariro ring plains, New Zealand. N. Z. J. Geol. and Geophys., 40.

Cronin, S.J., Neall, V.E., Stewart, R.B., Palmer, A.S., 1996. A multiple parameter approach to andesitic tephra correlation, Ruapehu volcano, New Zealand. J. Volcanol. and Geotherm. Res., 72: 199-215.

Cronin, S.J., Neall, V.E., Lecointre, J.A., Palmer, A.S., in press(b). Changes in Whangaehu River lahar characteristics during the 1995 eruption sequence, Ruapehu volcano, New Zealand. J. Volcanol. and Geotherm. Res.

Cronin, S.J., Neall, V.E., Palmer, A.S., Stewart, R.B., in press(a). Methods of identifying late Quaternary rhyolitic tephras on the ring plains of Ruapehu and Tongariro volcanoes, New Zealand. N. Z. J. Geol. and Geophys, 40.

Department of Statistics, 1992. 1991 Census of Population and Dwellings, Waikato/Bay of Plenty Regional Report. Department of Statistics, Wellington, N.Z.

Donoghue, S.L., 1991. Late Quaternary volcanic stratigraphy of the south-eastern sector of Mount Ruapehu ring plain, New Zealand. Unpub. PhD thesis, Massey University, Palmerston North, New Zealand.

Donoghue, S.L., Neall, V.E., Palmer, A.S., 1995. Stratigraphy and chronology of late Quaternary andesitic tephra deposits, Tongariro Volcanic Centre, New Zealand. J. Roy. Soc. of N. Z., 25: 115-206.

Froggatt, P.C., Lowe, D.J., 1990. A review of late Quaternary silicic and some other tephra formations from New Zealand: their stratigraphy, nomenclature, distribution, volume, and age. N. Z. J. Geol. and Geophys, 33: 89-109.

Gregg, D.R., 1960. The geology of Tongariro Subdivision. N.Z. Geol. Survey Bull., 40: 151pp.

Grindley, G.W., 1960. Geological map of New Zealand, 1st ed., 1: 250 000, Sheet 8, Taupo. Dept. of Scientific and Industrial Res., Wellington.

Hackett, W.R., Houghton, B.F., 1989. A facies model for a Quaternary andesitic composite volcano: Ruapehu, New Zealand. Bull. Volcanol., 51: 51-68.

Hodgson, K.A., 1993. Late Quaternary lahars from Mt. Ruapehu in the Whangaehu River valley, North Island, New Zealand. Unpub. PhD thesis, Massey University, Palmerston North, New Zealand.

Mathews, W.H., 1967. A contribution to the geology of the Mount Tongariro massif, North Island, New Zealand. N. Z. J. Geol. and Geophys., 10: 1027-1038.

Nairn, I.A., Self, S., 1978. Explosive eruptions and pyroclastic avalanches from Ngauruhoe in February 1975. J. Volcanol. and Geotherm. Res., 3: 39-60.

Nairn, I.A., Wood, C.P, Hewson C.A.Y., 1979. Phreatic eruptions of Ruapehu: April 1975. N. Z. J. Geology and Geophys., 22: 155-173.

Palmer, B.A., Purves, A.M., Donoghue, S.L., 1993. Controls on the accumulation of a volcaniclastic fan, Ruapehu composite volcano, New Zealand. Bull. Volcanol., 55: 176-189.

Philippine Institute of Volcanology and Seismology, 1992. Pinatubo: Lava dome growth; pyroclastic flow deposits spawn destructive lahars and secondary explosions. Bull. Global Volc. Network 17(9): 8-10.

Pierson, T.C., Costa, J.E., 1987. A rheologic classification of subaerial sediment-water flows. G.S.A., Reviews in Engineering Geol. VII: 1-12.

Pierson, T.C., Janda, R.J., Thouret, J.-C., Borrero, C.A., 1990. Perturbation and melting of snow and ice by the 13 November 1985 eruption of Nevado del Ruiz, Colombia, and consequent mobilisation, flow and deposition of lahars. J. Volcanol. and Geotherm. Res., 41: 17-66.

Pierson, T.C., Janda, R.J., Umbal, J.V., Daag, A.S., 1992. Immediate and long-term hazards from lahars and excess sedimentation in rivers draining Mt. Pinatubo, Philippines. U.S.G.S. Water Resources Investigations Rep., 92-4039: 182-203.

Pierson, T.C., Scott, K.M., 1985. Downstream dilution of a lahar: transition from debris flow to hyperconcentrated streamflow. Water Resources Res., 21: 1511-1524.

Schuster, R.L., 1981. Effects of the eruptions on civil works and operations in the Pacific Northwest. *In*: Lipman, P.W.; Mullineaux D.R. (Eds.) The 1980 eruptions of Mount St. Helens, Washington. U.S.G.S. Prof. Pap. 1250: 701-718.

Smith, G.A. 1986: Coarse-grained nonmarine volcaniclastic sediment: Terminology and deposition process. G.S.A. Bull., 97: 1-10.

Smith, G.A., Fritz, W.J., 1989. Volcanic influences on terrestrial sedimentation. Geology 17: 375-376.

Stilwell, W.F., Hopkins, H.J., Appleton, W., 1954. Tangiwai railway disaster. Report of the Board of Inquiry. Government Printer, Wellington: 31pp.

Topping, W.W., 1973. Tephrostratigraphy and chronology of late Quaternary eruptives from the Tongariro Volcanic Centre, New Zealand. N. Z. J. Geol. and Geophys., 16: 397-423.

Topping, W.W., Kohn B.P., 1973. Rhyolitic tephra marker beds in the Tongariro area, North Island, New Zealand. N. Z. J. Geol. and Geophys., 16: 375-395.

Voight, B., 1990. The 1985 Nevado del Ruiz volcano catastrophe: anatomy and retrospection. J. Volcanol. and Geotherm. Res., 44: 349-386.

Water and Soils Division, Ministry of Works and Development, 1979. N. Z. Land Resource Inventory Worksheets, N102 Tokaanu and N112 Ngauruhoe and Bay of Plenty - Volcanic Region Landuse Capability Extended Legend (12pp). National Water and Soil Conservation Organisation, Ministry of Works and Development, Wellington, N.Z.

Wilson, C.J.N., Switzur, R.V., Ward, A.P., 1988. A new ^{14}C age for the Oruanui (Wairakei) eruption, New Zealand. Geol. Mag., 125: 297-300.

Wilson, C.J.N., Houghton, B.F., Lanphere, M.A., Weaver, S.D., 1992. A new radiometric age estimate for the Rotoehu Ash from Mayor Island volcano, New Zealand. N. Z. J. Geol. and Geophys., 35: 371-374.

Wilson, C.J.N., 1993. Stratigraphy, chronology, styles and dynamics of late Quaternary eruptions from Taupo Volcano, New Zealand. Phil. Trans. Roy. Soc. of London A 343: 205-306.

CHAPTER 7: GEOLOGY AND LANDSCAPE DEVELOPMENT OF THE NORTHEASTERN TONGARIRO VOLCANIC CENTRE

7.1 Introduction

In the three previous chapters, rhyolitic and andesitic tephrostratigraphy (developed in chapters 2 and 3) were used to establish a climate/soil development history and a history of lahars and landscape development by lahars in the study area. This chapter combines the results of the previous chapters and adds further information on other landscape and geological events on the ring plains to provide an overall synthesis of their geology and development.

This chapter comprises three parts: (7.2) a geological map of the northeastern Tongariro Volcanic Centre with accompanying notes, (7.3) a published paper entitled "Geological history of the northeastern ring plain of Ruapehu volcano, New Zealand", and (7.4) a summary geological synthesis of the entire study area.

The paper: *Geological history of the northeastern ring plain of Ruapehu volcano, New Zealand* by: Shane J. Cronin, V.E. Neall and A.S. Palmer, is published within Quaternary International Vol. 34-36. The contributions of each author to the study were as follows.

S. J. Cronin: Principal Investigator

Carried out all:	Field mapping, description and sampling
	Mineralogy analyses
	All other laboratory studies
	Preparation and writing of manuscript

V. E. Neall and A. S. Palmer: Advisors

Aided the study by:	discussion of results and methodology
	editing and discussion of the manuscript

7.2 Surficial geologic map of the northeastern Tongariro Volcanic Centre

The surficial geologic map of the northeastern Tongariro Volcanic Centre is presented in Fig. 7.1. Figure 7.2 demonstrates the stratigraphy of the mapping units and their relationship to tephra marker beds and previously mapped formations in the surrounding area.

7.2.1 Methods

The volcanic and volcaniclastic deposits and sediments within the area were mapped using field sheets of 1:25 000 scale. Field-section descriptions were supplemented with vertical aerial photographic interpretation to delineate surfaces. Stereo-pairs of 1981 black and white vertical aerial photographs at 1:25 000 scale were used.

MAP OF THE SURFICIAL GEOLOGY OF A PORTION OF THE NORTHEASTERN TONGARIRO VOLCANIC CENTRE

Legend

Laharic surfaces

- < 1.85 ka.
- > 1.85 ka
- > 5.3 ka
- > 9.7 ka, Ruapehu
- > 12 ka, Tongariro
- > 14.7 ka, Ruapehu
- > 14.7 ka, Tongariro and Ruapehu

Lavas

- < 14.7 ka, Tongariro
- > 14.7 ka, Ruapehu
- > 14.7 ka, Tongariro
- > 22.6 ka, Tongariro

Moraines

- > 10 ka moraines

Composite surfaces

- > 14.7 ka Tongariro lahar surface, covered by < 1.85 ka alluvium.
- > 14.7 ka lahar surface veneering > 22.6 ka lava, Tongariro.
- > 14.7 ka Ruapehu lahar surface, reworked and partially covered by < 10 ka alluvium.

Symbols

- Covered by up to 30 m of Taupo Ignimbrite
- Major roads
- Minor roads
- Power development tunnels
- Topographic contours 100 m intervals
- 47 State highways

Lake Taupo
Tokaanu
Tokaanu Power Station
Turangi
Hautu
Pihanga
Lake Rotoaira
Rangipo
Poutu Canal
Region not mapped
Mangahouhounui Stream
Puketarata Stream
Mangamate Stream
Oturere Stream
Makahikatoa Stream
Mangatawai Stream
Rangipo Power Station
Waihohonu Stream
Rangipo Dam
Tongariro River
Mangatoetoenui Stream
Waipakihi River
Te Piripiri Stream
Upper Waikato Stream
N
0 1 2 3 4 5 km
175° 40'
45'
50'
39° 00'
05'
10'
15'

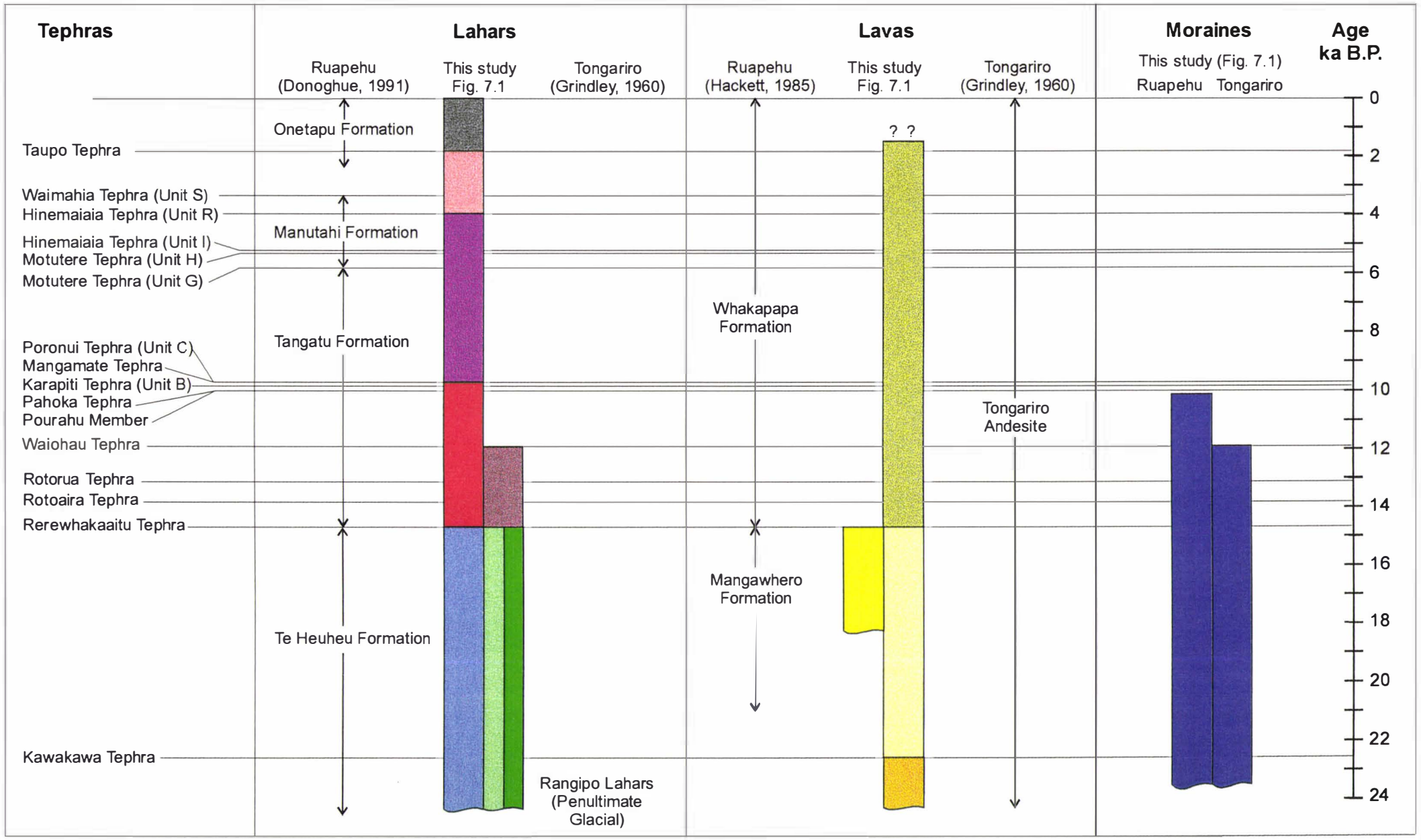

Fig 7.2 Legend of geologic units mapped in Fig. 7.1, showing their stratigraphic relationships to previously mapped formations and tephra marker beds.

The scale of the map presented in Fig. 7.1 is 1:100 000. The base map was prepared by scanning and digitising contours, rivers, roads and other features from NZMS 260 series topographic maps (1:50 000 scale), T19-Edition 2 (DOSLI, 1994) and T20-Edition 1 (DOSLI, 1982).

The study area was mostly limited to the ring plain and lower slopes of the Ruapehu and Tongariro volcanoes but also included the lower Tongariro River valley. Areas were delineated and mapped according to their age (determined by cover-bed stratigraphy), their lithology, and the volcano from which they were derived (Tongariro or Ruapehu).

7.2.2 Laharic surfaces

Seven laharic surfaces are mapped in the studied area. Each surface is delimited by the deposits of the youngest lahar preserved on it. The ages of these lahars are interpreted from tephra marker beds which under- and overlie them (Fig. 7.2). The stratigraphy of these surfaces was presented in Chapters 5 and 6.

7.2.2A *Ruapehu-derived lahar surfaces*

The youngest lahar surface (<1.85 ka B.P.) has been inundated by at least one lahar since the eruption of the Taupo Tephra. In Chapter 6 it was postulated that late Holocene lahars in the Tongariro catchment were derived from Ruapehu volcano. Thus lahar deposits forming this surface are correlated to the Onetapu Formation (after Donoghue, 1991; Hodgson, 1993). The > 1.85 ka surface, if it were derived from the same source, is between Onetapu Formation and Manutahi Formation in age (Fig. 7.2) and comprises a newly recognised Ruapehu lahar surface.

Ruapehu-sourced lahars mapped by Donoghue (1991) as the Tangatu Formation, are here mapped as two separate surfaces. The youngest and smaller surface comprises a lahar deposit in the order of 5.2-5.3 ka (R1, Chapter 5). This surface is preserved along the Mangatoetoenui Stream and a small remnant is preserved immediately south of Turangi. The other Tangatu Formation surface mapped here comprises multiple lahars which are > 9.7 ka in age. This surface occurs on the northeastern Ruapehu ring plain between the Te Piripiri and Ohinepango Streams and is also mapped over large areas from Turangi south to Rangipo.

Large areas of Te Heuheu Formation occur on the northeastern Ruapehu ring plain between Te Piripiri and Upper Waikato Streams and are mapped as the > 14.7 ka (Ruapehu) surface. A portion of this surface has been eroded and reworked by the Holocene/recent activity of streams crossing the area and so is mapped as a composite surface. North of the Waihohonu Stream, throughout the area where the Tongariro River cuts through the Tongariro volcano ring plain, Te Heuheu Formation lahar deposits are also interbedded with contemporaneous lahar deposits derived from Tongariro volcano. In this area it is impossible to differentiate the lahar deposits from the two volcanoes or a boundary between them. Consequently, this surface is mapped as containing lahars from both volcanoes, but is probably dominated by Tongariro-sourced lahars.

7.2.2B *Tongariro-derived lahar surfaces*

The lahars of the Tongariro ring plain were mapped by Grindley (1960) as the Rangipo Lahars and were thought to be of Penultimate Glacial age. Here the eastern Tongariro ring plain is mapped mostly as Last Glacial-age lahar deposits with smaller areas of early post-glacial lahars.

The youngest lahar surfaces derived from Tongariro volcano comprise lahar deposits which are > 12 ka in age (Fig. 7.2). These surfaces are mapped beside the upper portion of the Waihohonu Stream and along the Oturere and Makahikatoa Streams. These lahar deposits interdigitate with and are covered by Tangatu Formation lahar deposits (derived from Ruapehu volcano) in the lower Waihohonu Stream and along the Tongariro River.

The remaining eastern Tongariro ring plain mostly comprises surfaces composed of lahar deposits > 14.7 ka in age. This is mapped in two areas. The first area is mapped as a simple lahar surface comprising dominantly Tongariro volcano-derived lahar deposits > 14.7 ka in age. This surface is mapped on the Tongariro ring plain sector between the Mangamate Stream and Lake Rotoaira. This surface probably also includes subordinate lahar deposits derived from Ruapehu volcano, particularly in areas close to the Tongariro River. The second area (between the Waihohonu and Mangamate Streams) is mapped as a composite surface. This surface comprises lahar deposits >14.7 ka in age which veneer Tongariro-sourced lava flows which are >22.6 ka B.P. in age. In the present stream valleys the lahar deposit cover can be up to tens of metres thick, whilst on some ridge tops and other isolated areas the lahar veneer is absent. The lahar deposits are mostly derived from Tongariro volcano, but probably also include lahar deposits derived from Ruapehu volcano, particularly at the southern part of the mapped area and near the Tongariro River.

7.2.3 Lavas

Lava flows derived from both volcanoes were mapped on the ring plains and were dated by their tephra coverbeds. The petrology of some the lavas was also described in order to characterise them and to correlate exposures.

7.2.3A *Ruapehu-derived lavas*

On the northeastern Ruapehu ring plain several lava flows are mapped. All of these flows have similar coverbed sequences and their oldest coverbed is the Rerewhakaaitu Tephra (Fig. 7.2). These lava flows also have very similar lithologies. They all have a porphyritic-aphanitic texture and contain abundant glomerocrysts. They are all two-pyroxene andesites, with a phenocryst assemblage dominated by large, lath-shaped plagioclase crystals (Table 7.1). Plagioclase phenocrysts display strong oscillatory zoning. Orthopyroxene is the dominant ferromagnesian phenocryst with around twice the modal % of clinopyroxene.

Table 7.1 Mineralogy and locations of lava sampled from the ring plains of northeastern Tongariro Volcanic Centre.

Sample	NZMS 260 reference	Mapping Unit	Phenocryst modal %					Location
			PL	CPX	OPX	TM	OL	
93.14	T20/442146	> 14.7 ka Ruapehu	60	17	18	5	-	Flow north of Mangatoetoenui Stream
93.165	T20/448159	"	46	19	35	<1	-	"
93.23	T20/446127	"	62	11	26	1	-	Flow north of Te Piripiri Stream
93.106	T20/463122	"	57	13	29	1	-	Flow along Wharepu Stream
93.107	T20/435130	"	53	15	32	<1	-	Flow south of Te Piripiri Stream
95.5	T19/420243	< 14.7 ka Tongariro	32	24	30	10	3	Upper Oturere valley
95.8	T19/423339	"	40	17	37	6	-	Flow Southwest of Lake Rotoaira
93.19	T20/464174	> 22.6 ka Tongariro	53	18	26	3	-	Flow in mid-Waihohonu Stream beside State Highway 1
93.16	T20/492185	> 14.7 ka laharic surface veneering >22.6 ka lava, Tongariro	62	19	19	<1	-	Flow within lower Waihohonu Stream
94.8	T20/506185	"	54	12	31	1	2	Within Tongariro River channel, downstream of Rangipo Dam
94.31	T20/499178	"	58	9	32	1	-	At Rangipo Dam
94.33	T19/528227	"	50	13	35	2	-	Tongariro River, downstream of Tree Trunk Gorge
94.36	T19/520221	"	34	16	49	1	-	Tongariro River, upstream of Tree Trunk Gorge
94.55	T19/506238	"	63	32	4	1	-	Flow in lower Mangatawai Stream
94.75	T19/535246	"	41	10	44	1	4	Tongariro River, Pillars of Hercules
95.16	T19/550331	"	44	19	33	1	3	Tongariro River, on Rangipo Prison Farm
95.10	T19/448326	> 22.6 Tongariro	54	11	32	3	-	South of Lake Rotoaira
95.12	T19/466298	"	54	8	29	9	-	North of Mangahouhounui Stream
94.80	T19/536376	Unmapped Pihanga flow	<1	14	20	1	65	Tongariro River at Poutu Pool

PI = Plagioclase, CPX = Clinopyroxene, OPX = Orthopyroxene, TM = Titanomagnetite, OL = Olivine.

Titanomagnetite occurs in association with pyroxene phenocrysts and within glomerocrysts. Glomerocrysts are made up of 20 to 100+ crystals of all four phenocryst phases. Two types of glomerocrysts were observed, those comprising few (20-30) large crystals, and others comprising larger numbers of smaller crystals which were dominantly plagioclase. The groundmass is dominated by (80-95% by volume) small laths of plagioclase with minor orthopyroxene and clinopyroxene crystals.

Based on their mineralogy, these lavas appear to belong to the Type 1 class (plagioclase-pyroxene phyric lavas) of Graham and Hackett (1987). The minimum age of these lavas (determined from their oldest coverbed, Fig. 7.2) indicate that these flows correlate to the Mangawhero Formation of Hackett (1985).

7.2.3B *Tongariro-derived lavas*

The Tongariro massif was previously mapped as a single unit, Tongariro Andesite, which spanned the Quaternary in age (Grindley, 1960). In this study, three Tongariro-derived lava surfaces are mapped in addition to a composite surface comprising lavas and lahar deposits.

The oldest lava surfaces are those overlain by the Kawakawa Tephra, indicating a minimum age of 22.6 ka B.P. The lava flow beside the Waihohonu Stream has the Okaia Tephra below it, providing an age bracket of 22.6 - c. 23 ka (Section 5.10). The other lava surface mapped with the same minimum age (northeastern Tongariro volcano) has K-Ar ages ranging between 105 and 130 ka for samples taken higher on the cone (Hobden *et al.*, 1996). If one believes the radiometric ages, then this indicates that the northeastern Tongariro lava surface has an unconformable coverbed sequence.

Samples from both areas have a very similar mineralogy to one another and to the Ruapehu lavas described in the last section (Table 7.1). However, these samples have a finer-grained, plagioclase-dominated groundmass, and glomerocrysts comprising fewer crystals (10-20) than the Ruapehu flows described above. These lavas also fit within the Type 1 classification of Graham and Hackett (1987).

Lavas comprising the surface which is mapped as the composite of >14.7 ka lahars veneering >22.6 ka lava, also derive their minimum age from being overlain by the Kawakawa Tephra. However, given that this sector of the Tongariro cone is K-Ar dated at between 65 and 130 ka (Hobden *et al.*, 1996) these lavas are probably of similar or greater age. Samples from some of these flows have a pyroxene-dominant mineralogy rather than plagioclase-dominant. Three of the samples also contain a small percentage of large olivine phenocrysts. All samples have a very fine-grained groundmass comprised of laths of plagioclase and interstitial brown glass. These mineralogical features indicate that some of these lavas were more basic than those described above. These lavas include both Type 1 (plagioclase-pyroxene phyric lavas) and Type 3 (pyroxene-phyric lavas) classifications of Graham and Hackett (1987) for Tongariro Volcanic Centre lavas.

The > 14.7 ka (Tongariro) lavas mapped are overlain by the Rerewhakaaitu Tephra, indicating their minimum age (Fig. 7.2). However, samples from these flows

higher on the cone give K-Ar ages of 65-130 ka (Hobden *et al.*, 1996), indicating the coverbed sequences are potentially unconformable. No samples of these lavas were collected.

The disparity between the K-Ar ages of Hobden *et al.* (1996) and the coverbed sequences on the Tongariro lava surfaces, implies that these surfaces were exposed to intense physical weathering during the last stadial of the Last Glacial.

Two lava flows are mapped as < 14.7 ka. The flow southwest of Lake Rotoaira is immediately overlain by the Waiohau Tephra but the Rerewhakaaitu Tephra (present on the adjacent lava surface) does not occur. This provides an age range for this lava flow of between 14.7-11.9 ka B.P. The other flow mapped as < 14.7 ka occurs within the Oturere Valley. No coverbeds were found overlying this lava flow, which may indicate it is very young. Both of these two flows have a Type 3, pyroxene-dominant mineralogy, and the Oturere flow also contains olivine (Table 7.1).

7.2.4 Moraines

Parts of two sets of paired moraines were mapped in the study area based on their morphology. The moraines beside the Waihohonu Stream have been previously described by Mathews (1967) and those flanking the Mangatoetoenui Stream by McArthur and Shepherd (1990). Mathews (1967) estimated that the Waihohonu moraines were around 15 ka in age by comparison to the youngest moraines in the South Island. McArthur and Shepherd (1990) considered the Mangatoetoenui moraines to have been formed in multiple glacier advances and represented the last two stadials of the Last Glaciation.

In this study, tephra coverbeds on these two sets of moraines provide minimum ages for their stabilisation and the cessation of their construction (Fig. 7.2). The Waiohau Tephra occurs on the Waihohonu moraines providing a minimum age of stabilisation of 11.9 ka B.P. The oldest tephra on the Mangatoetoenui moraines is the Pourahu Member of the Bullot Formation indicating a minimum age of ca. 10 ka.

7.3 GEOLOGICAL HISTORY OF THE NORTH-EASTERN RING PLAIN OF RUAPEHU VOLCANO, NEW ZEALAND

Shane J. Cronin, Vincent E. Neall and Alan S. Palmer
Department of Soil Science, Massey University, Private Bag 11 222, Palmerston North, New Zealand

1996, Quaternary International 34-36: 21-28.

Abstract Continuous exposures along the Upper Waikato Stream provide new insights into the north-eastern ring plain of Ruapehu volcano, extending the known stratigraphy beyond 22.5 ka. Time control in the sequence is provided by five rhyolitic tephra units, erupted from central North Island volcanoes, comprising Kawakawa, Okaia,

Omataroa, Hauparu, and Rotoehu tephras. The sequence is dominated volumetrically by diamictons and fluvial deposits resulting both from volcanic events and periods of instability on the flanks of Ruapehu. Within the sequence are >60 individual andesitic lapilli units, derived primarily from Ruapehu volcano via mostly sub-plinian eruption mechanisms. An average eruption rate of more than one lapilli eruption per 1000 years is estimated for the *c.* 60 ka record. The style of deposition on the ring plain changes over time and appears to reflect climate change over the Last Glacial period. In periods of severe climatic conditions during marine $\delta^{18}O$ stage 4 (Porewan stadial), and the Last Glacial Maximum of marine $\delta^{18}O$ stage 2 (Ohakean), the north-eastern ring plain aggraded rapidly with deposition of thick continuous diamicton sequences. The other recognised cool period in the southern North Island, the stadial of late $\delta^{18}O$ stage 3 (Ratan), did not appear to induce major aggradation on the north-eastern ring plain. During periods of mild climate within the Last Glacial, deposition on the north-eastern ring plain was dominated by fall accession of either tephra, or material reworked from other parts of the ring plain by aeolian processes.

7.3.1 Introduction

Ruapehu volcano is an active andesitic composite volcano located at the southern end of the Taupo Volcanic Zone (TVZ) in the central North Island of New Zealand. Previous studies of the geological history of this volcano have mainly been confined to the present volcanic cone (e.g. Gregg, 1960; Hackett and Houghton, 1989), or to the younger (<22.5 ka) stratigraphy preserved on the ring plain, where a more complete record of events at the volcano are recorded, both spatially and temporally (e.g. Palmer, 1991; Donoghue *et al.*, 1995).

This paper presents a summary of the stratigraphy preserved in the north-eastern sector of the Ruapehu ring plain and describes events occurring on the volcano and this sector of the ring plain for the period 22.5 ka to *c.* 80 ka.

7.3.2 Geologic setting

The Tongariro Volcanic Centre (TgVC) at the southern terminus of TVZ is composed of five composite andesitic volcanoes, as well as a number of outlying smaller vents. Ruapehu volcano is the largest in the TgVC and at 2797 m is the highest peak in the North Island. Tongariro volcano is also a large massif which lies to the north of Ruapehu. Both volcanoes have been historically active. The current Ruapehu massif comprises a volume of 110 km^3 (Hackett and Houghton, 1989) with a surrounding volcaniclastic ring plain of similar volume. Ruapehu is directly underlain by Tertiary marine sediments with Mesozoic metamorphosed greywacke (schist) occurring at greater depths. The Ruapehu ring plain deposits extend down drainage channels into Tertiary hill country to the south and west, interfinger with the Tongariro ring plain to the north, and are confined in the east by the Kaimanawa Mountains.

7.3.3 Site of study

The Upper Waikato Stream drains the north-eastern flanks of Ruapehu volcano and is immediately north of the watershed boundary where the present drainage from the eastern flanks of Ruapehu divides between the Whangaehu River to the south and the Tongariro River system to the north (Fig. 7.3).

Between State Highway 1 and the Tongariro River, Upper Waikato Stream has cut deeply through the ring plain deposits of Ruapehu volcano, exposing in near continuous sections a record of deposition spanning an estimated 80 000 years.

7.3.4 Stratigraphy

The stratigraphy of the deposits in the age range of 22.5 ka to the present has been described by Topping (1973) and Donoghue (1995). Beyond 22.5 ka there is very little published information on the Ruapehu and Tongariro ring plains. Topping (1973) describes these older deposits as the Rangipo lahars on the Tongariro ring plain, and the Waimarino lahars on the Ruapehu ring plain. This study focuses on the deposits older than the regional marker horizon of the Kawakawa Tephra, dated at 22 590 ± 230 years BP (Wilson *et al.*, 1988). The composite stratigraphic sequence preserved in Upper Waikato Stream cuttings beneath the Kawakawa Tephra is shown in Fig. 7.4.

7.3.4A *Age*

Time control is provided by the presence of five distal rhyolitic tephra layers interbedded with sediments in the depositional sequence. These are identified here as the Taupo sourced Kawakawa and Okaia Tephras, and the Okataina Volcano-sourced Omataroa Tephra, Hauparu Tephra, and Rotoehu Ash (Howorth, 1975; Froggatt and Lowe, 1990). The ages of these units are given in Table 7.2, and their stratigraphic position in Fig. 7.4.

Table 7.2 Rhyolitic tephra identified within the northeastern ring plain sequence, Ruapehu.

Tephra name	Source *	Age (B.P.)	Reference for age
Kawakawa Tephra	TVC	22 590 ± 230†	Wilson *et al.* (1988)
Okaia Tephra	TVC	ca. 23 000‡	Froggatt and Lowe (1990)
Omataroa Tephra	OVC	28 220 ± 630†	"
Hauparu Tephra	OVC	35 870 ± 1270†	"
Rotoehu Ash	OVC	64 000 ± 4000§	Wilson *et al.* (1992)

[a] TVC = Taupo Volcanic Centre; OVC = Okataina Volcanic Centre.

† Denotes ^{14}C ages on old half life basis.

‡ Estimated stratigraphic age.

§ Whole rock K-Ar age.

The Kawakawa Tephra occurs in this area as a 0.2 to 0.5 m deposit. Abundant accretionary lapilli are contained within the fall layers of the deposit, characteristic of this

tephra (Self and Healy, 1987). The older four tephras do not occur as visible layers in the sequence. They were identified as thin zones of rhyolitic glass enrichment within fine-grained andesitic ash. The identification of these microscopic tephra layers was elucidated using a combination of major element glass chemistry, ferromagnesian mineralogy, and stratigraphy. The major element chemistry was determined for polished individual grains on a JEOL-733 electron microprobe following the procedures and analytical conditions of Froggatt and Gosson (1982), and Froggatt (1983). A 20 μm beam diameter was used when possible, otherwise a 10 μm beam was used with a beam current of 8 nA at an accelerating voltage of 15 kV. Between 10 and 20 individual glass shards were analysed for each tephra layer.

The glass chemistry was compared with published glass analyses carried out under the same analytical conditions (Froggatt, 1983; Froggatt and Rogers, 1990; Pillans and Wright, 1992; Stokes *et al.*, 1992; and Pillans *et al.*, 1993). Similarity coefficients, and coefficients of variation (Borchardt *et al.*, 1971) were calculated to compare the unknown samples with large volume tephra units in the general time frame. The glass chemistry provided good matches with stratigraphically consistent correlations. The presence of cummingtonite within the layer identified as Rotoehu Ash gave further evidence of its identification based on glass chemistry (Froggatt and Lowe, 1990). The time planes provided by the rhyolitic tephra horizons enable a reconstruction of the events building up the north-eastern sector of Ruapehu ring plain.

Near the base of the sequence a lignite deposit is exposed. Given the time control provided by the rhyolitic tephras above, this lignite may be equivalent in age to one of two other lignite deposits found adjacent to this area. McGlone and Topping (1983) describe two lignite deposits each representing warm periods during marine $\delta^{18}O$ stage 5a and 5c. Further palynology work will confirm whether the lignite deposit can be correlated to one of these warm periods at approximately 80 ka and 100ka respectively (See Section 7.3.9).

7.3.4B *Sequence*

The stratigraphic column is divided into three parts (Fig. 7.4), each representing periods of different types of deposition on the north-eastern sector of the ring plain. The oldest part of the sequence (column C in Fig. 7.4) contains a cemented diamicton unit at the base. This unit forms the valley floor and its base is not seen. Overlying this basal diamicton is a deposit of dark brown and black, fibrous, firm, and centimetre to decimetre-scale laminar-bedded lignite. Interbedded within this lignite, as well as immediately above and below, are hornblende-rich andesitic, lapilli and ash layers. These tephra layers vary in thickness from centimetres to tens of centimetres and are not exposed in many other localities; hence their distribution is poorly known. Interbedded within the lignite, as well as above it, are centimetre-scale finely-bedded fluvial sands. Above the lignite deposit the remainder of column C is composed of stacked grey metre-thick diamictons as well as bedded sands, silts, and gravels.

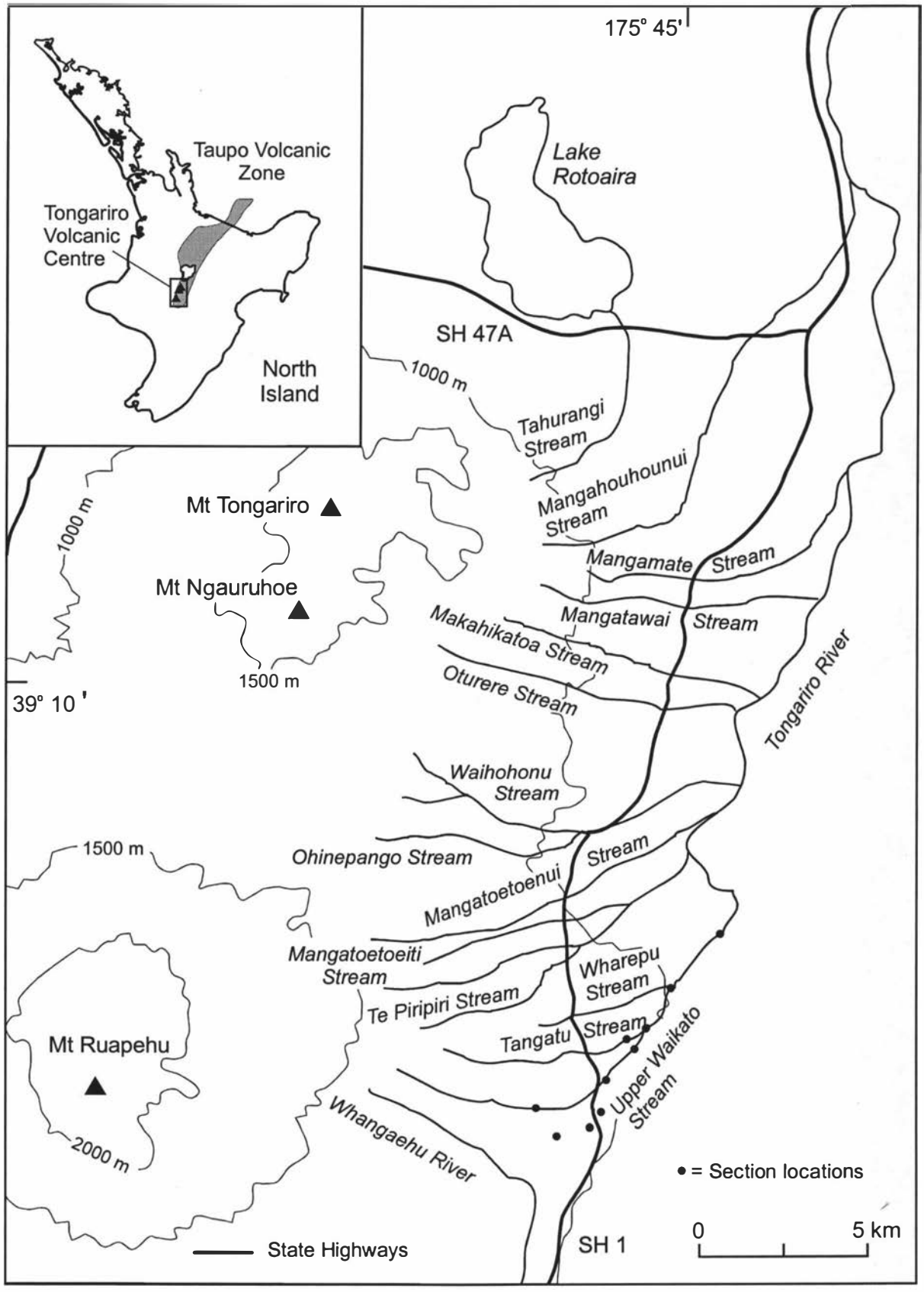

Figure 7.3 Location of Tongariro Volcanic Centre including Mts. Tongariro, Ngauruhoe and Ruapehu, and the streams dissecting the eastern Ruapehu and Tongariro ring plains. Upper Waikato Stream section locations marked by dots.

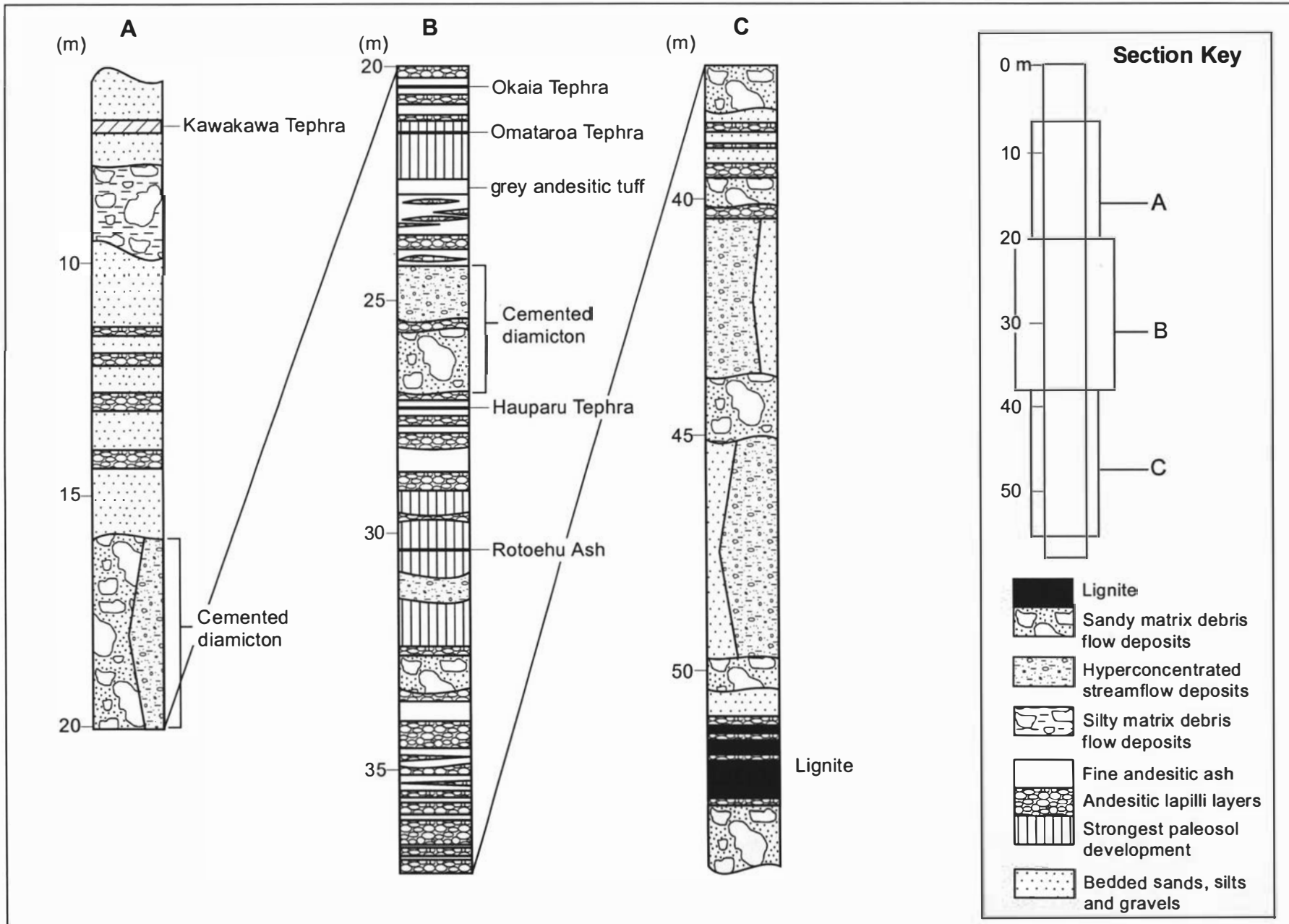

Figure 7.4 Composite stratigraphic columns of the northeastern Ruapehu ring plain sequence below the regional marker horizon of the Kawakawa Tephra.

These deposits are unconsolidated and there is no evidence for significant pause between the emplacement of each unit. The mechanisms of emplacement range from stream flow through hyperconcentrated flow and debris flow. There are a few andesitic lapilli layers interbedded near the top of this part of the sequence.

Above the stacked diamictons in column C the nature of the deposits, and hence the style of deposition changes markedly. Column B shows that deposits on this sector of the ring plain now consist dominantly of andesitic pumice lapilli and fine ash. The occasional diamicton unit still occurs but these appear to be separated by significant thicknesses of lapilli and fine ash. The cemented diamicton in the central part of column B contains up to 50% by volume pumice clasts and a pumice lapilli layer occurs between two of the flow units of this deposit. At the base of column B the sequence consists of many andesitic pumice lapilli layers stacked on top of one another with very little fine ash between each layer. Further up the column there are greater thicknesses of fine ash material between each pumice lapilli unit. The ash is brown to yellowish brown in colour, loam to clay loam in texture, very firm in consistence, and has a coarse blocky soil structure when dry. Root rhizomorphs are present throughout the ash and these occur in the greatest concentration where the ash is darker in colour and has more evidence of soil structure and soil development (indicated on column B as the zones of strong weathering). The grey andesitic tuff unit (Fig. 7.4) is firmly cemented, shower-bedded and contains accretionary lapilli. This unit is a locally important marker horizon.

Column A shows the upper portion of the sequence, the nature of deposition inferred to have again changed. At this time deposition on this part of the ring plain consisted of stacked diamictons of debris, hyperconcentrated, and stream flow origin. There appears to have been little or no time between depositional events. Thick (0.5 m) andesitic lapilli units are interbedded between and within the diamictons and fluvial deposits (column A, Fig. 7.4). Above the Kawakawa Tephra, fluvial aggradation deposits of the Hinuera Formation are described by Topping and Kohn (1973) in the Ruapehu and Tongariro area.

7.3.5 Lithology

7.3.5A *Diamictons*

Volumetrically this sequence is dominated by diamicton deposits. These vary considerably in their nature and inferred style of deposition. At one end of the depositional series are bedded silts, sands, and gravels. These are well sorted within individual layers but are poorly sorted as a whole, with layers of differing grain size bedded on top of one another. These deposits reflect a stream flow origin where turbulent, dilute (Newtonian) flow mechanisms transport the sediment (Smith, 1986; Pierson and Costa, 1987). At the other end of the scale are debris flow deposits which are poorly sorted and display no bedding. Often these deposits contain very large clasts within a fine sand matrix. These deposits have been transported and deposited by a much more concentrated (plastic or non-Newtonian) flow mechanism. Laminar flow

occurs under these conditions and sediment is supported and transported by a strong matrix (Smith, 1986; Pierson and Costa, 1987). Between these two extremes of deposit are a wide range of deposits intermediate in character. These deposits show varying amounts of planar bedding and varying degrees of sorting, with generally a finer grain size than debris flows. These units are termed hyperconcentrated flow deposits and are considered to have been deposited via an intermediate concentration (but still plastic and non-Newtonian) flow mechanism. Turbulence and matrix strength both play a role in transporting and depositing sediment in these flows (Smith, 1986; Pierson and Costa, 1987). There exists a wide range of deposits transitional in character between these three types. Table 7.3 outlines the characteristic features of the surface flow sediments within the northeastern ring plain sequence, and relates the observed (purely descriptive) types of deposits with their features and inferred flow mechanisms.

Table 7.3 Surface-flow sediment lithotypes within the northeastern Ruapehu ring plain area, with their characteristic properties and inferred mode of deposition.

Sediment type	Observed features	Inferred flow type (Smith, 1986)
Cemented diamictons	- firmly cemented - sand matrix - matrix- and clast-supported - pumice lapilli rich (up to 50% by vol.) - maximum clast diameter 1-3 m - composed of several flow units - massive and planar fabric preserved	Debris flow and hyperconcentrated flow
Sandy matrix diamictons	- unconsolidated - fine-coarse sand matrix - matrix- and clast-supported - pumice lapilli poor, dominated by lithic clasts - maximum clast diameter 1 m - massive and planar fabric preserved	Debris flow, hyperconcentrated flow, and transitional to stream flow
Silty matrix diamictons	- unconsolidated - greasy, allophane rich, silt loam matrix - matrix-supported - maximum clast diameter 2 m - can contain hydrothermally altered clasts	Debris flow
Bedded silts and sands, and gravels	- unconsolidated, dominantly clast-supported - planar laminated and low angle cross-bedded - pumice and lithic rich zones - highly variable grainsize, silt, sand, and pebbles in well sorted layers and lenses - maximum clast diameter 0.2m	Stream flow and transitional to hyperconcentrated flow

7.3.5B *Andesitic Tephra*

Andesitic tephra deposits are common throughout the entire sequence. More than 60 individual lapilli-grade units are described in the sequence, and thick deposits of fine ash occur in parts of it. The andesitic lapilli units are dominantly pumice that is highly vesicular with very fine vesicles, intermixed with <10% wall-rock lithic lapilli. The lapilli layers are generally thickest immediately to the east of Ruapehu volcano, which is consistent with the prevailing westerly wind direction. Close to source there is no

evidence of these tephra layers and their preservation on the ring plain is patchy, thus the best way to describe their original distribution and volume is by comparison to better studied younger tephra layers of the Bullot Formation (Donoghue *et al.*, 1995). Several analogous layers can be found which give an idea of the approximate dimensions of these eruptives. The lapilli layers would appear to be mostly of a sub-plinian origin, although plinian eruptives cannot be ruled out as the dispersion of the deposits is not well known.

The tephra contain phenocrysts of plagioclase + orthopyroxene + clinopyroxene > titanomagnetite ± olivine ± hornblende. This assemblage accounts for 90% of the andesitic units in the sequence. Hornblende and olivine occur only in small quantities (<2% by volume) in most of the units. Two other ferromagnesian mineral assemblages are observed in the andesitic tephra which can be characterised as, hornblende-dominant or olivine-dominant assemblages:

Olivine > Orthopyroxene + Clinopyroxene > Titanomagnetite

Hornblende > Orthopyroxene + Clinopyroxene > Titanomagnetite

These assemblages are restricted in their occurrence within the sequence. Two tephra layers at 12 m depth in the sequence (Column A, Fig. 7.4) have an olivine-dominated ferromagnesian assemblage, while two tephra layers at the very base of the sequence within lignite (Column C, Fig 7.4) contain a hornblende dominated assemblage.

Andesitic lapilli falls occur throughout the sequence, and the rate of eruption is > one sub-plinian lapilli eruption per 1000 years for a period of approximately 60 000 years.

Thick deposits of fine andesitic ash also occur in parts of the sequence and these are thought to represent the slow accumulation of fine ash directly from many eruptions as well as wind-blown fine ash reworked from other parts of the ring plain.

7.3.6 Interpretation of geological history

The relationship between the interpreted geological history of the north-eastern ring plain, the $\delta^{18}O$ record of deep sea cores, and the record of loess deposition and paleosol development of the southern North Island is summarised in Fig. 7.5.

The lignite in the lower part of the sequence is thought to represent deposition during marine $\delta^{18}O$ stage 5a, the Otamangakau interstadial period of McGlone and Topping (1983) around 80 ka (See Section 7.3.9). The organic materials accumulated slowly in a bog with occasional deposition of fluvial fine sands, and hornblende-rich tephra falls. The source of these hornblende-rich tephras could be either Tongariro or Ruapehu volcano, both of which were potentially active at the time. No hornblende-rich tephras have yet been described from Ruapehu whereas younger Tongariro-sourced tephras occasionally contain appreciable hornblende (Lowe, 1988; Donoghue *et al.*, 1991; Donoghue *et al.*, 1995). This suggests that Tongariro Volcano is the most likely source for these tephras.

The stacked diamictons and bedded silts, sands and gravels above the lignite represent a period of rapid aggradation on the north-eastern sector of the ring plain.

Aggradation without significant pause would imply that the slopes of Ruapehu were unstable, with much loose rock material available for transport and deposition to the north-east by lahars and stream flow. There are few interbedded lapilli units within these sediments and also little primary pumice within the sediments themselves. This indicates that these aggradation deposits are not likely to be the result of large scale eruptive events on Ruapehu volcano. This does not rule out the role of small scale eruptive events which are not recorded in the stratigraphic record as tephra deposits, but which have the potential to produce lahar and flood depositional events. A good example of this were the lahars produced during the eruptions of Ruapehu in 1975 (Nairn *et al.*, 1979), an eruption which was not accompanied by a tephra unit preserved on the ring plain. Small scale eruptives could potentially have produced the stack of diamictons and bedded deposits described here, but it is here considered that other environmental factors also played a major part.

Aggradation was taking place prior to the eruption of the Rotoehu Ash at *ca.*64 ka (Wilson *et al.*, 1992) and occurred during marine $\delta^{18}O$ stage 4 (Porewan stadial). The cooler climate of this period possibly accelerated physical weathering processes on Ruapehu, thus providing abundant material for redeposition on the north-eastern ring plain. The mechanism of this redeposition may have been small scale eruptives or simply slope failures and floods during storm events. The presence of a greater area of snow and ice on the higher slopes of the volcano in the cooler climate of δ^{18} isotope stage 4 may have also provided a ready water supply for producing lahars and floods in small scale eruptions, such as was observed in the 1985 eruption of Nevado del Ruiz (Pierson *et al.*, 1990).

Above the stacked diamictons, the deposits on this sector of the ring plain consist dominantly of andesitic pumice lapilli and fine ash beds. Occasional diamicton units occur but appear to be separated by significant periods of time and hence do not suggest major instability on the volcano. Deposition of the pumice-rich cemented diamicton unit (in the central part of column B, Fig. 7.4), which contains an andesitic pumice lapilli layer between flow units, probably was initiated by a large tephra-producing eruption on Ruapehu volcano.

At the base of the sequence represented by column B, the eruption rate of pumice lapilli falls on this sector of the ring plain appear to have been very high because there is little, or no fine ash between each lapilli layer and the lapilli units are often very thick and stacked on top of one another. Such a high eruption rate occurred in late marine $\delta^{18}O$ stage 4, corresponding to the period encompassed by the previously-named middle Tongariro Subgroup tephras (Leamy *et al.*, 1973; Milne and Smalley, 1979) which are mapped as occurring on top of the Porewa loess in the Rangitikei region to the south of Mt Ruapehu. Distal andesitic ash is also mapped on top of a correlative of the Porewa loess in the Hawkes Bay region to the east of Mt. Ruapehu (A.P. Hammond, *pers. comm.*, 1994). Thus the lapilli layers found on the north-eastern ring plain are probably proximal correlatives of the middle Tongariro Subgroup tephras.

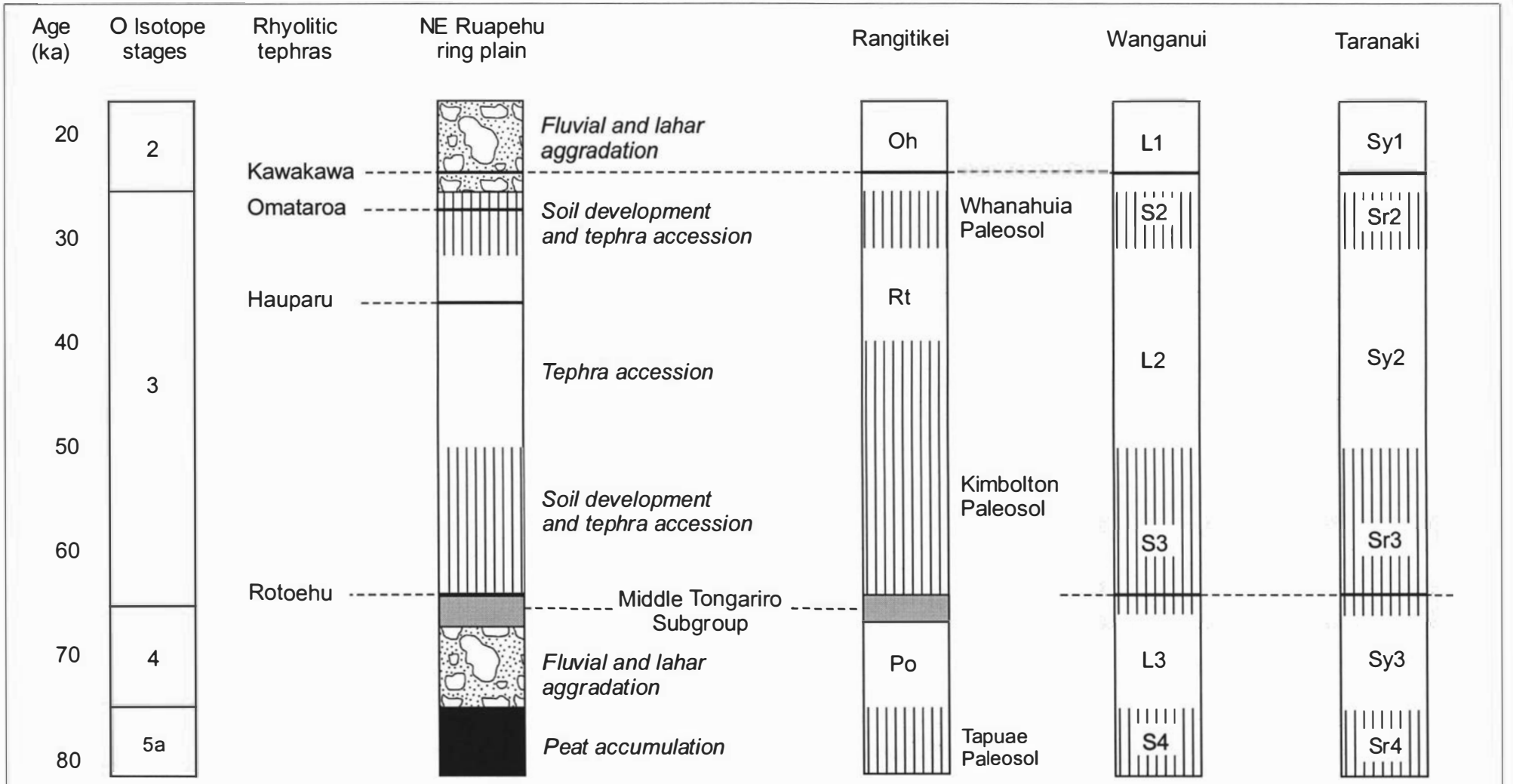

Figure 7.5 Comparison of the northeastern Ruapehu ring-plain landscape events with deep sea O isotope record (Shakleton *et al.*, 1990), rhyolitic tephra marker beds (Froggatt and Lowe, 1990), and southern North Island loess stratigraphy from the Rangitikei valley (Leamy *et al.*, 1973; Milne and Smalley, 1979), Wanganui (Pillans, 1988; 1994), and Taranaki (Alloway *et al.*, 1988). Oh = Ohakea loess, Rt = Rata loess and Po = Porewa loess, L1 = loess 1, S2 = buried soil 2 etc. Sy1 = loess 1 correlative, Sr2 = buried soil 2 correaltive etc.

Above these stacked pumice lapilli beds, the eruption rate of lapilli grade units appears to have slowed, indicated by greater thicknesses of fine ash between each lapilli unit. This may indicate that the dispersal axes of eruptives changed at this time or there was a reduction in magnitude or frequency of eruptive events. Given that the sites studied are directly down wind of the volcano under the prevailing westerly winds, it is unlikely that eruptives were deposited in different directions for the extended periods of time represented by this sequence. Therefore it is more likely that there was a reduction in the magnitude and/or the frequency of eruptive events at this time. Coupled with this apparent slowing of eruption rate or reduction in magnitude of the eruptive events, the degree of weathering and paleosol development within the fine ash increases, as the soil surface was accreting more slowly. The strongly weathered zone extends to just above the level of the Rotoehu Ash. This paleosol appears to have formed at the same time as the paleosol developed in the Porewa loess throughout the southern North Island (Leamy *et al.*, 1973; Milne and Smalley, 1979; Palmer, 1985; Pillans, 1988) during early marine $\delta^{18}O$ stage 3.

During the subsequent stadial period in mid-marine $\delta^{18}O$ stage 3 (Ratan) there is no expression of major aggradation on the north-eastern ring plain. The diamicton bracketed by the Hauparu and Omataroa tephras contains andesitic lapilli and appears to have been generated by eruptive rather than climatic processes, in contrast to the earlier diamictons. Deposition continued with accretion of fine ash and pumice lapilli beds. The weathering and soil development within fine ash deposited in this period is, however, very weak. This indicates that, either the eruption or accumulation rate was too high to allow soil development, or soil development was affected by cooler climate conditions during this period. The fine ash nature of the deposits and the thickness of ash between dated rhyolitic tephra layers would suggest a relatively slow deposition rate, indicating soil development was probably slowed by cool climate conditions.

The absence of appreciable aggradation deposits on the north-eastern sector of the ring plain at this time may indicate that the climate during the mid-marine $\delta^{18}O$ stage 3 stadial was not as severe as during the marine $\delta^{18}O$ stage 4 stadial. This is supported by pollen evidence from the area. McGlone and Topping (1983) and McGlone (1985) proposed a "cool interstadial" climate in the Ruapehu area during the time of the deposition of the Rata loess rather than a full stadial period. In Taranaki, andic deposits record peaks of aerosolic quartz accumulation indicative of cool climate in marine $\delta^{18}O$ stages 2 and 4, but negligible amounts in stage 3 (Alloway *et al.,* 1992). This also indicates the climate was not as severe in marine $\delta^{18}O$ stage 3 in comparison with that of stages 2 and 4.

Above the grey tuff unit in column B, the fine ash exhibits much stronger weathering. Root rhizomorphs become abundant and finely-disseminated charcoal layers are present. Near the top of this strongly weathered zone is the Omataroa Tephra, dated at 28 220 ± 630 BP (Froggatt and Lowe, 1990). This paleosol development correlates with the paleosol in the Rata loess in the southern North Island (Leamy *et al.*, 1973; Milne and Smalley, 1979; Palmer, 1985; Pillans, 1988), developed during late marine $\delta^{18}O$ stage

3. The fine ash in this part of the sequence is not interbedded with any lapilli layers and appears to have accumulated slowly, thus enhancing the paleosol and weathering features.

Weathering features become less pronounced above the Omataroa Tephra, potentially indicating deteriorating climate with the onset of $\delta^{18}O$ stage 2 (Last Glacial Maximum; Pillans *et al.*, 1993).

Above the Okaia Tephra, rapid aggradation of diamictons began on the north-eastern ring plain, again indicating instability on the slopes of Ruapehu volcano. These deposits accumulated during marine $\delta^{18}O$ stage 2. Throughout the aggradation sequence, represented by column A, andesitic lapilli continued to be erupted, indicating Ruapehu was active throughout the early part of the Last Glacial Maximum.

7.3.7 Discussion and Conclusions

The north-eastern Ruapehu ring plain sequence not only reflects the volcanic history of Ruapehu volcano but also indicates the response of the volcano-ring plain system to global climate oscillations.

Periods of severe-cold climate during the Last Glacial have caused large scale aggradation on the ring plain, with more frequent occurrences of lahars and deposition dominated by surface flow mechanisms. These processes appear to attain their maximum volume and frequency during marine $\delta^{18}O$ stages 2 and 4 (Fig. 7.5). The climate during mid-marine $\delta^{18}O$ stage 3 may not have been so severe, because no widespread aggradation is noted in the deposits of this age on the north-eastern ring plain. The climate-related aggradation may be driven by increased physical weathering on the higher slopes of Ruapehu volcano.

The aggradation deposits to some degree mask the purely eruptive or volcanic-triggered events recorded on the ring plain. Only deposits from the very large tephra eruptions are preserved in this environment; the smaller tephra units and fine ash deposits are mostly reworked by the wind or entrained in successive lahars and stream flow deposits.

In the milder periods on the north-eastern ring plain, deposition reflects the eruptive and volcanic-triggered events occurring on Ruapehu volcano. Deposition is dominated by fall processes, primary fall ash and lapilli deposition and aeolian redistribution of fine ash on the ring plain. Diamicton deposits are still present in this sector but the time between each lahar event is much greater than during $\delta^{18}O$ stages 2 and 4.

7.3.8 Acknowledgements

This work forms part of the Ph.D. research of one of the authors (SJC). The authors gratefully acknowledge funding from the New Zealand Vice-Chancellors' Committee, Massey University Graduate Research Fund, the Helen E. Akers Scholarship Fund, and

the Department of Soil Science of Massey University. Thanks are also due to B.V. Alloway, W.R. Hackett, and B.F. Houghton for their thoughtful and insightful reviews, which greatly improved the manuscript.

7.3.9 Subsequent comments on the paper

A recent analysis of the palynoflora within the lignite deposit at the base of the Upper Waikato Stream sequence has led to a slight modification of its estimated age. The lignite contains a palynoflora composed of shrub and grassland species, indicative of a cool and stormy climate (McGlone, pers. comm., 1995). Thus its correlation to $\delta^{18}O$ stage 5a in the paper (a relatively warm period) is not supported. Instead it is now considered (see Chapter 5) that the lignite was deposited immediately after $\delta^{18}O$ stage 5a, within $\delta^{18}O$ stage 4 (or the Porewan stadial of the Last Glacial). Consequently the record preserved on the northeastern ring plain extends back only to the Porewan stadial (represented by the Porewan loess, Loess 3 and Sr3 on Fig. 7.5).

In addition, the identification methods of the interbedded rhyolitic tephras have been improved over those described in the paper (see Chapter 2).

7.4 SUMMARY GEOLOGICAL SYNTHESIS OF THE NORTHEASTERN TONGARIRO VOLCANIC CENTRE

This synthesis concentrates on the events which occurred on the ring plains rather than on the Tongariro and Ruapehu volcano slopes.

7.4.1 c. 75 000 - 64 000 years ago

The record from this period is preserved only in the Upper Waikato Stream sequences described in Section 7.3 and 5.13 (Chapter 5). This interval encompassed the antepenultimate stadial of the Last Glacial (the Porewan stadial), thus the periglacial climate of this time had a large influence on ring plain sedimentation. Palynoflora within a lignite deposit from this sequence indicates that the climate was cool and stormy during this time (Section 5.13, and 7.3.9).

The northeastern Ruapehu ring plain during this interval was aggrading rapidly with deposits from many lahars across it. These lahars were mostly non-cohesive, sandy matrix flows exhibiting both hyperconcentrated streamflow and debris flow sedimentation styles. Reworking of these lahar deposits probably occurred soon after their emplacement and large thicknesses of alluvial gravelly sands are associated with many of the lahar deposits. The lahars during this time were likely to be in response to greater physical weathering on the volcano slopes and consequently larger loads of sediment within the upper stream catchments. Glaciers were probably present on the cone and supplied sediment (from till and outwash) and water (from ice melt and kettle lakes) to lahars. Lahar-triggering mechanisms probably included; eruptions from either Ruapehu

or Tongariro, storms, glacial lake breakouts, avalanches and possibly small flank collapses.

During the main period of ring-plain aggradation by lahars, the frequency of large tephra eruptions from either Ruapehu or Tongariro appears to have been low. However, hornblende-rich tephras below the lahar deposit sequence may indicate that in the early part of this interval Tongariro volcano was actively erupting (Section 3.4.7 and 7.3.6). In addition, following the main period of lahar aggradation, but prior to 64 ka, it appears that there was a major period of eruptive activity from Ruapehu volcano (Fig. 7.6). Large numbers of thick lapilli layers interbedded within fine andesitic ash, indicate that large and frequent eruptions were occurring at Ruapehu (Table 5.3, Sections 4.10 and 7.3.6). Fewer lahar deposits preserved in this part of the sequence imply that the climate had begun to ameliorate and the volcano slopes were more stable, despite these frequent and large tephra eruptions.

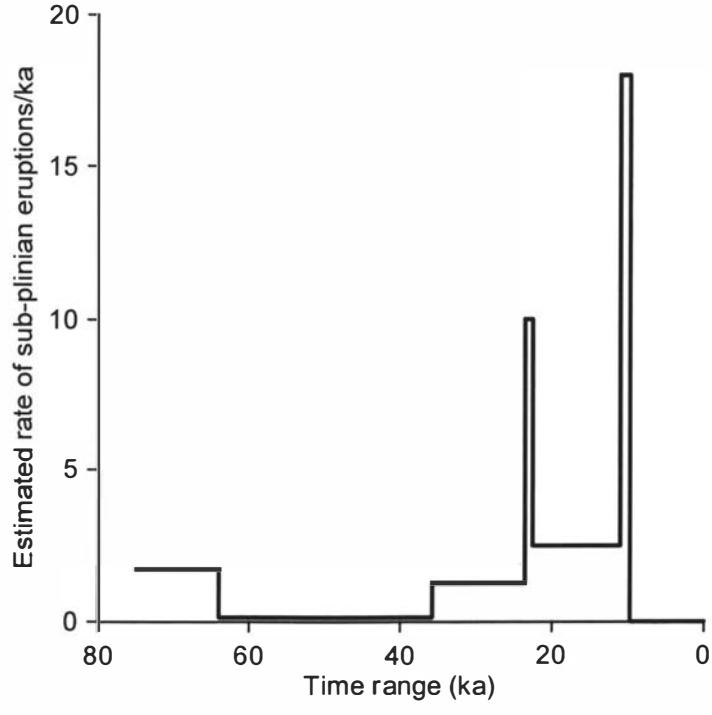

Figure 7.6. Summary diagram of the estimated rate (per ka) of lapilli-producing sub-plinian eruptions of Ruapehu and Tongariro volcanoes for the last 75 ka. Based on the ring plain record of Topping (1973), Donoghue *et al.,* (1995) and Cronin *et al.*, (1996).

7.4.2 64 000 - 36 000 years ago

The most complete record of this interval is also preserved in the Upper Waikato Stream sequences. During this period, very little lahar deposition occurred on the northeastern Ruapehu ring plain. The deposits of only a single lahar are preserved at only a few localities (R13, Section 5.9). This was probably related to stabilised landscapes in the

mild and settled climatic conditions prevailing during this interval in the area (McGlone and Topping, 1983).

A very low frequency (1 per 7 000 years) of large tephra eruptions from Ruapehu was recorded in this period (Fig. 7.6, Table 5.3, Sections 4.10 and 7.3.6). However, accretion of fine ash appears to have occurred throughout the interval, indicating frequent low-magnitude eruptions, from either Ruapehu or Tongariro. Soil development indicates that during this interval, the northeastern Ruapehu ring plain was a stable landscape surface, with low rates of accretion (Section 4.10). Stronger soil development in the earlier part of this interval corresponded in age to soil development in loess sequences throughout the lower North Island (Sections 4.10 and 7.3.6), during a period of warmer and more settled climate.

7.4.3 36 000 - 23 000 years ago

The full record of this period is also preserved only in the Upper Waikato Stream sequences. As in the preceding interval, deposition on the northeastern Ruapehu ring plain was dominated by accession of tephras. However, two lahars, closely spaced in time, inundated the area. These lahars were contemporaneous with and probably related to large scale tephra eruptions of Ruapehu (R12, Sections 5.9 and 5.13).

Large-scale tephra eruptions of Ruapehu were much more frequent in this period compared to the last, with an average of 1 per 800 years (Fig. 7.6, Table 5.3, Sections 4.10 and 7.3.6). However, the overall frequency of large scale eruptions was not uniform throughout the entire interval. The rate was high early in the period, but very low in the latter stages. Smaller scale eruptions (probably from both Ruapehu and Tongariro) occurred throughout the entire interval and resulted in continuous and slow accretion of the ring-plain surface.

Soil development was strongest in the latter stages of the 36 - 23 ka interval due to the rate of large scale tephra eruptions being at their lowest, thus the soil surface was accreting slowly. This period of strong soil development corresponds to a period of widespread soil development in loess sequences throughout the lower North Island (Section 4.10).

7.4.4 23 000 - 15 000 years ago

This was a period of major construction of both the Tongariro and Ruapehu ring plains due to both volcanic activity and climatic instability. On both ring plains deposits of this interval probably comprise a larger volume than those of any other interval described. This interval corresponds with the period of greatest climatic and landscape instability in the North Island over the last 120 ka (Pillans, *et al.* 1993). Response to this cooler and stormier climate on the ring plains was deposition of large amounts of sediment by lahars and streams (Section 5.13). Thick deposits of many lahars were deposited over the entire ring plain study area (R11, R10 and R09 on the Ruapehu ring plain, T3 and T4 on

the Tongariro ring plain; Section 5.12, Fig 5.7). In addition to lahar sedimentation, all of the streams in the area were transporting and depositing large quantities of sediment as well as reworking lahar deposits. On the Tongariro ring plain, particularly in its northern portion, emplacement of the Oruanui Ignimbrite contributed large volumes of material which was reworked and preserved extensively as Hinuera Formation alluvium (Sections 5.11 and 5.13) and remobilised by wind as Mokai Sand.

Eruptive activity of Ruapehu volcano in this interval was also very high, contributing to construction of the ring plains by large additions of tephra as well as generation of lahars. The voluminous middle and lower Bullot Formation tephras from Ruapehu volcano were erupted between 22.6 and 14.7 ka B.P. (Donoghue *et al.*, 1995). In addition, between the eruptions of Okaia and Kawakawa Tephras (22.6 ka B.P. to ca. 23 ka) several more thick pumice lapilli layers were erupted and preserved between lahar and fluvial deposits (Fig. 7.6, Section 3.4, Fig. 3.6). Soil development in this interval was minimal due to climatic instability (i.e. scant vegetation cover) and rapid aggradation of ring plain surfaces with lahar, fluvial and pumice tephra deposits.

A large lava flow from Tongariro volcano occurred in the early part of this interval. This flow was emplaced between the ring plains of Ruapehu and Tongariro creating a boundary between them (Section 5.12). Other lava flows on the northeastern Ruapehu ring plain may have also been emplaced during this interval (Section 7.2.3A).

7.4.5 15 000 - 9 700 years ago

In this interval the high rate of large tephra eruptions from Ruapehu volcano continued with large thicknesses of upper Bullot Formation tephras deposited on the northeastern Ruapehu and southeastern Tongariro ring plains (Donoghue *et al.*, 1995). Tongariro volcano was also extremely active in this period, with the eruptions of the Rotoaira, Pahoka and Mangamate Tephras (Topping, 1973). The maximum rate of large lapilli-producing eruptions was between 10 and 9.7 ka B.P. (Fig. 7.6), when at least six sub-plinian tephras were erupted from Tongariro (Mangamate Tephra).

Many lahars continued to occur throughout this interval, although they were confined to narrow sectors of the ring plains. On the Ruapehu ring plain, lahar deposition was centred around the Mangatoetoenui - Te Piripiri Streams area and on the Tongariro ring plain, around the Oturere - Makahikatoa Streams (R08 - R02 and T1, Section 5.12). These lahars were related to the frequent tephra eruptions of both volcanoes in this interval (Section 5.13). The major portion of the ring plains in between were unaffected by lahar and fluvial deposition and had relatively stable surfaces showing periods of soil development punctuated by deposition of thick tephra layers. The absence of widespread fluvial and lahar aggradation of the ring plains in this interval compared to the last, corresponds with post Otiran climatic amelioration (McGlone and Topping, 1977).

During this interval, lahars caused major aggradation in the lower Tongariro River, resulting in extensive laharic surfaces. These deposits ceased accumulating at around 9 700 years ago (Section 6.9.2A).

Another event that occurred during this interval was between 14.7 and 11.9 ka B.P., when a lava flow was emplaced on the northern flanks of Tongariro, reaching the ring plain (Section 7.2.3B).

7.4.6 9 700 - 2 500 years ago

During this interval most of the surfaces of both ring plains were stable with slow accretion of tephra from small eruptions of Ruapehu and Tongariro forming the Papakai Formation (Topping, 1973; Donoghue *et al.*, 1995). Soil development was strong throughout this interval with the combination of a mild climate (McGlone and Topping, 1977) and slow soil surface accretion. A single lahar occurred during this period but deposition was confined close to the Mangatoetoenui Stream (R01, Section 5.12). This lahar was probably related to a small eruption of Ruapehu (Section 5.13).

In the Tongariro River the extensive laharic surface constructed in the preceding interval was incised and in places a small laharic surface was constructed at ca. 5.2 ka (Section 6.9.2B and 6.10.4).

7.4.7 2 500 years ago - present

Tephra accretion and soil development continued throughout this interval with deposition of the Mangatawai Tephra, Tufa Trig Formation and Ngauruhoe Formation (Topping, 1973; Donoghue *et al.*, 1995). However, this was interrupted by the emplacement of large volumes of Taupo Ignimbrite. The Ignimbrite was up to 30 m thick in the Tongariro River valley and in many places on the ring plain, levelling surfaces of formerly differing ages (Section 6.9.2A).

In the Tongariro River incision continued, particularly following infilling of the river valley with Taupo Ignimbrite. At least seven small lahars occurred in this interval, some producing depositional surfaces in the lower Tongariro River, others documented only in historic records and two in 1995 which left deposits along the Mangatoetoenui Stream (6.9.2B). All of the pre-1995 lahars in this interval appear to have flowed down the Mangatoetoenui Stream. These lahars were all probably related to eruptions of Ruapehu.

7.5 Combined References

Alloway, B.V., Stewart, R.B., Neall, V.E. and Vucetich, C.G., 1992. Climate of the Last Glaciation in New Zealand, based on aerosolic quartz influx in an andesitic terrain. Quat. Res., 38: 170-179.

Borchardt, G.A., Harward, M.E. and Schmitt, R.A., 1971. Correlation of ash deposits by activation analysis of glass separates. Quat. Res., 1: 247-260.

Cronin, S.J., Neall, V.E., Stewart, R.B., Palmer, A.S., 1996. A multiple-parameter approach to andesitic tephra correlation, Ruapehu volcano, New Zealand. J. Volcanol. and Geotherm. Res., 72: 199-215.

Donoghue, S.L., 1991. Late Quaternary volcanic stratigraphy of the south-eastern sector of Mount Ruapehu ring plain, New Zealand. Unpub. PhD. thesis, Massey University, Palmerston North, N. Z.

Donoghue, S.L., Neall, V.E., Palmer, A.S., 1995. Stratigraphy and chronology of andesitic tephra deposits, Tongariro Volcanic Centre, New Zealand. J. Roy. Soc. N. Z., 25: 115-206.

Donoghue, S.L., Stewart, R.B. and Palmer, A.S., 1991. Morphology and chemistry of olivine phenocrysts of Mangamate Tephra, Tongariro Volcanic Centre, New Zealand. J. Roy. Soc. N. Z., 21: 225-236.

DOSLI (Department of Survey and Land Information), 1982. NZMS 260, T20 Ruapehu, Edition 1. Wellington N.Z.

DOSLI (Department of Survey and Land Information), 1994. Topomap Tongariro. Infomap 260, T19, Edition 2. Wellington N.Z.

Froggatt, P.C. and Gosson, G.J., 1982. Techniques for the preparation of tephra samples for mineral or chemical analysis and radiometric dating. Geology Dept., Victoria University of Wellington Publ., 23: 12 pp.

Froggatt, P.C., 1983. Towards a comprehensive Upper Quaternary tephra and ignimbrite stratigraphy in New Zealand using electron microprobe analysis of glass shards. Quat. Res., 19: 188-200.

Froggatt, P.C. and Lowe, D.J., 1990. A review of late Quaternary silicic and some other tephra formations from New Zealand: their stratigraphy, nomenclature, distribution, volume, and age. N. Z. J. Geol and Geophys., 33: 89-109.

Froggatt, P.C. and Rogers, G.M., 1990. Tephrostratigraphy of high altitude peat bogs along the axial ranges, North Island, New Zealand. N. Z. J. Geol. and Geophys., 33: 111-124.

Graham, I.J., Hackett, W.R., 1987. Petrology of calc-alkaline lavas from Ruapehu volcano and related vents, Taupo Volcanic Zone, New Zealand. J. of Petrology, 28: 531-567.

Gregg, D.R., 1960. The geology of Tongariro Subdivision. N. Z. Geological Survey Bull., 40: 152 pp.

Grindley, G.W., 1960. Geological map of New Zealand, 1st ed., 1: 250 000, Sheet 8, Taupo. D.S.I.R., Wellington.

Hackett, W.R., 1985. Geology and petrology of Ruapehu volcano and related vents. Unpub. thesis Victoria University of Wellington: 312 pp.

Hackett, W.R. and Houghton, B.F., 1989. A facies model for a Quaternary andesitic composite volcano: Ruapehu, New Zealand. Bull. Volcanol., 51: 51-68.

Hobden, B. J., Houghton, B.F., Lanphere, M.A. and Nairn, I.A., 1996. Growth of the Tongariro volcanic complex: new evidence from K-Ar age determinations. N.Z. J. Geol. and Geophys., 39: 151-154.

Hodgson, K.A., 1993. Late Quaternary lahars from Mount Ruapehu in the Whangaehu River valley. Unpub. PhD. thesis, Massey University, Palmerston North, N.Z.

Howorth, R., 1975. New formations of Late Pleistocene tephras from Okataina Volcanic Centre, New Zealand. N. Z. J. Geol. and Geophys., 18: 683-712.

Leamy, M.L., Milne, J.D.G., Pullar, W.A. and Bruce, J.G., 1973. Paleopedology and soil stratigraphy in the New Zealand Quaternary succession. N. Z. J. Geol. and Geophys., 16: 723-744.

Lowe, D.J., 1988. Stratigraphy, age, composition, and correlation of late Quaternary tephras interbedded with organic sediments in Waikato lakes, North Island, New Zealand., N. Z. J. Geol. and Geophys., 31: 125-165.

Mathews, W.H., 1967. A contribution to the geology of the Mount Tongariro massif, North Island, New Zealand. N.Z. J. Geol. and Geophys., 10: 1027-1038.

McArthur, J.L. and Shepherd, M.J., 1990. Late Quaternary glaciation of Mt. Ruapehu, North Island, New Zealand. J. Roy. Soc. N. Z., 20: 287-296.

McGlone, M.S. and Topping, W.W., 1983. Late Quaternary vegetation, Tongariro region, central North Island, New Zealand. N. Z. J. of Botany, 21: 53-76.

McGlone, M.S., 1985. Biostratigraphy of the Last Interglacial - Glacial cycle, southern North Island, New Zealand. *In*: Pillans, B.J. (ed.) Proceedings of the second CLIMANZ conference. Geology Dept., Victoria University of Wellington, Publ., 31: 17-31.

Milne, J.D.G. and Smalley, I.J., 1979. Loess deposits in the southern part of the North Island of New Zealand: an outline stratigraphy. Acta Geologica Academiae Scientarium Hungaricae, 22: 197-204.

Nairn, I.A., Wood, C.P. and Hewson, C.A.Y., 1979. Phreatic eruptions of Ruapehu: April 1975. N. Z. J. Geol. and Geophys., 22: 155-173.

Palmer, A.S., 1985. The Last Interglacial record in Wairarapa Valley, New Zealand. *In*: Pillans B.J. (ed.) Proceedings of the second CLIMANZ conference. Geology Dept., Victoria University of Wellington, Publ., 31: 32-36.

Palmer, B.A., 1991. Holocene lahar deposits in the Whakapapa catchment, northwestern ring plain, Ruapehu Volcano (North Island, New Zealand). N. Z. J. Geol. and Geophys., 34: 177-190.

Pierson, T.C. and Costa, J.E., 1987. A rheologic classification of subaerial sediment-water flows. Geol. Soc. of America, Reviews in Engineering Geology, VII: 1-12.

Pierson, T.C., Janda, R.J., Thouret, J-C. and Borrero, C.A., 1990. Perturbation and melting of snow and ice by the 13 November 1985 eruption of Nevado del Ruiz, Colombia, and consequent mobilisation, flow and deposition of lahars. J. Volcanol. and Geotherm. Res., 41: 17-66.

Pillans, B.J., 1988. Loess chronology in Wanganui Basin, New Zealand. *In:* Eden, D.N. and Furkert, R.J. (eds) Loess - Its Distribution Geology and Soils: 175-191. A.A. Balkema, Rotterdam.

Pillans, B.J., 1994. Direct marine-terrestrial correlations, Wanganui Basin, New Zealand: The last 1 million years. Quat. Sci. Reviews, 13: 189-200.

Pillans, B.J. and Wright, I., 1992. Late Quaternary tephrostratigraphy from the southern Harve Trough - Bay of Plenty, northeast New Zealand. N. Z. J. Geol. and Geophys., 35: 129-143.

Pillans, B., McGlone, M., Palmer, A., Mildenhall, D., Alloway, B. and Berger, G., 1993. The Last Glacial Maximum in central and southern North Island: a paleoenvironmental reconstruction using the Kawakawa tephra formation as a chronostratigraphic marker. Palaeo., Palaeo., Palaeo., 101: 283-304.

Self, S. and Healy, J., 1987. Wairakei Formation, New Zealand: stratigraphy and correlation. N. Z. J. of Geol. and Geophys., 30: 73-86.

Shackleton, N.J., Berger, A. and Peltier, W.R., 1990. An alternative astronomical calibration of the lower Pleistocene timescale based on ODP Site 677. Trans. Roy. Soc. of Edinburgh: Earth Sciences, 81: 251-261.

Smith, G.A., 1986. Coarse-grained nonmarine volcaniclastic sediment: Terminology and deposition process. G. S. A. Bull., 97: 1-10.

Stokes, S., Lowe, D.J. and Froggatt, P.C., 1992. Discriminant function analysis and correlation of Late Quaternary rhyolitic tephra deposits from Taupo and Okataina volcanoes, New Zealand, using glass shard major element composition. Quat. Inter., 13/14: 103-117.

Topping, W.W., 1973. Tephrostratigraphy and chronology of late Quaternary eruptives from the Tongariro Volcanic Centre, New Zealand. N. Z. J. Geol. and Geophys., 16: 397-423.

Topping, W.W. and Kohn, B.P., 1973. Rhyolitic tephra marker beds in the Tongariro area, North Island, New Zealand. N. Z. J. Geol. and Geophys., 16: 375-395.

Wilson, C.J.N., Switzur, R.V. and Ward, A.P., 1988. A new ^{14}C age for the Oruanui (Wairakei) eruption, New Zealand. Geol. Mag., 125: 297-300.

Wilson, C.J.N., Houghton, B.F., Lanphere, M.A. and Weaver, S.D. (1992). A new radiometric age estimate for the Rotoehu Ash from Mayor Island volcano, New Zealand. N. Z. J. of Geol. and Geophys., 35: 371-374.

CHAPTER 8: CONCLUSIONS

8.1 Fulfilment of study objectives - Tephrochronology groundwork

Chapter 1 outlined the original objectives of this study as well as identifying areas in which the study could contribute to knowledge gained from past studies in and around the study area. Underpinning all of these objectives was the need to establish a chronostratigraphic framework for the ring-plain sequences. This was eventually provided by a stratigraphy of interbedded andesitic and rhyolitic tephras.

For sequences < 22.6 ka B.P. a tephrochronologic framework had been established in past studies (Topping, 1973; Topping and Kohn, 1973; Donoghue *et al.*, 1995). Consequently, in this interval the object of field and laboratory study was to correlate tephras from new sequences to tephras that were already known to occur in the area. For andesitic tephras this was readily achieved using field appearance and stratigraphic criteria. However, rhyolitic tephras were not as easily identified, instead laboratory-based geochemical methods were required. When existing methods were found to be inadequate for precise identification of these rhyolitic tephras, an existing but practically untested statistical method was attempted. This formed the basis of Chapter 2 and resulted in much more precise and quantitative rhyolitic tephra identification.

Sequences > 22.6 ka B.P. had not been studied in the area prior to this study and consequently their tephrochronologic framework was unknown. To establish a chronology, rhyolitic tephras were initially sought in the sequences. These were only found after channel sampling and microscopic analysis to identify rhyolitic glass concentration layers within fine-grained andesitic ash sequences. These glass concentrations were correlated with tephras known from the central North Island using the methods described in Chapter 2. Once a rhyolitic tephrochronology was established for this time range in this area it was supplemented by establishment of a new andesitic tephrochronology.

Chapter 3 describes the development of the andesitic tephrochronology. The first part of the approach was to test whether the discriminant function analysis (DFA) method used for the rhyolitic tephras in Chapter 2 could be used to discriminate andesitic tephras, and which mineral phases were best for the purpose. This was tested by examining different methods and geochemistry of different mineral phases to distinguish andesitic tephras from two different sources (Egmont volcano and Ruapehu volcano). Once these methods were proven, they were applied, along with several other parameters, to establish andesitic marker tephras in the > 22.6 ka B.P. sequence on the northeastern Ruapehu ring plain. These marker tephras were then used to correlate the > 22.6 ka B.P. sequence.

8.2 Fulfilment of study objectives - Specific objectives

The realisation of the original objectives and planned contributions of this study form Chapters 4 - 7 of this thesis. Individual planned objectives and contributions are as follows:

8.2.1 *An improved assessment of the lahar hazards from Ruapehu volcano*

Lahar deposits on the northeastern Ruapehu ring plain and along the Tongariro River were mapped and dated using interbedded tephra layers. This enabled the age, number, frequency, and distribution of Ruapehu-sourced lahars to be assessed on the northeastern Ruapehu ring plain (Chapter 5) and along the Tongariro River (Chapter 6). Dating and mapping lahar surfaces led to the development of a lahar hazard map for the entire Tongariro catchment which includes the northeastern Ruapehu ring plain (Chapter 6).

Ruapehu volcano was the source of most lahars in the Tongariro catchment post-14.7 ka, and the source of all Holocene lahars. Eight lahar hazard zones were delineated in the Tongariro catchment ranging from 1 in > 15 000 to 1 in 35 years. Ruapehu-sourced lahars occur in every hazard zone and Ruapehu is the sole source of lahars in the youngest six zones, ranging between 1 in 10 000 to 1 in 35 years. The Mangatoetoenui catchment has the greatest lahar hazard on the northeastern Ruapehu ring plain. The Upper Waikato Stream also has a high potential lahar hazard if capture of the Whangaehu River were to occur.

8.2.2 *An assessment of the lahar hazards on the eastern Tongariro ring plain and the Tongariro River*

The number, age, frequency and distribution of the lahars on the Tongariro ring plain were assessed using the same mapping methods as on the Ruapehu ring plain and along the Tongariro River (Chapter 5). A lahar hazard map for the Tongariro ring plain is included in the map produced for the entire catchment (Chapter 6).

The eastern Tongariro ring plain is almost entirely within a 1 in > 15 000 year lahar hazard zone. Small areas of the ring plain, surrounding the Waihohonu, Oturere and Makahikatoa Streams have a greater hazard of 1 in 12 000 years. Consequently, Tongariro-sourced lahars contribute only to the two hazard zones with the longest return periods of the eight zones mapped along the Tongariro River.

8.2.3 *A better understanding of the eruptive history (particularly that of tephra eruptives) of the two volcanoes*

This study was the first to examine sequences older than the 22.6 ka B.P. Kawakawa Tephra in the area. A tephra eruptive history of both volcanoes (but mostly Ruapehu)

further back in time has therefore been obtained (Chapter 3; Section 5.13; Table 5.3; Section 7.4, Fig. 7.6).

From c. 75 - 64 ka, there was 1 large-scale (thick pumice lapilli-producing) eruption per 600 years on average from Ruapehu, but in the period immediately prior to 64 ka the rate was much higher. Probable Tongariro-sourced tephras were limited to the earliest part of this time interval.

In the interval 64 - 36 ka there was a very low frequency of large tephra eruptions from Ruapehu, averaging 1 per 7 000 years.

Between 36 and c. 23 ka the average rate of large Ruapehu eruptions was again higher, at 1 per 800 years. The rate was much higher early in the interval and very low in the latter stages.

From c. 23 to 22.6 ka the rate of large Ruapehu eruptions was extremely high at 1 per 100 years. This eruption rate was equivalent or higher than that of the Bullot Formation (described by Donoghue *et al.*, 1995), and probably indicates the start of that eruptive period.

Throughout the entire 75-22.6 ka period small scale eruptions were occurring frequently, probably from both volcanoes. These are recorded by accumulations of fine ash with soil development reflecting the slow rate of surface accretion.

8.2.4 *An overall synthesis of the landscape development of the northeastern Ruapehu and eastern Tongariro ring plains*

Using the ring plain stratigraphy developed to meet the previous objectives, ring plain construction was examined over time and in the context of the late Quaternary geologic history of the lower North Island. This resulted in the development of a construction history of the northeastern Ruapehu ring plain from c. 75 - 22.6 ka (Section 7.3), and for both ring plains from 22.6 ka B.P. to the present. (Chapter 5). Landscape stability and paleosol development in the c.75 - 22.6 ka sequence was also elucidated (Chapter 4).

A summary geologic synthesis (Section 7.4) combines all of the above information as well as additional data from geological mapping (Section 7.2).

8.3 Additional contributions made by this study

During the process of meeting the prime objectives of this study, other significant developments were made in the following areas:

8.3.1 *Rhyolitic tephra identification*

In previous studies, rhyolitic tephras have been identified using mineralogy (e.g. Lowe, 1988), titanomagnetite chemistry (e.g. Kohn, 1970) and glass chemistry (e.g. Froggatt, 1983). Electron microprobe-determined glass chemistry has proved to be the most successful tool, particularly when mineralogy and stratigraphic data are lacking.

Comparison and discrimination of glass chemistry was initially by graphical and numeric means (e.g. Borchardt *et al.*, 1971; Froggatt, 1983). Later studies demonstrated the potential for using canonical discriminant function analysis (DFA) to discriminate glass chemistry from different sources and different tephras (e.g. Stokes and Lowe, 1988; Stokes *et al.*, 1992; Shane and Froggatt, 1994). However, although these methods were used to *discriminate* tephras, they were not proved nor developed in a practical study in which the aim was to *identify* tephras.

In Chapter 2 a DFA model was developed for potential tephra correlatives in the area (the point where previous studies had reached). Following on from this, unknown tephras were identified using probabilities of their classification to tephras in the model. This was the first practical demonstration of these techniques on New Zealand tephras. In addition, methods of improving the identification of the tephras were tried, including addition of correctly classified previously unknown tephras to the original model, and treatment of some unknowns as mixed tephras.

8.3.2 *Andesitic tephra discrimination*

The DFA methods used for rhyolitic tephra discrimination had never been used for andesitic tephras in New Zealand. In the first part of Chapter 3 (Section 3.3) the DFA methods were tested on electron microprobe-determined chemistry of various phenocryst phases to discriminate between two volcanic sources (Ruapehu and Egmont volcanoes) and then between individual tephras of one of the sources (Egmont). This study established that these discriminations were possible and that titanomagnetite was the best mineral phase for this purpose.

In the second part of Chapter 3 (Section 3.4) the use of DFA and clustering techniques were demonstrated for development of an andesitic tephrostratigraphy in a previously unknown sequence. These techniques were shown to be able to distinguish marker tephras which could be used in correlation.

8.3.3 *Halloysite/allophane formation in andesitic tephras*

In Chapter 4 (Section 4.9), a two stage weathering process was shown to account for an apparently unusual combination of 2:1 allophane and halloysite present in a paleosol sequence developed into andesitic tephras. Most studies of weathering tephras had not taken such a process into serious consideration.

It is commonly considered (e.g. Parfitt *et al.*, 1984; Singleton *et al.*, 1989) that soil solution Si/Al ratios determine whether 2:1 allophane, 1:1 allophane or halloysite is formed from weathering tephras. Soil solutions high in Si promote formation of 1:1 allophane and halloysite, low Si:Al ratios promote 2:1 allophane. In andesitic tephras, lower Si:Al ratios normally promote the formation of 2:1 allophane (e.g. Kirkman 1981; Lowe, 1986). This occurred in the Ruapehu tephra sequence studied when the tephra/soil surface was originally accreting. Later rapid burial of this weathered material

by 20 m of lahar deposits and tephras created poor drainage conditions within it. In addition, weathering of the overburden resulted in large amounts of dissolved silica leaching downward into the buried tephra. This resulted in ongoing weathering of remaining andesitic glass into halloysite rather than the 2:1 allophane previously formed at the soil surface.

8.3.4 *Relationship of ring-plain construction to late Quaternary climate change*

A well constrained rhyolitic tephrochronology was developed for the Ruapehu and Tongariro ring-plain sequences in Chapter 2. This enabled examination of the ring plains' depositional history in relation to other records of late Quaternary climate change in the lower North Island.

In Section 4.10, periods of paleosol development in the Ruapehu ring-plain sequence were correlated to periods of relatively warm climate and widespread soil development in the lower North Island. In Section 7.3 and 5.13, periods of large scale and widespread lahar and streamflow deposition on the ring plains were correlated to the last and antepenultimate stadials of the Last Glacial (Ohakean and Porewan stadials).

The Ruapehu and Tongariro ring plains therefore record a composite history of both volcanic events and late Quaternary climate change.

8.4 Potential future work

A) An examination of the so-called middle Tongariro Subgroup tephras (Milne and Smalley, 1979) preserved in loess sections to the south, east and west of the study area. Correlation of these to their near source equivalents would prove valuable in providing further chronology for the loess sequences. In addition, the provenance and correlation of tephras in loess sequences to the west of Ruapehu (which could contain tephras from both Egmont and the Tongariro Volcanic Centre) could be established.

B) A pedological and mineralogical investigation of the Papakai Formation around the entire Tongariro Volcanic Centre. This study would provide valuable information on soil-forming and weathering processes within andesitic tephra of the same age in areas of different drainage and climate. It may also provide additional information about the climate in this area during the Holocene.

C) A detailed investigation of the upper ring-plain portions of the Upper Waikato Stream and the Whangaehu River. The purpose of this study would be to (1) identify definitely if lahars from the Whangaehu River have entered the Upper Waikato Stream, and (2) examine the potential for this to happen in the future, following the events of 1995.

D) Investigate the physical volcanology of the Mangamate Tephra, Bullot Formation and older tephras. This would provide information on column height, eruption rates and

potential distributions of these larger events from Ruapehu and Tongariro. Information such as this could be used to predict and prepare for the effects of larger eruptions of either of the two volcanoes in future.

E) Investigation of the large lava flow(s) along the Tongariro River. This unit has not been adequately dated, nor has its origin been completely determined. Is it a series of large flows derived from Tongariro volcano or are the flows from satellite vents or a fissure along the eastern TVZ boundary fault close to the present course of the Tongariro River?

8.5 References

Borchardt, G.A..; Harward, M.E.; Schmitt, R.A., 1971. Correlation of ash deposits by activation analysis of glass separates. Quat. Res. 1: 247-260.

Donoghue, S.L.; Neall, V.E.; Palmer, A.S., 1995. Stratigraphy and chronology of late Quaternary andesitic tephra deposits, Tongariro Volcanic Centre, New Zealand. J. Roy. Soc. N. Z. 25: 115-206.

Froggatt, P.C., 1983. Towards a comprehensive Upper Quaternary tephra and ignimbrite stratigraphy in New Zealand using electron microprobe analysis of glass shards. Quat. Res. 19: 188-200.

Kirkman, J.H., 1981. Morphology and structure of halloysite in New Zealand tephras. Clays and Clay Min., 29, 1-9.

Kohn, B.P., 1970. Identification of New Zealand tephra layers by emission spectrographic analysis of their titanomagnetites. Lithos 3: 361-368.

Lowe, D.J., 1986. Controls on the rates of weathering and clay mineral genesis in airfall tephras: a review and New Zealand case study. In: Colman, S.M., and Dethier, D.P. (eds) Rates of chemical weathering of rocks and minerals. Academic Press, Orlando, pp. 265-330.

Lowe, D.J., 1988. Stratigraphy, age, composition, and correlation of late Quaternary tephras interbedded with organic sediments in Waikato lakes, North Island, New Zealand. N. Z. J. of Geol. and Geophys. 31: 125-165.

Milne, J.D.G. and Smalley, I.J., 1979. Loess deposits in the southern part of the North Island of New Zealand: an outline stratigraphy. Acta Geologica Academiae Scientarium Hungaricae, 22: 197-204.

Parfitt, R.L., Saigusa, M. and Cowie, J.D., 1984. Allophane and halloysite formation in a volcanic ash bed under different moisture conditions. Soil Sci., 138, 360-364.

Shane, P.A.R., Froggatt, P.C., 1994. Discriminant function analysis of glass chemistry of New Zealand and North American tephra deposits. Quat. Res. 41: 70-81.

Singleton, P.L., McLeod, M. and Percival, H.J., 1989. Allophane and halloysite content and soil solution silicon in soils from rhyolitic volcanic material, New Zealand. Australian J. of Soil Res., 27, 67-77.

Stokes, S.: Lowe, D.J., 1988. Discriminant function analysis of late Quaternary tephras from five volcanoes in New Zealand using glass shard major element chemistry. Quat. Res. 30: 270-283.

Stokes, S.; Lowe, D.J.; Froggatt, P.C., 1992. Discriminant function analysis and correlation of Late Quaternary rhyolitic tephra deposits from Taupo and Okataina volcanoes, New Zealand, using glass shard major element composition. Quat. Inter. 13/14: 103-117.

Topping, W.W., 1973. Tephrostratigraphy and chronology of late Quaternary eruptives from the Tongariro Volcanic Centre, New Zealand. N. Z. J. Geol. and Geophys., 16: 397-423.

Topping, W.W., Kohn, B.P., 1973. Rhyolitic tephra marker beds in the Tongariro area, North Island, New Zealand. N.Z. J. Geol. and Geophys., 16: 375-395.

APPENDIX 1: SAS PROGRAMS USED IN THIS STUDY

A1.1 Programs

The analyses within Chapter 2 were all carried out using SAS Release 6.11 for Windows 95. Chapter 3 analyses were carried out using SAS Release 5.0 on a UNIX system.

A) Glass data were entered from tab-delimited text files, constructed in the following format: Sample // Group // SiO_2 // TiO_2 // Al_2O_3 // FeO // CaO // Na_2O // K_2O.
Consequently, the Data Step required for all of the programs was:

```
data libname.sas-dataset-name;
        infile "absolute address of text file";
        input sample group sio2 tio2 al2o3 feo cao na2o k2o;
run;
```

The sample field was a number individually identifying each analysis of each sample. The group field was an integer code, each number represented a different tephra. The other fields contained the log-transformed oxide values.

B) To construct discriminant models the following program step was used:

```
proc discrim data=libname.sas-dataset-name outstat=libname.outstat-dataset-name ncan=5
                listerr distance simple;
        class group;
        var sio2 tio2 al2o3 feo cao na2o k2o;
        id sample;
run;
```

The "outstat" option was used to store the discriminant model parameters which were required to test the unknown samples against. The number of canonical variables was the lesser number of 1-(number of tephra groups) and 1-(number of oxide predictors). The "listerr" option prints the observations that were classified incorrectly and lists their probabilities of classification to each of the tephra groups in the discriminant model. The "distance" option prints the Mahalanobis (D^2) distances between tephra groups in the model. The "simple" option prints means and standard deviations of each of the tephra groups.

C) To produce the plots of canonical variates for the discriminant models the following program steps were used:

```
proc candisc data=libname.sas-dataset-name out=libname.outcan-dataset-name;
        class group;
        var sio2 tio2 al2o3 feo cao na2o k2o;
run;
proc plot data=libname.outcan-dataset-name;
        plot can2*can1=group / href=0 vref=0;
run;
```

All canonical variables are stored in the "out" dataset by the first part of the procedure. The second part of the procedure plots the first two canonical variables from the "out" dataset.

D) To test unknown analyses against the discriminant models the following program step was used:

```
proc discrim data=libname.outstat-dataset-name testdata=libname.test-dataset-name
                testout=libname.testout-dataset-name testlist;
        class group;
        var sio2 tio2 al2o3 feo cao na2o k2o;
        testclass group;
        testid sample;
run;
```

This program uses the "outstat" dataset created when the discriminant model was initially constructed and tests the unknown analyses (test-dataset) against it. The "testlist" option prints probabilities of classification of all of the unknown samples with each of the tephra groups in the discriminant model.

E) To establish the variables which discriminate between tephra groups the most by stepwise DFA, the following program step was used:

```
proc stepdisc data=libname.sas-dataset-name stepwise;
        class group;
        var sio2 tio2 al2o3 feo cao na2o k2o;
run;
```

F) To carry out clustering analysis of the tephra samples the following program steps were used:

```
proc cluster data=libname.sas-dataset-name method=wards ccc pseudo;
        var sio2 tio2 al2o3 feo cao na2o k2o;
        copy group;
proc tree ncl=(number of clusters you suspect) out=libname.outclus-dataset;
        copy sio2 tio2 al2o3 feo cao na2o k2o group;
proc freq;
        tables cluster*group;
```

The first program step carries out the clustering process using a minimum variance method. The second step plots a tree diagram to help interpret the number of clusters present. The third step produces a table comparing the cluster groupings with those which you have pre-defined. Usually a "candisc" step was added to this procedure to evaluate the efficiency of the clustering, with the class=cluster.

Note: For each program or data step the list of variables was customised for the particular mineral or glass phase being considered.

A1.2 Reference

SAS Institute Inc., 1989. SAS users guide: statistics. Version 6 Edition. Cary N.C., SAS Institute Inc., 1028 pp.

Appendix 2: Rhyolitic glass analyses

All of the glass analyses carried out in this study follow.
Samples are listed in the same order as Table 2.2 (Chapter 2).
The analyses are in a raw form (not normalised).

Sample	Location	Analysis	SiO2	TiO2	Al2O3	FeO	MgO	CaO	Na2O	K2O
Sample 93.5	T20/465127	1	76.050	0.529	11.899	0.792	0.190	0.732	4.027	3.524
		2	75.563	0.278	12.225	1.059	0.161	0.995	4.156	3.107
		3	76.593	0.509	12.004	1.109	0.120	1.069	4.128	3.825
		4	76.788	0.345	11.923	1.049	0.108	1.038	4.183	3.687
		5	76.175	0.522	12.126	0.897	0.065	1.153	4.237	3.826
		6	78.617	0.748	12.012	0.909	0.191	1.084	4.236	3.443
		7	75.637	0.316	12.064	1.032	0.121	1.048	3.896	3.783
		8	76.511	0.340	12.005	0.992	0.122	1.323	4.146	3.320
		Mean	76.492	0.448	12.032	0.980	0.135	1.055	4.126	3.564
Sample 93.6	T20/453129	1	77.442	0.187	12.734	1.029	0.232	0.910	4.301	3.333
		2	73.210	0.175	11.845	1.074	0.226	0.925	4.158	3.156
		3	75.842	0.163	12.403	1.093	0.221	0.984	4.302	3.429
		4	74.592	0.164	12.058	1.031	0.128	0.965	4.352	3.478
		5	75.656	0.168	12.384	0.973	0.134	0.900	4.314	3.357
		6	79.033	0.170	12.604	0.906	0.234	0.998	4.152	3.303
		7	78.614	0.088	12.381	0.902	0.215	0.834	3.876	3.386
		8	77.977	0.205	12.357	1.010	0.161	0.962	4.225	3.359
		9	76.916	0.229	12.157	1.124	0.141	0.925	4.147	3.135
		10	79.594	0.222	11.887	0.926	0.197	0.887	4.346	3.428
		Mean	76.888	0.177	12.281	1.007	0.189	0.929	4.217	3.336
Sample 93.7	T20/430127	1	77.655	0.694	12.323	0.830	0.174	0.957	3.956	3.977
		2	74.621	0.232	11.480	0.982	0.191	1.045	4.190	3.417
		3	76.167	0.599	11.639	0.718	0.187	0.931	3.995	3.087
		4	75.672	0.319	12.235	0.918	0.124	0.909	4.149	3.037
		5	75.572	0.269	11.826	0.763	0.212	0.728	4.175	3.226
		6	75.186	0.414	11.945	0.889	0.072	0.815	4.035	2.949
		7	74.603	0.209	12.058	0.783	0.231	0.991	3.942	3.066
		8	74.134	0.217	12.338	0.855	0.144	0.708	3.713	3.138
		9	75.609	0.208	12.017	1.155	0.154	0.894	4.056	3.393
		Mean	75.469	0.351	11.985	0.877	0.165	0.886	4.023	3.254
Sample 93.8	T20/435129	1	76.975	0.557	12.197	0.832	0.186	1.350	4.403	3.687
		2	77.440	0.624	11.961	1.093	0.136	1.613	4.079	3.379
		3	71.812	0.861	11.792	0.935	0.122	1.947	3.962	3.359
		4	77.496	0.243	12.469	1.260	0.156	0.828	4.240	3.684
		5	74.878	1.094	12.002	1.217	0.152	1.071	3.925	3.684
		6	77.166	0.000	12.542	0.989	0.180	1.678	4.123	3.316
		7	77.280	0.074	12.337	0.976	0.235	1.331	4.105	3.682
		8	74.892	0.491	11.523	1.177	0.172	1.127	4.072	3.210
		9	78.737	0.866	11.978	1.082	0.163	0.814	4.144	3.625
		10	73.917	1.471	11.972	0.980	0.177	0.384	3.956	3.578
		11	77.022	1.320	11.678	1.111	0.101	1.026	4.171	3.958
		12	78.007	0.926	12.231	0.933	0.183	0.952	4.102	3.778
		13	77.894	0.301	11.901	1.021	0.114	1.935	4.069	3.235
		14	75.064	0.936	11.304	1.001	0.145	1.242	3.902	3.329
		Mixed								
Sample 93.9	T20/498157	1	74.197	0.106	12.017	0.987	0.074	0.755	4.220	3.457
		2	75.680	0.110	12.022	0.964	0.065	0.535	4.135	3.721
		3	73.492	0.167	12.266	1.058	0.202	0.877	4.420	3.499
		4	74.504	0.075	11.851	0.945	0.084	0.536	4.164	3.776
		5	74.445	0.130	11.949	1.168	0.118	0.725	4.451	3.305
		6	73.919	0.113	11.804	1.192	0.166	0.601	4.323	3.296
		7	73.278	0.125	11.950	1.066	0.132	0.577	4.023	3.311
		8	76.138	0.106	12.164	0.913	0.074	0.561	4.200	3.745
		9	75.713	0.179	11.949	1.080	0.128	0.655	4.278	3.458
		10	73.635	0.120	12.255	1.337	0.186	0.856	4.187	3.250
		11	73.199	0.266	11.818	1.131	0.147	0.764	4.288	3.831
		Mean	74.382	0.136	12.004	1.076	0.125	0.677	4.244	3.514

Appendix 2: Rhyolitic glass

Sample 93.32	T20/469100	1	74.862	0.147	11.925	0.868	0.052	0.658	3.791	4.428
		2	74.338	0.131	12.169	0.844	0.067	0.764	3.950	4.266
		3	74.872	0.078	12.390	0.954	0.109	0.698	3.979	4.347
		4	75.023	0.131	12.363	0.882	0.048	0.717	4.059	4.191
		5	74.542	0.090	12.069	0.870	0.064	0.554	3.792	4.408
		6	71.756	0.122	12.010	0.838	0.072	0.634	3.766	4.161
		Mean	74.232	0.117	12.154	0.876	0.069	0.671	3.890	4.300
Sample 93.59	T19/505248	1	78.011	0.229	13.106	1.280	0.257	1.559	4.150	2.814
		2	74.733	0.196	12.353	0.773	0.129	0.717	3.707	4.056
		3	74.021	0.125	12.101	1.111	0.197	0.869	4.291	3.421
		4	78.826	0.272	13.324	1.336	0.278	1.370	4.091	3.528
		5	75.769	0.246	12.403	0.752	0.063	0.638	3.744	4.620
		6	75.989	0.136	12.285	0.780	0.045	0.738	3.911	4.186
		7	76.539	0.129	12.338	0.928	0.082	0.523	3.993	4.375
		8	76.667	0.128	11.801	0.996	0.070	0.649	4.041	4.031
		9	75.320	0.273	12.318	0.981	0.109	0.991	4.117	3.685
		10	78.489	0.159	12.307	1.075	0.156	0.933	4.124	3.455
		Mixed								
Sample 94.7	T20/465127	1	75.627	0.114	12.012	1.017	0.162	0.898	3.874	3.310
		2	76.161	0.104	12.152	0.988	0.143	0.834	3.749	3.200
		3	72.616	0.101	11.572	2.004	0.192	0.829	3.756	3.154
		4	75.023	0.260	11.801	0.883	0.168	0.871	3.946	3.087
		5	76.403	0.186	12.429	0.834	0.150	0.928	3.858	3.263
		6	72.965	0.147	11.638	0.737	0.083	0.839	3.632	2.901
		7	76.166	0.163	12.166	1.052	0.175	0.913	3.848	3.132
		8	76.104	0.176	12.235	0.972	0.141	1.121	3.571	3.398
		9	74.466	0.155	11.854	0.972	0.115	0.965	4.003	3.118
		Mean	75.059	0.156	11.984	1.051	0.148	0.911	3.804	3.174
Sample 94.9	T20/468162	1	76.328	0.214	12.883	1.740	0.198	1.380	3.912	3.028
		2	74.926	0.184	12.729	1.530	0.174	1.418	3.942	2.925
		3	72.836	0.148	11.768	1.315	0.134	1.043	3.604	2.904
		4	75.351	0.237	12.771	1.528	0.147	1.220	3.933	2.854
		5	75.859	0.190	12.776	1.506	0.200	1.454	3.938	2.893
		6	75.876	0.181	12.891	1.616	0.179	1.396	3.885	3.138
		7	74.500	0.189	12.802	1.548	0.165	1.410	4.026	2.895
		8	72.239	0.244	11.820	1.492	0.189	1.272	3.931	2.981
		9	76.376	0.179	12.921	1.577	0.194	1.519	4.207	3.172
		10	72.517	0.308	12.559	1.321	0.255	1.365	4.236	2.717
		Mean	74.681	0.207	12.592	1.517	0.184	1.348	3.961	2.951
Sample 94.21	T19/481211	1	73.883	0.206	11.760	1.015	0.185	1.013	3.752	3.270
		2	73.903	0.207	12.042	0.998	0.237	0.854	3.944	3.029
		3	75.398	0.198	12.014	0.922	0.161	0.863	3.781	3.482
		4	75.472	0.175	12.628	0.972	0.187	1.274	4.144	3.119
		5	76.873	0.157	11.933	0.879	0.197	0.888	3.939	3.282
		6	75.862	0.216	11.066	1.147	0.121	0.663	3.531	3.364
		7	72.994	0.093	11.640	0.871	0.209	0.927	3.791	2.907
		8	74.943	0.198	12.201	1.171	0.195	0.888	3.938	3.167
		9	74.222	0.095	12.026	0.964	0.145	0.787	3.797	3.583
		Mean	74.839	0.172	11.923	0.993	0.182	0.906	3.846	3.245
Sample 94.24	T19/486211	1	75.850	0.179	12.800	1.456	0.167	1.531	4.065	2.920
		2	75.608	0.256	12.941	1.766	0.172	1.433	4.022	2.909
		3	75.050	0.187	12.873	1.570	0.162	1.546	3.984	3.188
		4	72.989	0.269	12.590	1.448	0.240	1.498	3.960	3.022
		5	74.509	0.215	12.765	1.543	0.246	1.651	3.884	3.123
		6	74.391	0.242	12.786	1.501	0.209	1.484	4.039	3.075
		7	75.569	0.214	12.877	1.762	0.156	1.402	3.936	2.867
		8	75.009	0.243	12.686	1.786	0.161	1.262	4.220	2.986
		9	71.286	0.171	16.033	1.339	0.144	2.982	4.779	2.329
		10	72.349	0.258	12.495	1.604	0.168	1.332	4.058	2.945
		Mean	74.261	0.223	13.085	1.578	0.183	1.612	4.095	2.936
Sample 94.27	T19/485221	1	79.743	0.057	12.912	1.125	0.078	0.702	3.679	3.991
		2	74.259	0.155	11.758	1.002	0.050	0.724	3.602	4.070
		3	75.002	0.214	11.848	0.959	0.134	0.851	3.901	3.109
		4	75.289	0.158	11.792	1.097	0.125	1.053	3.883	3.144
		5	77.128	0.109	12.314	0.882	0.096	0.795	3.775	3.958
		6	77.463	0.149	12.317	1.139	0.202	0.838	4.013	3.056
		7	75.757	0.222	11.997	1.067	0.158	0.834	4.002	3.193

		8	75.999	0.103	12.190	0.868	0.071	0.833	3.865	3.387
		9	76.081	0.158	12.170	1.039	0.101	0.982	4.017	3.299
		Mean	76.302	0.147	12.144	1.020	0.113	0.846	3.860	3.467
Sample 94.28	T19/495220	1	73.280	0.052	11.670	1.174	0.080	0.755	3.381	3.166
		2	74.430	0.061	11.824	0.941	0.131	0.755	3.660	3.792
		3	71.086	0.106	11.596	1.357	0.072	0.828	3.796	3.041
		4	73.820	0.103	11.752	0.904	0.126	0.702	3.128	4.248
		5	74.483	0.115	11.754	1.197	0.121	0.778	3.737	3.956
		6	70.450	0.102	11.309	1.111	0.105	0.972	3.551	3.016
		7	73.917	0.128	11.680	1.067	0.106	0.664	3.761	3.525
		8	72.529	0.070	11.663	0.906	0.114	0.791	3.715	3.602
		9	71.928	0.128	11.423	1.199	0.167	0.573	3.652	3.443
		10	70.504	0.164	11.583	1.257	0.145	0.982	3.637	3.108
		Mixed								
Sample 94.29	T19/495220	1	73.167	0.073	11.836	1.089	0.123	0.709	2.672	3.505
		2	72.856	0.157	11.542	1.190	0.045	0.759	3.107	3.575
		3	72.770	0.105	11.552	1.003	0.043	0.732	3.282	3.774
		4	73.401	0.219	12.000	1.311	0.106	0.944	3.488	3.316
		5	73.704	0.174	12.088	1.374	0.164	0.871	3.517	3.424
		Mixed								
Sample 94.37	T19/485238	1	76.275	0.147	12.248	1.058	0.116	0.929	4.022	3.319
		2	73.883	0.090	11.687	1.055	0.178	0.856	3.969	2.951
		3	73.701	0.181	11.499	1.113	0.171	0.880	3.777	2.834
		4	78.023	0.107	12.327	1.127	0.140	0.897	4.095	3.347
		5	76.217	0.157	12.014	0.928	0.174	0.958	4.208	3.145
		6	76.923	0.158	12.411	1.137	0.184	0.867	3.890	3.252
		7	76.462	0.105	12.176	1.155	0.242	0.965	3.767	3.104
		8	74.827	0.144	12.423	1.040	0.170	1.092	3.874	3.038
		9	77.566	0.113	12.040	0.904	0.146	0.795	3.859	3.280
		10	74.951	0.158	11.833	0.961	0.183	0.931	3.941	3.107
		Mean	75.883	0.136	12.066	1.048	0.170	0.917	3.940	3.138
Sample 94.47	T19/496238	1	76.533	0.120	11.293	1.270	0.055	0.636	3.491	3.813
		2	76.019	0.105	11.427	0.922	0.003	0.607	3.777	3.707
		3	75.026	0.169	11.337	0.964	0.043	0.563	3.665	3.718
		4	75.729	0.151	11.268	0.975	0.044	0.510	3.647	3.972
		5	75.787	0.145	11.389	1.058	0.078	0.489	3.649	3.496
		6	76.166	0.175	11.368	1.043	0.094	0.390	3.713	3.775
		7	75.920	0.175	11.418	0.863	0.034	0.360	3.664	3.678
		8	74.862	0.137	11.123	1.006	0.074	0.377	3.461	3.753
		9	75.598	0.251	11.412	0.961	0.098	0.396	3.845	3.538
		10	75.021	0.122	11.232	0.988	0.137	0.393	3.528	3.727
		Mean	75.666	0.155	11.327	1.005	0.066	0.472	3.644	3.718
Sample 94.51	T19/504237	1	76.588	0.178	12.134	0.799	0.148	0.871	3.414	2.963
		2	73.653	0.203	11.639	1.008	0.198	0.842	3.662	3.246
		3	75.575	0.179	11.992	0.753	0.140	0.916	3.791	3.168
		4	76.264	0.176	12.149	0.892	0.168	0.795	3.578	3.417
		5	75.477	0.122	12.090	0.860	0.138	0.919	3.909	3.019
		6	73.925	0.186	11.759	0.835	0.112	0.820	3.811	3.016
		7	72.491	0.180	11.540	1.058	0.172	0.950	3.669	2.868
		8	72.490	0.177	11.518	1.104	0.112	0.888	3.788	3.002
		9	70.811	0.124	11.312	1.060	0.103	0.716	3.572	2.803
		Mean	74.142	0.169	11.793	0.930	0.143	0.857	3.688	3.056
Sample 94.58	T19/505248	1	75.099	0.054	12.014	0.759	0.098	0.856	3.962	3.152
		2	75.708	0.128	11.926	0.887	0.189	0.961	4.084	3.215
		3	73.637	0.119	11.646	0.637	0.119	0.832	3.734	3.099
		4	75.082	0.126	11.821	0.733	0.126	0.768	3.640	3.747
		5	73.992	0.148	11.869	0.570	0.121	1.094	4.108	2.943
		6	72.901	0.096	11.766	1.098	0.274	1.062	3.623	3.182
		7	76.702	0.192	12.349	0.792	0.111	0.941	3.932	3.330
		8	72.265	0.077	11.496	0.783	0.193	0.886	3.476	3.002
		9	72.113	0.077	12.394	0.537	0.093	0.871	4.323	2.590
		Mean	74.167	0.113	11.920	0.755	0.147	0.919	3.876	3.140
Sample 94.71	T19/488242	1	75.523	0.036	12.082	0.799	0.142	0.854	3.511	4.088
		2	73.692	0.173	12.096	0.819	0.134	0.791	3.620	4.152
		3	76.017	0.189	12.372	0.906	0.171	0.979	4.054	3.284
		4	76.783	0.115	12.066	1.063	0.148	0.892	4.149	3.048
		5	74.283	0.105	11.962	0.981	0.170	0.944	3.854	3.327

		6	76.948	0.130	11.994	1.039	0.162	0.970	3.853	3.447
		7	74.888	0.136	12.089	0.748	0.164	0.909	3.873	3.337
		8	75.921	0.173	12.439	1.102	0.086	0.935	3.919	3.888
		9	74.191	0.060	12.172	0.971	0.123	0.688	3.844	3.860
		10	73.835	0.093	12.198	0.923	0.090	1.000	3.957	4.090
		Mixed								
Sample 94.74	T19/499247	1	77.275	0.134	12.184	1.110	0.174	0.880	3.980	3.133
		2	76.234	0.104	11.997	1.248	0.129	0.921	3.804	3.137
		3	74.633	0.108	11.938	0.975	0.161	0.764	4.425	3.099
		4	75.454	0.160	12.015	0.996	0.146	0.818	3.891	3.174
		5	76.484	0.307	12.061	0.912	0.210	0.877	3.777	3.178
		6	74.212	0.225	11.823	1.076	0.186	0.831	3.902	2.904
		7	75.794	0.336	12.131	0.935	0.177	0.823	3.897	3.062
		8	75.541	0.115	12.137	0.884	0.110	0.867	3.990	3.161
		9	74.963	0.107	12.323	1.045	0.131	0.811	4.173	3.239
		10	75.025	0.130	12.053	1.084	0.162	0.829	4.022	3.324
		Mean	75.562	0.173	12.066	1.027	0.159	0.842	3.986	3.141
Sample 94.79	T19/364544	1	75.220	0.338	13.638	1.889	0.255	1.441	3.849	2.987
		2	74.605	0.405	13.438	2.140	0.335	1.461	4.057	3.013
		3	74.716	0.285	13.377	1.992	0.303	1.388	4.150	2.891
		4	75.099	0.384	13.207	1.976	0.359	1.402	4.136	2.938
		5	75.133	0.254	13.345	1.897	0.320	1.412	4.036	2.998
		6	74.998	0.345	13.002	1.995	0.338	1.442	4.112	2.901
		Mean	74.962	0.335	13.335	1.982	0.318	1.424	4.057	2.955
Sample 95.2	T19/430238	1	75.323	0.201	11.770	0.844	0.155	0.896	3.878	2.920
		2	76.403	0.221	12.033	0.939	0.191	0.894	3.848	3.221
		3	74.617	0.145	11.975	0.886	0.134	0.871	4.193	2.934
		4	74.023	0.173	11.920	1.002	0.116	0.898	3.916	3.008
		5	76.586	0.130	12.206	1.177	0.186	0.914	3.668	3.772
		6	71.486	0.183	11.352	0.891	0.123	0.827	3.670	2.825
		7	75.139	0.184	11.883	1.125	0.204	0.883	3.958	3.231
		8	76.564	0.131	12.139	1.013	0.151	0.869	2.956	3.488
		9	76.362	0.182	12.329	0.997	0.121	0.898	3.991	3.073
		Mean	75.167	0.172	11.956	0.986	0.153	0.883	3.786	3.164
Sample 95.3	T19/430238	1	74.844	0.112	12.187	1.084	0.059	0.641	3.538	4.144
		2	73.657	0.063	11.775	0.867	0.033	0.581	3.473	4.116
		3	74.676	0.080	11.900	0.873	0.078	0.671	3.549	3.898
		4	73.806	0.165	11.796	0.907	0.058	0.603	3.621	4.039
		5	75.048	0.094	12.345	1.006	0.060	0.779	3.718	3.860
		6	72.598	0.109	11.932	1.004	0.084	0.682	3.542	3.793
		7	74.831	0.169	12.290	0.861	0.135	1.014	3.971	2.883
		8	75.977	0.296	12.212	1.192	0.241	1.196	3.854	3.160
		Mean	74.430	0.136	12.055	0.974	0.094	0.771	3.658	3.737
Sample 95.6	T19423339	1	75.755	0.114	12.105	1.184	0.220	0.956	3.889	3.163
		2	75.375	0.133	11.969	1.038	0.233	0.905	3.940	3.285
		3	73.722	0.201	11.846	0.987	0.124	0.862	3.869	3.099
		4	75.129	0.165	11.752	1.056	0.206	0.980	4.070	3.162
		5	73.909	0.123	11.647	1.096	0.124	0.921	3.783	3.253
		6	76.427	0.190	12.141	1.062	0.236	1.042	4.044	3.174
		7	74.366	0.206	12.156	1.020	0.190	0.985	3.828	3.218
		8	74.891	0.161	11.854	1.098	0.144	0.834	3.902	3.160
		9	73.660	0.142	11.989	1.069	0.205	0.938	3.837	3.051
		10	75.950	0.110	11.935	1.118	0.151	0.941	3.861	3.255
		Mean	74.918	0.155	11.939	1.073	0.183	0.936	3.902	3.182
Sample 95.9	T19/448326	1	74.315	0.261	11.550	0.857	0.154	0.852	4.003	3.049
		2	73.074	0.205	11.616	0.844	0.117	0.910	3.848	2.841
		3	74.463	0.240	11.602	1.025	0.252	0.874	3.784	3.035
		4	75.748	0.179	12.264	0.928	0.158	0.782	3.908	3.577
		5	73.373	0.094	11.978	1.068	0.140	0.851	3.677	2.909
		6	76.560	0.212	12.346	1.070	0.165	0.867	3.969	3.348
		7	76.747	0.146	12.178	0.924	0.195	0.904	3.825	3.236
		8	76.238	0.179	12.245	0.964	0.177	0.925	4.300	3.114
		9	74.495	0.246	12.009	1.120	0.204	0.958	4.053	3.174
		10	72.904	0.167	11.770	1.080	0.176	0.958	3.848	2.963
		Mean	74.792	0.193	11.956	0.988	0.174	0.888	3.922	3.125
Sample 95.13	T19/549328	1	79.480	0.119	12.638	1.026	0.106	1.032	3.710	3.034
		2	74.747	0.164	11.955	0.979	0.131	0.928	3.834	2.860

		3	75.815	0.114	12.027	0.898	0.154	0.893	3.825	3.050
		4	71.140	0.123	11.304	0.881	0.122	0.862	3.660	2.757
		5	71.762	0.242	11.439	1.018	0.198	0.918	3.558	2.836
		6	74.703	0.182	11.812	0.983	0.239	0.789	3.798	3.161
		7	73.479	0.130	11.549	1.016	0.145	0.905	3.813	2.935
		8	75.169	0.178	11.705	1.091	0.191	0.878	3.936	3.211
		9	71.442	0.213	11.494	1.041	0.196	0.904	3.656	2.723
		Mean	74.193	0.163	11.769	0.993	0.165	0.901	3.754	2.952
Sample 93.1	T20/455088	1	74.231	0.670	11.539	1.210	0.142	0.926	3.954	3.422
		2	73.136	0.384	11.953	1.233	0.121	1.285	3.949	3.332
		3	72.679	0.583	11.949	1.249	0.121	1.287	3.945	3.247
		4	73.000	0.224	11.425	1.029	0.248	1.141	3.800	3.169
		5	73.659	0.354	11.741	1.278	0.068	1.229	3.941	3.356
		6	75.709	0.329	11.653	1.162	0.130	1.595	3.968	3.189
		7	75.540	0.261	11.655	1.234	0.109	1.455	4.051	3.243
		8	76.139	0.833	11.453	1.224	0.106	1.264	3.577	3.332
		9	73.218	0.297	11.828	1.290	0.153	1.603	4.108	2.996
		10	75.809	0.653	11.650	1.099	0.083	1.283	3.969	3.403
		Mean	74.312	0.459	11.685	1.201	0.128	1.307	3.926	3.269
Sample 93.3	T20/465095	1	70.768	0.173	11.753	1.175	0.185	0.949	4.003	3.159
		2	70.197	0.191	11.648	1.286	0.116	1.160	4.030	2.882
		3	73.239	0.132	12.168	1.258	0.158	1.052	4.071	3.202
		4	73.307	0.055	11.634	1.249	0.154	0.970	4.138	3.249
		5	74.545	0.148	11.684	1.374	0.109	0.983	3.979	3.141
		6	72.958	0.144	11.979	1.328	0.157	1.127	4.247	3.196
		7	72.515	0.325	12.145	1.133	0.114	0.987	4.263	3.302
		8	73.907	0.200	12.197	1.226	0.164	1.064	4.250	3.153
		9	75.796	0.125	11.757	1.240	0.143	1.068	4.016	3.228
		10	75.877	0.098	11.365	1.050	0.076	1.021	3.841	3.230
		Mean	73.311	0.159	11.833	1.232	0.138	1.038	4.084	3.174
Sample 93.17	T20/461170	1	72.683	0.205	12.208	1.259	0.156	1.148	3.938	2.798
		2	75.642	0.120	12.252	1.071	0.139	0.936	4.184	3.268
		3	75.094	0.146	12.090	1.156	0.142	1.134	4.304	2.963
		4	74.458	0.136	11.842	0.950	0.095	0.693	3.746	3.993
		5	73.607	0.181	12.368	0.998	0.195	1.070	4.357	3.007
		6	73.175	0.236	11.785	1.424	0.181	1.057	4.026	2.791
		7	73.396	0.115	12.002	1.142	0.151	0.975	4.103	2.999
		8	74.019	0.225	12.098	1.435	0.225	1.034	4.236	3.003
		9	72.013	0.141	11.904	1.465	0.147	1.060	3.877	2.820
		10	73.893	0.137	12.258	1.455	0.190	1.038	4.281	3.154
		11	74.964	0.263	12.149	1.400	0.151	1.130	4.140	2.955
		Mean	73.904	0.173	12.087	1.250	0.161	1.025	4.108	3.068
Sample 93.33	T20/469100	1	72.696	0.276	11.862	1.374	0.244	1.514	3.577	3.285
		2	72.563	0.221	11.229	1.164	0.150	1.032	3.912	3.340
		4	75.141	0.154	12.016	1.164	0.088	1.107	4.018	2.986
		5	71.388	0.321	11.598	1.320	0.142	1.186	4.125	2.990
		6	77.992	0.200	11.974	1.299	0.154	1.519	4.132	3.597
		7	77.409	0.143	11.733	1.218	0.122	1.093	4.126	3.412
		8	75.353	0.236	11.997	1.078	0.116	0.911	3.750	4.313
		9	70.170	0.274	11.658	1.156	0.156	1.076	3.741	2.983
		10	73.820	0.083	12.594	1.434	0.175	1.237	4.206	3.067
		11	76.510	0.142	12.510	1.322	0.144	1.357	4.182	3.466
		Mean	74.304	0.205	11.917	1.253	0.149	1.203	3.977	3.344
Sample 7.37	T20/469100	1	73.665	0.158	12.710	1.206	0.099	1.507	3.385	3.547
		2	73.105	0.268	12.042	1.824	0.120	1.317	2.832	3.509
		3	74.123	0.156	12.265	1.645	0.142	1.332	3.698	3.269
		4	73.125	0.251	12.740	1.468	0.125	1.471	3.889	3.358
		5	73.235	0.136	12.059	1.338	0.145	1.358	3.678	3.332
		6	73.200	0.200	12.111	1.665	0.163	1.451	3.587	3.457
		7	72.995	0.430	11.998	1.540	0.251	1.265	3.900	3.698
		8	74.023	0.235	12.457	1.568	0.099	1.315	3.547	2.998
		Mean	73.434	0.229	12.298	1.532	0.143	1.377	3.565	3.396
Sample 7.36	T20/469100	1	75.829	0.202	13.487	1.672	0.247	1.659	3.692	2.982
		2	74.655	0.289	13.383	1.866	0.274	1.678	4.101	2.782
		3	74.569	0.216	12.998	1.532	0.257	1.699	3.889	3.204
		4	74.587	0.247	13.258	1.665	0.243	1.637	3.952	2.936
		5	74.897	0.302	13.498	1.567	0.236	1.521	3.265	2.568
		6	75.112	0.256	13.003	1.587	0.213	1.563	3.777	2.886

Appendix 2: Rhyolitic glass

		Mean	74.942	0.252	13.271	1.648	0.245	1.626	3.779	2.893
Sample 9.37	T20/468102	1	72.100	0.242	12.624	1.561	0.107	1.370	3.353	3.422
		2	71.256	0.109	12.188	1.317	0.170	1.193	2.829	3.698
		3	71.590	0.172	12.293	1.737	0.163	1.192	3.086	3.609
		4	71.845	0.117	12.073	1.605	0.128	1.318	3.389	3.643
		5	73.379	0.192	12.139	2.019	0.137	1.269	2.775	3.500
		6	72.169	0.395	12.118	1.520	0.167	1.331	3.419	3.452
		7	73.057	0.150	12.329	1.954	0.107	1.214	3.041	3.410
		8	72.475	0.000	12.120	2.032	0.126	1.117	3.290	3.758
		9	71.924	0.000	12.019	2.082	0.112	1.247	3.717	3.680
		10	71.750	0.000	12.321	1.549	0.156	1.431	3.628	3.535
		Mean	72.155	0.138	12.222	1.738	0.137	1.268	3.253	3.571
Sample 9.36	T20/468102	1	72.618	0.208	12.510	1.625	0.147	1.292	3.126	3.639
		2	72.802	0.217	12.418	1.965	0.102	1.253	3.319	3.721
		3	73.310	0.190	12.376	1.675	0.132	1.232	3.318	3.642
		4	72.724	0.163	12.414	1.226	0.210	1.158	3.011	3.600
		5	73.265	0.278	12.567	1.368	0.218	1.366	3.215	3.555
		6	74.777	0.189	13.035	1.333	0.158	1.255	3.215	3.368
		Mean	73.249	0.208	12.553	1.532	0.161	1.259	3.201	3.588
Sample 9.35	T20/468102	1	73.673	0.192	13.234	1.822	0.268	1.521	3.886	2.636
		2	73.254	0.162	12.280	1.824	0.082	1.307	3.444	3.633
		3	74.216	0.187	13.005	1.668	0.125	1.406	3.446	2.949
		4	74.365	0.236	13.458	1.664	0.147	1.456	3.584	3.640
		5	73.998	0.205	13.612	1.624	0.179	1.258	3.845	3.514
		6	73.257	0.166	12.998	1.512	0.166	1.367	2.994	3.446
		7	74.111	0.114	12.359	1.699	0.135	1.357	3.489	3.495
		8	74.369	0.178	13.547	1.521	0.232	1.266	3.487	3.651
		9	75.002	0.154	13.200	1.478	0.148	1.312	3.265	2.846
		10	73.334	0.125	12.690	1.588	0.197	1.389	3.658	3.235
		Mean	73.958	0.172	13.038	1.640	0.168	1.364	3.510	3.305
Sample 9.33	T20/468102	1	74.508	0.164	11.854	1.213	0.078	1.095	3.152	3.043
		2	72.846	0.183	11.597	1.064	0.100	1.001	3.189	3.106
		3	72.836	0.173	11.451	1.283	0.201	0.824	2.273	3.430
		4	72.440	0.183	11.280	1.205	0.157	0.688	2.792	3.626
		5	73.491	0.109	12.130	1.165	0.131	1.011	3.076	2.785
		6	73.162	0.152	12.085	1.206	0.129	1.050	3.287	2.762
		7	73.190	0.097	12.061	1.248	0.157	0.915	3.051	2.942
		8	74.178	0.101	12.093	1.335	0.156	1.123	3.038	2.959
		9	74.396	0.060	11.659	1.124	0.141	0.970	2.608	2.747
		Mean	73.450	0.136	11.801	1.205	0.139	0.964	2.941	3.044
Sample 9.25	T20/468102	1	70.521	0.379	12.285	2.180	0.350	1.660	3.019	3.820
		2	73.076	0.393	12.531	2.608	0.412	1.446	3.552	3.681
		3	73.144	0.449	12.401	2.663	0.415	1.656	2.886	3.283
		4	76.662	0.309	13.279	2.002	0.285	1.393	4.148	2.796
		5	75.783	0.372	13.299	2.125	0.261	1.662	2.298	2.855
		6	77.303	0.275	13.089	1.892	0.223	1.212	4.084	3.026
		7	76.158	0.248	13.041	1.498	0.176	1.275	4.142	2.745
		8	75.974	0.253	13.125	1.637	0.192	1.295	4.232	2.808
		Mean	74.828	0.335	12.881	2.076	0.289	1.450	3.545	3.127
Sample 9.22	T20/468102	1	75.663	0.293	13.352	2.121	0.265	1.554	4.078	2.846
		2	72.623	0.241	12.922	2.073	0.299	1.474	3.515	2.638
		3	75.509	0.093	12.773	1.965	0.097	1.368	3.353	3.731
		4	74.301	0.078	12.382	1.738	0.036	1.174	3.524	3.365
		5	74.605	0.405	13.438	2.140	0.335	1.461	4.057	3.013
		6	74.716	0.285	13.377	1.992	0.303	1.388	4.150	2.891
		Mean	74.570	0.233	13.041	2.005	0.223	1.403	3.780	3.081
Sample 9.21	T20/468102	1	76.538	0.210	12.141	1.090	0.118	1.042	3.361	3.040
		2	76.252	0.167	11.865	1.038	0.134	0.969	3.696	3.044
		3	78.179	0.162	12.245	1.124	0.170	0.875	3.656	3.124
		4	75.750	0.137	11.849	1.070	0.192	1.066	2.936	2.710
		5	76.087	0.062	11.854	1.251	0.137	0.851	3.333	3.015
		6	76.019	0.105	11.427	0.922	0.003	0.607	3.777	3.707
		7	75.026	0.169	11.337	0.964	0.043	0.563	3.665	3.718
		8	75.729	0.151	11.268	0.975	0.044	0.510	3.647	3.972
		Mean	76.198	0.145	11.748	1.054	0.105	0.810	3.509	3.291
Sample 14.23	T20/477112	1	76.213	0.328	13.295	2.025	0.298	1.504	3.699	2.830

	2	75.990	0.320	13.343	1.918	0.290	1.971	3.808	2.709
	3	75.515	0.345	13.110	1.930	0.264	1.494	3.914	3.239
	4	74.176	0.134	12.690	1.643	0.113	1.227	3.206	2.785
	5	74.758	0.246	12.528	1.499	0.128	1.209	3.418	2.710
	6	74.677	0.145	12.899	1.589	0.163	1.338	3.712	2.933
	7	76.197	0.313	13.750	1.942	0.293	1.663	3.951	2.800
	8	76.205	0.228	13.093	2.266	0.258	1.584	3.929	2.801
	Mean	75.466	0.257	13.089	1.852	0.226	1.499	3.705	2.851
Sample 14.22 T20/477112	1	72.115	0.124	11.262	1.086	0.162	1.081	3.021	2.824
	2	74.828	0.152	11.671	1.197	0.144	1.009	3.004	2.975
	3	75.123	0.145	11.833	0.949	0.150	1.078	3.222	3.001
	4	74.408	0.102	11.849	0.885	0.070	0.960	3.290	3.016
	5	76.287	0.137	12.317	1.082	0.116	1.038	2.542	3.047
	6	74.345	0.165	11.968	1.114	0.118	0.887	2.676	2.837
	7	77.982	0.121	12.506	1.217	0.184	1.048	3.582	3.196
	Mean	75.013	0.135	11.915	1.076	0.135	1.014	3.048	2.985

APPENDIX 3: ANDESITIC TEPHRAS

3.1 Ferromagnesian mineral assemblages

The following table presents modal ferromagnesian mineralogy of all the andesitic tephras sampled in this study. Counts of 400 grains were made on mineral separates.

Sample	Location	Section	Unit or correlation	OPX	CPX	TM	HB	OL
93.23	T20/461096	45		56	39	5	0	0
93.24	T20/464098	46		59	40	1	0	0
93.25	"	"		41	37	3	0	19
93.26	"	"	Marker Unit 1	8	36	1	0	56
93.27	"	"	Marker Unit 1	16	48	1	0	36
93.28	T20/465099	47		51	48	0	0	2
93.29	T20/469102	9		57	43	0	0	0
93.30	T20/466096	5		54	45	0	0	0
93.31	"	"		47	51	0	0	2
93.34	T20/469100	7		50	49	0	0	1
93.36	"	"		53	47	0	0	0
93.38	"	"		59	34	1	0	6
93.39	"	"	Marker Unit 2	39	50	10	2	0
93.40	"	"		56	44	0	0	0
93.41	T20/468102	9		44	54	0	0	2
93.42	"	"		47	52	1	0	0
93.43	"	"		57	34	9	0	0
93.44	"	"		58	33	9	0	0
93.45	"	"		57	29	14	0	0
93.46	"	"		51	31	18	0	0
93.47	"	"	Marker Unit 3	49	40	11	0	0
93.48	"	"		63	22	15	0	0
93.49	"	"		67	19	15	0	0
93.50	"	"		66	20	15	0	0
93.51	"	"		52	43	4	1	0
93.52	T20/468102	10	Marker Unit 4	54	39	6	1	0
93.53	"	"		59	41	1	0	0
93.54	"	"		55	40	2	0	3
93.55	"	"		55	42	3	1	0
93.56	"	"		58	41	1	0	0
93.57	"	"		59	29	12	0	0
93.58	"	"		72	15	13	0	0
93.60	T20/477112	14		49	51	1	0	0
93.61	"	"	(93.37)	49	43	9	0	0
93.62	"	"	(93.38)	65	28	1	0	6
93.63	"	"	(93.40)	58	41	1	0	1
93.64	"	"	(93.40)	47	52	1	0	1
93.65	"	"	(93.42)	54	44	1	0	2
93.66	"	"		65	29	5	0	1
93.67	"	"		53	43	4	0	1
93.68	"	"		68	22	10	0	1
93.69	"	"		66	26	8	0	0
93.70	"	"	Marker Unit 3	57	41	2	0	0
93.71	"	"	(93.48)	66	28	6	0	0
93.72	"	"	(93.49)	57	27	16	0	0
93.73	"	"	(93.51)	49	40	8	2	1
93.74	"	"	Marker Unit 4	56	39	5	0	0
93.75	"	"		52	47	1	0	0
93.76	"	"		56	42	2	0	0
93.77	"	"		62	27	11	0	0
93.78	"	"		75	12	14	0	0
93.79	"	"		59	40	2	0	0

93.80	"	"		61	30	9	0	0
93.81	"	"		63	34	3	0	0
93.82	"	"		43	56	2	0	1
93.83	"	"		49	50	1	0	0
93.84	"	"		73	22	5	0	0
93.85	"	"	Marker Unit 5	50	41	9	0	1
93.86	"	"		51	37	12	0	0
93.87	"	"		61	36	4	0	0
93.88	"	"		60	37	3	0	0
93.89	"	"	Marker Unit 6	27	33	9	31	0
93.91	"	"	Marker Unit 7	55	39	1	5	0
94.2	T20/455088	-	Bullot Fm.	68	24	8	0	0
94.4	T20/469102	9	L1 Bullot Fm.	69	28	3	0	0
94.13	T20/496157	51		76	20	4	0	0
94.15	T20/463097	-	Bullot Fm.	47	10	15	28	0
94.16	"	-	"	78	13	9	0	0
94.17	"	-	"	66	26	8	0	0
94.18	T20/498184	53	?Bullot Fm.	66	24	9	1	0
94.20	T19/484209	54	"	71	22	4	0	3
94.22	T19/481211	55	(94.31)	36	31	7	26	0
94.31	T19/495220	59	(94.22)	37	14	9	40	0
94.32	T20/477112	14	Marker Unit 7	20	6	8	66	0
94.41	T19/491239	-	Rotoaira Tephra	78	19	3	0	0
94.43	T19/496238	66	Bullot Fm.	71	28	<1	<1	0
94.44	"	"	"	75	25	<1	0	0
94.45	"	"	"	72	24	4	<1	0
94.46	"	"	(94.22&31)	39	34	27	0	0
94.79	T19/364544	73	Poutu Tephra	63	29	7	0	1

3.2 Hornblende analyses

All analyses are listed in a raw form (not normalised).

Sample	Location	Section	Analysis	SiO2	TiO2	Al2O3	FeO	MnO	MgO	CaO	Na2O	K2O
Sample 93.39	T20/469100	7	1	44.665	1.192	13.032	13.215	0.171	15.805	10.682	2.840	0.217
			2	38.562	2.272	12.035	12.349	0.421	12.403	11.561	2.078	0.768
			3	39.565	2.225	12.821	12.959	0.348	12.773	11.694	2.161	0.844
			Mean	40.931	1.896	12.629	12.841	0.313	13.660	11.312	2.360	0.610
Sample 93.48	T20/468102	9	1	39.885	3.106	11.854	12.020	0.402	13.520	11.169	2.428	0.951
			2	38.493	2.965	11.211	12.913	0.361	12.903	11.270	2.325	0.890
Sample 93.51	T20/468102	9	1	41.877	2.039	13.772	11.474	0.089	14.617	10.957	2.398	0.415
			2	42.615	1.941	13.611	12.109	0.152	14.819	10.824	2.438	0.360
			3	41.589	1.759	13.368	12.598	0.255	13.932	10.691	2.358	0.382
			4	41.504	1.710	13.048	11.264	0.318	14.330	10.723	2.410	0.430
			5	42.194	2.126	13.976	11.608	0.420	14.762	11.128	2.433	0.331
			6	40.067	2.054	13.269	11.321	0.260	13.863	10.574	2.238	0.411
			7	41.245	3.305	11.261	11.856	0.333	14.673	11.192	2.546	0.815
			8	41.473	3.301	11.707	11.459	0.206	14.344	11.089	2.524	0.915
			9	41.103	3.546	11.620	11.116	0.524	14.282	11.272	2.269	0.893
			Mean	41.519	2.420	12.848	11.645	0.284	14.402	10.939	2.402	0.550
Sample 93.52	T20/468102	10	1	42.820	1.168	12.634	13.569	0.180	14.161	11.084	2.040	0.225
			2	42.945	1.228	12.232	14.141	0.387	13.373	10.775	1.976	0.295
			3	43.290	1.261	11.770	14.338	0.579	13.823	10.424	1.913	0.263
			4	42.051	1.215	12.006	14.515	0.172	13.527	10.602	2.014	0.173
			5	41.725	1.194	12.094	13.928	0.369	13.407	10.500	1.920	0.341
			6	40.830	1.199	12.079	13.755	0.318	13.093	10.592	1.873	0.325
			Mean	42.277	1.211	12.136	14.041	0.334	13.564	10.663	1.956	0.270
Sample 93.55	T20/468102	10	1	35.407	2.973	11.795	12.297	0.258	11.878	12.190	2.258	0.936
			2	37.311	3.369	11.968	12.102	0.217	11.708	12.321	2.420	0.975
			3	39.803	2.930	13.340	12.406	0.229	13.137	11.985	2.542	1.039
			Mean	37.507	3.091	12.368	12.268	0.235	12.241	12.165	2.407	0.983
Sample 93.71	T20/477112	14	1	39.540	2.967	9.925	11.727	0.482	13.630	10.293	2.187	0.758
Sample 93.73	T20/477112	14	1	40.694	2.110	13.755	11.241	0.187	14.492	11.052	2.300	0.387
			2	37.426	2.153	12.407	11.705	0.313	12.793	10.885	1.951	0.297
			3	40.770	2.038	13.368	12.032	0.297	14.674	10.835	2.349	0.348
			4	41.085	2.018	13.117	11.816	0.282	14.543	10.556	2.327	0.340
			5	39.621	1.883	13.057	11.675	0.192	14.477	10.633	2.095	0.371
			6	40.477	2.016	13.542	10.875	0.196	14.468	11.063	2.300	0.398
			7	41.163	1.990	13.481	11.900	0.342	14.677	11.266	2.292	0.350
			8	40.863	2.062	13.577	11.505	0.451	14.756	11.013	2.445	0.308
			9	40.818	2.034	13.220	11.417	0.306	14.555	10.961	2.357	0.317
			10	40.594	2.169	13.580	12.018	0.420	14.637	10.795	2.408	0.313
			11	40.453	3.109	12.517	12.955	0.355	13.446	10.989	2.561	0.844
			12	40.595	2.010	13.709	11.938	0.266	14.666	10.975	2.669	0.324
			Mean	40.380	2.133	13.278	11.756	0.301	14.349	10.919	2.338	0.383
Sample 93.75	T20/477112	14	1	40.764	2.269	11.681	11.717	0.467	13.886	11.787	2.425	0.749
			2	42.518	2.149	11.900	12.145	0.372	14.661	11.948	2.690	0.743
			3	41.933	3.085	12.150	11.366	0.297	14.269	11.426	2.638	0.730
			4	43.624	3.262	12.457	11.954	0.312	14.683	11.341	2.659	0.759
			Mean	42.210	2.691	12.047	11.796	0.362	14.375	11.626	2.603	0.745
Sample 93.89	T20/477112	14	1	41.637	2.180	13.451	11.151	0.188	14.937	12.239	2.565	0.856
			2	41.062	2.790	12.499	12.785	0.279	13.272	11.854	2.493	0.884
			3	40.784	2.014	13.681	11.425	0.121	13.779	12.467	2.358	0.933
			4	36.875	2.132	13.902	12.434	0.151	11.961	12.361	2.332	0.810
			5	41.979	2.787	11.532	13.134	0.373	13.283	12.201	2.625	0.827
			6	41.056	2.109	13.644	14.557	0.380	12.778	12.392	2.607	0.764
			7	40.159	1.971	14.230	13.105	0.206	12.848	12.541	2.487	0.928
			8	41.546	2.490	12.084	13.113	0.423	12.681	11.795	2.665	0.766
			9	44.438	3.081	10.475	11.446	0.421	14.632	11.983	2.395	0.759
			10	42.613	1.907	13.347	10.551	0.212	14.955	12.752	2.580	0.957
			Mean	41.215	2.346	12.885	12.370	0.275	13.513	12.259	2.511	0.848
Sample 93.90	T20/477112	14	1	41.845	1.743	13.223	12.900	0.250	13.661	11.295	2.644	0.699
			2	38.954	1.850	11.738	13.529	0.242	12.319	11.594	1.855	0.767

Appendix 3.2: Hornblende analyses

			3	39.785	2.719	8.082	12.095	0.501	13.193	11.323	1.659	0.790
			4	38.381	2.579	12.453	13.656	0.326	11.983	11.090	2.615	0.733
			Mean	39.741	2.223	11.374	13.045	0.330	12.789	11.326	2.193	0.747
Sample 93.91	T20/477112	14	1	41.030	2.489	11.101	12.323	0.375	13.477	11.819	2.454	0.648
			2	43.698	2.918	10.792	11.713	0.504	14.527	11.910	2.570	0.739
			3	42.780	3.122	11.802	12.194	0.507	14.053	11.713	2.623	0.748
			4	41.701	2.224	14.352	11.780	0.173	14.632	12.104	2.545	0.938
			5	42.739	2.306	14.220	12.205	0.145	14.032	12.733	2.508	0.890
			6	40.861	2.281	14.028	12.880	0.323	13.433	12.594	2.444	0.832
			7	42.703	3.070	12.369	13.065	0.519	13.625	12.435	2.872	0.907
			8	40.427	2.055	12.999	11.021	0.265	14.956	12.573	2.563	0.921
			9	43.738	2.012	14.289	10.122	0.232	16.407	11.372	2.885	0.886
			10	39.626	2.050	13.034	10.459	0.063	14.600	12.262	2.377	0.904
			Mean	41.930	2.453	12.899	11.776	0.311	14.374	12.152	2.584	0.841
Sample 94.15	T20/463097	52	1	43.937	2.431	10.585	11.745	0.202	14.499	10.975	2.230	0.277
			2	45.061	2.458	11.108	12.158	0.245	14.998	10.960	2.279	0.333
			3	45.070	2.143	11.218	12.341	0.224	15.053	10.931	2.289	0.335
			4	43.937	2.314	10.900	12.258	0.238	14.524	11.183	2.044	0.388
			5	44.144	2.432	11.809	12.815	0.163	14.491	10.953	2.349	0.361
			Mean	44.430	2.356	11.124	12.263	0.214	14.713	11.000	2.238	0.339
Sample 94.18	T20/498184	53	1	41.015	2.162	13.023	12.125	0.097	14.446	10.924	2.208	0.329
			2	41.241	2.170	13.087	12.021	0.211	14.655	11.305	2.209	0.408
			3	40.385	1.790	12.656	10.906	0.261	14.471	10.957	2.197	0.356
			4	41.797	2.074	13.057	12.513	0.199	14.526	10.978	2.391	0.331
			Mean	41.110	2.049	12.956	11.891	0.192	14.525	11.041	2.251	0.356
Sample 94.22	T19/481211	55	1	46.023	1.746	9.129	13.958	0.407	13.497	10.918	1.765	0.322
			2	44.588	1.685	9.607	14.838	0.293	13.671	10.876	1.812	0.296
			3	45.905	1.341	8.542	13.606	0.355	14.116	10.331	1.400	0.416
			4	44.626	1.422	9.156	13.824	0.369	13.607	10.190	1.643	0.337
			5	45.176	1.801	9.575	13.166	0.268	14.016	10.948	1.646	0.363
			6	47.106	1.299	7.443	12.733	0.280	15.729	10.568	1.281	0.244
			Mean	45.571	1.549	8.909	13.688	0.329	14.106	10.639	1.591	0.330
Sample 94.31	T19/495220	59	1	44.845	1.204	11.357	13.874	0.484	13.982	10.677	1.948	0.219
			2	43.904	2.289	10.810	13.469	0.276	13.911	10.719	2.243	0.321
			3	44.054	1.319	12.312	13.677	0.306	13.689	10.748	2.420	0.380
			4	44.429	1.613	10.548	11.995	0.312	14.086	10.938	2.191	0.333
			5	42.430	1.402	11.312	12.043	0.207	14.128	10.827	2.093	0.276
			6	44.191	1.421	12.248	11.005	0.214	14.849	10.955	2.258	0.340
			Mean	43.976	1.541	11.431	12.677	0.300	14.108	10.811	2.192	0.312
Sample 94.43	T19/496238	66	1	43.372	1.195	12.530	14.917	0.948	13.144	10.511	1.932	0.381
			2	41.124	1.306	12.446	15.285	0.509	12.246	10.356	1.793	0.370
			3	40.582	1.523	12.809	12.933	0.354	13.105	11.181	2.122	0.310
			4	40.934	1.686	13.726	13.974	0.183	13.499	11.082	2.401	0.337
			5	41.973	1.664	9.901	14.280	0.377	13.363	10.223	1.971	0.233
			6	41.486	1.416	10.680	13.746	0.455	13.325	10.705	1.907	0.336
			Mean	41.579	1.465	12.015	14.189	0.471	13.114	10.676	2.021	0.328
Sample 94.45	T19/496238	66	1	41.092	1.428	13.813	12.641	0.329	14.281	10.903	2.416	0.324
			2	42.314	1.553	13.244	13.143	0.182	14.479	11.171	2.173	0.278
			3	43.101	1.594	13.083	12.169	0.260	14.935	11.114	2.264	0.203
			4	41.419	1.645	13.638	11.396	0.141	14.876	10.815	2.311	0.293
			5	44.565	0.958	9.896	16.091	0.681	13.331	10.261	1.585	0.375
			6	42.369	1.256	12.675	11.644	0.135	15.502	10.793	2.141	0.244
			7	41.706	1.464	14.105	12.071	0.274	14.226	10.804	2.422	0.285
			Mean	42.367	1.414	12.922	12.736	0.286	14.519	10.837	2.187	0.286
Sample 94.46	T19/496238	66	1	40.721	2.851	11.133	10.830	0.252	14.487	11.597	2.368	0.806
			2	41.669	2.610	11.317	11.679	0.316	15.010	11.479	2.534	0.633
			3	41.659	2.811	11.113	11.513	0.254	14.513	11.326	2.293	0.837
			4	41.925	2.974	11.051	10.917	0.233	14.910	11.282	2.426	0.795
			5	41.017	2.528	11.049	11.109	0.334	14.401	11.340	2.342	0.701
			6	40.452	2.476	11.486	12.258	0.324	13.877	11.210	2.118	0.738
			7	43.502	3.011	11.659	11.712	0.450	14.677	11.333	2.521	0.774
			Mean	41.564	2.752	11.258	11.431	0.309	14.554	11.367	2.372	0.755
Sample 94.47 (Rhyolitic)	T19/496238	66	1	45.625	1.330	6.683	15.811	0.531	13.287	10.166	1.531	0.303
			2	45.112	1.393	6.369	16.534	0.604	12.483	10.132	1.436	0.327
			3	44.111	1.865	7.853	14.480	0.474	13.609	10.569	1.539	0.220
			Mean	44.949	1.529	6.968	15.608	0.536	13.126	10.289	1.502	0.283

3.3 Olivine analyses

All analyses are listed in a raw form (not normalised).

Sample	Location	Section	Analysis	SiO2	TiO2	Al2O3	FeO	MnO	MgO	CaO	Na2O	K2O
Sample 93.25	T20/464098	46	1resorbed	37.947	0.012	0.000	21.649	0.190	39.953	0.119	0.005	0.029
			2resorbed	39.090	0.000	0.007	18.170	0.125	43.692	0.133	0.058	0.026
			1	39.674	0.062	0.008	11.806	0.284	47.596	0.186	0.050	0.035
			2	40.235	0.100	0.035	12.237	0.331	47.465	0.100	0.035	0.109
			3	40.832	0.029	0.049	15.408	0.260	46.610	0.153	0.051	0.024
			4	41.481	0.029	0.015	12.442	0.266	48.663	0.177	0.049	0.051
			5	41.462	0.021	0.052	12.876	0.228	48.540	0.133	0.005	0.020
			Mean	40.737	0.048	0.032	12.954	0.274	47.775	0.150	0.038	0.048
Sample 93.26	T20/464098	46	1	39.200	0.021	0.097	14.765	0.529	45.887	0.152	0.031	0.002
			2	39.512	0.034	0.050	14.514	0.468	45.969	0.178	0.090	0.010
			3	39.394	0.070	0.083	15.626	0.288	45.407	0.118	0.013	0.025
			4	38.805	0.053	0.014	15.306	0.159	45.285	0.146	0.057	0.039
			5	39.633	0.053	0.045	14.676	0.027	46.170	0.180	0.035	0.044
			6	39.686	0.009	0.055	13.826	0.085	45.844	0.149	0.029	0.053
			7	39.212	0.245	0.018	14.872	0.105	45.598	0.167	0.002	0.087
			8	39.354	0.066	0.015	14.816	0.326	44.984	0.159	0.068	0.035
			9	39.689	0.074	0.061	14.402	0.071	46.199	0.129	0.001	0.043
			10	39.370	0.039	0.019	15.136	0.019	45.900	0.128	0.005	0.029
			Mean	39.386	0.066	0.046	14.794	0.208	45.724	0.151	0.033	0.037
Sample 93.27	T20/464098	46	1	39.120	0.040	0.015	14.819	0.509	45.762	0.158	0.002	0.015
			2	39.323	0.057	0.059	15.647	0.393	45.808	0.160	0.000	0.031
			3	38.974	0.027	0.066	14.613	0.319	45.413	0.218	0.044	0.037
			4	39.985	0.000	0.074	13.881	0.466	46.403	0.205	0.031	0.008
			5	39.735	0.001	0.079	14.988	0.301	45.332	0.195	0.005	0.017
			6	40.290	0.000	0.051	14.349	0.659	46.067	0.141	0.037	0.026
			7	40.088	0.000	0.115	14.481	0.384	46.105	0.188	0.001	0.031
			8	39.963	0.000	0.057	15.493	0.528	40.089	0.145	0.008	0.076
			9	39.439	0.094	0.059	14.013	0.252	46.607	0.155	0.000	0.043
			10	39.308	0.005	0.039	15.836	0.370	45.153	0.166	0.000	0.001
			Mean	39.623	0.022	0.061	14.812	0.418	45.274	0.173	0.013	0.029
Sample 93.28	T20/465099	47	1resorbed	37.820	0.049	0.000	23.829	0.430	38.142	0.146	0.005	0.051
			2resorbed	35.922	0.000	0.019	23.503	0.391	37.540	0.158	0.000	0.059
			1	38.018	0.000	0.013	18.166	0.272	43.807	0.130	0.083	0.027
			2	38.001	0.056	0.116	18.618	0.174	42.628	0.139	0.013	0.032
Sample 93.31	T20/466096	5	1	38.200	0.012	0.063	21.276	0.358	39.613	0.156	0.037	0.003
			2	38.157	0.002	0.076	20.525	0.318	40.809	0.142	0.037	0.017
			3	38.036	0.000	0.043	19.359	0.378	40.925	0.100	0.071	0.000
			4	35.920	0.070	0.077	20.715	0.304	37.892	0.156	0.239	0.095
			Mean	37.578	0.021	0.065	20.469	0.340	39.810	0.139	0.096	0.029
Sample 93.34	T20/469100	7	1	39.006	0.078	0.051	16.481	0.313	47.662	0.104	0.000	0.009
			2	39.444	0.031	0.015	15.039	0.284	46.085	0.124	0.000	0.041
			3	39.159	0.030	0.018	15.085	0.264	47.255	0.149	0.000	0.012
			4	40.288	0.058	0.036	12.968	0.209	46.560	0.157	0.011	0.006
			Mean	39.474	0.049	0.030	14.893	0.268	46.891	0.134	0.003	0.017
Sample 93.38	T20/469100	7	1resorbed	37.827	0.055	0.106	25.870	0.622	36.703	0.159	0.113	0.053
			1	41.053	0.123	0.042	9.753	0.256	49.300	0.152	0.013	0.039
			2	40.307	0.061	0.060	11.468	0.260	47.998	0.199	0.029	0.053
			3	39.419	0.005	0.067	13.450	0.263	46.319	0.154	0.000	0.026
			4	40.048	0.048	0.012	11.061	0.490	48.455	0.191	0.000	0.027
			5	39.967	0.013	0.016	16.007	0.343	45.334	0.109	0.089	0.011
			Mean	40.159	0.050	0.039	12.348	0.322	47.481	0.161	0.026	0.031
Sample 93.41	T20/468102	9	1	39.264	0.000	0.018	12.556	0.200	45.544	0.137	0.028	0.024
			2	39.234	0.020	0.088	16.118	0.265	43.130	0.137	0.000	0.037
			3	39.152	0.048	0.017	15.840	0.303	44.091	0.132	0.000	0.000
			4	38.377	0.075	0.132	18.183	0.262	41.520	0.100	0.007	0.025
			5	39.733	0.000	0.017	16.611	0.182	44.058	0.181	0.086	0.048
			Mean	39.152	0.029	0.054	15.862	0.242	43.669	0.137	0.024	0.027

Appendix 3.3: Olivine analyses

Sample 93.44	T20/468102	9	1resorbed	38.366	0.016	0.035	26.864	0.429	35.010	0.087	0.003	0.031
			2resorbed	38.510	0.047	0.000	26.965	0.532	35.077	0.069	0.001	0.047
			1	40.593	0.032	0.056	17.205	0.346	43.407	0.139	0.005	0.016
			2	40.028	0.039	0.011	17.300	0.295	43.016	0.098	0.056	0.041
Sample 93.54	T20/468102	10	1	38.973	0.000	0.016	13.097	0.231	46.030	0.167	0.011	0.023
			2	39.854	0.000	0.208	12.091	0.203	47.247	0.141	0.085	0.010
			3	39.154	0.011	0.014	13.924	0.199	45.506	0.144	0.058	0.009
			4	38.293	0.086	0.095	17.940	0.268	41.761	0.122	0.078	0.007
			Mean	39.069	0.024	0.083	14.263	0.225	45.136	0.144	0.058	0.012
Sample 93.60	T20/477112	14	1	39.254	0.030	0.009	12.403	0.224	47.222	0.166	0.070	0.037
			2	39.982	0.075	0.012	12.225	0.277	47.632	0.135	0.073	0.043
			3	39.828	0.128	0.062	12.621	0.197	47.547	0.196	0.139	0.045
			4	38.610	0.061	0.088	18.547	0.252	43.273	0.180	0.104	0.064
			5	38.971	0.048	0.047	16.325	0.269	43.140	0.146	0.070	0.043
Sample 93.62	T20/477112	14	1	38.619	0.064	0.015	8.500	0.136	51.163	0.156	0.067	0.052
			2	38.232	0.000	0.069	8.496	0.117	52.488	0.131	0.012	0.047
			3	36.979	0.051	0.067	13.970	0.171	46.301	0.114	0.056	0.002
			4	37.459	0.039	0.055	14.115	0.298	47.498	0.169	0.092	0.000
			5	37.612	0.025	0.010	13.846	0.260	47.395	0.147	0.055	0.018
			6	36.863	0.115	0.001	11.823	0.313	49.300	0.181	0.058	0.027
			Mean	37.228	0.058	0.033	13.439	0.261	47.624	0.153	0.065	0.012
Sample 93.63	T20/477112	14	1	36.203	0.123	0.045	22.252	0.298	39.614	0.099	0.065	0.044
			2	38.549	0.005	0.046	14.057	0.116	47.669	0.112	0.000	0.004
			3	36.820	0.002	0.000	13.757	0.263	46.787	0.124	0.000	0.002
			4	39.259	0.028	0.000	11.022	0.190	49.080	0.125	0.011	0.027
Sample 93.65	T20/477112	14	1	39.778	0.091	0.074	14.115	0.183	46.203	0.081	0.066	0.018
			2	40.818	0.112	0.069	14.191	0.149	46.535	0.113	0.013	0.000
			3	40.050	0.046	0.000	11.890	0.209	47.921	0.135	0.000	0.007
			4	39.856	0.033	0.000	11.205	0.167	48.208	0.092	0.000	0.016
			Mean	40.126	0.071	0.036	12.850	0.177	47.217	0.105	0.020	0.010
Sample 93.67	T20/477112	14	1	38.507	0.010	0.000	18.549	0.210	43.155	0.100	0.101	0.026
			2	39.563	0.057	0.040	17.745	0.192	42.841	0.124	0.077	0.035
			3	36.638	0.068	0.018	18.131	0.329	42.189	0.138	0.000	0.042
			4	37.750	0.054	0.059	17.386	0.314	42.863	0.133	0.101	0.030
			Mean	38.115	0.047	0.029	17.953	0.261	42.762	0.124	0.070	0.033
Sample 93.68	T20/477112	14	1	40.023	0.015	0.065	17.973	0.371	43.747	0.123	0.050	0.018
			2	39.422	0.052	0.168	17.853	0.252	45.803	0.421	0.030	0.000
			3	39.460	0.024	0.011	17.086	0.353	44.393	0.150	0.084	0.023
			4	37.240	0.011	0.074	19.531	0.346	43.195	0.136	0.073	0.022
			Mean	39.036	0.026	0.080	18.111	0.331	44.285	0.208	0.059	0.016
Sample 93.70	T20/477112	14	1	36.074	0.254	0.293	29.819	0.318	30.813	0.309	0.053	0.031
			2	35.435	0.120	0.014	31.139	0.536	28.757	0.283	0.004	0.046
			3	35.566	0.069	0.516	29.289	0.636	29.271	0.283	0.402	0.041
			4	35.989	0.060	0.000	27.177	0.625	34.342	0.187	0.084	0.054
			5	36.485	0.032	0.057	27.146	0.584	34.285	0.393	0.200	0.084
			6	34.994	0.122	0.204	31.220	0.466	27.644	0.317	0.168	0.024
			Mean	35.757	0.110	0.181	29.298	0.528	30.852	0.295	0.152	0.047
Sample 93.71	T20/477112		1	35.369	0.100	0.563	31.548	0.341	27.134	0.356	0.084	0.036
			2	35.460	0.136	0.430	31.048	0.511	27.458	0.378	0.095	0.030
			3	35.681	0.111	0.251	29.746	0.506	30.066	0.312	0.138	0.044
			4	35.256	0.112	0.325	31.056	0.458	29.687	0.310	0.106	0.021
			5	35.487	0.105	0.465	29.998	0.347	29.874	0.398	0.068	0.059
			6	35.540	0.121	0.402	30.157	0.503	29.325	0.398	0.098	0.041
			Mean	35.466	0.114	0.406	30.592	0.444	28.924	0.359	0.098	0.039
Sample 93.77	T20/477112	14	1	41.438	0.152	0.017	13.766	0.247	46.510	0.183	0.037	0.053
			2	41.302	0.025	0.015	13.691	0.265	46.839	0.191	0.045	0.057
			3	40.576	0.012	0.069	12.016	1.973	46.598	0.164	0.042	1.528
Sample 93.82	T20/477112	14	1	36.179	0.029	0.154	18.471	0.434	42.790	0.238	0.088	0.151

			2	34.925	0.028	0.040	19.079	0.335	42.308	0.151	0.071	0.055
			3	33.552	0.011	0.098	21.213	0.298	39.985	0.149	0.091	0.017
Sample 93.85	T20/477112	14	1	36.119	0.014	0.108	24.502	0.436	37.754	0.066	0.145	0.041
			2	35.601	0.035	0.035	24.029	0.428	38.989	0.101	0.047	0.048
			3	35.985	0.014	0.098	23.684	0.425	38.647	0.095	0.102	0.045
			4	35.998	0.016	0.112	23.268	0.462	38.654	0.035	0.078	0.044
			5	36.002	0.025	0.105	24.125	0.465	38.264	0.037	0.089	0.046
			6	35.654	0.056	0.065	24.517	0.425	37.724	0.105	0.067	0.048
			7	35.458	0.023	0.099	24.056	0.402	38.025	0.095	0.098	0.041
			8	36.015	0.012	1.070	24.265	0.414	37.951	0.102	0.068	0.039
			Mean	35.854	0.024	0.212	24.056	0.432	38.251	0.080	0.087	0.044

Appendix 3.4 Titanomagnetite analyses

All analyses are in a raw form (not normalised).

Sample	Location	Section	Analysis	SiO2	TiO2	Al2O3	FeO	MnO	MgO	CaO	Na2O	K2O	Cr2O3	NiO
Sample 93.24	T20/464098	46	1	0.064	11.691	3.046	72.650	0.285	2.823	0.095	0.239	0.052	0.776	0.138
			2	0.150	10.532	3.181	75.910	0.188	1.415	0.148	0.300	0.000	0.081	0.047
			3	0.290	12.030	3.351	71.196	0.329	3.233	0.166	0.359	0.014	0.569	0.176
			4	0.059	11.042	3.216	72.686	0.191	3.152	0.046	0.092	0.069	0.081	0.131
			5	0.076	11.383	3.161	71.688	0.277	2.961	0.058	0.051	0.003	0.293	0.199
			Mean	0.128	11.336	3.191	72.826	0.254	2.717	0.103	0.208	0.028	0.360	0.138
Sample 93.25	T20/464098	46	1	0.066	13.254	2.506	74.933	0.381	3.387	0.073	0.002	0.023	0.229	0.004
			2	0.082	11.627	2.232	79.062	0.658	2.204	0.083	0.227	0.029	0.444	0.106
			3	0.128	13.372	2.251	75.805	0.347	3.686	0.048	0.175	0.050	0.120	0.000
			4	0.097	15.027	2.373	76.633	0.309	2.452	0.043	0.089	0.036	0.215	0.065
			5	0.121	15.125	2.730	73.923	0.456	3.502	0.070	0.006	0.025	0.130	0.064
			6	0.125	10.717	3.335	77.494	0.377	3.090	0.027	0.012	0.029	0.260	0.037
			7	0.229	11.988	2.262	77.921	0.425	2.275	0.141	0.146	0.025	0.160	0.078
			8	0.159	14.266	2.368	74.968	0.433	2.778	0.021	0.088	0.014	0.167	0.056
			Mean	0.126	13.172	2.507	76.342	0.423	2.922	0.063	0.093	0.029	0.216	0.051
Sample 93.26	T20/464098	46	1	0.158	8.125	2.501	80.265	0.564	1.025	0.088	0.112	0.045	0.215	0.062
			2	0.256	8.698	2.013	80.999	0.441	1.115	0.078	0.165	0.088	0.258	0.098
			3	0.142	9.003	1.854	80.698	0.235	1.698	0.089	0.188	0.068	0.232	0.254
			4	0.111	8.995	1.764	81.254	0.336	1.995	0.056	0.165	0.035	0.247	0.158
			5	0.198	8.269	1.846	80.005	0.289	1.654	0.021	0.121	0.056	0.332	0.114
			6	0.225	8.784	1.655	80.568	0.364	1.567	0.091	0.133	0.130	0.395	0.102
			Mean	0.182	8.646	1.939	80.632	0.372	1.509	0.071	0.147	0.070	0.280	0.131
Sample 93.27	T20/464098	46	1	0.144	9.052	2.001	81.051	0.429	1.581	0.091	0.083	0.019	0.065	0.066
			2	0.388	8.458	1.451	80.574	0.407	1.803	0.067	0.138	0.041	0.722	0.000
			3	0.717	8.357	0.876	81.255	0.324	1.225	0.094	0.134	0.035	0.205	0.174
			4	0.298	8.671	1.687	81.600	0.322	1.665	0.099	0.143	0.440	0.360	0.191
			5	0.265	8.798	2.087	80.998	0.345	1.582	0.068	0.152	0.029	0.265	0.115
			6	0.154	9.045	2.258	80.254	0.399	1.396	0.024	0.199	0.023	0.030	0.098
			Mean	0.328	8.730	1.727	80.955	0.371	1.542	0.074	0.142	0.098	0.275	0.107
Sample 93.38	T20/469100	7	1	0.065	8.752	4.222	75.048	0.385	3.946	0.087	0.065	0.000	0.920	0.170
			2	0.042	8.928	4.504	74.376	0.274	4.050	0.069	0.000	0.021	1.322	0.105
			3	0.107	9.646	3.834	77.449	0.346	3.083	0.042	0.000	0.031	0.632	0.055
			4	0.086	9.545	4.277	77.194	0.429	3.191	0.046	0.209	0.033	0.521	0.189
			5	0.144	9.569	4.224	77.703	0.418	2.853	0.046	0.127	0.010	0.476	0.057
			Mean	0.089	9.288	4.212	76.354	0.370	3.425	0.058	0.080	0.019	0.774	0.115
Sample 93.39	T20/469100	7	1	0.102	15.260	1.201	73.025	0.531	2.160	0.052	0.000	0.018	0.153	0.051
			2	0.050	15.897	1.115	73.254	0.315	1.882	0.028	0.080	0.050	0.175	0.093
			3	0.020	15.555	0.706	73.598	0.225	1.890	0.060	0.057	0.000	0.068	0.000
			4	0.136	15.334	1.327	73.300	0.242	1.160	0.042	0.000	0.042	0.141	0.023
			5	0.216	15.722	1.241	74.218	0.474	1.258	0.038	0.000	0.023	0.089	0.033
			6	0.059	16.002	1.315	72.598	0.256	1.357	0.025	0.057	0.015	0.155	0.048
			Mean	0.097	15.628	1.151	73.332	0.341	1.618	0.041	0.032	0.025	0.130	0.041
Sample 93.43	T20/468102	9	1	0.096	13.935	2.652	71.589	0.510	2.720	0.106	0.188	0.000	0.178	0.034
			2	0.096	14.193	2.773	71.559	0.419	2.697	0.041	0.008	0.000	0.394	0.091
			3	0.157	14.225	2.765	71.904	0.415	2.643	0.067	0.119	0.000	0.349	0.094
			4	0.127	14.684	2.602	72.474	0.458	2.381	0.042	0.097	0.000	0.476	0.095
			Mean	0.119	14.259	2.698	71.882	0.451	2.610	0.064	0.103	0.000	0.349	0.079
Sample 93.44	T20/468102	9	1	0.165	9.688	3.733	74.084	2.783	3.382	0.055	0.008	0.770	0.085	0.165
			2	0.211	10.425	3.843	73.270	0.403	3.214	0.008	0.162	0.016	0.260	0.198
			3	0.233	10.363	3.946	73.948	0.334	3.235	0.032	0.175	0.154	0.202	0.139
			4	0.162	10.049	4.172	75.763	0.388	3.157	0.051	0.073	0.048	0.123	0.155
			5	0.261	10.005	3.855	72.278	0.258	3.338	0.084	0.149	0.037	0.041	0.147
			6	0.168	9.801	3.979	75.587	0.323	3.260	0.056	0.191	0.013	0.131	0.162
			Mean	0.200	10.055	3.921	74.155	0.748	3.264	0.048	0.126	0.173	0.140	0.161
Sample 93.45	T20/468102	9	1	0.129	7.472	6.856	76.346	0.222	4.255	0.043	0.158	0.023	0.301	0.006
			2	0.132	7.468	7.068	77.093	0.312	3.815	0.037	0.000	0.047	0.850	0.355
			3	0.194	12.341	3.271	78.028	0.324	2.868	0.065	0.254	0.009	0.122	0.098
			4	0.153	12.037	3.228	75.130	0.398	3.006	0.108	0.194	0.035	0.054	0.000

Appendix 3.4: Titanomagnetite analyses

			5	0.167	12.806	2.892	76.952	0.443	2.686	0.109	0.177	0.030	0.134	0.204
			6	0.114	12.664	3.066	77.152	0.476	2.609	0.052	0.087	0.037	0.141	0.072
			Mean	0.157	12.462	3.114	76.816	0.410	2.792	0.084	0.178	0.028	0.113	0.094
Sample 93.46	T20/468102	9	1	0.072	11.065	3.446	72.767	0.383	3.050	0.000	0.269	0.000	0.182	0.262
			2	0.075	10.459	3.384	72.334	0.338	2.966	0.000	0.000	0.007	0.074	0.116
			3	0.178	11.169	3.404	74.536	0.417	2.907	0.010	0.012	0.005	0.267	0.007
			4	0.181	11.537	3.388	72.604	0.456	2.800	0.011	0.117	0.005	0.147	0.177
			5	0.143	11.611	3.285	71.670	0.395	2.781	0.000	0.057	0.015	0.155	0.018
			6	0.218	11.046	3.523	74.197	0.361	3.244	0.004	0.000	0.042	0.161	0.123
			Mean	0.145	11.148	3.405	73.018	0.392	2.958	0.004	0.076	0.012	0.164	0.117
Sample 93.47	T20/468102	9	1	0.053	8.380	6.032	76.190	0.311	3.750	0.097	0.085	0.023	1.160	0.111
			2	0.034	8.196	6.071	77.164	0.186	4.054	0.079	0.096	0.023	1.170	0.100
			3	0.126	8.819	5.357	78.235	0.248	3.654	0.110	0.079	0.007	0.392	0.247
			4	0.363	8.763	5.616	77.391	0.389	3.893	0.090	0.342	0.000	0.856	0.055
			5	0.108	8.650	5.425	79.506	0.289	4.139	0.128	0.164	0.036	0.473	0.106
			6	0.136	8.608	4.990	78.559	0.450	3.815	0.074	0.073	0.012	0.538	0.078
			Mean	0.137	8.569	5.582	77.841	0.312	3.884	0.096	0.140	0.017	0.765	0.116
Sample 93.48	T20/468102	9	1	0.226	9.423	4.627	74.929	0.284	3.509	0.036	0.139	0.023	0.450	0.000
			2	0.054	7.177	3.467	81.476	0.785	2.751	0.077	0.218	0.053	0.118	0.007
			3	0.139	9.226	4.507	76.258	0.245	3.305	0.008	0.000	0.027	0.134	0.106
			4	0.192	9.198	4.602	76.826	0.267	3.551	0.037	0.002	0.012	0.448	0.000
			5	0.134	8.969	4.477	76.863	0.301	3.488	0.079	0.013	0.017	0.209	0.060
			Mean	0.149	8.799	4.336	77.270	0.376	3.321	0.047	0.074	0.026	0.272	0.035
Sample 93.49	T20/468102	9	1	0.062	8.734	4.358	81.060	0.387	3.553	0.046	0.165	0.000	0.255	0.103
			2	0.129	8.644	4.528	77.981	0.403	3.737	0.049	0.235	0.004	0.143	0.026
			3	0.159	8.594	4.609	79.361	0.337	3.590	0.054	0.265	0.019	0.448	0.030
			4	0.147	8.721	4.596	78.311	0.438	3.550	0.049	0.208	0.000	0.224	0.154
			5	0.121	8.651	4.295	78.439	0.277	3.252	0.058	0.164	0.040	0.289	0.035
			6	0.085	8.633	4.882	77.992	0.326	3.689	0.030	0.134	0.021	0.115	0.113
			Mean	0.117	8.663	4.545	78.857	0.361	3.562	0.048	0.195	0.014	0.246	0.077
Sample 93.50	T20/468102	9	1	0.166	10.861	3.261	77.722	0.468	2.691	0.089	0.199	0.021	0.229	0.000
			2	0.127	13.272	2.684	78.850	0.622	2.412	0.070	0.209	0.006	0.097	0.022
			3	0.042	13.014	2.782	77.845	0.583	2.161	0.024	0.003	0.058	0.217	0.180
			4	0.124	12.987	2.881	77.854	0.382	2.617	0.070	0.187	0.030	0.081	0.029
			5	0.036	10.829	3.122	80.272	0.493	2.912	0.021	0.000	0.054	0.025	0.073
			6	0.021	9.374	4.379	81.128	0.287	3.065	0.116	0.000	0.014	0.093	0.071
			Mean	0.086	11.723	3.185	78.945	0.473	2.643	0.065	0.100	0.031	0.124	0.063
Sample 93.51	T20/468102	9	1	0.108	8.397	3.879	79.537	0.323	3.334	0.044	0.143	0.027	0.396	0.215
			2	0.137	8.868	3.746	79.203	0.424	3.245	0.000	0.082	0.055	0.203	0.155
			3	0.137	9.080	3.778	77.719	0.392	3.225	0.035	0.000	0.052	0.050	0.283
			4	0.189	8.690	3.407	77.837	0.282	3.005	0.105	0.000	0.042	0.168	0.039
			5	0.182	9.008	3.967	78.818	0.389	3.223	0.025	0.008	0.024	0.184	0.225
			Mean	0.151	8.809	3.755	78.623	0.362	3.206	0.042	0.047	0.040	0.200	0.183
Sample 93.52	T20/468102	10	1	0.167	7.828	4.515	78.222	0.372	3.649	0.117	0.150	0.000	0.925	0.127
			2	0.184	7.518	3.617	74.289	0.252	2.501	0.093	0.009	0.014	0.864	0.254
			3	0.484	7.921	4.842	77.113	0.338	3.883	0.045	0.605	0.022	0.577	0.118
			4	0.475	7.763	5.256	76.502	0.375	3.827	0.026	0.504	0.009	0.796	0.245
			5	0.508	8.018	5.411	78.048	0.407	3.730	0.091	0.723	0.002	0.570	0.229
			6	0.505	7.738	5.140	77.826	0.308	3.864	0.071	0.490	0.014	0.556	0.174
			Mean	0.387	7.798	4.797	77.000	0.342	3.576	0.074	0.414	0.010	0.715	0.191
Sample 93.53	T20/468102	10	1	0.138	9.475	4.974	76.666	0.298	2.400	0.048	0.000	0.007	0.375	0.129
			2	0.153	8.516	5.051	74.663	0.303	3.393	0.051	0.002	0.007	1.050	0.091
Sample 93.54	T20/468102	10	1	0.151	9.475	3.535	71.564	0.305	3.411	0.208	0.002	0.013	0.568	0.114
			2	0.147	10.259	3.579	71.035	0.332	3.125	0.070	0.168	0.024	0.740	0.098
			3	0.072	9.810	3.549	71.505	0.344	3.150	0.020	0.000	0.022	0.717	0.094
			4	0.176	9.911	3.845	72.889	0.270	3.413	0.048	0.093	0.030	0.998	0.071
			Mean	0.137	9.864	3.627	71.748	0.313	3.275	0.087	0.066	0.022	0.756	0.094
Sample 93.55	T20/468102	10	1	0.126	12.801	2.956	75.422	0.282	2.425	0.035	0.077	0.005	0.263	0.122
			2	0.281	12.248	3.042	75.073	0.368	2.725	0.032	0.268	0.000	0.540	0.169
			3	0.189	10.243	3.336	76.203	0.222	3.016	0.025	0.251	0.000	0.477	0.104
			Mean	0.199	11.764	3.111	75.566	0.291	2.722	0.031	0.199	0.002	0.427	0.132
Sample 93.57	T20/468102	10	1	0.134	10.197	3.348	74.069	0.294	2.857	0.045	0.000	0.030	0.459	0.116
			2	0.167	10.279	3.498	74.154	0.322	3.181	0.036	0.113	0.019	0.373	0.000

Appendix 3.4: Titanomagnetite analyses

			3	0.080	10.590	3.423	73.334	0.359	3.192	0.002	0.181	0.075	0.337	0.029
			4	0.129	10.068	3.608	74.440	0.425	3.216	0.026	0.000	0.023	0.368	0.000
			5	0.107	10.472	3.268	73.414	0.411	3.057	0.038	0.013	0.065	0.201	0.020
			6	0.158	10.095	3.417	74.138	0.348	2.965	0.027	0.081	0.027	0.497	0.000
			Mean	0.129	10.284	3.427	73.925	0.360	3.078	0.029	0.065	0.040	0.373	0.028
Sample 93.58	T20/468102	10	1	0.069	12.096	3.033	74.382	0.344	2.382	0.054	0.336	0.060	0.162	0.119
			2	0.060	12.133	3.123	73.764	0.344	2.422	0.045	0.162	0.016	0.092	0.155
			3	0.039	11.993	3.064	72.638	0.338	2.421	0.050	0.000	0.040	0.128	0.018
			4	0.064	11.659	2.530	72.793	0.357	2.180	0.073	0.000	0.062	0.091	0.064
			5	0.141	12.279	2.801	74.147	0.348	1.849	0.056	0.092	0.035	0.218	0.004
			6	0.401	12.300	2.993	73.298	0.379	2.588	0.075	0.001	0.045	0.000	0.031
			Mean	0.129	12.077	2.924	73.504	0.352	2.307	0.059	0.099	0.043	0.115	0.065
Sample 93.61	T20/477112	14	1	0.137	9.401	4.246	71.746	0.351	3.129	0.186	0.142	0.061	0.295	0.134
			2	0.151	9.277	3.965	73.577	0.417	2.178	0.191	0.141	0.035	0.339	0.075
			3	0.127	8.589	3.783	74.333	0.669	3.073	0.063	0.000	0.028	0.235	0.088
			4	0.221	8.551	3.630	74.541	0.664	3.127	0.059	0.201	0.067	0.300	0.119
			5	0.177	9.104	4.504	73.108	0.346	3.175	0.026	0.000	0.065	0.672	0.093
			6	0.112	8.514	5.068	73.333	0.425	3.094	0.029	0.128	0.055	0.412	0.000
			Mean	0.154	8.906	4.199	73.440	0.479	2.963	0.092	0.102	0.052	0.376	0.085
Sample 93.62	T20/477112	14	1	0.195	8.637	4.734	71.337	0.284	3.716	0.251	0.075	0.017	2.231	0.165
			2	0.122	8.682	4.793	72.131	0.323	3.422	0.271	0.004	0.000	1.788	0.169
			3	0.056	9.286	4.422	75.708	0.422	3.365	0.090	0.173	0.041	0.488	0.188
			4	0.055	9.084	4.398	75.206	0.260	3.642	0.074	0.222	0.020	0.440	0.108
			5	0.100	9.060	4.386	76.958	0.472	3.095	0.108	0.126	0.077	0.389	0.154
			6	0.040	8.973	4.250	76.123	0.243	3.578	0.110	0.105	0.093	0.394	0.146
			Mean	0.095	8.954	4.497	74.577	0.334	3.470	0.151	0.118	0.041	0.955	0.155
Sample 93.63	T20/477112	14	1	0.194	13.461	2.468	73.919	0.428	2.540	0.047	0.013	0.011	0.249	0.098
			2	0.162	13.895	2.673	73.194	0.362	2.644	0.024	0.112	0.000	0.234	0.084
			3	0.177	13.097	2.464	71.750	0.378	2.914	0.144	0.090	0.046	0.419	0.245
			Mean	0.178	13.484	2.535	72.954	0.389	2.699	0.072	0.072	0.019	0.301	0.142
Sample 93.65	T20/477112	14	1	0.191	12.698	3.074	72.225	0.414	3.525	0.073	0.003	0.006	0.335	0.168
			2	0.169	12.071	3.148	71.726	0.397	3.342	0.040	0.010	0.026	0.221	0.119
			3	0.299	12.677	3.242	71.745	0.337	3.596	0.108	0.083	0.025	0.358	0.113
			Mean	0.220	12.482	3.155	71.899	0.383	3.488	0.074	0.032	0.019	0.305	0.133
Sample 93.66	T20/477112	14	1	0.252	11.207	2.977	73.905	0.427	2.857	0.080	0.171	0.007	0.330	0.089
			2	0.136	11.361	3.185	73.615	0.583	3.024	0.003	0.334	0.020	0.382	0.046
			3	0.270	10.946	3.268	71.518	0.326	2.896	0.009	0.193	0.035	0.523	0.011
			4	0.187	11.190	3.266	72.344	0.333	3.068	0.000	0.248	0.007	0.310	0.000
			5	0.083	10.892	3.229	71.603	0.396	2.961	0.066	0.168	0.015	0.605	0.050
			Mean	0.186	11.119	3.185	72.597	0.413	2.961	0.032	0.223	0.017	0.430	0.039
Sample 93.67	T20/477112	14	1	0.093	12.469	2.997	73.785	0.292	2.522	0.092	0.013	0.018	0.166	0.140
			2	0.099	12.198	3.040	74.392	0.271	2.269	0.057	0.192	0.016	0.125	0.130
			3	0.134	11.603	3.065	74.805	0.343	2.486	0.075	0.060	0.008	0.000	0.245
			4	0.097	9.284	4.334	72.928	0.221	3.543	0.096	0.005	0.021	0.125	0.149
			5	0.152	13.798	3.153	73.027	0.334	2.296	0.044	0.067	0.048	0.343	0.113
			Mean	0.115	11.870	3.318	73.787	0.292	2.623	0.073	0.067	0.022	0.152	0.155
Sample 93.68	T20/477112	14	1	0.108	9.353	3.877	75.147	0.266	3.505	0.054	0.115	0.040	0.300	0.101
			2	0.059	10.193	4.364	76.134	0.344	3.328	0.072	0.009	0.006	0.145	0.106
			3	0.128	10.222	4.100	76.229	0.366	3.313	0.075	0.170	0.040	0.222	0.149
			4	0.185	10.294	4.419	75.427	0.380	2.899	0.088	0.159	0.017	0.227	0.065
			5	0.076	10.097	4.194	76.650	0.287	2.986	0.049	0.005	0.001	0.384	0.124
			Mean	0.111	10.032	4.191	75.917	0.329	3.206	0.068	0.092	0.021	0.256	0.109
Sample 93.69	T20/477112	14	1	0.123	9.878	3.940	73.899	0.467	3.492	0.053	0.000	0.037	0.285	0.080
			2	0.101	9.796	3.863	71.916	0.358	3.470	0.017	0.095	0.033	0.492	0.167
			3	0.086	9.792	3.888	73.193	0.415	3.522	0.060	0.053	0.038	0.221	0.178
			4	0.244	10.136	4.187	73.747	0.527	3.697	0.025	0.285	0.037	0.385	0.120
			5	0.046	10.117	3.666	72.404	0.286	3.262	0.023	0.004	0.034	0.188	0.040
			Mean	0.120	9.944	3.909	73.032	0.411	3.489	0.036	0.087	0.036	0.314	0.117
Sample 93.70	T20/477112	14	1	0.075	7.775	5.170	76.721	0.350	3.762	0.020	0.000	0.018	1.240	0.149
			2	0.038	6.628	5.792	76.720	0.390	3.632	0.000	0.011	0.021	1.735	0.146
			3	0.057	9.048	4.610	76.465	0.372	3.704	0.016	0.064	0.037	0.679	0.171
			4	0.088	8.662	4.638	74.720	0.362	3.648	0.054	0.049	0.022	1.008	0.144
			5	0.137	8.275	5.554	75.105	0.228	4.106	0.094	0.076	0.000	1.208	0.118
			Mean	0.079	8.078	5.153	75.946	0.340	3.770	0.037	0.040	0.020	1.174	0.146

Appendix 3.4: Titanomagnetite analyses

Sample 93.71	T20/477112	14	1	0.192	8.659	5.540	74.731	0.376	3.133	0.032	0.050	0.001	0.655	0.147
			2	0.248	9.062	4.349	75.617	0.414	3.127	0.075	0.100	0.006	0.395	0.109
			3	0.100	8.862	5.916	76.227	0.376	3.398	0.045	0.118	0.023	0.749	0.000
			4	0.170	9.042	4.993	76.009	0.420	3.757	0.068	0.000	0.000	0.508	0.066
			5	0.118	8.714	4.767	76.283	0.362	3.486	0.043	0.000	0.008	0.692	0.055
			Mean	0.166	8.868	5.113	75.773	0.390	3.380	0.053	0.054	0.008	0.600	0.075
Sample 93.72	T20/477112	14	1	0.146	8.429	4.713	73.152	0.263	3.511	0.092	0.060	0.072	0.201	0.166
			2	0.069	9.264	4.618	73.909	0.345	3.294	0.110	0.264	0.014	0.115	0.065
			3	0.199	8.757	4.477	74.937	0.271	3.051	0.042	0.000	0.020	0.148	0.035
			4	0.227	8.934	4.493	76.585	0.332	3.064	0.054	0.182	0.002	0.123	0.015
			5	0.076	9.326	4.301	77.194	0.283	2.876	0.058	0.000	0.000	0.000	0.096
			6	0.141	9.245	4.657	77.033	0.313	3.113	0.073	0.112	0.000	0.153	0.050
			7	0.066	9.099	4.233	77.102	0.491	3.334	0.060	0.067	0.000	0.083	0.000
			Mean	0.132	9.008	4.499	75.702	0.328	3.178	0.070	0.098	0.015	0.118	0.061
Sample 93.73	T20/477112	14	1	0.082	10.606	3.015	78.327	0.516	2.356	0.055	0.116	0.030	0.082	0.032
			2	0.116	10.290	3.138	78.353	0.497	2.387	0.054	0.129	0.000	0.176	0.026
			3	0.078	9.976	3.198	79.005	0.927	2.702	0.007	0.047	0.044	0.356	0.129
			4	0.091	9.327	3.217	78.979	0.449	2.771	0.044	0.107	0.012	0.194	0.039
			5	0.001	8.586	3.787	78.540	0.392	3.196	0.045	0.007	0.019	0.138	0.113
			6	0.068	10.497	2.835	78.635	0.765	2.559	0.059	0.170	0.000	0.229	0.142
			7	0.074	10.315	2.881	79.208	0.498	2.448	0.020	0.211	0.024	0.118	0.073
			Mean	0.073	9.942	3.153	78.721	0.578	2.631	0.041	0.112	0.018	0.185	0.079
Sample 93.74	T20/477112	14	1	0.112	7.572	4.908	74.600	0.272	3.664	0.036	0.005	0.000	0.905	0.231
			2	0.105	7.796	5.016	74.661	0.346	3.406	0.064	0.000	0.020	0.787	0.085
			3	0.128	7.852	5.073	74.946	0.291	3.776	0.042	0.096	0.029	0.913	0.008
			4	0.149	7.777	5.275	75.274	0.361	3.661	0.041	0.000	0.018	0.477	0.121
			5	0.141	7.933	4.798	74.792	0.342	3.775	0.057	0.326	0.010	0.850	0.079
			6	0.113	7.751	4.648	73.467	0.419	3.741	0.044	0.217	0.042	0.696	0.079
			Mean	0.125	7.780	4.953	74.623	0.339	3.671	0.047	0.107	0.020	0.771	0.101
Sample 93.76	T20/477112	14	1	0.146	8.393	4.967	73.745	0.245	3.470	0.208	0.050	0.022	1.754	0.153
			2	0.013	6.965	6.886	70.919	0.337	4.234	0.110	0.003	0.000	2.954	0.038
			3	0.145	10.130	4.423	73.979	0.344	3.244	0.039	0.140	0.000	0.554	0.138
			4	0.083	9.007	5.602	73.345	0.255	3.366	0.040	0.012	0.000	0.387	0.102
			5	0.102	9.054	6.095	73.659	0.416	3.606	0.091	0.121	0.000	0.278	0.133
			6	0.191	8.215	6.048	72.452	0.318	4.086	0.050	0.007	0.000	0.644	0.075
			Mean	0.113	8.627	5.670	73.017	0.319	3.668	0.090	0.056	0.004	1.095	0.107
Sample 93.77	T20/477112	14	1	0.136	9.187	3.068	75.764	0.390	2.413	0.061	0.056	0.025	0.321	0.121
			2	0.186	9.571	3.434	73.568	0.358	2.476	0.096	0.073	0.013	0.426	0.077
			3	0.261	9.196	3.833	75.294	0.292	3.094	0.070	0.105	0.034	0.033	0.127
			4	0.168	9.752	3.518	74.560	0.265	2.661	0.065	0.327	0.017	0.472	0.121
			5	0.217	9.468	4.692	73.719	0.418	3.045	0.055	0.365	0.027	1.045	0.000
			6	0.140	9.616	4.511	74.002	0.325	2.759	0.051	0.134	0.037	0.349	0.098
			Mean	0.185	9.465	3.843	74.485	0.341	2.741	0.066	0.177	0.026	0.441	0.091
Sample 93.78	T20/477112	14	1	0.152	11.492	3.148	71.313	0.290	2.697	0.060	0.113	0.023	0.382	0.100
			2	0.136	12.317	3.107	72.652	0.364	2.558	0.042	0.113	0.000	0.063	0.004
			3	0.099	12.045	2.864	72.389	0.457	2.632	0.057	0.000	0.033	0.303	0.059
			4	0.102	12.590	2.928	71.496	0.465	2.508	0.029	0.000	0.032	0.063	0.055
			5	0.158	12.427	2.867	75.373	0.341	1.849	0.066	0.000	0.016	0.334	0.009
			6	0.074	12.169	2.678	71.797	0.351	2.028	0.012	0.063	0.000	0.011	0.167
			Mean	0.120	12.173	2.932	72.503	0.378	2.379	0.044	0.048	0.017	0.193	0.066
Sample 93.79	T20/477112	14	1	0.020	10.905	3.931	72.338	0.360	2.622	0.000	0.000	0.011	0.182	0.141
			2	0.004	9.655	3.530	72.257	0.316	2.857	0.000	0.068	0.017	0.201	0.203
			3	0.124	9.448	3.525	74.830	0.426	2.830	0.019	0.121	0.026	0.338	0.003
			4	0.111	9.745	3.404	73.883	0.275	3.143	0.049	0.214	0.019	0.128	0.000
			5	0.061	9.484	4.105	75.692	0.248	3.308	0.024	0.193	0.016	0.163	0.000
			6	0.003	9.220	3.866	75.772	0.541	3.313	0.046	0.122	0.013	0.371	0.057
			7	0.019	9.300	4.098	74.945	0.413	3.150	0.040	0.312	0.040	0.326	0.000
			Mean	0.049	9.680	3.780	74.245	0.368	3.032	0.025	0.147	0.020	0.244	0.058
Sample 93.80	T20/477112	14	1	0.127	8.383	3.774	71.401	0.290	3.112	0.054	0.203	0.018	0.673	0.083
			2	0.223	8.161	3.976	72.201	0.322	3.243	0.080	0.210	0.016	0.805	0.097
			3	0.148	8.818	4.677	73.308	0.287	3.428	0.050	0.078	0.029	0.678	0.085
			4	0.131	8.843	4.676	72.237	0.312	3.397	0.046	0.096	0.033	0.678	0.167
			5	0.140	8.539	4.756	72.036	0.281	3.349	0.047	0.000	0.018	0.734	0.045
			Mean	0.154	8.549	4.372	72.237	0.298	3.306	0.055	0.117	0.023	0.714	0.095

Appendix 3.4: Titanomagnetite analyses

Sample 93.81	T20/477112	14	1	0.088	8.889	4.824	73.095	0.305	3.245	0.141	0.130	0.024	0.677	0.114
			2	0.206	8.894	3.850	72.533	0.568	3.190	0.209	0.000	0.034	0.641	0.234
			3	0.351	8.965	4.730	72.499	0.265	3.056	0.103	0.330	0.048	0.814	0.169
			4	0.186	8.754	4.868	72.985	0.431	3.326	0.126	0.228	0.011	0.420	0.134
			5	0.289	8.917	5.036	75.734	0.259	3.400	0.075	0.202	0.008	0.734	0.140
			6	0.149	8.678	4.603	74.009	0.340	3.599	0.045	0.189	0.000	0.831	0.095
			Mean	0.212	8.850	4.652	73.476	0.361	3.303	0.117	0.180	0.021	0.686	0.148
Sample 93.85	T20/477112	14	1	1.118	9.482	5.579	77.683	0.442	3.234	0.026	0.000	0.053	0.613	0.100
			2	0.153	8.262	5.687	75.843	0.368	3.313	0.065	0.049	0.005	0.459	0.155
			3	0.091	7.844	5.597	77.374	0.362	3.270	0.065	0.121	0.015	0.123	0.076
			4	0.108	8.121	5.347	74.795	0.239	3.242	0.055	0.124	0.013	0.558	0.193
			5	0.130	8.253	5.457	76.605	0.232	3.189	0.074	0.000	0.000	0.300	0.122
			6	0.050	8.072	5.369	76.567	0.450	3.113	0.030	0.000	0.015	0.321	0.170
			7	0.149	7.689	5.206	75.524	0.185	2.747	0.032	0.000	0.044	0.493	0.162
			Mean	0.257	8.246	5.463	76.342	0.325	3.158	0.050	0.042	0.021	0.410	0.140
Sample 93.86	T20/477112	14	1	0.291	7.812	5.366	75.436	0.380	3.383	0.044	0.083	0.020	0.320	0.031
			2	0.063	7.836	5.417	75.190	0.350	3.273	0.051	0.000	0.024	0.227	0.004
			3	0.104	8.156	5.358	76.492	0.250	3.480	0.047	0.009	0.013	0.306	0.000
			4	0.070	7.576	5.705	76.447	0.296	3.087	0.039	0.000	0.035	0.236	0.046
			5	0.121	7.835	5.249	75.392	0.361	3.283	0.066	0.000	0.039	0.196	0.042
			6	0.224	8.144	5.159	75.055	0.379	3.338	0.057	0.000	0.027	0.129	0.000
			Mean	0.146	7.893	5.376	75.669	0.336	3.307	0.051	0.015	0.026	0.236	0.021
Sample 93.87	T20/477112	14	1	0.166	8.675	3.260	77.240	0.207	2.251	0.083	0.000	0.065	0.189	0.128
			2	0.148	8.551	3.322	75.435	0.217	2.258	0.058	0.005	0.020	0.196	0.106
			3	0.185	8.566	3.431	76.824	0.395	2.290	0.086	0.001	0.028	0.549	0.187
			4	0.145	8.065	3.508	77.470	0.454	2.785	0.124	0.103	0.018	0.293	0.090
			5	0.126	8.434	3.374	75.478	0.346	2.952	0.051	0.155	0.024	0.197	0.077
			6	0.102	8.357	3.367	75.870	0.261	2.629	0.100	0.000	0.041	0.068	0.088
			Mean	0.145	8.441	3.377	76.386	0.313	2.528	0.084	0.044	0.033	0.249	0.113
Sample 93.88	T20/477112	14	1	0.085	6.554	2.674	77.581	0.209	1.753	0.097	0.136	0.017	0.975	0.290
			2	0.147	7.438	2.997	78.837	0.366	1.912	0.070	0.000	0.041	0.337	0.110
Sample 93.89	T20/477112	14	1	0.020	21.450	0.706	68.764	0.225	1.890	0.060	0.057	0.000	0.068	0.000
			2	0.013	21.634	0.793	67.725	0.263	1.905	0.101	0.221	0.013	0.185	0.000
			3	0.045	21.590	0.714	68.530	0.137	1.971	0.123	0.213	0.010	0.137	0.046
			4	0.026	21.888	0.758	69.025	0.133	1.912	0.147	0.068	0.025	0.158	0.048
			5	0.023	21.368	0.702	67.897	0.258	1.889	0.125	0.221	0.054	0.111	0.009
			6	0.068	21.547	0.788	67.998	0.225	1.928	0.098	0.167	0.014	0.215	0.012
			Mean	0.033	21.580	0.744	68.323	0.207	1.916	0.109	0.158	0.019	0.146	0.019
Sample 93.91	T20/477112	14	1	0.198	11.078	3.479	75.877	0.383	2.953	0.037	0.121	0.010	0.000	0.097
			2	0.067	11.006	3.509	75.397	0.352	2.864	0.044	0.270	0.012	0.286	0.129
Sample 94.2	T20/455088	-	1	0.117	12.148	2.849	75.248	0.290	2.849	0.066	0.222	0.036	0.289	0.108
			2	0.116	11.443	3.162	74.930	0.449	2.977	0.097	0.281	0.032	0.221	0.009
			3	0.387	11.050	3.804	73.801	0.341	2.949	0.069	0.288	0.026	0.063	0.092
			4	0.233	11.356	3.484	74.641	0.409	3.327	0.107	0.460	0.064	0.389	0.129
			5	0.240	11.057	3.629	74.812	0.325	3.260	0.101	0.158	0.073	0.279	0.261
			6	0.177	12.090	3.136	75.044	0.414	2.961	0.062	0.240	0.044	0.367	0.053
			Mean	0.212	11.524	3.344	74.746	0.371	3.054	0.084	0.275	0.046	0.268	0.109
Sample 94.4	T20/469102	9	1	0.112	12.691	2.838	72.873	0.401	2.826	0.071	0.003	0.006	0.695	0.159
			2	0.134	12.725	2.749	72.201	0.325	2.874	0.085	0.000	0.038	0.778	0.157
			3	0.164	12.881	2.857	72.826	0.451	2.854	0.061	0.012	0.024	0.967	0.113
			4	0.139	12.488	2.772	73.833	0.358	2.553	0.062	0.290	0.014	2.159	0.156
			5	0.111	12.685	2.690	72.670	0.363	2.993	0.049	0.000	0.013	0.888	0.165
			Mean	0.132	12.694	2.781	72.881	0.380	2.820	0.066	0.061	0.019	1.097	0.150
Sample 94.13	T20/496157	51	1	0.341	9.784	2.863	71.946	0.368	2.427	0.177	0.119	0.040	0.359	0.082
			2	0.197	9.528	3.609	75.460	0.417	3.079	0.056	0.348	0.055	0.496	0.170
			3	0.300	9.536	3.534	75.653	0.313	2.974	0.086	0.412	0.006	0.408	0.109
			4	0.370	7.653	4.963	74.810	0.545	3.597	0.032	0.504	0.081	0.260	0.150
			5	0.240	7.828	5.063	75.869	0.360	3.467	0.045	0.371	0.012	0.396	0.187
			6	0.398	7.838	4.721	75.828	0.347	3.449	0.113	0.249	0.000	0.474	0.147
			Mean	0.308	8.695	4.126	74.928	0.392	3.166	0.085	0.334	0.032	0.399	0.141
Sample 94.15	T20/463097	-	1	0.131	6.964	4.255	79.809	0.415	3.231	0.030	0.001	0.002	0.139	0.382
			2	0.075	7.215	4.512	80.209	0.401	3.068	0.058	0.000	0.000	0.123	0.318
			3	0.244	7.469	4.211	78.315	0.366	2.824	0.027	0.075	0.002	0.000	0.262
			4	0.171	7.169	4.420	80.409	0.273	3.065	0.027	0.102	0.007	0.014	0.374

Appendix 3.4: Titanomagnetite analyses

		5	0.129	7.052	4.271	77.857	0.553	2.862	0.022	0.006	0.014	0.142	0.119
		6	0.114	6.926	4.440	78.167	0.329	2.857	0.048	0.000	0.023	0.050	0.166
		Mean	0.144	7.133	4.352	79.128	0.390	2.985	0.035	0.031	0.008	0.078	0.270
Sample 94.16	T20/463097	-	1	0.071	8.547	3.438	80.490	0.329	2.604	0.059	0.000	0.048	0.066	0.006
			2	0.061	9.143	2.878	79.208	0.376	2.456	0.017	0.490	0.010	0.210	0.090
			3	0.154	9.500	2.728	78.471	0.381	2.218	0.026	0.008	0.022	0.058	0.110
			4	0.178	8.384	3.399	78.382	0.319	2.791	0.067	0.138	0.009	0.092	0.045
			5	0.070	8.276	3.434	77.815	0.299	2.752	0.099	0.059	0.023	0.019	0.042
			6	0.230	9.220	3.449	76.361	0.269	2.881	0.058	0.408	0.038	0.000	0.000
			Mean	0.127	8.845	3.221	78.455	0.329	2.617	0.054	0.184	0.025	0.074	0.049
Sample 94.17	T20/463097	-	1	0.178	8.486	3.285	77.041	0.412	3.068	0.189	0.047	0.000	0.236	0.122
			2	0.124	8.730	3.262	76.470	0.436	3.034	0.158	0.075	0.000	0.100	0.039
			3	0.174	9.142	2.913	76.429	0.325	3.027	0.076	0.221	0.029	0.163	0.153
			4	0.172	8.585	3.169	79.089	0.368	3.033	0.121	0.000	0.011	0.106	0.085
			5	0.406	9.375	3.170	78.498	0.398	3.075	0.139	0.076	0.009	0.125	0.057
			Mean	0.211	8.864	3.160	77.505	0.388	3.047	0.137	0.084	0.010	0.146	0.091
Sample 94.18	T20/498184	53	1	0.130	8.886	2.836	78.639	0.446	2.182	0.078	0.051	0.007	0.261	0.184
			2	0.147	9.101	2.853	78.138	0.421	2.300	0.082	0.084	0.021	0.409	0.184
			3	0.257	9.364	2.685	77.943	0.454	2.390	0.107	0.165	0.017	0.346	0.213
			4	0.164	8.967	2.437	82.107	0.399	2.251	0.100	0.150	0.071	0.341	0.235
			Mean	0.175	9.080	2.703	79.207	0.430	2.281	0.092	0.113	0.029	0.339	0.204
Sample 94.22	T19/481211	55	1	0.639	6.614	2.936	78.826	0.410	2.473	0.110	0.876	0.049	0.956	0.233
			2	0.361	6.551	2.670	80.201	0.456	1.944	0.067	0.426	0.032	0.898	0.241
			3	0.358	4.709	3.359	79.385	0.458	1.488	0.080	0.493	0.045	0.718	0.219
			Mean	0.453	5.958	2.988	79.471	0.441	1.968	0.086	0.598	0.042	0.857	0.231
Sample 94.31	T19/495220	59	1	0.155	5.886	3.544	79.209	0.561	2.190	0.054	0.252	0.096	0.183	0.138
			2	0.205	6.231	3.885	79.874	0.480	2.594	0.046	0.393	0.018	0.332	0.214
			3	1.399	6.227	3.444	76.714	0.464	2.793	0.108	0.196	0.011	0.327	0.230
			4	0.109	6.561	3.376	78.639	0.887	2.069	0.050	0.013	0.302	0.386	0.362
			5	0.568	6.422	3.408	79.459	0.402	1.885	0.268	0.485	0.021	0.220	0.135
			6	0.175	6.538	3.680	79.380	0.340	2.280	0.059	0.448	0.015	0.177	0.195
			Mean	0.435	6.311	3.556	78.879	0.522	2.302	0.098	0.298	0.077	0.271	0.212
Sample 94.45	T19/496238	66	1	0.063	7.093	2.357	82.463	0.673	1.789	0.137	0.162	0.022	0.000	0.115
			2	0.265	7.940	1.246	79.189	0.664	0.736	0.400	0.337	0.045	0.111	0.047
			3	0.362	6.830	2.053	80.866	0.574	1.478	0.137	0.447	0.060	0.036	0.137
			4	0.717	6.262	2.360	84.179	0.709	2.039	0.145	0.740	0.034	0.116	0.123
			Mean	0.352	7.031	2.004	81.674	0.655	1.511	0.205	0.422	0.040	0.066	0.106
Sample 94.79	T19/364544	73	1	0.122	13.233	1.971	75.269	0.233	1.118	0.089	0.000	0.026	0.376	0.119
			2	0.092	12.381	2.977	77.863	0.438	2.588	0.056	0.119	0.024	0.187	0.123
			3	0.425	13.032	2.282	77.867	1.022	1.452	0.098	0.486	0.081	0.395	0.169
			4	0.475	12.603	2.335	77.414	1.031	1.459	0.166	0.574	0.059	0.291	0.218
			Mean	0.279	12.812	2.391	77.103	0.681	1.654	0.102	0.295	0.048	0.312	0.157

3.5 Analyses of other phases

All analyses are in a raw form (not normalised).

3.5.1 Chromite

Sample	Location	Section	Analysis	SiO2	TiO2	Al2O3	FeO	MnO	MgO	CaO	Na2O	K2O	Cr2O3	NiO
Sample 93.28	T20/465099	47	1	0.171	3.434	13.774	49.795	0.179	7.638	0.030	0.064	0.057	19.472	0.313
Sample 93.31	T20/466096	5	1	0.669	1.415	10.371	46.440	0.295	7.401	0.096	0.314	0.046	27.857	0.247
			2	0.000	1.155	9.262	42.565	0.339	6.343	0.083	0.013	0.020	31.112	0.134
			3	0.181	3.750	10.425	50.921	0.328	6.230	0.057	0.006	0.006	18.743	0.282
			Mean	0.283	2.107	10.019	46.642	0.321	6.658	0.079	0.111	0.024	25.904	0.221
Sample 93.56	T20/468102	10	1	0.085	5.317	7.478	67.042	0.486	3.951	0.082	0.188	0.026	7.972	0.076
			2	0.162	5.579	7.548	67.921	0.267	4.267	0.109	0.186	0.022	7.756	0.040
Sample 93.63	T20/477112	14	1	0.481	4.758	7.568	62.560	0.353	4.864	0.073	0.316	0.063	12.154	0.283

3.5.2 Clinopyroxene

				SiO2	TiO2	Al2O3	FeO	MnO	MgO	CaO	Na2O	K2O
Sample 93.26	T20/464098	46		51.789	0.156	1.273	4.737	0.042	18.744	20.089	0.225	0.046
Sample 93.31	T20/466096	5		50.273	0.399	2.459	8.477	0.395	15.281	20.629	0.390	0.026
Sample 93.38	T20/469100	7	1	49.034	0.544	3.454	9.680	0.550	14.289	20.098	0.388	0.235
			2	49.818	0.577	2.331	9.350	0.552	15.603	19.059	0.361	0.011
Sample 93.39	"	"		46.641	0.574	2.511	11.376	0.466	13.052	18.119	0.381	0.026
Sample 93.54	T20/468102	10		53.070	0.133	1.558	3.871	0.084	19.295	19.650	0.316	0.043
Sample 93.65	T20/477112	14	1	49.828	0.684	3.655	9.689	0.186	14.372	19.633	0.405	0.015
			2	50.154	0.513	2.070	10.085	0.318	14.796	19.494	0.401	0.032
Sample 93.72	"	"		52.596	0.666	3.226	10.453	0.312	15.944	18.811	0.268	0.024
Sample 93.75	"	"		51.637	0.560	3.793	9.191	0.277	15.501	20.101	0.453	0.038
Sample 93.76	"	"		54.189	0.354	2.357	9.436	0.200	16.015	19.500	0.007	0.000
Sample 93.85	"	"		47.689	0.495	2.029	9.653	0.298	15.002	19.828	0.298	0.040
Sample 93.89	"	"		51.322	0.538	2.316	10.588	0.255	16.235	17.580	0.358	0.024
Sample 93.90	"	"	1	45.908	0.553	0.280	12.020	0.378	13.587	17.229	0.000	0.065
			2	47.857	0.487	2.071	10.000	0.000	14.400	17.842	0.397	0.077
Sample 93.91	"	"		50.916	0.419	1.943	9.168	0.314	14.616	20.208	0.471	0.036
Sample 94.31	T19/495220	59		50.541	0.374	2.076	8.763	0.436	13.570	20.474	0.481	0.052
Sample 94.43	T19/496238	66		50.433	0.498	1.891	10.152	0.549	15.377	19.670	0.267	0.022
Sample 94.45	"	"	1	51.436	0.232	1.285	9.643	0.748	15.161	20.327	0.377	0.028
			2	48.899	0.375	2.013	8.755	0.656	14.120	20.432	0.355	0.027

3.5.3 Orthopyroxene

				SiO2	TiO2	Al2O3	FeO	MnO	MgO	CaO	Na2O	K2O
Sample 93.39	T20/469100	7		51.508	0.183	1.603	21.383	0.697	22.808	1.298	0.012	0.021
Sample 93.48	T20/468102	9		51.683	0.271	1.597	17.540	0.595	25.843	1.614	0.093	0.042
Sample 93.50	"	"		51.226	0.278	0.872	21.038	0.403	24.520	1.833	0.000	0.000
Sample 93.51	"	"		52.370	0.379	1.130	18.807	0.592	25.651	1.365	0.002	0.023
Sample 93.52	T20/468102	10	1	52.755	0.245	1.140	19.186	0.485	24.091	1.692	0.044	0.010
			2	52.534	0.309	1.453	16.690	0.469	26.030	1.576	0.007	0.016
Sample 93.54	"	"		51.392	0.573	4.821	12.719	0.263	28.184	1.284	0.037	0.008
Sample 93.63	T20/477112	14		49.565	0.246	2.126	14.528	0.278	25.495	1.133	0.047	0.087
Sample 93.69	"	"		45.959	1.742	1.786	24.686	0.457	23.476	1.477	0.000	0.027
Sample 93.70	"	"		51.294	0.262	2.018	17.403	0.741	25.189	1.463	0.278	0.038
Sample 93.71	"	"	1	52.624	0.257	1.380	19.069	0.534	24.717	1.780	0.185	0.059
			2	51.905	0.334	2.589	18.476	0.549	25.249	1.629	0.092	0.025
			3	51.331	0.170	2.109	18.249	0.448	23.562	1.538	0.048	0.000
Sample 93.73	"	"	1	54.189	0.313	1.406	20.280	0.508	23.715	1.532	0.107	0.068
			2	51.644	0.297	1.719	19.747	0.575	24.244	1.676	0.055	0.010
Sample 93.75	"	"	1	50.767	0.394	1.268	25.532	0.721	19.921	1.495	0.042	0.019
			2	53.634	0.188	1.930	18.272	0.551	25.270	1.776	0.168	0.042
			3	53.060	0.211	1.539	18.754	0.442	24.826	1.795	0.039	0.027
			4	51.524	0.261	1.416	21.644	0.516	22.625	1.652	0.376	0.040
			5	52.730	0.252	1.043	17.468	0.377	23.050	1.750	0.137	0.051
			6	50.634	0.310	2.170	19.011	0.359	23.186	1.989	0.085	0.064
Sample 93.82	"	"		48.649	0.132	1.037	13.96	0.421	27.94	0.731	0.092	0.035
Sample 93.89	"	"		52.333	0.302	1.868	19.39	0.522	23.72	1.622	0.099	0.069
Sample 94.15	T20/463097	-		53.447	0.306	1.410	22.357	0.795	22.656	1.440	0.139	0.017

Sample 94.43	T19/496238	66	1	52.398	0.269	1.212	19.297	0.587	24.961	1.596	0.069	0.039
			2	52.792	0.241	1.353	23.254	0.873	20.247	1.553	0.077	0.000
			3	53.534	0.169	0.772	18.897	0.708	25.121	1.439	0.033	0.020
			4	54.651	0.171	0.738	14.354	0.589	27.954	1.471	0.069	0.009
			5	51.762	0.314	1.014	19.404	0.662	24.651	1.567	0.000	0.021
Sample 94.45	"	"	1	52.439	0.161	0.673	20.360	1.180	24.009	1.038	0.000	0.032
			2	53.364	0.227	0.684	18.928	0.979	25.272	0.988	0.080	0.019
Sample 94.46	"	"	1	52.056	0.237	0.992	23.166	0.628	21.032	2.829	0.080	0.000
			2	53.135	0.191	2.994	12.737	0.224	28.448	1.892	0.054	0.054
			3	48.358	0.172	0.928	25.58	0.866	20.5	0.961	0.165	0.082
			4	52.023	0.156	1.164	20.511	0.765	23.754	1.354	0.093	0.067
			5	52.156	0.295	0.765	20.688	0.936	23.427	1.712	0.000	0.050
Sample 94.79	T19/364544	73		52.936	0.792	7.267	16.824	0.353	14.912	2.900	1.283	1.732

3.5.4 Andesitic glass

				SiO2	TiO2	Al2O3	FeO	MgO	CaO	Na2O	K2O
Sample 93.25	T20/464098	46	1	68.005	2.367	12.123	6.151	1.561	2.487	1.789	2.635
			2	64.833	0.913	15.185	6.178	1.392	4.759	1.885	2.082
			3	69.299	0.735	14.264	4.016	0.526	2.791	2.059	2.964
			4	67.151	0.767	14.420	4.614	1.325	4.034	4.492	1.621
Sample 93.26	T20/464098	46	1	60.428	0.941	19.278	4.268	1.635	7.356	4.306	2.217
			2	60.551	0.977	18.865	3.938	2.077	7.103	4.212	2.105
			3	63.918	1.258	15.276	5.341	2.778	5.504	3.896	2.766
			4	60.952	0.886	18.753	4.448	1.873	6.723	4.303	2.135
			5	63.651	1.205	15.720	5.624	2.320	5.659	4.045	2.688
			6	65.023	1.122	14.108	5.501	2.319	5.548	3.852	3.133
			7	64.071	1.023	15.507	5.080	2.553	5.066	4.264	2.999
			8	64.292	1.303	15.091	5.319	2.794	5.106	4.069	2.945
			9	63.909	1.174	15.255	5.748	2.541	5.412	3.855	2.817
			10	63.799	1.283	15.058	5.865	2.824	5.593	3.919	2.889
Sample 93.39	T20/469100	7	1	63.050	1.644	13.341	11.034	2.588	4.311	2.886	0.268
			2	62.504	1.197	14.452	10.150	2.470	4.102	3.025	1.383
			3	63.205	1.845	13.987	10.955	2.251	3.204	2.204	1.642
Sample 93.72	T20/477112	14	1	62.932	0.781	16.264	6.163	1.741	5.380	3.166	1.531
			2	61.996	1.077	15.804	4.865	2.220	5.877	4.169	2.743
			3	60.875	1.105	14.777	5.288	3.013	5.293	3.736	2.825
Sample 93.84	T20/477112	14	1	59.037	1.331	15.266	7.112	2.661	5.629	3.055	1.975
			2	58.355	1.062	16.482	5.903	2.548	5.639	3.617	1.768
			3	56.410	0.960	16.051	6.870	2.840	5.458	3.639	1.898
			4	56.791	0.940	15.904	7.238	2.923	5.935	3.699	1.776
Sample 93.89	T20/477112	14	1	63.985	1.024	15.363	7.188	1.758	5.766	4.372	1.919
			2	63.135	0.999	14.794	6.524	1.654	5.118	4.136	2.118
			3	62.703	0.967	14.808	6.177	1.757	4.805	4.283	2.056
			4	63.549	0.819	15.065	6.797	1.796	4.999	4.326	2.221
			5	62.287	1.123	14.819	6.404	1.748	5.042	3.906	2.145
Sample 93.91	T20/477112	14	1	62.077	1.274	13.453	5.295	1.613	4.679	3.705	2.438
			2	62.485	1.130	13.950	6.390	2.221	5.185	3.578	2.444
			3	61.695	1.127	15.200	6.059	1.777	5.760	4.030	2.051
			4	64.966	1.350	14.266	6.492	2.049	5.263	4.000	2.391
			5	63.471	1.233	14.760	6.260	2.097	5.480	3.707	2.407
			6	63.785	1.242	13.932	6.278	1.905	5.215	3.877	2.526
			7	64.503	1.126	13.992	6.329	1.960	5.091	3.734	2.396
			8	62.677	1.126	14.142	6.319	2.069	5.041	3.654	2.416
Sample 94.46	T19/496238	66	1	65.793	0.630	14.819	3.910	1.418	3.947	3.895	2.509
			2	63.858	0.968	15.335	5.788	1.788	4.888	3.994	2.073
			3	64.326	1.043	15.060	6.358	1.521	4.866	3.727	2.558
Sample 94.79	T19/364544	73	1	64.649	1.213	12.073	6.969	2.548	2.883	2.312	2.803
			2	62.324	1.684	13.024	6.584	2.262	2.954	2.540	2.777
			3	63.709	1.848	12.574	5.984	2.616	2.984	2.154	2.978
			4	63.537	1.174	12.250	6.950	2.567	3.514	2.652	3.060

3.5.5 Plagioclase

				SiO2	TiO2	Al2O3	FeO	MgO	CaO	Na2O	K2O
Sample 93.25	T20/464098	46	1	52.067	0.036	27.982	0.423	0.075	11.614	4.596	0.240
			2	56.978	0.133	27.224	0.833	0.129	10.976	3.778	0.678
			3	52.744	0.078	29.174	0.440	0.073	11.909	4.781	0.216
Sample 93.80	T20/477112	14	1	49.899	0.039	30.616	0.748	0.057	14.143	3.888	0.117
			2	57.891	0.358	23.944	1.102	0.321	9.998	3.145	0.684
			3	48.098	0.113	31.247	0.608	0.131	15.425	2.954	0.068
			4	51.819	0.173	25.598	1.498	0.091	10.687	5.716	0.404
Sample 93.89	T20/477112	14	1	46.220	0.077	30.989	0.655	0.081	16.973	2.416	0.067
			2	53.316	0.060	28.289	0.619	0.221	10.871	4.745	0.320
			3	52.697	0.088	29.794	0.743	0.101	13.221	3.194	0.293
			4	52.165	0.131	29.899	0.672	0.195	13.951	3.024	0.247
			5	54.062	0.050	28.227	0.635	0.100	11.564	4.967	0.303
Sample 93.91	T20/477112	14	1	49.939	0.000	27.051	0.612	0.000	11.360	4.706	0.116
			2	55.203	0.121	27.331	0.550	0.065	10.097	4.777	0.345
			3	52.148	0.000	30.480	0.281	0.009	13.476	4.351	0.148

3.5.6 Ilmenite

				SiO2	TiO2	Al2O3	FeO	MnO	MgO	CaO	Na2O	K2O	Cr2O3	NiO
Sample 93.25	T20/464098	46	1	0.086	44.015	0.285	48.396	0.370	4.032	0.076	0.361	0.015	0.777	0.148
			2	0	44.006	0.216	48.710	0.423	3.917	0.067	0.000	0.014	0.083	0.14
			3	0.117	46.701	0.365	44.227	0.331	6.530	0.082	0.186	0.039	0.054	0.156
			4	0.015	43.481	0.428	48.857	0.438	4.247	0.079	0.005	0.008	0.145	0.114
			5	0.052	44.531	0.270	48.483	0.359	4.140	0.061	0.087	0.040	0.062	0.149
Sample 93.51	T20/468102	9		0.186	36.568	0.590	55.435	0.254	2.705	0.114	0.005	0.013	0.068	0.049
Sample 93.88	T20/477112	14	1	0.702	28.867	0.690	58.933	0.101	1.603	0.377	0.010	0.020	0.155	0.048
			2	0.106	28.968	0.536	58.457	0.134	1.459	0.160	0.080	0.026	0.243	0.068
Sample 94.4	T20/468102	9	1	0.081	42.528	0.335	47.238	0.227	4.141	0.280	0.074	0.023	0.311	0.265
			2	0.000	46.474	0.100	46.924	2.071	0.935	0.073	0.097	0.029	0.262	0.227
Sample 94.22	T19/481211	55	1	0.262	28.556	0.633	60.858	0.234	1.858	0.172	0.526	0.034	0.233	0.117
			2	0.110	32.024	0.652	58.834	0.182	1.952	0.124	0.081	0.014	0.177	0.098
Sample 94.41	T19/491239	-	1	0.071	47.027	0.227	46.423	0.474	3.342	0.104	0.006	0.025	0.027	0.008
			2	0.065	46.263	0.188	45.401	0.428	3.348	0.076	0.000	0.027	0.249	0
			3	0.150	45.547	0.280	45.190	0.459	3.366	0.053	0.196	0.044	0.033	0.025
			4	0.065	46.292	0.269	46.690	0.493	3.380	0.050	0.086	0.020	0.168	0.057
			5	0.018	45.955	0.294	45.067	0.467	3.525	0.085	0.000	0.023	0.064	0
Sample 94.46	T19/496238	66	1	0.124	43.404	0.523	46.330	0.839	2.353	0.203	0.424	0.111	0.097	0.02
			2	0.194	42.194	0.270	46.628	0.321	2.772	0.077	0.125	0.044	0.095	0.076
			3	0.151	44.127	0.401	51.117	0.385	2.624	0.416	0.129	0.024	0.133	0.109
			4	0.130	45.452	0.207	49.338	0.501	2.689	0.139	0.092	0.049	0.284	0.117

3.5.7 Spinel

				SiO2	TiO2	Al2O3	FeO	MnO	MgO	CaO	Na2O	K2O	Cr2O3	NiO
Sample 93.53	T20/468102	10	1	0.000	1.167	51.245	34.108	0.174	12.404	0.020	0.000	0.000	0.100	0.049
			2	0.000	0.975	51.657	33.825	0.313	12.608	0.011	0.000	0.004	0.232	0
Sample 93.83	T20/477112	14		1.361	0.791	42.720	39.567	0.242	9.305	0.224	0.147	0.103	0.056	0.049

APPENDIX 4: SELECTED FIELD SECTION DESCRIPTIONS

Of the > 120 sections described during the course of this study the following 60 are listed in order to characterise the stratigraphy within each stream or sector of the ring plains studied. The sections from which samples were taken for further analysis are also listed. The section numbers used are those assigned during the original field work and are consistent with the numbering system used throughout the thesis. The following indicates the section numbers describing each stream sector:

Upper Waikato Stream	3, 4, 5, 7, 9, 10, 14, 45, 46, 47
Tangatu Stream	11
Wharepu Stream	17, 18
Te Piripiri Stream	22, 24, 26, 30
Mangatoetoenui Stream	32, 34, 35, 37
Ohinepango Stream	38, 41, 42
Waihohonu Stream	40, 44, 53
Oturere Stream	54, 56, 81
Makahikatoa Stream	58, 59, 60
Mangatawai Stream	64, 66
Mangamate Stream	68
Puketarata Stream	91
Mangahouhounui Stream	93
Tauhurangi Stream	82, 83, 88, 89
Tongariro River	50, 51, 72, 73, 76, 78, 95-105

In the "correlation and samples taken column", Marker tephra units 1-7 from Chapter 3, and lahar episodes R01-R15 and T1-T4 from Chapter 5 are indicated as well as correlations to other, previously defined tephra formations. Samples taken and referred to in this study are also indicated, as are correlations between the samples.

Section 3
Upper Waikato Stream T20 465095
True left bank of southern-most tributary of the Upper Waikato Stream, 50m east of State Highway 1, approx 2 km north of Tukino Skifield access road.

Unit Depth (mm)	Cum. depth (m)	Correlation and samples taken	Description
300-500		Taupo Ignimbrite	White fine pumice ash with intermixed pumice lapilli and blocks. Occasional charcoal fragments present. Undulating basal contact.
280	0.78	Papakai Formation	Unconformable upper contact. Greasy, fine ash, dark greyish brown (2.5Y 4/2), with vertical crack development and evidence of root channels.
90			Reworked red-stained, olive brown (2.5Y 4/4), and grey fine lithic and pumice lapilli
140	1.01	Mangamate Tephra (MT), Poutu Lapilli	Normally graded coarse ash and fine lapilli. Grey and olive brown poorly vesicular pumice.
160-190			Reworked coarse ash and fine pumice and lithic lapilli grey and reddish brown, crossbedded in places.
110-140		MT, Wharepu Tephra	Coarse grey and olive brown ash and fine lapilli, poorly vesicular pumice. Upper contact erosive. Lower 50 mm reddish brown.
20			Yellow brown fine ash
10		MT, Ohinepango Tephra	Dark grey med-coarse ash
90		"	Fine pumice lapilli, olive brown, dark grey and yellowish red (5YR 4/8)
130		MT, Waihohonu Lapilli	Banded layers of med-coarse lithic and poorly vesicular ash, bands dominated by grey, yellowish red, and olive brown.
180	1.77	MT, Oturere Lapilli	Dark grey, olive brown and yellowish brown (10YR5/6) ungraded med pumice and lithic lapilli.
120			Dark yellowish brown fine ash with scattered yellowish brown pumice.
50		Pahoka Tephra	Greyish brown coarse ash and fine lapilli, some pale brown banding evident within some of the poorly vesicular pumice.
80			Brown and greyish brown med-fine ash with scattered lapilli interbedded.
80	2.10	Bullot Formation (BT), Pourahu Member	Coarse-fine pale yellow and yellowish brown pumice lapilli and grey lithic lapilli.
20			Grey coarse ash with occasional lapilli interbedded.
20			Yellowish brown fine pumice angular lapilli and grey lithic coarse ash.
30			Olive grey med-coarse ash and occasional fine pumice lapilli.
10			Yellow brown fine ash
30			grey medium lithic ash
40			Brown fine-med pumice lapilli and grey lithic lapilli.
20			Yellowish brown fine angular pumice lapilli and coarse ash.
20			Greyish brown coarse pumice ash.
50			Yellowish red fine-med pumice lapilli and occasional grey lithic coarse ash.
40			Dark purplish black lithic coarse ash and fine lapilli.
40			Brown pumice med-fine pumice lapilli reversely graded with coarse ash at the base.
10	2.43	BT, M1	Greyish brown med-fine ash
10		"	Yellowish brown coarse ash and fine pumice lapilli.
10		"	Fine-med yellowish brown ash with occasional fine pumice lapilli.
20			Purplish black coarse lithic ash and fine lapilli.
40			Greyish brown coarse ash and fine pumice and lithic lapilli.
20			Purplish grey coarse ash and fine lithic lapilli.
10			Strong brown soft pumice lapilli and coarse ash.
20			Purplish black coarse ash and fine lithic lapilli.
50	2.61	BT, L17?	Strong brown med-fine pumice lapilli with occasional grey lithic fine lapilli intermixed.
20			Strong brown pumice coarse ash and fine lapilli.
60			Dark greyish brown coarse ash and occasional lithic lapilli.
100	2.79	BT, L16?	Yellowish red (5YR 5/6) pumice fine-med lapilli and few grey fine lithic lapilli.
10			Grey med-coarse lithic ash.
10			Greyish brown fine ash.
10			Purplish grey med lithic ash.
10			Strong brown fine pumice lapilli and coarse ash.
10			Purplish black med-fine lithic lapilli.
50		BT, M3?	Yellowish brown coarse ash and fine pumice lapilli, reversely graded.
20		"	Purplish black med-coarse ash.
30			Greyish brown coarse-med ash and fine lithic lapilli.
80	3.02	"	Yellowish red pumice fine-med lapilli with few grey fine lithic lapilli.
20			Grey coarse lithic ash.
50		BT, L14?	Normally graded greyish brown coarse pumice ash and fine lapilli.
50			Greyish brown coarse-med ash with occasional fine lapilli intermixed, lower 10 mm fine lapilli dominant.

40			Dark purplish black coarse ash and fine lapilli.
20			Yellowish brown coarse pumice ash and fine lapilli.
20			Purplish black coarse ash and fine lithic lapilli.
20			Greyish brown pumice coarse ash.
10			Purplish black coarse lithic ash.
20			Brown fine pumice lapilli.
10			Grey med lithic ash.
20			Yellowish brown med ash with occasional pumice lapilli.
10			Grey med lithic ash.
30			Greyish brown med-coarse ash mixed with many fine pumice lapilli.
20			Brownish yellow pumice fine lapilli and coarse ash, with few grey lithic lapilli.
80	3.44	Rerewhakaaitu Tephra	Greyish brown coarse pumice and lithic ash and fine lapilli. White fine ash interbedded within the base 5-10 mm thick.
10			grey coarse lithic ash.
10			Greyish brown med ash and fine pumice lapilli.
10			Grey coarse lithic ash.
30			Yellowish brown pumice fine-med lapilli and few grey lithic fine lapilli.
50			Grey med-coarse ash variable lower boundary.
100	3.65	BT, L7?	Yellowish brown coarse pumice ash to med lapilli, shower bedded.
20			Grey med lithic ash.
850	4.50	Hinuera Formation, Sample 93.3	Bedded silts sands and pebbles, sub-rounded and poorly sorted as a whole. Dominantly greyish brown in colour with clasts of pumice and grey lithic andesite. Thin layers of reworked white and pink fine rhyolitic ash interbedded in parts of unit.
1000	5.50		Dark grey andesite lithic med-coarse sands laminated and cross-bedded. Layers and lenses of cobbles and pebbles interbedded. Lower contact is an angular unconformity.
1200		R10	Greasy silty matrix diamicton. Matrix supported with pebble to boulder sized clasts. Clasts are heterolithologic, often soft and multi-coloured and appear hydrothermally altered. Lower part of unit contains large (1 m) diameter boulders. Matrix colour yellow to yellowish brown.
250		R10	Similar to unit above, except matrix is pale yellow and there are no boulder sized clasts.
3000+	9.95		Bedded sands silts and gravels, in lenses and layers. Med-coarse sands and fine pebbles sub-rounded and sub angular. Base into stream.

Section 4

Upper Waikato Stream, T20 466095

True left bank 50m downstream from Section 3. Cover-beds are the same as section 3 and this description is taken from the base of the distinctive R10 diamicton.

Unit Depth (mm)	Cum. depth (m)	Correlation and samples taken	Description
100	*c*.7.0		Bedded silt and sand, with yellow and greyish brown pebbly lenses.
50			Gravels with intermixed sand.
50			Dark red and yellowish brown coarse pumice ash and fine lapilli. Normally graded with grey lithic coarse ash interbedded toward the base.
2000-2500			Bedded sands silts and gravels, rounded heterolithologic clasts. Cross-stratified in places, colours range from dark brown to greyish brown sands.
50	9.65	(=93.24)	Coarse pumice ash and fine lapilli, ungraded, soft, yellow and pale yellow.
200			Fine grey sand with occasional interbedded pumice pebbles.
150		(=93.25)	Reverse graded brown and olive brown fine-med pumice lapilli.
10			Brownish grey fine ash.
400			Grey and pale olive brown coarse-med ash alternating layers of colour dominated by the grey lithic or olive brown pumice ash. Shower-bedded.
100		(=93.26, Marker Unit 1)	Bedded coarse ash and fine lapilli, strong shower-bedding with grey and olive brown colours on a 30 mm scale.
10-150	10.66	(=93.27, Marker Unit 1)	Yellow fine pumice lapilli.
2000			Bedded silts, gravels and sands, brown and greyish brown. Beds and lenses of sub-rounded pebbles and occasional cobbles. Multiple coloured hetero-lithologic pebbles, highly weathered. Laminated and cross bedded. Basal 200 mm gravelly.
500			Purplish grey and purple silty matrix diamicton. Sparse multi-coloured clasts within matrix and mostly of pebble size. Few large boulders near base of unit.
200		(=93.28 and 93.30)	Strong brown and yellow, soft, pumice fine lapilli, with few intermixed grey lithics.
30			Purplish grey fine ash.

50		(=93.29 and 93.31)	Coarse-med pumice ash, strong brown top and base mostly grey lithic ash.
2000+	15.44		Silt sand and gravel beds, 50 mm scale beds mostly greyish brown and brown in colour. Lenses of pebbles and occasional small cobbles. Cross-bedded and planar bedded. Sharp contact onto lithified diamicton unit.

Section 5
Upper Waikato Stream, T20 466096
True left bank 100 m downstream from Section 4. Description taken from lowest andesitic tephra described at Section 4.

Unit Depth (mm)	Cum. depth (m)	Correlation and samples taken	Description
40	14.00	93.30	Yellow and yellowish brown pumice fine-med lapilli. Reversely graded.
10			Grey fine ash.
300		93.31	Shower bedded fine-med pumice lapilli, yellowish brown and grey. 20 mm lithic rich layer of fine lapilli.
1000	15.31		Bedded silts sands and gravels, in layers and lenses. Grey and greyish brown in colour with multi-coloured pumice and lithic pebbles.
1200		R11	Sharp upper contact. Sandy-matrix diamicton, matrix of fine-coarse sand supporting clasts of pebble to boulder in size. Yellow pumice clasts in finer size range and grey lava in larger size range. Highly lithified unit. Grey and greyish brown matrix colour.
600		"	Sharp contacts with upper and lower units. Sandy matrix diamicton with maximum clast size of cobbles and pebbles. Grey and greyish brown matrix.
400		"	Sandy-matrix diamicton, fine grained, clasts of mostly pebble in size. Sharp contact with units above and below.
1500	19.01	"	Sandy-matrix diamicton, with dominantly cobble sized clasts supported within matrix. Crude horizontal fabric preserved in the base of this bed. Grey and greyish brown in colour. base obscured by talus.

Section 7
Upper Waikato Stream, T20 469100
True right bank of southern tributary, 200 m upstream of junction between the two tributaries. Description taken from above Kawakawa Tephra.

Unit Depth (mm)	Cum. depth (m)	Correlation and samples taken	Description
20	*c.* 9.0		Yellow brown coarse ash and fine pumice lapilli.
30		93.32, Rerewhakaaitu Tephra	Greyish brown and yellow brown fine lapilli and coarse ash with pocketing interbedded white fine rhyolitic ash.
10			Yellow brown fine pumice lapilli.
20-200			Pinching and swelling diamicton, coarse-fine sand matrix supporting mostly pebble clasts with occasional boulders. Unconformable lower contact, undulating.
20			Yellow brown fine pumice lapilli.
10			Grey medium lithic ash.
10			Yellow brown fine greasy ash.
50			Strong brown fine-med pumice lapilli with few grey lithic lapilli.
20			Grey and brownish grey medium ash.
40	9.38	93.33, Kawakawa Tephra	Fine yellow pumice ash 20 mm at the top of the unit, underlain by 10 mm pink fine ash and 20 mm further pale yellow fine ash.
50			Grey and brownish grey bedded med sand and pebbles.
250			Yellow brown and brownish grey loose sands containing yellow pumice pebbles, unbedded.
400		R10	Pink and grey, greasy, silt-matrix diamicton, multi-coloured pumice and weathered lithic clasts supported in the matrix. Cobble and boulder clasts also common.
500		"	Brown and dark yellow brown greasy silt-matrix diamicton, containing multi-coloured pumice pebble clasts.
700		"	As above, but separated by a sharp even contact from the above unit.
350	11.73	93.34 (=93.31)	Shower bedded strong brown and yellow brown fine-med pumice lapilli. 10 mm zone of grey lithic lapilli 100 mm above base and reversely graded base.
1200			Grey and greyish brown silt, sand and gravel beds, 2-3 cm scale planar bedding and cross-bedded.
200		R11	Greyish brown and grey sandy matrix diamicton, coarse-fine sand matrix supporting pebble clasts, grey red and yellow pumice and lithic clasts.
1200		"	Normally graded grey and greyish brown sandy matrix diamicton, matrix supporting pebble clasts at the top and cobble clasts at the

			base. Clast rich unit with most of clasts grey and lithic, around 10% of clasts yellow pumice pebbles. Strongly lithified.
1500		"	Three to four layers of finer grained diamicton units. Sandy matrix with clasts of yellow pumice and dominantly grey lithic pebbles. Strings of cobbles seen and a horizontal fabric preserved. Strongly lithified.
2000	17.83	"	Sandy-matrix diamicton, no yellow pumice clasts entirely grey lithic pebbles. Strings of cobbles and occasionally huge boulders. Several units pinching in and out with sharp contacts between. Firmly lithified.
100		93.36	Dark red and yellow pumice med-fine lapilli, very firm and cemented.
500			Bedded grown and greyish brown med-fine sand with interbedded yellow pumice in layers and lenses.
150		93.37	Reddish brown and red coarse pumice ash firmly cemented, and shower-bedded.
200			Yellow brown and brown fine ash with occasional yellow pumice lapilli intermixed.
200		93.38	Yellow brown and red stained fine-med pumice lapilli, shower-bedded with few grey lithic fine lapilli.
1000			Brown and dark brown fine ash with paleosol development evident. Greasy fine ash with abundant, finely disseminated charcoal present in the upper 300 mm. Abundant root channels seen as well as vertical cracking and coarse blocky structure. Some intermixed grey and yellow pumice and lithic lapilli near base.
150	20.13	93.39, Marker Unit 2	Grey and dark grey firmly-cemented fine ash. Extremely hard and breaks up into brittle slabs along shower bedding. Accretionary lapilli within two of the shower beds, 2-5 mm in diameter.
600			Brown and brownish grey fine ash, firm, with little paleosol development.
300		93.40	Yellow and strong brown fine-med pumice lapilli, soft, with occasional fine grey lithic lapilli.
1500		R12	Uniformly fine grained diamicton. Greyish brown sandy and silty matrix with grey lithic pebble sized clasts. Distinctive content of around 20 % yellow pumice fine pebbles. Horizontal fabric observed and unit is firmly lithified.
			Base of section into stream.

Section 9
Upper Waikato Stream, T20 468102
True left bank of north tributary, 40 m upstream of junction of two tributaries. Description taken from above R10.

Unit Depth (mm)	Cum. depth (m)	Correlation and samples taken	Description
1500	*c*.5.0		Grey and yellow brown bedded fine-coarse sands and fine gravels, unconsolidated, with planar 10-50 mm scale bedding.
600		R10	Yellow brown greasy silt-matrix diamicton. Pebble-cobble clasts supported by the matrix. Multi-coloured pumice and weathered lithic clasts.
1500		"	Yellow brown and pale yellow silt-matrix diamicton with large grey and red boulder clasts as well as multi-coloured pebble clasts supported by the matrix.
3000			Grey, brownish grey and brown bedded sands, silts and gravels, planar and cross bedded layers, bedding on a 10-100 mm scale. Yellow and yellow brown pumice pebbles common scattered within silts and sands as well as in lenses.
300	10.40	93.29	Yellow brown and yellow fine-med soft pumice lapilli, normally graded with scattered fine grey lithic lapilli.
4000			Bedded silts, sands, and gravels, brown with grey and multi-coloured pumice and lithic pebbles. Planar and cross-bedded on a 50 mm scale.
1500	15.90	R12	Grey and greyish brown sand- and silt-matrix diamicton. Grey lithic pebbly clasts and abundant (>20%) yellow pumice clasts supported by the matrix. Weak planar fabric and firmly lithified.
20			Yellow brown fine ash with mixed in fine yellow pumice lapilli.
20			Grey lithic fine lapilli with yellow brown fine ash intermixed.
120		93.41	Strong brown and yellow brown fine pumice lapilli with intermixed grey lithic lapilli.
1000-1500		R12	Firmly lithified diamicton. Grey and greyish brown sandy matrix supporting huge boulder clasts. Abundant large clasts as well as up to 60% of matrix made up of yellow pumice lapilli.
500		93.42	Yellow and yellow brown fine pumice lapilli ungraded and shower-bedded. Occasional grey lithic fine lapilli also present.
100			Grey and greyish brown fine ash, firm.
40			Yellow brown and strong brown fine-med pumice lapilli.
150			Grey and greyish brown fine ash with 5% scattered fine yellow pumice lapilli.

500	18.85		Reddish brown fine ash firm with paleosol development. Abundant brown stained root channels and rare finely dispersed charcoal.
50		93.43	Yellow and strong brown fine-med pumice lapilli with abundant dark grey lithics and coarse ash sized black free pyroxene crystals.
150			Massive brown fine ash with few scattered fine yellow pumice lapilli, common root channels.
20			Yellow and yellow brown fine pumice lapilli with abundant coarse black free pyroxene crystals.
100			Reddish brown fine ash with common root channels.
40		93.44	Yellow and yellow brown fine pumice lapilli intermixed with grey lithic lapilli, 5-10% free black coarse ash sized pyroxene crystals.
250			Reddish brown fine ash with scattered fine yellow pumice lapilli and black free pyroxene crystals, also common root channels.
350			Grey and greyish brown fine ash firm with common yellow pumice and grey lithic lapilli scattered throughout.
350			Reddish brown and brown fine ash, greasy vertical cracking and some blocky structure, common root channels.
50		93.45	Yellow and yellow brown fine pumice lapilli with intermixed grey fine lithic lapilli.
400		R13	Firm diamicton unit, silt and sand matrix supporting mostly grey lithic pebble clasts, also less common pebbles of red and yellow pumice. Erosive lower contact.
50		93.46	Yellow brown and strong brown fine pumice lapilli with intermixed grey lithic lapilli.
300	19.96	93.47, Marker Unit 3	Strong brown stained fine pumice lapilli and coarse ash shower-bedded with two distinctive grey lithic dominated zones 10 mm thick 20 mm apart, and 50 mm from the top of the unit.
100			Grey fine ash with scattered fine yellow pumice and grey lithic lapilli.
50		93.48	Yellow brown and strong brown fine pumice lapilli with intermixed grey lithic fine lapilli and black coarse ash sized free pyroxene crystals.
30			Grey fine ash, firm.
50		93.49	Yellow brown and strong brown fine pumice lapilli with intermixed grey lithic fine lapilli and black coarse ash sized free pyroxene crystals.
10			Brown fine ash
200		93.50	Yellow brown and strong brown fine-med pumice lapilli with intermixed grey lithic fine lapilli and black coarse ash sized free pyroxene crystals, concentrated toward the top of the unit.
50			Grey fine ash with scattered 5% yellow pumice lapilli and black pyroxene crystals.
50		93.51	Yellow and yellow brown med-fine pumice lapilli with intermixed grey lithic fine lapilli.
200+			Grey and pinkish grey fine ash with scattered 5% yellow pumice lapilli and black pyroxene crystals.
	20.70		Base into stream.

Section 10
Upper Waikato Stream, T20 468103
True right bank of stream 50 m downstream of the junction of the two tributaries. Description taken from above the R13 diamicton in section 9.

Unit Depth (mm)	Cum. depth (m)	Correlation and samples taken	Description
50	*c.* 26.5		Yellow and strong brown fine pumice lapilli with grey lithic coarse ash and black free pyroxene crystals intermixed.
50			Brown and reddish brown fine ash with root channels.
800		R13	Sandy-matrix diamicton. Upper 0-400 mm reworked and partially bedded lower part massive with grey lithic pebble and cobble clasts supported in matrix of grey coarse-med sand, uncemented.
100			Olive brown and grey fine ash, firm.
200	27.65	Marker Unit 3	Strong brown fine pumice lapilli and coarse ash with distinctive 10 mm thick grey lithic dominated layers 20 mm apart 40 mm from the top of the unit.
50			Grey greasy fine ash.
100		(=93.48)	Strong brown medium pumice lapilli with intermixed grey lithic lapilli.
50			Grey greasy fine ash.
200		(=93.50)	Yellow and strong brown fine pumice lapilli with mixed grey fine lithic lapilli.
50			Greyish brown greasy fine ash.
30		(=93.51)	Yellow and pale brown fine pumice lapilli with grey lithic fine lapilli and black free pyroxene crystals intermixed.
70			Grey fine ash with scattered fine yellow pumice lapilli intermixed.
200			Brown fine ash firm with root channels.
100		93.52, Marker Unit 4	Pale brown and strong brown med-coarse pumice lapilli with grey lithic fine lapilli and black free pyroxene crystals intermixed.

200			Bedded silt and sand with intermixed yellow pumice fine lapilli.
60		93.53	Strong brown fine pumice lapilli and coarse ash.
10			Grey fine lithic ash.
30		93.54	Strong brown and reddish brown coarse-med pumice lapilli.
150			Alternating 30 mm layers of olive brown and yellow fine pumice lapilli.
150			Grey lithic coarse ash and strong brown fine lithic lapilli.
120			Pale brown and strong brown alternating 30 mm layers of fine pumice lapilli.
200			Many thin (10 mm) layers of brown, grey, yellow, and pale brown fine pumice lapilli and coarse ash.
1200	31.52	R14	Sandy-matrix diamicton. Matrix supporting grey clasts of pebble to small boulder in size. Brown to greyish brown clasts and matrix. Ungraded and with no bedding. Sharp planar lower contact.
100			Dark grey and strong brown coarse-med pumice lapilli in a matrix of grey coarse ash.
50			Grey coarse lithic ash and fine lapilli.
100			Brown fine pumice lapilli and coarse ash.
90			Pale brown and grey coarse ash and fine pumice lapilli.
50		93.58	Strong brown and pale brown fine pumice lapilli with intermixed grey lithic fine lapilli.
200			Sandy matrix diamicton, pebble clasts supported in greyish brown med-coarse sand.
20			Pale brown and yellow fine pumice lapilli.
1500+	33.63	R15	Grey sandy-matrix diamicton, pebble and cobble clasts supported in med-coarse sand matrix, unbedded and uncemented. Base into stream.

Section 11
Tangatu Stream, T20 470110
True left bank of stream, 500m downstream of state highway 1.

Unit Depth (mm)	Cum. depth (m)	Correlation and samples taken	Description
400		Makahikatoa Sand	Brown and greyish brown med-fine sand, present soil development.
450		Taupo Ignimbrite	White fine ash matrix supporting white pumice block and lapilli clasts. Charcoal present near base.
300	1.15	Mangatawai Tephra	Brown and greyish brown fine greasy ash with several black and purplish grey fine-coarse ash beds. Yellowish brown beech leaves preserved in some of the ash layers.
100		Papakai Formation	Brown and yellow brown fine greasy ash with strong paleosol development.
30	1.28	Waimahia Tephra	Cream-cakes of fine white ash.
300		Papakai Formation	Yellow brown fine greasy ash.
150	1.73	Hinemaiaia Tephra within Papakai Formation	Coarse white pumice ash scattered throughout brown fine ash. Unconformable lower contact.
1200-1500			Bedded sands, silts and gravels. Greyish brown and brown, planar bedded and cross bedded, with layers and lenses of grey lithic and yellow pumice pebbles. 10 cm scale bedding.
1500			Brown silt-matrix diamicton. Large boulder clasts supported within matrix as well as grey pebbles and cobbles.
500+		R10	Yellow brown sandy and silty matrix diamicton. Fine grained with dominantly pebble clasts. Firm matrix supporting multi-coloured pumice and weathered lithic clasts.
	5.23		Base into stream.

Section 14
Upper Waikato Stream, T20 477112
True left bank of stream, 300 m upstream of junction with Tangatu Stream. Description taken from Bullot Formation member containing Rerewhakaaitu Tephra.

Unit Depth (mm)	Cum. depth (m)	Correlation and samples taken	Description
50	*c.* 7.0	93.59, Rerewhakaaitu Tephra	Greyish brown coarse ash and fine lithic lapilli containing cream-cakes of up to 20 mm thick of white fine rhyolitic ash.
30			Strong brown and yellow brown fine-med pumice lapilli.
10			Grey coarse ash.
0-50			Eroded yellow brown and strong brown fine, soft pumice lapilli.
400-500			Grey and greyish brown bedded sands and gravels in planar layers and lenses. Variable thickness and unconformable contacts.
400		93.60	Yellow brown and strong brown fine-med pumice lapilli with few grey fine lithic lapilli interbedded.
2000	9.99	R10/R11	Brown silt and sand matrix diamicton. Matrix supports clasts of pebble to boulder in size. Multi-coloured lithic and pumice clasts abundant.

			Massive and unbedded, boulders concentrated toward the base.
10			Yellow medium pumice lapilli in a matrix of brown fine ash.
20			Dark greyish brown fine ash.
20			Yellow coarse pumice ash and fine pumice lapilli.
30			Grey fine ash.
20			Yellow medium pumice lapilli.
30			Grey fine ash.
50			Dark greyish brown fine ash with scattered fine yellow pumice lapilli.
200		93.61 (=93.37)	Olive grey coarse ash, shower-bedded and ungraded.
50			Brown fine ash with scattered yellow fine-pumice lapilli and coarse ash.
100		93.62 (=93.38)	Yellow brown fine and soft pumice lapilli.
1000	11.49		Brown and greyish brown fine ash, greasy and with common root channels. Finely disseminated charcoal present in the upper 200 mm. Weak blocky structure developed near top. Lower 200 mm contains scattered yellow and yellow brown fine pumice lapilli (5%).
150-200		Marker unit 2	Pale grey and light brownish grey hardened fine ash tuff unit. Shower-bedded fine and med ash. Breaks into brittle slabs along beds.
400		93.63 (=93.40)	Yellow and yellow brown fine-med pumice lapilli with intermixed grey fine lithic lapilli.
150			Brown fine ash with scattered yellow brown fine pumice lapilli.
200		93.64 (=93.40)	Yellow brown med-fine pumice lapilli and grey lithic fine lapilli.
1400	13.84	R12	Massive diamicton. Silt and sand-matrix supporting pebble to boulder clasts. Abundant grey lithic and yellow pumice clasts. Firmly lithified.
50		93.65 (=93.42)	Yellow and brown fine pumice lapilli and coarse ash.
350			Greyish brown fine ash with scattered coarse yellow pumice ash (10%)
50			Yellow brown fine pumice lapilli and coarse ash.
20			Greyish brown fine ash.
40		93.66	Yellow and yellow brown med-fine pumice lapilli.
200			Greyish brown fine ash with abundant root channels and few scattered yellow fine pumice lapilli.
100		93.67	Yellow and strong brown med pumice lapilli, with grey fine lithic lapilli.
50			Reddish brown fine ash with root channels.
50		93.68	Yellow fine pumice lapilli with grey fine lithic lapilli and black coarse ash sized pyroxene crystals.
200			Dark red fine ash with scattered fine yellow pumice lapilli (5%), and root channels.
50	15.00	93.69	Yellow pumice lapilli with abundant black coarse ash grade pyroxene crystals.
400			Dark red fine ash with scattered fine yellow soft pumice lapilli, some root channels
150			Yellow and grey fine pumice lapilli mixed with fine brown ash.
100			Dark red fine greasy ash with scattered fine yellow soft pumice lapilli, some root channels.
1000-1200	16.85		Bedded silts and fine sands, laminated and cross-bedded, lenses and layers rich in pebbles. Dusky red and greyish brown.
20			Grey and Yellow brown coarse ash.
300			Pink fine ash, firm, and contains root channels.
300		R13	Firm silt matrix diamicton, grey red and yellow pebble to cobble-sized clasts supported by the matrix.
150			Greyish brown fine ash with intermixed yellow brown fine pumice lapilli.
200	17.82	93.70 (=93.47), Marker unit 3	Red coarse pumice ash and fine lapilli with grey lithic lapilli and black coarse ash grade pyroxene crystals intermixed. 3 distinctive grey 10 mm layers separated by 20 mm near the top of the unit.
70			Grey fine ash with scattered fine yellow pumice lapilli.
200		93.71, (=93.48)	Strong brown and yellow brown med-fine, soft, pumice lapilli with grey lithic lapilli and black coarse ash grade pyroxene crystals intermixed.
50			Greyish brown and grey fine ash with scattered fine yellow pumice lapilli.
250		93.72, (=93.49)	Yellow brown and pink fine-med pumice lapilli with grey lithic lapilli and black coarse ash grade pyroxene crystals intermixed.
70			Grey fine ash.
50		93.73, (=93.51)	Yellow and yellow brown fine-med pumice lapilli.
100			Grey and greyish brown fine ash with 5% yellow fine pumice lapilli intermixed.
50	18.66	93.74, Marker Unit 4	Yellow brown pumice lapilli with intermixed grey fine lithic lapilli.
10			grey coarse ash.
50		93.75	Yellow and greyish brown and black pumice and lithic fine lapilli, lithic rich unit.
200			Brown and greyish brown fine ash with scattered fine yellow pumice lapilli.
20			Yellow pumice coarse ash and fine lapilli with intermixed grey fine lithic lapilli.
200			Greyish brown fine ash with scattered fine yellow pumice lapilli.

20			Brown and yellowish brown fine pumice lapilli.
30			Grey med ash and greyish brown and black coarse lithic ash.
100	19.29	93.76	Brown and strong brown fine-med pumice lapilli, firm lapilli.
40			Greyish brown med-coarse ash and grey lithic fine lapilli.
50		93.77	Yellow and yellow brown fine pumice lapilli with intermixed fine grey lithic lapilli.
100			Brown and yellow brown fine ash with scattered yellow brown fine pumice lapilli.
200			Brownish grey med-coarse ash with scattered grey lithic and yellow pumice fine lapilli.
30			Brown fine ash with scattered yellow brown fine pumice lapilli
20			Grey coarse ash.
30			Brown coarse ash.
30			Yellow brown fine pumice lapilli with intermixed grey coarse lithic ash.
30			Brown coarse ash.
10			Dark grey lithic med ash.
40	19.87	93.78	Yellow and yellow brown fine pumice lapilli with 50% intermixed grey lithic fine lapilli.
10			Grey fine lithic ash.
30			Yellow and yellow brown fine pumice lapilli with intermixed grey coarse lithic ash.
40			Grey med ash with scattered yellow fine pumice lapilli.
20			Brownish grey fine ash with scattered yellow fine pumice lapilli.
40			Grey med ash with scattered yellow fine pumice lapilli.
250			Brownish grey med ash with scattered yellow fine pumice lapilli.
20			Yellow brown fine pumice lapilli with intermixed grey lithic coarse ash.
250			Greyish brown and grey fine-coarse ash with scattered yellow fine pumice and grey lithic lapilli.
100	20.63	93.79	Yellow brown strong brown, greyish brown and black med-coarse pumice lapilli.
200		93.80	Strong brown and yellow brown fine-med pumice lapilli.
10			Brown firm, fine ash.
100			Brown and greyish brown med-coarse ash and fine pumice lapilli.
50		93.81	Brown and yellow brown fine-med pumice lapilli with grey fine lithic lapilli.
1500		R14	Sandy matrix diamicton, grey and brownish grey med-coarse sand supporting grey and red lithic pebbles-boulders. Poorly sorted, unconsolidated and unbedded. Some faint planar fabric.
600			Bedded sands and pebbles, 30 mm scale planar and cross bedding. Greyish brown with lenses of yellow and strong brown pumice pebbles.
50	23.14	93.82	Black stained yellow fine-med pumice lapilli.
100			Grey and brownish grey med-fine ash with scattered fine yellow pumice lapilli.
40		93.83	Black stained, yellow brown fine-med pumice lapilli.
400		93.84	Greyish brown, yellow and grey fine-med shower-bedded pumice lapilli.
50			Grey med coarse-fine ash.
20			Brownish grey fine ash.
50		93.85, Marker Unit 5	Normally graded yellow and grey pumice and lithic fine lapilli and coarse ash.
500			Grey bedded sands and gravels in lenses and layers with yellow pumice pebbles.
1000		R15	Grey and greyish brown diamicton. Coarse-fine sand matrix supporting pebble-cobble clasts and some small boulders. Planar fabric preserved with cobble strings.
200	25.50	93.86	Brown, brownish grey and yellow med-coarse pumice lapilli, shower-bedded, lower 100 mm has intermixed grey med ash or sand.
5000		R15	Several 1 m thick diamicton units interbedded with bedded silts sands and gravels in layers and cross beds. Diamictons have matrices of coarse-med sand supporting pebble-cobble clasts with occasional boulder. Unconsolidated and overall planar fabric preserved with cobble strings. Dominantly grey and brownish grey lithic with occasional red lithic clasts.
2500		"	Coarse grained diamicton. Coarse-med grey sand matrix supporting large grey angular boulder and cobble clasts. Weak planar fabric.
5000		"	Grey and greyish brown planar diamictons and interbedded finely bedded sands and gravels. Sandy matrix supporting lithic pebble and cobble clasts.
5000			Bedded sands and gravels, grey and brownish grey, planar and cross bedded in layers and lenses. Upper half dominantly gravels and lower half dominantly sands.
1000			Pale brownish grey firm, fine sand, massive unbedded with 5 % scattered fine yellow pumice lapilli.
500-1000		"	Variable thickness dark grey diamicton. Sandy matrix supporting

			pebble-boulder lithic clasts.
1000			Grey and olive grey well sorted planar bedded med sand.
50			Grey coarse-med ash.
50	46.10	93.87	White and strong brown stained fine pumice lapilli.
100		93.88	Pinkish white and grey fine pumice lapilli.
300			Fibrous dark brown and black firm lignite. Finely bedded 10 mm scale, planar bedding. Sampled at 50 mm intervals.
20		93.90	White and pale grey med ash.
300			Fibrous pale brown and dark brown lignite planar laminated.
40		93.89, Marker Unit 6	Grey and pinkish grey coarse ash and fine pumice and lithic lapilli.
20			Brown lignite.
100			Finely laminated brown lignite and grey fine-med sand.
150			Dark brown and pale brown laminated lignite.
100		93.91, Marker Unit 7	Grey and pinkish grey med pumice ash.
400			Bedded fine-coarse pale grey sands.
1000+		R15	Coarse sand matrix diamicton, large boulder-pebble clasts supported within the matrix. Brownish grey unbedded, massive and very firmly consolidated.
	48.63		Base into stream.

Section 17
Wharepu Stream, T20 463122
True left bank of stream, 50 m upstream of western power pylons, approximately 500 m downstream of State Highway 1.

Unit Depth (mm)	Cum. depth (m)	Correlation and samples taken	Description
800		Ngauruhoe Formation	Brown and greyish brown fine-med ash, friable, with present soil development.
100-250		Taupo Ignimbrite	White fine-med pumice ash supporting clasts of white pumice lapilli and blocks. Charcoal fragments dispersed throughout.
300		Mangatawai Tephra	Dark brown and brown fine greasy ash with paleosol development and paleo-root channels. The lower 100 mm contains several 10-20 mm thick fine-med purplish black and black ash beds. Yellow brown beech leaves are preserved within some of these layers.
100		Papakai Formation (Pp)	Yellowish brown fine greasy ash, friable, with paleosol development.
20	1.47	Waimahia Tephra within Pp	Cream-cakes of greyish white fine ash interbedded within yellow brown greasy fine ash.
150		Pp	Brown greasy fine ash.
100	1.72	Hinemaiaia Tephra within Pp	Scattered med-coarse white pumiceous ash within brown greasy fine ash.
200		Pp	Brown fine greasy ash.
40	1.96	Motutere Tephra within Pp	Pale brown med-fine ash in cream-cakes within brown greasy fine ash.
50		Pp	Brown fine greasy ash, strong brown staining at basal contact.
30			Grey coarse ash.
50	2.09	Mangamate Tephra (MT), Poutu Lapilli	Strong brown and grey lithic and poorly vesicular pumice lapilli with grey coarse ash base.
500		MT, Wharepu Tephra	Shower-bedded fine-med poorly vesicular pumice and lithic lapilli. Grey, strong brown and greyish brown. Strong brown and reddish brown basal 30 mm of fine lapilli, distinctive.
20			Yellow brown fine firm ash.
10			Dark grey coarse ash.
260		MT, Waihohonu Lapilli	Grey brownish grey and strong brown fine pumice and lithic lapilli. Strong shower bedding and alternating 10-50 mm layers dominated by the different colours.
400-500		MT, Oturere Lapilli	Coarse-med grey, brownish grey and strong brown pumice and lithic lapilli, shower-bedded but ungraded.
150			Yellow brown fine ash with yellow pumice fine lapilli scattered through a zone in the middle of the unit.
50	3.58	Pahoka Tephra	Distinctive platy olive grey fine pumice lapilli.
100			Dark yellowish brown fine ash with scattered fine yellow pumice lapilli.
50	3.73	Bullot Formation (BT), Pourahu Tephra	Pale brown coarse pumice lapilli.
50			Normally graded coarse ash-med lapilli, yellow pumice and grey lithic lapilli intermixed.
50			Brownish grey coarse ash and fine lapilli.
10			Yellow brown fine ash and scattered fine pumice lapilli.
10			Grey lithic coarse ash.
50			Pale brown pumice and grey lithic med lapilli
30			Grey med lithic lapilli.
30	3.96	BT, M1?	10 mm olive grey med ash over 10 mm yellow fine pumice lapilli, over 10 mm grey coarse ash.
40			Brownish grey fine-med lapilli.
30			Yellowish brown fine ash with scattered coarse pumice and lithic yellow and grey ash.

50			Strong brown and grey pumice and lithic med-coarse lapilli.
20			Yellowish brown fine pumice lapilli.
30			Grey lithic fine lapilli.
10			Yellow brown coarse pumice ash.
10			Grey fine lithic lapilli.
30			Strong brown and grey med pumice and lithic lapilli.
20			Brownish grey coarse pumice ash and fine lapilli.
100	4.30	BT, L17?	Strong brown and grey pumice and lithic med lapilli shower-bedded and ungraded.
30			Brownish grey pumice coarse ash and fine lapilli.
50			Brownish grey and grey fine pumice and lithic lapilli.
30			Dark grey coarse ash.
30			Brownish grey and grey coarse ash and fine lapilli.
120	4.56	BT, L16?	Strong brown coarse pumice lapilli with intermixed grey med lithic lapilli.
30			Brownish grey and grey coarse pumice and lithic ash.
50			Strong brown fine-med pumice lapilli and grey lithic fine lapilli.
150	4.79	BT, L15?	Strong brown and grey med pumice and lithic lapilli shower-bedded but ungraded.
0-10		Waiohau Tephra	Pocketing fine, white ash.
30			Brownish grey fine pumice lapilli.
20			Grey coarse ash.
50			Brownish grey, strong brown and grey fine pumice and lithic lapilli, normally graded.
20			Grey coarse lithic ash.
150		BT, L14	Strong brown med pumice lapilli, shower-bedded but ungraded.
50			Brownish grey coarse-med pumice ash.
10			Grey coarse ash.
4000+			Grey andesitic lava flow.
	9.10	93.106	Base into stream.

Section 18
Wharepu Stream, T20 465123
True left bank of stream 300m downstream of Section 17. Description taken from below L14? in Section 17.

Unit Depth (mm)	Cum. depth (m)	Correlation and samples taken	Description
1000	*c.* 5.0		Reworked ash and lapilli, in cm scale beds and layers and lenses. Grey brownish grey and pale olive brown pumice and lithic pebbles.
50			Dark purplish grey coarse ash and fine lapilli.
200			Reworked brownish grey coarse ash and fine lapilli wavy bedding.
40			Brownish grey fine lapilli.
10			Grey fine lapilli.
10			Brownish grey fine ash.
30			Reworked Brownish grey coarse ash and lapilli, wavy, fine bedding.
30			Strong brown and grey fine pumice and lithic med lapilli.
150			Reworked brownish grey coarse ash and fine lapilli mm scale beds and laminations.
20			Strong brown med pumice lapilli and grey lithic fine lapilli.
40			Reworked brownish grey ash and lapilli.
200	5.78		Reworked dark purplish grey coarse ash and fine lapilli, wavy and planar bedding.
40			Pale olive brown med-fine pumice lapilli.
400			Brownish grey reworked med-coarse ash and fine pumice lapilli mm scale wavy and planar beds.
250			Dark purplish grey reworked coarse lithic ash in planar cm scale beds.
50	6.52		Dark purplish grey fine lithic lapilli and olive brown pumice fine lapilli.
20			Olive brown coarse pumice ash and grey lithic coarse ash.
30			Grey coarse ash.
150			Strong brown med-coarse pumice lapilli with intermixed grey lithic fine lapilli.
250			Reworked brownish grey med-coarse pumice and lithic ash, in planar and wavy bedded layers.
50	7.02		Pale olive brown med pumice lapilli and grey lithic fine lapilli.
50			Grey and olive grey coarse-med ash.
20			Grey lithic med ash.
100			Shower-bedded olive brown and brownish grey coarse ash and fine pumice lapilli.
30			Brownish grey med-fine pumice lapilli.
10			Grey coarse lithic ash.
30			Strong brown fine pumice lapilli and grey fine lithic lapilli.
10			Brownish grey fine ash.
50	7.32		Brownish grey coarse pumice ash and fine lapilli.
1300			Reworked grey and pale olive brown coarse ash and fine pumice

			lapilli, planar and cross bedded on a mm scale.
150			Shower-bedded pale olive brown fine-med pumice lapilli.
1200			Grey sandy matrix diamicton. Brownish grey med-coarse sand supporting grey pebble to cobble clasts. Pinches and swells in thickness and has bouldery clasts concentrated in places.
1000+		R10	Silty matrix clast rich diamicton. Yellowish brown and pale brown firm silt matrix. Clasts mostly pebble-cobble in size and are multi-coloured pumice and lithics.
	10.97		Base into stream.

Section 22
Te Piripiri Stream, T20 453129
True right bank of southern tributary of stream, 20 m upstream of fork in southern sub-fork.

Unit Depth (mm)	Cum. depth (m)	Correlation and samples taken	Description
500		Taupo Ignimbrite	White and pale grey fine-coarse pumice ash with pumice lapilli and blocks. Charcoal fragments near base.
500		Mangatawai Tephra	Dark brownish grey and brown fine ash with paleosol development, lower half of unit contains several 10-30 mm thick grey and purplish grey ash beds. Abundant yellow brown beech leaves are preserved within some of the layers.
50	1.05	Papakai Formation (Pp)	Yellow brown and brown fine greasy ash with paleosol development.
20		"	Strong brown and yellow fine pumice lapilli and coarse ash.
50		"	Yellow brown fine ash.
20	1.14	Waimahia Tephra within Pp	Cream-cakes of white, fine rhyolitic ash within yellow brown and brown fine ash.
30		Pp	Yellow brown fine ash.
100	1.27	Hinemaiaia Tephra within Pp	White med-coarse pumice ash speckled within fine brown greasy ash.
400		Pp	Yellow brown and brown fine ash with intermixed grey lithic and poorly vesicular pumice fine lapilli near the base.
50	1.72	Mangamate Tephra (MT), Poutu Lapilli	Strong brown and grey pumice and lithic fine-med lapilli.
230		MT, Wharepu Tephra	Grey and brownish grey fine pumice and lithic lapilli and shower-bedded coarse ash. Distinctive strong brown basal 30 mm.
200		MT, Waihohonu Lapilli	Alternating coloured zones of grey and strong brown dominated coarse pumice and lithic ash, strong banded shower-bedding.
200		"	Grey and strong brown fine pumice and lithic lapilli and coarse ash, shower-bedded.
300		MT, Oturere Lapilli	Brownish grey and grey fine pumice and lithic lapilli and coarse ash.
50			Yellow brown fine ash with scattered fine yellow brown pumice lapilli.
50			Yellow brown fine ash with grey fine ash intermixed.
90	2.84	Pahoka Tephra	Olive grey platy blade like pumice fine lapilli and coarse ash. Normally graded onto olive grey and grey fine-med pumice and lithic lapilli.
100			Yellow brown fine pumice ash with scattered yellow brown fine pumice lapilli.
50	2.99	Bullot Formation (BT), Pourahu Member	Pale yellow and yellow brown coarse-med pumice lapilli.
50			Pale yellow and grey med-fine pumice and lithic lapilli and coarse ash.
30			Greyish brown fine pumice lapilli and coarse ash with few grey lithic fine lapilli.
30			Olive grey and grey pumice and lithic fine lapilli and coarse ash.
10			Pale brown fine ash and scattered fine lithic lapilli.
100	3.21		Brownish grey coarse ash with scattered med grey lithic lapilli.
50			Olive grey and yellow fine-med coarse pumice and lithic ash.
30			Olive brown fine ash and scattered fine pumice lapilli.
30			Grey coarse lithic ash and fine lapilli.
10			Olive brown coarse pumice ash and fine lapilli.
20			Grey fine lithic lapilli.
30			Olive brown fine-med pumice lapilli with few intermixed grey lithic fine lapilli.
10			Brownish grey med ash with scattered fine pumice lapilli.
50			Pale brown and yellow fine-med pumice lapilli with few grey lithic fine lapilli.
200	3.64		Brownish grey and yellow coarse pumice ash with intermixed grey lithic coarse ash.
30			Yellow brown fine pumice lapilli.
20			Grey fine lithic lapilli and coarse ash.
10			Brown fine ash.
70			Olive grey coarse lithic ash with scattered yellow fine pumice lapilli.
50			Strong brown and yellow fine pumice lapilli with few grey lithic fine lapilli.
100	3.92		Brownish grey coarse ash with scattered grey fine lithic lapilli.

50			Yellow and pale brown fine pumice lapilli with few grey lithic fine lapilli.
10			Grey fine lithic lapilli and coarse ash.
100			Yellow and yellow brown fine-med pumice lapilli with few grey lithic fine lapilli.
30			Brownish grey coarse ash with scattered yellow pumice and grey lithic fine lapilli.
30	4.14	93.6, Waiohau Tephra	White fine ash, semi-continuous layer with occasional yellow fine pumice lapilli mixed in.
20			Olive brown coarse pumice ash and fine lapilli.
20			Dark brownish grey fine ash with scattered fine yellow pumice lapilli.
50			Dark brownish grey fine pumice lapilli and coarse ash.
30			Grey and olive brown fine pumice and lithic lapilli.
20			Yellowish brown and yellow fine pumice lapilli.
50			Dark grey lithic coarse ash and fine lapilli.
30			Pale yellow med-fine pumice lapilli.
300	4.66		Shower-bedded grey and pale brownish grey coarse pumice and lithic ash.
100			Strong brown and yellow brown fine-med ungraded pumice lapilli.
500			Reworked pale brownish grey, grey and yellow pumice and lithic med-coarse ash. Layers of yellow and grey pumice and lithic lapilli also occur.
100	5.36		Pale olive brown med-fine pumice lapilli with scattered grey lithic fine lapilli.
100			Greyish brown coarse lithic ash.
150			Brownish grey coarse ash and fine pumice lapilli.
50			Pale brown fine pumice lapilli with scattered fine grey lithic lapilli.
1000		R10	Sandy matrix diamicton brownish grey matrix supporting clasts from pebble-boulder, clast rich in places.
1000+		"	Silt and sand-matrix diamicton. Greyish brown and brown matrix supporting heterolithologic, multicoloured clasts from pebble to large boulder.
	7.66		Base into stream.

Section 24
Te Piripiri Stream, T20 448137
True left bank of northern tributary stream, 1 km upstream from State Highway 1.

Unit Depth (mm)	Cum. depth (m)	Correlation and samples taken	Description
600		Makahikatoa Sand and Tufa Trig Formation with Kaharoa Tephra?	Brownish grey fine sand with interbedded 5-10 mm thick black fine-med ash beds interbedded throughout sand. At 300 mm depth white pocketing fine pumice ash preserved. Present soil development.
200		Taupo Ignimbrite	White pumice ash with interbedded pumice lapilli and blocks.
1000		Mangatawai Tephra	Dark brown and dark greyish brown greasy fine ash with paleosol development. In basal half of unit preserved several 10-20 mm black and purplish grey fine-med ash beds. Yellow brown beech leaves preserved within the ash.
50	1.85	Papakai Formation (Pp)	Greyish brown and yellow brown greasy fine ash.
20		"	Strong brown and pale yellow fine pumice lapilli.
200		"	Olive grey and greyish brown fine greasy ash.
20	2.09	Waimahia Tephra within Pp	Pocketing fine white pumice ash within greyish brown fine ash.
100		Pp	Greyish brown fine ash.
100	2.29	Hinemaiaia Tephra within Pp	White med-coarse pumice ash speckled within greyish brown fine greasy ash.
20		Pp	Strong brown fine pumice lapilli.
1000		"	Yellow brown greasy fine ash with strong brown and grey fine pumice and lithic lapilli intermixed toward the base of the unit.
100	3.41	Mangamate Tephra (MT), Poutu Lapilli	Strong brown and reddish brown lithic and poorly vesicular pumice lapilli.
1100		MT, Wharepu Tephra	Olive brown and greyish brown coarse pumice and lithic ash and fine lapilli. Shower-bedded and ungraded. Basal 100 mm strong brown fine pumice and lithic lapilli.
300	4.81	MT, Waihohonu Lapilli	Strong brown and grey fine-med pumice and lithic lapilli, reversely graded.
10			Brownish grey fine ash and fine pumice lapilli.
50			Dark grey med lithic shower-bedded ash.
60			Yellow brown and greyish brown fine ash and interbedded strong brown fine pumice lapilli.
40			Dark grey med-coarse lithic ash.
400	5.37	MT, Oturere Lapilli	Greyish brown, strong brown and grey fine-med pumice and lithic lapilli.
50			Yellow brown fine greasy ash and scattered grey fine lithic lapilli.
30			Pale yellow and grey fine pumice and lithic lapilli and coarse ash.

40			Pale brown fine ash with scattered fine yellow pumice lapilli.
50	5.54	Pahoka Tephra	Olive grey platy fine pumice lapilli.
20		"	Greyish brown fine ash with interbedded yellow fine pumice lapilli.
130		"	Olive grey platy coarse ash and fine-med pumice lapilli, normally graded.
10			Pale yellow and grey coarse ash.
500			Pale greyish brown silty and sandy matrix diamicton. Pebbles-boulders supported within the matrix. Poorly sorted and unbedded, erosive angular unconformity as basal contact.
200			Yellow brown fine ash and interbedded olive brown fine pumice lapilli.
50	6.45	Bullot Formation/ Pourahu Member	Pale yellow med pumice lapilli.
100		"	Olive brown and yellow fine-med pumice lapilli and coarse ash.
1000+		R07	Grey med sandy matrix diamicton. Greyish brown coarse-med sand matrix with clasts of pebble to small boulder.
	7.55		Base into stream.

Section 26

Te Piripiri Stream, T20 435129

True left bank of main northern tributary of stream 600 m upstream of where other tributaries join the main stream.

Description taken from base of Pahoka Tephra.

Unit Depth (mm)	Cum. depth (m)	Correlation and samples taken	Description
50	*c.* 3.0		Coarse pale yellow and grey pumice and lithic ash.
30			Olive brown fine pumice lapilli.
100			Yellow brown and pale brown fine ash with scattered grey lithic and pale brown pumice lapilli.
50	3.18	Bullot Formation (BT), Pourahu Member	Pale yellow and pale brown med-coarse pumice lapilli with scattered grey med lithic lapilli.
100			Pale brown and pale yellow coarse ash and fine pumice lapilli with scattered grey coarse lithic ash.
50			Greyish brown coarse pumice ash with grey lithic lapilli intermixed.
50			Yellow brown and grey pumice and lithic fine lapilli.
20			Grey lithic coarse ash.
20			Greyish brown coarse pumice and lithic ash.
30			Grey and greyish brown fine-med pumice and lithic lapilli.
30			Olive grey coarse-med pumice lapilli.
30			Grey coarse ash and fine lithic lapilli.
10	3.52	BT, M1?	Olive brown coarse pumice ash.
10		"	fine olive grey ash.
10			Grey bedded coarse lithic ash.
100			Reworked pale brown and olive brown fine-med ash.
50			Greyish brown and grey coarse pumice and lithic ash and fine lapilli.
30			Pale olive brown fine pumice lapilli and coarse ash with scattered grey lithic coarse ash.
10			Grey med lithic ash and scattered fine lithic lapilli.
30			Olive brown med-coarse pumice ash with scattered fine pumice lapilli.
50	3.79		Olive brown fine pumice lapilli with scattered grey lithic fine lapilli.
30			Yellow brown fine ash with scattered yellow brown fine pumice lapilli.
50			Grey and greyish brown coarse pumice and lithic ash and fine lapilli.
30			Dark brownish grey fine-med pumice lapilli.
30			Grey coarse ash.
50			Greyish brown and olive brown fine-med pumice lapilli with scattered fine grey lithic lapilli.
300	4.28		Brownish grey silty-matrix diamicton. Pebble clasts supported within the matrix, no bedding.
80			Yellow brown and strong brown med-coarse pumice lapilli with scattered grey lithic fine lapilli.
50			Brownish grey coarse pumice ash and fine lapilli.
100			Yellow and grey fine-med pumice and lithic lapilli.
20			Grey coarse lithic ash with scattered yellow fine pumice lapilli.
150			Grey fine-med ash with scattered yellow and yellow brown fine pumice lapilli.
50			Grey coarse lithic ash and fine lapilli.
150			Grey and greyish brown pumice and lithic, shower-bedded coarse ash and fine lapilli.
20			Yellow and yellow brown fine-med pumice lapilli.
20	5.02	93.8, Rerewhakaaitu Tephra	Grey coarse ash with scattered yellow pumice lapilli and interbedded white fine pumice ash 10 mm thick.
100			Reworked purplish grey med ash to fine lithic lapilli.
30			Grey med ash with scattered yellow fine pumice lapilli.
20			Pale brown and yellow pumice coarse ash with grey coarse lithic ash intermixed.

200			Reworked grey and brownish grey fine-med ash with layers of fine-med pumice lapilli within.
50			Yellow brown and olive brown fine-med pumice lapilli with scattered grey fine lithic lapilli.
300	5.72		Reworked black and purplish grey coarse lithic ash and fine lapilli, 10-20 mm planar bedding.
30			Pale olive brown fine-med pumice lapilli.
10			Grey coarse lithic ash.
10			Strong brown and pale yellow coarse pumice ash.
20			Greyish brown pumice med-coarse ash.
150			Reworked purplish grey and brownish grey lithic and pumice coarse ash and fine lapilli.
70			Strong brown and yellow fine-med pumice lapilli with scattered grey fine lithic lapilli.
150			Brownish grey bedded med-sands, 10-20 mm scale beds.
100	6.26		Pale olive brown and yellow fine pumice lapilli.
400			Brownish grey med sands with layers and lenses of brownish grey and yellow fine pumice lapilli. Planar and cross bedded.
10			Yellow brown silt.
600			Dark purplish grey coarse lithic ash and shower-bedded fine lapilli.
200			Pale olive brown and grey fine-med pumice and lithic lapilli.
1000		R09	Brownish grey sandy matrix diamicton. Pebble-boulder clasts supported within the matrix, grey clasts, unbedded. Angular unconformity as lower contact.
100			Strong brown and reddish brown fine soft pumice lapilli.
1000+	9.57	R10	Yellow brown silty and sandy matrix diamicton. Pinches and swells over lava flow. Clasts of pebble to huge lava boulders contained within matrix.
10000+			Grey andesite lava flow.
	19.57		Base into stream.

Section 30
Te Piripiri Stream, T20 486162
True left bank of stream where four-wheel-drive track crosses lower Stream, 1 km upstream from Tongariro River.

Unit Depth (mm)	Cum. depth (m)	Correlation and samples taken	Description
300		Ngauruhoe Formation	Brown and brownish grey fine-med ash, present soil development.
1000+		Taupo Ignimbrite	White fine-coarse pumice ash with pumice lapilli and blocks. Charcoal fragments near base and pink staining in places. Unit ramps over a hill and thickens in paleo-valley.
300	1.60	Mangatawai Tephra	Dark greyish brown fine ash with paleosol development lower half contains several grey and purplish grey fine-med ash, 10-20 mm layers.
100		Papakai Formation (Pp)	Yellow brown and brown fine ash with few scattered yellow brown fine pumice lapilli
20	1.72	Waimahia Tephra within Pp	White fine ash cream-cakes within fine greasy yellow brown ash.
30		Pp	Yellow brown fine ash.
50	1.80	Hinemaiaia Tephra within Pp	White coarse-med pumice ash scattered within yellow brown fine greasy ash.
50		Pp	Yellow brown fine ash.
20		"	Strong brown fine pumice lapilli.
100		"	Yellow brown fine ash.
20	1.99	Motutere Tephra within Pp	Pale brown and white fine pumice ash cream-cakes within yellow brown fine ash.
50		Pp	Yellow brown fine ash with scattered grey pumice lapilli. Strong brown stained base.
200-400		R02	Greyish brown med-coarse and matrix diamicton, angular grey and strong brown pebble-cobble clasts supported within the matrix. Very clast rich unit with abundant strong brown and pale brown pumice clasts present especially concentrated near the base of the unit.
250-400	2.84	Mangamate Tephra (MT), Poutu Lapilli	Strong brown and greyish brown and grey fine-med pumice and lithic lapilli, shower-bedded and ungraded.
400		MT, Wharepu Tephra	Upper 200 mm grey and olive grey med-coarse pumice ash shower-bedded, next 150 mm fine pumice lapilli of the same colour. Lower 50 mm strong brown fine pumice lapilli and coarse ash.
150		MT, Ohinepango Tephra?	Strong brown and grey pumice and lithic lapilli and coarse ash.
150			Brown and yellow brown fine, firm, greasy ash.
150			Grey and strong brown pumice and lithic med ash.
150			Grey and strong brown fine pumice and lithic lapilli and coarse ash.
10			Brown fine ash.
1000	4.85	MT, Waihohonu Lapilli	Alternating bands of grey and strong brown fine pumice and lithic lapilli and coarse ash. Shower-bedded but ungraded. Distinctive colour

			banding.
600-1000		R04	Grey and greyish brown fine sandy matrix diamicton. Pebble-cobble angular clasts, very clast rich almost clast supported. Unbedded, grey lithic clasts with occasional red and yellow clasts.
20			Yellow brown coarse pumice ash.
30			Grey lithic coarse ash.
300		MT, Oturere Lapilli	Reversely graded greyish brown, strong brown and grey fine-med pumice and lithic lapilli.
30	6.23	94.9, Karapiti Tephra	Olive grey fine-med ash containing thin (5 mm) white fine pumice ash.
4000+		R05-R09	Stacked sequence of diamicton units pinching in and out. Grey and greyish brown fine-coarse sandy matrices supporting clasts of pebble to boulders. Some of units have a horizontal fabric some are massive and unbedded. Lower units are very clast rich with huge boulders.
3000+		"	Yellow brown matrix diamicton, silt and sand matrix with pebble to large boulder clasts, grey clasts massive and unbedded.
	13.23		Base into stream.

Section 32
Mangatoetoenui Stream, T20 445145
True left bank of stream 1500 m upstream of State Highway 1. Description taken from below Papakai Formation.

Unit Depth (mm)	Cum. depth (m)	Correlation and samples taken	Description
200	*c.* 2.0	Mangamate Tephra (MT), Poutu Lapilli	Strong brown and grey fine-med pumice and lithic lapilli
1200		MT, Wharepu Tephra	Brownish grey and grey fine pumice and lithic lapilli and coarse ash. Shower-bedded but ungraded, lower 100 mm strong brown fine pumice and lithic fine lapilli.
20			Yellow brown firm, fine ash.
1000-2000		R03	Greyish brown diamicton. Fine-coarse sand matrix supporting clasts of pebble to boulder in size.
10			Yellow fine pumice lapilli.
30			Grey and strong brown coarse pumice and lithic ash.
200			Grey and strong brown mixed fine-med pumice and lithic lapilli.
100	5.56	MT, Waihohonu Lapilli	Alternating layers of grey and strong brown fine pumice and lithic lapilli.
3000-4000		R04-R09	Several diamicton units, greyish brown and grey sandy matrix supporting pebble to boulder clasts. Dominantly grey clasts, some units have planar fabric others are massive. Lower unit contains very large boulder clasts in a yellow brown and greyish brown silty and sandy matrix.
2000+			Grey andesite lava flow
	11.56		Base into stream.

Section 34
Mangatoetoenui Stream, T20 476160
True right bank of stream, next to the four-wheel-drive track and ford across the stream, 2 km downstream of S.H. 1.

Unit Depth (mm)	Cum. depth (m)	Correlation and samples taken	Description
400	*c.* 1.0	Mangatawai Tephra	Brown and dark brown fine ash with 20-30 mm beds of black and purplish grey med-fine ash.
100		Papakai Formation (Pp)	Yellow brown fine greasy ash with paleosol development.
30	1.13	Waimahia Tephra within Pp	White fine ash cream-cakes within yellow brown fine ash.
150		Pp	Olive brown and yellow brown greasy fine ash.
100	1.38	Hinemaiaia Tephra within Pp	White med-coarse pumice ash scattered within fine yellow brown ash.
80		Pp	Yellow brown fine greasy ash.
500		R01	Yellow brown, greyish brown and grey sandy matrix diamicton. Grey and few red scoriaceous pebble to small boulder clasts supported within the matrix.
150		Pp	Yellow brown fine ash with scattered yellow brown pumice and grey lithic fine lapilli.
40	2.15	Motutere Tephra within Pp	Fine pale brown and white pocketing pumice ash, almost a complete layer, within brown fine ash.
100		Pp	Greyish brown fine ash with scattered grey fine lithic lapilli.
200-400	2.65	Mangamate Tephra (MT), Poutu Lapilli	Strong brown, olive brown and grey fine pumice and lithic lapilli, shower-bedded but ungraded.
20			Grey coarse-med ash.
500		MT, Wharepu Tephra	Greyish brown and grey fine pumice lapilli and coarse ash, shower-bedded. Lower 150 mm strong brown fine pumice lapilli and coarse ash.

20			Yellow brown fine firm ash.
3000+		R03	Grey and pale olive grey sandy matrix diamictons. Pebble-boulder clasts supported within the matrix, mostly grey clasts, 2-3 units.
	6.19		Base into stream.

Section 35
Mangatoetoenui Stream, T20 476161
True left bank of stream, at 4WD ford in stream, 2 km downstream from State Highway 1.

Unit Depth (mm)	Cum. depth (m)	Correlation and samples taken	Description
400	*c.* 1.0	Mangatawai Tephra	Brown and dark brown fine ash with 20-30 mm thick layers of black and purplish grey fine-med ash.
50		Papakai Formation (Pp)	Yellow brown fine greasy ash.
20	1.07	Waimahia Tephra within Pp	White fine pumice ash cream-cakes within fine yellow brown fine ash.
50		Pp	Grey fine-med ash mixed within yellow brown fine ash.
100		"	Yellow brown fine ash.
50	1.27	Hinemaiaia Tephra within Pp	White med-coarse ash scattered within yellow brown fine ash.
150		Pp	Yellow brown fine greasy ash.
40	1.46	Motutere Tephra within Pp	Pale brown fine pumice ash cream-cakes within brown fine ash.
100		Pp	Greyish brown fine ash.
100-300	1.86	Mangamate Tephra (MT), Poutu Lapilli	Variable thickness strong brown and grey fine-med pumice lapilli.
400		MT, Wharepu Tephra	Upper 250 mm greyish brown and grey fine pumice and lithic lapilli and coarse ash, shower-bedded. Lower 150 mm strong brown fine pumice lapilli and coarse ash.
20			Yellow brown fine ash. Angular unconformity with sediments below.
0-1000		R03	Grey and brownish grey sandy matrix diamicton. Pebble-boulder grey lithic clasts supported by the matrix.
100	3.38	MT, Ohinepango Tephra	Coarse grey and strong brown ash, shower-bedded with alternating bands of colour.
800		MT, Waihohonu Lapilli	Strong brown yellow brown and grey fine-med pumice and lithic lapilli and coarse ash, shower-bedded in bands of colour.
500		R04	Grey brownish grey and grey sandy matrix diamicton, faint planar fabric observed, clasts sparse and pebble-small boulders supported within the matrix.
1000+		R05-R06	Grey sandy matrix diamictons (2 units) massive and unbedded pebble-small boulder clasts, grey lithic.
	5.68		Base onto track.

Section 37
Mangatoetoenui Stream, T20 465150
True left bank of stream 300 m downstream of State Highway 1, description from Poutu Lapilli.

Unit Depth (mm)	Cum. depth (m)	Correlation and samples taken	Description
300	*c.* 2.0	Mangamate Tephra (MT), Poutu Lapilli	Strong brown and grey fine-med pumice and lithic lapilli, shower-bedded.
30			Grey lithic med ash.
1000	3.03	MT, Wharepu Tephra	Brownish grey and grey fine-med pumice and lithic lapilli and coarse ash, strongly shower-bedded and ungraded. Basal 100 mm strong brown fine pumice lapilli.
20			Yellow brown fine, firm ash.
30			Grey med lithic ash.
800	3.88	MT, Waihohonu Lapilli	Grey, olive brown and strong brown fine-med pumice and lithic lapilli, shower bedded and ungraded.
50			Banded olive grey, brown and grey coarse-med pumice and lithic ash.
500	4.43	MT, Oturere Lapilli	Grey, brownish grey and strong brown fine-med pumice and lithic lapilli, shower-bedded.
100			Pale grey and pale brown fine ash with scattered soft pumice and lithic fine lapilli.
30			Greyish brown med ash and scattered fine lithic lapilli.
60			Upper half yellow brown fine-med ash, lower half yellow brown fine, soft pumice lapilli.
1000-1500	6.12	Pahoka Tephra	Over-thickened at this locality. Grey and olive grey platy coarse ash and fine lapilli, normally graded top. Lower 500-1000 mm olive grey, and pale yellow med-coarse pumice lapilli, with banded lapilli common.
200			Yellow brown fine ash.
300-500			Distinctive very pale yellow and grey pumice and lithic coarse ash and fine lapilli.
400	7.22	Bullot Formation, Pourahu	Pale yellow and pink fine ash, containing large pumice clasts of pale

		Member	yellow and pale olive, some clasts up to 250 mm diameter.
30		"	Pale yellow coarse-med pumice lapilli.
9000+		R07-R09	Grey, greyish brown and yellow brown matrix diamictons, several sandy matrix units. Pebble-boulder lithic clasts supported within matrix.
	16.25		Base obscured.

Section 38
Ohinepango Stream, T20 448164
True left bank of stream close to foot bridge across stream along track to Waihohonu Hut.

Unit Depth (mm)	Cum. depth (m)	Correlation and samples taken	Description
600		Makahikatoa Sand and Tufa Trig Formation	Brown and yellow brown fine-med sands with interbedded black and grey faint med-fine 5-10 mm ash layers.
200	0.80	Taupo Ignimbrite	White fine-coarse pumice ash with pumice lapilli and blocks intermixed. Occasional charcoal fragments.
400		Mangatawai Tephra	Dark brown and dark greyish brown fine greasy ash with soil development. Interbedded black and purplish black fine-med ash, some containing yellow brown beech leaves.
50		Papakai Formation (Pp)	Greyish brown greasy fine ash.
10	1.26	Waimahia Tephra within Pp	White pocketing fine ash within greyish brown fine ash.
400		Pp	Greyish brown and yellow brown fine greasy ash, with scattered occasional yellow brown and grey pumice and lithic fine lapilli.
50	1.71	Hinemaiaia Tephra within Pp	White med-coarse pumice ash scattered within greyish brown fine ash.
300		Pp	Yellow brown and greyish brown fine ash.
10	2.02	Motutere Tephra within Pp	Pale brown fine pumice ash within yellow brown fine ash.
150		Pp	Greyish brown and yellow brown fine ash with scattered fine grey lithic lapilli.
600	2.77	Mangamate Tephra (MT), Poutu Lapilli	Grey, olive grey and strong brown fine-med pumice and lithic lapilli, shower-bedded and normally graded.
10			Fine grey ash.
1200		MT, Wharepu Tephra	Olive grey and brownish grey fine-med pumice and lithic lapilli and coarse ash shower-bedded and ungraded. Lower 100 mm strong brown fine pumice lapilli.
20			Yellow brown fine, firm ash.
600			Reworked grey and strong brown med-coarse ash, planar bedded 20 mm scale.
50		MT, Waihohonu Lapilli	Grey and strong brown coarse pumice and lithic ash.
400	5.05	"	Olive grey, strong brown and brownish grey fine pumice and lithic lapilli and coarse ash, shower-bedded and reversely graded, banded strong brown and grey zones near base.
100		R04	Pale brownish grey silty and sandy matrix diamicton. Grey pebble clasts supported within matrix.
10			Yellow brown fine pumice lapilli.
10			Grey fine ash.
20			Grey coarse lithic ash.
30			Pale brown and yellow fine ash with scattered fine pumice lapilli.
20			Olive grey fine ash.
400	5.64	MT, Oturere Lapilli	Grey, brownish grey and strong brown fine-med pumice and lithic lapilli, shower-bedded but ungraded.
50			Pale yellow and grey fine-med ash grading into coarse pumice ash and lapilli of the same colours.
30			Yellow brown fine ash.
30			Yellow brown fine-med pumice lapilli with scattered grey fine lithic lapilli.
30			Greyish brown fine ash and fine lithic lapilli.
300	6.08	Pahoka Tephra	Upper 50 mm normally graded, olive grey platy med-coarse ash and fine lapilli. Lower 250 mm coarse-med pumice lapilli, olive grey and pale yellow with occasional banded pumice lapilli.
20			Yellow and grey coarse pumice and lithic ash.
250		R06	Grey sandy matrix diamicton. Grey pebble-cobble clasts supported within matrix, eroded lower contact.
20			Dark yellow brown fine ash.
100			Yellow brown and greyish brown fine pumice lapilli.
100			Yellow brown fine pumice ash.
20			Grey and greyish brown med lithic ash.
200	6.79	Bullot Formation, Pourahu Member	Poorly sorted yellow brown and pale brown fine-coarse lapilli. Lower 150 mm normally graded coarse pumice ash and fine lapilli of same colours, with scattered grey lithic coarse ash.
1500		R07	Grey and greyish brown sandy matrix diamicton. Pebble-boulder clasts supported within the matrix, grey, unbedded.

2500+		93.16a	Grey andesite lava flow
	10.79		Base into stream

Section 40
Waihohonu Stream, T20 415815
Moraine capped ridge behind Waihohonu Hut, at top of un-vegetated part of hill. Description taken from Oturere Lapilli.

Unit Depth (mm)	Cum. depth (m)	Correlation and samples taken	Description
500	c. 3.0	Mangamate Tephra, Oturere Lapilli	Greyish brown and grey fine-med pumice and lithic lapilli, shower-bedded and ungraded.
100			Yellow brown fine ash with scattered pale yellow and yellow brown fine pumice lapilli.
100	3.20	Pahoka Tephra	Pale olive grey and yellow fine pumice lapilli and coarse ash. Normally graded and platy coarse ash at top. Abundant yellow pumice.
10			Grey fine ash.
50			Brownish grey coarse pumice ash and fine pumice lapilli.
50			Greyish brown fine ash with scattered fine yellow pumice lapilli.
30	3.34	Bullot Formation, Pourahu Member?	Yellow brown med-fine pumice lapilli.
300			Greyish brown and grey bedded sands and pebbles.
100			Yellow, strong brown and grey med-coarse pumice and lithic lapilli.
30			Yellow brown and greyish brown med-coarse pumice ash.
100			Pale brown, yellow and greyish brown fine pumice lapilli with scattered fine grey lithic lapilli.
30			Grey and pale yellow fine pumice and lithic lapilli and coarse ash.
50			Grey, pale brown, and brownish grey fine-med pumice and lithic lapilli.
10	3.96	Waiohau Tephra	White fine pumice ash cream-cakes.
100			Black and greyish brown coarse lithic ash and fine lapilli.
500+			Grey and greyish brown sandy matrix diamicton or till. Grey pebble-boulder clasts.
	4.56		Base obscured

Section 41
Ohinepango Stream, T20 461170
True right bank of stream in a deep rut carved by a small tributary stream. 50 m west of State Highway 1.

Unit Depth (mm)	Cum. depth (m)	Correlation and samples taken	Description
400		Taupo Ignimbrite	White fine-coarse pumice ash with intermixed pumice lapilli and blocks. Charcoal fragments contained near base of unit.
500		Mangatawai Tephra	Brown and dark brown fine ash with paleosol development, Lower half has several interbedded black and purplish grey 20-30 mm, fine-med ash beds. Yellow brown beech leaves contained within some of the layers.
50		Papakai Formation (Pp)	Brown fine greasy ash.
10	0.96	Waimahia Tephra within Pp	Pocketing white fine pumice ash within brown fine ash.
200		Pp	Brown and yellow brown fine greasy ash.
60	1.22	Hinemaiaia Tephra within Pp	White med-coarse ash scattered within yellow brown fine ash.
250		Pp	Yellow brown fine ash with scattered fine yellow pumice lapilli.
10	1.48	Motutere Tephra within Pp	Pale brown fine pumice ash within yellow brown fine ash.
150		Pp	Yellow brown fine ash with scattered grey pumice and lithic lapilli.
400	2.03	Mangamate Tephra (MT), Poutu Lapilli	Grey, strong brown and olive brown fine-med pumice and lithic lapilli, shower-bedded.
20			Grey med lithic ash.
400		MT, Wharepu Tephra	Grey and brownish grey fine pumice and lithic lapilli, shower-bedded and ungraded. Lower 150 mm strong brown fine pumice lapilli.
10			Yellow brown fine ash.
100		MT, Ohinepango Tephra	Alternating beds of grey and strong brown coarse pumice and lithic ash.
10			Grey fine ash.
80		MT, Waihohonu Lapilli	Grey and strong brown fine pumice and lithic lapilli, alternating colour layers.
20			Black and dark grey coarse ash.
20			Pale brown and pale yellow fine ash with soft fine-med pumice lapilli.
20			Olive grey fine-med ash and fine lapilli, pumice and lithic.
500	3.21	MT, Oturere Lapilli	Grey, brownish grey and strong brown fine-med pumice lapilli, shower-bedded but ungraded.
50			Pale brown fine ash.
50-100			Pale yellow and grey coarse ash, pumice and lithic.
30			Pale brown fine ash.

30			Yellow and yellow brown soft pumice lapilli.
300	3.72	Pahoka Tephra	Pale olive grey and pale yellow fine-coarse pumice lapilli, shower bedded and normally graded. Platy coarse ash near top.
20			Pale yellow and grey coarse pumice and lithic ash.
300-500		R06	Yellow brown fine sandy diamicton, with intermixed large pumice blocks 200 mm diameter, as well as lithic pebbles and cobbles supported within the matrix.
100			Yellow brown and strong brown fine pumice lapilli and coarse ash, shower-bedded.
30			Yellow brown fine ash with scattered fine pumice lapilli.
100	4.47	Bullot Formation, Pourahu Member	Pale yellow and yellow brown fine-coarse pumice lapilli, with scattered grey fine lithic lapilli.
3000		R07	Clast rich diamicton, large boulder-pebble clasts with small amount of sandy and pebbly matrix. Grey, greyish brown and occasional red clasts and matrix. Erosive base, unconformity.
600			Bedded sands, silts and gravels planar and cross-bedded, grey, greyish brown and strong brown.
40	8.11	93.17, Kawakawa Tephra	White fine pumice ash shower-bedded.
400			Grey and brownish grey bedded sands.
1000	9.51	R10	Yellow brown and pale yellow greasy silt matrix diamicton, multi-coloured pebble-large boulder, lithic and pumice clasts, highly weathered or altered clasts.
1000		R10	Strong brown and reddish brown silty matrix diamicton, with abundant reddish and grey lava bomb clasts within it. Semi-detached bomb clasts.
450			Bedded fine sands and silts, cross-bedded. Brown and brownish grey with scattered yellow fine pumice lapilli.
80	11.04		Yellow brown and strong brown med-coarse pumice lapilli.
500			Grey and olive grey bedded sands with scattered yellow brown fine pumice lapilli.
100			Strong brown and yellow brown fine-med pumice lapilli with scattered grey lithic lapilli.
1000+		R11	Greyish brown and grey silt and sand matrix diamicton, with pebble-boulder, grey lithic clasts supported within the matrix.
	12.64		Base into stream.

Section 42

Ohinepango Stream, T20 462172

True right bank of stream, 50 m upstream from joining with Waihohonu Stream, immediately west of State Highway 1. Description taken from below Papakai Formation.

Unit Depth (mm)	Cum. depth (m)	Correlation and samples taken	Description
200	*c.* 2.0	Mangamate Tephra (MT), Poutu Lapilli	Strong brown and grey pumice and lithic fine-med lapilli, shower-bedded, eroded upper contact.
500		MT, Wharepu Tephra	Grey and brownish grey shower-bedded and ungraded fine-med pumice and lithic lapilli and coarse ash. Lower 200 mm strong brown fine pumice lapilli.
20			Yellow brown fine ash.
650	3.17	MT, Waihohonu Lapilli	Grey, strong brown, and olive grey fine pumice and lithic lapilli, shower-bedded. Lower part has alternating strong brown and grey dominated bands.
10			Greyish brown and pale grey fine pumice lapilli.
10			Brownish grey med-coarse ash.
450	3.64	MT, Oturere Lapilli	Grey, olive brown and yellow brown fine-med pumice lapilli, shower-bedded but ungraded.
80			Yellow brown and pink fine ash with interbedded med-coarse yellow and pale brown soft pumice lapilli.
40			Pink, grey and pale yellow med-coarse pumice ash.
120	3.88	Pahoka Tephra	Grey and pale yellow fine pumice and lithic lapilli and coarse ash.
50			Pale yellow fine ash and fine-med pumice lapilli.
2000-3000			Grey andesitic lava flow.
2000		R10	Strong brown silty matrix diamicton, large scoriaceous bombs-pebbles supported within the matrix, grey and reddish coloured clasts.
50			Strong brown fine pumice lapilli and coarse ash.
1000+			Brown and brownish grey bedded silts and fine sands with layers and lenses of multicoloured pumice pebbles.
	9.98		Base obscured

Section 44
Waihohonu Stream, T20 464174
Large road cutting on the western side of State Highway 1, immediately north of the bridge over the Waihohonu Stream.

Unit Depth (mm)	Cum. depth (m)	Correlation and samples taken	Description
400		Ngauruhoe Formation and Tufa Trig Formation	Dark brownish grey fine-med, friable ash with indistinct 10 mm thick grey and black fine-med ash beds.
400-1000	1.40	Taupo Ignimbrite	White fine-coarse pumice ash with intermixed pumice lapilli and blocks, charcoal fragments also present.
450-500		Mangatawai Tephra	Dark brown and greyish brown fine greasy ash with paleosol development, lower half of unit contains several black and purplish grey fine-med ash layers, often with preserved yellow brown beech leaves.
200		Papakai Formation (Pp)	Brown and greyish brown fine ash with paleosol development.
50		"	Greyish brown fine ash with pocketing black fine-med ash.
20	2.17	Waimahia Tephra within Pp	Cream-cakes of fine white pumice ash within brown fine greasy ash.
100		Pp	Yellow brown fine greasy ash with scattered fine yellow brown soft pumice lapilli.
50	2.32	Hinemaiaia Tephra within Pp	White med-coarse pumice ash scattered within yellow brown fine ash.
650		Pp	Yellow brown greasy fine ash with scattered yellow and grey fine pumice and lithic fine lapilli, more concentrated near the base. Uneven lower contact.
350			Reworked strong brown and grey pumice and lithic fine lapilli and coarse ash, eroded upper contact, planar and cross-bedded.
400	3.42	Mangamate Tephra (MT). Poutu Lapilli	Strong brown and grey fine pumice and lithic lapilli, shower-bedded but ungraded.
600		MT, Wharepu Tephra	Upper 450 mm, grey, greyish brown and some strong brown fine-med pumice lapilli, shower-bedded but ungraded. Lower 150 mm strong brown fine pumice lapilli.
20			Yellow brown fine, firm ash.
30		MT, Ohinepango Tephra	Greyish brown and strong brown med-coarse pumice and lithic ash.
30			Greyish brown reworked fine-med pumice and lithic lapilli, within med grey and greyish brown ash.
1000	5.10	MT, Waihohonu Lapilli	Strong brown, grey and greyish brown fine-med pumice and lithic lapilli and coarse ash with strong shower-bedding giving a banded colour appearance.
150			Greyish brown fine-med sand, with mixed grey sub-rounded pebbles, and occasional cobbles.
20			Strong brown and brown coarse ash and fine pumice lapilli.
450	5.72	MT, Oturere Member	Grey, greyish brown and strong brown med-fine pumice and lithic lapilli, shower-bedded but ungraded.
60			Yellow brown and pale brown fine ash with scattered grey-white soft pumice fine lapilli.
20			Yellow brown and strong brown fine pumice lapilli and coarse ash.
100-150			Grey and greyish brown sands and fine gravels planar bedded, sub-rounded clasts.
10			Strong brown fine-med pumice lapilli.
30			Greyish brown sand and fine, sub-rounded gravel.
350	6.34	Pahoka Tephra	Olive grey and pale yellow fine-med pumice lapilli and coarse ash, normally graded, upper part has very platy lapilli, and lower part contains occasional banded olive grey and pale yellow pumice lapilli.
20			Strong brown and yellow brown coarse pumice ash.
1200			Grey and greyish brown bedded sands and fine-coarse gravels, planar bedded 100-300 mm scale, sub-rounded clasts.
600-1300	8.86	R06	Greyish brown sandy matrix diamicton, abundant boulder-cobble clasts in upper half of unit and dominantly pebble clasts within the lower half, clasts supported within the matrix. Dominantly grey with occasional red lithic clasts.
50			Pale brown fine ash.
100			Pale brown fine-med pumice lapilli.
100	9.11	Bullot Formation, Pourahu Member	Pale brown and pinkish fine ash containing abundant coarse-med pumice lapilli within.
100-200		"	Pale yellow and pale brown fine-med pumice lapilli and coarse ash with scattered grey coarse lithic ash.
10			Brown fine silty layer.
3000+		R07	Greyish brown sandy and silty matrix diamicton. Pebble-large boulder clasts supported within the matrix, dominantly grey with occasional red clasts. Diamicton pinches out over lava, laps up onto side of lava. Angular unconformity with coverbeds below diamicton.
2000+		R09/T3	Brownish grey sand and silt matrix diamicton, dominantly multi-coloured and grey pumice and lithic pebble clasts with few grey lithic

			boulders, unconformable upper contact.
400	14.72	Kawakawa Tephra	Shower-bedded white and pale pink fine-med pumice ash. Upper 150 mm massive fine pale pink ash, onto 100 mm pale brown med ash with coarse ash horizons and accretionary lapilli present up to 15 mm in diameter. Onto 30 mm coarse white pumice ash, onto 20 mm pale brown fine ash, onto 30 mm fine white ash.
200			Dark greyish brown fine-med ash.
50			Yellow brown fine-coarse pumice lapilli intermixed within the scoriaceous top of the lava flow.
30000+		93.19	Grey andesite lava flow with red scoriaceous top, highly brecciated top.
	44.97		Base into stream on opposite side of road.

Section 45
Upper Waikato Stream, T20 461096
True left bank of northern tributary 500 m upstream of State Highway 1. Description taken from M1 marker sequence in Bullot Formation.

Unit Depth (mm)	Cum. depth (m)	Correlation and samples taken	Description
10	*c.* 4.0	Bullot formation, M1	Grey fine ash.
10		"	Yellow brown coarse pumice ash.
20		"	Yellow brown fine ash with scattered grey coarse lapilli.
30			Grey fine lithic lapilli and coarse ash.
30			Yellow brown coarse pumice ash and fine lapilli.
20			Grey coarse lithic ash.
40			Grey and yellow brown coarse ash and fine pumice and lithic lapilli.
150			Grey and strong brown fine-med pumice and lithic lapilli.
50			Grey and purplish grey med ash.
200	4.55		Strong brown fine-med pumice lapilli, shower-bedded with scattered grey lithic fine lapilli.
30			Grey and strong brown lithic and pumice med ash.
20			Strong brown and grey fine-med pumice and lithic lapilli.
50			Grey and brownish grey coarse-med pumice and lithic ash.
100	4.75		Strong brown and brownish grey fine-med pumice lapilli with scattered grey fine lithic lapilli.
20			Brownish grey med ash.
20			Strong brown and yellow brown fine pumice lapilli with scattered grey fine lithic lapilli.
20			Pale grey lithic med ash.
20			Strong brown fine-med pumice lapilli.
20			Purplish grey lithic coarse ash.
10			Brown coarse ash and fine pumice lapilli.
40			Purplish grey coarse ash with scattered yellow brown fine pumice ash.
20			Strong brown and yellow brown fine pumice lapilli with scattered fine grey lithic lapilli.
20			Brownish grey and grey coarse lithic and pumice ash.
30			Yellow brown and brown med pumice ash with sparse scattered grey fine lithic lapilli.
50	5.02	Waiohau Tephra?	Brownish grey and grey coarse pumice and lithic ash, contains a 10-20 mm pocketing white fine pumice ash.
100			Grey and brownish grey coarse pumice and lithic ash with scattered yellow brown and strong brown fine pumice lapilli.
80			Strong brown fine-med pumice lapilli, shower-bedded with scattered grey fine lithic lapilli.
20			Black lithic med-coarse ash.
400	5.64	Hinuera Formation	Bedded silt, sand and gravels, wavy and planar bedding 20-100 mm scale. Intermixed white fine pumice ash in places. Greyish brown and pale brown.
600			Brownish grey sand and fine gravel. Planar and wavy bedding on a 10-20 mm scale, unconsolidated with pumice and lithic pebbles.
500	6.74	R10	Eroded upper contact. Strong brown sand and silt matrix diamicton. Multi-coloured pebble and cobble clasts supported by the matrix. Clasts highly weathered lithic and pumice, heterolithologic.
100		"	Yellow brown silt matrix supporting clasts as described in the unit above.
1000		"	Greyish brown massive sandy matrix diamicton unit with fine pebbly clasts, dominated by grey lithic and pumice clasts with multi coloured pebbles also.
600	8.44	"	Yellow brown and fine sand and silt matrix diamicton with multi-coloured cobble and boulder clasts.
300			Bedded brown and greyish brown sands and gravels, wavy and planar bedded.
200			Pale brown and brown fine sands and silts 10-20 mm scale wavy and

			planar bedding.
200			Grey and brown sands and gravels cross bedded.
700		R10	Pale brown and pale yellow brown silt matrix diamicton with cobble and pebble clasts supported within the matrix.
3000	12.84		Bedded fluvial sands, gravels and silt layers, grey lithic and pumice pebbles. Well developed cross-stratification in some layers. Lenses of yellow pumice lapilli interbedded in places, and some layers slightly hardened.
250	12.99	93.23	Yellow brown pumice fine-med lapilli with few scattered fine grey lithic lapilli.
2000+			Bedded silt, sand, and gravel in lenses and layers. Yellow brown and brown silts with grey and greyish brown sands and gravels.
	14.99		Base into stream.

Section 46
Upper Waikato Stream, T20 464098
True left bank of northern tributary of stream, 300 m upstream from State Highway 1. Description taken from lowest Bullot Formation tephra preserved.

Unit Depth (mm)	Cum. depth (m)	Correlation and samples taken	Description
80	*c.* 6.0		Yellow brown and reddish brown fine-med pumice lapilli with scattered fine grey lithic lapilli.
20			Grey med-coarse ash.
300			Yellow brown, bedded fine med sand and silt, with occasional yellow brown fine pumice pebbles, weak planar beds.
500			Grey lithic, bedded sands and fine-coarse gravels, mostly grey lithic clasts with occasional red clast, cross-bedding, eroded lower contact.
50-200	7.02	R10	Variable top brown silt and sand matrix diamicton, containing multi-coloured pumice and weathered lithic pebble clasts supported within the matrix.
200		"	Yellow brown silt and fine sand matrix with fine pebbles-boulders supported within the matrix.
500		"	Massive pale brown silt and sand matrix diamicton with multi-coloured pumice and highly weathered lithic pebble-cobble clasts supported within the matrix.
2500			Strong brown, brownish grey and purplish grey bedded sands and gravels, well developed planar and cross-bedding on a 10-50 mm scale. Eroded lower contact.
0-50	10.27	93.24	Strong brown and yellow brown fine pumice lapilli, soft and porous.
200			Grey bedded sands and gravels as above.
200		93.25	Strong brown reversely graded coarse pumice ash-med lapilli, with scattered grey lithic fine lapilli.
10			Brown fine ash.
500	11.18	93.26, Marker Unit 1	Grey, olive grey and yellow coarse-med pumice and lithic ash, shower-bedded with distinctive banded appearance. Lower 100 mm coarse ash and fine pumice and lithic lapilli.
20	11.20	93.27, Marker Unit 1	Yellow fine pumice lapilli and coarse ash.
400			Brown and greyish brown bedded sands and gravels, planar and cross-bedded with multi-coloured heterolithologic pumice and lithic pebbles in layers and lenses.
500+		R11	Massive yellow brown and grey sand and silt matrix diamicton, grey and greyish brown lithic pebble-cobble clasts supported by the matrix.
	12.10		Base into stream.

Section 47
Upper Waikato Stream, T20 465099
True left bank of northern tributary, 100m upstream from State Highway 1, description taken from below Marker Unit 1.

Unit Depth (mm)	Cum. depth (m)	Correlation and samples taken	Description
2000	*c.* 10		Grey, and dark grey bedded sands and coarse gravels, wavy and planar bedding 200 mm scale beds.
1000			Grey and brownish grey bedded sands and fine gravels, cross-bedded and planar bedded on a 20-50 mm scale.
2000			Brown and strong brown bedded sands, silts and gravels, planar and cross-bedded with layers and lenses of multi-coloured pumice and lithic clasts, yellow pumice and grey lithic clasts dominant, 10-100 mm scale beds.
400	13.40	93.28	Yellow and yellow brown soft fine-med pumice lapilli, with sparse scattered grey lithic fine lapilli.
1500			Firm, bedded sands silts and gravels, grey and greyish brown planar and cross-bedded, 10-100 mm scale.

1000+		R11	Very hard grey and greyish brown sandy matrix diamicton. Grey pebble-boulder clasts supported within the matrix. Faint planar fabric.
	15.90		Base into stream.

Section 50
Tongariro River, T20 494965
Road cutting and cliff exposure on the true left bank of river at the end of Waipakihi Road near the river gauging station.

Unit Depth (mm)	Cum. Depth (m)	Correlation and samples taken	Description
1500		Taupo Ignimbrite	Fine-coarse white pumice ash with mixed pumice lapilli and blocks. Charcoal fragments contained within the lower part of the unit.
300		Mangatawai Tephra	Dark brown and greyish brown fine ash with paleosol development. Interbedded within this are several 10-20 mm beds of fine-med black and purplish grey ash. Some ash beds contain Yellow brown beech leaves preserved within.
600	2.40	Papakai Formation	Yellow brown and brown fine greasy ash with paleosol development and scattered yellow brown and grey fine pumice lapilli.
400-500		Mangamate Tephra (MT), Poutu Lapilli	Variable upper contact. Yellow brown and grey fine-med poorly vesicular pumice and lithic lapilli, shower-bedded and ungraded.
10			Black med lithic ash.
300-350	3.26	MT, Wharepu Tephra	Grey and greyish brown fine pumice and lithic lapilli and coarse ash, shower-bedded but ungraded. Basal 50 mm strong brown fine pumice.
10			Yellow brown fine, firm ash.
250-300		MT, Waihohonu Lapilli	Grey and strong brown alternating coloured. Shower-bands of pumice and lithic fine lapilli and coarse ash.
10			Brown fine ash.
250	3.83	"	Grey and strong brown fine pumice and lithic fine lapilli and coarse ash, shower-bedded and normally graded.
20			Pale yellow fine pumice lapilli and coarse ash.
50			Grey fine lapilli and coarse lithic ash.
20			Pale yellow and grey pumice and lithic coarse ash and fine lapilli.
10			Grey coarse lithic ash.
20			Yellow brown and brown fine ash with scattered fine yellow pumice lapilli.
20			Grey coarse-med lithic ash.
300	4.27	Mt, Oturere Lapilli	Grey and pale yellow fine-med pumice and lithic lapilli, shower-bedded and ungraded.
50			Brown and yellow brown greasy fine ash.
200		Pahoka Tephra	Grey and olive grey fine pumice lapilli and coarse ash, platy coarse ash at top of unit, normally graded. Occasional banded lapilli present, olive grey and pale yellow bands.
10			Pale brown coarse pumice ash.
10			Grey med-coarse lithic ash.
100-200			Yellow brown fine ash with scattered yellow fine pumice lapilli.
150-200	4.94	Bullot Formation, Pourahu Tephra	Yellow brown and pale yellow fine-med pumice lapilli and coarse ash, normally graded.
50			Grey lithic fine lapilli.
1500-2000		R07	Grey and yellow brown sand and silt matrix diamicton. Upper 1000 mm grey pebble-boulder clasts, very clast rich and almost clast supported in places. Lower part finer grained with matrix mostly supporting pebble clasts, grey and olive grey lithic and sparse poorly vesicular pumice. Lower part has faint planar fabric.
800		R08-R09	Yellow brown silt and grey sand matrix diamicton, planar fabric preserved. Yellow, strong brown and grey fine pebbly pumice and lithic clasts supported by the matrix.
1000	8.74	"	Yellow brown and greyish brown silt and sand matrix. Large boulder-pebble clasts supported by the matrix, reversely graded, upper part dominated by boulders and lower part by cobbles-pebble clasts.
4000-5000		"	Grey and brownish grey sandy and silt matrix diamicton with large boulder-pebble clasts. Massive and unbedded. Lower 2000 mm finer grained with largest clasts dominantly grey cobbles. Sharp contact to unit below.
1000+	14.70	"	Grey and greyish brown firm sandy matrix diamicton, grey angular lithic pebble-cobble clasts supported by the matrix. Faint planar fabric preserved.
5000			Obscured
2000+	21.70		Bedded and tilted greywacke rock, with base into river.

Section 51
Tongariro River, T20 496157
Large road cutting along the Waipakihi Road, after the crossing of the unnamed stream on the top of the large high surface.

Unit Depth (mm)	Cum. Depth (m)	Correlation and samples taken	Description
300		Ngauruhoe Formation	Brown greasy fine-med ash with present soil development.
200-1000		Taupo Ignimbrite	White fine-coarse pumice ash with pumice lapilli and blocks intermixed. Charcoal fragments intermixed near base of unit.
200-300	1.60	Mangatawai Tephra	Dark brown and greyish brown fine ash with paleosol development, and several interbedded black and purplish grey fine-med ash beds, 10-20 mm thick, some of the beds contain yellow brown beech leaves preserved within.
80		Papakai Formation (Pp)	Brown and yellow brown fine greasy ash with occasional scattered fine yellow pumice lapilli.
20-30	1.71	Waimahia Tephra within Pp	Pocketing white fine ash within yellow brown fine ash.
70		Pp	Yellow brown fine greasy ash.
100	1.88	Hinemaiaia Tephra within Pp	White med-coarse pumice ash scattered within yellow brown greasy fine ash.
250		Pp	Yellow brown greasy fine ash with scattered fine yellow pumice lapilli.
20-30	2.16	Motutere Tephra within Pp	Pale brown fine pumice ash cream-cakes.
100		Pp	Yellow brown fine ash with scattered grey fine lithic and pumice lapilli.
400-600	2.86	Mangamate Tephra (MT), Poutu Lapilli	Wavy upper contact. Strong brown, grey and greyish brown fine pumice and lithic lapilli, shower-bedded and weakly reversely graded.
10			Grey med lithic ash
300-400		MT, Wharepu Tephra	Grey and greyish brown fine pumice and lithic lapilli and coarse ash, shower-bedded and ungraded. Lower 100 mm strong brown fine pumice lapilli.
10			Brown fine firm ash.
20-50	3.33	Poronui Tephra	Grey med-coarse ash containing pocketing fine white pumice ash.
150			Alternating shower-bands of grey and strong brown med-coarse pumice and lithic ash.
200	3.68	MT, Waihohonu Lapilli	Strong brown, grey and greyish brown alternating bands of fine pumice and lithic lapilli.
10			Brown fine ash.
1000		"	Grey and strong brown coarse ash and fine-med pumice lapilli, shower-bedded with bands of alternating colours, ungraded.
10			Grey fine ash.
10-20			Grey and yellow brown pumice and lithic med ash.
40			Yellow brown fine ash with scattered grey and yellow brown fine pumice lapilli.
500	5.26	MT, Oturere Lapilli	Grey, greyish brown and strong brown fine-med pumice and lithic lapilli, shower-bedded but ungraded.
50-100			Yellow brown fine ash with scattered fine yellow and yellow brown pumice lapilli.
20			Yellow brown fine pumice lapilli.
50			Yellow brown fine ash.
400	5.83	Pahoka Tephra	Normally graded coarse ash-med pumice lapilli, olive grey and pale brown, with scattered banded pumice lapilli with grey and pale brown stripes. Platy pumice coarse ash at the top of the unit.
10			Pale yellow and grey pumice and lithic coarse ash.
40			Yellow brown fine ash.
50	5.93	Bullot formation, Pourahu Member?	Yellow brown pumice lapilli and coarse ash.
50			Yellow brown fine ash.
40			Strong brown and pale yellow fine-med pumice lapilli, with scattered grey fine lithic lapilli.
40			Grey and pale yellow coarse pumice and lithic ash.
30-40			Strong brown, pale yellow and yellow brown fine-med pumice lapilli.
50	6.17		Pale brown and pale greyish brown fine ash with scattered fine grey lithic lapilli.
20			Pale yellow and yellow brown pumice lapilli with scattered grey lithic coarse ash.
20			Grey fine ash.
20			Yellow brown fine pumice lapilli with scattered fine grey lithic lapilli.
50			Grey and greyish brown med-coarse lithic and pumice lapilli.
10			Olive grey and brown fine ash.
40			Greyish brown and purplish grey coarse lithic ash and fine lapilli.
10			Pale yellow coarse pumice ash.
20			Grey coarse lithic ash.
30	6.39		Yellow brown fine-med pumice lapilli with scattered grey lithic fine lapilli.
20-50			Grey coarse lithic ash.

50			Pale yellow fine pumice lapilli, reversely graded with grey coarse lithic ash.
20			Grey coarse ash and fine lithic lapilli.
10			Pale greyish brown and yellow brown fine ash with scattered yellow brown fine pumice lapilli.
300			Grey and pale yellow reworked pumice and lithic coarse ash and fine lithic lapilli, wavy and planar beds.
40	6.86		Strong brown fine pumice lapilli with scattered grey fine lithic lapilli.
30			Greyish brown and grey coarse-med ash.
100			Strong brown med-fine pumice lapilli with scattered grey fine lithic lapilli and med ash, shower-bedded and ungraded.
50-100			Purplish black coarse lithic ash and fine lapilli.
50			Grey and greyish brown med-coarse lithic ash.
40	7.18	Waiohau Tephra	Greyish brown med ash with interbedded white fine pumice ash.
10			Purplish grey med lithic ash.
300			Alternating layers of greyish brown and olive grey coarse lithic and pumice ash and fine lapilli.
30			Strong brown and pale yellow fine pumice lapilli.
200	7.72		Purplish black coarse lithic ash.
200			Greyish brown, grey and yellow brown fine-med shower-bedded pumice lapilli.
100			Pale yellow brown and brown fine-med ash with scattered coarse pumice ash.
50			Yellow and grey coarse pumice and lithic ash.
50			Brown and greyish brown fine ash.
30			Greyish brown and pale brown fine pumice lapilli with scattered grey lithic fine lapilli.
100	8.25		Normally graded grey and pale olive brown coarse pumice ash and fine lapilli.
50			Greyish brown and pale brown med-coarse pumice ash with scattered grey lithic med ash.
30			Pale yellow pumice fine lapilli with scattered grey lithic coarse ash.
30			Greyish brown fine ash.
10			Purplish grey fine ash.
150-200	8.57		Reversely graded yellow brown fine-med pumice lapilli with scattered fine grey lithic lapilli.
50			Pale yellow brown normally graded coarse pumice ash and fine lapilli, with scattered grey lithic coarse ash.
0-1000	9.62	R10	Brown silt and sand matrix diamicton, sparse grey angular lithic pebble-large boulder clasts supported by the matrix, angular unconformable lower contact.
500-1000		"	Brownish grey and brown sand and silt matrix firm diamicton. Weak planar fabric preserved and pebble clasts supported by the matrix. Grey lithic and yellow pumice clasts.
400			Greyish brown bedded sands and gravels, cross-bedded, sub-rounded grey lithic gravels.
1000	12.02	"	Massive firm yellow brown silt and sand matrix diamicton. Pebble-cobble clasts supported by the matrix, grey lithic and abundant yellow pumice clasts. At top of unit abundant yellow pumice pebbles with a faint horizontal fabric, the rest of the unit is massive and unbedded.
20-30	12.05	94.13	Yellow brown and yellow coarse pumice ash with scattered grey lithic coarse ash.
40			Brown fine ash.
3000		R11	Massive firm fine-grained diamicton. Brown silt and sand matrix supporting clasts of grey and red lithic and yellow pumice pebble clasts.
	15.09		Base obscured.

Section 53

Waihohonu Stream, T20 498184

True right bank of stream, 300 m upstream of where Pangara Stream meets Waihohonu Stream.

Unit Depth (mm)	Cum. Depth (m)	Correlation and samples taken	Description
1000-10000		Taupo Ignimbrite	White and pale grey fine-coarse ash with abundant pumice blocks and lapilli intermixed. Large charcoalised logs preserved especially near the base of the unit. Eroded angular contact into units below, angular unconformity.
200-350	10.35	Mangamate Tephra (MT), Waihohonu lapilli	Strong brown, greyish brown and grey coarse pumice and lithic ash and fine lapilli, shower-bedded with alternating coloured zones.
20			Grey and greyish brown fine-med ash.
20			Yellow brown and strong brown fine pumice lapilli and coarse ash.
30			Greyish brown med-coarse pumice ash.
450	10.87	MT, Oturere Lapilli	Reddish brown, and grey fine-med poorly vesicular pumice and lithic

			fine-med lapilli, shower-bedded but ungraded.
50			Fine yellow brown and greyish brown ash with scattered grey and yellow brown fine pumice and lithic lapilli.
50			Yellow brown, yellow and grey coarse pumice and lithic ash.
100			Yellow brown fine ash with scattered grey and yellow brown lithic and fine pumice lapilli.
200	11.27	Pahoka Tephra	Olive grey and pale brown platy coarse pumice ash and fine-med lapilli. Normally graded, with occasional olive grey and pale brown banded pumice lapilli, shower-bedded.
40			Brown and yellow brown fine ash.
150			Grey med-coarse sands with scattered yellow brown fine pumice lapilli, planar bedded on a 10 mm scale.
3000			Bedded greyish brown and grey sands and fine-coarse gravels. Planar bedded on a 100 mm scale.
1300	15.76		Bedded grey sands with scattered common pale brown pumice fine pebbles. Wavy bedded with occasional lenses of pumice pebbles.
40			Greyish brown and pale brown fine sand and silt, wavy bedded.
100-150	15.95	94.18	Strong brown fine-med pumice lapilli, interbedded within top of diamicton and as a discrete layer on top of diamicton.
5000-10000		R07-R09	Clast rich diamicton unit, dominating exposures all along this stream. Grey and occasional red lithic sub-rounded clasts, pebble-very large boulders. Matrix of greyish brown silt and fine sand, yellow pumice and grey lithic pebble clasts common. Matrix supported but very clast rich.
2000+	27.95	Tongariro andesite	Grey lava, base into stream

Section 54

Oturere Stream, T19 484209

Cutting on the western side of State Highway 1, 100 m south of crossing of Oturere stream. True left bank of Oturere stream valley.

Unit Depth (mm)	Cum. Depth (m)	Correlation and samples taken	Description
600-1000		Taupo Ignimbrite	White pumice, fine-coarse ash with mixed pumice lapilli and blocks, charcoal fragments preserved within base of unit.
400-500		Mangatawai Tephra	Dark brown and dark greyish brown fine ash with paleosol development. Interbedded black and purplish grey fine-med ash beds 10-20 mm thick with common pale brown beech leaves preserved within layers.
100	1.60	Papakai Formation (Pp)	Brown greasy, fine ash with paleosol development.
20	1.62	Waimahia Tephra within Pp	Cream-cakes of white, fine, pumice ash within brown greasy fine ash.
150		Pp	Dark greyish brown greasy fine ash.
100	1.87	Hinemaiaia Tephra within Pp	White, med-coarse pumice ash scattered within fine greasy greyish brown ash.
150		Pp	Yellow brown and brown greasy fine ash with vertical cracking, and paleosol development.
10-20	2.04	Motutere Tephra within Pp	Pale brown pumice fine ash cream-cakes within brown fine greasy ash.
100		Pp	Yellow brown and brown fine ash.
550	2.69	Mangamate Tephra (MT), Poutu Lapilli	Strong brown and grey fine-med poorly vesicular pumice and lithic lapilli, shower-bedded but ungraded.
40			Grey coarse-med lithic ash.
50		MT, Wharepu Tephra	Strong brown fine-med pumice lapilli.
150			Grey and strong brown 10 mm alternating layers of poorly vesicular pumice and lithic med-coarse ash. Reworked ash.
600		MT, Waihohonu Lapilli	Strong brown, greyish brown and grey fine-med pumice and lithic lapilli. Shower-bedded but ungraded. Lower 40 mm yellow brown pumice and lithic lapilli.
10			Greyish brown fine ash.
10			Grey med lithic ash.
10			Yellow brown med-coarse pumice ash.
10			Grey fine ash.
400	3.97	MT, Oturere Lapilli	Grey and greyish brown fine-med poorly vesicular pumice and lithic lapilli shower-bedded but ungraded.
150			Pale brown soft greasy fine ash with interbedded yellow brown and grey fine lapilli.
150	3.27	Pahoka Tephra	Grey, olive grey and pale brown fine-med pumice lapilli, shower-bedded, platy fine lapilli near top.
50			Brown fine ash, soft and greasy with scattered yellow brown fine pumice lapilli.
50			Pale yellow and grey coarse pumice and lithic ash.
100			Brown and yellow brown fine ash with scattered fine, soft, brown and yellow fine pumice lapilli.

50-100	3.57	Bullot Formation, Pourahu Member	Yellow brown and pale brown fine-med pumice lapilli with scattered grey lithic lapilli, shower-bedded.
100			Grey and pale greyish brown fine ash with interbedded yellow brown and grey fine pumice and lithic lapilli.
40			Yellow brown fine-med soft pumice lapilli with scattered grey fine lithic lapilli.
180			Grey and greyish brown fine ash with scattered yellow brown and grey pumice and lithic lapilli.
20			Yellow brown fine pumice lapilli.
100			Brown and pale brown fine-med ash with scattered yellow brown fine pumice lapilli.
80	4.09		Yellow brown and strong brown fine-med pumice lapilli with scattered grey lithic fine lapilli.
150			Yellow brown coarse pumice ash and fine lapilli with sparse, scattered grey lithic coarse ash.
100			Grey and few yellow brown coarse lithic and pumice ash and fine lapilli.
50			Brown and greyish brown fine greasy ash with scattered yellow brown and strong brown fine pumice lapilli.
20	4.41	Waiohau Tephra	Grey and greyish brown fine ash with pocketing white fine pumice ash.
80			Greyish brown and brown fine-coarse ash with sparse scattered fine yellow brown pumice lapilli.
100			Yellow brown fine pumice lapilli, shower-bedded with scattered fine grey lithic lapilli.
50			Grey fine-med ash with scattered fine yellow brown pumice lapilli.
30			Yellow brown, strong brown and grey med-coarse pumice and lithic ash.
30			Brown fine ash.
150	4.85		Pale brown and pale yellow pumice fine-med lapilli with scattered grey fine lithic lapilli, grey lithic rich zone in centre of unit.
40			Brown fine ash with scattered yellow brown fine pumice lapilli.
100			Yellow and pale yellow brown fine-med, soft pumice lapilli with scattered grey lithic coarse ash and fine lapilli.
10			Grey med lithic ash.
30			Yellow and pale yellow brown fine-med, soft pumice lapilli with scattered grey lithic coarse ash and fine lapilli.
10			Grey med lithic ash.
80	5.12		Yellow brown and pale brown fine pumice lapilli with scattered grey lithic fine lapilli.
180			Greyish brown and grey fine ash with scattered pale brown fine pumice lapilli.
20			Pale brown and yellow brown fine pumice lapilli with scattered grey lithic fine lapilli.
200			Brown and greyish brown fine ash with scattered grey and pale brown lithic and pumice fine lapilli.
50-60			Grey and greyish brown coarse lithic and pumice ash and fine lapilli.
50			Grey and greyish brown fine-med lithic ash.
50	5.68		Pale brown coarse pumice ash and fine lapilli, normally graded, with scattered grey lithic coarse ash and fine lapilli.
30			Yellow brown fine ash.
40			Yellow brown and grey coarse pumice and lithic ash mixed in equal proportions.
100			Grey and greyish brown fine ash with scattered pale brown fine pumice lapilli.
20			Greyish brown and yellow brown fine pumice lapilli.
20			Purplish grey fine ash.
120	6.01	94.20	Greyish brown and pale brown med-fine pumice and scattered lithic lapilli.
350			Brown and greyish brown fine ash with scattered grey and yellow brown lithic and pumice fine lapilli.
400			Grey and greyish brown fine ash or silt with occasional interbedded cobbles and yellow brown and grey lithic fine lapilli.
2000-3000		T1	Reworked diamicton, grey clast supported with a grey sandy matrix, pebble cobble and small boulder clasts.
4000+		T2	Eroded upper contact. Yellow brown. pale brown and greyish brown silt and sand matrix diamicton. Pebble-large boulder clasts supported within matrix, massive with no bedding, multi-coloured pebble clasts, larger clasts dominantly grey.
	13.76		Base obscured.

Section 56
Oturere Stream, T19 478213
True left bank of stream 500 m upstream of previous section.

Unit Depth (mm)	Cum. depth (m)	Correlation and sample taken	Description
500-3000		Taupo Ignimbrite	White and pale grey fine-coarse pumice ash with mixed pumice lapilli and blocks. Charcoal fragments preserved near base, thickens in paleo-valley.
800-1000	4.0	Mangatawai Tephra	Dark brown fine ash with paleosol development, several purplish grey and black ash beds, 10-30 mm thick interbedded within. Common pale brown beech leaves preserved within black ash layers.
500		Papakai Formation (Pp)	Yellow brown and dark brown fine greasy ash with paleosol development.
100	4.6	Hinemaiaia Tephra within Pp	White med-coarse pumice ash scattered within yellow brown fine greasy ash.
200		Pp	Yellow brown fine greasy ash.
10-20	4.82	Motutere Tephra within Pp	Pale brown fine ash cream-cakes within yellow brown fine ash.
100		Pp	Yellow brown fine ash.
200-500	5.42	Mangamate Tephra (MT), Poutu Lapilli	Uneven upper boundary. Strong brown and grey fine-med poorly vesicular pumice and lithic lapilli, shower-bedded but ungraded.
40			Grey lithic med-coarse ash.
50		MT, Wharepu Tephra	Strong brown fine pumice lapilli.
200-400		MT, Ohinepango Tephra	Grey and strong brown alternating layers of coarse pumice and lithic ash, shower-bedded.
300		MT, Waihohonu Lapilli	Grey, greyish brown and strong brown fine-med pumice and lithic lapilli, shower-bedded.
500		"	Grey and strong brown fine poorly vesicular pumice and lithic lapilli. Grey dominated at the top and strong brown at the base.
30			Grey lithic med ash.
20			Strong brown coarse pumice ash.
10			Grey coarse ash.
350-400	7.17	MT, Oturere Lapilli	Grey, greyish brown and strong brown fine-med poorly vesicular pumice and lithic lapilli, shower-bedded and ungraded.
50			Greyish brown fine ash with scattered yellow brown and pale brown fine pumice lapilli.
20			Yellow brown coarse pumice ash.
20			Greyish brown fine ash.
30			Strong brown and yellow brown fine pumice lapilli.
200	7.49	Pahoka Tephra	Grey and olive brown fine-med pumice lapilli, shower-bedded, with scattered banded grey and pale brown pumice lapilli.
10			Grey coarse lithic ash.
10			Yellow brown coarse pumice ash.
40			Yellow brown and brown fine ash.
80			Yellow brown and grey coarse pumice and lithic ash and fine lapilli, equal proportions of lithics and pumice.
40			Dark brown fine ash, with scattered yellow brown and brown fine pumice lapilli.
100	7.77	Bullot Formation, Pourahu Member	Yellow brown, pale brown and strong brown med-fine pumice lapilli, with scattered fine grey lithic lapilli.
40			Greyish brown fine ash with scattered grey and yellow brown fine lithic and pumice fine lapilli.
40			Strong brown fine pumice lapilli.
30			Grey lithic coarse-med ash.
10			Yellow brown coarse pumice ash.
40			Grey med-coarse lithic ash.
20			Yellow brown and pale brown fine soft pumice lapilli with scattered grey lithic lapilli.
50	8.00		Greyish brown and grey pumice and lithic med ash.
30			Grey coarse lithic ash.
30			Yellow brown and brown fine pumice lapilli with scattered grey coarse ash.
100			Brown and yellow brown fine ash with scattered, sparse yellow brown and grey fine pumice lapilli.
100	8.26		Strong brown and yellow brown med-fine pumice lapilli with scattered grey lithic lapilli.
150			Yellow brown fine ash with abundant yellow brown and grey lithic and pumice fine lapilli.
200			Grey, greyish brown and strong brown fine pumice and lithic lapilli, shower-bedded.
50			Yellow brown and brown fine ash with scattered pale brown and grey pumice and lithic fine lapilli.
150	8.76	94.21, Waiohau Tephra	Greyish brown and grey fine-med ash with scattered occasional yellow brown fine pumice lapilli. Pocketing white fine pumice ash within

			centre of unit 10-20 mm thick.
10			Strong brown, soft fine pumice lapilli.
20			Grey coarse lithic ash.
20			Yellow brown fine ash with scattered strong brown fine pumice lapilli.
100			Strong brown fine, soft pumice lapilli.
50			Brown and grey fine ash with scattered common grey coarse lithic ash and strong brown fine pumice lapilli.
80			Pale yellow fine pumice lapilli with scattered grey fine lithic lapilli.
40			Pale grey and yellow fine ash with scattered fine yellow brown pumice lapilli.
100	9.18		Pale yellow fine soft pumice lapilli with scattered grey lithic lapilli.
400			Grey and greyish brown bedded silts and sands with scattered and lenses of yellow brown fine pumice lapilli.
3000		T1	Eroded upper surface. Dark grey sandy matrix diamicton. Pebble-large boulder clasts supported within matrix, clasts and matrix grey, massive and unbedded.
500-1000		T2, pumice sample -94.22	Sharp upper contact. Pale brown and pale yellow silt and sand matrix diamicton, with clasts of yellow, yellow brown and grey pumice and lithic pebble clasts supported within the matrix.
200			Grey and yellow pumice and lithic bedded med-fine sand, 20 mm scale.
1000		T2	Yellow, greasy silt matrix diamicton. Grey, and pinkish grey pumice and lithic pebble clasts supported within the matrix. Bright distinctive appearance.
1000+		T3	Firm reddish grey lithic sand matrix diamicton, with pebble-cobble clasts supported within the matrix, massive and unbedded. Base obscured

Section 58
Makahikatoa Stream, T19 485221
True right bank of stream 500 m upstream of road. Description started at Mangamate Tephra.

Unit Depth (mm)	Cum. depth (m)	Correlation and samples taken	Description
300	*c.* 4.0	Mangamate Tephra (MT), Poutu Lapilli	Grey and strong brown alternating beds of coarse-med poorly vesicular pumice and lithic ash, 30 mm shower-beds.
150		MT, Wharepu Tephra	Strong brown, grey and greyish brown pumice and lithic fine-med lapilli, shower-bedded.
20		"	Strong brown fine pumice lapilli.
300		MT, Waihohonu Lapilli	Grey and strong brown fine pumice and lithic lapilli, shower-bedded, with grey dominated top and strong brown base.
20			Grey coarse-med lithic ash.
10			Strong brown coarse pumice ash.
10			Pale olive grey med ash.
60	4.57	MT, Oturere Lapilli	Greyish brown, grey and strong brown fine-med pumice and lithic lapilli shower-bedded and ungraded.
40			Yellow brown and pale greyish brown fine-med ash.
30			Yellow brown and grey pumice and lithic coarse ash.
250-300	4.94	Pahoka Tephra	Grey and olive brown fine-med pumice lapilli with scattered fine banded pumice lapilli. Shower-bedded but ungraded.
20			Brown fine-med ash with scattered grey and yellow brown fine lithic and pumice lapilli.
50			Yellow brown, pale brown and grey coarse pumice and lithic ash in equal proportions.
10			Brown fine ash with scattered yellow fine pumice lapilli.
50	5.07	Bullot Formation, Pourahu Member	Strong brown and yellow brown fine-med pumice lapilli, shower-bedded with scattered grey lithic fine lapilli.
50			Greyish brown fine ash with scattered yellow brown and pale brown fine pumice lapilli.
50	5.17		Strong brown and yellow brown fine-med pumice lapilli with scattered grey lithic fine lapilli.
20			Greyish brown fine ash.
10			Grey coarse lithic ash.
10			Strong brown coarse pumice ash.
10			Greyish brown fine ash.
20			Strong brown fine pumice lapilli.
40			Greyish brown fine ash with scattered fine strong brown pumice lapilli.
10			Grey coarse lithic ash.
20			Strong brown and grey pumice and lithic fine lapilli.
50			Brown and greyish brown fine ash.
100	5.46		Strong brown and yellow brown fine-med pumice lapilli with scattered grey fine lithic lapilli.
50			Yellow brown fine ash with scattered strong brown fine pumice lapilli.
20			Strong brown fine pumice lapilli.

100	5.61		Yellow brown and strong brown fine-med shower-bedded pumice lapilli with scattered grey lithic fine lapilli.
30			Brown fine ash with scattered yellow brown fine pumice lapilli.
40			Greyish brown fine-med ash.
10			Strong brown fine pumice lapilli.
10			Grey coarse lithic ash.
10			Greyish brown fine ash.
10			Strong brown fine pumice lapilli.
10			Grey fine lithic lapilli.
50			Greyish brown fine ash.
20			Strong brown and yellow brown coarse pumice ash.
20			Yellow brown fine ash.
30	5.85		Yellow brown and grey fine pumice and lithic lapilli and coarse ash.
20			Strong brown fine pumice lapilli.
100			Grey and dark grey fine-med lithic ash with scattered strong brown and pale brown pumice fine lapilli.
200			Yellow brown and yellow med pumice lapilli with grey med-coarse lithic ash interbedded at the top of the unit. Distinctive unit in this area.
400	6.57	94.27 Waiohau Tephra	Grey and pale greyish brown fine ash with scattered sparse yellow fine pumice lapilli. 10 mm cream-cakes of white fine pumice ash.
40			Yellow brown coarse pumice ash.
100			Greyish brown and yellow brown fine ash.
40			Strong brown and yellow brown fine pumice lapilli.
50			Yellow brown and strong brown fine ash with scattered strong brown fine pumice lapilli.
500			Greyish brown bedded sands and silts, planar bedded on 10-30 mm scale with interbedded yellow brown pumice pebbles in layers and lenses.
1000+		T1	Grey and strong brown sandy matrix diamicton. Clasts of sub-rounded and sub-angular pebble-large boulders supported within the matrix, grey clasts, unbedded.
	8.30		Base into stream.

Section 59

Makahikatoa Stream, T19 495220

True right bank of stream *c.* 800 m downstream of State Highway 1 at crossing of power pylons. Description taken from distinctive grey topped pumice lapilli unit described near the base of the previous section (above Waiohau Tephra).

Unit Depth (mm)	Cum. depth (m)	Correlation and samples taken	Description
150	*c.* 8.0		Strong brown and yellow brown fine-med pumice lapilli with scattered grey lithic fine lapilli and grey fine-med ash mixed in at the top of the unit.
4000-5000		T1	Grey and greyish brown silty and sandy matrix diamicton, with clasts of pebble to boulder supported by the matrix. Clasts, grey and red lithic as well as abundant multi-coloured pumice and weathered lithic pebbles.
200-3000		T2, pumice sample - 94.31	Variable thickness, eroded top. Yellow silty matrix diamicton with grey lithic and white, pink and yellow brown pumice clasts supported by the firm silty matrix. Distinctive unit.
200	16.20		Grey med-coarse lithic ash.
250			Pale greyish brown fine ash with scattered fine yellow and grey pumice and lithic lapilli.
20			Pale yellow and grey fine pumice and lithic lapilli.
40			Pale brownish grey fine ash with scattered fine yellow pumice lapilli.
50	16.56		Pale yellow and yellow brown fine pumice lapilli, soft with scattered grey fine lithic lapilli.
100			Pale grey fine ash, greasy.
30	16.69	94.28, Okareka Tephra	Yellow brown and pale grey bedded silts, with white fine pocketing pumice ash.
400			Pale brownish grey bedded fine silts and sands with planar and wavy bedding on a 10-30 mm scale.
150			Grey fine ash with scattered fine yellow pumice lapilli.
20			Grey and pale yellow fine pumice and lithic lapilli.
40			Pale grey fine ash.
20	17.32	94.29, TeRere Tephra	Pocketing wavy bedded fine white pumice ash.
250			Pale yellow and yellow brown fine pumice lapilli with scattered weathered pale grey lithic lapilli.
40			Pale greyish brown fine ash with scattered pale grey fine pumice lapilli.
50-100			Pale yellow and purplish grey fine pumice and lithic weathered lapilli.
150			Pale greyish brown fine ash with scattered grey and pale yellow fine pumice and weathered lithic lapilli.
50	17.66		White and pale yellow brown fine pumice lapilli with scattered grey lithic lapilli.

10			Greyish brown fine ash.
30			Pale yellow and grey fine pumice and lithic lapilli.
50			Greyish brown fine ash with scattered pale yellow fine pumice lapilli.
	17.75		Base into Stream

Section 60
Makahikatoa Stream, T19 504215
True left bank of stream *c.* 2 km downstream of State Highway 1. 100 m downstream of telephone line crossing.

Unit Depth (mm)	Cum. depth (m)	Correlation and samples taken	Description
	c. 4.0		Upper part obscured
150			Strong brown fine pumice lapilli and coarse ash, with scattered grey lithic lapilli.
250			Greyish brown greasy fine ash.
40			Greyish brown med-coarse pumice ash.
50			Grey med-coarse lithic ash.
20			Yellow brown fine ash.
50			Grey and pale yellow brown coarse pumice and lithic coarse ash.
10			Brown fine ash.
50	4.63		Yellow brown coarse pumice ash and fine lapilli with scattered grey coarse lithic ash.
300		Hinuera Formation	Greyish brown and brown fine ash with scattered yellow and yellow brown fine pumice lapilli. Contains white pumice ash.
20			Yellow brown fine pumice lapilli.
10			Grey fine ash.
40			Yellow brown fine pumice lapilli.
1200	6.20	Hinuera Formation	Brown and pale brown bedded silt and fine pumice sand with scattered strong brown and pale brown fine pumice lapilli, also few layers and lenses of pumice lapilli.
400			Strong brown and grey sandy matrix diamicton, pebble-cobble rounded clasts supported within the matrix.
6000-8000		Kawakawa Tephra, Oruanui Ignimbrite Member	Grey soft fine-med ash, massive, unbedded with very occasional cobble-pebble clast of andesite supported within. Scattered white coarse pumice ash.
10		Aokautere Ash Member	Pinkish white fine ash.
10		"	Pale brown med pumice ash.
10		"	Pale yellow and white med-fine pumice ash.
20	14.65	"	Pinkish brown fine pumice ash.
2000-3000+		T4	Sharp upper contact. Brown and yellow brown silty matrix diamicton. Pebble-boulder grey lithic clasts supported by the matrix. Some sites massive and unbedded others contain fluvial lenses and planar fabric.
	17.65		Base into stream

Section 64
Mangatawai Stream, T19 490239
True left bank of stream 50 m upstream of the State Highway 1 bridge over stream.

Unit Depth (mm)	Cum. depth (m)	Correlation and samples taken	Description
			Top obscured, coverbeds at road section.
200		T2	Brown silt and sand matrix diamicton, yellow strong brown, grey angular pebbly lithic clasts supported by the matrix.
300			Grey and greyish brown planar bedded sands and fine gravels, 30 mm scale beds.
1000		T3	Greyish brown sand and silt matrix diamicton. Pebble-cobble clasts supported by matrix, occasional boulders also present. Dominantly grey and few red lithic clasts with pumice pebble clasts also. Unbedded, massive.
10-20			Pale brown silt and fine sand.
1200			Grey, purplish grey, strong brown and brown fine-coarse sands and pebbles, pumice and lithic, planar bedded on 10-30 mm scale.
300	3.0	94.41, Rotoaira Tephra	Strong brown coarse-med pumice lapilli with scattered lithic med lapilli.
600		Hinuera Formation	Greyish brown, strong brown and grey fine-coarse bedded sands, planar bedded on a 10-30 mm scale.
1300		"	Grey and pale brown bedded sands and fine white pumice ash, planar and wavy bedded on a 10-30 mm scale.
1500+		T4	Greyish brown and grey sandy matrix diamicton, clast rich with cobble to boulder sized clasts supported within the matrix, grey lithic clasts.
	6.40		Base into stream.

Section 66
Mangatawai Stream, T19 496238
True left bank of stream 600 m downstream from State Highway 1, at crossing of westem-most power pylon line.

Unit Depth (mm)	Cum. depth (m)	Correlation and Samples taken	Description
200-1000		Taupo Ignimbrite	White fine-coarse pumice ash with mixed pumice lapilli and blocks, local over-thickening, contains fragments of charcoal within base.
400		Mangatawai Tephra	Black and purplish black 10-20 mm thick fine-med ash beds interbedded within dark brown, greasy, fine ash with paleosol development.
100	1.50	Papakai Formation (Pp)	Brown and yellow brown greasy fine ash.
10-20		Waimahia Tephra within Pp	Pocketing white fine pumice ash within brown greasy fine ash.
400		Pp	Brown and yellow brown fine ash with paleosol development, cracked vertically.
300-500	2.42	Mangamate Tephra (MT), Poutu Lapilli	Strong brown, and yellow brown fine-med poorly vesicular pumice and lithic lapilli, shower-bedded and ungraded.
4000		T1	Grey and greyish brown silty and sandy matrix diamicton. Pebble-large boulder clasts supported by matrix, grey sub-angular lithic clasts, massive unbedded.
300			Unconformable angular upper eroded contact. Pale purplish brown, pale brown and pale yellow bedded silt and fine sand, wavy and planar bedded on a 10 mm scale, with scattered fine pale yellow pumice lapilli.
150	6.87		Brown and dark brown fibrous lignite, with wood fragments, wavy and planar laminations on a 5-20 mm scale. Mgt(a) taken 20 mm from top, and (b) taken 20 mm above base.
200			Pale grey bedded silt and fine sand, planar and wavy bedded on a 10-20 mm scale, with scattered pale yellow fine pumice lapilli present.
50	7.12	94.43	Pale yellow fine, soft, pumice lapilli with scattered sparse grey lithic fine lapilli.
100			Pale yellow and pale grey silt and fine sand, planar and wavy bedded on a 10-20 mm scale, with scattered pale yellow fine pumice lapilli present.
30	7.25	94.44	Pale yellow fine pumice lapilli with few scattered pale grey lithic fine lapilli.
50			Pale yellow and pale grey silt and fine sand, planar and wavy bedded on a 10-20 mm scale.
80	7.38	94.45	Yellow and pale yellow fine pumice lapilli with few scattered pale grey lithic fine lapilli.
10			Purplish brown firm lignite.
50	7.44	94.46	Pale brown fine-med pumice ash.
300			Dark brown and brown firm lignite with large (>500 mm long, >200 mm diameter) wood fragments within. Wood sampled as (c) and lignite sampled in 50 mm intervals as (d)-(h).
50			Grey bedded fine sand planar 10 mm scale bedding.
100			Dark brown and brown lignite planar bedded, on a 10-30mm scale, firm. (I) sampled near top and (j) near base.
50	7.94	94.47, Rerewhakaaitu Tephra	White fine -med pumice ash.
150			Black and dark brow lignite, firm, bedded, planar and wavy bedding on a 10-30 mm scale. Sampled 2 cm from top and 2 cm from base.
10			Pale brown wavy bedded fine silt.
400	8.50		Dark brown and brown lignite and organic rich silts and fine sands. Sampled in the zones of most pure lignite.
1200			Pale grey and pale yellow bedded silts and fine sands with scattered pale yellow fine pumice lapilli. Planar and wavy bedded on a 5-30 mm scale, very finely laminated at base.
200-400		T3	Pale brown sandy matrix diamicton, pebble-cobble grey lithic clasts supported by matrix, unbedded.
1200			Massive, unbedded pale brown and pale olive silt and fine sand.
1500+		T3-T4	Greyish brown and brown silt and sandy matrix diamicton, clasts of grey and greyish brown lithic pebble-boulders supported by matrix, unbedded.
	12.80		Base into stream.

Section 68
Mangamate Stream, T19 505248
True left bank of stream 150-200 m upstream of crossing of eastern-most line of power pylons, *c.* 1 km downstream of State Highway 1.

Unit Depth (mm)	Cum. depth (m)	Correlation and samples taken	Description
400		Mangatawai Tephra	Dark brown fine greasy ash with interbedded purplish grey and black fine-med ash beds 10-20 mm thick.
150		Papakai Formation (Pp)	Brown and yellow brown fine greasy ash.
50	0.60	Hinemaiaia Tephra within Pp	Scattered white pumice med-coarse ash within brown fine greasy ash.
250		Pp	Brown and yellow brown fine ash with scattered grey and strong brown pumice and lithic lapilli in base of unit.
500	1.35	Mangamate Tephra (MT). Poutu Lapilli	Strong brown and grey fine-med pumice and lithic lapilli, shower-bedded but ungraded.
150		MT, Waihohonu Lapilli	Grey and strong brown med-coarse poorly vesicular pumice and lithic ash.
250		"	Strong brown and yellow brown and grey pumice and lithic lapilli.
50			Grey and greyish brown fine-med ash, 20 mm onto 30 mm of strong brown fine-med ash.
350	2.15	MT, Oturere Lapilli	Strong brown, greyish brown and grey fine-med poorly vesicular pumice and lithic lapilli, shower-bedded but ungraded.
20			Grey fine lithic lapilli.
50			Yellow brown fine ash.
30			Strong brown fine pumice lapilli and coarse ash.
300	2.55	Pahoka Tephra	Upper 150 mm grey and greyish brown coarse pumice ash, shower-bedded, lower 150 mm olive grey and pale brown fine-med pumice lapilli, with scattered banded pumice lapilli.
300			Greyish brown fine ash with scattered strong brown and grey fine pumice and lithic lapilli.
20-50	2.90		Yellow and yellow brown fine pumice lapilli, with scattered grey lithic lapilli.
50			Greyish brown and brown fine-med ash.
20			Strong brown and grey fine pumice and lithic lapilli.
50			Brown and grey fine-med ash.
10			Strong brown pumice lapilli.
50			Yellow brown and brown fine ash.
80	3.18		Strong brown fine pumice lapilli, with scattered grey fine lithic lapilli.
50			Strong brown fine ash with scattered fine pumice lapilli.
250			Grey and strong brown fine pumice and lithic lapilli, shower-bedded and ungraded.
20	3.50	94.58, Waiohau Tephra	Greyish brown fine-med ash with scattered grey and strong brown fine pumice and lithic lapilli, 30-40 mm cream-cakes of white fine rhyolitic ash interbedded.
300			Strong brown, greyish brown and grey med-coarse pumice and lithic ash, shower-bedded.
40			Strong brown fine ash.
100	3.94		Strong brown and reddish brown fine pumice lapilli with scattered fine grey lithic lapilli.
30			Strong brown and brown fine ash.
20			Strong brown fine pumice lapilli.
200	4.19	Rerewhakaaitu Tephra	Brown and greyish brown fine ash with interbedded cream-cakes of white fine pumice ash.
150			Yellow brown and strong brown normally graded med ash-fine pumice lapilli, with scattered grey lithic fine lapilli and coarse ash.
50			Grey, greyish brown and strong brown fine-med pumice ash.
150			Strong brown fine pumice lapilli.
200	4.74	Hinuera Formation	Brown, pale brown and white reworked fine ash with scattered fine strong brown pumice lapilli.
300			Grey med lithic ash with scattered strong brown fine-med pumice lapilli.
200			Pale grey soft greasy fine ash with scattered yellow brown and strong brown fine pumice lapilli.
500	5.74		Yellow brown and strong brown fine pumice lapilli, reworked, with scattered grey fine lithic lapilli.
200			Pink and pale yellow fine ash with scattered strong brown fine pumice lapilli.
1000		T4	Grey sandy matrix diamicton, pebble to boulder clasts supported within the matrix, massive and unbedded.
3000+		"	Sharp upper contact. Pale greyish brown and brown silty matrix diamicton. Sparse pebbly multi-coloured lithic and pumice clasts supported by matrix, massive and unbedded.
	9.94		Base into stream.

Section 72
Tongariro River, T19 356556
True left bank of river immediately downstream of "Sand Pool".

Unit Depth (mm)	Cum. depth (m)	Correlation and samples taken	Description
400			Grey bedded sand with scattered fine white pumice lapilli pebbles. Recent soil developing into top of unit, greyish brown and brown fine-coarse sand.
400	0.80	Taupo Ignimbrite	Fine-coarse pumice ash with mixed pumice lapilli and blocks, unconformable sharp lower contact.
2500-3000	3.80		Grey and pale brown diamicton, sand and fine pebble matrix supporting grey clasts of cobble to boulder size. Sub-rounded clasts, with a more well sorted matrix than unit below. Occasional interbedded lenses of sand and fine cross-bedded gravels.
4000+			Greyish brown and grey sandy matrix diamicton. Surface reworked in many places by river and fines depleted. Pebble-huge sub-rounded and sub-angular boulder clasts supported by matrix. Fine clasts grey, yellow and red lithic and occasional pumice larger clasts all grey lithic. Occasional huge boulder clasts up to 3 m diameter. Very firm, cemented? matrix.
	7.80		Base into stream.

Section 73
Tongariro River, T19 364544
True left bank of river, large cliff section at "Breakaway Pool"

Unit Depth (mm)	Cum. depth (m)	Correlation and samples taken	Description
5000		Taupo Ignimbrite	White pumice fine-coarse ash with mixed pumice lapilli and large pumice blocks, charcoal fragments and logs near base of unit. Upper 800 mm black present soil developed. Unconformable lower contact.
300	5.30	Mangamate Tephra, Poutu Lapilli	Strong brown and yellow brown fine pumice lapilli, with scattered grey lithic lapilli, shower-bedded and ungraded, irregular upper contact.
600-800		94.79, Karapiti Tephra	Yellow brown and pale yellow brown fine ash with paleosol development and paleo-root channels, white fine ash pocketing 10 mm near top.
800-1000	7.10		Grey sandy matrix diamicton, pebble-cobble clasts supported by matrix, cross bedded in places and with only faint planar fabric in other places.
800-1200			Grey and olive grey massive coarse-fine sand, poorly sorted, weak planar fabric, possible log casts present.
20			Wavy bedded pale brownish grey silt and fine sand.
1500	9.82		Grey, olive grey and pale greyish brown coarse-fine poorly sorted matrix diamicton, planar fabric with occasional cobble and small boulder clasts supported by matrix, empty log casts seen. Lower 500 mm massive with no planar fabric.
100-150			Pale greyish brown silt, massive with paleo-root channels.
1000			Grey and brownish grey fine-coarse sand, massive with faint planar fabric in places.
2000	12.97		Grey and greyish brown fine-coarse sand matrix diamicton with pebbly clasts supported by matrix, grey red and yellow brown pebble clasts. Planar fabric, and poorly sorted.
150			Pale grey fine sand, planar bedded.
30			Dark grey fine sand and silt with scattered yellow brown fine pumice lapilli.
30			Grey and pale brown planar bedded sand and silt.
50		Rotoaira Tephra	Strong brown and pale brown fine pumice lapilli with scattered grey lithic fine lapilli.
10		"	Dark grey fine-med lithic ash.
40	13.28	"	Grey, strong brown and yellow brown fine pumice and lithic lapilli, grey at top and strong brown and yellow brown soft pumice lapilli at base.
200		Hinuera Formation	Greyish brown and grey fine sand and silt with mixed in fine white pumice ash.
30			Grey and greyish brown fine sand and silt.
50			Pale brown fine ash with scattered grey and yellow brown fine pumice and lithic lapilli.
300			Greyish brown and grey sand and silt, planar bedded.
0-1700	14.56	Kawakawa Tephra/ Oruanui Ignimbrite Member	Pinkish pale brown fine ash with scattered coarse and med pumice ash within, occasional pumice clasts up to fine lapilli in size.
20		Aokautere Ash Member	Coarse white pumice ash

30		"	Pale pinkish brown fine ash with accretionary lapilli up to 10 mm in diameter.
40		"	White fine pumice lapilli, and accretionary lapilli within white fine pumice ash.
10		"	Pale brown fine pumice ash.
20		"	White fine pumice lapilli.
200-250		"	White and pale brown fine pumice ash with abundant accretionary lapilli 5-20 mm in diameter.
10			Brown fine ash.
4000+			Greyish brown sandy and silty matrix diamicton. Clasts of sub-angular pebble-boulders supported within the firmly cemented matrix.
	18.94		Base into river.

Section 76
Tongariro River, T19 533383
Road cutting on the western side of Sate Highway 1, 200 m south of the Trout Hatchery.

Unit Depth (mm)	Cum. depth (m)	Correlation and samples taken	Description
300-400		Taupo Ignimbrite	White and pale grey fine-coarse pumice ash with mixed white pumice lapilli and blocks, with present soil development.
400-450	0.85	Mangamate Tephra, Poutu Lapilli	Strong brown and yellow brown fine pumice lapilli, shower-bedded and ungraded with scattered grey fine lithic lapilli.
30			Pale grey med-coarse lithic ash.
100			Yellow brown and greyish brown coarse pumice ash and fine lapilli.
150			Greyish brown and yellow brown fine-med ash.
100	1.23		Yellow brown and strong brown fine pumice lapilli and coarse ash, with scattered grey lithic lapilli. Grey lithic fine lapilli rich zone near top of unit, 10 mm thick.
100			Pale brown fine ash.
10			Pale brown fine pumice lapilli.
450			Pale brown and yellow brown fine ash with paleosol development and scattered grey and yellow brown fine pumice and lithic lapilli.
40	1.83		Strong brown and yellow brown fine pumice lapilli
10			Dark grey med-fine ash.
10			Pale brown fine ash.
10			Dark grey med-fine ash.
40		Rotoaira Tephra	Strong brown fine pumice lapilli and coarse ash with scattered grey fine lithic lapilli.
10		"	Grey fine ash.
30	1.94	"	Strong brown and yellow brown fine pumice lapilli and coarse ash.
50			Pale brown fine ash.
2000+		Hinuera Formation	White, grey and pale pinkish brown pumice rich sands silts and gravels, cross-bedded and planar bedded on a 20-50 mm scale.
	3.99		Base obscured.

Section 78
Tongariro River, T19 404533
Disused pumice quarry at end of Admirals Reserve Road, off State Highway 1, 2 km south of Turangi.

Unit Depth (mm)	Cum. depth (m)	Correlation and samples taken	Description
1000-6000		Taupo Ignimbrite	White and pink fine-coarse pumice ash with mixed pumice lapilli and blocks and fragments of charcoal near base. Variable thickness and eroded irregular lower contact.
100	6.1	Mangamate Tephra, Poutu Member	Strong brown, yellow brown and grey fine pumice and lithic lapilli, shower-bedded and ungraded, with scattered grey fine lithic lapilli.
100			Grey and greyish brown coarse pumice and lithic ash and fine lapilli.
1200			Brown and yellow brown fine ash with scattered yellow brown fine pumice lapilli, paleosol development and paleo-root channels present.
50			Grey and strong brown fine pumice and lithic lapilli and coarse ash.
100			Pale brown fine ash.
500-2000+		Kawakawa Tephra/ Oruanui Ignimbrite Member	Pinkish brown and pale brown fine-med pumice ash with scattered white coarse pumice ash, massive, unwelded but firm.
	9.55		Base obscured.

Section 81
Oturere Stream, T19 430238
Exposure on the top of a lava flow on the true right side of Oturere valley, 500 m due west of Oturere Hut, within wilderness area.

Unit Depth (mm)	Cum. depth (m)	Correlation and samples taken	Description
100			Brown fine ash with scattered grey lithic coarse ash.
400		Mangamate Tephra, Oturere Lapilli	Grey and greyish brown fine lithic and poorly vesicular pumice lapilli and coarse ash, shower-bedded and ungraded.
300	0.80	Pahoka Tephra	Pale grey and pale olive brown fine-med pumice lapilli, shower-bedded, ungraded, with distinctive common banded pumice lapilli.
20			Dark grey fine lithic lapilli.
20			Brown fine ash.
10			Grey med-fine ash.
150			Yellow and grey fine pumice and lithic lapilli and coarse ash, reversely graded with equal proportions of pumice and lithics.
200	1.20	Bullot Formation, Pourahu Member	Greyish brown fine pumice lapilli, shower-bedded with scattered grey fine lithic lapilli.
50			Brown fine ash, with scattered pale yellow brown and grey fine pumice and lithic lapilli.
150			Greyish brown fine pumice lapilli, shower-bedded, with scattered fine grey lithic lapilli.
50			Grey and purplish grey fine lithic lapilli and coarse ash.
150			Pale greyish brown fine-med pumice lapilli, with scattered grey fine lithic lapilli, 10 mm grey med lithic ash zone 50 mm from top of unit.
20			Grey and pale brown fine-med ash.
300	1.92		Greyish brown and grey pumice and lithic coarse ash and fine lapilli.
50			Grey and yellow brown banded 10 mm layers of alternating colour, pumice and lithic coarse ash.
10			Yellow brown coarse pumice ash.
10			Dark grey fine-med ash.
10			Yellow coarse pumice ash.
20			Grey lithic and pumice coarse ash.
150	2.17		Yellow brown coarse pumice ash with scattered coarse lithic ash, shower-bedded.
150			Dark grey and greyish brown alternating zones of med ash and fine pumice and lithic lapilli, shower-bedded.
20			Yellow brown coarse pumice ash.
10			Grey coarse lithic ash.
20			Yellow brown coarse pumice ash.
10			Dark grey coarse lithic ash.
30-50	2.43	95.2, Waiohau Tephra	Grey med-coarse lithic ash with pocketing white fine pumice ash cream-cakes.
10			Yellow brown coarse pumice ash.
10			Dark grey coarse-med lithic ash.
10			Yellow brown coarse pumice ash.
10			Purplish grey med ash.
100			Yellow brown and greyish brown zones of shower-bedded fine pumice lapilli.
200			Greyish brown and grey alternating zones of fine-med pumice lapilli, shower-bedded.
10			Greyish brown fine ash.
1000	3.78		Yellow brown, yellow and pale greyish brown fine pumice lapilli, shower-bedded with scattered grey lithic fine lapilli.
50			Grey and greyish brown coarse pumice and lithic ash.
30			Greyish brown fine pumice lapilli.
300	4.16	95.3, Rerewhakaaitu Tephra	Greyish brown and grey shower-bedded coarse ash and fine pumice lapilli, alternating coloured zones, 5 mm cream-cakes of white fine pumice ash 30 mm from base.
10			Pale grey fine ash.
200			Greyish brown and grey coarse pumice and lithic ash and fine pumice lapilli, shower-bedded.
10			Greyish brown fine ash.
500			Greyish brown coarse pumice ash and fine lapilli with scattered grey fine lithic lapilli.
20			Yellow brown fine pumice lapilli with scattered grey fine lithic lapilli.
200	5.10		Grey and greyish brown med-coarse pumice and lithic ash, with scattered yellow brown fine pumice lapilli.
10			Grey fine ash.
30			Greyish brown coarse pumice ash.
10			Brown fine ash.
30			Greyish brown coarse pumice ash.
20			Greyish brown and yellow brown fine pumice lapilli.

10		Greyish brown coarse pumice and lithic ash.
10		Yellow brown coarse pumice ash
10		Dark grey fine ash.
70	5.30	Greyish brown coarse pumice ash and fine lapilli.
10		Brown and yellow brown fine ash.
40		Greyish brown and yellow brown med ash and fine pumice lapilli intermixed.
300	5.65	20-30 mm of dark grey fine-med ash intermixed within the top of yellow brown and yellow coarse-fine pumice lapilli, shower-bedded and reversely graded, with scattered grey fine lithic lapilli.
10		Grey fine ash.
100		Yellow brown and strong brown fine pumice lapilli.
150		Greyish brown and grey med-coarse sand with interbedded pale brown pumice and grey pebbles and cobbles.
200	6.11	Strong brown and yellow brown coarse-med pumice lapilli, with scattered grey fine lithic lapilli.
100		Olive greyish brown fine pumice lapilli, with scattered grey lithic fine lapilli.
150		Grey and greyish brown med-coarse sands with interbedded greyish brown and grey lithic and pumice pebbles.
4000+	10.36	Grey lava flow, base not seen.

Section 82
Mangatetipua Stream, T19 423339
Road side section on the southern side of State Highway 47A, large lava flow exposure 500 m west of road bridge over Mangatetipua Stream.

Unit Depth (mm)	Cum. depth (m)	Correlation and samples taken	Description
200-3000		Taupo Ignimbrite	White fine-med pumice ash mixed with white pumice lapilli and blocks, primary in some places, bedded and reworked in other places.
500	3.50	Mangatawai Tephra	Brown and greyish brown fine ash, purplish grey and black fine ash within lower 100 mm.
100		Papakai Formation (Pp)	Brown and yellow brown fine ash, greasy with paleosol development.
10-20	3.62	Waimahia Tephra within Pp	White fine pumice ash cream-cakes within brown fine ash.
300		Pp	Yellow brown fine ash.
50	3.97	Hinemaiaia Tephra within Pp	White coarse-med pumice lapilli scattered within fine brown ash.
300		Pp	Yellow brown fine ash, greasy.
500-800	5.07	Mangamate Tephra (MT). Poutu Lapilli	Strong brown and yellow brown fine-med pumice lapilli, shower-bedded and ungraded, with scattered grey fine lithic lapilli, upper part mixed within lower part of Papakai Tephra.
30			Grey med-coarse lithic ash.
50-100			Brown fine ash with scattered grey and yellow brown fine lithic and pumice lapilli.
400		MT, Te Rato Lapilli	Grey and greyish brown poorly vesicular fine-med pumice lapilli, shower-bedded and ungraded.
0-2000	7.60	95.6 Waiohau Tephra	Variable thickness yellow brown and brown fine ash, with scattered yellow brown pumice lapilli and occasional large lava clast, colluvial layer. Unconformable upper contact. Two apparent horizons of white fine pumice ash cream-cakes.
7000+		95.8	Grey and reddish grey scoriaceous and dense lava flow.
	14.60		Base obscured.

Section 83
Tahurangi/ Te Karo Streams, T19 448326
Large road cutting on the southern side of State Highway 47A, 500 m east of Rotoaira Trust Fishing camp jetty.

Unit Depth (mm)	Cum. depth (m)	Formation and Member	Description
200-300		Taupo Ignimbrite	White fine-coarse pumice with mixed pumice lapilli.
300		Mangatawai Tephra	Brown fine ash upper 150 mm, lower 150 mm grey and dark grey med-fine ash beds 10-30 mm thick interbedded with brown fine ash..
200		Papakai Formation (Pp)	Brown and yellow brown fine greasy ash.
50	0.85	Hinemaiaia Tephra within Pp	White med-coarse pumice ash scattered within yellow brown fine ash.
50-300		Pp	Yellow brown and brown fine greasy ash.
400-700		Mangamate Tephra (MT), Poutu Lapilli	Variable upper contact, yellow brown, strong brown and grey fine pumice and lithic lapilli, shower-bedded and ungraded.
30			Grey coarse-med ash.
20			Greyish brown fine ash.
400	2.30	MT, Te Rato Lapilli	Grey and pale greyish brown fine pumice and lithic lapilli, shower-

			bedded and ungraded.
100			Pale brown and yellow brown fine ash with scattered yellow brown and strong brown fine pumice lapilli.
200			Yellow brown fine ash.
20			Strong brown fine pumice lapilli.
20			Grey med-fine ash.
20			Strong brown fine pumice lapilli and coarse ash.
150			Greyish brown and brown fine ash with scattered strong brown fine pumice lapilli and coarse ash.
10	2.78	95.9, Waiohau Tephra	Pocketing white fine pumice ash cream-cakes, within greyish brown fine ash.
10			Black med lithic ash, pocketing within greyish brown fine ash.
20			Brown fine ash with scattered yellow brown pumice and grey lithic coarse ash.
40			Strong brown and yellow brown coarse pumice ash.
50			Greyish brown and yellow brown fine ash with scattered yellow brown fine pumice lapilli.
100	3.00		Yellow brown and strong brown fine pumice lapilli with brown fine ash intermixed toward base.
150			Greyish brown fine-med ash.
200-250		Rotoaira Tephra	Yellow brown and strong brown fine-med, soft pumice lapilli, with scattered grey fine lithic lapilli.
30		"	Black and dark grey med lithic ash.
80	3.51	"	Yellow brown and strong brown fine-med pumice lapilli, with scattered fine grey lithic lapilli.
20			Greyish brown med ash.
100			Yellow brown sand with interbedded grey and strong brown pebbles.
100	3.73	Kawakawa Tephra, Aokautere Ash Member	Pinkish pale brown fine-med pumice ash.
10		"	White med pumice ash.
10		"	Pale pink and pale grey fine pumice ash.
40		"	Alternating layers of pale yellow and pale pink fine and med pumice ash, with basal 10 mm fine pale pink ash.
400			Grey and greyish brown med sand, massive and well sorted.
20			Strong brown soft pumice lapilli.
400			Dark grey fine-coarse bedded sands, planar bedded.
1000+	4.61	95.10	Grey lava flow, base obscured.

Section 88
Unnamed stream between Tahurangi and Rahuituki Streams, T19 475304
True left bank of stream 20 m upstream of forestry road bridge, Te Ngoi forestry road.

Unit Depth (mm)	Cum. depth (m)	Correlation and samples taken	Description
400		Mangamate Tephra (MT), Poutu Lapilli	Strong brown fine pumice lapilli with scattered grey lithic fine lapilli, shower-bedded and ungraded.
70			Grey med lithic ash.
30			Greyish brown fine ash with scattered yellow brown fine pumice lapilli.
20			Grey med-fine ash.
10			Yellow brown coarse pumice ash.
60	0.59	MT, Oturere Lapilli	Grey med lithic ash, grading into 30 mm yellow brown coarse pumice ash with scattered grey coarse lithic ash.
30			Greyish brown fine ash with scattered yellow brown fine pumice lapilli.
100	0.62	MT, Te Rato Lapilli	Greyish brown and yellow brown fine pumice lapilli.
80			Greyish brown and pale brown fine ash with scattered fine grey and yellow brown pumice and lithic fine lapilli.
150			Yellow brown and strong brown coarse pumice ash.
250			Greyish brown fine ash with scattered yellow brown fine pumice lapilli.
100	1.10		Strong brown fine pumice lapilli, with scattered grey fine lithic lapilli, 10 mm grey lithic dominated layer near top of unit.
30			Greyish brown fine ash with scattered yellow brown fine pumice lapilli.
50			Yellow brown fine pumice lapilli.
600			Greyish brown fine ash with scattered yellow brown fine pumice lapilli.
100	1.88		Yellow brown and strong brown fine pumice lapilli, soft, with scattered fine grey lithic lapilli.
400			Greyish brown fine ash with scattered yellow brown fine pumice lapilli.
40			Grey med lithic ash.
100	2.42		Strong brown fine pumice lapilli with scattered grey ash.
20			Grey med ash.
200			Yellow brown fine-med pumice lapilli with scattered grey fine lithic lapilli.
10			Grey med lithic ash.
100	2.75		Yellow brown and strong brown fine pumice lapilli with scattered grey fine lithic lapilli.

100			Grey med lithic ash.
100-300		Kawakawa Tephra, Oruanui Ignimbrite Member	Pale brown fine-med massive unbedded ash with scattered coarse pale brown and white pumice ash.
500+		T4	Boulder rich diamicton, grey sandy matrix, firm and cemented with pebble-boulder clasts supported within, large grey boulder clasts.
	3.65		Base into stream.

Section 89
Poutu Canal, T19 497327
True left side of canal as it flows into Poutu Dam (basal part exposed 300 m further upstream on true right side of canal).

Unit Depth (mm)	Cum. depth (m)	Formation and Member	Description
			Top Obscured.
200	*c.* 2.0		Brown fine ash with scattered strong brown and yellow brown fine pumice lapilli.
30		Rotoaira Tephra	Yellow brown and strong brown fine pumice lapilli.
10		"	Grey med-coarse lithic ash.
120		"	Strong brown and yellow brown fine pumice lapilli, with scattered grey fine lithic lapilli.
200			Greyish brown fine ash with scattered strong brown fine pumice lapilli.
40			Strong brown and yellow brown fine pumice lapilli.
10			Grey coarse lithic ash.
50	2.46		Yellow brown and strong brown fine pumice lapilli with scattered grey fine lithic lapilli, shower-bedded.
10			Grey lithic fine-med ash.
30			Strong brown and yellow brown fine pumice lapilli.
250			Greyish brown with scattered grey and yellow brown fine pumice and lithic lapilli.
1000		Hinuera Formation	Grey and pale brown lithic and pumice sands and fine gravels, rich in pale brown pumice ash. Grey and brown pumice and lithic gravels, fine-coarse bedded in planar layers and lenses.
500	4.25	Kawakawa Tephra/ Oruanui Ignimbrite Member	Pale brown and white fine pumice ash with scattered white fine pumice lapilli, massive and unbedded, uneven upper contact.
15000+		T4	Grey sandy matrix diamictons, pebble-boulder grey lithic clasts supported by matrix. Many units, some massive and unbedded others with weak planar fabric.
	4.75		Base obscured.

Section 91
Puketarata Stream, T19 528289
True left bank of stream, below State Highway 1 bridge.

Unit Depth (mm)	Cum. depth (m)	Correlation and samples taken	Description
			Top obscured.
600	*c.* 4.0		Brown and greyish brown fine ash with scattered yellow brown fine pumice lapilli.
20			Yellow brown and strong brown fine pumice lapilli.
200			Greyish brown fine greasy ash.
50			Grey and greyish brown fine-med lithic ash.
30			Pale brown and greyish brown fine ash.
50	4.35	Rotoaira Tephra	Strong brown and yellow brown fine pumice lapilli with scattered fine lithic lapilli.
20		"	Grey fine ash.
50		"	Strong brown fine pumice lapilli with scattered grey fine lithic lapilli.
10-20		"	Grey fine-med ash.
50		"	Yellow brown and strong brown fine pumice lapilli, with scattered grey fine lithic lapilli.
250			Greyish brown and yellow brown fine, greasy ash with paleosol development.
1000+		T3/T4	Grey and brownish grey sandy matrix diamicton with pebble to large boulder clasts supported by matrix. Upper part reworked and fines depleted, clast supported with bedded grey and strong brown sand between grey lithic clasts.
	5.74		Base into stream.

Section 93
Mangahouhounui Stream, T19 512315
True right bank of stream where it is crossed by the Poutu canal, deep partially obscured section.

Unit Depth (mm)	Cum. depth (m)	Correlation and samples taken	Description
500		Mangamate Tephra, Poutu Lapilli	Strong brown and yellow brown fine pumice lapilli, shower-bedded and ungraded, scattered grey fine lithic lapilli.
2000			Partially obscured ash and lapilli beds, undescribed
2000		Hinuera Formation	Brownish grey, pale brown and grey bedded sands and gravels, planar and cross-bedded containing abundant pale brown and white pumice ash.
10000+		T4	Greyish brown and dark grey sandy matrix diamicton, massive and unbedded, pebble-large boulder clasts, grey and reddish grey angular lava clasts supported by the matrix. Potentially several diamicton units present.
	14.50		Base into stream.

Section 95
Tongariro River, T19 540397
Stag Pool, true right bank of river.

Unit Depth (mm)	Cum. depth (m)	Correlation and samples taken	Description
4000		Taupo Ignimbrite	White fine-coarse pumice ash with mixed pumice lapilli and blocks, Charcoal fragments and logs in base of unit.
500-2000			Variable lower contact pinches over paleo-topography planar upper contact. Grey and greyish brown sandy matrix diamicton with pebble-boulder clasts supported within the matrix.
0-1500			Lenses of bedded grey and greyish brown gravels and sands, rounded grey gravels and grey and yellow brown sands.
4000			Large boulder rich diamictons. Grey and greyish brown firm sandy matrix supporting clasts of pebble-boulder, grey sub-rounded boulders, two or more units.
	11.50		Base into river.

Section 96
Tongariro River, T19 549328
Road cutting along Rangipo Prison Farm road toward river, northern side of road, 300 m before bridge over river.

Unit Depth (mm)	Cum. depth (m)	Correlation and samples taken	Description
300-1000		Taupo Ignimbrite	White fine-coarse ash with mixed pumice lapilli and blocks, charcoal fragments within base.
200		Mangatawai Tephra	Dark brown fine ash with interbedded grey and purplish grey fine-med ash, pocketing in the base of the unit.
200		Papakai Formation	Brown fine greasy ash with paleosol development, scattered white coarse pumice ash.
200-400	1.80	Hinemaiaia Tephra	White and pale brown coarse pumice ash shower-bedded occasionally over-thickened.
500		Papakai Formation	Brown and yellow brown fine ash with grey fine pumice and lithic lapilli scattered within base of unit.
200-400		Mangamate Tephra (MT), Poutu Lapilli	Variable upper contact, strong brown and yellow brown fine pumice lapilli with scattered grey lithic lapilli, shower-bedded but ungraded.
10			Grey med lithic ash.
30			Greyish brown fine ash.
10-20	2.76	Poronui Tephra	White pocketing fine pumice ash, within grey fine greasy ash.
50			Greyish brown fine ash.
20			Grey med lithic ash.
20			Greyish brown fine ash.
10			Strong brown, yellow brown and grey fine pumice and lithic lapilli.
30	2.89	MT, Te Rato Lapilli	Grey coarse ash and fine pumice and lithic lapilli.
40			Greyish brown fine ash with scattered grey fine lithic lapilli.
20	2.95	Pahoka Tephra	Grey and olive pale brown fine pumice lapilli, with scattered occasional banded lapilli.
100			Greyish brown and brown fine, greasy ash with scattered yellow brown fine pumice lapilli.
500			Planar bedded gravels and sands, poorly sorted coarse and fine grey gravels and sand, sub-rounded and sub-angular, with scattered yellow brown fine pumice pebbles.
40			Greyish brown fine-med sand.
10-200			Sandy matrix pebbly diamicton, lenzoidal. Grey and greyish brown

			pebbles within greyish brown sandy matrix.
50			Greyish brown fine-med sand.
400-700	4.54		Grey and greyish brown planar bedded sands and gravels, 20-30 mm scale beds, poorly sorted, pebbles rich in layers and lenses.
20			Greyish brown fine ash.
20			Greyish brown and yellow brown fine pumice lapilli.
40			Greyish brown fine ash.
600			Grey and greyish brown sandy matrix diamicton, pebble-cobble clasts supported within the matrix, clast rich unit, massive and unbedded.
50			Brown fine ash.
40	5.31		Yellow brown and strong brown fine pumice lapilli with scattered grey fine lithic lapilli.
30			Brown fine ash.
60			Grey and strong brown fine lithic and pumice lapilli.
20			Greyish brown fine ash.
10	5.43	95.13 Waiohau Tephra	White fine pumice ash, pocketing in places and a continuous layer in other places.
250			Brown and gleyed pale brown fine ash with scattered pale brown coarse pumice ash.
30			Strong brown and grey coarse-med pumice and lithic ash.
200	5.91		Brown fine ash with paleosol development and root channels present.
15000+			Base of section seen at road bridge across the river. Greyish brown and grey med-coarse sand-matrix diamicton, pebble-large boulder clasts, massive and unbedded, sparse large boulders, firm unit.
	20.91		Base into stream.

Section 97
Tongariro River/ Whitikau Stream, T19 558336
Road cutting on the western side of the Rangipo Prison farm road next to the bridge across the Whitikau Stream.

Unit Depth (mm)	Cum. depth (m)	Correlation and samples taken	Description
400		Taupo Ignimbrite	White and pale grey fine-coarse pumice ash with mixed pumice lapilli and blocks.
50		Mangatawai Tephra	Dark brown and grey fine-med ash.
200		Papakai Formation (Pp)	Brown and yellow brown fine ash
200	0.85	Hinemaiaia Tephra	Pale yellow brown med-coarse pumice ash, shower-bedded.
300		Pp	Brown fine greasy ash with occasional white med pumice lapilli.
20	1.17	Motutere Tephra	Pale brown fine pumice ash, pocketing within brown fine ash.
150		Pp	Brown fine greasy ash with scattered grey fine lithic and pumice lapilli.
400-500		Mangamate Tephra (MT), Poutu Lapilli	Strong brown and fine pumice lapilli, shower-bedded and ungraded with scattered grey fine lithic lapilli.
100	1.92	Poronui Tephra	Greyish brown and grey fine-med ash with pocketing 10 mm thick fine white pumice ash.
30			Grey med lithic ash.
20			Greyish brown fine ash.
40		MT	Grey and yellow brown coarse pumice ash and fine lapilli.
100	2.11	Pahoka Tephra	Grey and pale olive brown fine pumice lapilli and coarse ash.
250			Greyish brown fine ash with scattered fine yellow brown fine pumice lapilli.
300-500			Grey and greyish brown sandy matrix diamicton, pebble sub-angular clasts supported within the matrix, planar fabric preserved.
20			Greyish brown fine ash with scattered fine yellow brown fine pumice lapilli.
40			Strong brown and yellow brown fine pumice lapilli.
20			Greyish brown fine ash with scattered fine yellow brown fine pumice lapilli.
40	2.98		Grey and strong brown coarse pumice and lithic ash and fine lapilli.
20			Greyish brown fine ash with scattered fine yellow brown fine pumice lapilli.
10	3.01	Waiohau Tephra	White fine pocketing fine pumice ash, within greyish brown fine ash.
250			Greyish brown fine ash with scattered fine yellow brown fine pumice lapilli.
40			Strong brown and grey coarse pumice and lithic ash and fine lapilli.
150			Greyish brown fine ash with scattered fine yellow brown fine pumice lapilli.
10-20			Yellow brown and grey fine pumice lapilli.
150	3.62		Greyish brown fine ash with scattered fine yellow brown fine pumice lapilli.
20			Strong brown coarse pumice ash.
30			Grey and strong brown coarse lithic and pumice ash and strong brown fine pumice lapilli.
20			Grey med lithic ash.
80	3.77		Strong brown and yellow brown fine pumice lapilli with scattered grey

			fine lithic lapilli.
20			Dark brown greasy fine ash.
100			Pale brown gleyed fine greasy ash.
600			Brown greasy fine ash.
500+	3.99	Kawakawa Tephra, Oruanui Ignimbrite Member	Pale brown and pink fine pumice ash with scattered white coarse pumice ash
10000-15000		95.16	Grey andesite lava flow.
	18.99		Base into stream.

Section 98
Tongariro River, T19 537411
True right bank of river between "The Rip" and "Hydro Pool" beside the walkway.

Unit Depth (mm)	Cum. depth (m)	Correlation and samples taken	Description
400		Taupo Ignimbrite	White fine-coarse pumice ash with mixed white pumice lapilli and blocks.
250			Grey and greyish brown sands and gravels.
300			Grey and greyish brown med sands, planar and wavy bedded.
50		Papakai Formation (Pp)	Yellow brown fine greasy ash with paleosol development.
200	1.20	Hinemaiaia Tephra within Pp	White fine pumice and coarse pumice ash scattered within fine brown greasy ash.
400		Pp	Brown and yellow brown greasy fine ash with paleosol development.
300			Grey and greyish brown fine-med sands, planar and wavy bedded.
1000+			Grey sandy matrix diamicton, pebble-boulder sub-rounded grey clasts supported within matrix, firm, massive and unbedded.
	2.90		Base into river.

Section 99
Tongariro River, T19 544423
Judges pool, exposure on true right bank of river, second terrace scarp.

Unit Depth (mm)	Cum. depth (m)	Correlation and samples taken	Description
1500			Grey and black med-coarse bedded sands, fine white Taupo pumice interbedded, wavy and planar bedded on a 20-50 mm scale
400		Taupo Ignimbrite	White fine-coarse pumice ash, poorly sorted and massive, sharp upper contact.
1200			Bedded coarse-med gravels, rounded grey clasts supported, with grey well sorted sand between clasts.
1000+			Grey sandy matrix diamicton, pebble-boulder sub-rounded grey clasts supported within matrix, massive and unbedded.
	3.10		Base obscured.

Section 100
Tongariro River, T19 545424
Judges Pool, True right bank of river, cliff exposure.

Unit Depth (mm)	Cum. depth (m)	Correlation and samples taken	Description
2000-30000		Taupo Ignimbrite	White fine-coarse pumice ash and mixed white pumice lapilli and blocks, massive with charcoal fragments and logs near base, upper part reworked and planar and cross-bedded.
1000		Papakai Formation	Yellow brown and brown fine greasy ash, with paleosol development.
400		Mangamate Tephra, Poutu Lapilli	Strong brown and yellow brown fine pumice lapilli with scattered grey fine lithic lapilli, shower-bedded and ungraded.
50-100		Poronui Tephra	Grey and greyish brown fine ash with pocketing fine white pumice ash.
200			Yellow brown and brown fine ash.
100-150			Grey med ash.
300			Greyish brown fine ash.
1000			Grey and greyish brown fine grained diamicton, sands, silts and fine gravels cross-bedded and planar bedded.
1500			Sharp upper and lower contact, unit as above but only planar bedded.
12000			Greyish brown fine-coarse sand massive and unbedded with faint planar fabric, several units separated by 10-50 mm greyish brown silt or fine sand, fine pebbles supported within the sandy matrix. Firm and bluff forming.
	16.60		Base obscured.

Section 101
Tongariro River, T19 538417
True left bank of river at cable-way across river.

Unit Depth (mm)	Cum. depth (m)	Correlation and samples taken	Description
500			Brownish black fine-coarse bedded sands with scattered fine white Taupo Pumice pebbles within, recent soil development in top.
2000			Clast supported pebble, cobble and small boulder deposit, sands between clasts. Pebbles of Taupo Pumice within.
1000			Grey and greyish brown sandy matrix diamicton, with pebble-boulder sub-rounded clasts supported by matrix, clast rich unit.
	3.50		Base into river.

Section 102
Tongariro River, T19 543427
True right bank of river, 100 m downstream of State Highway 1 bridge.

Unit Depth (mm)	Cum. depth (m)	Correlation and samples taken	Description
350			Brownish grey and grey bedded sands cross and planar bedded on a 20 mm scale, Taupo Pumice fine pebbles interbedded.
2100			Grey rounded cobbles and pebble and sand, clasts supported, loose and unconsolidated, very rudimentary soil development in top. Highly rounded in places with zones devoid of matrix and zones with sand matrix between clasts although not supporting clasts. Taupo Pumice fine pebbles present within top of deposit. 80-85 % andesite clasts and remainder greywacke clasts.
	2.45		Base into river

Section 103
Tongariro River, T19 540429
Swirl Pool, true left bank of river.

Unit Depth (mm)	Cum. depth (m)	Correlation and samples taken	Description
500-1500			Pale brown and grey fine sands and silts cross-bedded and containing Taupo Pumice fine pebbles. Alternating layers of silt and sand, bedded on a 10-50 mm scale. Present, recent soil development in top. Irregular lower contact.
0-500			Pale greyish brown and greyish brown silt and fine sand, massive and mottled with pale greyish brown colours, structureless with common root channels.
150-250			Coarse sandy matrix diamicton, pebble clasts supported within the matrix and with common scattered white fine Taupo pumice rounded pebbles, massive and unbedded.
2500+			Grey and greyish brown diamicton, in places matrix supported and in some places clast supported where its upper part is reworked. Grey sandy matrix firm where it is supporting, and grey sub-rounded and sub-angular pebble-boulder clasts, firm unit, massive with no bedding in all of the unit.
	4.65		Base into river.

Section 104
Tongariro River, T19 541435
Upper Island Pool, true right bank of river.

Unit Depth (mm)	Cum. depth (m)	Correlation and samples taken	Description
200			Black and brown fine sand and silt, with scattered white fine rounded Taupo Pumice lapilli, present soil development within this layer, friable and unbedded.
400			Bedded grey and greyish brown sands with scattered white fine Taupo Pumice pebbles, wavy bedded with 10-20 mm scale beds.
50			Fine gravel and sand layer with andesite, greywacke and Taupo Pumice fine-med pebbles and grey sand, clast supported.
50			Greyish brown fine sand with scattered fine Taupo Pumice fine pebbles.
50			Fine gravel and sand layer with andesite, greywacke and Taupo Pumice fine-med pebbles and grey sand, clast supported.
100			Greyish brown fine sand with scattered fine Taupo Pumice fine

			pebbles, 10 mm scale wavy bedding.
1500+			Grey pebbles, cobbles and boulders and coarse sand, clast supported but with matrix of coarse sand between clasts. Sparse Taupo Pumice pebbles within unit. Andesite and greywacke clasts, unconsolidated and unbedded.
	2.35		Base into river.

Section 105
Tongariro River, T19 524425
Stream running through western residential part of town, below major road culvert, highest terrace seen in town.

Unit Depth (mm)	Cum. depth (m)	Correlation and samples taken	Description
1000		Taupo Ignimbrite	White fine-coarse pumice ash with mixed white pumice lapilli and blocks, primary in places, reworked with grey sands in others.
1000		Papakai Formation and Hinemaiaia Tephra	Yellow brown and brown fine ash, paleosolic and greasy, 100-150 mm zone in centre of unit with scattered, sparse, white fine pumice lapilli, and coarse ash
300	2.3	Mangamate Tephra, Poutu Lapilli	Strong brown and yellow brown fine pumice lapilli with scattered grey fine lithic lapilli.
20			Greyish brown fine-med ash.
100			Greyish brown coarse pumice and lithic ash and fine lapilli.
50			Yellow brown fine ash.
200	2.57	Mangamate Tephra, Te Rato Lapilli	Grey, yellow brown and pale yellow fine pumice lapilli and coarse ash.
1000			Obscured.
2000			Grey and pale greyish brown fine grained diamicton. Sand and silt matrix supporting pebble clasts, planar fabric.
1000			Firm diamicton, Grey and greyish brown sandy matrix supporting clasts of pebble-cobble dominantly but also some boulders, massive and unbedded.
	6.57		Base into creek.